



Institute of Subsurface Engineering

Doctoral Thesis

Geological and multi-analytical
investigations on the predictability of
application scenarios for soft, clay-rich
sedimentary rock for CERN's future
subsurface infrastructure in the Geneva
Basin (Switzerland-France)

Dipl.-Ing. Maximilian Mathias Haas, B.Sc.

August 2022



EIDESSTÄTLICHE ERKLÄRUNG

Ich erkläre an Eides statt, dass ich diese Arbeit selbständig verfasst, andere als die angegebenen Quellen und Hilfsmittel nicht benutzt, und mich auch sonst keiner unerlaubten Hilfsmittel bedient habe.

Ich erkläre, dass ich die Richtlinien des Senats der Montanuniversität Leoben zu "Gute wissenschaftliche Praxis" gelesen, verstanden und befolgt habe.

Weiters erkläre ich, dass die elektronische und gedruckte Version der eingereichten wissenschaftlichen Abschlussarbeit formal und inhaltlich identisch sind.

Datum 02.08.2022

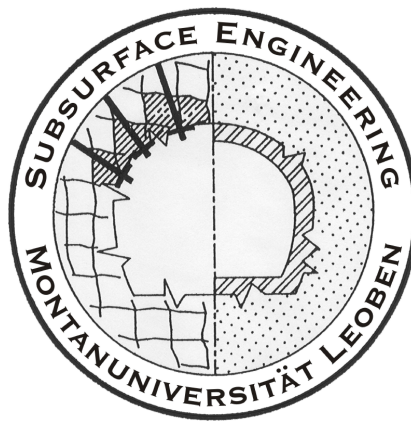
Unterschrift Verfasser/in
Maximilian Mathias Haas

MONTANUNIVERSITÄT LEOBEN

Geological and multi-analytical investigations on the
predictability of application scenarios for soft,
clay-rich sedimentary rock for CERN's future
subsurface infrastructure in the Geneva Basin
(Switzerland-France)

A DOCTORAL THESIS SUBMITTED IN FULFILLMENT
OF THE REQUIREMENTS FOR THE DEGREE OF
DOCTOR RERUM MONTANARUM (DR.MONT.)

TO THE
INSTITUTE OF SUBSURFACE ENGINEERING



Dipl.-Ing. Maximilian Mathias Haas, B.Sc.

ACADEMIC SUPERVISORS

Prof. Dr. Robert Galler

Montanuniversität Leoben

Prof. Dr. Michael Benedikt

European Organization for Nuclear Research

COLLABORATING SUPERVISORS

Prof. Dr. Andrea Moscariello

University of Geneva

Dr. Michael Plötze

Swiss Federal Institute of Technology Zurich

August 2022

Preamble

This cumulative doctoral research has been performed as part of the Future Circular Collider (FCC) study at the European Organization for Nuclear Research (CERN) in Geneva, Switzerland. The goal of this thesis was to (1) identify the encountered geology by CERN's proposed future subsurface infrastructure across the Geneva Basin and its associated geological hazards and (2) to develop a rock characterisation to predict application scenarios for its proposed excavated rock and soil.

The comprehensive, multi-analytical rock characterisation serves as a basis for the evaluation of application scenarios. It is based on the review of more than 600 wells, the digitisation and analysis of geophysical well-logs, as well as field and laboratory analyses across the domains of geochemistry, (clay) mineralogy, rock mechanics and petrophysics. These analyses were performed at the University of Geneva (UNIGE), the Swiss Federal Institute of Technology (ETH) Zurich, both Switzerland, and the Montanuniversität Leoben (MUL), Austria, respectively.

The thesis fulfills the formal requirements stated by the Montanuniversität Leoben for a cumulative doctoral thesis according to the document "*Curriculum für das Doktoratsstudium der montanistischen Wissenschaften an der Montanuniversität Leoben*". It consists of a collection of scientific manuscripts published in international peer-reviewed journals and conference proceedings as well as technical reports published on the open-access ZENODO platform.

This study has received funding from the European Union's Horizon 2020 research and innovation program under grant agreement number 951754.

“Who owns your time owns your mind. Change your time and you change your mind. Change your mind and you change your world.”

- José Argüelles

“I have always thirsted for knowledge, I have always been full of questions.”

- from *Siddhartha*, Hermann Hesse

Acknowledgements

A PhD is a journey; both a scientific and a personal one that has started by signing a piece of paper, a contract. Steps have been taken at different paces - sometimes slowly, sometimes too fast - often into foggy directions. Social and scientific contacts have been established and new scientific directions are explored with every upcoming challenge. Even though each step is decided by oneself, there are people, who guided and supported me: supervisors, colleagues, friends and family. While the ink of the signed contract holds more than I could have ever imagined, it has been the start of an experience I would not have wanted to miss. With the following paragraphs, I would like to mention all the like-minded people that supported me during my PhD journey, for which words can barely express my deepest gratitude.

First of all, I would like to sincerely thank Prof. Dr. Robert Galler (Montanuniversität Leoben, MUL), Prof. Dr. Michael Benedikt (CERN) and Dr. Johannes Gutleber (CERN) for giving me the unique opportunity to work on the Future Circular Collider study. Your trust and freedom for exploration, paired with your undeniable amount of communication made it possible to successfully perform this research.

Essential laboratory analyses would not have been possible without the dedicated support of my collaborating supervisors, Prof. Dr. Andrea Moscariello (University of Geneva, UNIGE) and Dr. Michael Plötze (Swiss Federal Institute of Technology Zurich, ETH), who both supported me throughout the analyses and gave me the incredible opportunity to conduct them on the highest scientific standards.

Thank you, Andrea, for providing me the UNIGE laboratory facilities, and supporting me with your relentless scientific and personal advice embedded in various conversations. Your plain attitude to solve administration problems within a very short time was something I truly appreciated. Our fruitful scientific discussions brought me on a next level of expertise, and your supervision during the rock core inspections in Boussens (France) was truly

something I would have definitely not wanted to miss. A big *Thank you* goes to the whole research team of the Geo-Energy Reservoir Geology and Sedimentary Basin Analysis institute at UNIGE, who supported me in facing the technical challenges of GIS (Dr. Luca Guglielmetti), Python and general coding (Dr. Lorenzo Perozzi), getting a first understanding of the basin's geological and petroleum history (Dr. Silvia Omodeo Sale), boosting my skills in Petrel and Techlog (Dr. Ovie Eruteya) and introducing me to the porosity and permeability measurement device (Dr. Aymeric Le Cottonnec). Thank you for the kind conversations we had in between the work loads in the offices, laboratories or during field trips (Dr. Yasin Makhoulfi, Sam Carmalt, Marc Perret, as well as various Bachelor and Master students). My deepest gratitude is bespoken to Dr. Antoine De Haller for his great practical and scientific support with the QEMSCAN measurements and the critical geochemical and mineralogical discussions, to Dr. Kalin Kouzmanov for his meticulous introduction to the portable XRF device, and to Dr. Dario Ventura for teaching me proper scientific writing. I would also like to thank Dr. Rossana Martini, Nino Isabella Valenzi and Frédéric Arlaud for condoning my occupancy of half the laboratory with rock sample boxes as well as Christine Lovis and Elisabeth Lagut for all the help with administration work. Finally, I would like to thank my dear colleague Davide Carraro for the congenial Kebab lunches that have always ended up in great discussions and personal exchanges.

Words can barely describe my gratitude for the incredible research trip to the Institute for Geotechnical Engineering (ClayLab) at ETH Zurich and the supervision I received by you, Michael. Our scientific discussions on clays and clay mineralogy together with the candid and trustworthy conversations have given me a boost of both personal and scientific self-confidence. A big *Thank you* goes to Annette Röthlisberger and Marion Rothaupt for bearing with me through all the glass washing and rinsing in the laboratory.

With respect to the geomechanical measurements, I would like to cordially thank Prof. Dr. Nina Gegenhuber,

Assoz.Prof. Dr. Marlène Villeneuve, Jörg Krainz and the Bachelor and Master students at Montanuniversität Leoben, who tremendously analysed and helped with the geomechanical measurements.

Dedicated acknowledgements is attributed to Prof. Dr. Alexander Puzrin (ETH Zurich), Prof. Dr. Sébastien Castellort (UNIGE), CERN's department leaders Benoit Delille and formerly Lluís Miralles for their administrative permissions to perform the laboratory analyses on behalf of CERN at these respective universities.

Rock sampling has been an integral part of this thesis and would not have been possible without the dedicated permission and support from Dr. Peter Hayoz (Swisstopo) at the Swiss core storage facility in Hochdorf. Thank you, Peter, for the kind lunches we had, eating MIGROS BBQ chicken on pallets to recharge our (and the machines') batteries after carrying around hundreds of kilograms of rock core material. I would also like to thank Dr. Caroline Nawratil de Bono (SIG) for her permission to visit and sample at ongoing drilling sites in the Geneva area.

This thesis has substantially benefited from review input and scientific discussions with the Swiss and French geological services and governmental institutions. I would like to thank the members of *Le Centre d'Etudes des Tunnels (CETU)*, Dr. Eric Prémat, Dr. Florent Robert, Dr. Laetitia D'Aloia Schwartzentruber and Dr. Laëticia Mongeard for their dedicated support and guidance with respect to the French legislation about excavated tunnel materials. This acknowledgement especially goes to the beneficial and highly appreciated input received by Dr. Jacques Burdin (Ingenieur Conseil) and extended discussions with Dr. Antoine Faure (SETEC-lerm).

I would also like to sincerely thank you, Dr. Richard Nolen-Hoeksema (retired), for your review of the manuscript and Prof. Dr. Jef Caers (Stanford University) for your valuable input on the statistical analysis as part of your courses.

A study such as the Future Circular Collider at CERN contains an incredible amount of people with different technical and cultural backgrounds, mindsets and manners. I would like to mention and thank the ones that supported me the most.

I would like to cordially thank Dr. Luigi Scibile for your

supervision and straightforward, efficient support and trust. Sincere acknowledgement goes to Dr. Luisa Ulrici for her support, in particular during the last year of my PhD. Further people at CERN who I would like to thank are: Dr. Volker Mertens, Dr. Frank Zimmermann, Pieter Mattelaer, Michael Poehler, Zacharie Antoine Arenas, Dr. Markus Widorski, Dr. Christian Theis, Dr. Nabil Mena, Jérémy Voiron and Charly Gasnier.

While the professional environment remains an essential part for scientific discussions, friends and family have often given me the necessary boost to keep on going in whatever environment, state of mind or language.

Some of the new friendships have started with a beer at the pub O'Brasseur or at CERN's restaurant during late evenings. However, one friendship started quite unconventionally during a professional ZOOM meeting. I would like to sincerely thank you, Dr. Jörg Herwanger (Sharp Reflections, Heriot-Watt University), for your relentless and personal support in continued exchanges embedded in a candid and courteous environment.

Furthermore, I would like to thank Ben Swatton for our *British English Friday lunches*, Araceli Alvarez Escobar and David Rodriguez Gomez for *las comidas de españolas*, Amelie Meyer for the *Café-causerie en français* and Stephanie, Emanuel, Lilly and Tim for the Austrian, Austro-Brazilian and German lunches, which contained a lot of laughter and brought a feeling of joy and relaxation. Last but not least, I would like to thank Elisabeth, Patrick and Maria for your unconditional and personal support. Greatest gratitude goes to Clairet for supporting and strengthening me to finish this thesis.

Abschließend möchte ich mich bei meinem Vater, meiner Großmutter und meiner Großcousine für eure sowohl persönliche als auch finanzielle Unterstützung während meines gesamten Studiums von Herzen bedanken.

Maximilian Haas
London, August 2022

Contents

Preamble	iii
Acknowledgements	vii
Contents	ix
List of Figures	xi
List of Tables	xix
Nomenclature	xxiv
Abstract	xxv
Résumé	xxvii
Zusammenfassung	xxix
1 General introduction	1
1.1 Motivation	1
1.2 Research objectives	1
1.3 Thesis outline	2
1.4 Excursus: particle physics as the driving factor for geoscientific investigations	3
2 Technical and legal framework for the applicability of excavated tunnel material in Europe	7
2.1 First initiatives of material management	7
2.2 State-of-the-art management	10
2.3 Application scenarios and technical challenges	13
2.4 Suggestions for the FCC’s material management concept for mechanized tunnelling	15
3 Materials and methods	21
3.1 Data review and rock sampling	21
3.2 Database setup and data analysis	29
3.3 Geophysical well-log analyses	32
3.4 Laboratory analyses	38
4 Large-scale geological investigations in the Geneva Basin	53
4.1 Introduction	53
4.2 Tectonic evolution and stratigraphic framework	53
4.3 Basin-wide stratigraphic evaluation in the context of CERN’s future subsurface infrastructure	59
4.4 Data coverage and interpretation of the depositional environment	69
4.5 Identification of geological hazards	73

5	Rock characterisation of the basin’s geological formations	81
5.1	Introduction	81
5.2	Lithotype characterisation based on geophysical well-logs	82
5.3	Rock classification scheme based on multi-proxy cross-correlations	84
5.3.1	Mineralogical composition and physico-chemical properties	84
5.3.2	Elemental distributions and alteration paths	108
5.3.3	Plasticity modelling and physico-chemical correlations	120
5.3.4	Petrophysical and geomechanical correlations	132
6	Predictability of application scenarios for clay-rich sedimentary rock	155
6.1	Introduction	155
6.2	Bricks and tiles production	156
6.3	Cement, concrete and lime production	157
6.4	Insulation material and glass production	162
6.5	Topsoil construction (agricultural use)	162
6.6	Landfilling and backfilling	164
6.7	Identification of essential rock properties, environmental pollutants and disposal	164
6.8	Analytical limitations and recommendations for minimum sets of analyses	176
7	Summary	183
8	Conclusions	189
9	Outlook	191
	References	199
	Technical reports	225
	Legislation, norms and guidelines	229
A	Peer-reviewed journal articles	231
A.1	Waste or valuable resource – a critical European review on re-using and managing tunnel excavation material	231
A.2	Applicability of excavated rock material: A European technical review implying opportunities for future tunnelling projects	244
A.3	Integrated geo-engineering rock characterisation for CERN’s Future Circular Collider subsurface infrastructure (Geneva Basin, Switzerland-France) from well-log, field and laboratory data	262
B	Peer-reviewed conference articles	307
B.1	Gestion des matériaux d’excavation potentiellement pollués aux hydrocarbures	307
B.2	Geochemical challenges for the construction of CERN’s 90-100 km subsurface infrastructure	320
B.3	A mineralogical re-use classification model of Molasse rock mass in the Geneva Basin	326
C	Non-peer-reviewed articles, data reports and database file	335
C.1	Wiederverwertung ausgehobener Molasse basierend auf geologischer Untergrundmodellierung	335
C.2	Microsoft Access database and data reports	345
D	Curriculum vitae	387

List of Figures

1.1	Research questions structured in four work packages (WP).	3
1.2	FCC milestones since its kick-off meeting in 2013. The data acquired as part of this study has a significant impact on the market survey and tendering after 2022 based on the evaluation of available data along the FCC subsurface layout. CDR=Conceptual Design Report, ESUPP=European Strategy Update for Particle Physics.	5
1.3	Subsurface layout of the FCC-eh tunnel with its main tunnel, caverns, shafts and galleries. By the time of the publication of this thesis, the layout of the tunnel evolved to a reduction from initially twelve to currently eight access points. Modified after Abada et al. (2019a).	5
1.4	The FCC's three initial layouts.	6
2.1	Flowchart for excavated materials specifying geology, processing techniques and laws. Mutual legislation should frame engineering application purposes. After Haas, Galler, et al. (2020).	16
2.2	Schematic on-line analysis of excavated rock and soil material on a tunnel boring machine (TBM) for mechanical excavation. After Haas, Galler, et al. (2020).	17
2.3	Conceptual design of a database plan for the management of excavated rock and soil framed by a legal European authority (green line). The red square indicates tasks to be conducted on-site, respectively in the subsurface and are framed by geological investigations discussed in chapter 4. Key highlights of this concept are integrated in the present study for the (technical) properties, quantities, and database setup in chapter 3, for the rock characterisation (application classes) with on-line sorting being replaced by proper rock sampling in chapter 5 and for the type of applicability scenarios and use-able rock materials in chapter 6. After Haas, Galler, et al. (2020).	18
2.4	Conceptual flowchart for subsurface infrastructure projects.	20
3.1	(A) Total amount of samples per outcrop, well and excavation site locations in the vicinity of the current FCC layout (blue circle). At each unique depth value, a new sample was introduced as digitised from well reports of wells SLHCxx, SPLxx and SPMxx, taken from the literature or measured as part of the present study. The flat bars refer to scientific studies (Table 3.1). (B) Distribution of the 756 analysed locations grouped by their respective purposes. The majority of hydrocarbon wells dates back to the exploration boom during 1970-1990 by various oil and gas operators. Civil engineering site investigations are predominantly associated to subsurface projects built for CERN. The latest wells (e.g., Geo-01 and Geo-02) are drilled based on recent geothermal exploration initiatives of the Swiss canton of Geneva.	22
3.2	A) The High-Luminosity LHC with main construction lots at Point 1 (Switzerland) and Point 5 (France). B) Subsurface layout of HL-LHC's Point 1 with sampled PM17 shaft. Modified after Mattelaer (2019) and Madinier et al. (2017).	23

3.3	Methodological approach depicting petrophysical calculations with revised stratigraphic log, associated geophysical well-logs and mineralogical laboratory results for well Gex-CD-01. White areas in QEMSCAN column represent no measurements. Note that the minerals illite, biotite and muscovite are summarized under the term “mica”. Remaining space in QEMSCAN column refers to other minerals. MD=measured depth (m), TVDSS=true vertical depth sub-sea (m). After Haas et al. (2022).	24
3.4	Borehole identification and workflow procedure relevant for the FCC subsurface infrastructure. The software packages Neuralog and Techlog were used for digitisation and analysis of geophysical well-logs, respectively. An ongoing spin-off project deals with the creation of the Geneva basin’s detailed 3D geological model for the FCC construction in the Petrel software. This model relies on data input from both digitised and measured data as part of this study.	25
3.5	Flowchart of rock sampling based on different sample types and associated laboratory measurements, which led to the identification of the FCC’s encountered geology, potential geological hazards, and the prediction of application scenarios. Landfilling and quarry backfilling are not considered as application scenarios (Haas, Galler, et al. 2020; Haas, Mongeard, et al. 2021). Colours link the sampling and analysis streams to the respective sample types. See text for abbreviations.	29
3.6	Database relationships among linked tables in the Microsoft Access software. The key-symbol next to the ID-fields (highlighted red box) denotes the unique primary key depicted by sample-ID or location-ID for the respective relationship to avoid duplicate entries.	31
3.7	GR values before (A) and after (B) normalization. Middle line in box plots depicts mean values, circles denote extreme values (outliers). The latest geothermal exploration wells (Geo-01, Geo-02, Thônex-1) were used as calibration for older, hydrocarbon exploration wells (Gex-CD-01, -03, -04, -06, -07 and Humilly-2) to normalize the data sets. After Haas et al. (2022).	35
3.8	Exemplified overview of drilled plugs on which petrophysical, geomechanical, geochemical, mineralogical and physico-chemical analyses were performed.	39
3.9	Selected samples with fraction $>400 \mu\text{m}$ of the glaciogenic deposits, Molasse Rouge, and Siderolithic formations as prepared for consecutive physico-chemical analyses. Note their different colours depending on type and amount of clay minerals.	44
4.1	Tectonic realms in the Geneva Basin for the FCC construction with analysed well and outcrop locations.	56
4.2	Lithotypes for wells Montfleury-2 and L112 as well as outcrops Mornex, Biollay, Nyoux and Sarzin-R for various geological formations encountered in the Geneva Basin based on QEMSCAN measurements. Mineral abbreviations: Qz=quartz, Fsp=feldspar, Cal=calcite, Dol=dolomite, Ank=ankerite. After Haas et al. (2022).	64
4.3	Lithotypes derived for wells Gex-CD-01 to -07 from the northern to southern parts of the FCC construction area. The FCC depth denoted between -100 and -300 m ASL. Mineral abbreviations: Qz = quartz, Fsp = feldspar, Cal = calcite, Dol = dolomite, Ank = ankerite. After Haas et al. (2022).	65
4.4	Wells Geo-02, Gex-CD-07 and Gex-CD-04 wells depicting respective QEMSCAN and XRD measurements compared with calculated shale volume from GR log. After Haas et al. (2022).	66
4.5	Wells Thônex-1 and Geo-01 depicting QEMSCAN measurements in comparison to calculated shale volume from GR logs.	67
4.6	Thin gypsum band (Fig. 5.5) encountered at an outcrop in the Molasse Rouge (Upper Chattian) formation. These bands occur at various outcrops with ranging thicknesses between 5 to 22 cm.	68
4.7	The FCC’s well data coverage map based on its current tunnel alignment based on 661 wells. The model will be updated following the results of future site investigations. After Haas et al. (2022).	72
4.8	Swellable montmorillonite (smectite) from XRD measurements for 6 wells. The northern wells (Gex-CD-07 and Peissy-I) show a high variability, depicting maximum smectite values of up to 17.2% by volume. After Haas et al. (2022).	75

4.9	Borehole Montfleury-2 in an anticline structure, depicting Pleistocene deposits confined in a topographic valley (Fig. 4.2). Respective rock samples are used amongst others for lithotype derivation. Modified after Haas et al. (2022).	76
4.10	Cross section A from North to South of the 7 Gex wells in the western part of the FCC's construction area with associated potential geological hazards. Values below well-ID depict topographic elevation in meters. The FCC's current perimeter depth intervals range between +100 and +300 m ASL. Modified after Haas et al. (2022).	77
4.11	Cross section B in NW to SE direction for wells Geo-01, Thônex-1, Geo-02, Humilly-2, Humilly-1, Salève-2, Salève-1, Savoie-109, Savoie-104 and Savoie-105 in the eastern part of the FCC's construction area with proposed geological hazards. Values below well-ID depict topographic elevation in meters. The FCC's current perimeter depth intervals range between +100 and +300 m ASL. Modified after Haas et al. (2022).	78
5.1	Calculated sand-silt-clay model for well Geo-01 showing volume estimates for sand, silt and wet/dry clay, formation water and clay-bound water (CBW). Note the impermeable zone based on the neutron and density logs along the Molasse Rouge formation. After Haas et al. (2022).	85
5.2	Matrix density and volumetric photoelectric factor for the derivation of lithotypes based on RHOB and PEF well-log calculations in well Geo-01. Numbers in brackets depict top and bottom of formation. After Haas et al. (2022).	86
5.3	Clay-type derivation using a Thomas-Stieber plot for eight formations. A trend towards dispersed shale is distinguished for the Hauterive Member of the Grand Essert Formation. Clay distribution for the Molasse Rouge ranges between the structural and dispersed types. After Haas et al. (2022).	87
5.4	Lithotypes derived for wells Geo-01, Geo-02, Thônex-1 and Humilly-2 in the northern part of the FCC construction area based on QEMSCAN analyses. The current FCC depths range between -100 and -300 m ASL. The transition to calcareous formations is well captured by the kink in blue curves (e.g. Geo-01 or Humilly-2 at ca. 0 and -50 m, respectively). Mineral abbreviations: Qz=quartz, Fsp=feldspar, Cal=calcite, Dol=dolomite, Ank=ankerite. After Haas et al. (2022).	88
5.5	Lithotypes analysed in the field and on rock cores encountered along the FCC's current tunnel alignment at different scales analysed from small-scale drilled plugs to rock cores and large-scale outcrops. A1-A2=Quaternary glaciogenic deposits, M1-M5=different marls as part of the Molasse Rouge formation, S1-S5=different sandstones as part of Molasse Rouge formation, S6=sandstone as part of the Siderolithic formation, often referred to as Gompholite, HC=hydrocarbon-bearing sandstone in the Molasse Rouge formation, C1-C2=different conglomerates as part of the Molasse Rouge formation, L=freshwater limestone as part of the Molasse Rouge formation, G1=sandstone as part of Siderolithic Formation, AG=gypsum layer in the Molasse Rouge. After Haas et al. (2022).	89
5.6	Major minerals based on XRD analyses. Note the occurrence of bassanite with 4.4% explicitly in the Geo-02-30 sample, which is not detectable in QEMSCAN analyses. The missing percentages refer to the sum of minor (trace) minerals $\leq 1\%$	92
5.7	Selected diffractograms of XRD powder samples measured from 4 to 80°2-theta angles along the depth of wells Geo-02 (grey area below curve) and Peissy-I (white area below curve) in the northern part of the FCC construction area. HC=hydrocarbon.	93
5.8	Peak separation in XRD diffractogram of a textured (S) and ethylene glycol (EG) treated sample at the Peissy-I well. Incorporation of ethylene glycol shifts the broad peak at ca. 7°2-theta to 6°2-theta (d001 value) from 14 to 17 Å.	93

5.9	(A) Image analyses and quartz grain-size distribution via QEMSCAN with associated modal mineralogy of various clay-rich samples in the Molasse Rouge formation. (B) Clay-rich (siltstone) samples depicting an increased amount of gypsum/anhydrite in the Grès et Marnes Gris à gypse formation, encountered at wells Geo-02 and Thônex-1, potentially subjected to swelling issues (see chapter 4.5).	95
5.10	Image analyses and quartz grain-size distribution via QEMSCAN for the violet marl (A) and freshwater limestone (B) with associated modal mineralogy of the Molasse Rouge formation.	97
5.11	Frame-colour-coded image analyses and quartz grain-size distribution via QEMSCAN with associated modal mineralogy of various sand-rich samples in the Molasse Rouge formation. HC=hydrocarbon.	101
5.12	Image analyses and quartz grain-size distribution via QEMSCAN for glaciogenic (A) and Siderolithic (B) samples with associated modal mineralogy.	102
5.13	Pore size distribution curves (left) and injected mercury volume versus pressure curves (right) measured on selected samples at the C-wells.	103
5.14	Pore size distribution curves (left) and injected mercury volume versus pressure curves (right) measured on selected samples at well Peissy-I.	104
5.15	Pore size distribution curves (left) and injected mercury volume versus pressure curves (right) measured on selected samples at wells Gex-CD-04, -05 and outcrops.	105
5.16	FTIR spectra for sandstone, siltstone, marl and freshwater limestone lithotypes of the Molasse Rouge, and gravel lithotype of the glaciogenic deposits formation. Samples are taken from wells Peissy-I, C1, Gex-CD-04, -05, -07, Geo-02 as well as outcrops Sarzin and Mornex. Absorption bands (after Bertaux et al. (1998), Marel & Beutelspacher (1976), and Sauer & Wuthier (1988)) attributed to organic compounds occur at 3'600-3'200 (O-H), 2'950-2'850 (C-H), 1'750 (C=O) ester, 1'655 (C=O) amide, 1'550 (N-H, C-N), 1'460 (CH ₂), 1'400-1'250 (P=O), 1'380 (CH ₃), 1'240 (C-N, N-H), 1'060 (P-O-C), and 925 (C=C) cm ⁻¹	107
5.17	Calculated correction coefficient on Ca element measured with pXRF and ICP-OES/-MS based on 40 Molasse Rouge samples in the Geo-02 well. (A) Ca content (ppm) before the correction. The slope yields a correction factor of 1.288. (B) Ca content (ppm) after the correction, showing a very good Pearson's correlation coefficient of 0.93 along the 1:1 line.	109
5.18	Calculated correction factors for elements Mg, Al, Ca, Ti, Fe, V, Cr, and Ni as a function of atomic number (Z).	110
5.19	Correction coefficient calculations applied for various elements essential for the identification of application scenarios and disposal classes.	111
5.20	Elemental molar ratios of 42 pXRF samples in well Geo-02 for the qualitative prediction of muscovite, K-feldspar, chlorite and biotite minerals based on Fe, Mg, K and Al in the Molasse Rouge formation, color-coded by depth intervals. No Na concentrations are required for this plot, as they are not measured by pXRF. Borehole Geo-02 represents predominantly sand-rich, clay-rich and marl samples. Numbers in brackets denote X and Y plot locations.	112
5.21	Comparison of elemental molar ratios of 42 pXRF samples in the Geo-02 well (top) and 378 ICP samples across multiple wells (bottom) for the prediction of muscovite, K-feldspar, chlorite and biotite minerals based on Fe, Mg, K and Al elemental distributions in the Molasse Rouge formation. No Na concentrations are required for this plot, as they are not measured by pXRF.	113
5.22	Characterisation of alteration diagrams based on ICP data for 378 samples. (A) Rock characterisation of shale and sandstone based on major elements as proposed by Herron (1988). (B) Zr-Al ₂ O ₃ -TiO ₂ weathered rock type characterisation after Garcia et al. (1994), valid for clastic sediments. ABS=average bulk sediment, CAS=calc-alkaline suite, SPG=strongly peraluminous granite.	114
5.23	Characterisation of alteration diagrams based on ICP data for 378 samples deriving alkali-alumina (K/Al and Na/Al) molar ratios after Davies & Whitehead (2006).	115

5.24	Alteration paths based on ICP data for 378 samples in the Quaternary glaciogenic deposits, Molasse Rouge and Siderolithic formations. (A) Alkali-feldspar alteration with respect to Fe, Mg, Na and K content, showing the alteration paths of AF to muscovite (blue arrow) and chlorite (red arrow). (B) Alkali-feldspar alteration with additional respect to Si, Na and K content. Chl=chlorite, Mu=muscovite, AF=alkali feldspar.	117
5.25	Alteration paths based on ICP data for 378 samples in the Quaternary glaciogenic deposits, Molasse Rouge and Siderolithic formations depicting the Ishikawa alteration index (AI) versus advanced argillic alteration index (AAAI) after Stanley (2017). Chl=chlorite, Mu=muscovite, AF=alkali feldspar.	118
5.26	Screeplot used for the determination of the optimal number of principal components comprising at least 80% of the total elemental ICP data variation. 3 PCs are chosen based on eigenvalues ≥ 1 depicted by the optimal "elbow point".	119
5.27	Pairwise PCA biplot for cross-correlation of polluting elements and those relevant for application scenarios, combining vector loadings and scores of 342 Molasse Rouge samples labelled according to their classified category at the FCC depth interval between 100 and 300 m ASL based on ICP data. The PC1 & PC2 axes denote 40.38% and 25.19% of the variance of the data set, respectively.	120
5.28	Plasticity diagram grouped into low, medium and high plasticity for Molasse Rouge and Siderolithic rock samples comparing measured and modelled liquid limits via Enslin-Neff analyses, following the approach after Dieng (2005). The U-line defines the upper limit for natural soil. The A-line depicts the border between silt and clay.	122
5.29	Comparison of four modelled liquid limits. Note the overestimation of values after Kahr & Madsen (1995) as compared with digitised values.	123
5.30	Temporal water absorption behaviour of sand-rich, clay-rich, marl and limestone samples in the Molasse Rouge, and sand-rich rock (sandstone) of the Siderolithic formation measured via Enslin-Neff. Analyses lasted for 24 h per sample for the derivation of plasticity indices after Dieng (2005). The depicted samples show no significant increase of water absorption after 4 minutes, while after 30 minutes most of the behaviour is associated to evaporation.	125
5.31	Correlated linear relationship for 27 Molasse Rouge samples based on total phyllosilicate content from XRD analyses and modelled liquid limits using BET surface areas, A_S . Limestone outliers (Mornex samples) are excluded from the linear fit. All samples contain a TOC $\leq 1\%$	126
5.32	Water absorption dependencies on total phyllosilicates based on 70 Molasse Rouge samples (left) and BET surface areas on 27 Molasse Rouge samples (right) with both linear (blue) and polynomial (red) correlations. Limestone outliers depicted in grey ellipses are excluded from fitting curves. The red area depicts the 95% confidence band ($y = \pm t_{\alpha/2}$) estimated standard error of prediction. All samples contain a TOC $\leq 1\%$	126
5.33	Water content from 1'168 digitised Molasse Rouge samples taken during the LEP and LHC site investigations from boreholes SPLx.xx, SLHCxx, SPMxx, and Lxxx, with x denoting consecutive well numbers.	127
5.34	(Top) Effective CEC from Cu-trien complex and sum of CEC ICP-OES analyses with respect to total phyllosilicate content. (Middle) Exchangeable cations Na, K, Ca and Mg. (Bottom) Exchangeable cations Al, Sr and Li. All at respective depth elevation levels relevant for the FCC range measured on 70 Molasse Rouge samples.	129
5.35	Digitised grain size distribution curves as measured on samples taken during LEP and LHC site investigations from the following borehole locations: SPLx.xx, SLHCxx, SPMxx, and Lxxx, with xx denoting the consecutive well numbers. Colours depict different trends depending on curve uniformity. Data compiled from Géotechnique Appliquée Dériaz & SA (GADZ) (1981a,b, 1982a,b, 1992, 1993a,b, 1996a,b).	133

5.36	PCA screeplot of clay data depicting the ideal number of principal components (3) based on the "elbow point". The three PC together make up ca. 79% of the total variation in the data sets comprising all physico-chemical, FTIR and XRD analyses.	134
5.37	Pairwise PCA 3D biplot of clay data for cross-correlations among total phyllosilicate, smectite, quartz, calcite, dolomite content with water absorption (Enslin-Neff), water adsorption (Keeling), CEC from Cu-(trien) and ICP-OES, TIC and TOC values. PC1, PC2 and PC3 denote 42.88%, 22.11% and 13.88% of the total variation along the components, respectively.	135
5.38	Porosity and permeability results measured on 170 plug samples with respect to their total clay and total carbonate contents. 93 samples comprise the sum of mineralogical data (XRD and/or QEMSCAN). Samples without mineralogical information are depicted in black colour. Symbol size represents increasing sample (borehole) depths (m).	135
5.39	Porosity versus rock quality index based on FZI calculations on 170 plug samples. 93 samples comprise summarised mineralogical data from XRD and QEMSCAN analyses, and respective total clay contents are colour-coded. Samples without mineralogical analysis are depicted in black colour.	136
5.40	Compressional (V_P) versus transversal (V_S) velocity and porosity with respect to total phyllosilicate content. Outliers are circled in pink colour and excluded from statistical fitting analyses.	137
5.41	PCA screeplot from petrophysics data on 170 Molasse Rouge samples for the identification of optimal principal components considering at least 80% of data variation.	138
5.42	PCA biplot of PC1 depicting 55.19% and PC2 with 14.55% of the total data variation from 170 Molasse Rouge samples for cross-correlation among petrophysical and mineralogical data. <i>COMB</i> refers to properties combining the results from both XRD and QEMSCAN.	139
5.43	Biplot of PC1 and PC3 with 13.67% of total data variation the same 170 Molasse Rouge samples.	140
5.44	Axial stress versus axial strain depicting the rock strength behaviour of clay-rich, sand-rich and marl rocks.	142
5.45	Uniaxial compressive strength (UCS) correlated with both compressional (triangle) and shear-wave (circle) velocities from 27 Molasse Rouge samples, together with correlated fitting lines.	143
5.46	Porosity correlated with uniaxial compressive strength (UCS), quartz content and respective grain densities (g/cm^3) from 27 Molasse Rouge samples.	143
5.47	Histogram of 152 measured and 499 digitised samples from the Molasse Rouge formation. For data sources see Table 3.1.	144
5.48	PCA screeplot based on 33 Molasse Rouge samples featuring quartz, calcite and total clay content correlated with petrophysical data V_P , V_S , and geomechanical data CAI, LAC, LBC, point load indices, and UCS with reference to quartz, calcite, total phyllosilicate and smectite contents. The screeplot depicts the optimum number of PCs as 4 based on the "elbow point" as the last point of eigenvalues ≥ 1 , and a total variation across the data set of $\geq 80\%$. These 4 PCs are depicted and discussed below. All samples contain a TOC $\leq 1\%$	145
5.49	Resulting PCA biplot for PC1 and PC2, based on 33 Molasse Rouge samples (Fig. 5.48) using the same input parameters. PC1 shows the largest total variation with 35.19%, and PC2 of 18.30%.	146
5.50	Short vectors in Fig. 5.49 are better represented in different PC domains, plotting PC2 together with PC3 yields 18.30% and 15.96%, respectively based on 33 Molasse Rouge samples (Fig. 5.48) using the same input parameters but having an increased representation of e.g. the total phyllosilicate content, LAC, LBC, and calcite vectors.	147
5.51	PC1 and PC4 with 35.19% and 8.71%, respectively based on 33 Molasse Rouge samples (Fig. 5.48) using the same input parameters but having an increased representation of e.g. the total phyllosilicate content, LAC, LBC, and calcite vectors.	148

5.52	428 Molasse Rouge from both measured and digitised analyses results of point load indices versus borehole (topographic) depth at various locations, color-coded by bulk density. Data compiled from reviewed well reports, originating from the LEP, LHC and HL-LHC site investigations, see Table 3.1.	151
5.53	Ratio of uniaxial compressive strength (UCS) and Brazilian tensile strength (BRA) to ratio of uniaxial compressive strength (UCS) and point load index (PL) with respective calcite content, calculated linear regression fit and outlier detection for the same 30 Molasse Rouge samples.	152
5.54	Correlation of UCS, Brazilian tensile strength, CAI, LAC, and LBC values for the same 30 Molasse Rouge samples with colour-coded total clay and quartz contents.	153
6.1	Augustinik diagrams based on ICP-MS/OES measurements. (A) 322 Molasse Rouge samples grouped by lithotypes at respective depths, predominantly located in the bricks and tiles windows for direct application. Note that if mixed with pollutants no direct usage is possible and requires further processing. (B) 51 samples from the Cretaceous, glaciogenic deposits, Siderolithic and topsoil formations, with glaciogenic and clay-rich limestone samples depicting the predominant potential to be further used as bricks or tiles. Note that areas outside of applicability scenarios imply further processing or disposal of the sedimentary raw material. $R_2O = K_2O + Na_2O$, $RO = CaO + MgO + MnO$	158
6.2	Box plots with thresholds of mineralogical parameters for selected application scenarios based on a comparison of XRD and QEMSCAN measurements. Applicability threshold limits compiled from BRGM (2009), Garbarino et al. (2018), Schorcht et al. (2013), and Setec-Lerm (2020). Glaciog. dep.=glaciogenic deposits, Sid=Siderolithic Formation; sst=sandstone, slst=siltstone, ls=limestone, cgl=conglomerate, gra=gravel.	160
6.3	CEC values derived from Cu-trien complex measurements with clay content from XRD analyses at respective depth elevation. All samples show CEC values ≥ 1 , relevant for the evaluation of application scenarios.	163
6.4	QEMSCAN analyses of 5 wells extending across the north/northwestern area of the FCC construction ring at its current elevation depth between 100 and 300 m above sea level, highlighting the vertical (220 m) and lateral (100 m to 4 km) heterogeneity of the Molasse Rouge formation. Each bar represents one sample, whereas minor minerals with volume concentrations below 2% were summarised with unclassified minerals. For statistical mineral distribution see Fig. 6.6.	165
6.5	Essential parameters for selected potential application scenarios. The bubble size and colour depict the number of parameters per category. Parameters are further elicited in the text, and based on national legislation (République Française 2003; Schweizerischer Bundesrat 2015), personal communication with experts and research of manufacturer's thresholds, or taken from Anger et al. (2015), BRGM (2009), Faure (2017), Fourvel (2018), Frar et al. (2014), Furlani et al. (2011), Garbarino et al. (2018), Haurine (2015), Haurine et al. (2016), Schorcht et al. (2013), Setec-Lerm (2020), Swiss Confederation (2021), and Wimmer-Frey & Schwaighofer (2002).	167
6.6	Statistical distribution of essential minerals based on QEMSCAN measurements for Geo-01, Geo-02, Gex-CD-02, -05 and -07 wells. The middle line in the box denotes the mean value. Black curves indicate the normal distribution of the data. Diamond symbols represent extreme values (outliers). A wider trend of increased quartz value in the northern part of the basin (Geo-01, Geo-02, Gex-CD-07) is observed. The Geo-01 profile is enriched in dolomite but shows lower values of plagioclase compared to other wells. Values of "other" minerals do not represent a large portion of the data set as indicated by the marginal difference between the "unclassified" and the sum ("unclassified" and "others") with < 2 vol%.	168
6.7	Fresh hydrocarbons (oil) encountered on raw tunnel face at Swiss Point 1 during HL-LHC excavation analysed via the PetroFLAG TM test. Modified after Voiron et al. (2020).	170

6.8	Polluting elements As, Pb, Ni and Cr_{total} including error bars based on pXRF data along well Geo-02 depth in the Molasse Rouge with respective threshold limits for Swiss disposal classes. Class A=non-polluted (green line), class B=polluted (orange line), class E=highly polluted and hazardous (red line).	171
6.9	Ion analyses based on cuvette tests across various boreholes, depicted in the proposed FCC depth range. In liquid form, mg/L is equivalent to mg/kg (ppm).	173
6.10	Pairwise cross-correlation of cuvette analyses with respective dependencies for F, Cr-VI, NH ₄ -N, NO ₂ -N and CN using Pearson's correlation coefficient for monotonic, linear relationships, and a significance level of 0.95.	174
6.11	Elemental department from QEMSCAN measurements for Mg and Cr exemplified by well Geo-02. Mass units in %.	175
6.12	(A) Longitudinal tunnel section along the FCC in clockwise direction based on identified geology, laboratory and field data. (B) Longitudinal tunnel section showing proposed grade of pollution with respect to disposal of the excavated raw material. Extrapolations in areas with no data coverage yield predictions of grades of pollution, also marked as "?". For zoomed-in areas see cross sections A and B in chapter 4. The pollution follows the trend identified in geochemical and cuvette analyses. Faults are excluded for increased readability. FCC layout after (Abada et al. 2019a).	177
6.13	Augustinik diagram comparison of elemental data from QEMSCAN, pXRF and ICP measurements, plotted in application scenarios.	180
6.14	Suggestions of minimum sets of easily-applicable and cost-efficient analyses streams for a successful prediction of application scenarios or disposal.	181

List of Tables

2.1	LEP's initial volume for its excavated materials after CERN (1982).	9
2.2	Swiss and French disposal classes with associated chemical pollutant thresholds.	12
2.3	Purification methods during the HL-LHC excavation.	12
3.1	Data compilation with performed work (R=review, A=analysis, D=digitisation) of industrial and academic third-party sources across the FCC's construction area.	27
3.2	Sampled locations, types of laboratory analyses and number of samples acquired as new data and implemented into the database.	28
3.3	Measured ions complemented by the ICP-OES analysis (Hach Lange GmbH 2021).	48
3.4	Ranges for CAI and LAC thresholds. After Käsling et al. (2007).	52
4.1	Lithostratigraphic units and lithotypes across the Geneva Basin.	70
5.1	Engineering classifications of the Molasse Rouge rock used for the HL-LHC construction.	83
5.2	Mercury intrusion porosimetry results for samples at well C1.	106
5.3	Mercury intrusion porosimetry results for samples of Gex-CD-04 and -05 wells and Sarzin outcrop.	106
5.4	Mercury intrusion porosimetry results for samples at well Peissy-I.	108
A.1	Overview of authorship and metadata of the presented publication.	231
A.2	Overview of authorship and metadata of the presented publication.	244
A.3	Overview of authorship and metadata of the presented publication.	262
B.1	Overview of authorship and metadata of the presented publication.	307
B.2	Overview of authorship and metadata of the presented publication.	320
B.3	Overview of authorship and metadata of the presented publication.	326
C.1	Overview of authorship and metadata of the non-peer-reviewed <i>Berg- und Hüttenmännische Monatshefte</i>	336

Nomenclature

ACCESS	Commercial Microsoft database software	CETU	Centre d'Etudes des Tunnels, a central technical service to provide the French Ministry with expertise and methods related to the design, construction, maintenance, operation and safety of tunnels
ADECO-RS	Conventional tunnelling method and Italian equivalent of the New Austrian Tunnelling Method		
AFTES	Association Française des Tunnels et de l'Espace Souterrain, a multidisciplinary structure, which monitors and observes the design and construction of underground structures in France	CEVA	Tunnel de Champel, a former tunnelling project in Geneva
ASTM	American Society for Testing and Materials	CH1903+	Latest Swiss coordinate system
ATLAS	A Toroidal LHC ApparatuS, one of the detectors along the LHC	CLIC	Compact Linear Collider, an alternative study for a linear future particle accelerator at CERN
BBT	Brenner Base tunnel between Austria and Italy	CMS	Compact Muon Solenoid, one of the detectors along the LHC
BRA	Rock tensile strength measured via the geomechanical Brazilian tensile strength test	DHRO	Corrected bulk density, a petrophysical well-log
BRGM	The Bureau de recherches géologiques et minières, the French national reference institute in geosciences for raw materials and geological risks	DIN	Deutsches Institut für Normung
C&D	Construction and demolition (waste)	DRAGON	A former Austrian research project on the usage of excavated tunnel materials
CAI	CERCHAR abrasivity index, a geomechanical measure for rock abrasivity	DT	Delta-time (sonic), a petrophysical well-log
CALI	Caliper, a petrophysical well-log for borehole size	EEA	European Commission and the European Environmental
CBT	Ceneri Base Tunnel, a railway base tunnel in the Swiss canton of Ticino	EN	European Norm
CCS/CGRF	Local coordinate systems used by CERN	EPB-TBM	Earth Pressure Balanced tunnel boring machine
CDR	Conceptual Design Report	ESDAC	European Soil Data Center
CEC	Cation exchange capacity	ESUPP	European Strategy Update for Particle Physics, essential for future decisions on the FCC study
CERN	The European Organization for Nuclear Research	ETHZ	Swiss Federal Institute of Technology Zurich
		EU	European Union
		FCC	Future Circular Collider, the planned 90-100 km-long particle accelerator at CERN

FTIR	Fourier Transform Infrared spectroscopy, a qualitative analysis for minerals, amorphous substances and organic matter	K-40	Natural, radioactive potassium-40 isotope measured by the (spectral) gamma ray logging tool
GADZ	The Géotechnique Appliquée Dériaz SA, a company based in Geneva specialised in geotechnical and geological investigations	KAT	Koralm Tunnel, a railway tunnel currently under construction under the Koralpe mountain range in Austria
GB	Geneva Basin, the investigated region of this thesis	LAC	See LCPC
		LBC	See LCPC
GB	Geneva Basin, the investigated study area	LBT	Lötschberg Base Tunnel, a railway base tunnel through the Bernese Alps of Switzerland
GBT	Gotthard Base Tunnel, a railway tunnel through the Alps in Switzerland	LCPC	Laboratoire Central des Ponts et Chaussee, a geomechanical test for the abrasivity (LAC value) and breakability (LBC value) of rock
GESDEC	The Service de géologie, sols et déchets, the official geological survey institute of the canton of Geneva	LEP	Large Electron Positron, the particle accelerator hosted before the LHC in the 26.6 km subsurface infrastructure at CERN
GPE	Grand Paris Express tunnel system, a subsurface project extending the existing Paris metro infrastructure currently under construction	LHC	Large Hadron Collider, the 26.6 km-long particle accelerator currently running at CERN
GR	Gamma ray, a petrophysical well-log		
HL-LHC	High-Luminosity Large Hadron Collider, an upgrade of the LHC by an increased number of particle collisions per time	Lithotype	A rock defined on the basis of certain physical properties
		LLD	Deep latero-log resistivity, a petrophysical well-log
ICP	Inductively coupled plasma, written with MS (mass spectrometry) or OES (optical emission spectroscopy), a geochemical analysis	LLS	Shallow latero-log resistivity, a petrophysical well-log
In-situ	Rock analysed at its original place in the subsurface	LN	Long normal resistivity, a petrophysical well-log
ISDD	Dangerous waste according to French law	LV-03	Former Swiss coordinate system
ISDI	Inert, non-polluted waste according to French law	m ASL	meters above sea level
		MIP	Mercury intrusion porosimetry
ISDNDNI	Non-dangerous and non-inert waste according to French law	Molasse	A generic term in geology describing eroded rock material after an orogeny and a geological formation in the Geneva Basin
ISRM	International Society for Rock Mechanics and Rock Engineering	MSFL	Micro-spherically focused resistivity, a petrophysical well-log
Jura-FTB	Fold-and-thrust belt of the Jura mountain range	MUL	Montanuniversität Leoben

N ₂ -BET	Brunauer-Emmet-Teller analysis for the measurement of specific surface area	RQI	Rock quality index, a petrophysical parameter addressing the fluid flow of rock
NAFB	Northern Alpine Foreland Basin	SBT	Semmering Base Tunnel, a railway tunnel currently under construction beneath the Semmering Pass in Austria
NATM	New Austrian Tunnelling Method, a conventional tunnelling excavation technique	SIG	The Services Industriels de Genève, a Swiss infrastructure company responsible for drilling sites in the canton of Geneva
NeuraLog	Commercial software for the digitisation of geophysical well-logs	SMB	Swiss Molasse Basin
NEUT	Neutron (porosity), a petrophysical well-log	SN	Short normal resistivity, a petrophysical well-log
NGF-Lambert	Latest French coordinate system	SP	Spontaneous potential, a petrophysical well-log
NMR	Nuclear magnetic resonance, a petrophysical well-log	SPS	Super Proton Synchrotron, the first subsurface particle collider at CERN
NPHI	Neutron porosity, see NEUT	SSA	Specific surface area
OriginPro	Commercial software by OriginLab for advanced data analysis	STRATER	Commercial software by GoldenSoftware for the visualization of borehole information
PCA	Principal Component Analysis, a statistical method for the correlation of multi-dimensional data sets	SURFER	Commercial software by GoldenSoftware for the visualization of maps
PEF	Photoelectric (absorption) factor, a petrophysical well-log	Swisstopo	The Swiss Federal Office of Topography, responsible for Swiss geodata and topographic maps
PetroFLAG TM	A field measurement for the identification of hydrocarbons	TBM	Tunnel Boring Machine
PL	Point Load (index), a geomechanical parameter for rock strength	Techlog	Commercial software by Schlumberger for the 1D-analysis of geophysical well-logs
PS	Proton Synchrotron, the first surface particle collider at CERN	TELT	Tunnel Euralpin Lyon Turin SAS, a railway line from Lyon in France to Turin in Italy
QEMSCAN	Automated mineralogical and petrography detection (electron microscope), a mineral (image) phase analysis	TEN-T	Trans-European Transport Network (TEN-T), a European network of railway lines, roads, inland waterways, maritime shipping routes, ports, airports and railroad terminals
RHOB	Bulk density, a petrophysical well-log	Th	Natural, radioactive thorium as part of the thorium series measured by the (spectral) gamma ray logging tool
RHOMMA	Matrix density, a petrophysical well-log	TOC	Total organic carbon
RQD	Rock quality designation index, a geomechanical parameter addressing the quality of intact rock		
RQD	Rock quality designation index, a measure of rock quality (strength) measured on intact rock		

U	Natural, radioactive uranium as part of the uranium series measured by the (spectral) gamma ray logging tool
UCS	Uniaxial (unconfined) compressive strength, a geomechanical parameter for rock strength
UNIGE	University of Geneva
V_P, V_S	Compressional and shear wave velocity, both petrophysical parameters
V_{sh}	Volume of shale, a petrophysical parameter derived from GR or SP well-logs
w_{LL}	Critical water content (liquid limit) at which a fine-grained soil no longer flows like a liquid
w_{PL}	Critical water content (plastic limit) at which a fine-grained soil can no longer be remolded without cracking
w_{SL}	Critical water content (solid limit) at which a fine-grained soil no longer changes its volume upon drying
WGS84	The World Geodetic System 1984, a georeferenced coordinate system
XRD	X-ray diffraction, a mineralogical analysis
XRF	X-ray fluorescence, a (portable) geochemical analysis
ÖBB	Österreichische Bundesbahnen, the official Austrian railway company

Abstract

The European Organization for Nuclear Research (CERN) is currently undertaking a feasibility study to build the next-generation particle accelerator named the Future Circular Collider (FCC). The planned FCC will be hosted in a 90-100 km-long tunnel in the Geneva Basin extending across western Switzerland and adjacent France. Traditionally, excavated materials from tunnelling constructions have been treated as waste. Modern thinking has shifted toward finding beneficial uses for these excavated materials. The present study provides basin-scale stratigraphic and lithotype analyses to establish a rock classification scheme within the FCC footprint. The rock classification will help to identify geological hazards and predict the beneficial application uses for the excavated materials. This characterisation is based on a thorough review and digitisation of archive subsurface data as well as an extensive set of newly acquired field and laboratory analyses. These geomechanical, petrophysical, mineralogical, geochemical and physico-chemical analyses were performed on rock material sampled at well and outcrop locations along the FCC's planned subsurface alignment, and analysed in conjunction with geophysical well-log data, resulting in a catalogue of 2'461 samples. The FCC tunnel will intersect 13 geological formations, which are classified into 25 different lithotypes across the Geneva Basin. Three geological hazards are identified to affect tunnelling construction: (1) karstic intervals in the Mesozoic Grand Esert Formation's Neuchâtel Member, Vallorbe and Vuache formations, predominantly associated with fractured limestone; (2) swelling rock associated with anhydrite contents up to 13 wt.% in the Grès et Marnes Gris à gypse formation in the northern part of the basin and swelling rock associated with smectite contents of up to 17.2 wt.% in the clay-rich Molasse Rouge formation; (3) materials that contain hydrocarbons and heavy metals that must be either treated before used for beneficial purposes or treated as hazardous waste. The identified beneficial uses include predominantly brick and tile manufacturing. This study has successfully characterized the geological formations along the proposed alignment for the FCC tunnel. Analytical methods and schemes have been developed, tested and forecast the rocks to be encountered by proposed excavation machines and the beneficial uses for the excavated rock material.

Résumé

L'Organisation européenne pour la recherche nucléaire (CERN) réalise actuellement une étude de faisabilité en vue de la construction d'un accélérateur de particules de nouvelle génération, le Future Circular Collider (FCC). Le FCC prévu sera logé dans un tunnel circulaire de 90 à 100 km de circonférence dans le bassin de Genève, qui s'étend sur la Suisse occidentale et la France voisine. Traditionnellement, les matériaux d'excavation des tunnels ont été traités comme des déchets. La pensée moderne s'est orientée vers la recherche d'utilisations bénéfiques de ces matériaux d'excavation. La présente étude fournit des analyses stratigraphiques et lithologiques à l'échelle du bassin pour établir un schéma de classification des roches sur le tracé du FCC. La classification des roches permettra d'identifier les risques géologiques et de prédire les utilisations bénéfiques des matériaux excavés. Cette caractérisation est basée sur un examen approfondi et la numérisation des données souterraines archivées, ainsi que sur un ensemble complet d'analyses de terrain et de laboratoire récemment acquises. Les analyses géomécaniques, pétrographiques, minéralogiques, géochimiques et physico-chimiques ont été effectuées sur des échantillons de roches prélevés dans des puits et des affleurements le long du tracé souterrain prévu du FCC, et analysées conjointement avec les données géophysiques des puits, ce qui a permis de constituer un catalogue de 2'461 échantillons. Le tunnel du FCC traversera 13 formations géologiques, qui sont classées en 25 lithologies différentes dans le bassin de Genève. Trois risques géologiques sont identifiés pour affecter la construction du tunnel: (1) des intervalles karstiques dans le secteur de Neuchâtel de la formation mésozoïque du Grand Essert, ainsi que dans les formations de Vallorbe et du Vuache, principalement associés à des calcaires fracturés ; (2) des matériaux de gonflement associés à des teneurs en anhydrite allant jusqu'à 13% en poids dans les roches riches en argile de la formation Grès et Marnes Gris à gypse dans la partie nord du bassin et des matériaux de gonflement associés à des teneurs en smectite de 17.2% en poids dans la formation de Molasse Rouge riche en argile ; (3) les matériaux contenant des hydrocarbures et des métaux lourds qui doivent être traités avant d'être utilisés ou

traités comme des déchets dangereux. Il a été identifié la fabrication de briques et de tuiles comme des utilisations bénéfiques potentielles. Cette étude a permis de faire une caractérisation géologique le long du tracé proposé pour le tunnel du FCC. Des méthodes analytiques ont été développées et testées. On peut raisonnablement penser que les analyses testées et les schémas d'analyse développés ont la puissance nécessaire pour prédire quelles roches seront rencontrées lors de l'excavation et comment les matériaux excavés seront utilisés une fois que le projet sera passé à la phase de réalisation.

Zusammenfassung

Die Europäische Organisation für Kernforschung (CERN) führt derzeit eine Machbarkeitsstudie für den Bau eines zukünftigen Teilchenbeschleunigers mit dem Namen "Future Circular Collider" (FCC) durch. Der geplante FCC soll in einem kreisförmigen Tunnel mit einem Umfang von 90-100 km im Genfer Becken untergebracht werden, der sich durch die Westschweiz und das angrenzende Frankreich erstreckt. Rechtlich bedingt wird Aushubmaterial aus Tunneln als Abfall behandelt, jedoch der in dieser Studie präsentierte Ansatz zeigt, dass für die Ausbruchmaterialien des FCC nützliche Verwendungen gefunden werden können. Die vorliegende Studie liefert stratigraphische und lithotypische Analysen innerhalb des Genfer Beckens, um eine Gesteinsklassifizierung entlang der derzeit geplanten FCC Tunneltrasse zu erstellen. Die Gesteinsklassifizierung trägt dazu bei, geologische Gefahren zu identifizieren und Verwendungsmöglichkeiten des Aushubmaterials vorherzusagen. Die Gesteinscharakterisierung basiert auf einer gründlichen Recherche und Digitalisierung von archivierten Untergrunddaten sowie auf einer umfangreichen Reihe von neu gewonnenen Feld- und Laboranalysen. Diese geomechanischen, petrophysikalischen, mineralogischen, geochemischen und physikalisch-chemischen Analysen wurden an Gesteinsmaterial durchgeführt, das an Bohrlöchern und Aufschlüssen entlang des geplanten FCC-Tunnels entnommen und in Verbindung mit geophysikalischen Bohrlochdaten analysiert wurde, was zu einem Katalog von insgesamt 2'461 Proben führte. Der FCC-Tunnel wird 13 geologische Formationen durchqueren, die im Genfer Becken in 25 verschiedene Lithotypen unterteilt sind. Es wurden drei geologische Gefahren identifiziert, die den Tunnelbau beeinflussen könnten: (1) Karstintervalle in den mesozoischen Formationen Grand Essert, Neuchâtel Member, Vallorbe und Vuache, die überwiegend mit gebrochenem Kalkstein verbunden sind; (2) quellendes Gestein mit Anhydritgehalten von bis zu 13 Gew.% in überwiegend tonhaltigen Gesteinen der Grès et Marnes Gris à gypse Formation im nördlichen Teil des Beckens und quellendes Gestein mit Smektitgehalten von bis zu 17.2 Gew.% in der tonhaltigen Molasse Rouge Formation; sowie (3) Gestein,

das Kohlenwasserstoffe und Schwermetalle enthält und entweder vor einer nutzbringenden Verwendung behandelt oder als gefährlicher Abfall entsorgt werden muss. Die Herstellung von Ziegeln und Fliesen wurde als geeignet Verwendungszweck des auszuhebenden Gesteinsmaterials identifiziert. Im Rahmen dieser Studie wurden die geologischen Formationen entlang der vorgeschlagenen Trasse für den FCC-Tunnel erfolgreich charakterisiert. Es wurden Analysemethoden und -schema getestet und entwickelt, die das Aushubmaterial für mögliche Verwertungsszenarien erfolgreich prognostizieren.

1 General introduction

1.1 Motivation

The motivation for this study stemmed from technical and environmental challenges faced within the evaluation of a post-Large Hadron Collider (LHC) particle accelerator, currently named the Future Circular Collider (FCC), at the European Organization for Nuclear Research (CERN). The new particle accelerator machines are planned to be hosted in a 90-100-km long, quasi-circular tunnel in the Geneva Basin across the region Auvergne-Rhône-Alpe in eastern France and the canton of Geneva in western Switzerland. Driven by a resource-efficient and sustainable vision, the CERN FCC commissioned a geological evaluation, rock characterisation and detailed investigation to identify potential beneficial uses for the raw materials excavated from the tunnels.

The present study aims to deliver the scientific and technical basis for the development of a future excavation material management plan. The plan will be based on results from a comprehensive rock sampling plan and large-scale data sets including geochemistry, (clay) mineralogy, petrophysics and rock mechanics. The goal is to identify the essential rock properties for using the excavated materials successfully. Beneficial use applications might include brick making, road construction, concrete admixtures and so forth.

The Molasse lithostratigraphic units are likely to comprise approximately 90% of the estimated ca. 8 million m^3 of excavated rock and soil from the FCC. These units extend laterally 700 km across western Switzerland, southern Germany and eastern Austria (Bachmann et al. 1987; Kempf & Pross 2005; Kuhlemann 2000; Trümpy & Schweizerische Geologische Kommission 1980). Affecting 30.5% of Switzerland (Matter 1980; Sommaruga et al. 2012) and, except for Basel, all major Swiss cities as well as further European mega-cities including London in the United Kingdom, Paris in France, Munich in Germany or Vienna in Austria (Pfiffner 2020), this underlines the importance of finding sustainable uses for excavated, similar clay-rich, soft sedimentary deposits relevant for the FCC

and other projects worldwide in order to apply the developed identification and rock classification scheme herein on finding potential application scenarios.

1.2 Research objectives

The evaluation of application scenarios of excavated rock and soil is substantiated by a rock characterisation (lithotyping) of the encountered geological formations across the Geneva Basin. In order to identify geochemical, mineralogical, physico-chemical, petrophysical and geomechanical rock properties properly, a large set of field and laboratory analyses has been designed and executed. Objectives have been implemented in a scientific program over the course of 3 years, that are summarised in the following research questions framed by two main topics: (1) tunnelling and tunnel trajectory and (2) the excavated, clay-rich sedimentary materials and their application scenarios.

Tunnelling and tunnel trajectory

1. Which geological formations and lithotypes will be encountered across the Geneva Basin by the CERN future subsurface infrastructure (FCC) based on the current layout?
2. Do the identified geological formations pose geological hazards for tunnelling construction and allow predictions for future layout optimizations?
3. How does the existing and missing data coverage affect predictions for potential application scenarios materials in unsampled or undersampled depositional (geological) environments encountered by the FCC tunnel?

Excavated materials and application scenarios

1. What is the current technical and legal state of the art for using and managing excavated tunnel materials on a national and European scale?

2. How do the rock properties of each identified lithotype affect potential beneficial usage?
 - (a) Which analyses adequately address the essential rock properties required for determining a beneficial use of a material?
 - (b) Which physical and chemical properties, i.e. extreme (hazardous) parameters might cause pollution and limit usage applications in favor of material disposal?
 - (c) Do the identified application and disposal scenarios allow a link to the identified rock properties featured in the regional geotechnical classification?
3. What is the minimum set of field and laboratory analyses required for a successful identification of beneficial usages?
 - (a) What are the limitations of each analysis?
 - (b) How do the modern analysis tools used in the present study give an economic or technical advantage over past projects?
 - (c) How do the presented methods for analyzing excavated raw materials have environmental, engineering and economic benefits for the identification of beneficial uses and selected analysis programs for future site investigations?

1.3 Thesis outline

The aforementioned research questions are summarised in respective work packages (Fig. 1.1), which follow the thesis structure explained below. A brief excursus to *Particle physics as the driving factor for geoscientific investigations* in section 1.4 kicks off the introductory paragraphs providing the physical concept behind the subsurface construction, which ultimately influences the FCC subsurface layout.

Current European and national legislation on managing and using excavated tunnel material includes French and Swiss chemical pollutants that mandate potential disposal of the FCC's proposed excavated rock and soil. The review of past and current legislation includes criteria for

evaluating the beneficial use. In conjunction with a new technical concept to provide on-line analyses of excavated materials, the respective outcome is comprehensively discussed in two peer-reviewed publications (see Haas, Galler, et al. 2020; Haas, Plötze 2021b and in appendices A.1 and A.2, respectively). A brief summary of these publications is stated in chapter 2 and extended by a discussion of the lessons learned from past civil engineering projects at CERN when set into context with the FCC. Chapter 3 elaborates with (1) the compilation and digitisation of existing data, (2) rock sampling, (3) the setup and execution of an extensive sample plan and its associated development of a comprehensive database and (4) the measurement procedures and analyses of geochemical, mineralogical, physico-chemical, geomechanical and petrophysical properties.

Chapter 4 discusses the geological formations in the geographically defined *Geneva Basin* and further elucidates on the large-scale stratigraphy and potential geologic hazards to be encountered by the FCC tunnel. The findings of this chapter have been published in Haas et al. (2022) and in appendix A.3, respectively.

The detailed rock characterisation derived in chapter 5 incorporates the aforementioned analyses to characterise the encountered rock and soil for potential application scenarios of the FCC's intersected geological formations.

This forms the basis for the prediction of potential material application scenarios discussed in chapter 6.

Chapter 7 summarises all findings of this study and chapter 8 concludes on the proposed research questions. Finally, chapter 9 closes with an outlook for future research. Chapters 2 and 4-6 use substantial parts of Haas, Galler, et al. (2020), Haas, Mongeard, et al. (2021) and Haas et al. (2022).

Appendix B provides the published conference proceedings, and appendix C states the URL download link to the full data sets as well as the associated data reports published on the ZENODO platform. The password can be requested from the author or any reliable person involved in the FCC study.

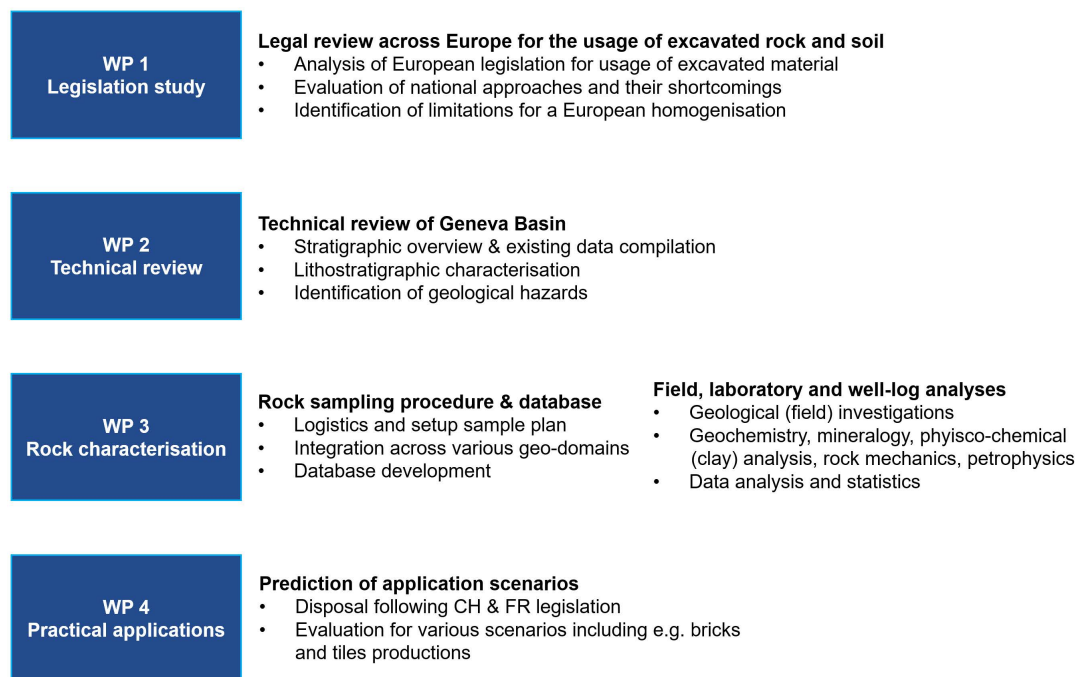


Fig. 1.1: Research questions structured in four work packages (WP).

1.4 Excursus: particle physics as the driving factor for geoscientific investigations

Particle accelerator machines have a long history at CERN. The first particle collider was the Proton Synchrotron (PS) built on the surface, and operated at proton energies of up to 28 GeV in an alternating gradient magnet design. The first subsurface collider machine was the Super Proton Synchrotron (SPS) in 1974 with maximum proton energies of 600 GeV in a tunnel with 7-km circumference. The tunnel was excavated by a tunnel boring machine (TBM) at a depth of ca. 50 m below ground level. Between 1983 and 1989, a 26.6-km circumference, quasi-circular subsurface infrastructure followed, which hosted the Large Electron Positron (LEP) collider and accelerated two opposed beams, each at energies of 55 GeV. As part of the LEP's upgrade later in 1996, additional superconducting radio-frequency (RF) modules paved the way for energies up to 100 GeV for both beams. The associated subsurface infrastructure was excavated at ca. 100 m below surface level by three TBMs and conventional drilling and blasting. In 1994, the CERN council approved the construction of the Large Hadron Collider (LHC), hosted

in LEP's underground facilities, in order to install superconducting magnets in a twin-ring structure for the acceleration of two Pb-beams, each at energies of 7 TeV. The first LHC physics experiments were run in 2007 culminating in the discovery of the Higgs-boson in 2012 (Higgs 1964; The Nobel Prize Committee 2013).

These examples show how the domains of particle physics and geoscientific investigations interact with tunnel design, planning and construction. This synergy has culminated recently with the High-Luminosity Large Hadron Collider (HL-LHC), whose excavation site played a crucial role for rock sampling in this study. Hence, it seems necessary once again to digress into the world of particle physics as the driving force behind tunnel design decisions and associated geoscientific investigations at CERN. The HL-LHC project receives the main focus, whose subsurface excavation finished in March 2020; as well as the FCC study, whose final tunnel alignment is still subject to refinement. The latest decisions based on particle physics considerations from the conceptual design report (Abada et al. 2019a,b,c,d) have been taken into account.

The High-Luminosity Large Hadron Collider

The HL-LHC upgrade aims to increase the current Large Hadron Collider's (LHC) luminosity, i.e. the number of

particle collisions per time, by installing more than 100 new superconducting magnets, 36 large Nb₃Sn magnets, 20 new RF cavities, as well as new system infrastructure close to the existing LHC detectors of Point 1 (ATLAS, Switzerland) and Point 5 (CMS, France). This required the excavation of additional shafts, caverns and tunnels comprising an approximate total length of 500 m from April 2018 to March 2020 and resulted in ca. 50'000 m³ of excavated rock and soil per construction lot (Joint Venture MARTI AG 2018). The new infrastructure is located between 6 to 7 m above the level of the existing LHC. The HL-LHC was excavated conventionally using the ADECO-RS method, an Italian equivalent to the New Austrian Tunnelling Method (NATM). Both perform simultaneous excavation tasks (Lunardi 2008, 2014; Lunardi et al. 2007). The selection of this tunnelling methods followed recommendations based on geotechnical site investigations between 2014 to 2016 in the form of seven boreholes (C1-C7) in close vicinity to the Swiss Point 1 in addition to wells that were drilled for LHC and LEP site investigations in the past. Respective data sets from these boreholes have been reviewed and incorporated into this thesis.

The Future Circular Collider

In 2013, CERN was granted a mandate to investigate the construction of a next-generation, post-LHC particle accelerator machine to be integrated into its existing particle physics laboratory infrastructure (Fig. 1.2).

This machine would be a circular collider, named the Future Circular Collider (FCC). Its construction will start off after 2030 and its first physics experiments are scheduled after 2042. The FCC is one of several possible competing colliders, for example, the Compact Linear Collider (CLIC) at CERN (CERN 2012) and the International Linear Collider (ILC) in Japan. Until the next meeting of the European Strategy Update for Particle Physics (ESUPP) in 2026, CERN will be focusing on detailed investigations to plan and construct the large-scale, 90- to 100-km circumference, circular tunnel infrastructure for the FCC (Fig. 1.3).

After various layout optimizations during the past 8 years (Fig. 1.4), CERN has completed the first feasibility stage of civil-engineering concepts of preliminary horizontal and vertical alignments for the FCC tunnels. The company

ILF consulting Engineers Austria GmbH conducted the work (Ariza & Dallapiazza 2018) that ultimately led to the conceptual design report (CDR) issued in four volumes in December 2018. The CDR provides the full scientific and engineering extents of the future accelerator machines, for example, potential new physics discoveries, new magnet design, ventilation and civil engineering considerations (Abada et al. 2019a,b,c,d). Unless otherwise stated, the following information has been adapted from these four volumes, as well as from personal communications with leading members of the FCC management. Particle physics experiments are driving the tunnel design, whose historical evolution and latest results are summarized, or sketched, in the following paragraphs.

The FCC construction includes excavating a quasi-circular subsurface tunnel, connected with various caverns, galleries and shafts that serve experimental, maintenance or service purposes (Fig. 1.3). The main tunnel features an external diameter of 6.5 m and a circumferential length of 97.75 km¹. The main tunnel sections are connected to surface sites along the ring at currently 12 points (labeled A through L), which have yet to have final locations. The beam transfer tunnels are 4 m in diameter and connect the FCC's main tunnel with the LHC accelerator complex at points B and L. Subsurface facilities include beam dump tunnels, beam dump connections, injection tunnels, junction and service caverns as well as small and large service and experimental shafts and caverns. The experimental structures host the large physics detectors.

Plans include to first set up the lepton collider, the FCC-ee (positron-electron) machine, in the 97.75-km quasi-circular tunnel, to study the structure of existing subatomic particles, e.g., electrons (quarks), in more detail. After 10-15 years of physics measurements, the hadron collider, the FCC-hh (proton-proton) machine follows, which aims for the discovery of as yet undiscovered particles. Both the FCC-ee and FCC-hh machines will be installed sequentially in the same subsurface infrastructure, and supersede the LHC and its upgrade, the HL-LHC, which would both remain as pre-accelerators. A third lepton-hadron machine, the FCC-eh (electron-hadron), runs in parallel to the FCC-hh and would follow the construction of an additional 9.1 km-long tunnel near point L.

¹While the final circumference is still subject to further changes, it is often expressed as the *90-100 km option*.

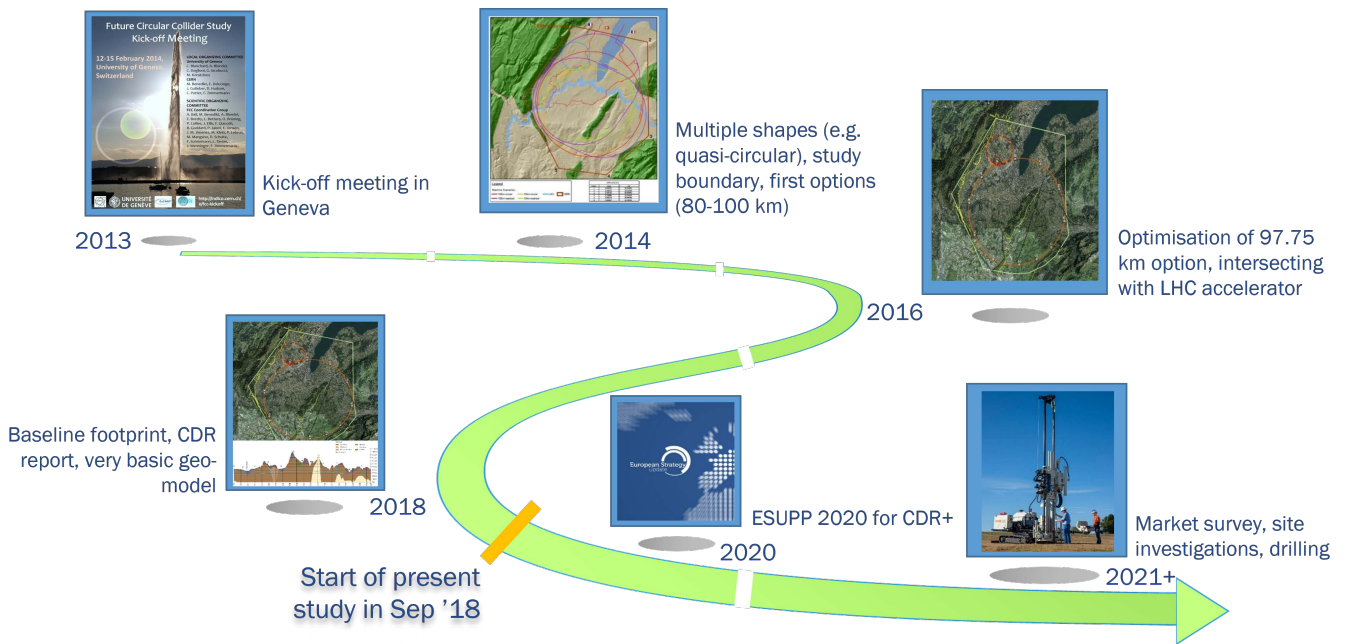


Fig. 1.2: FCC milestones since its kick-off meeting in 2013. The data acquired as part of this study has a significant impact on the market survey and tendering after 2022 based on the evaluation of available data along the FCC subsurface layout. CDR=Conceptual Design Report, ESUPP=European Strategy Update for Particle Physics.

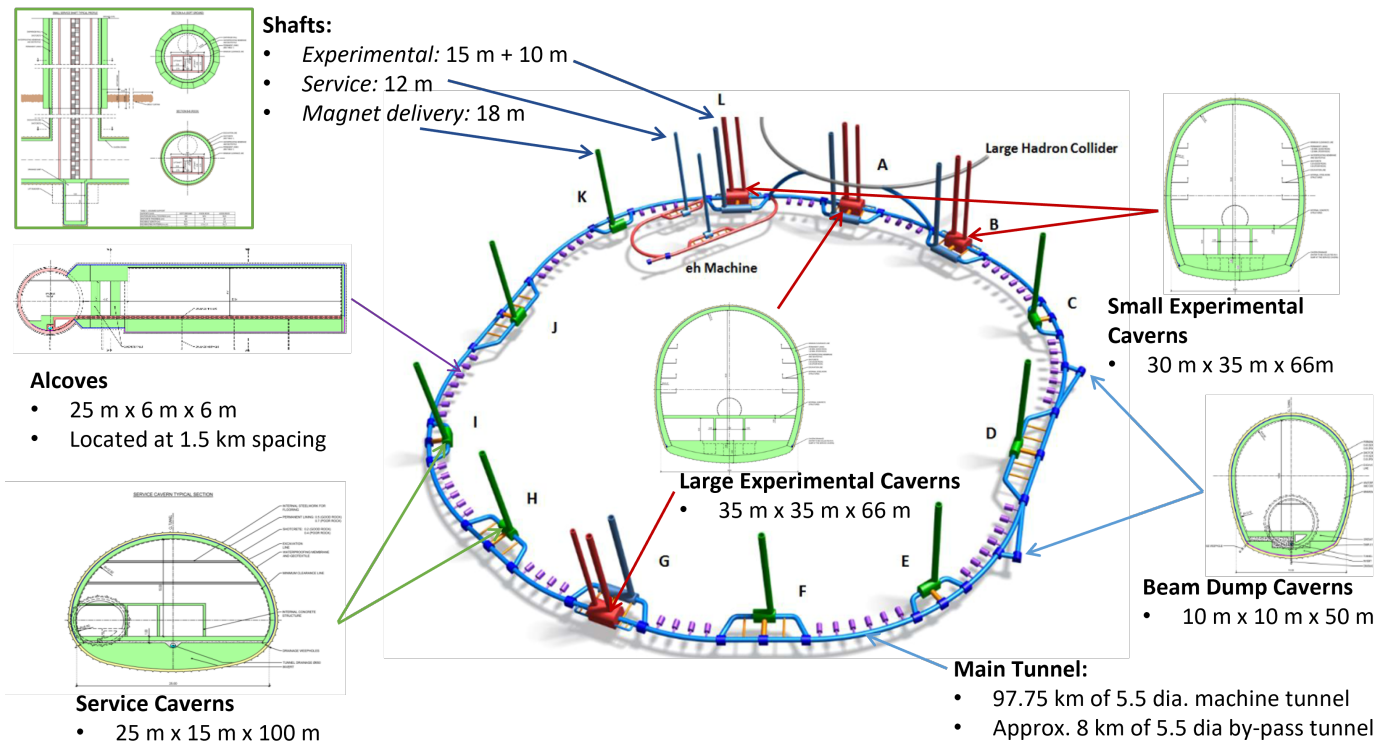


Fig. 1.3: Subsurface layout of the FCC-eh tunnel with its main tunnel, caverns, shafts and galleries. By the time of the publication of this thesis, the layout of the tunnel evolved to a reduction from initially twelve to currently eight access points. Modified after Abada et al. (2019a).

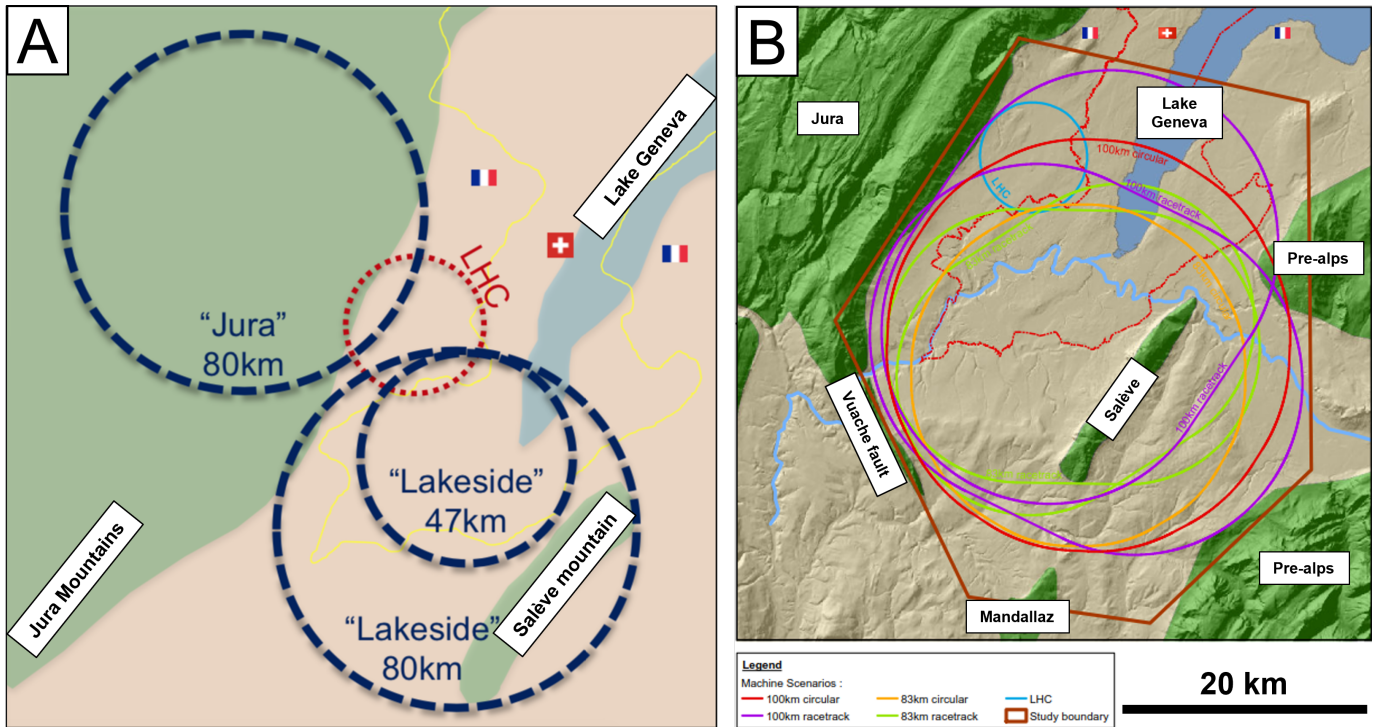


Fig. 1.4: (A) The FCC’s three initial layouts, the *Jura-80*, the *Lakeside-80*, and the *Lakeside-47* options. (B) Definition of the FCC’s study boundary (dark-red polygon) and various optimized 80-100 km subsurface tunnel layouts (multi-coloured circles). The current circumferential length of the tunnel as mentioned in the CDR is set to 97.75 km. Modified after CERN (2014) and Abada et al. (2019a).

The FCC’s feasibility phase is envisaged to last until 2026. Excavation of the first tunnel sectors is scheduled to last 4.5 years; full construction of tunnels and surface facilities is expected to last approximately 7 years. Latest considerations for the FCC’s excavation suggest an open-face shielded TBM assailing excavation tasks at several construction lots. Vertical shaft machines (VSM) excavate the glaciogenic deposits for shaft construction; the Molasse formations foresee single-pass pre-cast segmental lining, while the Mesozoic limestone formations will encounter conventional drill and blast for tunnelling construction. Proposed injection grouting behind the TBM as well as potential ground-freezing and diaphragm walling support the proposed advancement target of 25 m per day (Bruning et al. 2013). Physics equipment installation follows after excavation within 2-3 years. The FCC-ee machine will last approximately until 2055 (Benedikt et al. 2020).

This thesis investigates the proper characterisation of the excavated rock and soil from the FCC tunnels. The goal is to separate the excavated material into that which can be used beneficially and that which must be treated as waste. Results presented herein are based on available data and

published documents by the cut-off date of December 2021.

2 Technical and legal framework for the applicability of excavated tunnel material in Europe

This chapter is based on Haas, Galler, et al. (2020) and Haas, Mongeard, et al. (2021).

This section provides a short summary on the origin, history and actions that have led to the current state of the art of the technical and legal management and usage of excavated rock and soil. Focus has been spent on the review of subsurface construction projects across Europe and how they affected past underground constructions at CERN, to then apply the findings on the FCC. Unless otherwise referenced, text passages have been in parts or entirety taken from Haas, Galler, et al. (2020) and Haas, Mongeard, et al. (2021).

During the course of the literature review and discussions with industrial experts and project-specific on-site engineers, it occurred that legal and contractual documents as well as site-specific technical reports yielded a frayed terminology with respect to the handling of excavated material. These terms seemed not well defined, and often implied a legal status in case the excavated material was referred to as *waste*. This necessitated the introduction of proper terminology (Haas, Mongeard, et al. 2021) for consistency and coherence. Hence, throughout this study the terms *applicability*, *application*, *(beneficial) use* and *usage* are neutral terms for the handling of excavated material with no further legal implications¹. Although common but misleading, the term *re-use* should be avoided due to two predominant reasons: (1) the excavated material has never been used before when excavated and (2) it leads to the misconception with the term *recycling*. In case excavated material is inferred from a legal point of view, this is explicitly mentioned (Haas, Mongeard, et al. 2021).

¹Note that due to several iterations of terminology adaptations with journal peer-reviewers, and the resulting shift of publication dates for scientific manuscripts during the course of this thesis, the inclusion of the word *re-use* was unavoidable for the first peer-reviewed manuscript.

The subsurface infrastructure projects discussed in this chapter stretch across France, Switzerland, Austria, Italy and the United Kingdom. A full description of these case studies is provided in Haas, Mongeard, et al. (2021), and have been thoroughly investigated on a site-specific and state-of-the-art basis by analysing project related data, visiting dedicated construction sites, talking to project engineers, international experts, governmental entities and reviewing scientific literature. These case studies provide a variety of technical scenarios to use excavated material considering heterogeneous geological conditions, technical challenges for processing raw material and environmental issues such as heavy-metal ion concentrations, natural radioactivity or hydrocarbon contamination. However, for the FCC underground infrastructure, its associated construction and potential applications are set in the context of predominantly Swiss and French case studies since also previous civil engineering undertakings at CERN were located across France and Switzerland. Some CERN engineering data have not made it into the peer-reviewed literature. The exact volumes for excavated and used materials vary substantially in the literature and project reviews, because of advancements in construction, continuous improvements in material flow analyses and different (or no) measuring techniques in real-world projects.

2.1 First initiatives of material management

First beneficial use concepts were proposed in 1953 with landfilling as the ultimate solution, which was soon discovered to have a negative impact on the environment (Savage et al. 1994) as landfilling ranks at the bottom of valuable applicability scenarios. Environmental pollution since the 1970's caused European countries to develop institutional

and technical tools to deal with soil contamination related to landfilling, industrial and mining activities (Brombal et al. 2015). Most severe contamination problems stem from construction sites (Rahimzadeh et al. 2018).

The first innovative ideas on using tunnel excavation material apart from landfill date back to the 1990's when a lack of natural aggregates occurred in addition to environmental issues (Gertsch et al. 2000; Kwan & Jardine 1999). New constructions and extensions of Europe's tunnel network (TEN-T) opened up the potential for using excavated material sustainably (European Commission 2005) because underground constructions result in millions of cubic meters of excavated material that are potential resources for beneficial purposes (see e.g., DRAGON 2014). Driven by environmental regulations to minimize waste, there was a general shift toward sustainable construction practices over the last 30 years, and the recognition that excavated rock and soil could be used for beneficial purposes. Past studies focused on treating all construction and demolition (C&D) materials as waste rather than separating materials into their useful and waste components (Ghisellini et al. 2018). C&D waste makes up half of solid waste streams worldwide (Cochran et al. 2007; Dosal et al. 2012; Vázquez 2013). The material is considered as waste because either there is no market for it or it is too expensive to clean up in readiness for a useful purpose. Limiting factors such as legislation and management issues hamper additionally recycled products in the construction industry (Gangolells et al. 2014; Silva et al. 2016). However, a clear and precise review on how to describe, treat and track excavated material from a legal point of view has neither been addressed nor requested in a European framework. Even though the idea of continuous material loops thrives within a circular economy (Alhawari et al. 2021) and landfill mining has emerged as a useful source of usable materials (Altamura 2013; Andrews 2015), illegal landfill disposal continues today (Marzouk & Azab 2014; Pacheco-Torgal 2020).

Since its foundation in 1954, CERN has been planning and operating particle accelerators (L. Evans 2016). Compared to the SPS subsurface, the LEP's tunnel ran through the Jura foothills over a distance of 3 km, resulting in excavated material consisting of Mesozoic limestone formations besides the mixtures of sandstones, marls and conglomerates in the Molasse Rouge formation as well as gravelly sand, gravel and clay as part of the

glaciogenic deposits, and topsoil (see chapter 4). With an advancement speed of up to 58.3 m per day in the northern area of the Geneva Basin between Lac Léman (Lake Geneva) and the Jura mountains, the LEP was excavated with three TBMs and conventional drill and blast. In total, about 1 million m^3 of rock and soil were excavated as part of the LEP construction (CERN 1982). Large portions of the spoil were left in place to provide earth banks as visual and noise barriers. In search of deposit areas for the excavated material, CERN carried out prospections and legal explorations, leading to the identification of possible dumping sites and quarries in the Pays de Gex area in France (CERN 1982). Ultimately, more than 1 million m^3 of excavated material contributed predominantly to backfilling former gravel pits with an average individual capacity of ca. 200'000 m^3 , after official approval from respective legal authorities. The gravel pits were then covered with topsoil and transformed into about 20 ha of pasture land (CERN 1982). The LEP's initial machine alignment was reduced from 30.6 km to 26.6 km to avoid tunneling into deep Triassic anhydritic formations of the Jura mountains and potential tectonic faults identified during geological site investigations. This also reduced the length of the tunnel in the limestone under the Jura by 3 km. Thus, only 90'000 m^3 of excavated limestone under the Jura foothill was effectively used beneficially for road construction (Table 2.1). This example shows how drastically tunnel alignment influences ultimate usage of excavated material. Hence, while there is often a trade-off between choosing the best option for geotechnical tunnel design with respect to geology or tectonics and the best option to maximize the beneficial use of excavated material in complex geology projects, this argument is not valid for the rather simple geology and little tectonic activity as encountered in the Geneva Basin (see chapter 4). Having in mind the optimum connection points to the existing LHC particle accelerator to enable particle accelerations for the FCC, the target should address the resource-efficient and sustainable vision of maximizing the beneficial usage in the FCC study. Finding proper use cases for the excavated material of the LEP example caused also a public issue of concern, which required the open transport and supply of excavated material from construction sites. This was resolved by avoiding the main roads through inhabited urban areas, and following less travelled roads

Table 2.1: LEP’s initial volume for its excavated materials. After CERN (1982).

Construction lot	volume (m^3)
1	210’000
2	110’000
PA3	90’000
4	135’000
PA5	10’000
6	245’000
PA7	20’000
8	290’000
total	1’110’000

(CERN 1982). The fact that the change of the LEP layout was solely based on construction purposes show that the management and usage of excavated material was a non-priority issue back then. Little efforts and analyses have been spent to properly address the excavated rock and soil compared to the efforts taken as part of this thesis. On top of that, the change in perimeter of the LEP, in fact, reduced the amount of usable excavated tunnel material, which would hamper today’s construction approval when set into context for the FCC study because the environmental impact assessment (EIA) requires a clear plan that features suggestions and technically feasible procedures to use the proposed excavated material (Haas, Galler, et al. 2020). This also depicts a driving motivation for the present study, which means to identify whether more excavated material is usable than it was determined to be in the past having in mind both a similar geology and tunnel trajectory for the past and the FCC tunnels. From an economic point of view, usable materials generate income, whereas waste materials cost money.

Besides these regional examples at CERN, similar progress has been observed with respect to the management and usage of excavated material on national and European scales (Haas, Galler, et al. 2020; Haas, Mongeard, et al. 2021). In 1953, management plans called for disposal of excavation material in landfills. However, it soon became

apparent that landfilling resulted in negative impacts on the environment (Savage et al. 1994), and led to its exclusion from today’s list of management solutions (Haas, Galler, et al. 2020). Nonetheless, from the early 1950’s to 1990’s, landfilling was a government approved excavation-material management solution and used for the various CERN projects (Haas, Galler, et al. 2020). Despite landfilling being an approved application scenario, the practice caused environmental pollution and European countries developed technologies and new legislation to manage soil contamination related to landfilling, industrial or mining activities since the 1970’s (Brombal et al. 2015; Haas, Galler, et al. 2020; Haas, Mongeard, et al. 2021). A thorough summary of the elaborated laws, guidelines and regulations on the management and usage of excavated material is found in Haas, Galler, et al. (2020).

As a further consequence, the European Commission and the European Environmental Agency (EEA) were founded and the European Soil Data center (ESDAC) was established to survey and prevent European-wide soil contamination (Panagos et al. 2012), which was severe at contaminated construction sites (Rahimzadeh et al. 2018).

First innovative application ideas for tunnel excavation material occurred in the 1990’s when a scarcity of natural aggregates coincided with environmental issues (Gertsch et al. 2000; Kwan & Jardine 1999). This continued into the 2000’s, as the extension and subsequent constructions of Europe’s tunnel network (TEN-T) expanded the production of excavated material and necessitated a new management plan and sustainable and circular economy (AlpTransit Gotthard 2017; DRAGON 2014; European Commission 2005; Haas, Galler, et al. 2020; Voit 2013). The requirements of environmental impact assessments, environmental regulations, and a shift toward sustainable construction gave increased recognition to beneficial uses of excavated rock and soil (Haas, Galler, et al. 2020). Landfill mining has emerged as a useful source (Altamura 2013; Andrews 2015), whereas (illegal) landfill or disposal has seemed inevitable (Marzouk & Azab 2014; Pacheco-Torgal 2020). To encourage beneficial use and reduce the environmental impact on a tunnelling construction site, Haas, Galler, et al. (2020) suggest an on-line material flow analysis mounted on a tunnel boring machine (Fig. 2.3). This flow analysis is linked to a European database, which itself could be linked to industrial partners to check for local, regional

and national resource availability and potential application scenarios for expected, excavated rock types (Haas, Galler, et al. 2020).

2.2 State-of-the-art management

Input material for application purposes originates from construction and demolition (C&D) waste, i.e. excavated rock and soil, which has experienced recycling in a vast variety across Europe (Dahlbo et al. 2015; European Commission 2020). With estimations of more than 700 million tons of C&D waste produced each year in the European Union (EU) (Iacoboaia et al. 2019) and predictions of more than 800 million tonnes of excavated rock and soil within the next years (DRAGON 2014), European initiatives encourage the construction sector to find sustainable and resource-efficient uses for these otherwise waste materials. The Alpine countries of Austria, Switzerland, France and Italy produce a substantial portion of the excavated material because their mountainous regions promote a tunnel infrastructure for roads, railroads, water diversion and other needs. The geographically varied geological conditions demand site-specific applications of excavated materials (Ghisellini et al. 2018). Hence, for individual construction sites excavated material is analysed and processed either on-site, at dedicated sites or at industrial locations in the close vicinity (Haas, Galler, et al. 2020; Haas, Mongeard, et al. 2021).

Today, there are two reasons why excavated materials need to be processed: 1) legal regulations that dictate a reduction in waste from construction projects, and 2) proper preparation of the tunneling *waste* for feedstock in other industries, e.g., concrete mixtures. Several European construction sites have successfully used excavated material in various applications, of which the production of concrete and geopolymer rank the most prominent (Bellopede 2011; Blengini & Garbarino 2010; Clausi et al. 2018; Kumar et al. 2018; Leemann et al. 2005; Priyadharshini et al. 2017; Teuscher et al. 2007). These two applications required minimal pre-processing because the raw excavated material are already of good quality (Galler & Voit 2014; Resch et al. 2009). However, more sophisticated application scenarios require the geological materials to undergo advanced analyses and processing because they are not

immediately, or directly, amenable as feedstock for the intended use. Nevertheless, the guiding principle of European policies and initiatives is for the construction sector to be efficient and not wasteful of resources.

The Alpine countries of Austria, Switzerland, France and Italy produce a large share of excavated material because of their tunnel infrastructure. These materials come from a variety of complex, high mountain-related geological and tunnelling conditions. Their project analyses and review has revealed that these conditions have justified a general trend towards site-specific application scenarios (Ghisellini et al. 2018), which is still the current case. For each construction site, material is analysed and specifically prepared for processing in factories either on-site or nearby. Several researchers revealed environmental advantage when using excavated rock and soil on-site (Cabello Eras et al. 2013; Chittoori et al. 2012; Hilda et al. 1998; Kenley & Harfield 2011). To make their case, they cite the elimination of transportation off site, the diminution of pollutants and the on-site recycling of the excavation material.

The presence of polluted material plays a major factor during excavation. This impacts landfill prices depending on regulatory national thresholds and integration of risk in the mechanism for adjusting execution time. Research has shown that economic benefits from using the excavated material result in reduced costs tending to be lower than investing in new material or disposing excavated material (Ritter et al. 2013) leading to a reduction of material management costs by up to 85% (Chittoori et al. 2012). However, there are limited data available about using untreated excavated rock and soil across the EU (Magnusson et al. 2015).

In the past ten years, there has been a general trend toward a resource-efficient strategy in the European Union, in alignment with the Europe-2020 initiative. This trend has been observed for the use of excavated tunnel materials (Moreno & García-Álvarez 2018). European strategies include the reduction and closure of landfills for excavated rock and soil to foster on-site use (European Environment Agency 2009). The EU's ten-year strategy invested great efforts in smart, sustainable and inclusive growth (European Commission 2010) for a transition toward a resource-efficient, low-carbon economy to achieve sustainable growth by 2020 (European Commission 2012). It is mentioned that treatment and excavation of natural

resources should be in accordance with protecting the environment and pursuing a circular economy (Geissdoerfer et al. 2017; Mathieux et al. 2017).

The Roadmap to a Resource-efficient Europe visualises that “...by 2050 the EU’s economy has grown in a way that respects resource constraints and planetary boundaries, thus contributing to global economic transformation” (European Commission 2011). It connects resource policies to initiatives such as the Raw Materials Initiative and suggests using excavated material as raw material input for construction (European Commission 2008a,b). The EU Thematic Strategy on the Sustainable Use of Natural Resources outlined decoupling resource usage and economic growth (European Commission 2016a,b). In the Sustainable Consumption and Production and Sustainable Industrial Policy the European Commission aimed to give further impetus to resource-efficiency and eco-innovative production processes, to reduce dependency on raw materials and to encourage optimal, high-quality usage (European Commission 2008a; Velis & Brunner 2013). The European goal has been set to use at least 70% of excavated material (Vieira & Pereira 2015). The target was missed stating only 50% for 2019 (European Commission 2018). France has implemented this plan into national legislation and constituted that 70% of excavated rock and soil material must be used per region (République Française 2015).

Between 2000 and 2010, European initiatives (see extensive list in Haas, Galler, et al. 2020) proposed a clear direction to efficient use of resources causing increased commencements of national legislation and guidelines. Even though legal considerations were thriving, its resulting heterogeneity and bad communication of future legislation are still one of today’s key issues (Mittal & Sangwan 2014). The European Union waste concept is defined in the Waste Framework Directive 2008 and sets out measures to protect the environment by reducing the overall European impacts of resource use and efficiency (European Commission 2008a,b). Legislatively excavated rock and soil are considered to be waste and thus their dispositions are controlled by the Waste Management Act. The objective definition of waste is not fulfilled for tunnel excavation material recycled on construction sites according to EU directives. This waste definition also includes naturally occurring clean or contaminated soil, stone, rock and similar materials, which have been excavated as a result of site activities (LawInsider 2022). To use excavation material

from tunnelling construction sites, it is necessary to reach the end of waste status but this status is automatically attributed on tunnelling construction sites. Waste can be recycled if the same requirements as for primary raw material is fulfilled. Hence, excavation material from tunnelling construction sites should no longer be classified as waste material but as possible raw material, or feedstock, for industrial and construction applications. The fact that most excavated material is not available in a form for instant usage and that possibilities for recycling must be carefully measured, and satisfies the objective’s definition of waste. Legal waste terminology is regulated by federal governments and EU directives must be transposed into national law of each member state. A comprehensive list of legislation, guidelines and recommendations for Austria, Switzerland, France and Italy within the scope of using excavated rock and soil from underground tunnelling sites is summarised in Haas, Galler, et al. (2020).

Based on the two individual regional application cases (Haas, Galler, et al. 2020), Haas, Mongeard, et al. (2021) elaborated a mutual technical basis that aims to be applicable across international construction sites dealing with the engineering rock characterisation of excavated tunnel material. The most significant parameters were identified and set into context with a various number of laboratory and geophysical well-log analyses for the subsequent evaluation of application scenarios. A new approach was to identify relevant parameters in-situ by exploiting the analyses of geophysical well-logs. Such an approach has never been attempted before in the context of characterising rock for finding potential beneficial use scenarios.

Subsurface infrastructure projects have paved the way to potential resources and the derivation of sophisticated concepts on how to use excavated tunnel material. Today’s goal of subsurface projects is to maximize the use of excavated material, produce sustainable products and minimize landfilling. The status of waste is a tool to control environmental impacts, and the valorisation of waste is strongly encouraged. However, despite recent stipulations across Europe caused by various initiatives of the European Commission to increase sustainability, excavated rock and soil are still considered waste (Haas, Galler, et al. 2020). This fact hampers legislation procedures and efficient technical application scenarios as a potential resource, and is also not in line with legislation to be pursued

Table 2.2: Swiss and French disposal classes with associated chemical pollutant thresholds relevant for the FCC in the Geneva Basin. ISDI=inert waste, ISDND=non-inert & non-hazardous waste, ISDD=dangerous waste. *Approximate industry prices based on HL-LHC project as of year 2018. **Standardised leaching test to be applied after standard EN 12457-2 (European Norm (EN) 2003a). Values refer to dry substances according to the Swiss Ordinance on the Limitation and Disposal of Waste ("OLED") (Swiss Confederation 2016), the French Order of 15 February 2016 on non-hazardous waste storage facilities, JORF n°0069 (République Française 2016), and French Order of 12 December 2014 on the conditions of admission of inert waste in facilities falling under headings 2515, 2516, 2517, the inert waste storage facilities falling under heading 2760 of the nomenclature of classified facilities (République Française 2014a), and JORF n0289 of 14 December 2014 page 21032, text n11 (République Française 2014b). Valid for excavated material with more than 99 wt% of loose or solid rock. Modified after Haas, Mongeard, et al. (2021).

Country	Disposal classes	Price* (CH & EUR/ton)	HC _{C5-C10} (mg/kg)	HC _{C10-C40} (mg/kg)	Cr _{total} (mg/kg)	Cr(VI) (mg/kg)	Ni (mg/kg)
Switzerland	A	25	<1	<50	<50	-	<50
	B	60	1-10	50-500	50-500	-	50-500
	E	150	10-100	500-5'000	500-1'000	<0.5	-
	E+	200*	>100	>5'000	-	>0.5	-
Total organic carbon (mg/kg)							
France	ISDI	3	<500	<0.5**	-	<0.4	
	ISDND	60	50'000	10-70**	-	10-40	
	ISDD	140	60'000	>70**	-	>40	

Table 2.3: Purification methods during the HL-LHC excavation.

method	price (EUR/ton)
Hydrocarbon removal	80 (Point 1)
	60-80 (Point 5)
cement factory	80
desorption (removal of pollutants)	110
incineration	300

by, for instance, the mining industry, which treat their respective "excavated material" according to mining laws. On top of that, quarries are often used for backfilling excavated material from tunnelling construction sites, and declared as a successful application solution. National guidelines and recommendations bear potential to serve as a basis for a homogeneous European legislation; or at least within the European Union. Technical limitations imply physical and chemical characterisation of excavated rock and soil as well as their positioning in relation to inert waste thresholds. Respective analyses have to be conducted as part of material flow analyses if performed on-site. While a dedicated European authority has been suggested to undertake responsibility for the material management and govern a technical database obliged to aim for resource-efficient application scenarios and public awareness across Europe (Haas, Galler, et al. 2020), the present study's goal also aims at finding the minimum set of required parameters, laboratory and field analyses to derive an engineering rock characterisation that allows predictions for potential application scenarios as early as during feasibility phases of subsurface construction projects.

This also includes geophysical well-logs during site investigations.

2.3 Application scenarios and technical challenges

During construction, the inspection of excavated material is usually conducted by a geologist in conventional excavation, by different camera types in mechanized tunnelling at the tunnel face (Wenighofer & Galler 2017) or analysed with sensors for petrographical descriptions of rock material (Robben & Wotruba 2019). This allows for a separation of excavated rock into technical application classes. Subsequently, the material must be characterised by laboratory analyses, sorted, processed, and potentially temporarily stored if environmental pollutants are encountered. The operation of processing plants under different conditions as well as high demands upon quality control then follows a developed material management plan (Burdin et al. 2017; Voit 2013). Excavated material is analysed chemically, mineralogically and geomechanically and prepared for processing on first a small-scale and then large-scale scenarios in laboratories and construction sites. The literature review has shown that each tunnelling project has developed individual concepts adapted to local geological conditions. These analyses characterise the material for engineering purposes into subsequent application classes. Reconciliation of these analyses with national and European legislation classify excavated material as waste, if they leave the construction site requiring technical procedures such as processing (washing, crushing, sieving) and treating (chemically and/or physio-mechanically) conducive to removal of waste status in favour of environmental sustainability (Blengini & Garbarino 2010; Dahlbo et al. 2015). The definition of excavated material as waste per se does not hamper its potential applications but rather leads to rigorous engineering procedures and laboratory analyses aiming for compliance with legal thresholds and regulations upon removal of polluting substances (Rios 2018; Ritter et al. 2013; Ritzén & Sandström 2017; Rodríguez et al. 2007) for individual tunnelling construction sites. An extensive discussion on these subsurface construction sites is found in Haas, Mongeard, et al. (2021), whereas focus is spent on CERN's High-Luminosity LHC project in the following. The High Luminosity Large

Hadron Collider (HL-LHC) project involved the construction of complex underground infrastructures in the Geneva Basin on both sides of the French-Swiss border, adjacent to existing underground infrastructure of the Large Hadron Collider operated at CERN (Fern et al. 2018; Voiron et al. 2020). Swiss Point 1 site comprised the construction of a shaft with an internal diameter of about 12 m to a depth of 60 m (PM17), a cavern of 18 m in diameter and 45 to 50 m in length (US/UW17) as well as a main gallery of 50 m² section and a length of 300 m, both connected to secondary galleries of 50 to 70 m in length (UA/UPR 13 & 17 and UL 13 & 17). Underlying geology comprised Molasse units, which were deposited as detrital formations during the alpine orogeny (Moscariello et al. 2020; Oxburgh 1981). A geotechnical classification based on HL-LHC Point 1 data (Switzerland) subdivides the Molasse Rouge into very weak marl, weak marl, medium-weak marl, weak sandstone, medium-strong sandstone and strong sandstone formations (Fern et al. 2018). These six categories were based on uniaxial compressive strength, Young's modulus and Atterberg limits and were used for first trends of application scenarios for excavated material. The Molasse lithostratigraphic unit contains natural hydrocarbons originating from natural degradation of organic material accumulated as lenses and layers of variable extent and thickness (Voiron et al. 2020). It should be noted that such lenses had already been encountered at CERN during the civil engineering work for excavation of the currently operational Large Hadron Collider (LHC), with hydrocarbon contents ranging from 700 to 2'800 ppm. As to be seen in chapter 4, the distribution of hydrocarbons will also likely have a crucial environmental impact on the FCC construction and its materials' application scenarios on a larger, basin-wide extent. At Point 1, C_{10} to C_{40} hydrocarbons were detected in both solid and liquid state during excavation via a PetroFLAG test. It comprised an inexpensive and environmental-friendly portable field device for determining a probable contamination of a 10 g material sample. Concentrations of hydrocarbons C_{10} to C_{40} were evaluated in the laboratory according to the SN EN 14039 standard, with results available within 3 to 10 days. Concentrations of C_5 to C_{10} hydrocarbons were also evaluated according to the measurement of purgeable organic compounds in water by gas chromatography. Within the Swiss legal framework, these results were considered to further decide on the quality of material to judge further

applications or disposal. Any contamination were assessed at the end of each excavation step by the geotechnical engineer in charge of geological monitoring of the project. Excavated material was transported to the surface via a six cubic metre skip and dumped on the surface site in a weather-protected hall.

The HL-LHC project, ultimately, exhibits a small-scale prototype for Swiss and French legislation considerations for the FCC study (Voiron et al. 2020). On top of that, due to different national legislation in France (Point 5) and Switzerland (Point 1), the management of the HL-LHC's excavated material was treated separately at each construction site, handled by regional Swiss and French earth work companies. Table 2.2 shows the three classes (K1, K2, K3) in France for the disposal of excavated material, with K1 containing the most and K3 the least hazardous material. For French Point 5, company NABAFFA delivered the excavated rock and soil to Chevry (France) as K3 material, and to Lyon (France) as K1 material to a regional biocentre for biological treatment to remove the hydrocarbon pollution, ultimately turning the K1 into K3 material prior to final disposal. On the contrary in Switzerland, four disposal classes exist for excavated material, respectively classes A, B, E, and E+. For Swiss Point 1, additional sub-classes, B+ and B-, were introduced due to the higher concentration of hydrocarbon pollution lacking heavy-metal ions, hence not necessarily declared as E class material (Voiron et al. 2020). The B- materials was determined as slightly polluted materials, within the low limit and could be used for backfilling on the project site in accordance with the local GESDEC agreement; whereas the B+ quality materials was also determined as slightly polluted materials but in the upper limit of type B landfills in accordance with article 19 of the Swiss OLEP regulations (Swiss Confederation 2016). With respect to the on-site mixture of excavated class B material, its further usage on-site was not allowed and direct disposal was imperative. For the class E and E+ of hydrocarbon-polluted material mixed with class B heavy-metal polluted material, no special treatment was required and direct disposal was allowed. However, for class E and E+ hydrocarbon-polluted material *and* class E heavy-metal polluted material, direct disposal was strictly forbidden and the material was treated as hazardous waste, leading to its purifying biological treatment. Table 2.3 states the procedure for purification and subsequent disposal at French Point 5,

and shared, in particular, hydrocarbon purification with Swiss Point 1. Exceptional for Swiss Point 1, some excavated material was also delivered to a local cement factory for the production of concrete with the material requiring further processing. For both Point 1 and Point 5, CERN was the owner of the excavated material upon disposal, then following the release of owner rights. The same legal ownership would apply to the FCC's excavated material. Excavated material at the HL-LHC project required a thorough purification linked to chemical pollutants such as nickel and chromium. For the HL-LHC construction sites in Switzerland (Point 1), the total excavated material was about 50'000 m³. Original pollution was estimated at 25%, whereas an actual 35% were encountered (status February, 2020). Excavated material was sent to a local concrete producer for Point 1 material and local soil purification companies for Point 5. Based on Swiss and French legislation (République et Canton de Genève 2016; République Française 2003, 2015; Swiss Confederation 1983, 1989, 1998, 2005, 2016), the grade of pollution was significantly higher at LHC access Point 5 compared to Point 1. Swiss disposal classes for Point 1 were applied as respectively A, B (i.e. B- and B+), E and E+ classified material. For Point 5 French acceptance thresholds classified as ISDI (inert waste), ISDND (non-inert non-hazardous waste) and ISDD (dangerous waste). The project marks a crucial local example, as similar situations might occur for the FCC project. Based on instructions given by the engineer to the contractor, final destinations of excavated material were specific disposal or used on-site depending on the degree of pollution. Unpolluted but surplus material was disposed as unpolluted excavated material in accordance with Swiss legislation. Particularly in the constructing tunnels, it was found that excavated material contained traces of pollution measured by laboratory tests that were not previously detectable. In accordance with the Swiss precautionary principle, all excavated material was considered potentially polluted and transported to sheltered temporary storage areas, thus causing increased space constraints. The management of potentially polluted excavation material required increased monitoring during excavation continuously until use or final disposal. The different stocks were defined according to the origin of the material (per excavated structure) and were spatially

separated by modular concrete blocks. Based on laboratory results and in accordance with the regulatory thresholds defined by Swiss authorities for hydrocarbons, four application classes were identified: grade A material used for backfilling on-site or disposal as unpolluted material; grade B- material as very low-polluted material within the lower limit used for backfilling on the project site; grade B+ material as slightly polluted within the upper limits shipped to type B material; and grade E material shipped to a cement factory. Class E material was integrated into the flour preparation mix used in the homogenisation bed of the kilns, composed of a fraction of 30 to 40% Molasse material from the project, and limestone and siliceous material delivered by other quarries (Voiron et al. 2020), i.e. processed and prepared with additives. The HL-LHC project was a good example for showing the legal and technical harmonization of stakeholders and authorities as implementations for appropriate use of excavated material was necessary. This development was conducted in close collaboration with associated Swiss authorities and governmental entities (Vernus et al. 2017; Voiron et al. 2020). The legal and technical reconciliation was an inevitable step towards a successful use of excavated material and a proper use of excavated material will be required for FCC encountering similar issues.

In France, companies and quarries need special authorization to accept material for landfilling featured. The *formulaire installation classie pour la protection de l'environnement (ICPE)* is required to authorize companies and quarries to use excavated material for landfilling, which is then approved by the *directions Régionales de l'Environnement, de l'Aménagement et du Logement (DREAL)*. Upon authorization, the waste status is removed. However, in case no authorization is given, the quarry becomes an ISDI storage place for inert waste.

2.4 Suggestions for the FCC's material management concept for mechanized tunnelling

Applicability depends on geotechnical, petrophysical, mineralogical and chemical properties of excavated rock and soil and its underlying material management boundary conditions (Fig. 2.1). Excavated material has a strategic

impact on sustainable management of limited mineral resources, higher resource-efficiency and a sustainable environment. A material flow analysis concept with expected masses of excavated material should be prepared during feasibility phase of any underground project. Within the scope of an underground project, the constructor captures data of the subsurface via methods of site investigations.

Drilling samples or geophysical well-logs should be analysed to obtain essential information regarding complex geological situation, potentially incorporated even before construction (Haas, Mongeard, et al. 2021). Based on the resulting geological profile, volume and properties of the future excavated material can be estimated in advance and fine-tuned as construction progresses. The concept is based on an on-line database derived by continuous analyses on a conveyor belt attached to a TBM (Fig. 2.2), and considers an environmental and sustainable storage of oversupply in excavated material to cover future demands and the usage of less quality material. Transport routes, material specific processing, intermediate storage and landfilling should be taken into consideration in terms of CO_2 emission but are negligible for on-line analyses. The material management concept is a basis to prepare delivery contracts with potential purchasers. The proposed on-line database contains a matrix with integrated specific requirement lists for relevant and possible parameters for usage at local and global level linked to economic and environmental transport routes. Processing of raw material could distinguish between hard, soft and mixed rock, different mineral phases and would combine its transport to eligible industrial consumers. The individual utilization scenarios could be derived from a requirement matrix such as a risk mitigation matrix. Using the database, the constructor can thus immediately determine the utilization potential of the subsurface. Technical data would be continuously updated and linked to mutual legal contamination thresholds or trans-national transport legislation registered in the database. Intermediate purchasers and material processing companies would be eligible to access the database and specifically store their demands and requirements such as material properties, time of demand, volume or maximum transport distances. This would also allow for proper statistics for future data analyses and the planning of future international projects. Excavated material would be classified by real-time comparison with the required specifications in the on-line database and framed

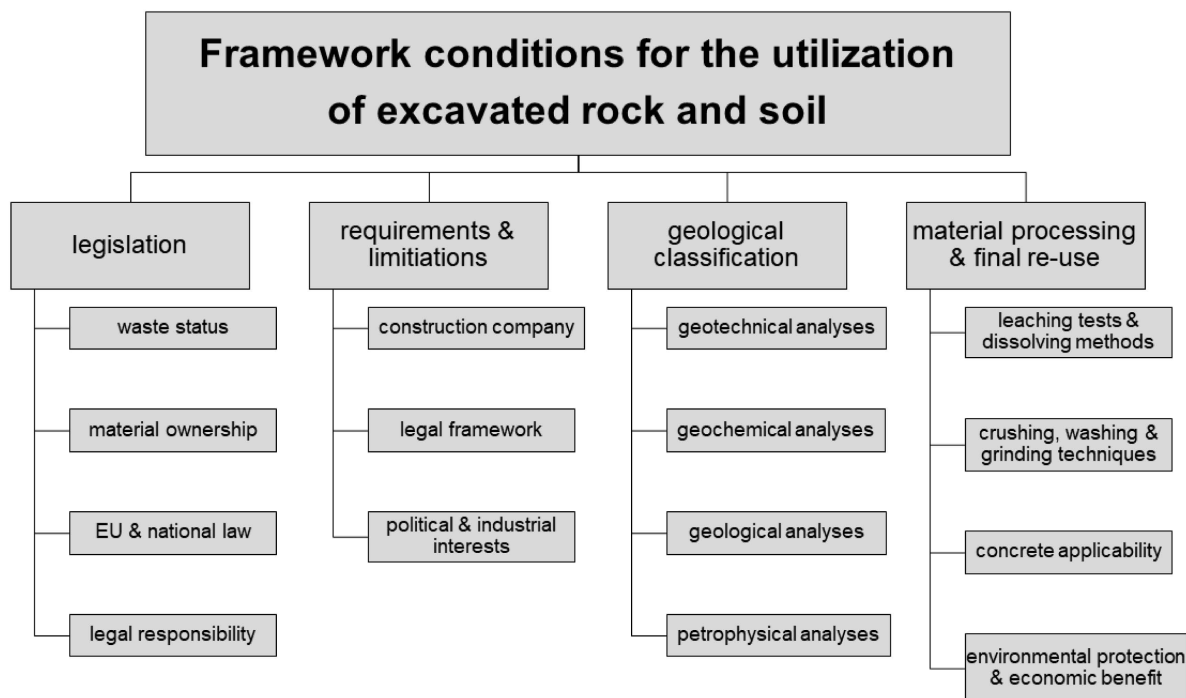


Fig. 2.1: Flowchart for excavated materials specifying geology, processing techniques and laws. Mutual legislation should frame engineering application purposes. After Haas, Galler, et al. (2020).

by one European authority. It could be argued that legislation drives the requirements of technical concepts, whereas it must be considered that natural resources need to be pre-processed for construction material anyway. Economic applicability benefits would result from earnings by selling certain material quality and from savings, first from the substitution of purchased aggregates for the internal needs of the site with the excavated material and second, through reduced landfill costs. Technical application concepts have become a mandatory part of environmental impact assessment procedures to receive construction approval. Thus, sorting excavated material is possible before start of construction during site investigations. In case properties of excavated material do not comply with quality requirements or industrial standards for application on-site, the material should be used for embankments (landfilling). However, this should be overcome by iterating the processes in the red dashed square (Fig. 2.3).

On-line analyses ease the process of waste avoidance due to characterising the material on a conveyor belt without touching the surface leading to avoidance of waste status and tracking material flows. This would give improved insights into rare and critical metals (Ayres & Talens Peiró

2013) also linking it to construction information models (BIM). Industries must be incorporated by the European applicability authority and support classification models including geotechnical, petrophysical, geological, mineralogical and chemical parameters in their laws. The new authority should be responsible for the material usage and waste management, who emphasises the development of a material flow analysis and governs a technical database. It should be the goal to maximise valorisation for final products to avoid landfilling. Application goals set to 90% or beyond should be outlined as a European standard and are likely achievable within a mutual legal and technical framework. The new and innovative technologies should be used for an on-line analysis of excavated material on tunnel boring machines. Such a concept has not been suggested before and bears potential for resource-efficient and sophisticated usage collected in a single process. The concept of on-line analyses on the TBM, respectively conveyor belt additionally saves time by avoiding sending samples to laboratories. There exist little European efforts to homogenize the underlying legislation or set the basis for a technical ground in terms of an overarching rock classification (see chapter 5 and in AlpTransit Gotthard (2017),

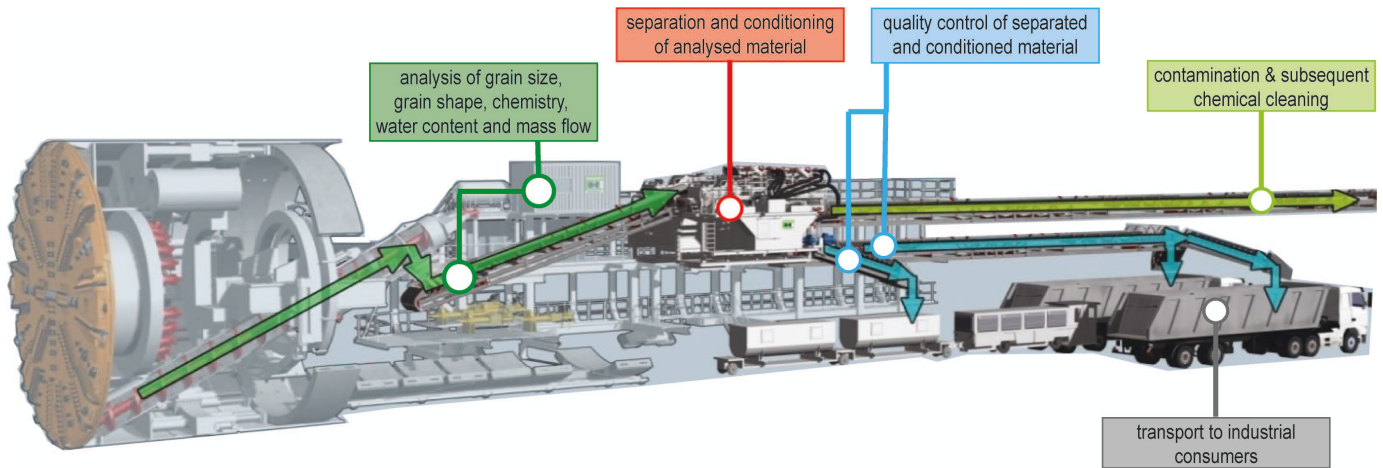


Fig. 2.2: Schematic on-line analysis of excavated rock and soil material on a tunnel boring machine (TBM) for mechanical excavation. After Haas, Galler, et al. (2020).

Barra Caracciolo et al. (2017), Bellopede (2011), Blengini & Garbarino (2010), Burdin & Monin (2009), Haas, Mongeard, et al. (2021), Priyadharshini et al. (2017), Teuscher et al. (2007), Tokgöz (2013), Voit & Zimmermann (2015), and N. Zhang et al. (2020)).

The setup of a material management plan (German: *Marschplan*, French: *la gestion des matériaux excavés*) includes technical concepts of excavated material from construction sites to processing facilities as well as usable material. Two contractual types of implementations exist for the management of excavated material. Either they are part of the main construction contract or they are treated as an individual contract as given for the Löttschberg, Gotthard or Lyon-Turin projects. An advantage of the former option is a reduction of involved people and therefore, offers efficient coordination. However, the latter option might lead to technically feasible results as it usually includes a specialized company in the field of use. Responsibility is always accounted to the client, i.e. in the case of FCC it would be CERN, which must deal with management of excavation material and final use or disposal. The present study has performed a vast amount of sample analyses along the current FCC layout. These results will be further used for planning an optimised usage already before construction. It is recommended that the spoil management is part of tendering documents to avoid the following issues: (1) usage of material unlikely to be fully integrated into the project, (2) contractors having less control over nature, quantity and quality of spoil even though they are the main decision makers on-site,

and (3) hampered communication among parties on-site concerning spoil management. Important considerations in addition is the required area of (temporary) disposal. The chemical and mineralogical analyses for rock are of uttermost importance. With respect to the FCC and its encountered sedimentary rock, the physico-chemical behaviour needs to be investigated based on an elaborated analysis flowchart.

Fig. 2.4 shows a conceptual flowchart for subsurface infrastructure projects deriving and deciding on applications for excavated material based on (1) legislation, (2) data availability and (3) rock characterisation. Essential rock parameters issue from geophysical well-logs, petrophysical, geomechanical, mineralogical, chemical and clay analyses. For each set of parameters (4), laboratory analyses are shown on the left-hand side, and well log equivalent parameters on the right-hand side, respectively. These analyses lead to suggestions of tunnelling excavation techniques (5a). Vice-versa and/or in parallel, excavation techniques based on experience from regional projects are evaluated (5b), leading to two distinguished rock classes with respect to excavation method and applicability of excavated material (6). Depending on excavation technique, excavated material is processed and scenarios for the application of excavated material (7) are derived. The plasticity behaviour is crucial for sedimentary rock, as is the hardness for metamorphic or magmatic rock (e.g. CAI or Los Angeles values). These European application scenarios from worldwide subsurface construction sites have successfully represented solutions across various types of

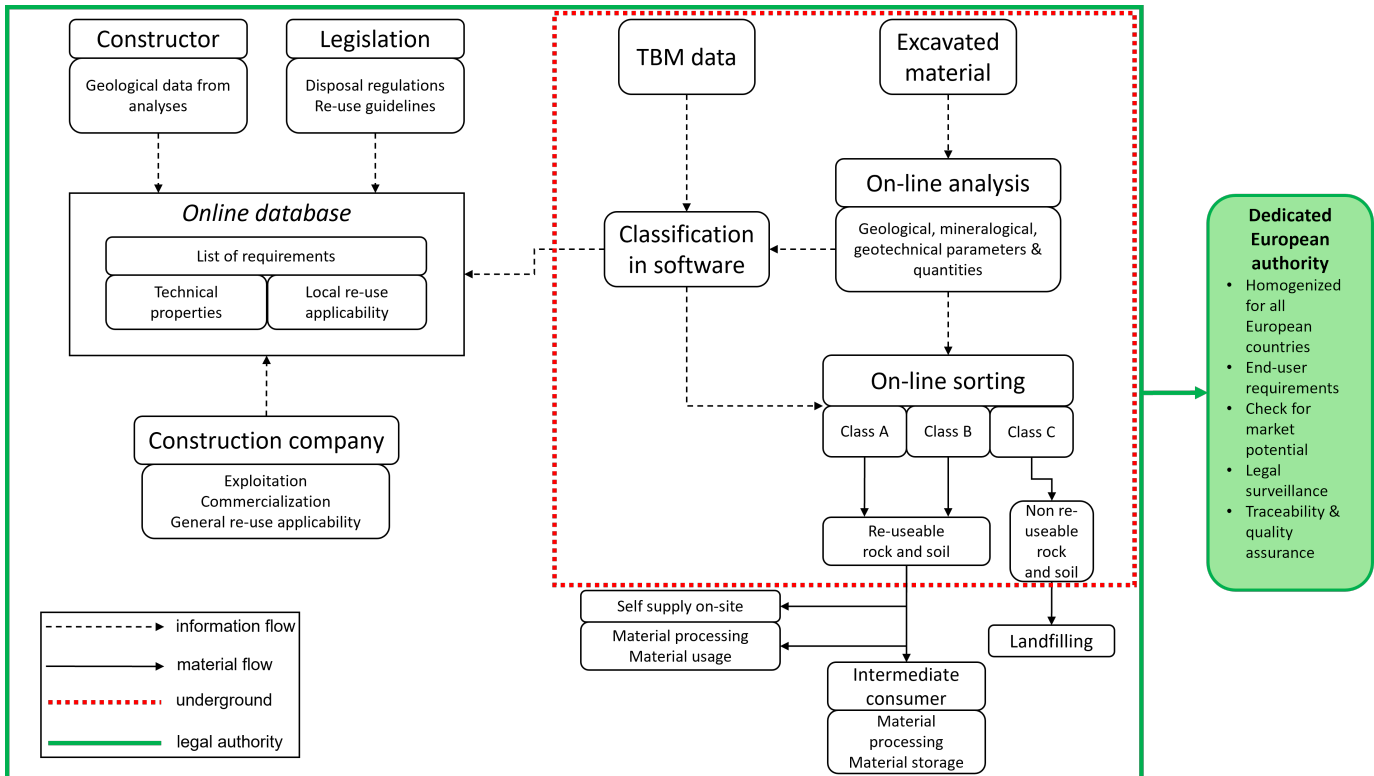


Fig. 2.3: Conceptual design of a database plan for the management of excavated rock and soil framed by a legal European authority (green line). The red square indicates tasks to be conducted on-site, respectively in the subsurface and are framed by geological investigations discussed in chapter 4. Key highlights of this concept are integrated in the present study for the (technical) properties, quantities, and database setup in chapter 3, for the rock characterisation (application classes) with on-line sorting being replaced by proper rock sampling in chapter 5 and for the type of applicability scenarios and use-able rock materials in chapter 6. After Haas, Galler, et al. (2020).

rock, both metamorphic and magmatic, as well as sedimentary.

For the FCC's excavated material, the pollution percentage is likely to be expected at least 25% or higher. This is based on encountered pollution at the HL LHC project, which exceeded up to 35%. With certain high hydrocarbon accumulations in both the Molasse Rouge as well as Mesozoic limestone formations (see sections 4 and 4.5), higher grades of pollution are likely. Hence, this is not a best- or worst-case scenario but rather a realistic one. The excavated material could be used for brick production or agricultural use. However, further studies would need to be performed for the latter. Most of the (polluted) material will likely have to be either cleaned from environmental pollutants such as Ni, Cr and hydrocarbons via chemical or biological treatments or disposed in classes (A), B, E or E+ for Switzerland, and (K3), K2 and K1 for France, respectively. There exists a tendency with an increasing grade of pollution increasing towards the south-east based on the well report reviews and stratigraphic

evaluations (see chapter 4). Extra costs might occur due to trans-national (French-Swiss) transport of waste. From a contractor's perspective, the excavated material should be moved to France given its economic benefit and the well-established Basel convention. This would have to be verified by both Swiss and French institutions GESDEC and CETU. From a client's (CERN) perspective, it would be economically more efficient to reduce the amount of Swiss shafts, and move them to France given the lower national disposal costs. Eventually, it is recommended that spoil management should be already implemented as part of the tendering documents at a planning stage, in order to avoid the following potential issues:

1. the evaluation of application scenarios for excavated spoil and its minimization of waste is unlikely to be fully integrated into the project,
2. contractors have less control over the nature, quantity and quality of spoil being processed and managed, although they are the main decision makers on-site,

and

3. the communication between different parties concerning spoil management is hampered, also with respect to legal national entities.

The following chapters consecutively identify the encountered geology and rock types to evaluate and predict potential application scenarios for the clay-rich sedimentary raw materials in the Geneva Basin. The results and discussion aim to derive an application rock classification, in order to capture the physico-chemical behaviour of the FCC's encountered rock, proposedly strongly influenced by natural clays and clay minerals. This is based on improved methods and technologies used herein compared to past projects. Important details are resolved in higher resolution than previous work that allows for an increased identification and awareness of what is safe and unsafe, hazardous or non-hazardous as well as rock and soil material predicted to be polluted or clean.

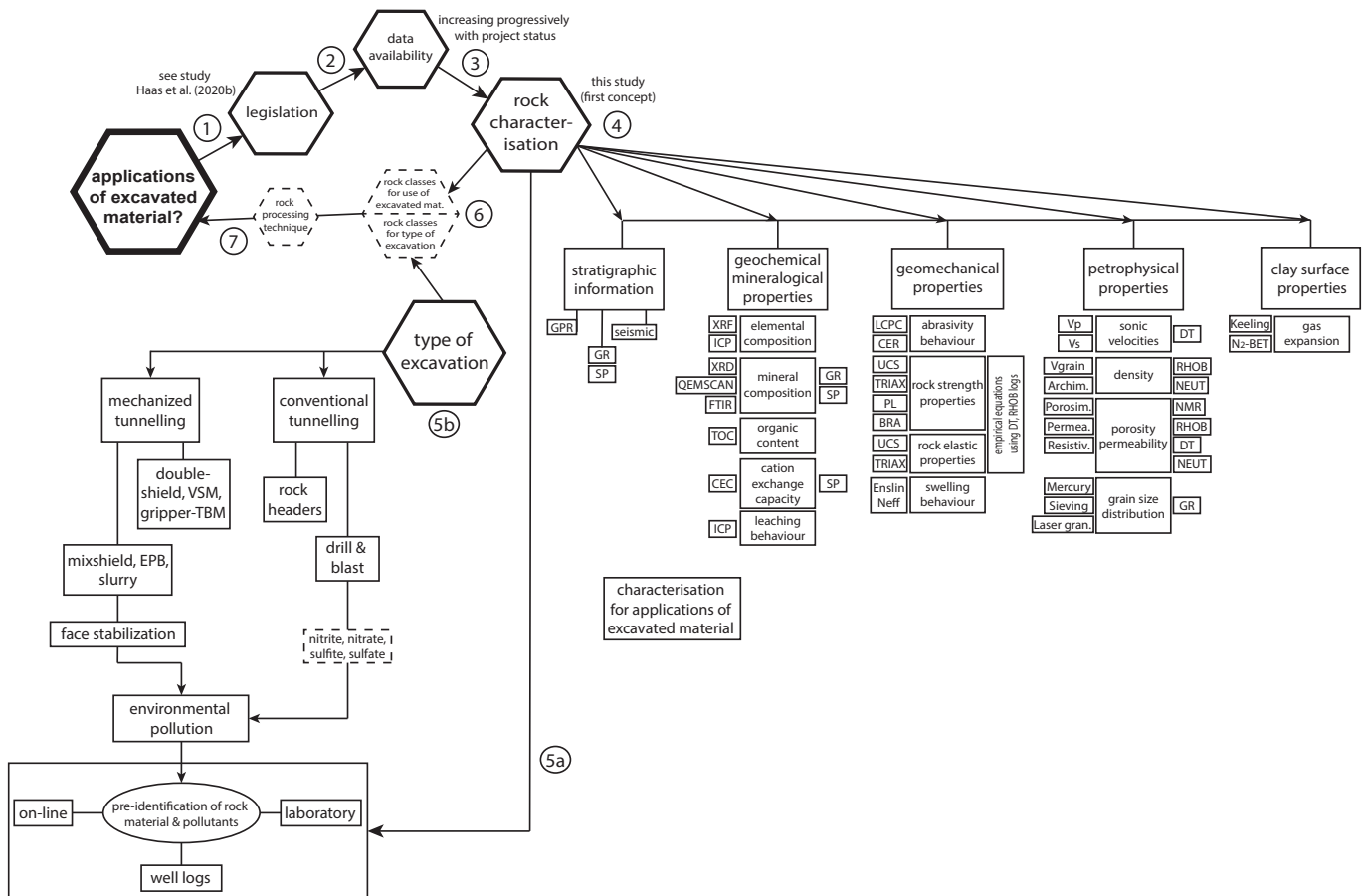


Fig. 2.4: Conceptual flowchart for subsurface infrastructure projects. See text for explanations. GPR=ground penetrating radar, GR=gamma ray log, SP=spontaneous potential log, DT=delta-time (sonic) log, RHOB=bulk density log, NEUT=neutron porosity log, NMR=nuclear magnetic resonance log, XRF=X-ray fluorescence, ICP=inductively coupled plasma, XRD=X-ray diffraction, QEMSCAN=automated mineralogical and petrography detection (electron microscope), FTIR=Fourier Transform Infrared spectroscopy, TOC=total organic carbon, CEC=cation exchange capacity, LCPC=Laboratoire Central des Ponts et Chaussées abrasivity, UCS=uniaxial compressive strength, TRIAX=triaxial compressive strength, PL=point load, BRA=Brazilian tensile strength, V_P =compressional (P-wave) velocity, V_S =shear (S-wave) velocity, V_{grain} =grain volume, archim.=porosity measurement after Archimedes principle, porosim=porosity measurement after Boyle's law, permea.=permeability measurement with permeameter, mercury=high-pressure mercury intrusion porosimetry, resistiv.=resistivity measurements, laser gran=laser granulometry for fine-grained material, N₂-BET=Brunauer-Emmett-Teller specific surface area, Keeling=water vapour adsorption after Keeling et al. (1980), Enslin-Neff=water uptake capacity. These analyses are described and discussed in chapters 3, 5, 4, and 6. After Haas, Mongeard, et al. (2021).

3 Materials and methods

This chapter is partially based on Haas, De Haller, Le Cottonnec, et al. (2021b), Haas, Gegenhuber, et al. (2021), and Haas & Plötze (2021b) as well as Haas et al. (2022).

The measurement of mineralogical geochemical, physico-chemical, petrophysical and geomechanical rock properties of the FCC's excavated material required sophisticated rock sampling of the Quaternary glaciogenic deposits, the Molasse Rouge, Grès et Marnes Gris à gypse, and Siderolithic formations to guide a proper rock characterisation. This was preceded by a thorough review of well, outcrop and excavation sites across the Geneva Basin, associated with the identification of available rock material. This chapter is split into four sections. The first section elucidates on the review, digitisation, rock sampling and data compilation procedures of various industrial and literature sources. The second explains the data organisation, processing and database development together with the statistical methods used for data analysis. The third section describes the geophysical well-log digitisation, the calculations and models as applied in Haas et al. (2022). The last section elaborates on the theoretical background of the geochemical, mineralogical, physico-chemical, petrophysical and rock mechanics analyses and describes their practical procedures performed in the field and laboratory. Text passages of this chapter were published in scientific manuscripts and technical reports, and were therefore adopted literally, in entirety or in parts from Haas et al. (2022), Haas, De Haller, Le Cottonnec, et al. (2021b), and Haas & Plötze (2021b) and Haas, Gegenhuber, et al. (2021). Parts of the acquired data were partly uploaded to the ZENODO platform under Haas & Plötze (2021a), Haas, Krainz, et al. (2021) and Haas, De Haller, Le Cottonnec, et al. (2021a) within CERN's *Mining the Future* industrial competition. The full database file containing all laboratory results, borehole locations and associated well reports are downloadable from the link provided in the appendix C.2 upon password request of the author or a reliable person involved in the FCC study. Data interpretations are comprehensively discussed in the following

chapters 4, 5 and 6.

3.1 Data review and rock sampling

An essential step in a feasibility study for a tunnelling project is the collection, preparation and review of all available data. For this purpose, wells, outcrops and excavation sites were reviewed across the whole Geneva Basin in France and Switzerland (Fig. 3.4). New sampling locations (Fig. 3.1) were selected for rock sampling. Existing ones were reviewed and digitised within a 2- to 5-km range outside the FCC's planned quasi-circular perimeter (Abada et al. 2019a; Benedikt et al. 2020). Geology not covered by the FCC's footprint but likely to be encountered inside the FCC construction ring was reviewed from third-party well reports that contained useful stratigraphic information, geophysical well-logs, core data or rock cores for analyses (Table 3.1). More than 2'000 boreholes were drilled across the Geneva Basin by Swiss (the Swiss Federal Office of Topography, Swisstopo, and the *Services Industriels de Genève*); and the French (*Bureau de Recherches Géologiques et Minières*) state surveys, as well as several oil and gas companies for geothermal, hydrocarbon and hydrogeological exploration. Among all well reports, technical reports and data sets available from BRGM's online Infoterre database, literature reviews, CERN civil engineering works during the SPS, LEP, LHC and HL-LHC site investigation programs, ongoing geothermal studies¹, former and ongoing drilling campaigns, 756 locations were considered useful for the FCC's current subsurface layout based on available stratigraphic information, rock cores or well-log data. With the oldest well drilled in 1831 and data reviews spanning over a time period of 190 years, the goal was to maximise the data coverage. The goal was to sample and analyze adequately the rock heterogeneity to be encountered by the tunnel route. The data were analyzed in three laboratories: the Swiss Federal Institute of Technology Zurich, the University of Geneva (both

¹Note that due to increased readability, capitalised letters of geothermal wells were avoided throughout this document. Hence, *GEo-01* becomes *Geo-01*.

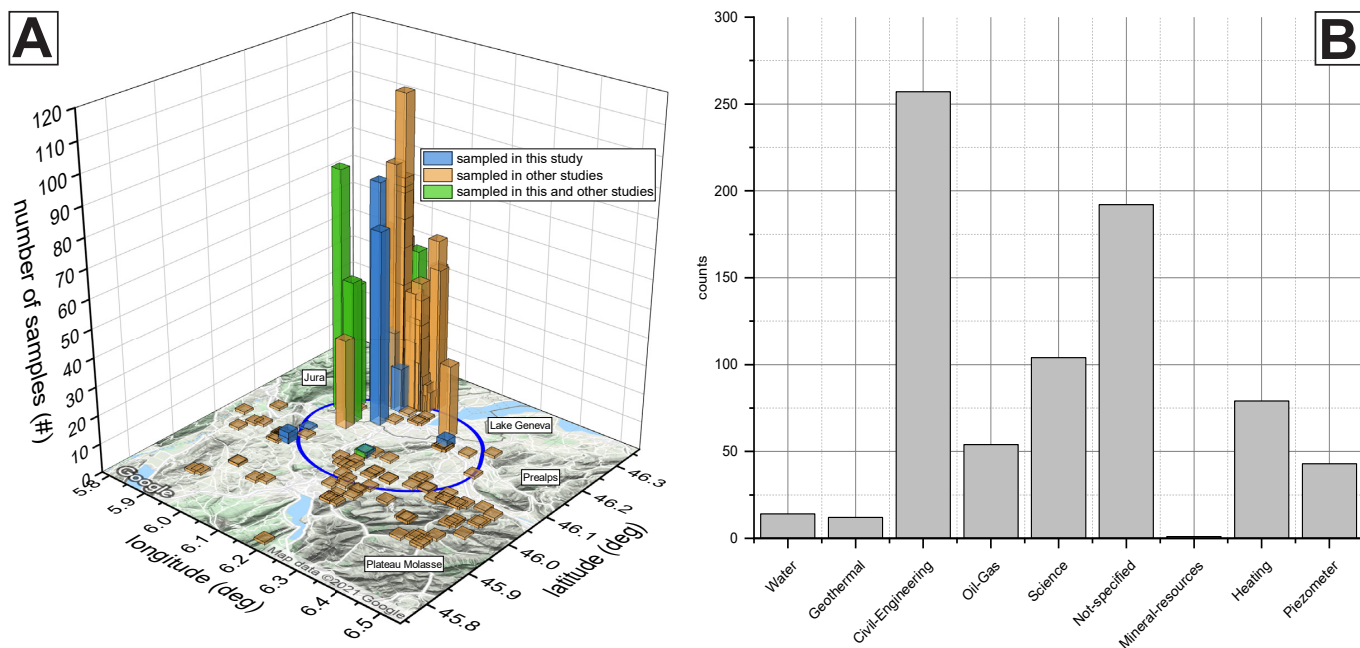


Fig. 3.1: (A) Total amount of samples per outcrop, well and excavation site locations in the vicinity of the current FCC layout (blue circle). At each unique depth value, a new sample was introduced as digitised from well reports of wells SLHCxx, SPLxx and SPMxx, taken from the literature or measured as part of the present study. The flat bars refer to scientific studies (Table 3.1). (B) Distribution of the 756 analysed locations grouped by their respective purposes. The majority of hydrocarbon wells dates back to the exploration boom during 1970-1990 by various oil and gas operators. Civil engineering site investigations are predominantly associated to subsurface projects built for CERN. The latest wells (e.g., Geo-01 and Geo-02) are drilled based on recent geothermal exploration initiatives of the Swiss canton of Geneva.

Switzerland) and the Montanuniversität Leoben (Austria).

Rock sampling along the current FCC subsurface layout focused on the depth interval from 100 to 300 m above sea level (m ASL) (Abada et al. 2019a,b,c,d). This led to the analyses of newly acquired rock samples and digitised samples.

The newly acquired samples were taken from various locations across the basin based on the data review. These sample locations are briefly described in the following. Wells Peissy-I, Montfleury-2 and L112 are located in the northern region of the Geneva Basin and their full-cores were stored at the rock core facility in Hochdorf (Switzerland). The Peissy-I and Montfleury-2 wells were purposed for hydrocarbon exploration, while the L112 well was drilled for CERN's LHC site investigations. For the HL-LHC site investigations, boreholes C1 to C6 at the Swiss HL-LHC Point 1 in Meyrin were analysed (Fig. 3.2, 4.1).

Half-cored rock samples from wells Gex-CD-01 to -07 ("Gex-wells") were stored at the rock core facility in

Boussens (France). British Petrol (BP) France drilled these boreholes between 1982 and 1983 to constrain the depth domains and properties of the Lower Freshwater Molasse unit (Chattian/Oligocene) and calcareous basement bedrock (Lower Cretaceous) for hydrocarbon exploration. The Gex-wells extend across the two French departments Ain and Haute-Savoie at the western edge of the Geneva Basin along the Jura mountains. Eventually, cutting samples were taken along ongoing drilling progress of the geothermal well Geo-02 close to the city centre of Geneva.

Sedimentological and geological core descriptions were carried out on all rock samples in the field in order to establish a reference lithotypes Haas et al. (2022). Lithotypes were based on visual features such as texture, colour, consistency, composition and sedimentary structures, and then cross-checked with well report documentation (e.g. Lagotala 1945; Wegmüller et al. 1995) and geophysical well-logs to identify associated well-log patterns (Fig. 3.3). The geomechanical laboratory tests required proper

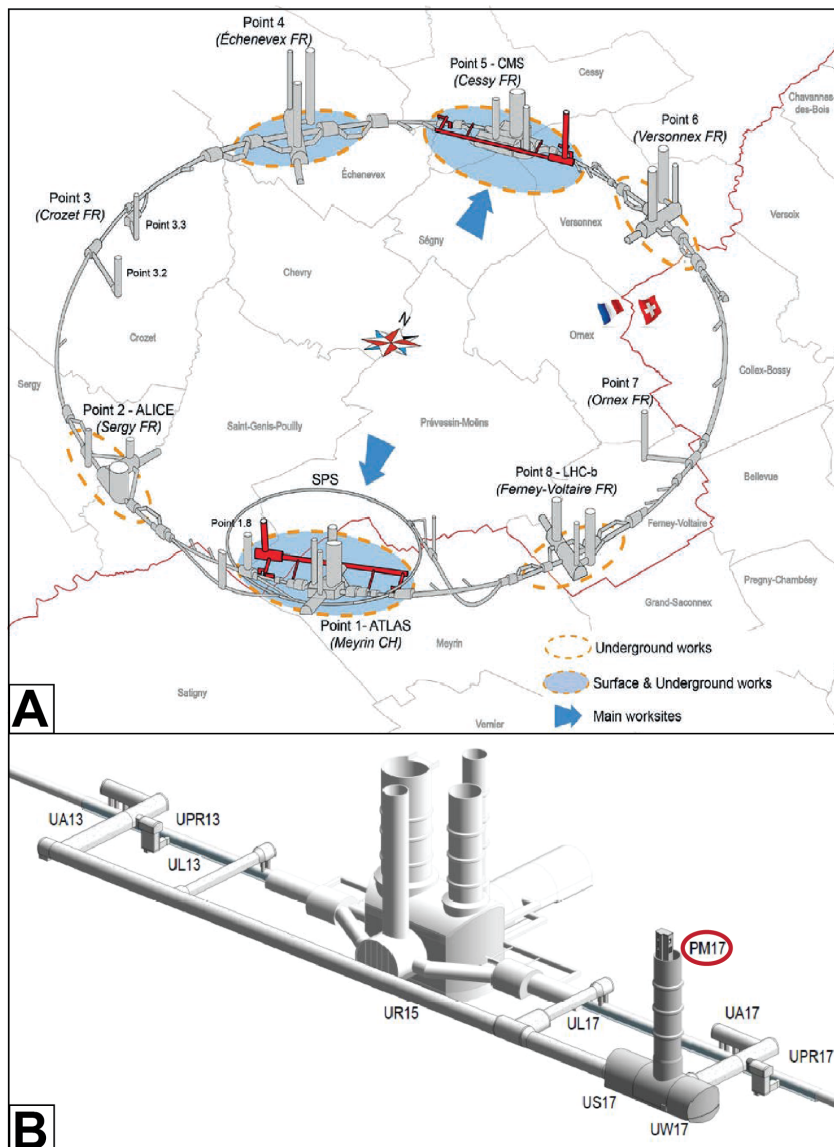


Fig. 3.2: A) The High-Luminosity LHC with main construction lots at Point 1 (Switzerland) and Point 5 (France). B) Subsurface layout of HL-LHC's Point 1 with sampled PM17 shaft. Modified after Mattelaer (2019) and Madinier et al. (2017).

orientation of the sample and each core was marked with a red (right hand-side) and blue (left hand-side) line to indicate top and bottom.

Digitised samples came from various data sources (Fig. 3.1, Table 3.1). The company *ORIGIN* gathered a dense grid of samples during excavation of shaft PM17, cavern US17 and tunnel UR15 (Fig. 3.2) at the HL-LHC Point 1. These samples were analysed for chemical pollutants at the laboratory of the University of Lausanne on behalf of *ORIGIN* and CERN as required by Swiss legislation (Swiss Confederation 2016). Data were extracted from

spoil records simultaneously with excavation advancement from October 2018 to March 2020.

The local survey company *Géotechnique Appliquée Dériaz SA (GADZ)* performed geotechnical and geological laboratory, field and in-situ borehole measurements as part of former civil engineering works on behalf of CERN. From CERN's LEP construction, the first GADZ report dated back to 1981 and initiated the (industrial) Molasse deposit characterisation for the subsequent construction of the LEP and the LHC (Table 5.1). Site investigations for the LEP and the LHC yielded associated technical reports (e.g. Fern et al. 2018), which were digitised. The digitised samples came from data reports for wells

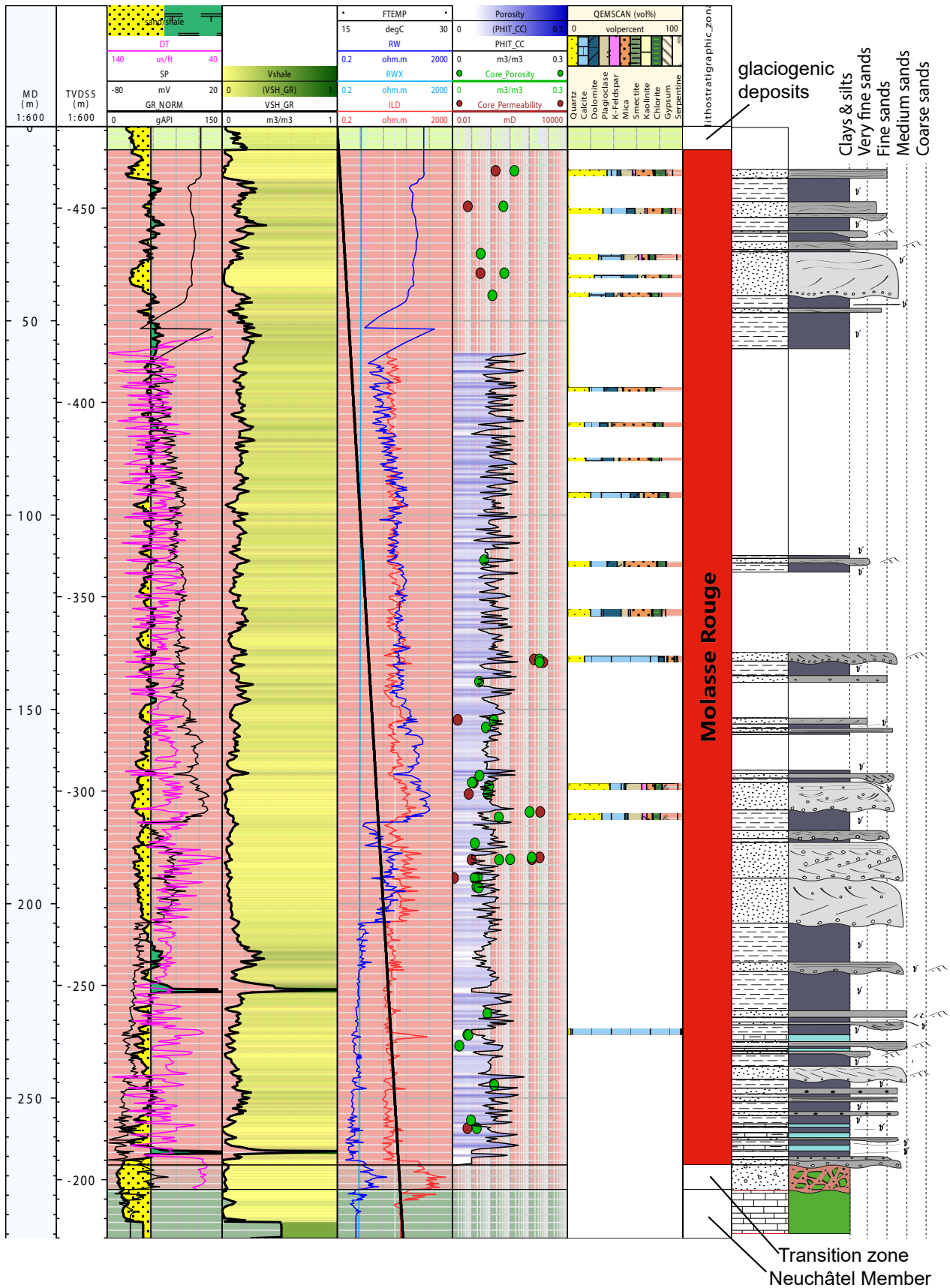


Fig. 3.3: Methodological approach depicting petrophysical calculations with revised stratigraphic log, associated geophysical well-logs and mineralogical laboratory results for well Gex-CD-01. White areas in QEMSCAN column represent no measurements. Note that the minerals illite, biotite and muscovite are summarized under the term “mica”. Remaining space in QEMSCAN column refers to other minerals. MD=measured depth (m), TVDSS=true vertical depth sub-sea (m). After Haas et al. (2022).

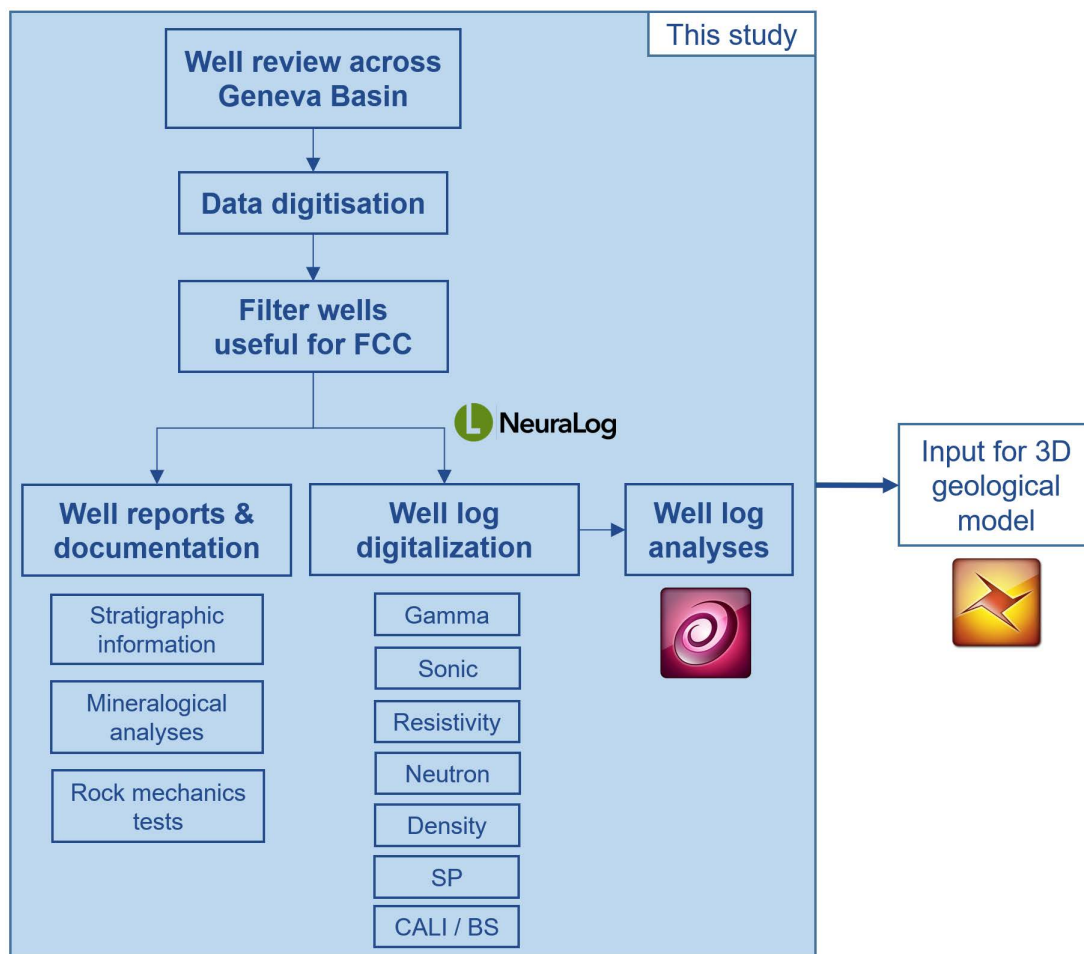


Fig. 3.4: Borehole identification and workflow procedure relevant for the FCC subsurface infrastructure. The software packages Neuralog and Techlog were used for digitisation and analysis of geophysical well-logs, respectively. An ongoing spin-off project deals with the creation of the Geneva basin's detailed 3D geological model for the FCC construction in the Petrel software. This model relies on data input from both digitised and measured data as part of this study.

SLHC $_{xx}$, SPM $_{xx}$, SPL $_{xx}$, F $_{xx}$ and L $_{xxx}$ with xx denoting the consecutive well numbers. These data included X-ray diffraction analyses, ultrasonic compressional and shear-wave velocity analyses, and a large set of geomechanical parameters such as wet, dry and solid specific weights, uniaxial compressive strength (UCS), cohesion and friction angle, rock quality designation index (RQD), Young's modulus, modulus of stiffness, point load index, void ratio (an alternative measurement of porosity), water content, Atterberg limits, water saturation, CERCHAR analyses, swelling tests as well as stress, strength and dilatometer results of triaxial compressive strength tests. The technical reports by GADZ also include stratigraphic borehole descriptions, depth relation and geological time in the nearby area of the FCC shafts. However, in the reports' appendices no coordinates are supplied for the boreholes, and can only be extracted manually from a

map. In some reports, pictures of outcrops are attached in the appendix to estimate where they occur in the area. The *Services Industriels de Genève* (SIG) and *Service de géologie, sols et déchets* (GESDEC) provided crucial geophysical well-log data and technical reports from the Thônex-1, Geo-01, Geo-01-DAS (vertical seismic profile well, abbreviated as "VSP" samples in the database) and Geo-02 wells close to the city of Geneva. These data sets were acquired through the University of Geneva (UNIGE), with the new well-log data being used as a reference for correlation with older wells (Fig. 3.7).

The University of Geneva has collected large data sets of geophysical well-logs and rock cuttings from geothermal wells as part of scientific studies across the Geneva Basin during the past decades. Among various research studies, this included 145 QEMSCAN samples from wells Geo-01, Thônex-1, Humilly-2 extracted from Brentini (2018)

and Pierdona (2018) and Rusillon (2018), and 97 X-ray diffraction results as part of the study by Schegg (1993). The company *ROCKSOIL* operating at the HL-LHC Point 5 in Cessy (France) depicts the French equivalent to Swiss Point 1. Rock samples were sent to the *EUROFINS* laboratory close to Lyon (France) on behalf of CERN checking for chemical pollutants according to French disposal classes (Haas, De Haller, Moscariello, et al. 2020; Haas, Galler, et al. 2020; République Française 2015). Their reports were reviewed and a few samples were taken for an initial comparison at the beginning of the study. However, due to its location outside of the proposed FCC perimeter, these samples were not further considered. Even though no sample data were available from BRGM's online website *Infoterre*, it provided stratigraphic data only. These boreholes were chosen based on their status as *verified* and *documented*. Hence, wells that were in the FCC's vicinity but did not contain any documented and verified geological information were neglected. The extracted wells follow the well notation of "BSSxxxxxxx" with x 's denoting consecutive well numbers.

Eventually, the present study has resulted in a large data set with a total of 2'461 samples (Table 3.2, 3.5) for the westernmost Swiss Molasse Basin (SMB). This is unique in its extent and comparable to, for instance, the eastern regions of the SMB with 1'500 Molasse samples from 18 locations as featured in a thermal diagenesis study by Monnier (1982); or 175 marl samples in the Molasse formations investigated for their swelling behaviour by Madsen & Kahr (1985) at 10 locations. Out of the 2'461 samples, 1'143 refer to newly acquired data and 1'318 to digitised data across the Quaternary glaciogenic deposits, the Grès et Marnes Gris à gypse, Molasse Rouge and Siderolithic formations. No samples were neither taken nor analysed for the various Mesozoic limestone formations.

Rock material of the newly acquired sample branch was further analysed in various laboratory analyses. Depending on sample type and inferred analyses, two different sample preparations (Fig. 3.5) were conducted. For the first preparation, drill cuttings explicitly from well Geo-02 were washed, sieved under water and dried at 45 °C for 48 h to prevent clay degradation. Dried samples were crushed in an agate mortar and sieved with a <400 μm

mesh. These samples were then analysed via portable X-ray fluorescence (pXRF), automated mineralogy and petrography scanning (QEMSCAN) and Inductively Coupled Plasma Mass Spectroscopy / Optical Emission Spectroscopy (ICP-MS/OES).

The second preparation included full- and half-cores from wells Montfleury-2, Peissy-I and Gex-CD-01 to -07. These samples were used to drill plug samples with a diameter of 2.54 cm (1 inch) and a length between 2 to 8 cm for petrophysical analyses and geomechanical tests as well as mineralogical and physico-chemical analyses by using the crushed sample remains. This provided a full set of all measurements for selected samples, comprising geochemical, mineralogical, petrophysical, physico-chemical and geomechanical results.

For the milling of plug samples, a jaw crusher was first used to receive a grain size of <400 μm for each sample. Second, an agate mill crushed the sample further to a grain size <63 μm . These two fractions were particularly required for the physico-chemical analyses. For the Fourier-transform infrared spectroscopy (FTIR) and X-ray diffraction (XRD) measurements, a <20 μm fine-grained material required a third step of milling the <400 μm fraction in a vibrating McCrone mill with agate balls, flushing them with ethanol and briefly drying the sample-ethanol solution in a 65 °C oven between 1 to 3 h depending on solution volume to consequently receive the <20 μm fraction. For the <400 μm and <63 μm fractions, respective sieves were used to check the grain size after each milling step. For fractions <400 μm and <63 μm , the water content was determined to calculate the dry mass after Standards DIN EN 12880 (European Norm (EN) 2001) and DIN EN ISO 17892 (European Norm (EN) 2015), formerly replacing DIN 18121-1 (Deutsches Institut für Normung (DIN) 1998). However, the <20 μm fraction was excluded from these calculations, since the calculations of X-ray diffractograms and Fourier transform infrared spectra do not require dry mass corrections. The water content based on humid and dry masses was calculated according to:

$$w (\%) = \frac{m_{humid} - m_{dry}}{m_{humid}} \cdot 100 \quad (3.1)$$

Table 3.1: Data compilation with performed work (R=review, A=analysis, D=digitisation) of industrial and academic third-party sources across the FCC’s construction area.

country	data	data treatment	location	entity	data owner	data source
	HL-LHC Point 1 spoil record reports, construction reports (PDF, XLS)	R-A-D	PM17, US17, UR15	ORIGIN	CERN	ORIGIN (2020)
Switzerland	Technical reports (PDF)	R-A-D	SLHC, SPM, SPL, F, L, C1-C7 wells	GADZ	CERN	Géotechnique Appliquée Dériaz & SA (GADZ) (1981a,b, 1982a,b, 1992, 1993a,b, 1996a,b, 1997, 2015a,b,c,d, 2016a,b,c), Gervaise (1972), and Lanterno et al. (1981)
	Well reports, well-logs (PDF, LAS)	R-A-D	Thônex-1, Geo-01, Geo-01-DAS (VSP), Geo-02	SIG, GESDEC	SIG, GESDEC, UNIGE	Chablais & Rusillon (2018), Chablais & Savoy (2019), Charollais et al. (2007), Clerc et al. (2015), Etat de Genève (1994), and Services Industriels de Genève (SIG) (2019)
	Scientific studies (PDF, XLS)	R-A-D	Montfleury-2, Peissy-I, Thônex-1, Humilly-2, Geo-01, Geo-01-DAS (VSP), Geo-02, various outcrops (Fig. 3.1)	SIG, GESDEC	SIG, GESDEC, UNIGE	Brentini (2018), Charollais et al. (2007, 2013), Jenny et al. (1995), Pierdona (2018), Rusillon (2018), Schegg (1993), Schegg (1992), and Wegmüller et al. (1995)
	Various well files (XLS)	R-A	eastern Geneva Basin	BRGM	public	BRGM (2021)
France	Well reports (PDF)	R-A-D	Gex-CD-01 to -07	BP France	UNIGE, BP France	Doumer & British Petrol (France) (1983a,b,c,d,e,f,g)

Table 3.2: Sampled locations, types of laboratory analyses and number of samples acquired as new data and implemented into the database. UNIGE=University of Geneva, ETH Zurich=Swiss Federal Institute of Technology Zurich, MUL=Montanuniversität Leoben.

laboratory	properties (analysis)	sample number	location (well/ <i>outcrop</i>)
UNIGE	Major-elements (portable XRF)	42	HL-LHC Point 1 (C1-C3, C5-C7), Geo-01-DAS, Geo-02, Montfleury-2, Peissy-I, Gex-CD-01 to -07, <i>Sarzin, Mornex, Nyoux, Biollay, Verney</i>
	Trace-elements (ICP-MS/OES)	375	
	Mineral phases (QEMSCAN)	439	
	Mineral phases (optical microscopy)	284	
	Porosity & permeability (gas absorption)	173	
ETH Zurich	Leaching elements (ICP-OES)	74	HL-LHC Point 1 (C1-C6), Geo-02, Peissy-I, Gex-CD-04, Gex-CD-05, Gex-CD-07, <i>Sarzin, Mornex</i>
	Cation exchange capacity (copper complex)	70	
	Exchangeable ions (ICP-OES)	76	
	Anions (photometry)	44	
	Mineral phases (FTIR)	31	
	Mineral phases (XRD)	79	
	Specific outer surface area (N ₂ -BET)	30	
	Specific inner surface area (water vapor adsorption)	59	
	Pore throat size & distribution (MIP)	30	
	Water uptake capacity (Enslin-Neff)	70	
Carbon content (thermal/acid treatment)	78		
MUL	P- & S-wave velocities (ultrasonic tests)	282	HL-LHC Point 1 (C1-C6), Peissy-I, Gex-CD-01 to -07, <i>Sarzin, Mornex</i>
	Abrasivity (CERCHAR)	147	
	Abrasivity & breakability (LCPC)	65	
	Tensile strength (Brazilian test)	99	
	Strength index (point load test)	116	
	Uniaxial compressive strength (UCS)	153	

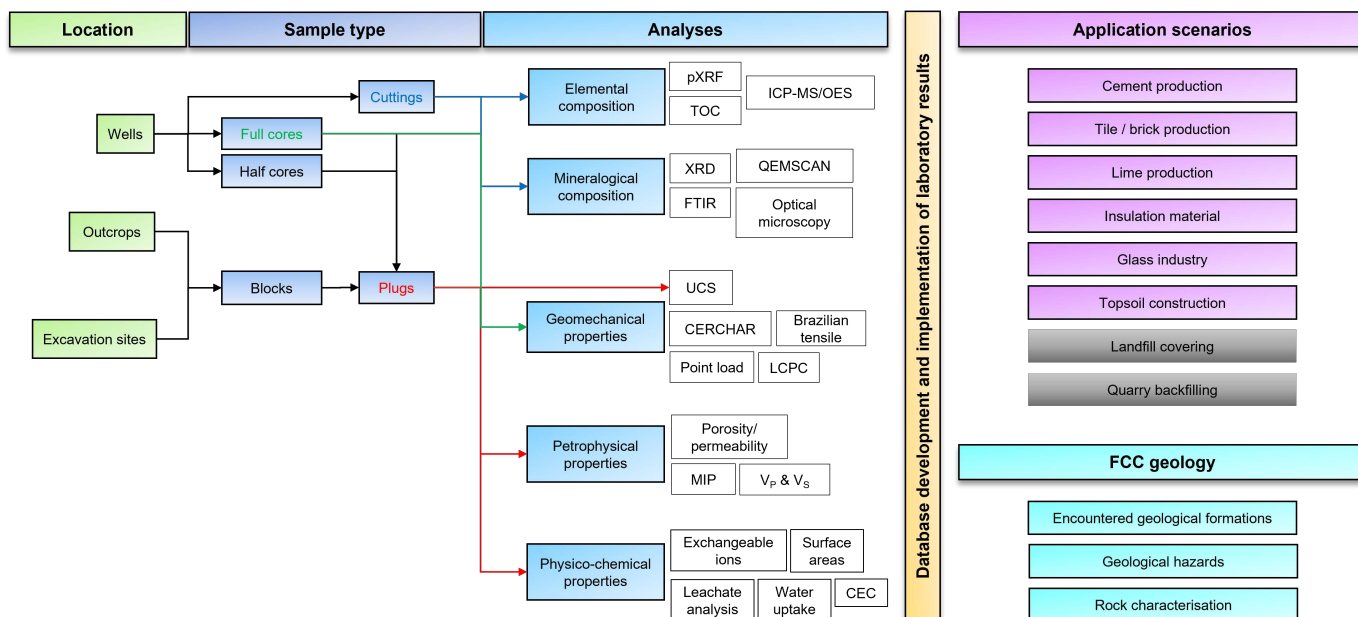


Fig. 3.5: Flowchart of rock sampling based on different sample types and associated laboratory measurements, which led to the identification of the FCC's encountered geology, potential geological hazards, and the prediction of application scenarios. Landfilling and quarry backfilling are not considered as application scenarios (Haas, Galler, et al. 2020; Haas, Mongeard, et al. 2021). Colours link the sampling and analysis streams to the respective sample types. See text for abbreviations.

3.2 Database setup and data analysis

The database was developed in Microsoft Access and consisted of a vast set of different tables, linked among each other via unique identifiers (IDs) referring to either sample-ID or location-ID using the *Structured Query Language (SQL)*. Various SQL-queries facilitated subsequent data analysis and took advantage of the minimum amount of required tables. This allowed for quick and efficient access to data tables, which are briefly stated in the following.

Each location-ID was uniquely defined as wells, outcrops and excavation sites, and contained the relevant local and geological metadata such as well name set as the location-ID, drilling purpose, measured and true vertical depth, available third-party samples and samples taken within the scope of this study, longitude, latitude, elevation, kelly-bushing reference level from digitised geophysical logs' well headers, encountered geological hazards such as gaseous and bituminous hydrocarbons, karstic features, anhydrite and pyrite occurrences, and data source references, respectively.

Digitised geological information from well reports was

summarised in a chronostratigraphic information table and included era, period, series/epoch and stage/age, lithostratigraphic descriptions, rock types from well reports and field descriptions from own inspections in the field.

The digitised and new samples were given unique sample-IDs stored in a separate table, which was linked to the location-ID table. Metadata of a single sample contained information on top and bottom depths in case of cm-long rock cores, sample type such as core, plug or cuttings, chronostratigraphic and lithostratigraphic information, sample photo, date of sampling, name of the sampled core box (in case available), rock descriptions from well reports and own descriptions from this study's field inspections. Ultimately, associated geological hazards were tagged to each sample, such as, gaseous and bituminous hydrocarbons, karstic features, anhydrite and pyrite occurrences.

Separate tables for each laboratory analysis were linked to the sample-ID and locations-ID tables, in order to guarantee unique data entries (Fig. 3.6) and allow for quick data table combinations. Metadata of each analysis included the type and date of analysis, name of analysing instrument, time and duration of analysis, name of the sampler, and analysing scientist.

The digitised data from the various third-party sources

were incorporated in separate tables in the database, except for the water content, uniaxial compressive strength and point load indices that were implemented together with own laboratory measurements in respective tables. Ultimately, the connections among various tables and analysis results required the setup of three different relationship types in the database:

1. $1 \langle \rangle 1$ (one to one): one single data set refers to another single data set; for instance, a GPS location (longitude, latitude, elevation) to a well;
2. $1 \langle \rangle n$ (one to many): one single data set refers to multiple data sets; for instance, one well contains multiple rock samples;
3. $m \langle \rangle n$ (many to many): m data sets refer to n data sets; for instance, various geological formations at different locations.

Distinct challenges emerged from a sophisticated data homogenisation across old and recent wells including digitised and new samples spanning over a period of 190 years with one well dating back to the year 1831, as well as a logical structure of data entries and connections to avoid data redundancy. The comparability among digitised and newly measured data ultimately required the introduction of an appositely devised unified English translated stratigraphical and engineering terminology, in particular for the Mesozoic formations, to homogenise outdated Swiss and French stratigraphic terms (Graf & Burkhalter 2016; Strasser et al. 2016). An essential condition of the database was to create as few tables and columns as necessary to avoid data redundancy based on the fact to efficiently diminish the required computational power and to keep the data structure logical and neat. This implied that derived or calculated data were not saved as such preventing potential data entry contradictions. Such calculated data excluded, for instance, the thickness of a specific lithology, which depicted the subtraction of its top and bottom depths. This was usually calculated after extraction of the database and specific data processing and analysis in R, Python, MATLAB codes, or commercial software such as GoldenSoftware's STRATER and SURFER, as well as Schlumberger's Techlog software suite, and OriginPro. To avoid working in five geographic coordinate systems, all geo-referenced data were transformed to the global World

Geodetic System 1984 (WGS84) system as longitude, latitude and elevation using respective calculations (Federal Office of Topography (swisstopo) 2016; Ibarrola & Jones 2016). The five coordinate systems were:

1. the Swiss LV-03 [CH1903] and LV-95 [CH1903+] coordinate systems,
2. the French NGF-Lambert-93 [RGF-93] coordinate system, and
3. the CERN (CCS and CGRF) coordinate systems.

While geophysical well-logs were not incorporated in the database but linked externally to respective software products in LAS file format, the underlying borehole folder structure was developed as follows: general summaries about the wells (*Well summary*), *Well-logs*, *Geological tops*, *Deviation*, *Seismic*, *Core*, *Operations* and *Production*. Seismic, core, operations and production as part of this study were not considered. However, this folder structure was honored for the upload to the respective data link in appendix C.2.

The next step was to use this database for data analysis. Statistical methods included principal component analysis (PCA), outlier detection tests (e.g. Grubb's test), and hypothesis tests. The principal component analysis (PCA) served as a robust technique for reducing the dimension of the data sets, while preserving as much variability, i.e. statistical information as possible. New uncorrelated variables (principal components) were created that successively maximized variance, and reduced to solve an eigenvalue/eigenvector problem. The new variables were linear functions and defined by the data sets themselves. The earliest literature on PCA dates back to F.R.S. (1901) and Hotelling (1933). An extensive mathematical derivation and application of the PC analysis is also found in e.g. Diamantaras & Kung (1996), J. Jackson (1991), and Jolliffe (2002) or Flury (1988). By maximizing the amount of parameters and data points per sample for a robust rock classification (see chapter 5), a crucial issue during data processing was the fact on how to treat missing data for PCA. Listwise and pairwise deletion are the most common techniques to handle missing data (Peugh & Enders 2004). It is important that in the vast majority of cases, the assumption to using either of these techniques is that the data is *missing completely at random* (MCAR). This

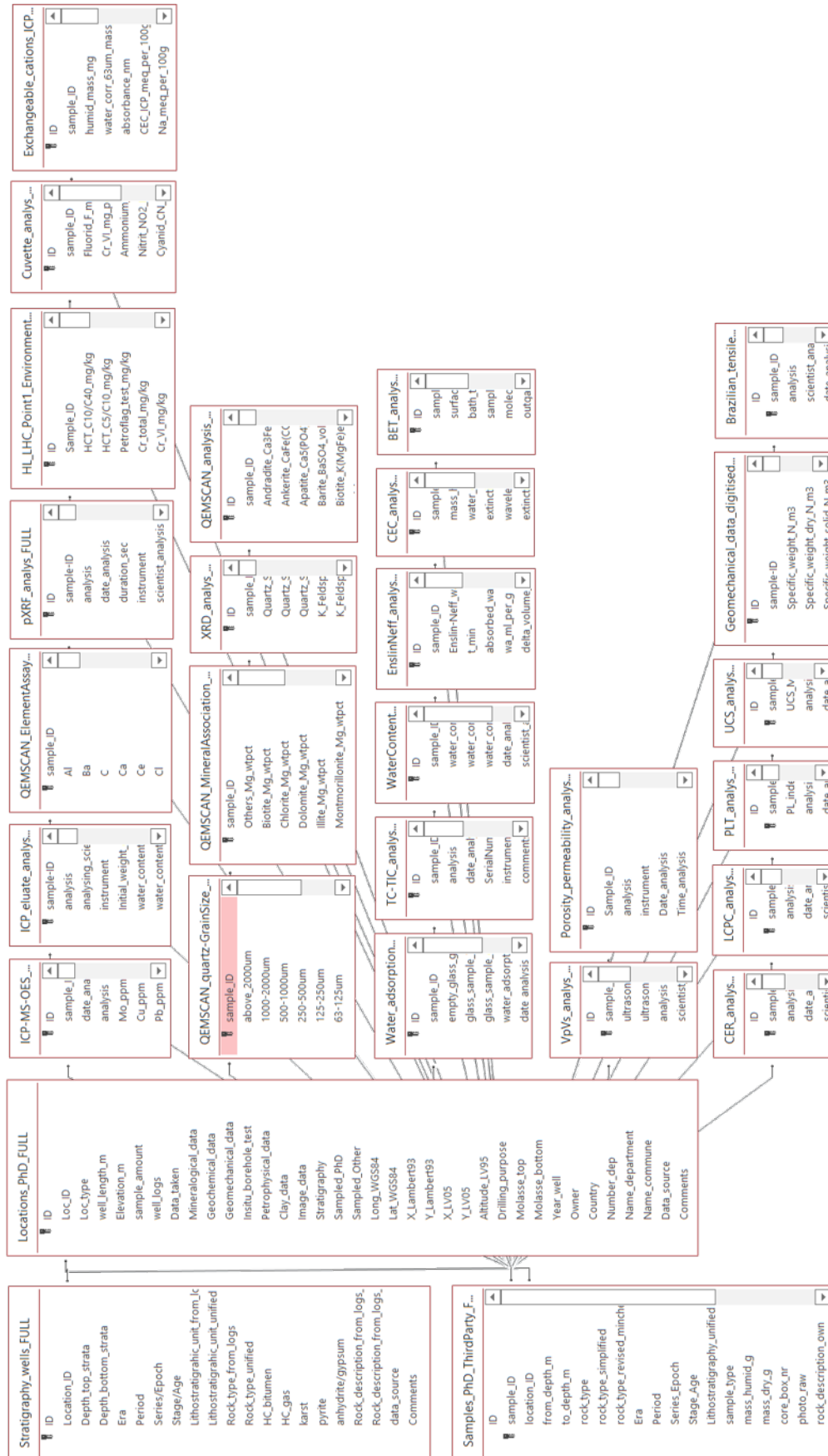


Fig. 3.6: Database relationships among linked tables in the Microsoft Access software. The key-symbol next to the ID-fields (highlighted red box) denotes the unique primary key depicted by sample-ID or location-ID for the respective relationship to avoid duplicate entries.

means that the probability of missing data on their dependent variable is unrelated to other independent variables as well as the dependent variable itself (Peugh & Enders 2004).

Listwise deletion (complete-case analysis) removes all data for a case that has one or more missing values. It is commonly disadvantageous to use listwise deletion since the assumptions of MCAR are typically rare to support. Hence, listwise deletion methods result in biased output parameters (Peugh & Enders 2004).

On the contrary, pairwise deletion (available-case analysis) attempts to minimize the loss that occurs in listwise deletion. Pairwise deletion works similar to a correlation matrix. Essentially, a correlation measures the strength of a (linear) relationship between two variables. For each pair of variables, the correlation coefficient takes that data into account. Thus, pairwise deletion maximizes all data available on an analysis-by-analysis basis, and is, therefore, not biased. Though this technique is typically preferred over listwise deletion, it also assumes that the missing data are MCAR. A disadvantage with the use of pairwise deletion is that the standard of errors computed by most software packages uses the average sample size across analyses. This tends to produce standard of errors that are under- or overestimated (Abonazel et al. 2018; Peugh & Enders 2004). Various researchers have associated pairwise deletion as a source for non-positive definite matrices in multivariate and contemporary statistical analyses such as structural equation modelling (Little 1992; Marsh 1998; Wothke 1993). Pairwise deletion offered the most reliable option of treating missing data without bias or loss of information and was used as the preferred technique for data analysis (Peugh & Enders 2004).

For the detection of outliers, the Grubb's hypothesis test, or often called maximum normed residual test, was applied (Grubbs 1969; Stefansky 1972). This test detects outliers in univariate data sets, whose data entries show a normal distribution. Outliers might refer to a geological trend but the present study was not dedicated to e.g., geological provenance analysis. Hence, outliers were excluded. The removal of outliers was also a given premise for the performed statistical methods. Prior to their removal, potential mis-measurements or geological trends were carefully investigated. In general, data distribution was mostly associated to bimodal or undersampled type, and aligned to a more Gaussian (normal) distribution with increasing

values as expected.

3.3 Geophysical well-log analyses

A geophysical log depicts a continuous plot of a measured property as a function of the measured depth along a well. Interpretation of these logs is referred to as *formation evaluation* and is based on transforming measured, raw log data into interpretable data, either empirically via experiments, theoretically via petrophysical models, or via a combination of both (Pickett 1974; Schlumberger 2021). The use of geophysical well-logs for the present study was based on two reasons: (1) to evaluate lithotypes and geological formations and possible associated geological hazards, and (2) to test a novel approach for correlating laboratory analyses to predictions of beneficial-use applications before any site investigations.

Well-logs were digitised between 0 and ca. 1'000 m ASL from 47 wells selected cover the FCC's construction depth interval, which is between 100 to 300 m ASL in its current subsurface alignment. Deeper geological formations and logging intervals not relevant for the FCC were omitted. The digitisation led to a cumulative length of 106.53 km of quality-checked (QC) logging curves using the NeuraLog software package, and were outputted in LAS file format for further processing in Schlumberger Techlog software. Out of 106.53 km, ca. 37 km were used for the stratigraphic evaluation and lithotype association with encountered geological units by the FCC (see Haas et al. (2022)). Digital 1D depth profiles for each log trace were created and hung from the topographic surface level down to respective depths related to the FCC. The output of quality-control (QC) reports (see download link in appendix C.2) allowed final editing and checks of digitised well-logs. Low QC values of 70-80% hereby did not imply an erroneous or low-quality curve digitisation, but was because some well-logs such as the neutron and density logs were restricted to certain depth intervals. Gamma ray (GR) and spontaneous potential (SP) logs occasionally did not start from the surface but at deeper levels, e.g. at 40 m depth as observed in wells C2 and C3. This led to an apparently low QC value, even though the full range of well-logs was captured, but the upper 40 m were interpreted as missing by the software.

Well-logs were predominantly acquired by the companies Schlumberger, Hydrolog or Hydro-Geo Environnement

over a time span of 70 years. The digitisation of well-logs featured the gamma-ray (GR), sonic transit-time (DT) or inverse V_P , compressional (V_p) and shear-wave (V_s) velocity, caliper (CALI), spontaneous potential (SP), bulk and matrix densities (RHOB, RHOMMA), photoelectric absorption factor (P_e), corrected density (DRHO), neutron porosity (NPHI) as well as different types of resistivity logs including the short normal (SN), long normal (LN), latero-log shallow (LLS), latero-log deep (LLD) and micro-spherically focused (MSFL) logs. For some wells, e.g. Chaleyriat-1, only calcareous material was encountered as part of Mesozoic limestone formations and excluded any Molasse formations. In this case, well-log resistivity curves were not digitised but only the GR, CALI, SONIC and SP logs. During digitisation, some misfit and log-shift was compensated by stretching and squeezing of log curves but could not be completely resolve discrepancies because of bad original paper quality, often loosely glued, or poorly scanned PDF files across a few meters. Some DT well-logs from the 1960's were not digitised because of either low image quality, missing units and calibrations, or unreasonable (spiky) log curve shapes.

Except for the digitised CALI log, each well-log type is briefly described in the following paragraphs. Unless otherwise stated, theoretical background information was taken from Darling (2005) and Ellis & Singer (2007) and Asquith et al. (2004). An extensive interpretation of the well-log data presented herein is found in Haas et al. (2022), respectively appendix A.3. It should be noted that the terminology used in the framework of this study follows the common petrophysical notations according to which (Ellis & Singer 2007):

1. the term mica refers to minerals that do not contribute to clay volume due to its low cation exchange capacity;
2. the term shale is considered to be a fine-grained rock composed of silt and clay minerals, whereas silt is predominantly quartz but may contain feldspar and organic matter.

Gamma ray and spontaneous potential logs

The gamma ray (GR) and spontaneous potential (SP) logs were used as lithology logs to map shale-dominated versus sand-dominated intervals. The GR log measures natural radioactivity in a geological formation, originating primarily from clay minerals, which are naturally radioactive,

or contain radioactive ions. The main source of natural radioactivity is potassium, ^{40}K , attributed to both the feldspar's potassium-rich end-members and mica, one of the nine sheet silicate groups (Jasmund & Lagaly 1993). Clay minerals such as illite, montmorillonite, muscovite and biotite are, in addition to ^{40}K , responsible for thorium, ^{232}Th , encountered in most shales. Three types of nuclear radiation are essential for applications of nuclear physics logging tools such as the GR log. While α and β radiation play an ancillary role in logging applications, the principle of γ radiation is exploited for the GR, as well as for the RHOB and NPHI logging tools as further described below.

Commonly, GR logging depicts the sum of all three major radioactive isotopes, while spectral GR measures each of the uranium, thorium, and potassium concentrations separately. A GR logging tool excites an atom's nucleus by a photon emitted from the detector. The excited atom emits gamma rays at characteristic energy levels, which uniquely identify the element in a given geological formation (R. Evans 1967). On one hand, this makes the GR tool ideal for elemental identification purposes even in cased boreholes, since the emitted photons pass through metallic or plastic matter. On the other hand, pore fluids play a minor role as they have lower atomic numbers and are less excited. The detection of gamma rays is a two-step process. In the first process, the gamma rays interact with the detector material, converting some or all of their energy into ionizing radiation (energetic electrons). In the second process, the electrons are converted to an observable electrical signal.

Among the three types of nuclear radiation, α and β radiation are predominantly characterised by the Compton scattering effect, whereas γ radiation is characterised by the excited atomic number and its amount of energy, which is differentiated among the photoelectric effect (below 100 keV), Compton scattering (around 450 keV) and pair production (above 1.022 MeV). For gamma rays in the energy range of hundreds of keV, the primary interaction is Compton scattering but the photoelectric factor plays an important role for geological formations, as it is exploited by the photoelectric absorption factor, P_e , logging tool. This factor is a direct indicator of lithology. In general, the material is characterised by the number of particles per unit volume, with which the flux of γ radiation may interact. By passing through material, only a certain fraction of the

incident particles have undergone interactions. The cross section is defined as the apparent area each target nucleus represents for the incoming γ beam. The unit of this cross section is *barn* given in 10^{-24}cm^2 .

There exist three types of gamma ray detectors. The first one is called the gas ionization counter. The second and most common one refers to the scintillation detector, mostly built of sodium iodide doped with a thallium impurity, NaI (Tl), and predominantly encountered in well-log measurements as part of the present study. This material shows solid gamma ray absorption properties and rapid scintillation decay times ($\approx 0.23 \mu\text{s}$). The third type of device, the solid state detector, is rarely found in logging applications (Melcher et al. 1991).

Due to the variability of GR log measurements within a time-frame of 70 years, different log units hampered the process of homogenizing the data set. Some of the GR logs were formerly measured in microgram Radon per ton (μgRt^{-1}), which required re-calculation to common log units adopted by the American Petroleum Institute (gAPI). Hence, unit conversion between μgRt^{-1} and gAPI was applied according to (Crain 2021):

$$GR_{log} = GR_{\mu\text{gRt}^{-1}} \cdot 10 \quad (3.2)$$

with GR_{log} being the converted gamma ray log value in gAPI and $GR_{\mu\text{gRt}^{-1}}$ being the original gamma ray log value in μgRt^{-1} . Different GR tool calibrations among older wells for hydrocarbon exploration required normalization (Fig. 3.7) based on the geothermal wells drilled recently. The new (geothermal) wells offered increased tool sensitivity. Hence, old wells were adapted accordingly despite removing potential shale- and sand-influenced (geological) trends. The gamma ray index was calculated based on GR logs applying different models depending on geological formations for the derivation of shale volume (V_{sh}). The Stieber Miocene/Pliocene Model was applied for the Quaternary deposits, the Tertiary Larionov Model for the Molasse Rouge, Grès et Marnes Gris à gypse and Siderolithic formations, and the Larionov Model for underlying Mesozoic formations, according to (Schön 2015):

$$I_{GR} = \frac{GR - GR_{min}}{GR_{max} - GR_{min}} \quad (3.3)$$

$$V_{sh} = \frac{I_{GR}}{3 - 2 \cdot I_{GR}} \quad (3.4)$$

$$V_{sh} = 0.083 \cdot (2^{\{3.7 \cdot I_{GR}\}} - 1) \quad (3.5)$$

$$V_{sh} = 0.33 \cdot (2^{(2 \cdot I_{GR})} - 1) \quad (3.6)$$

where the GR_{min} -value of 10 gAPI was set as the average sand-dominated zone, and the GR_{max} -value of 100 gAPI refers to an average shale-dominated zone.

Mineralogical analyses were used to correlate GR_{min} and GR_{max} values to the Molasse Rouge and Grès et Marnes Gris à gypse formations. High quartz-value intervals were chosen as clean (sand-dominated) zones and respective high fractions of clay minerals in shale-dominated zones. Wells Geo-01 and Geo-02 ran spectral GR logs (SGR), which were used to identify the type of clay, i.e. dispersed, structural or laminated. The spectral GR also proved to be a valuable identifier for shale volume estimates. However, U was excluded and only K and Th were used in patches for the calculation of V_{sh} from spectral GR logs. This arises from the fact that U is very soluble in sedimentary rocks, leading to transport of U by pore fluid and precipitation far away from the geological origin, hence deflecting the real shale volume of that location.

The spontaneous potential (SP) log measures the difference of voltage between an electrode lowered in a non-cased borehole and a surface electrode, involving two predominant processes: (1) the electrochemical potential and (2) the cation selectivity of shales. Typically, rocks are considered insulators, whereas the detectable conductivity refers to material filling up the pore space, i.e. clay minerals, graphite, metal or metal sulfides (Tittman 1987). The mechanism behind it depends upon the presence of dissolved salts in a pore fluid, e.g. water.

A spontaneous potential is caused by the diffusion of dissolved ions in the fluids inside the borehole and in the formation, considering the diffusion of Na^+ and Cl^- ions from the region of higher concentration to that of lower concentration (Ladd 1998; Revil, Leroy 2004). In a mixture of clay minerals and pore space containing hydraulic water flow, cations diffuse along the charged surfaces from high to low concentration, while the negative Cl ions are excluded. Such a diffusion process, which is referred to as the membrane potential, tends to accumulate a positive charge on the low ionic concentration side of the shale barrier (membrane), producing an attendant electric field. The measurement is then basically a direct current (dc)

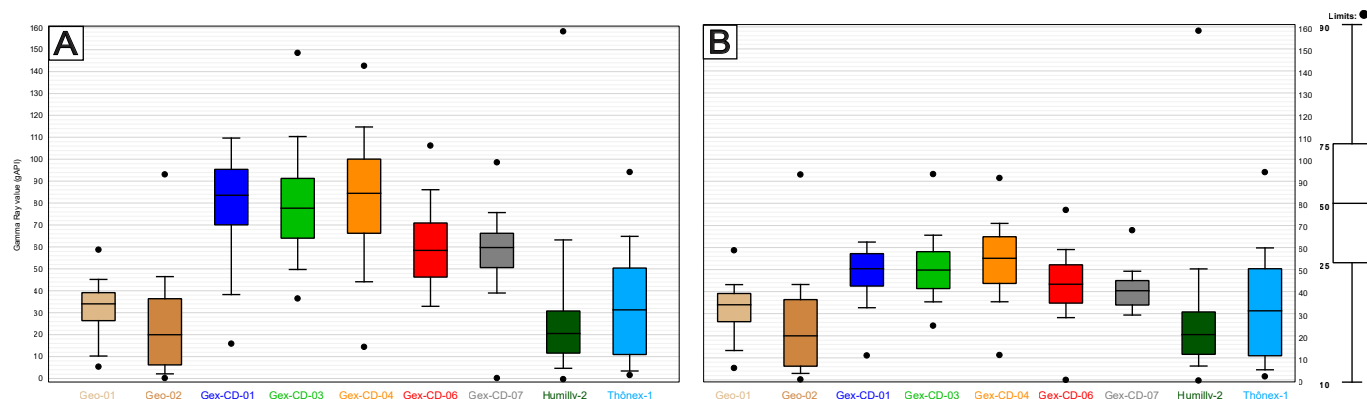


Fig. 3.7: GR values before (A) and after (B) normalization. Middle line in box plots depicts mean values, circles denote extreme values (outliers). The latest geothermal exploration wells (Geo-01, Geo-02, Thônex-1) were used as calibration for older, hydrocarbon exploration wells (Gex-CD-01, -03, -04, -06, -07 and Humilly-2) to normalize the data sets. After Haas et al. (2022).

voltage, for which it is assumed that unwanted sources are constant or slowly varying with time and depth. For further information on the electrical effect of clay in core samples, Hill & Milburn (1956) and Waxman & Smits (1968) are recommended.

A mathematical derivation of the electrochemical and membrane potentials, with the latter contributing the most to the SP potential applying the concepts of mobility and diffusion (Nernst-Einstein relation), is found in Ellis & Singer (2007). Considering the hydraulic flow, respectively diffusion of ions, SP logs were used to identify (clean) permeable zones for this study. SP logs allowed the determination of formation water resistivity and were used to calculate shale volumes. Clay minerals indicate a visible increase of spontaneous potential.

SP log measurements were run and displayed in increments of 20, 10 or 5 mV. Despite different well-logging campaigns tailored to different exploration purposes, either a GR or SP log was run in most of the 47 digitised wells. This allowed a first distinction of sand- and shale-dominated depth intervals based on the two eligible approaches of shale volume calculations.

Density and neutron logs

Similar to the GR log, the density (RHOB) and neutron (NPHI) logs are part of the nuclear physics logs. The density log measures the electron density, and the neutron log measures the neutron density of hydrogen along a borehole path. Both logs target the determination of total porosity. Neutron logs are affected by shale, which causes the log

to measure the additional hydrogen of clay minerals as an additional porosity. This results in the *shale effect*, for which porosity estimations tend to be higher compared to the true porosity.

Cross-plots of neutron and density logs depict a common procedure to determine both lithology distinctions and the identification of gas-bearing zones in the hydrocarbon industry (see e.g., Tang et al. 2013). The effect that density porosity tends to be higher due to the lower density of gas with respect to oil or water is exploited when intersected with the neutron porosity showing lower values. This is due to the fact that neutron logs are commonly calibrated with water-bearing sandstone formations. Hence, the neutron device assumes a water-filled formation, when it is gas-filled. Ultimately, the lower content of hydrogen in gas then reads lower values compared to those in oil or water.

A second technique envisaged by cross-plots is the derivation of lithologies. They allow for simple derivation of common lithologies, i.e. sandstone-limestone-dolomite models. For more complex lithologies inferring more than three or different components, the derivation of M-N plots combining the density, neutron and sonic log leads to a successful identification (see Haas et al. (2022)). The M-parameter required the input of transit time of the formation fluid, bulk density and fluid density as well as the value of transit-time at a specific borehole depth. The N-parameter used the neutron porosity of the formation fluid, the neutron porosity at a specific depth as well as the bulk density and fluid density. It is common that the formation parameters are replaced by respective matrix values

to obtain the minerals. The M-N ratio then follows defined lithology trends.

Another possibility for complex lithology detection used herein is the exploitation of the photoelectric absorption factor logging tool emitting gamma rays stemming from the photoelectric effect, as part of the density logging tool. The photoelectric effect results from the interaction of a gamma ray with an atom in the material at lower energies below 100 keV. In this process, the incident gamma ray disappears and transfers its energy to a bound electron. If the incident gamma ray energy is large enough, the electron is ejected from the atom and begins interacting with the adjacent material. Normally the ejected electron is replaced by another less tightly bound electron with the accompanying emission of a characteristic X-ray fluorescence. Based on these low-energy gamma ray interactions, the P_e was derived from the photoelectric factor (PEF) log that was run in well Geo-01 (Haas et al. 2022). This allowed for a lithology distinction based on atomic numbers (Z) according to (Ellis & Singer 2007):

$$P_e = \left(\frac{Z}{10} \right)^{3.6} \quad (3.7)$$

Bulk density logs were run in a vast number of boreholes, while apparent matrix density was run explicitly in geothermal well Geo-01. Results from early density logging tools deployed between 1960 and 1985, in particular in the Gex-CD-xx wells, were measured in units of counts per second (CPS) and no reliable calibration to density or porosity, as well as compensation for borehole effects was found in the well documentation. Hence, CPS density logs were predominantly used to qualitatively check encountered lithologies rather than to derive quantitative porosity calculations, despite them being the preferred logs for porosity derivations. In the geothermal wells, corrected density logs (DRHO) were used to check the original bulk density log (RHOB), whereas a value above 0.2 g/cm^3 was considered erroneous and the RHOB log was discarded in these intervals (Asquith et al. 2004; McPhee et al. 2015). Erroneous intervals were common since density logs require constant borehole wall contact, which was not the case in washout and mudcake zones for well Geo-01.

Density and neutron logs run in wells Thônex-1, Humilly-2, Geo-01 and Geo-02 allowed the identification of permeable zones. An overlap of these two curves indicated

permeable, i.e. possible sand-dominated depth intervals, whereas a clear separation indicated impermeable, i.e. possible shale-dominated intervals. Measured mineralogical data supported the identification of these respective intervals by using them as calibration indicators (Adams 2005). A true separation was not encountered due to the heterogeneous nature of the Molasse formations. In addition, neutron porosity versus bulk density enabled the derivation of clay types, i.e. occurrences of laminated, dispersed or structural shale. These findings were used for the sand-silt-clay model (Haas et al. 2022) and substantiated a first qualitative estimate of sand-silt-clay encountered at well Geo-01.

Acoustic travel-time log

Delta-transit time logs (DT) are used for different purposes in either transmission or reflection mode. For the former, a DT logging tool transmits acoustic energy in a frequency range of ca. 20 kHz in short bursts deriving the travel-time (slowness) of compressional (V_p) and transversal (V_s) elastic waves passing through a geological formation in a borehole between a source and a receiver. For geotechnical applications and geomechanical modelling, the DT log in transmission mode is used for the evaluation of cement bond to steel casing, the detection of fractures and for the empirical calculation of mechanical earth models (MEMs) by estimating mechanical rock properties such as the uniaxial compressive strength (UCS) and dynamic Young's modulus (E_{dyn}) from inserting V_p and V_s into respective equations for elasticity (Chang et al. 2006a; Herwanger et al. 2016; Herwanger & Horne 2009; Renli et al. 2019). Furthermore, the DT log is commonly used for the calculation of friction angles from V_p measurements (Lal 1999), empirical modelling of shear-wave velocities (Castagna, Backus 1993) or for seismic-to-well ties in combination with 2D or 3D seismic surveys as shown in various hydrocarbon exploration studies.

DT logs run in transmission mode were used as a second-choice porosity log because the density log was either erroneous or not initially part of the logging campaign. Together with neutron and density logs, neutron-sonic cross-plots were used as an indicator for dolomitic rocks, while density-sonic cross-plots exploited another possibility of lithology detection. However, it should be mentioned that the latter cross-plots were the least-favourable option, since the lines of sandstone, limestone and dolomite

lie very closely to each other and hamper a clear lithology separation.

In reflection mode, DT logging tool devices use frequencies at 500 kHz or higher hosting one single device that contains both transmitter and receiver. This mode is used for acoustic imaging. For this study, no acoustic imaging logs have been investigated and the DT logging tools are exclusively referred to in transmission mode.

For the present study, total (PHIT) and effective (PHIE) porosities were calculated using the sonic log and were calibrated to laboratory measurements in the Molasse Rouge formation. The DT porosity reflects PHIT and PHIE and accounts for the matrix in a given rock, i.e. intergranular and intercrystalline porosity. Porosity calculations based on the sonic log were performed using the Wyllie time-average equation (Wyllie et al. 1956):

$$\Delta t = \Delta t_{solid} (1 - \phi) + \Delta t_{fluid} \cdot \phi \quad (3.8)$$

Average values yielded Δt_{solid} of 47.5 $\mu\text{s}/\text{ft}$ and Δt_{fluid} of 189 $\mu\text{s}/\text{ft}$ for the Molasse Rouge formation. For effective porosity, the shale volume was subtracted from total porosity. No porosity calculations were performed in the Quaternary glaciogenic deposits and Mesozoic limestone formations.

Besides the Wyllie time-average equation, there exist various empirical methods for porosity estimations from compressional slowness, as summarised, for instance, in Mavko et al. (2009).

Electrode and induction logs

The general term of resistivity logs summarises two categories: electrode and induction logs. For the present study, electrode logs such as the short-normal (SN), long-normal (LN), laterologs (LL3, LL7) as well as induction logs such as the deep induction log (ILD, ID) and shallow induction log (ILS, IS) for the younger (geothermal) wells were analysed. Electrical devices respond predominantly to fluid content of a geological formation rather than the rock matrix, which is considered an insulator. The presence of clays, however, decreases the rock's resistivity. It is important to differentiate among three distinct regions of the measuring environment and their respective resistivity values stated in brackets below. The mud resistivity R_m

depicts lower values than R_{xo} and R_t . The mud filtrate resistivity, R_{mf} is usually retrieved from the well-log header. These regions include:

1. the borehole or mud environment (R_m),
2. the invaded zone (R_{xo}) and
3. the undisturbed formation (R_t).

Electrical devices consist of metallic electrodes, which utilise low-frequency current sources, often below 1 kHz to insert a current into a geological formation from a borehole. The spacing between the current electrode and voltage electrode gives a first hint of respective tool names, e.g., the short-normal (SN) in case of 16 inch spacing, and the long-normal (LN) for 64 inch spacing.

Induction devices use medium frequency (several tens of kHz) of alternating current to energise transmitter coils in the sonde, which induce eddy currents in the formation, proportional to the formation conductivity. The magnitude of the induced currents is measured by receiver coils in the tool that detect the magnetic field generated by the induced currents (Ellis & Singer 2007). Similarly, two-coil induction logging device consist of a transmitter coil excited by an alternating current of medium frequency (ca. 20 kHz) and a receiver coil. An industry standard depicted Schlumberger's standard deep reading array known as the 6FF40 as it consists of six coils, three transmitter and three receiver, respectively, with fixed radial and vertical focusing (FF). For the well-logs analysed as part of this study, the 6FF40 log was the most common induction tool. For the evaluation and interpretation of these resistivity logs, formation temperature corrections were required. The R_{mf} and R_m readings were converted to the values they would have at formation temperature, estimated from a recorded bottom hole temperature or from regional geothermal gradients (Chelle-Michou et al. 2017; Makhloufi et al. 2018). Unless provided in well reports, the gradient method (Crain 2021) was used for calculating the formation temperature, FTEMP, assuming a surface temperature of 15 °C with a gradient of 3 °C per 100 m. This seemed reasonable since in-situ temperature for the exploitation of geothermal energy significantly increases at ca. 1'000 m below the surface in the Mesozoic limestone formations (Chelle-Michou et al. 2017), with a geothermal gradient of 27 °C per km (Schegg & Leu 1996). However,

these depths do not intersect the FCC subsurface perimeter.

Most of the digitized logs explained above were obtained by the company Schlumberger deploying the 6FF40 induction tool, a short normal (SN) 16-inch, a long normal (LN) 64-inch tool as well as shallow (15'0") and medium (18'8") laterologs. They were formerly run along specific intervals for hydrocarbon detection, and used for water resistivity calculation and quality control across logged formations. Water resistivity was calculated for the derivation of the sand-silt-clay model in the Molasse Rouge formation considering FTEMP and concentrations of Na, K and Ca taken from laboratory analyses. Uninvaded (true) resistivity (R_t) was taken from deep resistivity curves (LN, LLD, ILD), while invaded resistivity (R_i) was derived from shallow resistivity logs (SN, LLS). Flushed zone resistivity (R_{xo}) commonly taken from a micro-spherically focused (MSFL) log was only available in Gex-CD-07 and $R_{xo} = R_i$ was assumed for the invaded zone due to unavailable data.

3.4 Laboratory analyses

The following paragraphs provide descriptions of the performed geochemical, mineralogical, petrophysical, geomechanical and physico-chemical laboratory analyses. Unless otherwise stated, theoretical explanations were taken from Bartsch & Sachs (2018), Bigham et al. (1989), Chapman et al. (2017), Chave (2017), Dinnebier & Billinge (2008), Fjaer et al. (2008), Jaeger et al. (2007), Jasmund & Lagaly (1993), Ma (2019), McPhee et al. (2015), Mishra & Datta-Gupta (2017), Moore & Reynolds (1989), Pecharsky & Zavalij (2009), Schlumberger (2006), Schön (2015), Singh & Goel (1999), Sparks et al. (1996), Ulery & Drees (2008), and Zoback (2007) and Herwanger (2011). Further theoretical information and mathematical derivations of statistical methods are found therein.

Measurement values below the limit of detection were set to respective limits for data analysis. In order to exploit the maximum amount of measurements per sample after initial rock sampling and sample preparation (Fig. 3.8), an analysis flow as follows was developed: the first measurements included petrophysical analyses for porosity, permeability and grain density as well as compressional and shear-wave velocities on plug samples; second, on these plugs uniaxial compressive strength, point load, Brazilian

tensile strength, CERCHAR and LCPC abrasivity tests were performed; ultimately, these now crushed rock samples were split into respective mesh fractions for consecutive geochemical, mineralogical and physico-chemical analyses.

Geochemical analyses

The elemental analysis and distribution of glaciogenic deposit and Molasse Rouge samples allowed for conclusions on the chemical composition of rock material. These analyses are introduced in the following paragraphs and were required for the identification of the major and minor (trace) elements as well as chemical pollutants to evaluate for potential application scenarios, e.g., tile or brick production. Element ratios were calculated rather than individual element concentrations to provide robust results with respect to nugget effects, and because these ratios were required for the derivation of Augustinik diagrams (Augustinik 1957). These diagrams depict the chemical alteration, argillosity (Al_2O_3/SiO_2 ratio), alkali (Na_2O , K_2O), alkaline earth (MgO , CaO) and transition metals (Fe_2O_3 , MnO). The elemental results also served as the basis for geochemical (alteration) diagrams that drove the subsequent rock characterisation and for cross-correlations among field (pXRF) and laboratory (ICP) data following the linear regression method by Mauriohooho et al. (2016).

Major elements via portable X-ray fluorescence (pXRF)

Portable X-ray fluorescence (pXRF) measurements allowed for a fast and low-cost multi-elemental quantitative analysis of rocks for the derivation of major oxide minerals. The pXRF device contains a detector and a radioactive cesium (Cs) source, which generates X-rays to excite electrons in the atom's outer shell into higher states of energy, ultimately pushing them out of their orbits. Electrons from the inner shell compensate the energy loss and occupy these orbits by emitting fluorescence, which depicts the difference of energy level by the two electrons given by the electromagnetic radiation (Bremsstrahlung). This difference is unique for an atomic number, i.e. element.

A portable Thermo Fisher Scientific Inc. NITON XL3t 900 Analyzer was used to measure 42 powder rock samples ($<400 \mu m$) explicitly in well Geo-02. About 2-3 g of



Fig. 3.8: Exemplified overview of drilled plugs on which petrophysical, geomechanical, geochemical, mineralogical and physico-chemical analyses were performed.

the $<400\ \mu\text{m}$ powder was placed in a cup, pressed with a piston and then covered by a plastic foil. All samples were analysed in three runs, each with 120 seconds measurement time, whereas the average of all three runs was taken for subsequent data analysis. Before each measurement, the 8 mm beam hole was cleaned with ethanol. The detection limit was given by 3σ standard deviation of a measurement. Precision was given by 2σ . An element was detected at a minimum of 1.5 times the precision in parts per million (ppm), i.e. mg/kg. Counts and energy of the detected X-rays were measured via energy-dispersive spectroscopy. The device was used in Mining Cu/Zn testing mode designed for soil and rock samples. This mode provided the most reliable results for metal concentrations $>1\%$ and included the measurement of the following 34 elements: Mg, Al, Si, P, S, Cl, As, K, Ca, Ti, V, Cr, Mn, Fe, Co, Ni, Cu, Zn, W, Pb, Bi, Zr, Nb, Mo, Sn, Ba, Sb, Cd, Pd, Sr, Rb, Se, Ag and Au.

Trace elements via ICP-MS/OES

For the detection of trace-elements via inductively coupled plasma mass spectroscopy (ICP-MS) and optical emission spectroscopy (ICP-OES), samples were outsourced to the certified laboratory *Bureau Veritas* in Poland and Canada, following analysis packages PRP70-250, EN004, PULSW, SHP-01, DY105, MA250, LF300-Si element and TC007 as

specified in the technical product catalogues *Bureau Veritas* (2015, 2018a,b, 2019a,b), *Geostats PTY LTD Mining Industry Consultants* (2020a,b,c,d), *Leco* (2007), *Perkin Elmer SCIEX Instruments* (2020), and *Spectro Ciros Vision* (2004)). This allowed for subsequent calculations of oxides, comparisons with portable XRF measurements, elemental alteration (GER) diagrams, and the prediction of application scenarios via respective elemental ratios.

Plug and cutting samples were crushed to $\geq 70\%$ passing a 2 mm mesh. 250 g of the crushed material were pulverized $\geq 85\%$ to a fraction of $75\ \mu\text{m}$ and dried in a $105\ ^\circ\text{C}$ oven for 48 h. Multi-acid digestion for ultra-trace analysis via ICP-MS was used for the identification of the following 59 elements: Mo, Cu, Pb, Zn, Ag, Ni, Co, Mn, Fe, As, U, Th, Sr, Cd, Sb, Bi, V, Ca, P, La, Cr, Mg, Ba, Ti, Al, Na, K, W, Zr, Sn, Be, Sc, S, Y, Ce, Pr, Nd, Sm, Eu, Gd, Tb, Dy, Ho, Er, Tm, Yb, Lu, Hf, Li, Rb, Ta, Nb, Cs, Ga, In, Re, Se, Te, Tl, Si (SiO_2). Four acid digestions with 0.25 g of the $75\ \mu\text{m}$ sample fraction were heated in HNO_3 , HClO_4 and HF until fuming. The residue was dissolved in HCl and analysed in a *Perkin Elmer Sciex Instruments ELAN 9000 ICP-MS* device. For the identification of silica, a *Spectro Ciros Vision* high-performance ICP-OES device (LiB02/LiB407 fusion analysis) was used.

Leachate analysis via ICP-OES

Leaching characteristics contributed to the evaluation of dissolved ions relevant for disposal considerations as well as uses such as in quarry backfilling, topsoil construction and agricultural, as stated in e.g. Swiss and French legislation (Association Française des Tunnels Et De L'Espace Souterrain (AFTES) 2019; Haas, Galler, et al. 2020; République et Canton de Genève 2016; République Française 2015; Swiss Confederation 1998, 2016; Vernus et al. 2017). These ultimate scenarios also required measuring respective ions by cuvette tests, which are described in the section below. For leaching analysis, the ICP-OES constituted a simple and high-precision state-of-the-art device.

The measurement procedure followed DIN EN 12457-2 (European Norm (EN) 2003a) with minor changes for water content corrections and initial dry masses for the eluate-solution (L) and dry-mass (S) ratio. Before analysis, the H_2O content was determined and served as a proxy for dry mass weights. According to the standard, the L/S ratio should not exceed 10, which resulted in initial weights of about 5 g of the $<400 \mu\text{m}$ sample fraction.

The centrifuge cup including the dry sample powder was filled with millipore- H_2O up to 50 ml. The samples were shaken for exact 24 h in an automatic shaker according to the standard to guarantee sufficient dispersion. The shaken samples were centrifuged at 3'800 RPM for 20 minutes in a Heraeus centrifuge. Then, the centrifuged samples were filtered with $<0.45 \mu\text{m}$ PES vaccine filters and the resulting 10 ml liquid was filled up with 2% of dissolved HNO_3 acid in a 50 ml cup to prevent heavy-metal precipitation. The prepared samples were stored in a refrigerator at 5 °C, and analysed in the ICP-OES device the next day. Results were calculated according to (European Norm (EN) 2003a):

$$A = C \cdot \left(\frac{L}{M_T} + \frac{FG}{100} \right), \quad (3.9)$$

with A being the leaching substance (mg/L), respectively release (mg/kg) at an L/S ratio of 10, C the concentration (mg/l) of the eluate solution, L depicting the volume of leaching conditioning substance (l), FG the humid mass (% related to dry mass) and M_T stating the dry mass (kg) of the sample. In total, twelve leaching substances were analysed, namely As, Cd, Co, Cr, Cu, Hg, Ni, Pb, Sb, Sn, Tl and Zn. In case values were below detection, these were

set to the detection limit.

Carbon content via thermal-acid treatment

Carbon determination contributed to the evaluation of the total organic and inorganic carbon content relevant for the evaluation of application scenarios. The test was performed according to DIN EN 15936 (European Norm (EN) 2020b) in a multi EA 4000 device by Analytik Jena, whose results on total carbon (TC), total inorganic carbon (TIC) and, via the indirect difference method, total organic carbon (TOC) content, allowed for conclusions on organic matter content relevant for the evaluation of tile and brick production. A $CaCO_3$ reference sample was used as a standard for all analyses.

The analysis was conducted on one sample, which was split into two sub-samples of different initial weights. For the TIC determination, about 50 mg of a 105 °C dried $<400 \mu\text{m}$ sample was placed on a ceramic sample holder and treated with 35% H_3PO_4 acid, while under oxygen atmosphere leading to decomposition. The resulting CO_2 gas was detected via non-dispersive infrared (NDIR), which was used to calculate the total inorganic carbon content. For the TC content, the second 105 °C dried $<400 \mu\text{m}$ sub-sample of 300 mg was burned in a 1'300 °C oven and the release of CO_2 was detected by NDIR. The TOC content was calculated indirectly by subtracting the TIC from the TC content in the multi EA Analytik Jena software.

Besides these measurements, carbon determination was also measured as part of the analysis packages outsourced to the laboratory *Bureau Veritas*. For these total organic carbon analyses, a Leco CS230 Carbon/Sulfur Series device was employed on the dried 75 μm samples that were produced for the former ICP-MS/OES analyses.

Mineralogical analyses

Mineral phases via XRD

X-ray diffraction (XRD) has become the most common method to determine crystalline mineral phases qualitatively and quantitatively, which in conjunction with automated mineralogy and petrography scanning (QEM-SCAN) were required for the identification of minerals to predict various application scenarios. XRD exploits Bragg's equation to derive the characteristic crystal lattice interplanar spacing, d , from incident X-rays diffracted

at atoms, oriented along parallel lattice planes for a given mineral phase.

The method applied herein followed standard DIN EN 13925-1/-2 (European Norm (EN) 2003b,c) and was performed with a D8 Advance Bruker AXS/D XRD device. The instrument used Co-K α radiation generated at 35 kV at a current of 40 mA with dynamic beam optimisation using an automatic theta compensating divergence slit and a motorised anti-scatter screen. The diffractometer was equipped with primary and secondary soller slits, and an energy-dispersive LynxEye XE-T line detector. Qualitative phase analysis was conducted with the software DIFFRAC.EVA v4.3 (Bruker AXS). The minerals were identified by peak positions and relative intensities in the X-ray diffraction pattern compared with the PDF2 database (International Centre for Diffraction Data (ICDD) 1998). For quantitative analyses, randomly oriented Ca-exchanged samples (G. Zhang et al. 2003) were scanned from 4° to 80°2 θ with steps of 0.02°2 θ at 2-s intervals using a Bragg-Brentano X-ray diffractometer (Bruker AXS D8 Advance, Germany). Quantitative mineral analyses were performed via Rietveld analysis of XRD patterns using the program Profex/BGMN V4.2.4 (Doebelin, Kleeberg 2015). This full pattern-fitting method calculated X-ray diffraction patterns based on crystallographic data of each mineral phase and its iterative adjustment (least-square fit) to the measured diffractogram. In the refinement phase, specific parameters and the phase content were adapted to minimize the difference between the calculated and the measured X-ray diffractogram.

Four (4) different types of samples were prepared and analysed. About 1-2 g of <20 μm powder was mixed in a mortar and sieved through a 200 μm mesh for random grain orientation.

1. The powder was placed into a powder sample holder (XRD-P) and carefully distributed by irregularly tapping with a razorblade to form a flat specimen surface and to maximise random grain orientation.
2. For the clay mineral XRD analysis, between 0.2 to 0.6 g of the same powder were placed on a glass disc, which was cleaned with (CH₃)₂CO (acetone) beforehand. The powder was mixed with 2-3 drops of distilled H₂O, and the resulting paste was smeared with a spatula on the disc for proper clay mineral orientation to receive a textured sample (XRD-S).
3. In order to identify inner crystalline swellable clay minerals and cause a separation of the illite-smectite peaks (12-32 Å), each XRD-S sample was placed in a 65 °C oven in ethylene glycol atmosphere in a desiccator overnight (XRD-EG). On the next day, the XRD-EG sample was measured within a timeframe of 1 hour before the ethylene glycol evaporated.
4. For the identification of kaolinite, two XRD-S samples were treated with hydrazine (XRD-HZ) leading to a distinct peak-shift in the diffractogram due to the incorporation of hydrazine molecules into the kaolinite crystal lattice (Jasmund & Lagaly 1993). For selected samples, the XRD-S/EG samples were heated up to 550 °C to induce a clear peak separation of kaolinite from chlorite between 7 and 14 Å based on the instability of kaolinite above 500 °C (Jasmund & Lagaly 1993).

Clay mineral peak separation is thoroughly described in Brindley & Brown (1980).

Besides the newly measured samples as part of this study, XRD results of 97 samples were implemented as part of the study by Schegg (1993). Schegg (1993) conducted bulk XRD mineralogy and analyses of relative content of phyllosilicates in the <2 μm fraction of shale and sandstone samples in the Haute-Savoie region and around Geneva investigating the paleogeothermal conditions and diagenetic evolution of the Swiss and French Molasse Basin sediments. While these analyses were used for qualitative comparisons, quantitative mineral phase results were consulted explicitly for the bulk mineralogy.

Mineral phases via FTIR

The Fourier-transform infrared (FTIR), i.e. mid-infrared (MIR, 2.5-40 μm) spectroscopy, allowed for qualitative conclusions on organic matter, whose thresholds were required for the evaluation of application scenarios. The FTIR method is complementary to the carbon determination method and the detection of amorphous and crystallized mineral phases based on measured interferograms following Lambert-Beer's (Bouguer-Lambert-Beer's) law (Beer 1852; Bouguer 1729; Lambert 1760) for clay-rich rock (Josh et al. 2019). Energy in the mid-infrared field (MIR, 2.5-40 μm) sets molecules in vibrations and the amount of transmitted energy allows conclusions on

the presence of kaolinite (hydroxyl groups in aluminosilicates). Organic matter (OM), i.e. total organic carbon (TOC), carbonates (CO_3^{2-}) such as calcite and dolomite, quartz (i.e. silicate minerals) and gibbsite show wave numbers at 3'696-3'620, 3'000-2'850, 1'600-1'268 (1'427) and for the latter two between wave numbers 1'270-951 and down to 450 cm^{-1} , respectively. Organic matter, which is qualitatively not identifiable during thermal or acid treatment analysis, is sub-divided into C-C stretching of aromatics and alkene double bonds, C=O stretching of secondary amides and COO asymmetric stretching of metal carboxylates between 1'756 to 1'600 cm^{-1} .

The applied potassium-bromide (KBr) disc method ensured that the Bouguer-Lambert-Beer's law was valid (Bertaux et al. 1998) for the qualitative analysis of mineral phases. KBr discs provide a robust method for the FTIR analysis because the material attracts less water. The approach was based on successful former studies performed on calcite, dolomite, aragonite, amorphous silica, silica polymorphs, quartz and clay minerals (e.g. Chester, Elderfield 1967, 1968; Duyckaerts 1959; Fröhlich 1989; Pichard, Fröhlich 1986; Van der Marel, Beutelspacher 1976). They analysed evenly dispersed solid components at low concentration in a non-absorbing medium using monochromatic light (Van der Marel, Beutelspacher 1976) according to:

$$I = I_0 \cdot e^{-acl}, \quad (3.10)$$

where I is the intensity of transmitted light, I_0 the intensity of incident light, a is the absorption coefficient, c being the concentration (mol/L), and l depicts the length of the sample cell (cm). Rock-forming minerals contain their fundamental molecular vibration bands in the *MIR* region (Farmer 1974; Salisbury 1993), yielding spectra along the wavenumber in cm^{-1} on the x-axis and percentage of transmission in $\%T$ on the y-axis.

The measurement preceded a thorough sample preparation, drying 1 mg of a $<20 \mu m$ sample at 105 °C, and subsequent mixing with 199 mg of KBr on a high-precision 5-digit scale. The 200 mg powder mixture provided enough material to subsequently press a disk. The powder mixture was stirred for ca. 1 minute, placed in an agate mortar and slowly mixed for another 3 minutes without applying pressure to avoid crushing of grain particles before the homogeneous powder mixture was subjected to a vacuum for 7.5 minutes. Once evacuated, a 10'000-kg load was

applied onto the sample for 2 minutes while holding the vacuum. The result was a pressed KBr pill, which was inserted in a Perkin Elmer Spectrum One device using the program Spectrum V5.3.1 for analysis. The background for an empty sample holder was determined before the measurement run. Each analysis measured 20 runs and summed up the partial Fourier-transformed spectra to a full transmission spectrum.

Mineral phases and elements via QEM-SCAN

Automated mineralogy and petrography scanning (QEM-SCAN) was originally developed by CSIRO in Australia in the 1970's for the mineral exploration and mining industry to guide decisions in mineral processing and metal refining (Miller et al. 1982; Reid et al. 1984). It enabled the quantification of minerals, i.e. gold, in complex ores (Goodall et al. 2005) by measuring chemical composition, fabric, distribution, texture, angularity and porosity of rock material. For this study, the method was used to correlate mineral phases with XRD analyses and derive elemental mapping distributions for result comparisons with geochemical analyses to predict application scenarios.

An FEI QEMSCAN® Quanta 650F instrument was used to identify the modal mineralogy, texture, and lithotypes. The instrument uses a scanning electron microscope (SEM) equipped with two energy-dispersive X-ray (EDX) spectroscopy detectors, which measures secondary X-ray spectra to determine elemental compositions. Individual X-ray spectra were compared to an X-ray EDS spectra library comprising a specific mineral name, assigned to each individual acquisition point (Gottlieb et al. 2000), and stemmed from the combination of back-scattered electron (BSE) contrast and EDS spectra providing information about the elemental composition. The results yielded respective minerals, mineral distributions and proposed rock types. This non-destructive analytical technique also enabled in-situ high-resolution elemental mapping with analytical points below 2 μm (Pirrie et al. 2004). Elemental mapping derived a statistical distribution from the EDS spectra.

Measurements were performed at an acceleration voltage of 15 kV with a 10 nA probe current on polished thin sections, which were carbon-coated beforehand using a Quorum Q150T S/E/ES graphite coating device (Quorum Technologies n.d.). X-ray acquisition time was set to 10

ms per pixel using a point-spacing of 2.5 and 5 μm . Each section was scanned on a 1.5×1.5 cm area at 10 μm resolution. Up to 122 individual view fields were measured in each sample, depicting 1.5 mm per single field. Areal capture of the beam is set to 500 pixels in order to not consider dust particles. About 1000 photons per pixel were used to fasten the measurement procedure. Detection limit is given in the range of 2 to 2.5 wt%.

Data processing and analyses were performed using the FEI iDiscover software and stored in a dedicated *species identification protocol (SIP)* job file. Due to physical mixed-layer clays and grain boundaries, which were not necessarily in compliance with the compared EDS spectra library, results contained a certain portion of unclassified minerals. Besides the newly measured samples, results of an additional 145 QEMSCAN samples of wells Geo-01, Thônex-1, Humilly-2 as part of the studies by Brentini (2018) and Pierdona (2018) and Rusillon (2018) were incorporated. The same FEI QEMSCAN Quanta 650F device was used and the samples were re-run with the same *SIP* file settings to guarantee reasonable comparison. Minor adaptations were taken for the measuring background due to their embedments in gypsum/anhydrite.

Mineral phases via optical microscopy

Optical microscopy qualitatively supported the QEMSCAN measurements, and allowed for the identification of transparent and opaque minerals in the same thin section samples prior to their carbon-coating in transmitted and reflected polarized light. These analyses were primarily used for cross-checking with the QEMSCAN analysis results, rather than performing a detailed thin-section analysis.

An OLYMPUS BX61 optical microscope was used operating with lenses at 2.5 \times , 5 \times , 10 \times , 20 \times and 40 \times magnification. Photographic documentation was conducted with a mounted OLYMPUS DP27 digital camera using a shutter speed of 1/80 s at ISO 100 and white-balance. Samples were analysed in plain-polarized transmitted (T-PPL), reflected light (R-PPL) and in cross-polarized transmitted (T-XPL) light modes in the OLYMPUS Stream Motion software. Image settings in these three specific modes were chosen depending on thin section glass thickness, using a 6.30 \times magnification for samples of well Geo-02, and 3.15 \times magnification for all other samples:

1. R/PPL: on average 3.333 milliseconds (ms) exposure, white-balanced, 9V light source,
2. T/PPL: on average 72.00 microseconds exposure, white-balanced, 12V light source,
3. T/XPL: on average 1053 milliseconds (ms), white-balanced, 12V light source.

Before image storage, proper scaling reference was applied for post-processing and the final image was stored in TIFF-format with approximately $16'262 \times 10'938$ pixels, yielding file sizes of ca. 512 MB on average. Each thin section measurement took about 3 min per analysis mode on average. All thin section images are uploaded in their high-resolution, original format onto the database link stated in appendix C.2.

Physico-chemical analyses

The physico-chemical behaviour of clay-rich rock is predominantly influenced by the type and amount of clay minerals. This deemed necessary to conduct specific analyses whose results were predominantly influenced by the physico-chemical behaviour of clay minerals (Fig. 3.9) that substantially impact the prediction of application scenarios for the FCC's excavated materials. Potential beneficial scenarios range from cement, tiles, bricks and lime production to topsoil construction. In a non-beneficial context, the scenarios also include disposal, landfilling and quarry backfilling. The characteristic physico-chemical properties allowed further for a subsequent correlation with various laboratory analyses for the underlying rock classification scheme introduced in chapter 5. In tunnelling, swelling is mostly associated with osmotic swelling, caused by the deconsolidation of clay minerals and their subsequent incorporation of water molecules (Wanninger-Huber 2019). A supporting measurement for the quantification of swellable clay minerals are specific surface area (SSA) analyses (Madsen & Kahr 1993) and Enslin-Neff analyses conducted and described below.

Therefore, the complex physico-chemical behaviour and analysis of clay minerals, i.e. phyllosilicates necessitate a brief introduction of their crystal structures, physical and chemical behaviour and clarification of shale, clay and clay mineral terminology across the various disciplines of geosciences including tunnelling.



Fig. 3.9: Selected samples with fraction $>400 \mu\text{m}$ of the glaciogenic deposits, Molasse Rouge, and Siderolithic formations as prepared for consecutive physico-chemical analyses. Note their different colours depending on type and amount of clay minerals.

Clay minerals belong to the family of phyllosilicates and contain continuous two-dimensional tetrahedral sheets (Brindley & Pedro 1972). They are hydrous aluminosilicates that form commonly from the weathering of feldspars and micas. They are deposited with sandy sediments. Authigenic clay minerals form within the pore space of rock after deposition and during cementation, causing a variety of issues with respect to reduced permeability, pore throat size, ion diffusion and leaching (McPhee et al. 2015). Four groups of clay minerals are distinguished according to their three-dimensional arrangements of atoms: (1) the kaolin group; (2) the smectite group; (3) illite; and (4) chlorite. These clay mineral groups can occur together in mixed layers.

Their crystal structure consists of combinations of sheets made of silica (SiO_2) and $\text{Al}(\text{OH})_3$ with di-octahedral and $\text{Mg}(\text{OH})_2$ with tri-octahedral, bonded by water molecules or positive ions. In the silica, the Si^{4+} ions are tetrahedrally coordinated with oxygen atoms and partially replaced by Al^{3+} . In the alumina, the Al^{3+} are octahedrally coordinated with oxygen and hydroxyl anions and often replaced by Mg^{2+} , Fe^{2+} , Ca^{2+} , Li^+ or K^+ cations. These silica and alumina sheets extend indefinitely in a and b crystal axis directions, and are

stacked along their respective c axis in composite layers of either two (1:1) or three (2:1) sheets, which are held together by van der Waals forces and hydrogen bonds, i.e. exchangeable cations and/or water molecules. These exchangeable cations are attracted due to the negative net charge on the clay surface because of substitution in the clay crystals of atoms of lower positive valence. The negative charge is balanced by the cations, which are termed *exchangeable* and dependant on the geological environment and the type of fluid flow. However, not all cations are exchangeable, as this is the case, for instance, for K^+ in mica. The excess negative charge is neutralized by the adsorption of hydrated cations, which are too large to fit inside the crystal lattice. In an ionic solution, these cations exchange with other ions in solution.

For the clay mineral's ability of attracting cations, the cation exchange capacity (CEC) depicts one of their most important properties. The capability of clay minerals to attract, retain or hold exchangeable cations has a significant influence on cation retention and diffusion of charged and uncharged molecules. The CEC measurement is prone to pH, soil texture, and organic matter content. A high pH value increases the amount of negative charges on clay mineral's surfaces because of the additional

negative charge at the edges due to hydrolyses, and hence correlates with high CEC values (Foth 1991). The ionic strength of the soil solution impacts the CEC value drastically, especially in weathered soils containing Al- and Fe-oxides, hydroxides or amorphous clay (Robertson et al. 1999).

Clay minerals consisting of three sheets, e.g. smectite (montmorillonite), cause major issues by incorporating water molecules into their crystal lattice and increasing their respective volume by a process called swelling (McPhee et al. 2015). Two main types of swelling are differentiated for clay minerals (smectites): (1) intra-crystalline swelling due to hydration of exchangeable ions in the inter-layer and (2) osmotic swelling due to a difference of ion concentrations at the clay mineral surface compared to a lower concentration in the pore water solution. These two types of clay swelling are reversible, whereas the irreversible third type refers to anhydrite swelling incorporating water by the formation of gypsum. Intra-crystalline and osmotic swelling cause a volume increase of up to 200% (Jasmund & Lagaly 1993). Anhydrite swelling depicts volume increases up to 61% (Anagnostou 2007; Steiner 1993).

Different disciplines have uniquely defined the size of clay particles, and it is for this reason that *fine-grained* is used in the definition rather than a precise value (Guggenheim et al. 2006). Although clays are phyllosilicates, they do comprise components that impart plasticity, and harden when dried or fired. Guggenheim & R. T. Martin (1995) stated a definition of the term *clay* and distinguished the terms *clay minerals* from *phyllosilicates*. Clay minerals form a sub-group of the phyllosilicate (silicate minerals) family. Micas such as muscovite and biotite are included in the phyllosilicate. Guggenheim & R. Martin (1996) further defined the term *clay* in an engineering context referring to "...a naturally occurring material composed primarily of fine-grained minerals, which is generally plastic at appropriate water contents and will harden when dried or fired...".

The present study follows the terminology stated by Guggenheim et al. (2006) (also mentioned in e.g., Bergaya & Lagaly (2013), Brindley & Brown (1980), Moore & Reynolds (1989) and Spooner (2014)) because the goal of the present study is to predict hazards to an engineering process, that is, tunnelling. According to Guggenheim et al. (2006), the term *shale* depicts a rock defined as a

finely laminated, sedimentary rock composed primarily of clay, mud and silt; while the term *clay* refers to the grain size in this study, and it is explicitly mentioned in case the term is used to refer to rock consisting predominantly of clay minerals. Furthermore, the term interstratified clay minerals, formerly called *mixed-layer* clay minerals, was used for the description of stacked layers of more than one clay mineral (e.g. illite-smectite, I/S, or kaolinite-smectite, K/S) within a crystal. This is essentially a mineral intergrowth with the first clay mineral name depicting the lower *d*-spacing value of the crystal lattice (S. Fiore et al. 2013) and excludes physical mixtures at the boundary of grains. These *physical mixed-layer* clay minerals are noted as such in the present study to describe QEMSCAN results.

Specific outer and inner surface areas via gas adsorption

The physico-chemical behavior and quantification of swellable clay minerals were associated with the measurement of their specific surface areas (SSA) via the adsorption of gas. The multi-layer BET adsorption method after Brunauer et al. (1938), i.e. DIN ISO 9277 (Deutsches Institut für Normung (DIN) 2014), measured the specific outer surface via gaseous N_2 -adsorption. BET-analysis preparation took about 1 day, while the second day was dedicated to sample measurement. On the first day, the 150 °C dried sample was weighed in a sample tube, whose end was attached to a VacPrep 061 vacuum pump. Heating elements increased the temperature gradually starting at 25 °C up to 150 °C with a temperature gradient of 25 °C/30 min. The pump operated overnight for 15 h at constant temperature of 150 °C in a heating element under vacuum ranging between 150 and 300 mtorr. On the second day, the evacuated sample tube was cooled down for ca. 1 h under room temperature. Afterwards, the sample tube was flushed with nitrogen gas for about 30 seconds at 0.5 bar. Subsequently, the sample was weighed on a medium-precision scale (4 digits), and immediately put in the Quantachrome Autosorb-1MP N_2 -adsorption measurement device for sample analysis.

Data processing and analysis was performed using the ASiQwin Version 3.01 software applying the multi-point BET method (nitrogen on silicates as adsorbate), which included 11 points in a relative P/P_0 range of 0.1 to 0.3,

in order to calculate specific outer surface areas based on equation (Allen 1990):

$$\frac{P}{V(P_0 - P)} = \frac{1}{CV_m} + \frac{C - 1}{CV_m} \cdot \frac{P}{P_0}, \quad (3.11)$$

with P and P_0 being the vapour pressure and saturation vapour pressure (bar), respectively, V depicting the total adsorbant volume, V_m the volume of a mono-layer and C being a constant. The results were plotted in a $\frac{1}{(W(P_0/P-1))}$ versus relative pressure P/P_0 diagram to conclude on the specific outer surface area in m^2/g .

While the multi-point BET method yielded the quantification of the specific outer surface originating from non-swelling clay minerals, the one-point vapor adsorption method after Keeling et al. (1980) provided insights about the specific inner surface area of swellable clay minerals by adsorbing H_2O molecules in their interlayers. For the analysis, a $<63 \mu m$ sample of 4 g was subjected to a 76% saturated NaCl solution under atmospheric pressure in a sealed plastic box. A small fan at the glass lid's bottom dispensed the gaseous NaCl homogeneously. The sample was kept under a 76% NaCl atmosphere for three continuous weeks. After the third week, random samples were checked for mass equilibrium occasionally within two to three days. Once adsorption was saturated, the samples were weighed on a high-precision (5-digits) scale. Afterwards, the sample was dried upon constant weight in a 105 °C oven and the difference of humid, NaCl-adsorbed and dried masses yielded the water adsorption according to:

$$w_{ads}(wt\%) = \frac{m_{NaCl} - m_{dry}}{m_{dry} - m_{glass}} \cdot 100 \quad (3.12)$$

Water uptake capacity via Enslin-Neff

The Enslin-Neff measurement was performed to analyse the water uptake capacity under free swelling conditions (Kugler et al. 2002; Madsen & Nüesch 1991; Neff 2005; Neff. H. 1959) and its associated temporal behaviour of rock-water interaction. The Enslin-Neff measurement followed standard DIN 18132 (Deutsches Institut für Normung (DIN) 2012) and served as an important basis for the rock characterisation proposed in chapter 5. Eventually, the Enslin-Neff data allowed for modelled plasticity behaviour of clay-rich rock after Dieng (2005) and Petkovšek

et al. (2009). This made it possible to compare older analyses conducted during LEP and LHC constructions with new ones measured herein.

About 1 g of a $<400 \mu m$ sample was placed in the Enslin-Neff apparatus and its free water uptake was recorded in time intervals up to 1'440 minutes. The maximum water absorption reading, w_{max} , served for the calculation of the water absorption capacity, w_a (wt.%), corrected by the dry mass, m_{dry} , according to:

$$w_a(wt\%) = \frac{w_{max}}{m_{dry}} \cdot 100 \quad (3.13)$$

Cation exchange capacity via $[Cu(trien)]^{2+}$ complex

The effective cation exchange capacity (CEC) was analysed based on the method proposed by Meier & Kahr (1999) via the $[Cu(trien)]^{2+}$ complex for the replacement of methylene blue values required for the prediction of application scenarios. This yielded a direct CEC measurement based on the ion concentration decrease in the exchanging solution. The CEC originates from negative charges carried by soil particles, commonly clay, organic matter and sesquioxides. These charges are commonly grouped into two categories: (1) permanent (pH independent) and (2) variable (pH dependent), and depend on whether ambient conditions (pH or salts) in the soil solution affect their magnitudes (Sumner & Miller 1996).

The Cu(II) ion forms stable, violet-blue complexes with the oligoamines triethylenetetramine (trien), tetraethylenamine (tetren), and pentaethylenhexamine (penten), which are connected via four and five N atoms to Cu. The maximum light extinction of these complexes ranges at pH values of 5 to 10. The maximum absorption is not affected by other cations or anions (free salts) at low salt concentration (Cheng 1962), and compared to other methods, the Cu(II) complexes with triethylenetetramine and tetraethylenepentamine allowed a rapid and reliable CEC measurement via photometric analysis (Kahr & Madsen 1995).

The sample solution was mixed with a $[Cu(trien)]^{2+}$ complex and analysed via photometry. 800 mg of a $<63 \mu m$ milled air dried sample were mixed with 20 ml ultra-pure milliQ- H_2O and treated in an ultrasound UP 200H device for 3 minutes to disperse the clay aggregates at a pH between 7 to 8. Then, 5.0 ml of 0.01 mol $[Cu(trien)]^{2+}$

complex solution were added. The remaining volume was filled up with ultra-pure milliQ- H_2O to 50 ml. Each sample was shaken overhead $30\times$ and left for sedimentation and exchange for about 1 h. After sedimentation, the supernatant solution was filled into a centrifuge tube and centrifuged at 13'000 RPM for 20 minutes in an Eppendorf Minispin centrifuge. After centrifugation, the clear supernatant was analyzed for the Cu-trien index cation concentrations, and for the exchangeable cations (described below). Determining the CEC requires centrifuging of the sample in order to reach cation saturation, removal of excess salt, and high displacement of the index cation (Jaynes & Bigham 1986). Ca. 1 ml of the centrifuged solution was pipetted into the measuring cuvette QS282. Then, measured concentrations were used to calculate CEC values and exchangeable cations values. The extinction at 578.0 nm was analysed via a Spectral-Photometer DR 6000 by Hach Lange device and compared with the extinction value of a blind solution without any sample material. Ultimately, effective cation exchange capacity was calculated according to:

$$CEC = \frac{(Ext_{blind} - Ext_{sample}) \cdot 200 \cdot 100}{m_{sample}}, \quad (3.14)$$

where Ext_{blind} and Ext_{sample} depict respective extinction values (nm) of the blind and actual sample, and m_{sample} depicts the sample mass (g). All calculations were corrected by the water content of each $<63 \mu\text{m}$ sample.

Exchangeable cations via ICP-OES

The measurement of exchangeable cations (Gaines & Thomas 1953) provided additional insights into the cation exchange behaviour and alternative CEC input for the evaluation of application scenarios. Analyses continued with the centrifuged supernatant of the CEC $[Cu(trien)]^{2+}$ complex samples using the same Agilent 5110 ICP-OES device. The solution was filtered with $<0.45 \mu\text{m}$ PES vaccine filters, acidized with 2% HNO_3 and quantified the exchanged cations Na^+ , K^+ , Mg^{2+} , Ca^{2+} , Sr^{2+} , Li^{2+} and Al^{3+} . Condition settings were adapted to 10 s of reading time and 15 s of stabilization time. Viewing mode was set to radial with a viewing height of 15 mm. For each sample run, a blank sample and 3 standards were used for calibration, followed by a quality control spike

blank sample and a copper blank sample. Apart from a different centrifuge speed of 4'500 RPM in the Heraeus centrifuge, the same sample preparation procedure as for the leachate analysis was applied. The difference in centrifuge speed is justified by the standard for eluate treatment. In addition, the exchangeable cation analysis aimed for the qualification of cations, while for the eluate analysis at lower speed more colloidal remained in the supernatant, which then counted into the measurement.

Ion analyses via cuvette tests

While the exchangeable cations via ICP-OES allowed the quantification of cations, it excluded the ones listed in Table 3.3 whose additional quantification was necessary for the identification of disposal class and potential issues with application solutions (Association Française des Tunnels Et De L'Espace Souterrain (AFTES) 2019; Haas, Galler, et al. 2020; République et Canton de Genève 2016; République Française 2015; Swiss Confederation 1998, 2016; Vernus et al. 2017). For each ion, the company Hach Lange (Hach Lange GmbH 2021) provided standardised cuvette tests that were analysed in the Spectral-Photometer DR 6000 photometrically. Depending on the analysed substance, the cuvette tests took between 1 and 15 minutes upon receipt of the final concentration results (mg/L).

Petrophysical analyses

Porosity, permeability and grain density via gas expansion

The pressure-decay unsteady-state method (Jones 1972, 1997; Schlumberger 2021) after the modified Darcy's law (Cunningham, Williams 1980; Whitaker 1986) was applied to measure effective porosity, absolute (single fluid) permeability and grain density with the AP-608 Automated permeameter and porosimeter (Chablais & Moscardello 2012; Coretest Systems Inc. 2008, 2011).

Plug samples were saturated in an inert gas such as nitrogen and helium. The latter served as an ideal gas optimized for medium to high permeability values, whereas nitrogen was used for fine-grained Molasse Rouge (clay-rich) samples expecting permeability values below 0.05 mD. Expecting low permeability values favour the unsteady-state over the steady-state method (McPhee et al. 2015). Before

Table 3.3: Measured ions complemented by the ICP-OES analysis (Hach Lange GmbH 2021).

test-ID	parameters	detection range (mg/L)	method	standard
LCK323	Fluoride F^-	0.1-2.5	SPADNS	-
LCK315	Cyanide free CN^-	0.01-0.6	Babituric Acid-Pyridine	-
LCK341	Nitrite NO_2^-N	0.015-0.6	Diazotisation	DIN EN 26777 (European Norm (EN) 1993)
LCK304	Ammonium NH_4N	0.015-2.0	Indophenol Blue	DIN 38406-5 (Deutsches Institut für Normung (DIN) 1983)
LCK313	Chromium Cr^{6+}	0.03-1.0	Diphenylcarbazide	DIN 38405-24 (Deutsches Institut für Normung (DIN) 1987)

each set of measurements, a leakage test was performed to guarantee safe sealing of the machine equipment. The differential pressure across the plug sample was measured as a function of time and solved for permeability. The measurement analysed the equivalent liquid permeability, slip and turbulence factors. Pore volume measurements were retrieved using gas expansion based on Boyle's law, also named *Mariotte's law* in Europe (Daintith 2014).

Grain densities were measured using a grain volume chamber. Before a set of measurements, calibration was conducted using standardised steel cylinders yielding a reference volume of 10.99 cm^3 on average. During each measurement, temperature was maintained constant at $58.3 \text{ }^\circ\text{C}$. Nitrogen and helium viscosities were used for respective calculations. Results were corrected for the Klinkenberg (Klinkenberg 1941) and Forchheimer effect (Forchheimer 1901)). In contrast to flowing liquids, the velocity of gas flowing through a porous medium is not zero at the wall but represents a slight increase. The Klinkenberg effect provided a robust approximation of liquid permeability based on measured gas permeability. It compensated for gas slippage within pores when gas flows along the pores' walls. The Forchheimer equations accounted for the additional non-Darcy pressure drop across the plug samples due to turbulent (inertial) flow. This pressure drop occurs ancillary to the Darcy viscous pressure differential for a

viscous flow regime. Both effects and subsequent mathematical equations used for the measurement were performed following the work of Jones (1972) and Tanikawa & Shimamoto (2006):

$$k_g = k_l \left(1 + \frac{4cl}{r} \right) = k_l \left(1 + \frac{c\kappa}{\pi\sqrt{2}r^3} \frac{T}{p} \right) = k_l \left(1 + \frac{b}{p} \right) \quad (3.15)$$

given, that

$$b = \frac{c\kappa}{\pi\sqrt{2}r^3} \quad (3.16)$$

where k_g is the permeability of gas (m^2), k_l depicts the permeability of liquid (m^2), l is the mean free path of gas molecules (m), r is the pore radius (m), κ the Boltzmann's constant (JK^{-1}), T the temperature (K), c is a constant, p depicts the pore pressure (Pa), and b the Klinkenberg slip factor (Pa). Corrected permeability results were outputted in units of mD.

Pore size distribution and porosity via mercury intrusion

Based on mercury intrusion porosimetry (MIP) pore throat size distribution was calculated from (capillary) mercury pressure curves (Pickell et al. 1966; Ritter, Drake

1945; Swanson 1979). Effective and total porosity were derived according to standard DIN ISO 15901-1 (Deutsches Institut für Normung (DIN) 2019) on plug samples using the cylindrical-plate grain shape model. The measurements were conducted to conclude on correlations with permeability, porosity, leachate analyses, and to substantiate the rock characterisation as described in chapter 5. The measurement exploited the non-wettable liquid behaviour of mercury, which depicted a contact angle at the transition of solid to liquid of $>90^\circ$. Mercury intruded into a porous material under increasing pressure, which was inversely proportional to the pore radius. By monitoring the mercury-intruded volume and pressure at intrusion, the pore volume distribution was derived as a function of pore radius. For the measurement, the following conditions were assumed:

1. the mercury's surface tension and angle of wettability remained constant,
2. the system was in equilibrium,
3. pores had a cylindrical shape, and
4. the solid rock material was not deformed under pressure.

Depending on expected porosity values, ϕ , initial mass weights of ca. 1 g (high ϕ) or ca. 3 g (low ϕ) were loaded into a dilatometer flask and evacuated in the macro-pore unit of the pressure porosimeter for 10 min. In order to cover the range of pore sizes between 2 to 10^6 nm, two POROTEC PASCAL devices with different pressure ranges were used. The dilatometer flask was filled with mercury under vacuum up to a certain volume in the measuring capillary using the pressure of the low-pressure device slowly increasing up to 400 kPa to cover pore diameters between 1 to 100 μm . Afterwards, the dilatometer flask was removed from the macro-pore unit at air-out pressure, weighed and placed in the micro-pore unit of the high-pressure porosimeter to further induce the mercury into the smallest pores (POROTEC GmbH (now Microtrac) 2021) using high-pressure oil at up to 400 MPa to cover the pore size range between 2 nm to 1 μm . During the process of high-pressure injection, the rate of pressure increase was automatically adjusted in an advanced procedure with lower rates at lower pressure levels and during measured intrusions. The pore size distribution was determined according to (Washburn 1921):

$$r = \frac{-2\gamma\cos(\theta)}{p}, \quad (3.17)$$

where γ depicts the mercury surface tension (N/m), p the applied absolute pressure (MPa), r the pore radius (nm), and θ states the wetting angle ($^\circ$). Assuming a mercury surface tension of 4'800 N/m, an average angle of wettability of 141.3° , and cylindrical pore shapes, this results in the equation:

$$r = \frac{7500}{p}, \quad (3.18)$$

with r being the final pore radius for each sample.

Compressional and shear wave velocities via ultrasonic measurements

The compressional (V_P) and shear wave (V_S) velocities were determined via ultrasonic measurements and guided the rock characterisation introduced in chapter 5. The test procedure followed the American Society for Testing and Materials (American Society for Testing and Materials (ASTM) 1976) and International Society for Rock Mechanics and Rock Engineering (International Society for Rock Mechanics (ISRM) 1978) standards. Samples were fixed between a transmitter and receiver with a contact ultrasonic gel on both sides. A continuous pressure of 5 bar was applied.

Transducers comprised piezo-ceramic systems (Geotron Elektrik) designed for compressional and shear wave measurements. A Dirac impulse was sent from a signal generator to the transducer through the sample, and resulted in a mechanical pulse. The arriving signal was visualized via a storage oscilloscope (Clevscope), and measurements of first arrivals and velocities were automated (Gegenhuber 2015), whereas for each measurement cycle, delay time between electrical impulse and mechanical pulse (dead time) was determined and corrected. The onset of V_P and V_S was detected with the Akaike Information Criterion Picker (AIC). AIC depicts an auto-regressive method, which divides each measurement into local stationary segments. The sections before and after the onset of a specific waveform stated the two different stationary processes. A phase onset was identified by the position, at which the AIC values showed a minimum (least-square fit). The detected

AIC global and local minima referred to the onset of compressional and shear wave arrivals, respectively.

Geomechanical tests

Rock mechanics tests involved uniaxial compressive strength (UCS), point load (PL), Brazilian tensile strength (BRA), LCPC and CERCHAR tests. These results served as a link between both the geotechnical rock characterisation after Fern et al. (2018) and the derived multidisciplinary rock characterisation for the prediction of application scenarios.

Uniaxial compressive strength via UCS

The unconfined compressive strength (UCS) test was performed to measure the uniaxial compressive strength of a cylindrical rock sample. The UCS value depicted a quantitative strength measure. Although uniaxial stress conditions predominate in the middle of the core, they fade out towards the border of the sample, and create a rather inhomogeneous stress state. Hence, while the actual state of stress in the rock core is not homogeneously uniaxial due to frictional forces along the interface between core and platens, the procedure conducted was sufficient to retrieve reasonable UCS values. Respective solutions for the stress-state problem were stated by Chau (1997) and applied by e.g., Edelman (1949) and Filon & Ewing (1901) and Pickett (1944).

A UCS sample was drilled with a 25 mm diameter drill bit honoring a length to diameter ratio of 2:1. The specimen was positioned accordingly to obtain plane-parallel surfaces, and then dried for 19 h at 45 °C. The sample was inserted in a computer-controlled servo-hydraulic MTS 815 testing apparatus with a load frame of type 315.02, and a machine rigidity of 9 MN/mm. For specimen with a length-diameter ratio less than 2:1, ISRM correction factors were applied accordingly (International Society for Rock Mechanics (ISRM) 1979). The upper plate was loaded with a low axial force and spherical support. Loading up to rock failure was controlled with a rate of 0.5 mm/min. The UCS value (MPa) was then calculated using the maximum force F_{max} (N) and test specimen cross-sectional area A (mm^2) according to:

$$UCS = \frac{F_{max}}{A}. \quad (3.19)$$

Strength index via point load test

The point load strength index (PLI) allowed for a fast measurement of rock strength index. The PLI was conducted as a potential quick and cost-efficient application as a field measurement (on-site) on variable sizes of rock specimen for a first and quick characterisation of rock strength. This allowed for further correlations with the uniaxial compressive strength and uniaxial tensile strength (Thuro & Plinninger 2001). The procedure was applied according to the ISRM standard (International Society for Rock Mechanics (ISRM) 1972a), and followed the method proposed by Franklin (1985). A sample was drilled using a 50 mm diameter drill bit to receive a sample with the dimensions $3 < h_{ideal} < 4$ cm and dried for approx. 1 day at 45 °C. The same servo-hydraulic rock testing press type MTS 815 device as for the UCS test was used, and applied an axial pressure with a control mode of 1.35 mm/min upon rock failure. The load applied to the sample was converted to the uncorrected point load strength, I_S (MPa), according to:

$$I_S = \frac{P}{D_e^2}, \quad (3.20)$$

where P was the applied load (N) and D_e the equivalent core diameter (mm), calculated via:

$$D_e^2 = 4 \frac{A}{\pi}, \quad (3.21)$$

with A being the minimum cross-sectional area (mm^2) of a plane through the platen contact points. The corrected point load strength index (MPa) equivalent to point load index for a 50 mm diameter sample was calculated according to:

$$I_{S(50)} = F \cdot I_S \quad (3.22)$$

with F being the geometric correction factor (-) following:

$$F = \left(\frac{D_e}{50} \right)^{0.45}. \quad (3.23)$$

The mean value of $I_{S(50)}$ was calculated by removing the two highest and lowest values from 10+ valid tests. In case fewer results were retrieved, the highest and lowest

results were removed, and the mean was calculated from the remaining results. In order to calculate mean values, test results were grouped based on similar sample locations and lithology. This provided mean values, $I_{S(50)}$, on a location and lithology basis for further correlations with UCS values according to:

$$UCS = c \cdot I_{S(50)}, \quad (3.24)$$

with c being the correlation factor (unitless) ranging from 20 to 25.

Tensile strength via Brazilian tensile test

The Brazilian tensile test (BRA) depicted an indirect method to derive the uniaxial tensile strength of a rock specimen. Tensile strength was calculated via equations that assumed isotropic rock material properties (Claesson & Bohlooli 2002). As shown by several researchers, this approach was valid despite the presence of anisotropy in sedimentary rocks (see citeMcLamore1967, Seto1997, Istvan1997). A 50 mm diameter drill bit was used to retrieve a sample with dimensions of 2.5 ± 0.2 cm, which was then dried for ca. 1 day at 45 °C. A circular rock disc sample was prepared and subjected to compression between two curved platens in the servo-hydraulic rock testing system type MTS 815. During test procedure, it was assumed that the platens were rigid compared to the rock, and followed a linear applied load distribution. The testing machine applied up to 2'850 kN of axial compressive forces and 1'340 kN of tensile forces onto the rock specimens. The control mode was regulated at 3 mm/min. The uniaxial tensile strength σ_t (MPa) was calculated using the failure load F_A (kN), at which a tensile crack developed according to:

$$\sigma_t = \frac{2F_a}{\pi D l} = 0.636 \frac{F_A}{D l}, \quad (3.25)$$

with D depicting the sample diameter (mm) and l the sample length (mm).

Abrasivity and breakability via LCPC and CERCHAR

The *Laboratoire Central des Ponts et Chaussee* (LCPC) test was used to derive the abrasivity of rock samples. The

test was considered important for the evaluation of application scenarios and correlations with other geomechanical and petrophysical laboratory analyses. It allowed conclusions on both abrasivity of the material and influence of grain size (Thuro et al. 2007). Test equipment consisted of an electric motor, which rotated a rectangular metal wing of standardised steel hardness (Rockwell B60-75) at 4'500 RPM for 5 minutes. The metal wing was immersed in a steel container filled with 500 g of air-dried sample material of grain sizes between 4 to 6.3 mm. In order to determine the abrasiveness, the metal wing was weighed before and after the measurement, and the weight difference yielded the LCPC abrasivity coefficient (LAC), and LCPC breakability coefficient (LBC) of rock material according to:

$$LAC = \frac{m_{F0} - m_F}{m_{sample}}, \quad (3.26)$$

and

$$LBC = \frac{100 \cdot m_{1.6}}{m_{sample}}, \quad (3.27)$$

with m_{F0} being the mass (g) of the metal impeller prior to the test and m_F (g) after the test, m_{sample} depicting the mass (g) of the sample and $m_{1.6}$ the mass (g) of the sample material after the test below a fraction of 1.6 mm. For each sample run, a new metal wing was mounted. Originally introduced by the *Laboratoire du Centre d'Etudes et Recherches des Charbonnages CERCHAR* institute and published by Valantin (1974), the CERCHAR test is a measure of rock abrasivity (Centre d'Etudes et Recherches de Charbonnages de France (CERCHAR) 1986; Plinninger & Thuro 2004; Prieto 2012) and allows for further correlations with the LCPC test results. According to the ISRM standard (Alber et al. 2014), the CERCHAR abrasivity index (CAI) ranges from 0.1 (extremely low abrasivity) to >5.0 (extremely high abrasivity).

For the CERCHAR test, samples were prepared using remaining rock cores and sawing off a suitable piece. Plane-parallel surfaces for clamping were prepared, and the sample was dried at 45 °C. The measurement procedure followed standard NFP94-430-1 (Association française de normalisation (AFNOR) 2000). A sample's surface of a 10 mm rock piece was scratched 5 times with a rate of 1

Table 3.4: Ranges for CAI and LAC thresholds. After Käsling et al. (2007).

LAC (g/t)	CAI (-)	classification
0-50	0-0.3	not abrasive
50-100	0.3-0.5	not very abrasive
100-250	0.5-1.0	slightly abrasive
250-500	1.0-2.0	medium abrasive
500-1250	2.0-4.0	very abrasive
1250-2000	4.0-6.0	extremely abrasive

mm/s under a static load of 7 kg, using a defined test pin (Rockwell hardness HRC 54-56) at 5 different locations on the sample with a pin direction normal to the foliation on the sample's sawn surface. The wear of the steel testing pin was checked under a microscope with a computer-aided image processing program. Each test pin was examined four times at different angles (0 °, 90 °, 180 °, 270 °), and the average value was calculated. It has been common practice in Austria that CERCHAR tests are performed on sawn (cut) sample surfaces. In 2014, the ISRM proposed an empirical correlation between the cut and rough CAI values (Ulusay 2015) that was applied according to:

$$CAI_{rough} = CAI_{cut} \cdot 1.14. \quad (3.28)$$

From these mean values, the total wear mean values (μm) were calculated and divided by 100 to obtain the CAI value. For both the CERCHAR and LCPC tests, specified ranges were used to name the level of abrasivity (Table 3.4).

4 Large-scale geological investigations in the Geneva Basin

This chapter is based on Haas et al. (2022).

4.1 Introduction

The FCC's ongoing feasibility phase requires the identification of encountered geological formations and the investigation of rock characteristics at its currently planned depth intervals between 100 and 300 m ASL for its main tunnel. Subsurface designs are still subject to changes as additional information is acquired but the current results impact admission into the subsequent technical design phase, associated environmental impact assessments, and ultimately, well placement for upcoming site investigations based on currently available data.

During the past decades, the Geneva Basin (GB) has been the subject of vast geological research with a strong focus on hydrocarbon exploration from the 1970's to the 1990's (Bachmann et al. 1982; Lemcke 1967), as potentially economic reservoirs were identified in the eastern (Austrian and German) equivalents of the NAFB (Bartenstein 1978; Brink et al. 1992; Gross et al. 2018; Gusterhuber et al. 2014; Sachsenhofer et al. 2010; Schulz et al. 2002; Wehner et al. 1983). This early phase of research was followed by renewed interest for groundwater resources (Keller 1992) and hydrocarbon distribution (Do Couto et al. 2021). Based on these extensive research and industrial explorations by various companies, available well-log data sets and core descriptions from adjacent basins have been available to decipher the stratigraphic evolution, phases of basin uplift and erosion as well as a geo-engineering classifications (Amir et al. 2020; Brentini 2018; Brink et al. 1992; Chelle-Michou et al. 2017; Clerc & Moscariello 2020; Clerc et al. 2015; Fern et al. 2018; Kaelin et al. 1992; Makhloufi et al. 2018; Moscariello 2018b, 2019; Moscariello et al. 2020; Rusillon 2018). The collection and review of these data sets (see chapter 3) allowed for a large-scale geological investigations across the basin, and

are contemplated by data gathered explicitly on behalf of this study (Haas et al. 2022).

A distinct lack of stratigraphic analysis and lithotype identification has remained for depths ranging from 0 to 1'000 meters above sea level (m ASL) in the Geneva Basin's subsurface. Compared to the knowledge amassed on corresponding sectors of the NAFB in e.g. Austria, Germany, eastern Switzerland and eastern France (Amir et al. 2020), this lack of high-resolution information hampers the FCC subsurface prediction for construction and design purposes. For this purpose, analyses have been focused on the FCC construction intervals with each data type presented from local to regional scales. Visual geological rock core inspections show the highest resolution in the order of millimetres, followed by a resolution decrease down to an average point density of 15.24 cm given by geophysical well-logs.

The following sections first derive the tectonic evolution of the NAFB and the Mesozoic deposits of the Jura, followed by a stratigraphic analysis related to the GB marking the essential geological formations intersected by the FCC, and their associated geological hazards with respect to tunnelling construction. Text passages have been taken and published in Haas et al. (2022).

4.2 Tectonic evolution and stratigraphic framework

The Geneva Basin (GB) constitutes the south-westernmost part of the Northern Alpine Foreland Basin (NAFB), which has been the object of intensive research over the past fifty years with a particular focus on its tectono-sedimentary evolution and associated potential for mineral and geo-energy resources as well as geo-engineering purposes, both at regional (Haas et al. 2022; Ziegler 1990) and local scales (Berger 1996; Doppler 1989). The NAFB's

western part has been thoroughly investigated along country borders, which makes it common to use different geographical terms in the literature, such as the *Bassin Franco-Genevois* or the *Savoy Molasse Bassin* (Deville et al. 1994) in French-speaking countries. These terms predominantly refer to the most western Swiss Molasse Basin (SMB) including the adjacent French Molasse Basin (FMB) to the west. A more recent geographical notation uses the term Geneva Basin (Moscariello 2019) for parts of the SMB, extending it by emphasizing the region around the city of Geneva in western Switzerland and its surrounding French departments Ain and Haute-Savoie. For the present study, the term Geneva Basin (Moscariello 2019) is used to emphasise the geographical area as part of both the SMB and FMB, and is bordered by the Jura mountains in the north/northwest, the Prealps in the east, the Salève massif in the south and the Vuache Fault system in the south/southwest (Fig. 4.1).

Tectonic evolution

The NAFB is located north of the Alps and extends approximately from Lake Geneva (Lac Léman) in western Switzerland, across Bavaria in southern Germany, to the east towards Vienna in Austria, reaching up to 700 km in lateral extent for its Oligocene–Miocene infill (Kempf & Pross 2005). The NAFB evolved from a foredeep to a negative-alpha basin controlled by rollback mechanisms of a proposed European slab (Schlunegger & Kissling 2015) during the Paleogene and Neogene due to flexural bending of the European Plate under increasing orogenic load by the advancing Alpine thrust wedge (Allen et al. 1991; Burkhard & Sommaruga 1998; Homewood et al. 1986; Karner & Watts 1983; Pfiffner 1986, 2021). The term “negative-alpha” describes a basin that formed on top of an orogenic wedge (Fuller et al. 2006; Willett & Schlunegger 2010). The NAFB’s tectonic origin relates to crustal loading in proximity of the uplifting Alpine orogen (Mock & Herwegh 2017; Schlunegger & Mosar 2011).

The basin and the associated orogenic belt show different tectonic patterns along their east–west extent, distinguishing Swiss, southern German and Austrian sectors (Willett & Schlunegger 2010). Sommaruga et al. (2012) described a notable decrease in structural complexity expressed in Mesozoic lithologies from west to east along the NAFB, substantiated by different deformation styles. In the western, wedge-top part of the basin, thrusting and

long-wavelength, evaporite-cored detachment folds relate to thin-skinned detachment tectonics (Sommaruga 1999, 2011; Sommaruga et al. 2012), whereas the eastern, non-detached part is comprised of normal faults related to Jurassic extension and subsidence of the epicontinental European shelf (Sommaruga et al. 2012; Stauble & Pfiffner 1991; Wetzel et al. 2003). The Fernschub hypothesis, originally proposed by Buxtorf (1916), confirmed a detachment of foreland sediments along a Triassic evaporite unit (Laubscher 1961), leaving the SMB as the NAFB’s westernmost area relatively undeformed compared with its conjugate eastern German and Austrian equivalents.

Predominant conjugate NNE–SSW and NW–SE-trending strike-slip fault zones cut the western SMB and extend into the Jura fold-and thrust belt (FTB), e.g. Vuache Fault (Fig. 4.1) (Gorin et al. 2003; Ibele 2011; Sommaruga 1999), limited to the sedimentary cover (Courboulex et al. 1999; Thouvenot et al. 1998). The Alpine orogen forms a tapered, double-vergent wedge to the NNW and SSE, with both the Jura FTB and SMB being decoupled from the basement over a basal *décollement* (Mosar 1999). The Vuache and Dent de Vaulion Fault systems extend from the SMB into the Jura and are conjugate with SE–NW-striking dextral faults (Burkhard 1990; Burkhard & Sommaruga 1998; Sommaruga 1997, 1999, 2011; Sommaruga et al. 2017).

From a tectonic point of view, there are two major structural units in the impacted FCC construction area: the Mesozoic of the Jura plus the Cenozoic (Molasse) of the Geneva Basin in the northwest, and the thrustured Mesozoic of the Salève plus the Cenozoic (Molasse) of the Bornes Plateau in the southeast. The Mesozoic deposits of the Jura form the substrate of the Cenozoic NAFB, which lies passively on top (cross-section X–Y, Fig. 4.1). Today both the Mesozoic and the Cenozoic deposits structurally form a single tectonic unit.

The geographically-defined GB is tectonically delimited by the Jura and the Mesozoic sedimentary Helvetic and Penninic units, and is internally divided into two tectonic subunits: (1) the Plateau Molasse and (2) the Subalpine Molasse (Burkhard 1990; Mock & Herwegh 2017; Pfiffner 1986). The slightly deformed Plateau Molasse is up to 50 km wide and is affected by faults and folds (Gorin et al. 2003), with exemptions towards the west suggesting a convergence of Alpine and Jura structures (Burkhard 1990). This required progressive sedimentation

within the basin to guarantee mechanical integrity (Fuller et al. 2006). Thrusting of the Subalpine Molasse started in the Oligocene (Schlunegger et al. 1997) and lasted until approximately 5 Ma (Von Hagke et al. 2012). After an early deformation phase in the Late Oligocene (Kempf & Pross 2005; Kuhlemann et al. 2002; Kuhlemann & Kempf 2002), principal tectonic shortening occurred in the Jura FTB between 12 and 4 Ma (Becker 2000), followed by progressive minor deformation in Pliocene–Quaternary times (Madritsch et al. 2010).

For consecutive stratigraphic development and sedimentation, two predominant hypotheses persist on the creation of accommodation for Molasse deposits: the first one is the argument of sea-level changes impacting sediment supply, reflected by the two mega-sequences (Home-wood et al. 1986; Trümpy & Schweizerische Geologische Kommission 1980) of marine to terrestrial deposits (Bachmann & Müller 1991, 1992; Lemcke 1984); the second one attributes the main role to tectonics and Alpine uplift in driving sediment accumulation, whereby the establishment of terrestrial environments would have followed increased sediment supply from the orogen and marine conditions would have been tied to lesser sediment influx (Kuhlemann 2000; Oxburgh 1981; Schlunegger et al. 2001; Schlunegger & Hinderer 2001). Both hypotheses hinge on sediment supply as proximate control on patterns of deposition (Kuhlemann et al. 2002; Schlunegger & Hinderer 2001; Schlunegger & Mosar 2011). For the Central Alps, a third hypothesis favours a slab-rollback mechanism to explain foreland plate flexure and accommodation space creation (Schlunegger & Kissling 2015), substantiated by a delayed rebound-type, erosional response to surface uplift, and represented by larger sediment fluxes and shifts to more proximal facies (Schlunegger & Castellort 2016). Large sediment influx could have controlled the establishment of (fluvial) fans. These fans further prograded over several tens of kilometres, merging distally with an axial fluvial system, which linked the Tethys to the Black Sea (Kuhlemann et al. 2002; Sinclair et al. 1991). Early post-collisional Alpine history was characterized by increased sedimentation rates at the Rupelian/Chattian transition, attributed to isostatic readjustment (Kuhlemann et al. 2002). Further increases in sedimentation rate took place later during the Aquitanian (23–21 Ma) and late Burdigalian (ca. 18–16.4 Ma), followed by decreased rates in early to middle Burdigalian (21–19 Ma) and Langhian to

Serravalian times (16.4–12 Ma) (Garefalakis & Schlunegger 2019; Kuhlemann et al. 2002).

While the swift increase in sediment discharge in the Eastern Alps is explained by the termination of E-W extension (Dunkl & Demény 1997) and subsequent minor uplift recorded by a regional regression (Winkler-Hermaden 1958), the Western Alps record a rather slower reduction (Kuhlemann et al. 2002) due to an extensional tectonic regime (Pfiffner 1986; Schlunegger 1999; Schmid et al. 1996). Basin inversion of the SMB between 11 and 10 Ma (Kaelin 1997) changed the drainage pattern to an easterly direction and was intensified by folding and thrusting of the Swiss Jura Mountains (Kuhlemann et al. 2002). Still ongoing basin uplift started in latest Miocene times in the Swiss and Western Alps (Kuhlemann et al. 2002).

Stratigraphic framework

The Geneva Basin covers the Molasse and Quaternary deposits of the SMB and FMB, as well as the sediments of the Jura, and is stratigraphically delimited by the latter and by the Helvetic and Penninic units. The Jura and the SMB consist of folded Mesozoic and Cenozoic successions, which are detached from the pre-Triassic basement (Sommaruga 1997). The Jura mountains border the current FCC perimeter in its north-western direction, consisting of calcareous, Mesozoic rocks of 250 Ma, making up about 6% of the excavated limestone (Haas et al. 2022). This mountain chain was folded in late Miocene to early Pliocene and is divided into the Plateau Jura, entirely on French territory, and the Folded Jura delimited by symmetric to asymmetric folds depicting the boundary transition to the overlying Molasse units at about 55 Ma (Do Couto et al. 2021; Moscariello 2019; Moscariello et al. 2020; Pfiffner 2020). The main tectonic structure intersected by the FCC is the Geneva Basin as part of the most-western Swiss Molasse Basin, making up about 90% of the proposed excavated material.

For the present study and the GB's geographical realm, the Jura's subdivision into the external and internal Jura domains plays an important role, while the third subdivision as the Tabular Jura is significant for the realms only around the southern Black Forest and Vosges basement. With the external Jura consisting of flat areas and plateaus delimited to the north, the internal Jura,

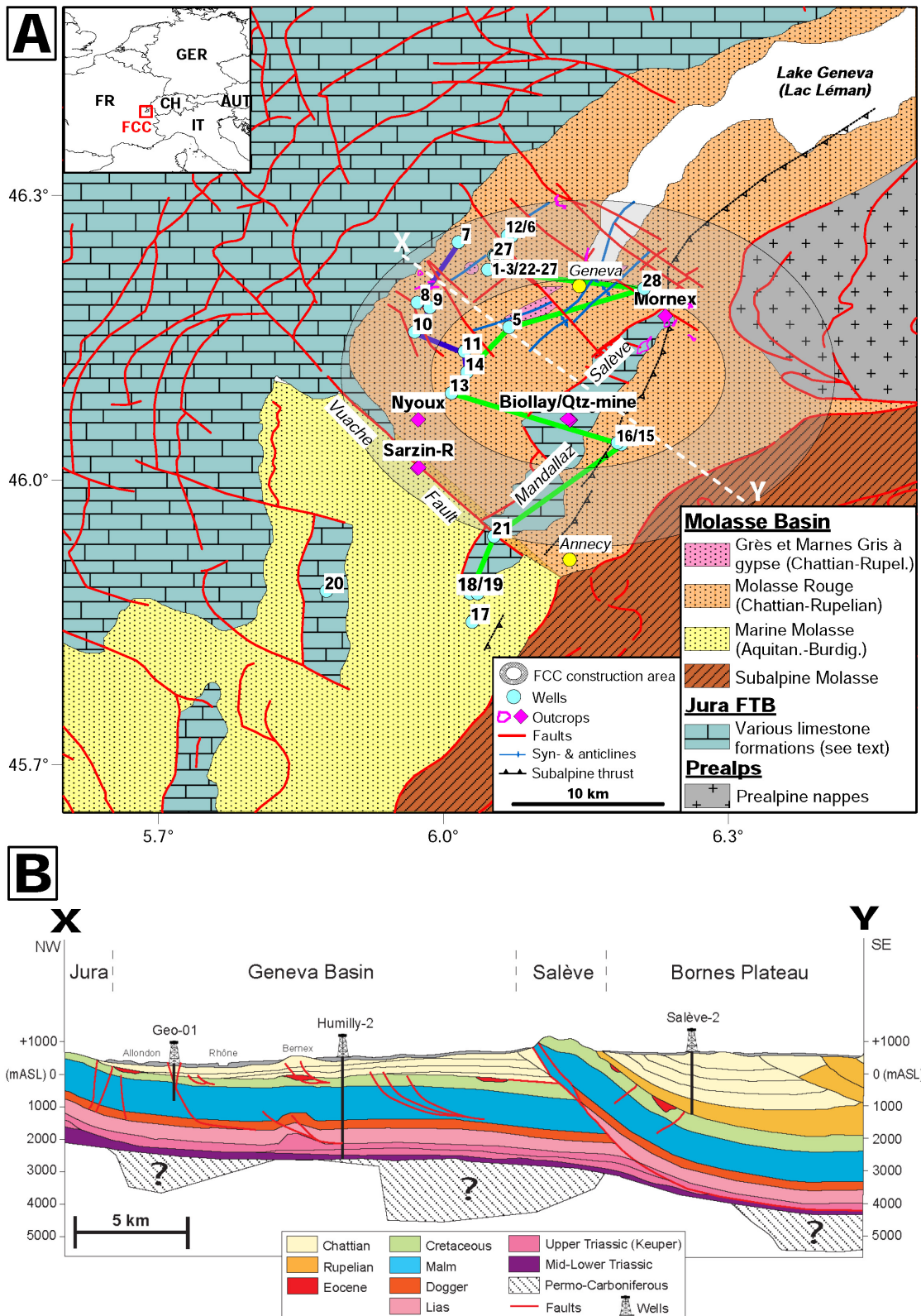


Fig. 4.1: Tectonic realms in the Geneva Basin for the FCC construction with analysed well and outcrop locations. Molasse units make up ca. 90% of the FCC's currently proposed subsurface layout. Note that the overlying Quaternary deposits are neglected for increased readability. The blue line depicts cross section A (Fig. 4.10), the green line refers to cross section B (Fig. 4.11). The Salève and Mandallaz limestone as commonly referred to in technical reports are part of the Jura. FTB=fold-and-thrust belt. B) The white profile X-Y displays a large-scale cross section through the Geneva Basin based on chronostratigraphic units. The Burdigalian Molasse belongs to the Upper Marine Molasse and is hereby noted *Marine Molasse*. The FCC's current subsurface alignment is foreseen between 100 to 300 m ASL. Well-IDs: 1-3=C1-C3, 4=Geo-01, 5=Geo-02, 6-12=Gex-CD-01 to -07, 13/14=Humilly-1/-2, 15/16=Salève-1/-2, 17/18-21=Savoie-101/-104-109, 22-27=SLHC20-25, 28=Thônex-1. After Haas et al. (2022).

also referred to as folded Jura or *Haute Chaîne*, represents thrust-related folds and sinistral faults, whose orientation gradually changes from a N-S in the eastern Jura to a WNW-ESE direction in the western Jura (Sommaruga 1997, 1999). The Mesozoic formations describe the general evolution from a shallow, peritidal platform to deeper-water shelf environments followed by the evolution of a carbonate platform, and its subsequent drowning in order to prevail in pelagic conditions (Sommaruga 1997; Strasser et al. 2016). During the Mesozoic, the Jura and the western SMB were part of the Alpine Tethys passive margin and comprised approximately 2 km of alternating limestone and marl (Sommaruga et al. 2012). Oligocene and Miocene alternating fluvial, lacustrine and marine Molasse sediments onlap the underlying Mesozoic rocks towards the northwest (Sommaruga 1997, 1999; Sommaruga et al. 2012).

Lower Cretaceous units, formerly termed Urgonien, are dominated by carbonate sedimentation, and marked by increasing clastic input associated to Valanginian sea-level fall (Haq 2014). Variations of relative sea-level of both tectonic and eustatic origin drastically controlled the development of depositional environments. The common lateral and vertical changes in facies and sedimentation rates as well as numerous hiatuses within the formations witness a complex interplay of tectonics, climate, and sea level that controlled the Jura during the Cretaceous (Strasser et al. 2016). One of these hiatuses reflects 72 My separating rocks of Aptian age in the GB (Brentini 2018; Rusillon 2018) from the overlying Siderolithic Formation of proposed Late Eocene age (Charollais et al. 2007). This hiatus resulted probably from subaerial exposure and consequent development of an erosive and deep karst system at the top of the Mesozoic series, which play a predominant role in the aquifer drainage systems of Cretaceous and Jurassic limestone across the GB (Moscariello 2018b), as well as for 6% of the FCC's current subsurface perimeter.

Deformation processes folded the Jura mountains to their current state from the Miocene to the Pliocene. The boundary between foreland and Jura is in general a thrust zone. Jura mountains contain Mesozoic cover rocks, uncoupled from the European basement and folded in Late Miocene to Early Pliocene times. During the Mesozoic, the Jura and the western SMB were part of the Alpine Tethys passive margin and comprised approximately 2 km of alternating limestone and marl (Sommaruga et al.

2012). Oligocene and Miocene alternating fluvial, lacustrine and marine Molasse sediments onlap the underlying Mesozoic rocks towards the northwest (Sommaruga 1997, 1999; Sommaruga et al. 2012). Two units are further distinguished: (1) the Plateau Jura comprising sub-horizontal Mesozoic rocks separated by narrow dislocation belts entirely on French territory, and (2) the Folded Jura depicting symmetric and asymmetric folds. The boundary between the Jura and the Swiss Molasse Basin is associated to the outcrop boundary between the Mesozoic and Cenozoic formations. The folded Jura continues southward into the external part of the French Subalpine Chains.

The Molasse Basin reaches its deepest depths between 5'000 to 6'000 m at the southern side below the Alpine nappes. Towards the southwest, the basin becomes narrower and shallower. Three sub-units are commonly differentiated: (1) the Autochthonous Molasse (Plateau Molasse) comprising flat-lying Oligocene to Upper Miocene formations affected by folds, (2) a north-dipping monocline depicting the transition into the Folded Molasse, whose structure is made of steep folds and anticlines intersected by thrusts and (3) the Subalpine Molasse towards the west of the Geneva Basin and made of slabs of south-dipping Oligocene to Lower Miocene formations. The boundary between the Autochthonous and Subalpine Molasse is a south-dipping thrust. The Plateau Molasse consists of Oligocene to Upper-Miocene formations and north-dipping monoclines and steep anticlinal folds representing the transition to the folded Molasse (Burkhard 1990; Haas et al. 2022; Sommaruga 1997; Sommaruga et al. 2012).

The infill of the SMB comprises two regressive, coarsening-upward sedimentary mega-sequences, each marking a transition from marine to continental conditions (Matter 1980; Sinclair & Allen 1992; Sinclair et al. 1991). The two mega-sequences are composed of four predominant lithostratigraphic units (Lemcke 1988; Matter 1980): (1) the Lower Marine Molasse (LMM), (2) the Lower Freshwater Molasse (LFM), (3) the Upper Marine Molasse (UMM) and (4) the Upper Freshwater Molasse (UFM). Informal terms often used in a regional context of the LFM also refer to the Molasse Rouge and Marnes bariolées as well as the Grès et Marnes Gris à gypse, whereas the latter shows an increased content of gypsum (Haas et al. 2022). For the northern/northeastern SMB, Freshwater-Brackish Molasse (SBM) evolved between the UMM and UFM (Bachmann & Müller 1992; Lemcke et al. 1953). The eastern German and

Austrian Molasse basins were subjected to marine conditions until Burdigalian times (Lemcke 1984), which makes the LFM terminology for terrestrial deposits only reasonable for the SMB and western Bavaria due to prevailing marine conditions to the east (Kuhlemann et al. 2002).

The total sedimentary cover in the western SMB consists of up to 5'000 m of Mesozoic and Cenozoic successions overlying the basin's crystalline basement (Clerc & Moscarello 2020; Gorin et al. 1993). Molasse deposition started in the Rupelian (34–30 Ma) as LMM and Chattian to Aquitanian (30–20 Ma) as LFM (Strunck & Matter 2002), marking the transition from an underfilled to an overfilled foreland basin (Erdős et al. 2019; Sinclair & Allen 1992). A Burdigalian (20–17 Ma) transgression that established the “Burdigalian Seaway” (Garefalakis & Schlunegger 2019) was probably caused by reduced sediment discharge (Kuhlemann et al. 2002) and marked the start of the second megasequence with accumulation of the UMM (Keller 1989, 1992) under marine conditions onto a truncated surface of LFM (Allen et al. 1991; Herb 1988; Kempf & Pross 2005; Matter 1980; Sinclair & Allen 1992). Molasse deposition in the Langhian to Serravalian (<17 Ma) accumulated fluvial floodplain and braidplain to lacustrine siliciclastics of the UFM in an overfilled basin, terminating marine conditions (Diem 1986; Sinclair & Allen 1992). Fluvial deposits of large alluvial megafans not only in the western SMB, but particularly in the central/eastern SMB were formed during the overfilled stage (Frisch et al. 1998; Kaelin & Kempf 2009; Ortner et al. 2015; Schlunegger & Castelltort 2016) despite decreasing sediment discharge until 11 Ma (Kuhlemann et al. 2002). After 11 Ma, sedimentation terminated in the western part of the NAFB due to folding and uplift of the Swiss Jura (Kuhlemann et al. 2002). The Freshwater units (LFM and UFM) were accumulated in terrestrial settings, consisting mainly of alluvial and fluvial-fan deposits along the southern basin margin and fluvio-lacustrine sediments in the central and external parts of the SMB (Kempf & Pross 2005). Kilometre-thick conglomerate successions were deposited by alluvial fans at the basin margin, while sand- and mud-dominated successions extended farther basinward (Kempf & Matter 1999; Schlunegger et al. 1997; Spiegel et al. 2001). The marine lithostratigraphic units are predominantly composed of shallow-marine siliciclastics deposited in tide- and storm-influenced environments (Kempf & Pross 2005). To the east, the SMB persisted in

an underfilled stage until at least 17 Ma, when sedimentation of sandstone and marlstone occurred under brackish to shallow-marine conditions (Hinsch 2013; Lemcke et al. 1953; Mock et al. 2020). Alluvial fans were missing in this eastern part of the NAFB due to the paleo-Inn river transporting clastic debris further to the east (Frisch et al. 1998; Kuhlemann et al. 2002). During UFM deposition, sediments originated from the central Alps and from massifs adjoining to the basin (Füchtbauer 1959). Molasse and Quaternary deposits accumulated on top of 2 km of Lower Triassic to Upper Cretaceous shallow-marine sediments, which are not outcropping in the eastern SMB (Charollais et al. 2007, 2013; Sommaruga 1997; Sommaruga et al. 2012).

A drastic base-level drop (Brenchley 1992; Lemcke 1988) of possible eustatic origin occurred around 28.5 Ma (Abreu & Anderson 1998; Haq et al. 1987) and caused an LMM regression towards the east (Bachmann & Müller 1992; Lemcke 1988; Zweigel et al. 1998). The LMM and lowermost LFM lithostratigraphic successions define a shallowing trend towards the top, indicated by an increase in sediment grain size (Diem 1986). The LMM-LFM transition in the western SMB is part of the Subalpine Molasse, documenting conditions at the southern basin margin (Kempf & Pross 2005). The study by Kempf & Pross (2005) emphasised the role of sediment supply for the transition of marine to terrestrial sedimentation in the northern Alpine foreland. In contrast to its eastern continuation, the western SMB lacks UFM units, which suggests complete erosion of this lithostratigraphic unit. Several researchers derived erosion thickness maps for the Late Miocene and post-Miocene times using apatite fission tracks, vitrinite reflectance, shale compaction and porosity measurements (Kaelin et al. 1992; Mazurek et al. 2006; Schegg 1993); Cederbom et al. (2004) proposed erosion up to 1'500 m for the Swiss Molasse Plateau and 3'000 m for the Subalpine Molasse as part of the SMB. They further mark the onset of erosion at 5 Ma, shortly before tectonic basin inversion. In the GB, the Cenozoic succession consists explicitly of Oligocene to Early Miocene LFM deposits. The overlying UMM is found in the adjacent Bellegarde and Rumilly basins to the west and southwest of the Vuache Fault (Amir et al. 2020; Charollais et al. 2007; Paolacci 2012). At the Bornes Plateau, the thrustured Subalpine Molasse is encountered at the front of the Subalpine units (Charollais et al. 2007; Paolacci 2012) continuing in front of the Prealpine

units into the Lake Geneva encountering lacustrine sediments as inferred from seismic data (Dupuis 2009). Accumulation of Molasse sediments took place during Jura deformation and in Late Miocene as the basin was detached from its basement (Cederbom et al. 2008). This suggests that erosion did not start before Pliocene times (Cederbom et al. 2004), but was associated to the 10–4 Ma Jura FTB shortening phase (Ziegler & Fraefel 2009). These Molasse deposits are composed of sandstone, marl and intercalations of anhydrite/gypsum and conglomerates (Wildi et al. 2017) tied to erosion of the Western Alps (Oxburgh 1981), sea-level changes (Bachmann & Müller 1992) or possibly a combination of both (Schlunegger & Mosar 2011). They constitute more than 90% of the subsurface domain to be intersected by the FCC's current layout.

Glacial erosion and deposition shaped the central part of the GB during the Middle and Late Pleistocene (Arn 1984). Associated Quaternary deposits comprise the GB's cover as intersected by about 4% of the current FCC subsurface layout. A recent revision of the old nomenclature for Switzerland's glacial periods (*Günz, Mindel, Riss, Würm*) introduced the terms post-glacial and interglacial deposits with a new stratigraphic classification taking into account not only lithological but also geomorphological features of these deposits (Graf & Burkhalter 2016).

A distinct geomorphological element in the GB depicts the *Petit Lac* at the southwestern termination representing the remains of a sub-glacial tunnel valley, which formed underneath the Rhône Glacier by sub-glacial meltwater (Fiore 2007; Moscariello 1996; Moscariello et al. 1998; Van der Vegt et al. 2012). Borehole data gave hints that the Rhône Glacier was responsible for incising and removing older Quaternary sediments reaching the underlying Molasse deposits during the Last Glacial Maximum (LGM). In the subsurface, this incision deviates towards the SE. On the surface, the buried incision is observed by the narrow Aire valley reflecting a branch of the Arve River located SE of the elongated Molasse ridge (*Berneux*, Fig. 4.1). It is assumed that the Rhône Glacier tunnel valley was gradually filled by a thick succession of proglacial lake deposits (Moscariello 1996) and accumulated in the large lake formed at the front of the melting LGM glacier (Moscariello 2018b). The downstream segment was filled with a mixed succession of subglacial, lacustrine, and proglacial deposits generated by the Arve Glacier (Moscariello 2018a,b).

Low-relief ridges, perpendicular to the main valley axis represent the sub-aqueous frontal moraines formed during temporary re-advances of the glacier during the glacial withdrawal phase. Large, flat-bottomed incision bordering the *Soral-Laconnex* sub-aqueous moraine resulted from meltwater discharge generated by the Arve Glacier, which carved a narrow spillway between the glacier and the northern slope. The spillway merged with the proglacial/lacustrine deposits and formed the flat morphology of the SW part of the Geneva area. The natural separation between the buried tunnel valley and its partly filled portion (*Petit Lac*) depicts a narrow ridge today. To the SE, this ridge forms an apron dipping to the SW, interpreted as a frontal moraine related to the Rhône Glacier, most likely formed in sub-aqueous(?) and sub-glacial(?) conditions (Moscariello 1996, 2018b).

The proglacial and paraglacial lake caused by the melting of the Rhône, Arve, and Jura glaciers gradually reduced its volume, which is represented in the terraced surfaces on both sides of the Lake Geneva (Burri 1981). These kame terraces formed in ephemeral lakes related to the LGM glacier at the ice front (Donzeau et al. 1997) in correspondence with probably lateral tributaries or supraglacial stream mouths (Moscariello et al. 1998). Lacustrine terraces formed during the evolution of syn- and postglacial lake levels after the disappearance of the Rhône Glacier, ultimately charging the sinuous Rhône River that incised cemented gravel deposits, which are locally known as the *Alluvion Ancienne*. Progressive incision of both the Rhône and Arve rivers shaped the central GB by various slopes of glacial origin towards the main axial drainage system represented by the *Petit Lac*. The Allondon River is likely associated with karst and fractured networks, whereby its associated deposits are the subject of current research.

4.3 Basin-wide stratigraphic evaluation in the context of CERN's future subsurface infrastructure

In the Geneva Basin, 22 geological formations and sub-units featuring 31 lithotypes are identified across 661 wells distributed within the FCC's construction area (Fig. 4.1). In the current layout, the FCC intersects 13 geological formations and their associated 25 lithotypes (Table 4.1). A

full description of each of these formations based on well report reviews and field inspection is stated in the following paragraphs in chronological order, and their geophysical well-log patterns are analysed, if available.

Balsthal Formation and Vellerat Formation

This Oxfordian interval is encountered by wells Brizon-1, Chaleyriat-1, Charmont-1 and Chatillon-1D close to the Jura in the western part of the GB, and by Humilly-2, La-Chandelière-1, La-Tailla, Musiège-1 and Thônex-1 comprising a dense series of alternating limestone, clayey to marly limestone and marl lithotypes. Except for well Chaleyriat-1 and La-Chandelière-1 with a starting depth at 18 m and 330 m extending down to 933 m and 726 m, respectively, average top depths among these wells range between 500 and 600 m. The limestone lithotype is very fine, grey-brown in colour, whereas the marl is very dark. Some depth levels are rich in organic matter. The microfacies consists of grey to brown mudstone with microbioclasts and micro-intraclasts, traces of dolomitisation, sometimes spongolitic. *Calcisphaerula*, filaments, *cadosina*, *reophax*, small miliolites, *spirillina*, *dentalina*, *saccocoma*, *textularia*, sponge spicules are present. The exact stratigraphic definition of these formations is under debate.

Blanc Limestone Formation

This Kimmeridgian (Portlandian) formation is encountered in wells Faucigny, La-Chandelière-1, La-Tailla, Mont-de-Boisy-1, Musiège-1, Salève-2, Savoie-104 and Savoie-105 and Thônex-1, as dolomitic, often clayey limestone lithotype. While wells close to the Jura encounter this formation at shallow depths of about 67 m, wells distributed towards the South of the FCC perimeter intersect it between 600 and 800 m and extend down to about 1'986 m. Savoie-104 contains dolomitic limestone, whereas in its neighbour, Savoie-105, the lithotype becomes more massive and less dolomitic, starting at a depth of 605 m and 647 m, respectively. In Thônex-1, the formation is encountered as marly limestone of supposedly Portlandian age at a depth of 1'678.60 m and extends down into the Oxfordian from 2'038.60 to 2'136 m as massive limestone.

Etiollets Formation with Tabalcon Limestone sub-unit

Massive, often dolomitic limestone banks developed as a carbonatic reef complex during the Kimmeridgian age in the Etiollets Formation comprise the Tabalcon Limestone sub-unit encountered in wells Chapery-1, Humilly-2, La-Balme-1, La-Chandelière-1, Musiège-1, Savoie-106, -107, -109 and Thônex-1. Chalk-white biotrititic limestone, and coral limestone are encountered, mingled in a microfacies of coarse bioclastic limestone and grey biomicrite. In between, crack-filling limestone occur, together with coarse debris of gastropods and lamellar branches, *thaumatoporella*, *baccinella*, *dascycladataceae*, solenopores, and miliolites (e.g., Jenny et al. 1995 a.o. well reports). The formation makes up a substantial portion of wells Savoie-106 and Savoie-107 starting from the top of the well down to 860 and 950 m depth, respectively, while for the other wells starting depths range between 846 and 1'100 m extending down to depths between 860 and up to 1'800 m in the Savoie wells, Humilly-2, Musiège-1, Chapery-1, Thônex-1 and La-Balme-1. The Etiollets Formation differs due to the absence of dolomitic composition, making it a pure, massive limestone. The Petit Salève is located 3 km to the south and the cuts in the Mint region are 8 km apart from the Thônex-1 well. The synthetic series is based on Deville's research (Deville et al. 1994) and also further elaborated in Charollais & Badoux (1990). The Thônex-1 correlation is straightforward as it depicts a good example of encountering all lithological units of the Cretaceous and Upper Jurassic limestones therein. Correlations among the Thônex-1 well and wells close to the Salève show an increased thickness of this reef limestone formation at the Salève compared with the northern part of the basin, which is in line with interpretations by Jenny et al. (1995). Furthermore, these authors describe the Tabalcon limestone in greater detail as fine white, beige, biotrititic limestone. Intercalations of dark beige micritic limestones occur more frequently at the base. Its microfacies comprises fine biotrititic recrystallised mudstone, sometimes dolomitised at the base of the formation. Small debris of echinoderms, corals and spine plants occur with abundant crevice-filling, sparse calcite. The full understanding of the Tabalcon sub-unit's base is still subject to current research, in particular for wells closer to the Salève.

Twannbach Formation and Goldberg Formation

The Late Kimmeridgian to Tithonian Twannbach Formation is comprised of dolomitic limestone and massive dolomite. The Goldberg Formation is of Early to Middle Berriasian age and bears massive, dolomitic, partly fine-grained limestone. Wells encountering these formations are Chapery-1, Geo-01, Humilly-2, La-Tailla, Musiège-1, Savoie-105, -107, -108, -109 and Thônex-1, restricted to the FCC's western region, terminated by the Salève and Mandallaz lineaments to the east and south-east. Average depths start at about 420 m and extend down to 1'680 m in Thônex-1.

Pierre-Châtel Formation

This Middle Berriasian formation consists of oolitic, often bioclastic, white to reddish limestone and marly interstratifications, and tends to become more massive towards the top yet impregnated by oolitic and bioclastic intercalations. The formation is encountered in the wells closer to the Jura towards the north/northwest. The formation comprises yellow-beige oolitic limestone in a microfacies of mudstone with dasyclitic algae, calcite veins, large complex foraminifera, and biological-etrinitic greystone.

Chambotte Formation and Vions Formation

These two formations of Berriasian age are mainly encountered by the northern wells close to the Jura. The Chambotte Formation intersects wells Faucigny, Geo-01, Humilly-2 and Thônex-1 comprising massive limestone, while Brizon-1, Chapery-1, Geo-01, La-Balme-1 and Thônex-1 account for the Vions Formation, comprised of marly to sandy limestone. Top depths for the Chambotte Formation start between 530 and 812 m, and extend down between 600 to 800 m, with an exception in Thônex-1 ranging between 1'583 and 1'600 m. Adjacent thereto, the Vions Formation extends down to 1'000 to 1'300 m, with exceptions in Geo-01 to 600 m and Thônex-1 to 1'615 m depth. The Vions Formation consists of biotrititic grey-brown or red sandstone limestone, intermingled with grey sandstone-marl. The microfacies comprises bioelastic mudstone with minor dolomitisation, and with 5-10%

of sandstone, partly occurring with bioclastic oolitic mudstone.

Vuache Formation

This Valanginian formation, formerly referred to as the Roux Limestone Formation (Charollais et al. 2007; Strasser et al. 2016), includes primarily sandy to marly limestone, sometimes dolomitic, and is encountered in Brizon-1, Chapery-1, Humilly-2 and La-Balme-1 at depths between 700 and 1'000 m, while in the SPM and L135 wells, top strata are exposed at shallow depths between 72 and 160 m in the northern part of the FCC's construction area. The Savoie, La-Tailla and Musiège-1 wells encounter these formations at depths varying between 342 and 470 m. In Thônex-1, the formation is restricted to intervals between 1'546.90 and 1'568.10 m. The formation consists of fine to lumpy grey limestone, sometimes brown in colour. Grey sandstone to marl with glauconia are identified. The microfacies consists of echinodermal packstone with bryozoans, fairly coarse, sometimes spongolytic. Traces of pyrite (crusts) and iron emigration occur. The formation shows very sandstone-like marls with 30% of fine quartz.

Grand Essert Formation with Hauterive Member and Neuchâtel Member

This formation consists of two members: the Late Valanginian to Early Hauterivian Hauterive Member, formerly referred to as the Marnes d'Hauterivian facies (Brentini 2018; Charollais et al. 2007) and the Early to Late Hauterivian Neuchâtel Member, formerly referred to as the Pierre Jaune de Neuchâtel facies (Charollais et al. 2007, 2013). The Hauterive Member is comprised of grey sandstone and black marl with glaucon. Yellow oolitic or lumpy limestone with glauconia are identified as well as red oolitic limestone with glauconia. Traces of pyrite are seen. The microfacies consists predominantly of mudstone. Spongolitic to bryozoic echinodermal limestones and molluscs together with lenticulina and textulariidae are encountered, with grains of glauconia and grey clayey micrite. Generally speaking, the formation appears to change between marly to sandy limestone, sometimes dolomitic, and predominantly ochre, bioclastic mudstone and highly recrystallized wackestone. The formation is encountered at 370 m in Brizon-1, 864 m in Chapery-1, 453 m in Geo-01, 286 m in Gex-CD-01, at 0 m in La-Chandelière-1, at

1'647 m in La-Tailla, 263 m in Musiège-1, at 356 m in Savoie-105, at 45 m in Savoie-108, 177 m in Savoie-109, at 107 m and 76.5 m in SPM1 and SPM15, and at 1'488 m in Thônex-1, respectively, becoming richer in clay before the overlying Neuchâtel Member.

The Neuchâtel Member consists of red-yellow limestone and sandstone, sometimes grey sandy marl and red limestone. Red sandstone limestone with glauconia. Microfacies: Echinodermal greystone, bioclastic mudstone, oolitic limestone shows silicification zones. Foraminifera and abundant bryozoans are encountered. Very sandstone-like marls with angular quartz (20%, 0.1-0.2 mm) occur. Predominantly, limestone is encountered with minor associated marl, and ochre-coloured, glauconite-bearing, bioclastic wackestone/packstone, encountered in wells Chapery-1, Geo-01, Gex-CD-01 and -06, L130, La-Balme-1, La-Tailla, Musiège-1, SPM2, SPM11, SPM15 and Thônex-1. Typical for this formation is its richness in bivalve shell fragments. Top depths range in the GB's northern wells between 120 and 430 m, whereas Thônex-1 marks an exception starting at 1'425 m. Top depths of about 800 m are common due to adjacent Jura mountains (Chapery-1) and associated elevated topography.

Rocher des Hirondelles Formation with Vallorbe Member

This Late Hauterivian to Late Barremian formation is encountered in wells Brizon-1, Chapery-1, Faucigny, Geo-01, Gex-CD-03, -04, -06, Grilly, Humilly-1, Humilly-2, L112, La-Balme-1, La-Tailla, Messery-1, Mont-de-Boisy-1, Musiège-1, Savoie-104, -105, -108, -109, SPM1-3, SPM5 and Thônex-1. In some well reports the differentiation between the Vallorbe Member and the Neuchâtel Member is not clear and sometimes refers to Barremian age. The main lithotype of this formation is massive limestone, often associated with sandstone and calcareous marlstone. Sandy-marly limestone is associated to the Vallorbe Member as well, when combined with the Neuchâtel Member. Together with the Late Hauterivian to Late Barremian Gorges de l'Orbe Formation, these two formations today represent the former Urgonien, as referred to in older well reports.

Transition zone and Siderolithic Formation

The Mesozoic-Cenozoic(?) Transition zone has been extensively researched in the past years. Its temporal relationship is not yet scientifically proven – as is its informal name used here – but the sandstone-bearing unit comprises an Eocene(?) siliclastic formation including karstic alterations. These have been erroneously combined with the Siderolithic Formation in older well reports. Latest considerations suggest that these lithologies could be part of the Perte-du-Rhône Formation, also referred to as *Gault*.

The Siderolithic Formation consists of continental sandstone likely deposited in a fluvial environment with the sedimentary source derived from the detrital Triassic of the eastern edge of the Central Massif (Conrad & Ducloz 1977). This zone has yet not been fully investigated, and ongoing, unpublished studies in conjunction with the Transition zone characterize it as an assembly of centimetric blocks of beige, glauconitic, bioclastic limestone of the Mesozoic basement, cemented by marly, glauconitic sandstone, with angular quartz on a multi-decimetres-scale, primarily encountered in all Gex wells at depths between 230 to 290 m and 395 to 412 m, respectively, in well Geo-02 between 630 and 714 m. Very fine cemented sandstone is associated with this limestone lithotype. Certain core samples in Gex-CD-02 show the presence of polygenic conglomerates with quartz and limestone, embedded or perforated in a ferruginous, ochre clay cement. The Siderolithic Formation has been formerly referred to as the *Gompholite* facies (e.g. Charollais et al. 2007, 2013) and is encountered in wells Charmont-1, Chatillon-1D, Faucigny, Geo-02, Gex-CD-02 to -06, Humilly-2, La-Chandelière-1, Musiège-1, Savoie-106 and 107 as well as Thônex-1. Fig. 5.5 (S6) shows an outcrop of the Siderolithic Formation in the northern part of the FCC construction area, yielding a high content of quartz (99%) in XRD analysis. A characteristic feature compared to the overlying Molasse Rouge sandstone lithotypes, is the fact that Siderolithic sandstones do not appear stratified on both a micro- and macroscopic scale. This facilitates their identification in the field on both outcrops and cored rock samples. According to Jenny et al. (1995) and Charollais et al. (2007), three types of colours are distinguished based on Fe concentrations. Earlier well reports and scientific studies (Charollais et al. 2013) reported that the Siderolithic sandstone infiltrates joints

of the underlying Mesozoic limestone (former *Urgonien*). They further report that the sandstone is commonly very fine with low-sphericity quartz crystals, embedded in a micritic, pyrite-rich matrix. Jenny et al. (1995) reported rare fossils (lithoclasts). However, these are not found in the respective Siderolithic outcrops in the present study. The GR log indicates a distinct offset to lower values in the respectively logged well-logs, while the SP log increase up to 10 mV across all wells for the Transition zone. The LN resistivity log shows a high offset from 20 to 2'000 Ohm*m, similar to the SN although in the order of 2 to 20 Ohm*m. Both logs, along the SP log, associate increased values to a higher clay content. The DT log depicts a decrease of travel-time, making the Siderolithic Formation a slow formation in terms of compressional wave velocity, substantiating its potentially karstic, porous characteristics. GR values (<57 gAPI) indicate sand-dominated intervals, which partly increase for a few meters when cemented with higher amounts of shale. This is also reflected by high resistivity values across all wells.

Mineralogical analyses (QEMSCAN) of related outcrops (Fig. 4.2) revealed an associated limestone lithotype. The Sarzin and Biollay outcrops (Siderolithic Formation) show a sandstone lithotype exceeding 90% in quartz by volume, with varying claystone content from 0 up to 34%. In contrast, the Mornex and Nyoux outcrops show a tendency towards a limestone lithotype.

Molasse Rouge

The Molasse Rouge, often informally referred to as Marnes bariolées, comprising a subset of the LFM (Charollais et al. 2007, 2013; Kissling 1974), is dated to Chattian age (Early Oligocene) and split into an Upper and Lower unit. The lower succession is dominated by clayey to partly silty limestone, making the Lower unit rich in clayey limestone from ca. 240 m down to the Transition zone in the Gex wells. Alternating thin beds of very fine to fine sandstone occur, rarely with medium and laminated, clayey siltstone or green, marly claystone. Nodular, highly bioturbated limestone with mollusc fragments were formerly correlated to the *Grilly* Formation (well Grilly) and interpreted as deposits of a palustrine environment (Charollais et al. 2007). Freshwater limestone intermingled with palustrine breccias is associated with the lower succession. The upper

succession is comprised predominantly of sandstone with intercalations of marlstone across all wells, excluding those closer to the Jura.

The sandstone of constant thickness is fine to medium-grained, showing a gradual decrease in grain size from top to bottom, with rather subangular grains and weak strength. This green-grey sandstone is comprised of quartz, feldspar, muscovite, and biotite, sometimes occurring with soft, clayey pebbles dispersed in a clayey matrix in layers. Encountered along the measured depth, the Savoie-109 well does exceptionally not transition into the Molasse Rouge, but directly into the limestone-bearing Rocher des Hironnelles' Vallorbe Member (Fig. 4.11), equivalent to those encountered in the adjacent Rumilly and Valserine basins further to the south of the Geneva Basin. This well only shows Molasse Rouge at its base, which is also reflected by its higher drilling altitude compared to that of adjacent wells in this cross section.

The Molasse Rouge formation is identified to consist of 13 lithotypes across all sampled wells (Fig. 4.10, 4.11, Table 4.1). This implies the necessity to define ranges for each mineral as measured by QEMSCAN and XRD analyses. Quartz, calcite and dolomite (ankerite) make up most of the formation with average values up to 80%, 50% and 25% by volume, respectively, but vary laterally across all wells from North to South. Calcite values reach up to 100% in Gex-CD-04 and -07 at about 200 m, representing the freshwater limestone lithotype (Fig. 4.3) associated to the Molasse Rouge. Total clay volumes are quantified up to 60% by volume (Fig. 4.4), constituting swelling potential in the Molasse Rouge.

The analysis of grain and bulk densities did not result in a sufficient differentiation among the samples, since the Molasse Rouge formation yields bulk density values in very close ranges between ca. 2.60 and 2.90 g/cm³, i.e. 2.55 to 3.13 g/cm³ based on well-logs (Fig. 5.2). These heterogeneous patterns are reflected in GR log values that vary between 5 to 100 gAPI across all wells. The DT log remains at averaged constant values of 50 μs/ft, decreasing up to 20 μs/ft before entering the underlying Siderolithic Formation and Transition zone in e.g. the Geo-01 well. Resistivity logs remain at average values between 20 and 200 Ohm*m, except for thin depth intervals of a few meters bearing hydrocarbons, hence showing increased values above 200 Ohm*m. NPHI and RHOB logs show separated log curves, making the Molasse Rouge appear impermeable

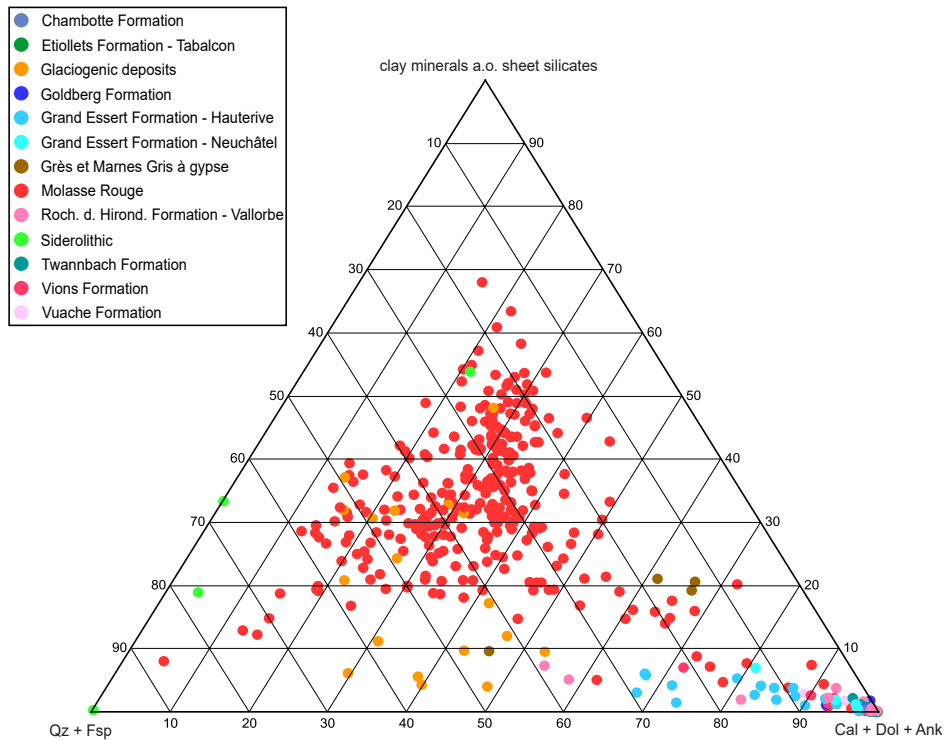


Fig. 4.2: Lithotypes for wells Montfleury-2 and L112 as well as outcrops Mornex, Biollay, Nyoux and Sarzin-R for various geological formations encountered in the Geneva Basin based on QEMSCAN measurements. Mineral abbreviations: Qz=quartz, Fsp=feldspar, Cal=calcite, Dol=dolomite, Ank=ankerite. After Haas et al. (2022).

due to its shale content (Fig. 4.5). Permeable zones are only detected below the Molasse Rouge in the Transition zone and Siderolithic Formation, suggesting compacted, sandstone-bearing intervals (Fig. 4.4, 4.5).

Grès et Marnes Gris à gypse

The Grès et Marnes Gris à gypse is part of the LFM Molasse formation and an equivalent to the Molasse Grise towards the northern area of the western SMB around Lausanne preserved in the foredeep of the GB. Jenny et al. (1995) characterise the Molasse Grise formation, respectively the Grès et Marnes Gris à gypse, as homogeneous, and reactive to HCl acid due to its carbonate content. Their claimed fibrous gypsum encounters are regularly encountered, mostly as thin layers. Based on well reports, the Grès et Marnes Gris à gypse is encountered only in the Thônex-1 well (Fig. 4.5), making the northern part of the FCC construction area more likely exposed to the Grès et Marnes Gris à gypse, and suggesting complete erosion towards the south.

The formation is dated to Late Oligocene (Middle/Upper Chattian) and is characterized by an increased amount

of anhydrite/gypsum, intercalated in sandstone and marlstone of various grain sizes (Haas et al. 2022). While the northern boreholes (e.g. Geo-01 and Salève-1) directly transition into Molasse Rouge, the Thônex-1 marks an exception with Grès et Marnes Gris à gypse being encountered between 73 and 364 m. This complies with the fact that Grès et Marnes Gris à gypse lenses have been geologically mapped in FCC's northern construction area and are delimited by the syn- and anticline structures (Fig. 4.1). Further wells encountering the Grès et Marnes Gris à gypse are Messery-1 and Mont-de-Boisy-1, ranging from 18 to 560.50 m and 748 to 1'774 m, respectively. On the contrary, the C1-C3 wells do not show any traces of gypsum in the north-northwestern part of the basin.

In the Thônex-1 and Geo-02 wells, QEMSCAN measurements yield up to 30% of gypsum by volume, occurring as anhydrite in the subsurface, and decreasing towards the underlying Molasse Rouge. This is a decisive characteristic, as the FCC fully intersects this formation in its currently planned subsurface alignment, raising concerns for operations and maintenance due to anhydrite swelling potential in these encountered lithologies (Fig. 4.4) for tunnelling construction.

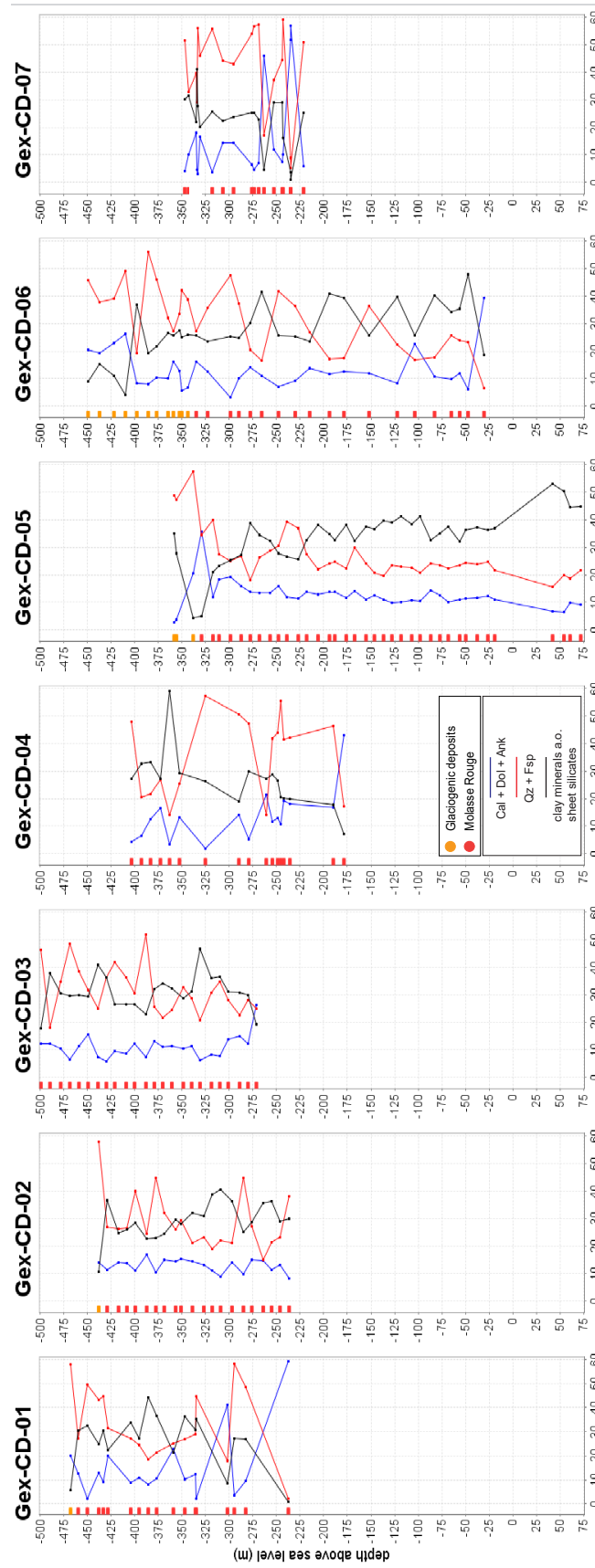


Fig. 4.3: Lithotypes derived for wells Gex-CD-01 to -07 from the northern to southern parts of the FCC construction area. The FCC depth denoted between -100 and -300 m ASL. Mineral abbreviations: Qz = quartz, Fsp = feldspar, Cal = calcite, Dol = dolomite, Ank = ankerite. After Haas et al. (2022).

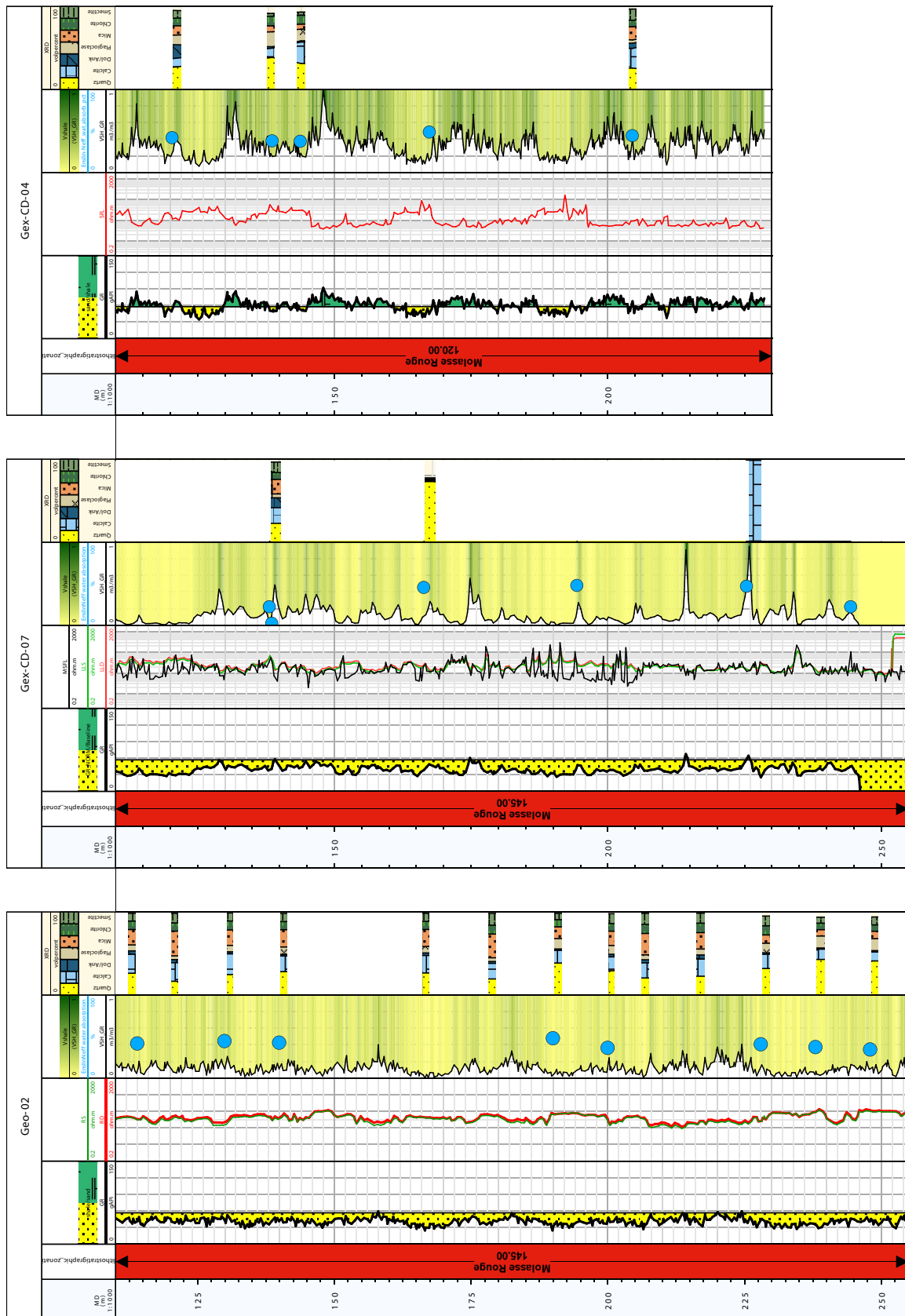


Fig. 4.4: Wells Geo-02, Gex-CD-07 and Gex-CD-04 wells depicting respective QEMSCAN and XRD measurements compared with calculated shale volume from GR log. After Haas et al. (2022).

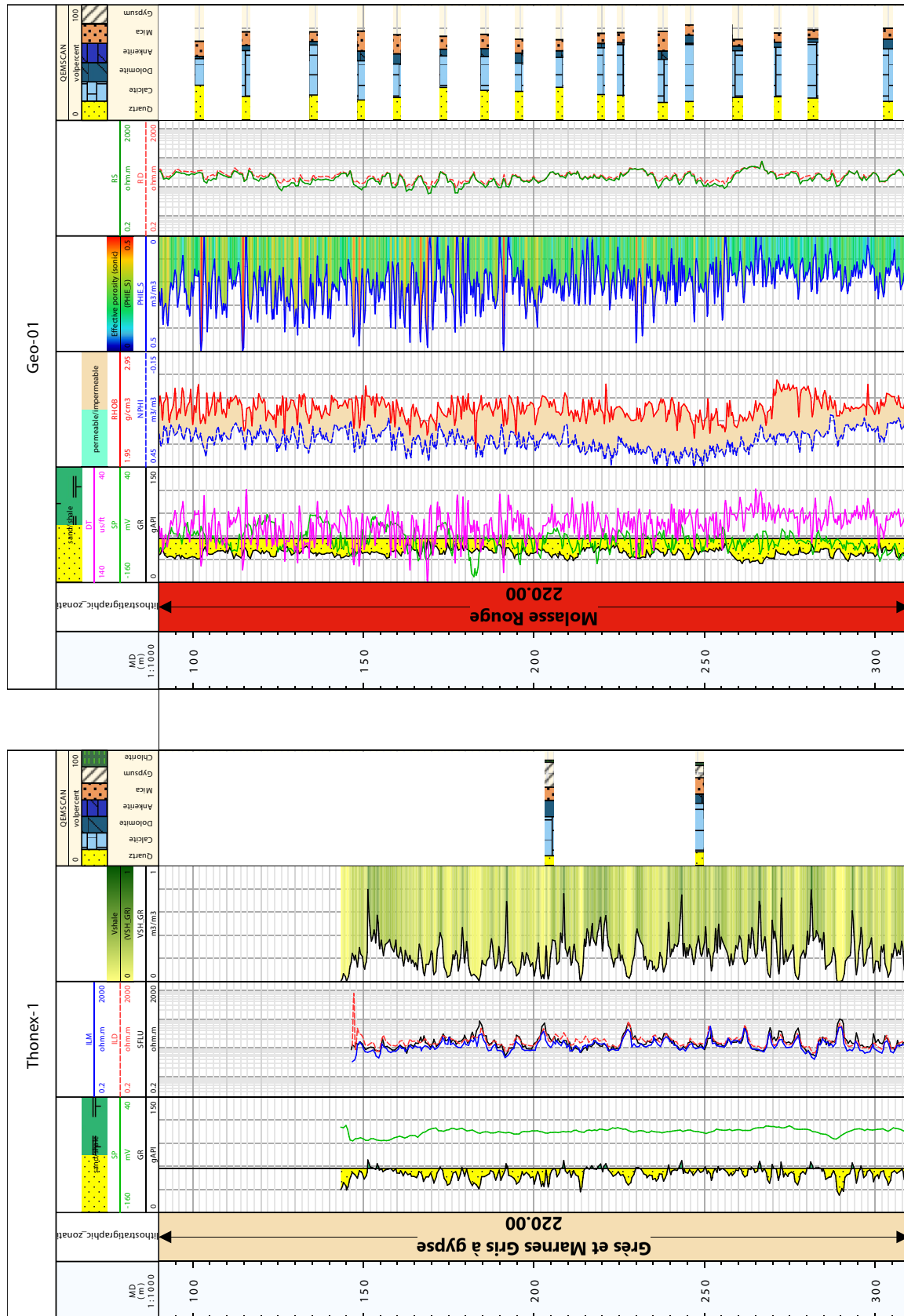


Fig. 4.5: Wells Thônex-1 and Geo-01 depicting QEMSCAN measurements in comparison to calculated shale volume from GR logs. Based on RHOBS-NPHI log crossovers, the Molasse Rouge appears impermeable. Note the increased gypsum concentration in the Thônex-1 well. Gypsum content is a good indicator to distinguish between the Molasse Rouge and Grès et Marnes Gris à gypse formations. The same depth interval of these two formations suggests the delimitation of the Grès et Marnes Gris à gypse formation by the syn- and anticline systems (Fig. 4.1). After Haas et al. (2022).



Fig. 4.6: Thin gypsum band (Fig. 5.5) encountered at an outcrop in the Molasse Rouge (Upper Chattian) formation. These bands occur at various outcrops with ranging thicknesses between 5 to 22 cm.

Well-log differences between the Molasse Rouge and Grès et Marnes Gris à gypse are difficult to establish, and only slightly visible in lower averaged SP values ranging around -20 mV in the Grès et Marnes Gris à gypse formation, compared to the Molasse Rouge of -10 to +20 mV.

Glaciogenic deposits

Glaciogenic sediments of Quaternary age, often mistakenly grouped as the *Moraine Formation* in various technical reports, summarise terminologically deposits that were influenced by glaciers, glacial erosion and deposition or subsequent geomorphological processes. These deposits formed during last pre-glacial, post-glacial, glacial and interglacial periods. They consist of compacted till made of sandy to clayey gravel mixtures, often with 0.5 to 2 cm-sized clasts of grey-beige plastic consistency and a mixture of fine-grained sand, embedded in a beige, clayey matrix.

These sediments are encountered by all wells and range from about 2 m to up to 110 m depth, overlying the Molasse Rouge or Grès et Marnes Gris à gypse in e.g., Thônex-1, Messery-1, Mont-de-Boisy-1. The greatest thicknesses are encountered at Gex-CD-05 and Gex-CD-06 with 37 and 110 m, respectively. These glacial deposits are typically irregular in thickness and lateral changes are caused by depositional or erosional processes. The post-glacial

sediments are mostly fluvial and lacustrine and show a harder consistency, while the LGM moraines depict till and show a more loose but sticky consistency. Interglacial deposits were formed between the glacial periods in the Late/Middle Pleistocene and occur either in cemented or unconsolidated form. The post-glacial deposits overlay these interglacial deposits. The latter consist of coarser gravel and sand, which is also commonly referred to as *Alluvion Ancienne*. These overlay fine-grained sediments in e.g., the Montfleury-2 well (Wegmüller et al. 1995). The post-glacial deposits consist of thick packages of variably cemented coarse gravel and sand, most likely deposited in a pro-glacial fluvial environment. These deposits are in-situ intercalated with dark-grey, clayey mudstones with traces of pollen.

GR logs show a tendency towards sandy intervals (low values) compared to the underlying Molasse Rouge, similar to the unconsolidated glacial sediments. Related DT logs show high values of 120 $\mu\text{s}/\text{ft}$, indicating loose, unconsolidated characteristics of these deposits. However, most logs show erroneous values since their data processing and theoretical analyses are based on consolidated rock, rather than loose, unconsolidated deposits.

Topsoil

Holocene (recent) topsoil commonly marks the first 2 m of wells, represented by gravelly to sandy, unconsolidated material. Among the well reports depicting topsoil descriptions over a period of 70 years, two terms are interchangeably used: the term *colluvium* referred to a mixture of eroded, unconsolidated slope deposits, while the obsolete term *alluvium* was often used to indicate fluvial deposits. These intervals are not logged.

Basin-wide stratigraphic investigations allowed for a lithotype identification of across the Geneva Basin. The topsoil, post- and interglacial unconsolidated deposits comprise a mixture of conglomerate and sandy to gravelly clay of fluvio-glacial origin (Haas et al. 2022). The lithotypes associated to the Molasse Rouge formation consist of irregular alternations of sandstone, often bearing hydrocarbons (Fig. 4.10, 4.11), siltstone and claystone, divided into an upper sandstone succession (Upper Chattian) and a lower clayey limestone succession (Lower Chattian). Layers of anhydrite/gypsum transition into pure (massive) limestone lithotypes in the underlying Mesozoic Jura units (Table 4.1, Haas et al. 2022). The Grès et Marnes Gris à gypse comprises higher amounts of anhydrite/gypsum and shows higher volumes of limestone lithotypes (Fig. 5.4) predominantly in the northern part of the FCC construction area and around well Humilly-2 when compared to the Molasse Rouge formation. The Siderolithic Formation and Transition zone consist of beige sandstone and karstic breccia with carbonate minerals of the substratum embedded in clayey sand. The Cenozoic Neuchâtel and Hauterivian members of the Grand Essert Formation feature massive limestones and ochre, bioclastic, glauconitic marls. Karstic limestones are encountered in the Cretaceous Vallorbe Member of the Rocher des Hirondelles Formation towards the FCC's southern construction area (Haas et al. 2022). They substantially vary in vertical and lateral extent and bear critical geological hazards and environmental contamination to be discussed further below.

4.4 Data coverage and interpretation of the depositional environment

A proper understanding of the spatial distribution of the identified Quaternary glaciogenic deposits and Cenozoic Grès et Marnes Gris à gypse, Molasse Rouge, and Siderolithic formations is crucial for the FCC's subsurface geo-engineering prospecting. Understanding the distribution and temporal succession across the basin allows extrapolating the lithostratigraphic and lithological information (lithotypes) from available wells to nearby areas that do not contain any data.

The stratigraphic evaluation reveals the following geological formations (top to bottom) across the Geneva Basin: Holocene topsoil, Quaternary post-glacial deposits and LGM moraines, inter-glacial and pre-glacial sediments, which overlie the Oligocene Molasse Rouge and Grès et Marnes Gris à gypse (LFM) followed by the Eocene(?) Siderolithic Formation. Then, the Transition zone (Perte-du-Rhône Formation?) marks the currently researched Cenozoic-Mesozoic stratigraphic boundary, before encountering the Jura units represented by the Cretaceous Vallorbe Formation, the Hauterive and Neuchâtel Members of the Grand Essert Formation and the Gorges de l'Orbe Formation (former Urgonien of Early Cretaceous) as well as the Vuache, Chambotte, Vions, Pierre-Châtel and Goldberg formations. The Twannbach, Etiollets and the currently debated Balsthal and Vellerat formations complete the Jurassic units.

The FCC's stratigraphic evaluation revealed 25 lithotypes across 13 geological formations that will be encountered by the FCC tunnel complex. Within the Geneva Basin, the FCC intersects in reverse chronostratigraphic order (top-to-bottom) of Holocene topsoil, Quaternary post-glacial deposits and LGM moraines, inter-glacial and pre-glacial sediments, which overlie the Oligocene Molasse Rouge and Grès et Marnes Gris à gypse (LFM) followed by the Eocene Siderolithic Formation. The Transition zone (Perte-du-Rhône Formation?) marks Cenozoic-Mesozoic stratigraphic boundary, before encountering the Jura units represented by the Cretaceous Vallorbe Formation, the Hauterive and Neuchâtel Members of the Grand Essert Formation and the Gorges de l'Orbe Formation (former Urgonien, Early Cretaceous) as well as the Vuache, Chambotte, Vions, Pierre-Châtel and Goldberg

Table 4.1: Lithostratigraphic units and lithotypes across the Geneva Basin. Transition zone currently under discussion. *Terminology currently under discussion. LGM=Last Glacial Maximum. After Haas et al. (2022).

Period	Epoch	Stage	Rock types	Lithostratigraphic notations	lithostratigraphy	lithotypes	abbreviation of lithotypes	Geological hazards	
Quaternary		Holocene	absent	absent	topsoil	topsoil	topsoil	none	
	Pleistocene	Late	silty-clayey gravel, conglomerate	Glaciogenic deposits, LGM moraines	post-glacial sediments, LGM moraines	clayey to (sometimes) sandy gravel mixtures, clasts with grey-beige plastic consistency	A3	active faults	
					cemented and unconsolidated, interglacial sediments	dark grey, clayey mud- and wackestone with pollen traces	A2	water-bearing aquifers	
	Middle			pre-glacial sediments	mixture of fine sand and sandstone embedded in clayey matrix	A1			
Paleogene	Oligocene	Serravalian	conglomerate	Upper Freshwater Molasse (UFM)				absent	
		Langhian	sandstone, marl	Upper Marine Molasse (UMM)	absent	absent	absent		
		Burdigalian	sandstone						
		Aquitanian	Molasse Grise						
		Chattian	Grès et Marnes Gris à gypse, Molasse Rouge (upper and lower succession)	Lower Freshwater Molasse (LFM), (Molasse Rouge, Grès et Marnes Gris à gypse)	Grès et Marnes Gris à gypse, Molasse Rouge as part of LFM	upper succession: sandstone (HC-bearing) with intercalations of marly siltstone.	S1, S2, S3, S4, S5; M1, M2, M3, M4, M5; AG; HC; L	swelling clays, anhydrite (AG), hydrocarbons (HC), active faults	
						lower succession: alternating thin beds of (very) fine sandstone to laminated clayey siltstone			
Rupelian	sandstone, conglomerate	Lower Marine Molasse (LMM)	-	conglomerate(?), part of Siderolithic(?)	C1, C2				
Eocene		sandstone	Siderolithic	Siderolithic	conglomerate with quartz and limestone in clayey cement	C1, C2, S6, G1			
Transition zone (Perte-du-Rhône Formation?)					Transition zone	karstic sandstone alternations(?)	KS	karst, hydrocarbons, active faults	
Cretaceous	Early	Barremian	limestone, often marly	Vallorbe Member of the Rocher des Hironnelles Formation and Gorges de l'Orbe Formation (both formerly Urgonien)	Vallorbe Member of the Rocher des Hironnelles Formation	massive limestone	ML		
		Hauterivian	marly to silty limestone	Vallorbe Member of the Rocher des Hironnelles Formation and Gorges de l'Orbe Formation (both formerly Urgonien), Hauterive Member and Neuchâtel Member	Vallorbe Member of the Rocher des Hironnelles Formation, Hauterive Member and Neuchâtel Member	marly-sandy limestone, sometimes dolomitic, mud-/wackestone; limestone with siltstone	MSLd, MLs		
		Valanginian	marl and sandstone alternations with intercalations of limestone	Hauterive Member, Vuache Formation	Hauterive Member, Vuache Formation	marly-sandy limestone, sometimes dolomitic	MSLd		
		Berriasian	limestone	Goldberg Formation, Chambotte Formation, Pierre-Châtel Formation, Vions Formation, Neuchâtel Member	Goldberg Formation, Chambotte Formation, Pierre-Châtel Formation, Vions Formation, Neuchâtel Member	massive limestone; marly-sandy limestone, biomicrite and wacke-/packestone	ML, MSL		
Jurassic	Late	Tithonian		Twannbach Formation	Twannbach Formation	massive, dolomitic, partly fine-grained limestone; massive dolomite	L, Ld, MD		
		Kimmeridgian		Twannbach Formation, Tabalcon sub-unit, Blanc Limestone	Twannbach Formation, Tabalcon sub-unit, Blanc Limestone	dolomitic, clayey limestone, sometimes massive	DCL, ML		
		Oxfordian		Balsthal Formation, Vellerat Formation*	Balsthal Formation, Vellerat Formation*	clayey to marly limestone and marlstone	CML, M1		

formations. The Twannbach, Etiollets and currently debated Balsthal and Vellerat formations complete the Jurassic units of the Jura. The FCC does not intersect the remaining Geneva Basin's stratigraphy such as the Goldberg, Chambotte, Pierre-Châtel and Twannbach formations as well as the Etiollet Formation's Tabalcon Limestone sub-unit, the Blanc Limestone, Balsthal and Vellerat formations.

Data coverage modelling

The FCC's current feasibility phase comprised the review and evaluation of existing wells, which allowed for a first interpretation of available stratigraphic data to deduce missing data zones. The modelling results aim at supporting optimal well placement for consecutive site investigations to further optimize the final tunnel alignment with respect to potential geological hazards. The geological hazards will determine the engineering efforts needed to minimize them while keeping to the alignments needed for the physics experiments.

Well density coverage modelling is based on wells located within a 2 km radius of the FCC's current layout. Wells located within the FCC ring perimeter and along a lateral extension of up to 2 km outside of the ring have been accounted for and filtered for a minimum depth of 10 m from topographic level to 300 m ASL (Fig. 4.7).

The results show a distinct lack of data (wells) between the southernmost point (Jura and Mandallaz limestone) and the easternmost point at the Bornes Plateau (Fig. 4.1), as well as to the east of Lake Geneva along the FCC footprint. Little data coverage is encountered in the western to south-western subsurface portions of the FCC's proposed construction area. It is suggested that future site investigations, e.g. seismic surveys and drilling campaigns, should first aim for these areas. Relevant correlation and laboratory data from this study should then be integrated with the gathered measurements. Assuming the same encountered stratigraphy and similar rock behaviour, no additional laboratory analyses would have to be conducted, as the information compiled for this study is abundant.

Interpretation of the depositional environment

Large-scale cross-sections help to identify the thickness and distribution of geological formations and interpolate stratigraphic information to zones, which have not yet been directly explored. The interpolation allows for predictions to conclude on different depositional environments that infer geological and environmental hazards to be discussed in the next section.

Fig. 4.10 and 4.11) show the thickness of the LFM succession decreasing towards the NW from over 1'000 m near the Salève to zero close to the Jura (Haas et al. 2022). An increasing trend is observed for the glaciogenic deposits, with higher encountered thicknesses of up to 130 m at well Gex-CD-06. It is suggested that these trends are linked to different depositional environments.

Haas et al. (2022) suggest two depositional environments under either marine or continental influences during Molasse deposition. Their border is suggested to be located close to the Thônex-1 well and lines up towards the north-west of the Salève mountain around wells Humilly-1 and Humilly-2. These three wells contain increased amounts of hydrocarbons. Based on cross section B, all wells show indices of hydrocarbons (bitumen) with larger amounts in the Geo-01, Geo-02, and Salève-2 wells (Fig. 4.11). No traces of gas were observed according to the well reports. This suggests local gas accumulations rather than laterally extensive gas horizons and complies with the minor success of industrial hydrocarbon exploration across the basin in the past. Local gas spots have been encountered at a depth of 90 m in the geothermal probe well drilled into the Molasse in Satigny (Do Couto et al. 2021).

A marine depositional environment seems reasonable that has produced these hydrocarbon accumulations. These hydrocarbon accumulations would go in line with increased gypsum contents towards the south-east (Thônex-1 well) being a remnant of evaporation in a marine environment. The LFM Molasse Rouge sediments overlap the Cretaceous formations in the Salève wells, while the Vuache Fault might have acted as a separation of continental and marine lithostratigraphic Molasse formations, separating the Chattian and Rupelian successions in the western part of the Geneva Basin. The Salève wells positioned close to the Vuache Fault encounter reduced thicknesses of Molasse Rouge sediments compared to the northern wells. This would substantiate the argument of two different settings

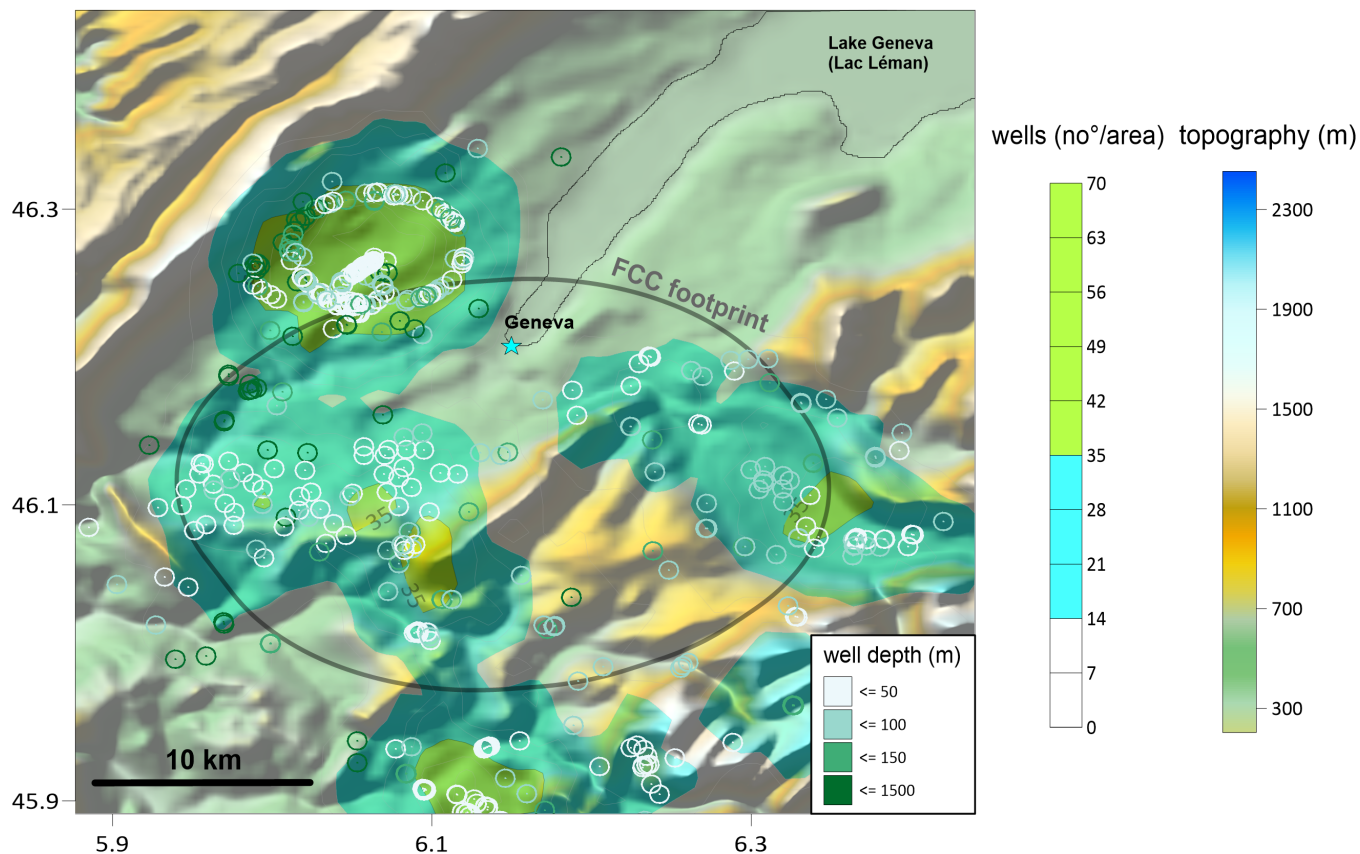


Fig. 4.7: The FCC's well data coverage map based on its current tunnel alignment based on 661 wells. The model will be updated following the results of future site investigations. After Haas et al. (2022).

across the Geneva Basin: a predominant continental environment in the north-east and a marine one in the south-west of Burdigalian(?) age, which might have been likely connected during the Chattian leading to thick accumulations of Molasse Rouge deposits in the north-eastern part of the Geneva (Moscarello et al. 2014). This suggests that the region to the west of the Salève may have been uplifted relative to the adjacent eastern Bornes Plateau (Fig. 4.1), potentially having caused less exposure to humid climate at the Bornes Plateau and complying with proposed influences of Molasse Rouge erosion in the literature. Increased hydrocarbon accumulations at the Bornes Plateau region south-east to the Salève underline the argument of a marine depositional environment. The Rupelian formations were deposited next to the Subalpine chain in the eastern part (Fig. 4.1), substantiating the view of uplift and causing erosion in the western part. However, the encountered Siderolithic Formation, which is likely to have been eroded to the east of the Salève, indicates thickening towards the Jura in the north-west. This would infer a (shallow) marine environment during its deposition in the hinterland

of the Geneva Basin and a continental environment in its foreland, likely to be part of karstic intervals and following an extension of the model proposed by Kaelin & Kempf (2009).

Based on depositional extrapolations, hydrocarbon accumulations would increase towards the south of the current FCC perimeter. Do Couto et al. (2021) investigated the origin of hydrocarbons based on rock eval pyrolysis and gas chromatography mass spectrometry, and concluded the majority on Carboniferous coals and shales of type III organic matter as part of the GB's Molasse formations. Bituminous occurrences are identified in wells Satigny and Geo-01 (this study) and on surface (e.g. Roulave stream), which is also in compliance with hydrocarbon occurrences at the HL-LHC Point 1 construction site as discussed in chapter 2 and in Voiron et al. (2020). These hydrocarbon indices might have followed migration paths created along fractured networks and fault systems such as the Vuache Fault as well as the northern syn- and anticline structures that also seem to delimit the Grès et Marnes Gris à gypse formation in the northern part of the basin around well

Thônex-1. However the fracture network and its potential link to hydrocarbon accumulations have not yet been fully investigated and are currently under research.

Hydrocarbon accumulations would have a negative impact on the FCC construction and its direct beneficial use of excavated materials in the realm of the GB towards the south-southwest because no direct beneficial use is applicable and purification of the raw material is required. Otherwise, the hydrocarbon-polluted material enforces disposal. In this region marine conditions would have prevailed during accumulation, meaning that hydrocarbon accumulations are not explicitly linked to the Cenozoic formations. Well Humilly-2 crossed the entire sedimentary sequence to reach the top of the Carboniferous at 3'051 m. It is located ca. 17 km from the Thônex-1 well with thicker successions of the Urgonian (Cretaceous limestone) than in Thônex-1. The thickness of this reef complex is difficult to estimate as it is poorly delineated at the base and top of the Tabalcon limestone sub-unit formation. This proposed reef limestone formation was initially suggested by Jenny et al. (1995) and identified as finely bioclastic distal talus formation of the Tabalcon limestone sub-unit as part of the pre-reef in the middle of the open sea. This formation remains hypothetical, and could not be identified in this study. However, it would suggest that hydrocarbon accumulations could potentially extend into deeper depth and into the Mesozoic limestone formations. About 16 km southeast, wells Thônex-1 and Faucigny-1 reached the Permo-Carboniferous basement at 4'600 m depth. An increased thickness of the Urgonian and Portland Kimmeridgian limestone is observed compared to wells Humilly-2 and Thônex-1. Do Couto et al. (2021) have revealed a higher risk assigned to the Permian and Carboniferous source rocks inside the gas window.

A decreasing trend of gypsum occurrences is identified towards the Jura, where limestone lithotypes prevail. This is an advantage for tunnelling advancement because it reduces the amount of potentially swellable rock. This could be substantiated by the argument of the Jura that was already folded when the area containing the Satigny wells was deposited (>10 Ma). Furthermore, the area's moderate water influx represented by paleo-rivers was lower than its evaporation. This process might have caused the accumulation of gypsum.

Two different pre-glacial trenches were identified. The identification of these trenches is essential as they might

be linked to the presence of rock with increased amounts of anhydrite (swelling potential) or the occurrence of groundwater aquifers. One large pre-glacial erosion trench is associated to rock that has often been referred to as *moraines* or *morainal debris* (Haas et al. 2022), and was encountered in the *Montfleury* trench at a depth of ca. 100 m under the Geneva airport (Switzerland); another trench was identified at a depth of ca. 50 m in the St. Genis-Pouilly area (France). This seems to depict the same trench, which was initially avoided by inclining the ring to remain under the top Molasse Rouge formation during previous civil engineering undertakings.

The identified hiatus of about 72 Ma (Allen et al. 1991; Sinclair & Allen 1992; Sinclair et al. 1991; Trümpy 1973) separates rocks of Aptian age (Brentini 2018; Rusillon 2018) from the overlying Siderolithic Formation of estimated Eocene(?) age. This hiatus comprises a hint towards the transition of the Siderolithic Formation and the Mesozoic-Cenozoic Transition Zone, which both represent karstic intervals that imply a geological hazard for tunnelling and could extend towards the south of the basin. The hiatus resulted probably from subaerial(?) exposure and consequent development of an erosive and deep karst system at the top of the Mesozoic series, which played a predominant role in the establishment of an aquifer drainage system within Cretaceous and Jurassic limestone across the GB. The drainage system potentially implies geological hazards for the FCC construction as karstic intervals, which are discussed further in the following sections.

4.5 Identification of geological hazards

Geological hazards such as swelling rocks, karstic intervals, aquifer horizons and active fault regimes play a crucial role for the successful construction of subsurface infrastructure. Swelling and karst intervals have been postulated as geological hazards in Bruning et al. (2013) and Agostini et al. (2016) as part of the LEP civil engineering undertakings. The LEP's initial circumference was reduced from 30.6 km to 26.6 km due to a change of the machine's position to avoid the deep Triassic anhydritic formations of the Jura mountains and potential tectonic faults based on results of site investigations. Ultimately, this reduced the length of the tunnel in the limestone under the Jura to 3 km in an optimised tunnel layout. Along the

3 km tunnel in the Mesozoic limestone formations, water ingresses of 100 L/s at pressures of up to 8.5 bar (Schopper 2009) required ground-freezing in the glaciogenic deposits at a depth of about 50 m (Bruning et al. 2013). This caused a delay of completion schedule of originally 36 months to 67 months (CERN 1989) and exemplifies the importance of the proper identification of geo-engineering hazards. Hence, the present study meticulously identifies and discusses these initial postulations and extends them across the full basin for the FCC construction.

Swelling is a geological hazard in tunnelling of clay-rich sedimentary deposits (Anagnostou 1993; Anagnostou et al. 2010; Einfalt et al. 1979; Einstein 1996; Kovári et al. 1987; Kovari et al. 1981a,b; Kovári & Vogelhuber 2014; Kovári et al. 2002) and has led to severe problems at tunnel construction sites worldwide, e.g., in the Jura Mountains of Switzerland and France, southern Germany, Spain, Poland, Italy and the U.S.A. (Alonso & Olivella 2008; Berdugo et al. 2009; Butscher et al. 2016; Kovári et al. 2002; Steiner 1993; Vrakas & Anagnostou 2016; Yilmaz 2001).

Another type of geological hazard is posed by karstic features that have caused water flooding at several subsurface construction sites (Alija et al. 2013; Li et al. 2020; Lv et al. 2020; Su et al. 2021), while aquifer tables and associated groundwater flow (Butscher et al. 2011; Hasegawa et al. 1993) have been well integrated in required environmental impact assessment studies (Huang et al. 2015) and contemplate, together with seismic activity studies (e.g. Rehbock-Sander, Jesel 2018), distinct hazards for subsurface construction projects.

The basin-wide geological investigations revealed potential geological hazards for the FCC and are stated in Table 4.1. The list provides ascertained occurrences of swelling rocks, karstified intervals, active faults, and water aquifers based on a lithostratigraphic subdivision of the subsurface. The identification of geological hazards is discussed below and would impact all subsequent project phases spanning over a period of over roughly ten years. As such, these factors would affect the optimal well placement prior to site investigations in the technical design phase, and excavation progress during the construction phase.

Swelling rocks

For the FCC swelling may be caused by anhydritic or clay-rich rocks. For the identification of anhydrite, QEM-SCAN is not the favoured mineralogical method because it analyses chemical compositions, which do not allow a differentiation between anhydrite and gypsum. This fact honors XRD analysis, which allows for the differentiation of anhydrite from gypsum and improved identification of fine-grained particles with respect to clay minerals. Both the Molasse Rouge and Grès et Marnes Gris à gypse formations bear a hazard for all three types of swelling: (1) intra-crystalline and (2) osmotic swelling due to the presence of smectite, and (3) anhydrite swelling (see chapter 3). To adequately address the swelling of rock, XRD and Enslin-Neff water absorption analyses need to be performed. The quantification of swelling rock will play a crucial role for optimum tunnel alignment to avoid severe tunnelling construction delays or safety concerns.

Anhydrite is encountered in wells Savoie-104, SPM2, SPM3, SPM5 and in the Savoie wells representing an anhydrite swelling hazard. The Grès et Marnes Gris à gypse contains a high amount of anhydrite/gypsum and smectites (Fig. 4.5) leading potentially to all three types of swelling. It is important to note that in the subsurface anhydrite occurs, while on the surface the stable form is gypsum with a transition temperature given at 40 degC (Anagnostou 1993; Klimchouk 1996; Kovari et al. 1981b; Rolnick 1954). The Balsthal/Vellerat formations might show a similar chemical composition as the Molasse Rouge for associated marl lithotypes, which bear swelling potential due to smectites, also encountered in the clayey limestone of the Etiollets Formation's Tabalcon Limestone sub-unit. Outcrop investigations in the north-northwestern FCC construction area yield various thin gypsum bands (Fig. 4.6) that are likely to occur as anhydrite in the subsurface due to its chemical instability (Klimchouk 1996). With respect to anhydrite swelling, dedicated laboratory swelling tests are required for geotechnical design calculations of the FCC's tunnel infrastructure. Former research successfully used such swelling test results to numerically retrieve design value estimates of swelling pressures for final tunnel lining optimizations (Kovári & Vogelhuber 2014).

The Molasse Rouge contains less anhydrite/gypsum but higher concentrations of smectite in clay, silty clay and clayey silt (Fig. 4.4) of up to 17.2% by volume (Fig. 4.8)

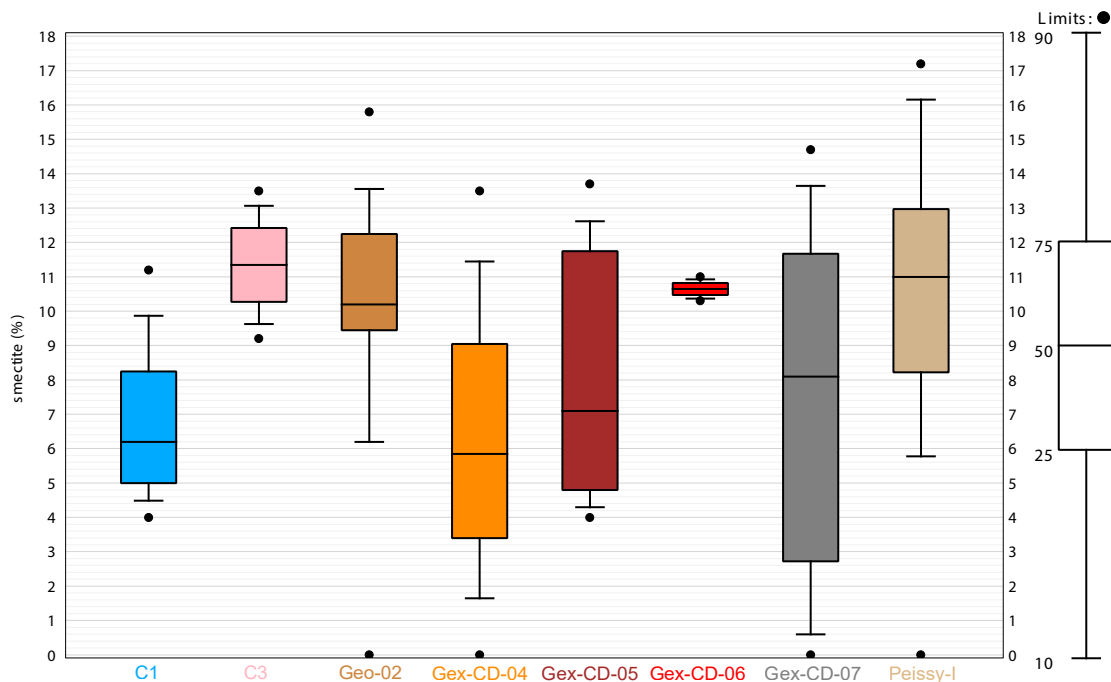


Fig. 4.8: Swellable montmorillonite (smectite) from XRD measurements for 6 wells. The northern wells (Gex-CD-07 and Peissy-I) show a high variability, depicting maximum smectite values of up to 17.2% by volume. After Haas et al. (2022).

making it prone to predominantly intra-crystalline and osmotic swelling. Apart from mineralogical analyses that quantify the amount of swellable components, the Enslin-Neff method relates to water absorption and swelling potential. The Molasse Rouge sandstone (S1-S6), mud- and siltstones (M1-M5) lithotypes show maximum Enslin-Neff water absorption of up to 58.9 wt.% (Geo-02, Fig. 4.4) leading to potential intra-crystalline and osmotic swelling. Minimum Enslin-Neff water absorption values of 2.8 wt.% are represented by hydrophobic, hydrocarbon-bearing sandstone (HC).

Detecting water absorption phenomena in geophysical well-logs is difficult, and only feasible in a qualitative manner via resistivity or neutron/density logs, potentially indicative of water/hydrocarbon-bearing rocks. Log responses to detect swelling potential are related to (swellable) clay content in the SP log, which indicates slightly lower values in the Grès et Marnes Gris à gypse formation compared to the Molasse Rouge. This is most likely related to higher contents of anhydrite/gypsum in the Grès et Marnes Gris à gypse formation, as also verified by QEMSCAN analysis, subjecting the type of voltage difference to the SP's membrane potential in the Molasse Rouge due to higher occurrences of clay, rather than the liquid junction potential. However, while

logs might indicate qualitatively the hazard of swelling, mineralogical analyses remain crucial for its quantification.

Karstified intervals

The detection of karstic features depicts an important hazard to be addressed for tunnelling in clay-rich, sedimentary rock (Solbakk 2020; Su et al. 2021). Karst was a significant litho-technical hazard during LEP subsurface construction in the 1970's, substantiated in documentation from SPM wells. During LEP construction, the karstic intervals led to severe water ingress during tunnelling. Reports of Salève wells have documented also rapid loss of mud circulation into fractured limestone, which ultimately caused a forced well closure (Conrad & Ducloz 1977; Géotechnique Appliquée Dériaz & SA (GADZ) 1981b, 1982b).

This has led to the assumption that karst formations are not restricted to the northern FCC construction area but could be encountered also in fractured limestone formations in the south. Karsting is possible in the Chambotte Formation, the Transition zone and the porous Siderolithic Formation (Fig. 4.3).

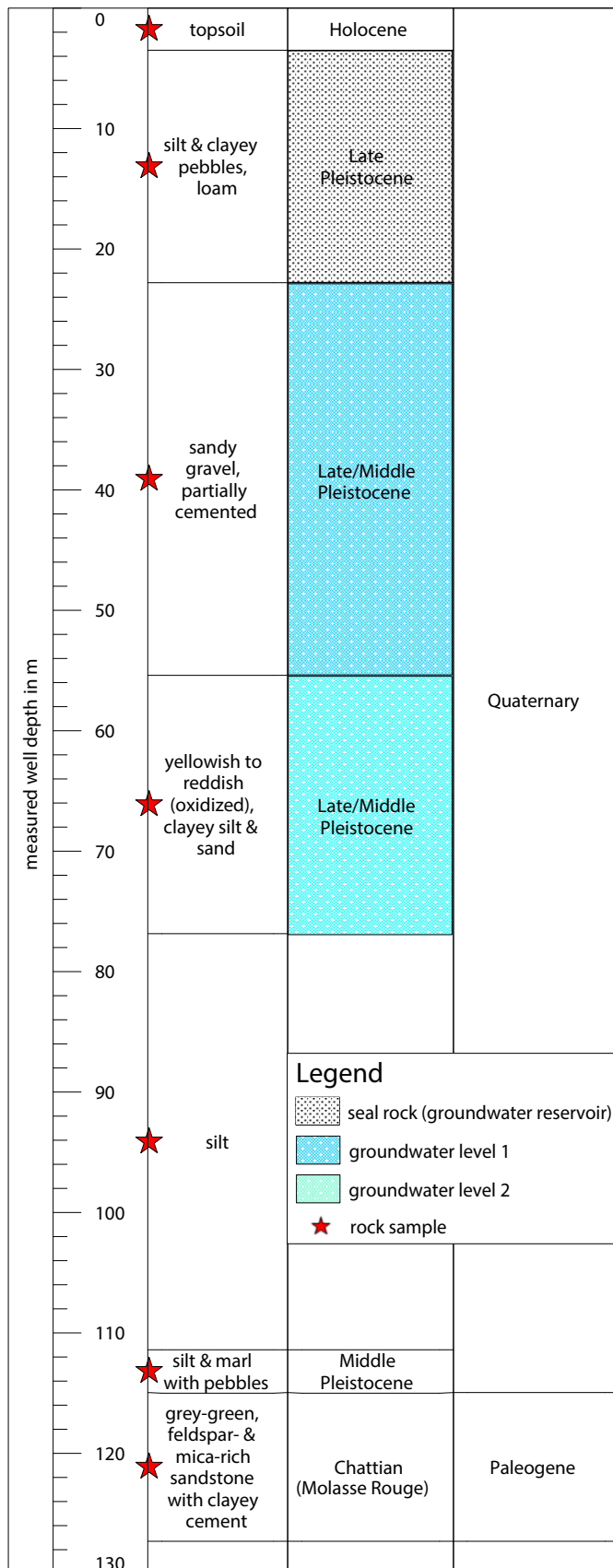


Fig. 4.9: Borehole Montfleury-2 in an anticline structure, depicting Pleistocene deposits confined in a topographic valley (Fig. 4.2). Respective rock samples are used amongst others for lithotype derivation. Modified after Haas et al. (2022).

Fault structures and water aquifers

The FCC's current footprint crosses several active faults, synclines and anticlines (Fig. 4.1), which presents the possibility of induced seismicity around the tunnel perimeter during construction. To the west/northwest, the upper Jura mountains impose a monotonic and isoclinic anticline formed by Alpine thrusting on a large thrust fault running along the Valserine valley (Burkhard 1990; Charollais et al. 2007; Moscariello et al. 2020; Sommaruga 2011; Wildi 1997).

One of the main active faults is represented by the sinistral strike-slip Vuache Fault in the southwestern corner of the FCC's planned construction area (Fig. 4.1). Another geological feature is represented by the Subalpine Thrust, which per se is not active but indicates a displacement in the spatial arrangement of encountered formations. The syn- and anticline structures observed in the northern part of the proposed FCC perimeter do not reflect an active fault scenario. The LEP construction layout avoided the Middle Jurassic and remained explicitly in the Cretaceous (Hauterivian, Valanginian, Berriasian, i.e. Urgonian) and in the upper part of the Malm. Boreholes and geophysical surveys showed that this foothill area was highly tectonised, and that tectonic faults along the perimeter were filled by Molasse Rouge or Siderolithic deposits (CERN 1982). These encountered faults control water drainage by acting as channels for the flow of seepage water towards the foothills springs (Moscariello 2018b).

The large erosional valleys located at the Valley of Aire and at Petit Lâc in the northern part of the FCC area are filled with unconsolidated, clayey sediments, usually referred to as mudstone of postglacial origin (J. Fiore et al. 2002; Moscariello et al. 1998), and would pose a substantial hazard for the FCC shaft construction due to affected groundwater aquifers (Fig. 4.9). These sediments represent one of the main water reservoirs in the Geneva Basin, implying the presence of water aquifers towards the northern part of the FCC construction. Above these deposits, the impermeable Late Pleistocene sediments likely seal these water reservoirs (Fig. 4.9).

The FCC tunnel should remain within the Molasse Rouge formation to avoid the Mesozoic karstic intervals since swelling rock is hardly completely avoidable along any footprint but karstic intervals are. The lithotypes encountered in the Molasse Rouge will serve as a weak rock for

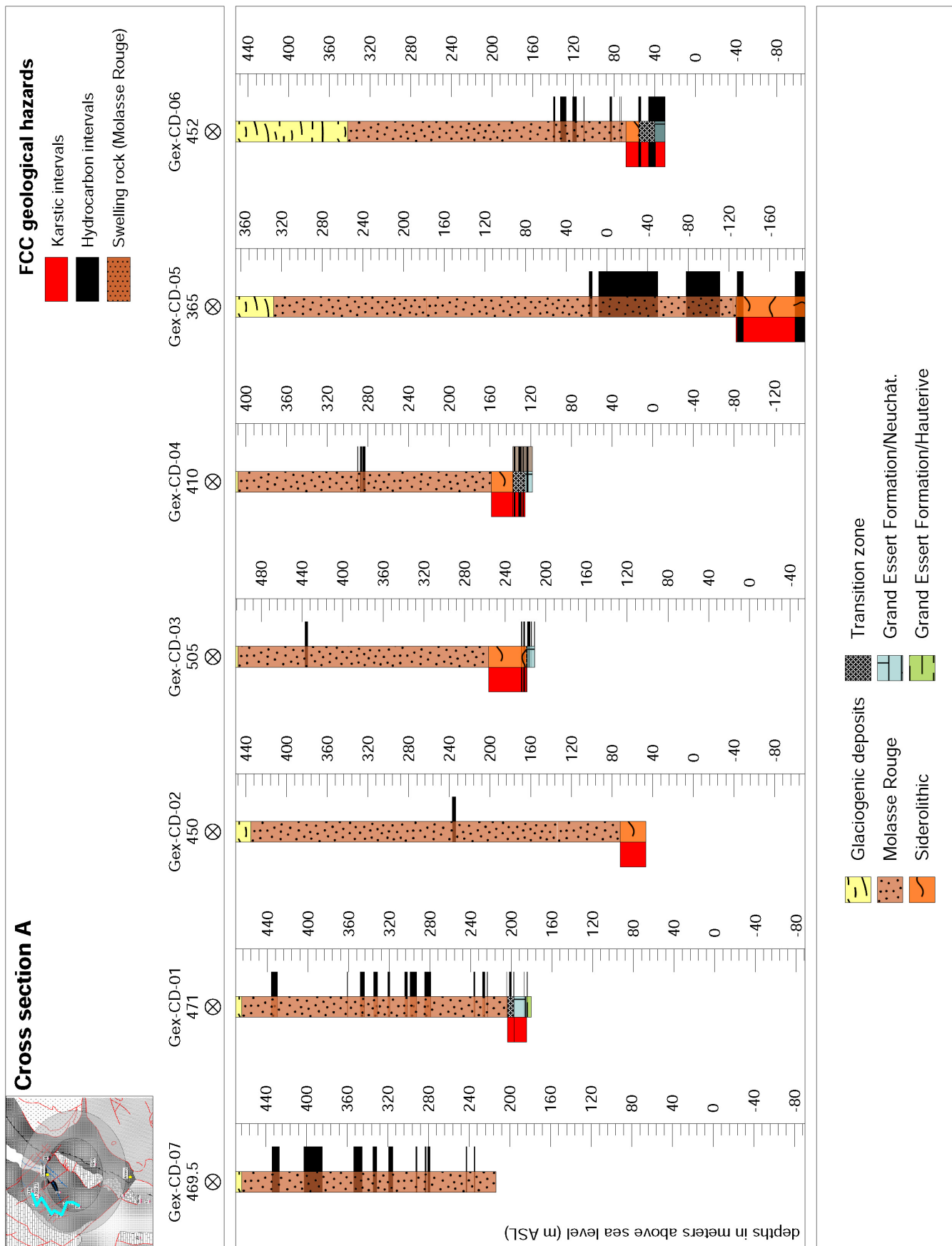


Fig. 4.10: Cross section A from North to South of the 7 Gex wells in the western part of the FCC’s construction area with associated potential geological hazards. Values below well-ID depict topographic elevation in meters. The FCC’s current perimeter depth intervals range between +100 and +300 m ASL. Modified after Haas et al. (2022).

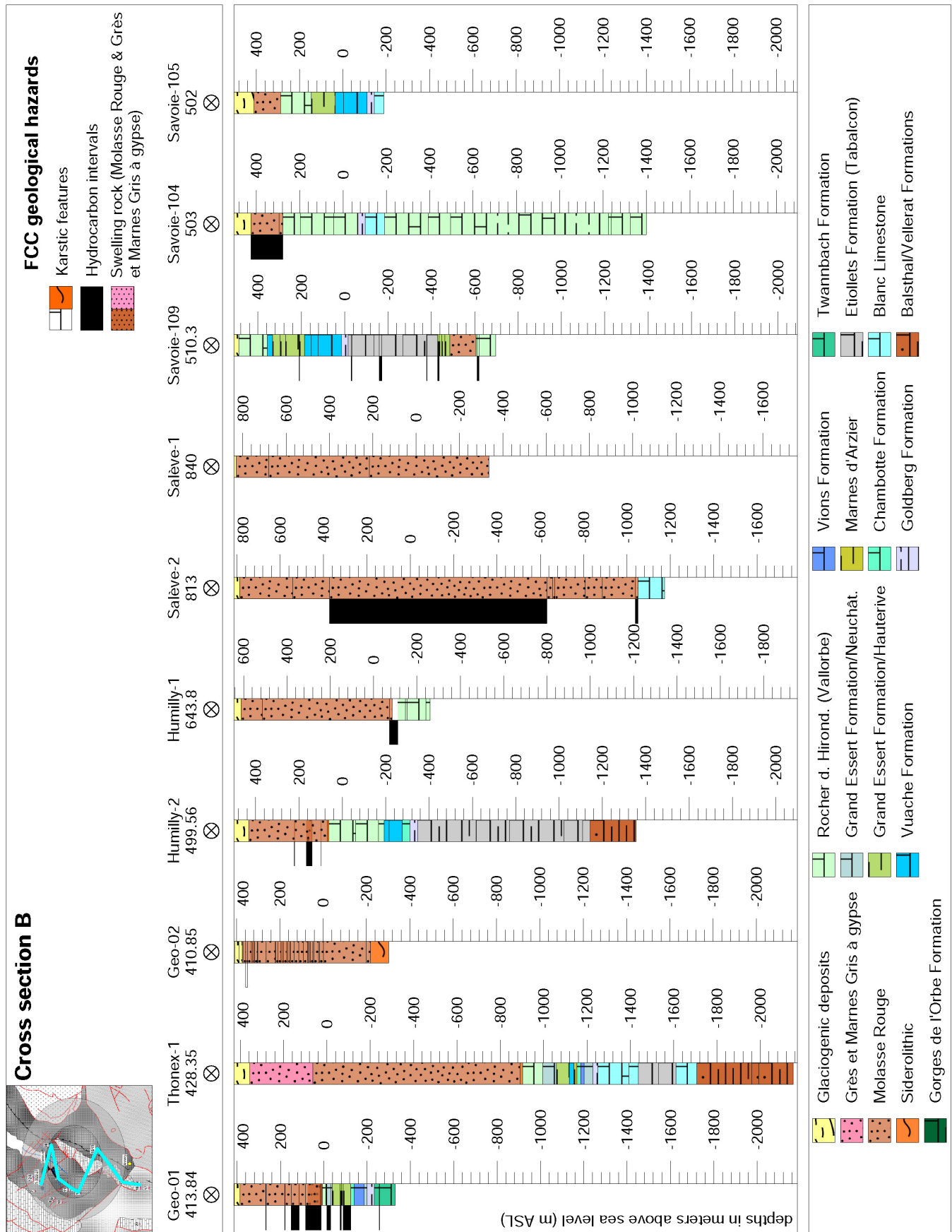


Fig. 4.11: Cross section B in NW to SE direction for wells Geo-01, Thônex-1, Geo-02, Humilly-2, Humilly-1, Salève-2, Salève-1, Savoie-109, Savoie-104 and Savoie-105 in the eastern part of the FCC’s construction area with proposed geological hazards. Values below well-ID depict topographic elevation in meters. The FCC’s current perimeter depth intervals range between +100 and +300 m ASL. Modified after Haas et al. (2022).

the construction in the *plain area*¹. The alignment should aim for a reduction in the overburden in the Jura foothills, which could be achieved by slightly tilting or moving the plane of the ring. New boreholes as part of the FCC's upcoming site investigations should focus on the yet unexplored (missing data) areas that would impose geological hazards. These areas are predominantly linked to the north/northwestern as well as south/south-western parts of the Geneva Basin.

¹A term used in former technical reports for the flat area around the Geneva city, and between the Geneva airport and the Jura mountains.

5 Rock characterisation of the basin's geological formations

5.1 Introduction

First rock investigations dated back to a study by Vernet (1958) half a century ago and were based on mineralogical XRD analyses of Molasse rock samples taken around the city of Lausanne and to the South towards the city of Geneva. A lithostratigraphic characterisation by Oxburgh (1981) followed as part of the wider Swiss Molasse Basin and the Northern Alpine Foreland Basin and introduced the terms Lower Freshwater and Lower Marine Molasse as well as Upper Freshwater and Upper Marine Molasse (see chapter 4). The Geneva Basin's stratigraphy has been further studied since in more detail introducing the lithostratigraphic units of the Mesozoic units, as well as the Cenozoic Grès et Marnes Gris à gypse, the Molasse Rouge, and the Siderolithic formations (Charollais et al. 2007, 2013; Strasser et al. 2016) together with the Quaternary glaciogenic deposits (Graf & Burkhalter 2016; Moscariello 1996, 2018a; Moscariello et al. 1998). This has been succeeded by a petrographical study on Molasse rock samples published by Jenny et al. (1995) in a similar area as today's specified Geneva Basin. Some of these lithostratigraphic terms have been used in simplified adaptations for the Cenozoic succession as part of engineering purposes (Amberg Engineering 2015; Bruning et al. 2013; CERN 1982).

CERN undertook a vast set of geological and geotechnical site investigations between 1980 and 1981 (CERN 1982) as part of the LEP subsurface infrastructure evaluation. Stratigraphic units such as the Cretaceous (Malm, Dogger, Lias) and the Triassic were investigated as part of several drilling campaigns. Three deep boreholes, one up to a depth of 1'000 m, encountered tectonic faults, which are identified karstified, empty or filled with mylonitic silt subjected to water loads (CERN 1982). With these subsurface engineering projects emerging in the 1980's, a geotechnical (engineering) rock classification was developed. These

geotechnical classes have been used for geotechnical design calculations but were merely set in basin-wide stratigraphic (depositional) or geological contexts. A geotechnical rock mass classification of the Molasse Rouge formation¹ in engineering reports has been initially categorized into four groups based on mineralogical content and uniaxial compressive strength (Table 5.1, 4-class). These results were documented in the HL-LHC's geotechnical baseline report (Madinier et al. 2017) and various other technical reports (e.g., Canzoneri et al. 2018). With continued progress and analysis of the HL-LHC geological and geotechnical site investigation results, the initial classification was updated (Table 5.1, 6-class) including also further geotechnical tests such as confined, unconfined compressive tests, Atterberg limits tests, shear, point load and Brazilian tensile tests, swelling and Lugeon permeability tests, the derivation of geological strength index (GSI) and by geophysical well-log data (GR, DT, V_P and V_S logs). These data sets together with an updated interpretation have been published in Fern et al. (2018) yielding a detailed geotechnical classification categorized into three marl and three sandstone classes of the Molasse Rouge formation. It must be noted that the terms *weathered Molasse* and *very hard sandstone* were used as two additional, unofficial classes explicitly on-site of both the LEP and HL-LHC constructions, referring to the lower and upper boundary of UCS values. These terms also occur in the HL-LHC geotechnical reports as outdated remnants.

In parallel to the geotechnical classification published by Fern et al. (2018) (Table 5.1), a first engineering characterisation for the FCC (Ariza & Dallapiazza 2018) introduced the terms *good* and *poor rock*, as well as *soft ground*. *Good* rock hereby refers to massive, fresh Molasse, Flysch and limestone rock, while *poor* rock implies their fractured

¹Note that in geotechnical reports the Molasse Rouge and Grès et Marnes Gris à gypse formations have not been differentiated. However, based on the data review (see chapter 3), the values correspond best with the Molasse Rouge formation.

equivalents. Soft ground includes Quaternary and Tertiary² soil specified as morainal debris (Ariza & Dallapiazza 2018). However, as discussed in chapter 4, terming all Quaternary deposits as *morainal debris* is erroneous because morainal debris includes just a small portion of the glaciogenic deposits (Table 4.1; Haas et al. 2022).

While these classification allowed for an estimate of geotechnical design parameters for the HL-LHC and FCC construction, its lateral and vertical extents have remained unconsidered. The characterisation is limited explicitly to data taken at the Swiss HL-LHC Point 1 in the northernmost part of the FCC perimeter. Furthermore, the classification lacks additional analyses as introduced herein, i.e. chemical impurities, organic content, and their respective link to samples of other formations such as the glaciogenic deposits and the Siderolithic formations. Neither of the previous rock characterisations was used for conclusions on potential beneficial usage scenarios. Hence, the following elaborations aim beyond existing rock characterisations across the Geneva Basin, and integrate a multi-proxy approach of the identification in the field from visual inspections, colour, texture and sedimentological characteristics, to geophysical well-logs and acquired geochemical, mineralogical, physico-chemical, petrophysical and geomechanical laboratory analyses (see chapter 3). These have not yet been available nor studied in such an extent, neither in former technical reports (CEREMA 2020) nor in the literature on the encountered rock materials.

The goal is to predict potential application scenarios of the FCC's proposed excavated rock and soil based on a newly developed rock characterisation. Its underlying geophysical well-log, laboratory and field analyses allow for empirical cross-correlations in order to suggest a minimum set of analyses to sufficiently characterise the properties of its clay-rich sedimentary raw materials for predictions on application scenarios discussed in chapter 6.

5.2 Lithotype characterisation based on geophysical well-logs

The digitisation and analysis of geophysical well-logs is based on the idea of characterising the in-situ rock for the

prediction of lithotypes and shale volume (total clay content) to qualitatively derive potential applications scenarios. Well-logs provide an ancillary level of understanding the rock behaviour, and an additional source of correlation for the heterogeneous rock composition on a macro-scale, contemplated by new laboratory analyses investigating the rock on a micro-scale. GR, SP and DT well-logs are an integral part of future site investigations, allowing for first qualitative conclusions prior to any laboratory analyses. The FCC's encountered geological formations as identified in chapter 4 depict the Cenozoic Grès et Marnes Gris à gypse, Molasse Rouge, Siderolithic formations, and the Cenozoic-Mesozoic Transition zone making up ca. 90% for its main tunnel. The glaciogenic deposits depict an additional 4% and are predominantly relevant for its shaft construction at shallow depths. The remaining 6% intersect the Mesozoic Vuache formation, the Vallorbe Member of the Rocher des Hirondelles Formation, and the Grand Essert Formation featuring both the Hauterive Member and the Neuchâtel Member for its proposed excavated volume estimations (Haas et al. 2022).

A sand-silt-clay model (Fig. 5.1) for well Geo-01 in the northern part of the basin was calculated to estimate volumes of sand, silt and (dry) clay, as well as respective clay-bound water and formation water. The results allow for conclusions on clay types, i.e. dispersed, laminated, or structural. They provide a correlation to the quantified volume with swelling clays in both the Molasse Rouge and the Grès et Marnes Gris à gypse formations. Required inputs for the sand-silt-clay model are neutron porosity, bulk density, true formation resistivity, flushed zone resistivity, formation temperature and water resistivity. The three-mineral model is calibrated to petrophysical and geochemical laboratory data, and includes quartz, calcite, and dolomite (Fig. 5.2).

The log lithotype model shows a quartz-dominated interval in the Hauterive Member and Neuchâtel Member, with a matrix density between 2.70 and 2.75 g/cm³ and a volumetric photoelectric factor between 4 to 8 b/cm³, influenced by the silty to clayey composition. The Molasse Rouge formation shows a heterogeneous apparent matrix density distribution between 2.55 to 3.13 g/cm³ with volumetric photoelectric factors of 4 to 16 b/cm³. Occurrences of muscovite are observed, and the mineral variations comply with the heterogeneity discovered by QEMSCAN and XRD analyses. The calcareous formations predominantly

²This term is officially no longer used in geological chronostratigraphy (Gradstein et al. 2004) but was hereby adapted from technical reports.

Table 5.1: Engineering classifications of the Molasse Rouge rock used for the HL-LHC construction. Mineral composition given in wt%. w =water content (%), w_{LL} =liquid limit (%), w_{PL} =plastic limit (%). σ_c =uniaxial compressive strength (MPa), E_S =stiffness (MPa), $\sigma_{ti,b}$ =Brazilian tensile strength (MPa), I_S =point load test index (MPa). V_P =compressional wave velocity (m/s), RQD=rock quality designation index. *4-type classification after Canzoneri et al. 2018. **6-type classification after Fern et al. 2018. ***French expression for *lumpy*.

rock classification (basic)*	rock classification (extended)**	mineral composition	geotechnical properties	rock descriptions
<i>grumeleuse</i> *** marl	very weak marl	-	$w \approx 8.6$, $w_{LL} \approx 51.4$, $w_{PL} \approx 25.0$, $\sigma_c \approx 3.7$, $E_S \approx 340$, $I_S \approx 0.22$, $v_P \approx 2240$, $RQD \approx 71$	numerous, closed micro-fissures; low stiffness; ductile behaviour; swelling potential
platty marl	weak (<i>laminated</i>) marl	clay: 45-60, quartz: 15-30, calcareous minerals: 20-30	$w \approx 6.7$, $w_{LL} \approx 48.0$, $w_{PL} \approx 23.0$, $\sigma_c \approx 8.0$, $E_S \approx 690$, $I_S \approx 0.33$, $v_P \approx 2500$, $RQD \approx 91$	micro-crystalline quartz; medium-high plasticity; mostly illite but smectite and chlorite up to 18%; minor micro-fissures; swelling potential
sandy marl	medium-weak marl	clay: 20-45, quartz: 20-40, calcite: 20-30	$w \approx 5.0$, $w_{LL} \approx 34.8$, $w_{PL} \approx 20.7$, $\sigma_c \approx 15.0$, $E_S \approx 1960$, $I_S \approx 0.57$, $v_P \approx 3040$, $RQD \approx 97$	well cemented; low-plasticity
sandstone	weak sandstone	clay: 5-20, quartz: 40-70, calcareous minerals: 5-45, feldspar: 5-10	$w \approx 7.8$, $\sigma_c \approx 10.8$, $E_S \approx 1230$, $I_S \approx 0.26$, $v_P \approx 2455$, $RQD \approx 96$	fine-grained; poorly cemented;
	medium sandstone		$w \approx 4.1$, $\sigma_c \approx 22.9$, $E_S \approx 3420$, $I_S \approx 0.7$, $v_P \approx 3340$, $RQD \approx 98$	
	strong sandstone		$w \approx 3.0$, $\sigma_c \approx 46.1$, $E_S \approx 9417$, $I_S \approx 1.59$, $v_P \approx 3955$, $RQD \approx 99$;	better-cemented grains; fewer discontinuities compared to the medium sandstone

lie inside the blue triangle (Fig. 5.2) with a tendency to both dolomite and calcite (Fig. 5.2). The glaciogenic deposits reflect a similar behaviour, with less variations for the matrix density ranging up only to 2.95 g/cm^3 , showing lesser abundance in muscovite and no tendencies to anhydrite or calcite.

Fig. 5.1 shows a high volume of clay-bound water at depth intervals from 130 to 140 m ASL and 150 to 200 m ASL. Clay-bound-water decreases upwards towards surface topography level. Water content (formation water) remains constant from 375 to 80 m ASL but shows an increasing trend between 70 and 20 m ASL, together with higher sand and reduced silt and clay content (Fig. 5.1). QEMSCAN and sand-silt-clay model results follow similar trends in the Molasse Rouge. The high amount of silt could be associated to the indication of low-permeable intervals in the NPHI-RHOB cross-plot, as well as V_{sh} log calculations depicting a similar trend.

The Molasse Rouge tends to contain both dispersed and structural shale, with single samples showing clean (sand-rich) zones. These clean zones are mostly related to porous, sand-rich rock (see section 5.3). The Mesozoic clayey limestone shows little content in clay minerals.

The log solid rock volumes correlate well with mineralogical analyses. The PEF log serves as a robust tool for a first rock type characterisation. Estimations of sand-silt-clay volumes and associated clay type (Fig. 5.3) confirm the applicability of a solid predictive approach based on well-logs. Apart from the feasible, predictive measure for the FCC site investigations prior to any laboratory analyses, it should be noted that the petrophysical log calculations are calibrated to mineralogical analyses that yield upper and lower boundaries of the GR shale- and sand-dominated intervals. Ultimately, this influences V_{sh} calculations, CEC, core porosity and core grain density inputs, which are suggested to be considered as future proxies.

Lithotyping solely based on petrophysical analyses suggests successful log calibration applied to compensate for the Molasse Rouge's heterogeneity and adequately define sand- and shale-bearing intervals if derived by the PEF log rather than the GR log. The GR log alone is not sufficient to properly distinguish between sand- and shale-dominated intervals due to the heterogeneity of the Molasse Rouge formation. The PEF log is commonly part of modern well-logging campaigns (part of the RHOB log)

and would prove to be a reliable indicator.

A clear distinction between the Molasse Rouge and Grès et Marnes Gris à gypse formations could not be established solely based on well-logs without explicit laboratory analyses (Fig. 5.4), since the difference of e.g., the SP log values by -20 mV reflects the error to be overcome by mineralogical analyses (Fig. 5.1). As identified in a geochemical-mineralogical well-logging study by La Vigne et al. (1994), shale formations are comprised of between 35% to 70% of clay minerals with formations containing close to 100% clay minerals are rare in nature. Using core-based mineralogical analysis to evaluate geochemical well-logs, the study by La Vigne et al. (1994) has shown clay mineral abundances in eight wells and have found that the shaliest formations contain only about 60% clay minerals. This is very similar to the Molasse Rouge samples and well-log analysis presented herein with total clay volumes of up to 58%.

5.3 Rock classification scheme based on multi-proxy cross-correlations

Chapter 4 investigated the large-scale basin's geology and intersected it with the currently planned FCC subsurface layout. This section aims to elucidate on a characterisation of sampled rock material on a micro-scale in the Cenozoic glaciogenic deposits, Molasse Rouge and Siderolithic formations. The rock characterisation follows the aforementioned rock features such as colour, odor, texture, consistency, sedimentological and geological features (Fig. 5.5) and extends it by the mineralogical, geochemical, petrophysical, and physico-chemical behaviour as analysed by the comprehensive set of laboratory analyses (see chapter 3) and respective cross-correlations among rock properties relevant for predicting potential application scenarios or disposal discussed in chapter 6.

5.3.1 Mineralogical composition and physico-chemical properties

QEMSCAN and XRD analyses are considered to be the predominant choice of mineralogical analyses because

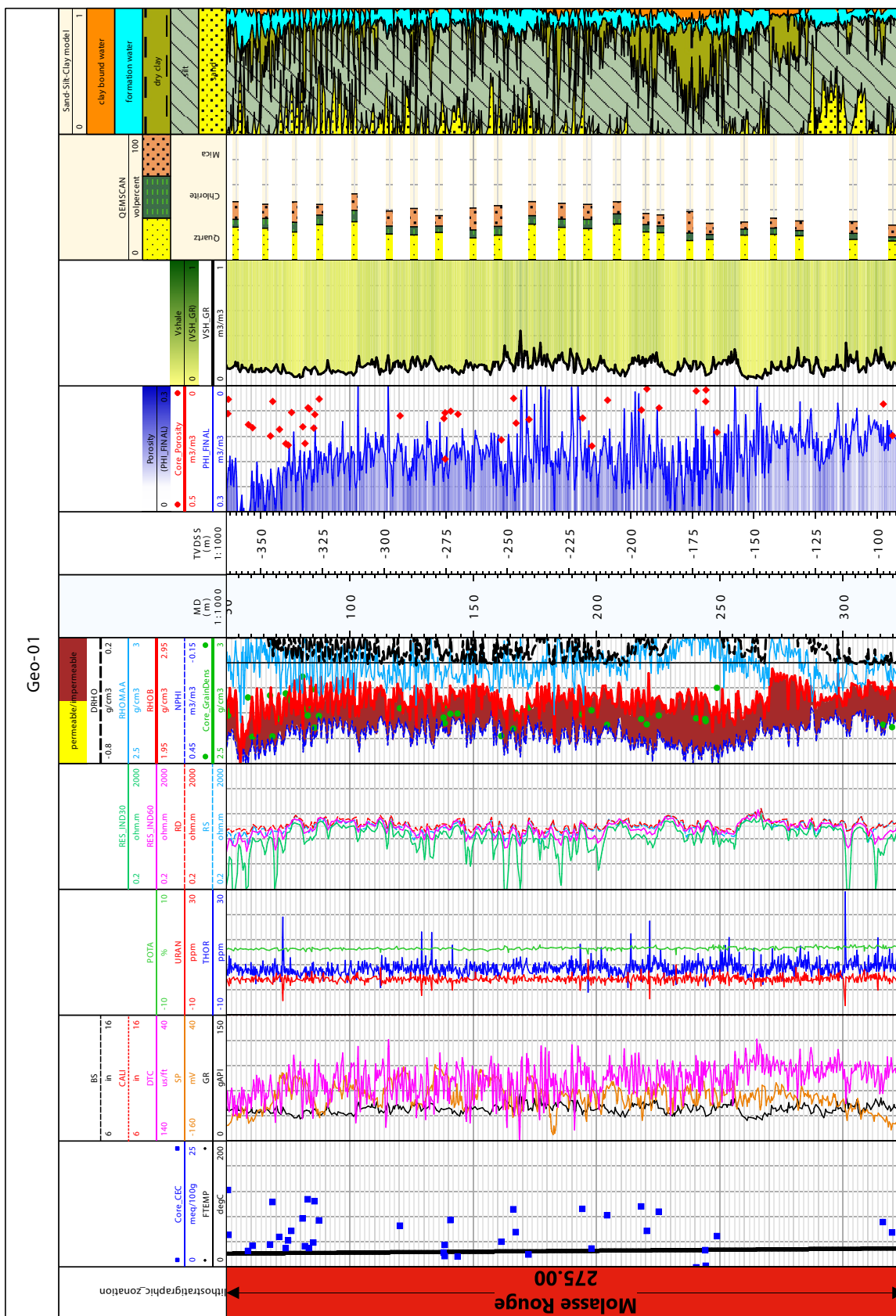


Fig. 5.1: Calculated sand-silt-clay model for well Geo-01 showing volume estimates for sand, silt and wet/dry clay, formation water and clay-bound water (CBW). Note the impermeable zone based on the neutron and density logs along the Molasse Rouge formation. After Haas et al. (2022).

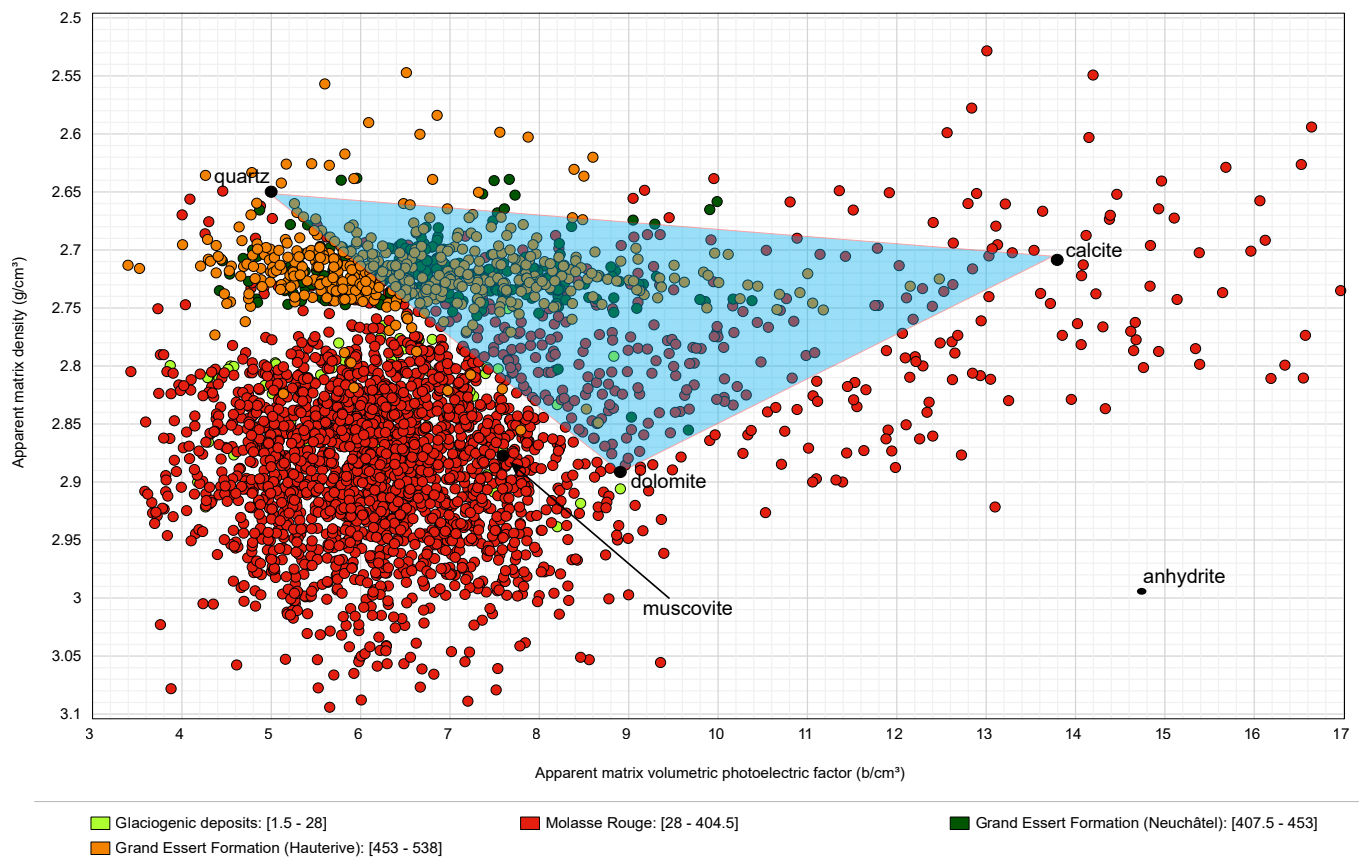


Fig. 5.2: Matrix density and volumetric photoelectric factor for the derivation of lithotypes based on RHOB and PEF well-log calculations in well Geo-01. Numbers in brackets depict top and bottom of formation. After Haas et al. (2022).



Fig. 5.3: Clay-type derivation using a Thomas-Stieber plot for eight formations. A trend towards dispersed shale is distinguished for the Hauterive Member of the Grand Essert Formation. Clay distribution for the Molasse Rouge ranges between the structural and dispersed types. After Haas et al. (2022).

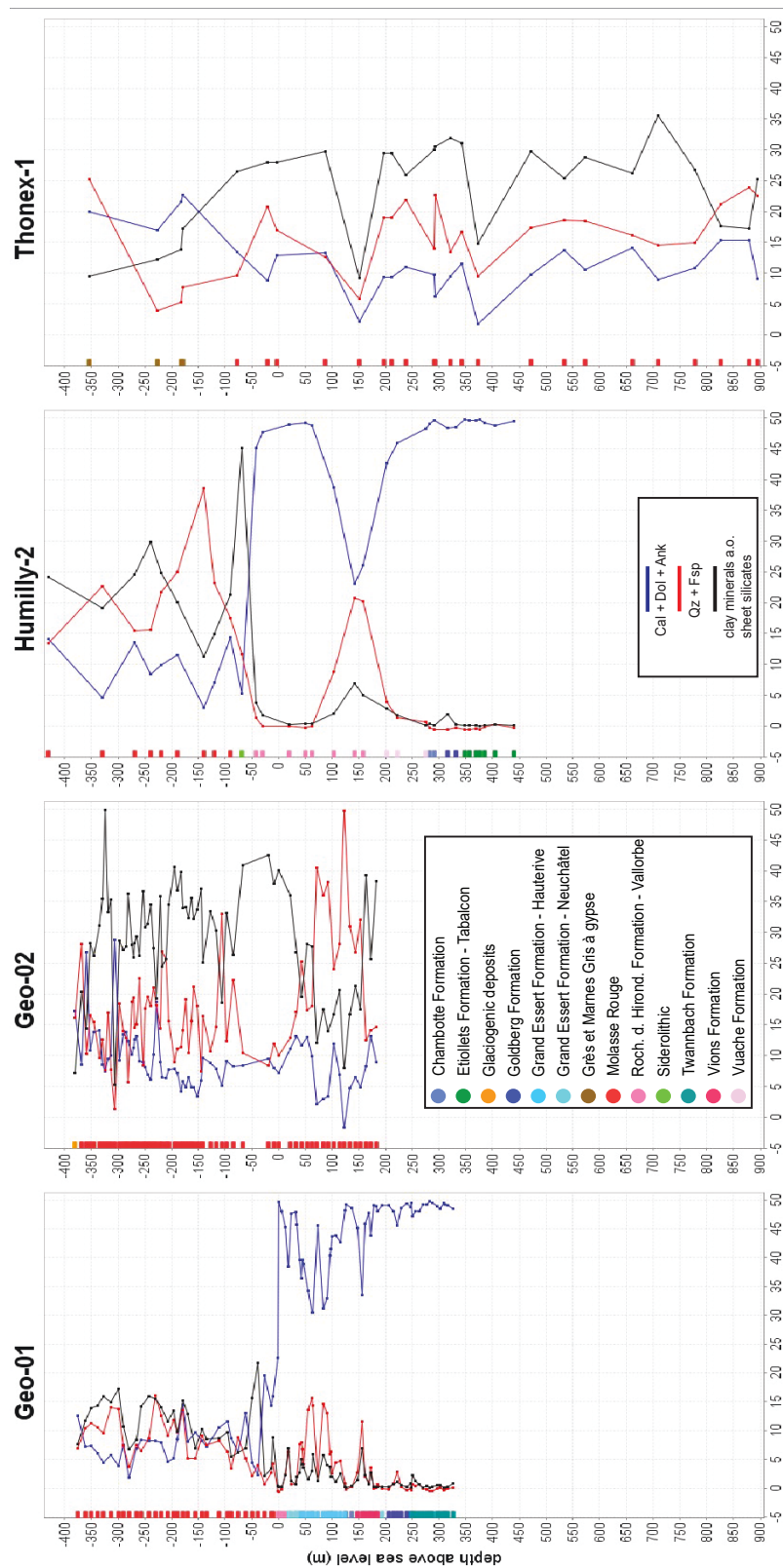


Fig. 5.4: Lithotypes derived for wells Geo-01, Geo-02, Thônex-1 and Humilly-2 in the northern part of the FCC construction area based on QEMSCAN analyses. The current FCC depths range between -100 and -300 m ASL. The transition to calcareous formations is well captured by the kink in blue curves (e.g. Geo-01 or Humilly-2 at ca. 0 and -50 m, respectively). Mineral abbreviations: Qz=quartz, Fsp=feldspar, Cal=calcite, Dol=dolomite, Ank=ankerite. After Haas et al. (2022).

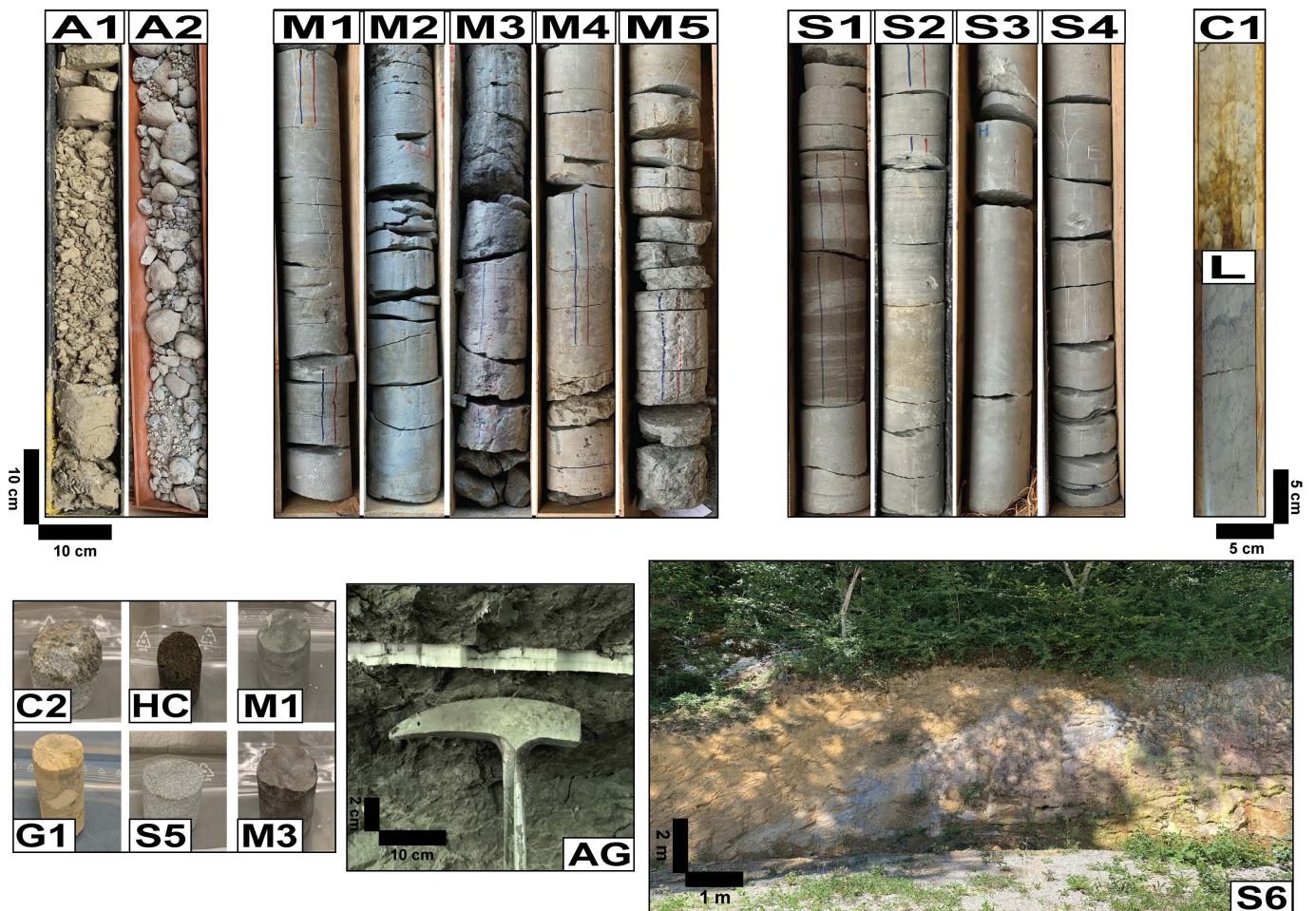


Fig. 5.5: Lithotypes analysed in the field and on rock cores encountered along the FCC's current tunnel alignment at different scales analysed from small-scale drilled plugs to rock cores and large-scale outcrops. A1-A2=Quaternary glaciogenic deposits, M1-M5=different marls as part of the Molasse Rouge formation, S1-S5=different sandstones as part of Molasse Rouge formation, S6=sandstone as part of the Siderolithic formation, often referred to as Gompholite, HC=hydrocarbon-bearing sandstone in the Molasse Rouge formation, C1-C2=different conglomerates as part of the Molasse Rouge formation, L=freshwater limestone as part of the Molasse Rouge formation, G1=sandstone as part of Siderolithic Formation, AG=gypsum layer in the Molasse Rouge. After Haas et al. (2022).

of the robustness of quantitative results for fine-grained material (XRD) and mineral distributions in image analysis (QEMSCAN). XRD analyses on powder (Fig. 5.7), textured and ethylene glycol treated samples provide a robust quantitative determination of mineral composition (Fig. 5.6, 5.8). QEMSCAN image analyses are used to investigate rock texture, quantitative mineralogy and grain size distributions of quartz. These two measurements mark the first laboratory analyses to be consecutively incorporated into the following discussion. Terms such as *sand-rich rocks* are used in case the rock contains more than 30% of quartz, and generalized terms characterise sand-rich, clay-rich, gravel, conglomerate, (violet) marl and (Freshwater) limestone lithotypes. This is based on the idea to not bias the rock classification scheme to samples with extreme values contradicting the behaviour when compared to samples containing a *clean* rock type. This is a necessary consequence of the heterogeneity of the Molasse Rouge sedimentary rock with cross-correlations of rock properties used to derive common rock patterns. The average transition depth between the glaciogenic deposits and Molasse Rouge formation lies at ca. 35 m for wells Geo-02 and Peissy-I (Fig. 5.7). X-ray diffractograms yield similar patterns within 10-20 m, whereas quantitative analyses show that the main differences originate from the clay mineral type and amount, quantified on textured (S) and ethylene glycol (EG) treated samples at 2-theta angles between 2 to 32°. The latter sample type allowed for the essential identification and quantification of smectite (montmorillonite, i.e. Ca-montmorillonite) by peak separation (Fig. 5.8). The main quantified minerals in XRD powder samples are albite, quartz, calcite, orthoclase, muscovite, clinocllore, antigorite, dolomite, gypsum, bassanite, ankerite, and phyllosilicates including clay minerals such as kaolinite, mica/illite, talc, serpentine, chlorite, and smectite in the form of Ca-montmorillonite when checking the type of exchangeable cations (Fig. 5.34).

The northern wells close to the FCC show varying mineral compositions based on their digitised data. All SLHC wells contain a substantial amount of clay minerals from 0 to 50% compared to the SPL boreholes. Wells SPM11 and L135 closer to the Jura mountains show increased calcite contents. All SLHC boreholes indicate a low chlorite and smectite but high illite content with the only exception at SLHC20. The limestone lithotype contains quartz

contents below 10% excluding outlier samples in L135 and SPM1. Wells in close vicinity to the FCC alignment are drilled up to a depth of 100 m. Wells located in the western area close to the Jura mountains have a depth greater than 100 m.

Smectite (montmorillonite) values in XRD samples reach up to 17.2% (Fig. 4.8) (Haas et al. 2022). Respective mean values range at ca. 6% (C1), 11.5% (C3), 10% (Geo-02), 6% (Gex-CD-04), 7% (Gex-CD-05), 10.8% (Gex-CD-06), 8% (Gex-CD-07), and 9% (Peissy-I). All described samples except the Mornex samples contain smectite, whereas values on average range between 7-12%. Samples G2-10 (high dolomite content), C1-02D and C1-04A contain smectite values below 4%. Pei-I-19C is likely associated with the violet marl category, represented by the violet colour and increased amounts of calcareous minerals compared to the sand-rich and clay-rock categories. A similar mineralogical pattern applies to Pei-I-19B. Except for sample Geo-02-248, no Geo-02 samples in XRD analyses contain any K-feldspar. Dolomite content progressively increases from samples in the north towards the south of the basin, when comparing the C1-C6 and Geo-02 samples with the ones from the Gex-CD-01, -04, -06 and -07 wells. It is observed that dolomite contents tend to be at a low level in the northern part of the basin with samples of the Peissy-I well showing dolomite contents between 5-10%. Samples Geo-02-130, -190 and -216 show one of the highest amounts of clay content with 53% on average.

Across all investigated formations, the classified sand-rich rocks contain predominantly the minerals quartz, K-feldspar and Na-plagioclase. These are contemplated by the minerals biotite, chlorite, illite, kaolinite, montmorillonite (smectite), muscovite, phlogopite, pyrophyllite, serpentine, talc and paragonite for clay-rich and marly rocks. The freshwater limestone rocks contain calcite, dolomite, ankerite and siderite.

Findings of kaolinite as well as the absence of the mineral corrensite in all XRD analyses contradict mineralogical analyses conducted as part of a thermal diagenesis study. Monnier (1982) has observed that during burial smectite disappears with the formation of interstratified minerals, and divided the smectite transformation into a first branch towards an irregular 2:1 mixed-layer silicate, and a second branch towards corrensite. He claims that the appearance of corrensite suggests an Mg-rich sedimentary

environment commonly found with anhydrite-bearing rocks nearby. However, the corrensite mineral has not been measured in this study questioning at least the second branch of smectite transformation. Anhydrite does occur abundantly in the Grès et Marnes Gris à gypse formation. This might substantiate the argument for the first branch for the smectite transformation and would also favour the hypothesis of a differentiation between western and eastern provinces (areas) of the GB with respect to its depositional subsidence and uplift scheme (see chapter 4). Illite occurs in increased quantities in Geo-02, Gex-CD-02 and -05. Comparing illite with smectite (montmorillonite) values suggests that the (irreversible) illite-smectite transition has occurred to a large portion and terminated in the northern part of the basin.

Clay-rich rock (siltstone)

Clay-rich rocks are exemplified by samples C1-04A (50.76 m), C1-15D (27.54 m), C1-18C (83.60 m), Pei-I-03C (41.72 m), G1-06 (111.60 m), G1-14 (168.85 m), as well as G7-10 (162.75 m), G7-15 (206.35 m), and G7-21 (234.65 m) at wells C1, Gex-CD-01 and -07. Samples C1-04A and C1-15D show similar mineralogical patterns (Fig. 5.6), with the major difference in their respective carbonate content represented predominantly by calcite and dolomite. C1-15D has distinctively more dolomite (ca. 10%), while sample C1-04A contains <5% but shows a higher calcite content of ca. 35% compared with C1-15D of ca. 20%. The quartz, total clay, K-feldspar and Na-plagioclase contents are similar with ca. 22%, 30-36%, 1-2% and ca. 5%, respectively. Samples C1-04A and C1-18C differ in their calcite content by 7% with ca. 35% in C1-04A versus ca. 28% in C1-18C. The major difference besides the lamination in sample C1-04A, is its value of ca. 1-2% of pyrite, which is 0% in sample C1-18C. In addition, C1-18C contains ca. 2% more dolomite, and the total clay content differs by ca. 5%. This distribution suggests a lower grade of carbonate (predominantly calcite) cementation in the C1-18C sample, compared to the C1-04A. C1-18C and G4-03 appear similar in the field, and also show similar mineralogical composition. Both contain between 24-27% quartz, 30-33% total clay, 2-4% K-feldspar; and a minor difference of Na-plagioclase with about 6% (C1-18C) versus 11% (G4-03). The predominant difference lies in the calcite contents depicted at 25% (C1-18C) versus 10% (G4-03). A distinct

feature is the low dolomite content of ca. 5% in C1-18C versus ca. 22% in G4-03.

The Geo-02-30 sample contains ca. 20% quartz, 0% K-feldspar, ca. 5% Na-plagioclase, ca. 30% calcite, 10% dolomite, 12% total clay and protrudes by its characteristic feature of ca. 16% gypsum and 4.4% bassanite, which are both unique minerals analysed among all XRD samples. This gypsum-enriched sample in well Geo-02 makes it only comparable to the samples TH-75, -201, and -250 m in Thônex-1 (Fig. 5.9) as part of the Grès et Marnes Gris à gypse formation (Fig. 4.11). The 30 m depth level for sample Geo-02-30 in well Geo-02 ranges at the same depth level as in the Thônex-1 well, making it likely that the basin contains increased amounts of gypsum compared to the underlying Molasse Rouge formation between 360 m ASL to 70 m ASL (Fig. 4.11). These increased gypsum contents are also represented by the AG lithotype depicting a fine layer of gypsum in the field (outcrop) close to Nyoux (Fig. 5.5). Although sample G5-17 shows similar mineralogical trends compared to samples C1-08C, C1-17C, C1-19B, C2-03A, Pei-I-08C and Pei-I-17B (Fig. 5.6), it occurs at a deeper borehole depth of 350 m compared to shallower depth levels of ca. 85 m on average for the aforementioned samples. G5-17 contains ca. 28% quartz, 2% K-feldspar, 8% Na-plagioclase, 15% calcite, 5% dolomite, and almost ca. 40% of total clay content (Fig. 5.6). The high amount of clay associates this sample to the clay-rich family with a smeary texture in the field. It is a good example of depicting similar mineralogical trends between clay- and sand-rich samples but a distinct difference in total clay content for the sake of either calcite or Na-plagioclase and K-feldspar. A similar mineralogical composition occurs for sample G7-17.

Based on their distinct beige colour, samples C1-16A (31.29 m), C3-01A (76.38 m), C3-03D (80.94 m), G1-04 (instead of G1-05; 42.50 m), Pei-I-02C (39.89 m), Pei-I-04C (50.56 m), Pei-I-10C (83.06 m), Pei-I-12C (87.59 m), Pei-I-15F (140.90 m), Geo-02-130 (130.00 m), Geo-02-190 (190.00 m), and Geo-02-216 (216.00 m) are summarised by its texture and colour in the field and titled *beige siltstone* depicting a sub-category of clay-rich rocks. Samples from well Geo-02 offer limited possibilities to be described visually in the field, as these were available as cuttings only. Hence, for the Geo-02 samples the XRD mineralogy (Fig. 5.6) is used as the main reference. Sample Geo-02-130 contains the least quartz amount with ca. 16% among all

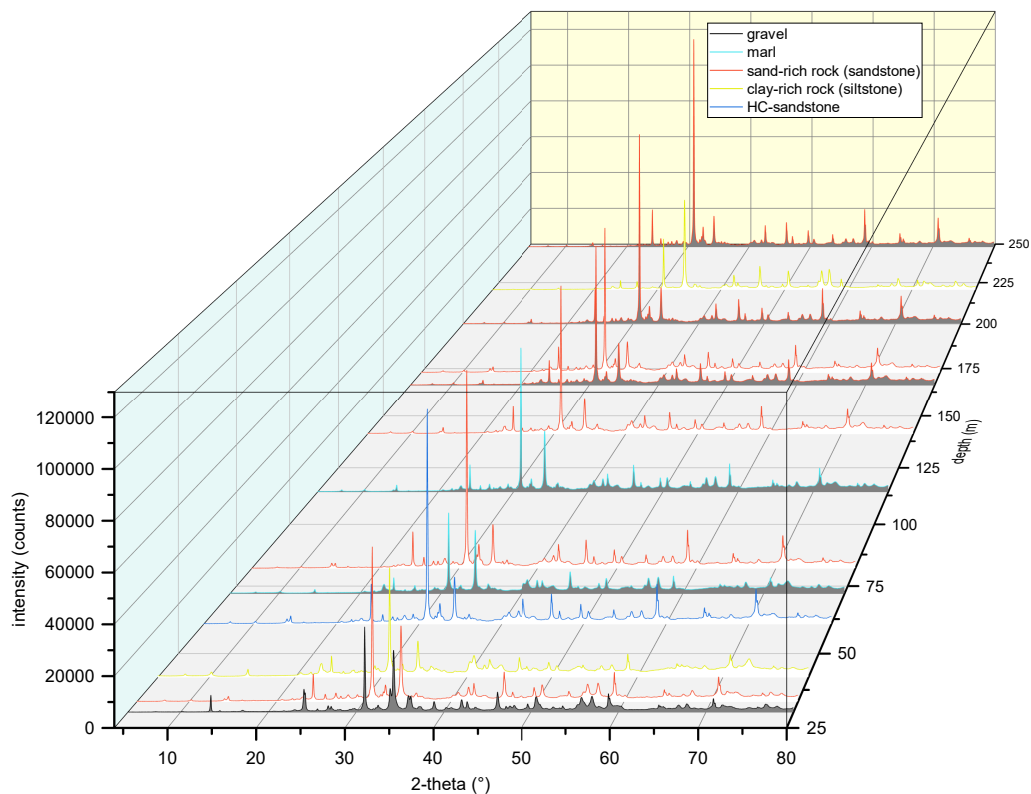


Fig. 5.7: Selected diffractograms of XRD powder samples measured from 4 to 80°2-theta angles along the depth of wells Geo-02 (grey area below curve) and Peissy-I (white area below curve) in the northern part of the FCC construction area. HC=hydrocarbon.

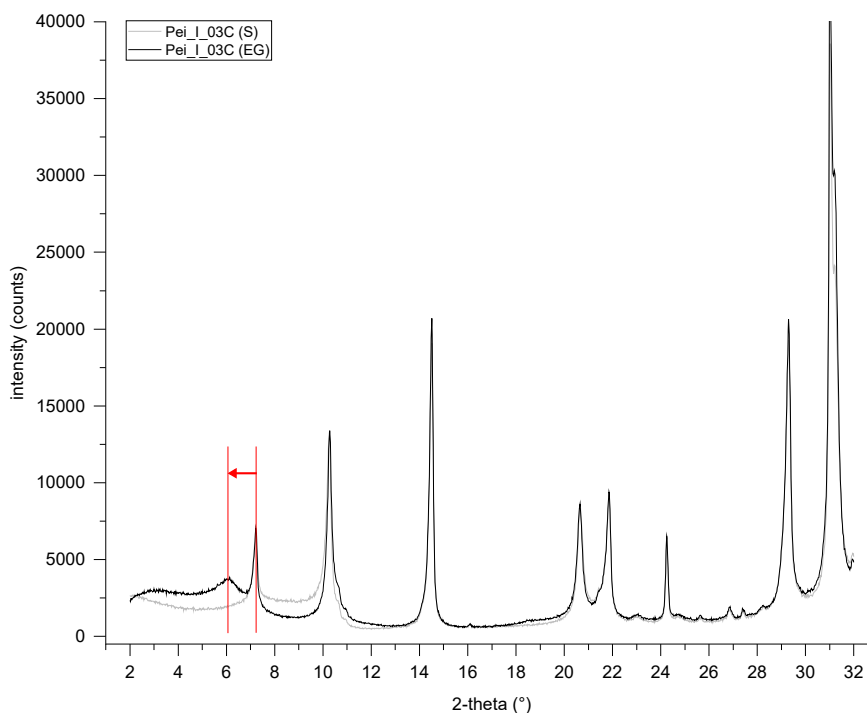


Fig. 5.8: Peak separation in XRD diffractogram of a textured (S) and ethylene glycol (EG) treated sample at the Peissy-I well. Incorporation of ethylene glycol shifts the broad peak at ca. 7°2-theta to 6°2-theta (d_{001} value) from 14 to 17 Å.

Geo-02 samples. With more than 50%, the Geo-02 samples contain the largest amount of total clay, while comprising a quartz content of <20% on average. Calcareous minerals depict values around 20%. Sample C1-16A contains slightly more calcite (ca. 20%) compared to C3-03D (ca. 15%), while both contain ca. 5% dolomite, making a difference in major carbonate minerals of ca. 5%. Ankerite and siderite play a minor role for total carbonate content with values ranging around or below 1%. C1-16A and C3-01A show similar mineralogical composition (Fig. 5.6). Pei-I-03C contains the highest amount of total clay across all XRD samples with ca. 60%. Despite it being similar in mineralogy compared to the violet marl, there is no distinct difference to sample Pei-I-04C in the field, which is attributed to the beige siltstone. The distinct feature of violet colour is missing in sample Pei-I-10C, which justifies its attribution to the beige siltstone category but appears weathered. This could be associated to the *weathered marl*, potentially depicting a transition between the (beige) siltstone and marl. Pei-I-12C shows similar mineralogical pattern compared to C3-01A, with the only difference of more dolomite and less calcite compared to C3-01A with ca. 10% versus ca. 3%, respectively. Pei-I-15F shows a similar mineralogical pattern compared to Pei-I-10C. This beige (M4) coloured lithotype is also encountered at Peissy-I at a depth between 82.50 and 83.46 m (Fig. 5.5).

Clay-rich samples show different types of cementation, being either cemented by calcite or clay minerals such as illite (or chlorite). Fig. 5.9 depicts 11 selected clay-rich samples across the Molasse Rouge formation at different depths in wells C1, Gex-CD-01 and -07. One sub-type of clay-rich rock is driven by increasing calcite content, i.e. cementation by calcite, while the second type is driven by predominantly illite cementation (Fig. 5.9). Quartz grain-size distributions show no notable differences in texture for both.

The type and grade of cementation seem to be two driving main factors for the characterisation of clay-rich rock. Both end members, either fully calcite-cemented (G1-14) or illite-cemented (C3-03D), are hereby noted in different classification terms: one end-member containing a large amount of calcite (calcareous minerals) is attributed rather to a marly lithotype with characteristics prone to marl. Similar to the violet marl (see below) it contains one of

the highest calcite contents. The second end-member comprises high amounts of illite and depicts a siltstone lithotype at various but always lower carbonate mineral contents compared to the violet marl. Most of the samples comprise a balance among the two extreme end-members having similar ratios of calcite (calcareous) minerals and clay minerals. A distinction in the field would only be possible by HCl acid treatment producing (more) CO_2 in case of calcite-rich marl samples.

All clay-rich rock samples depict quartz grain-size distributions settled at the lower end between 7.8-31 μm , with a few samples reaching into the 250-500 μm portion but none exceeding values above 500 μm . This makes clay-rich rocks generally very fine-grained in texture, which is also substantiated by the results of high-pressure mercury injection measurements (Table 5.2, 5.3, 5.4). All clay-rich rocks are comprised of small pore diameters with values between 4 to 50 nm as depicted by samples C1-04A, C1-15D, C1-16A, C1-18C, Pei-I-03C (Fig. 5.13, 5.14), in conjunction with low porosity and permeability values (Fig. 5.38) below 15% and 1 mD, respectively. This results in calculated flow zone indicator (FZI) slopes below 0.01 due to their high clay content and grade of cementation by either clay minerals (illite) or calcite (Fig. 5.9, 5.15) as elaborated in section 5.3.4.

Marl

Rocks consisting predominantly of calcareous minerals with clay minerals and quartz are classified as (violet) marl (Fig. 5.6) given their distinct violet colour inspected in the field. This classification type is best represented by samples G4-11 (148.85 m) and G4-25 (231.40 m) (Fig. 5.10). Further selected violet marl samples are G1-13 (161.70 m), G1-38 (236.60 m), G1-39 (233.70 m), G2-02b (228.85 m), G2-23 (300.00 m), G4-24 (223.10 m), G4-47 (204.50 m), G6-01 (316.30 m), G7-23 (166.40 m), Geo-02-82 (82.00 m), Geo-02-114 (114.00 m), Geo-02-178 (178.00 m), Geo-02-206 (206.00 m), Geo-02-228 (228.00 m), Pei-I-06C (68.73 m), Pei-I-11C (85.82 m), Pei-I-14A (124.61 m), Pei-I-14E (125.77 m), and Pei-I-19C (220.44 m).

G1-39 is used as an example instead of G1-38 sample, separated in depth by just 3.3 m located in the same formation at 233.30 m of well Gex-CD-01. The M1-M2 lithotypes depict different (clay-rich) marl- and siltstone that vary in colour and grain size from very fine to fine-grained in well Peissy-I at depth levels from 125.12 and 126.12 m and

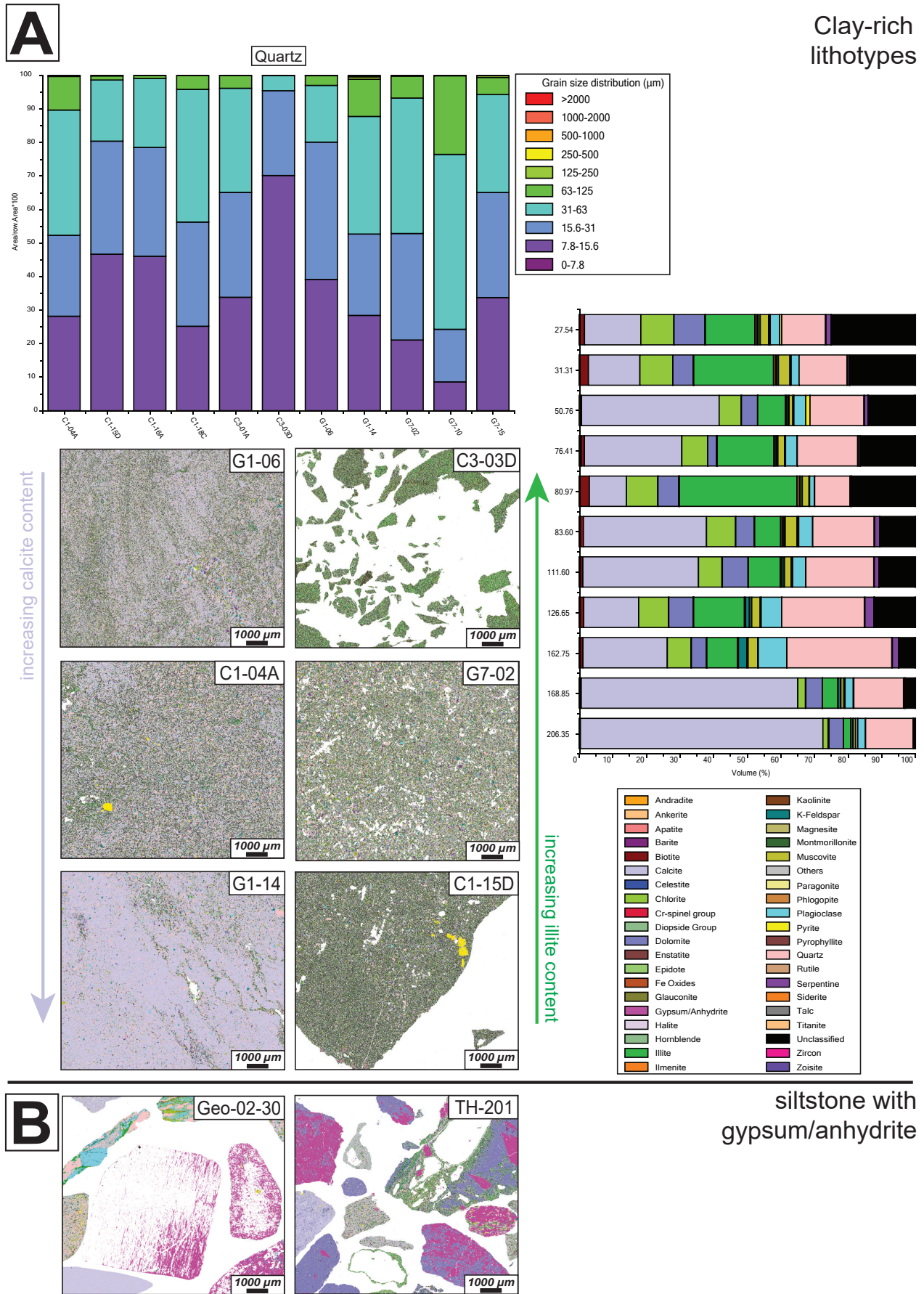


Fig. 5.9: (A) Image analyses and quartz grain-size distribution via QEMSCAN with associated modal mineralogy of various clay-rich samples in the Molasse Rouge formation. (B) Clay-rich (siltstone) samples depicting an increased amount of gypsum/anhydrite in the Grès et Marnes Gris à gypse formation, encountered at wells Geo-02 and Thônex-1, potentially subjected to swelling issues (see chapter 4.5).

between 42.30 and 42.90 m (Fig. 5.5), respectively, also depicting the transition among clay-rich rocks (siltstone) and (violet) marls. The category introduced herein would be comparable with the *lie-de-vin* rocks mentioned in the literature (Charollais et al. 2007).

All Geo-02 samples are solely based on mineralogy as there are no plugs available to inspect visually. The samples show similar mineralogical patterns when compared e.g. with sample G4-47. Sample G4-47 is defined as a typical violet marl sample based on its violet colour, and contains ca. 26% quartz, 2% K-feldspar, ca. 6% Na-plagioclase, ca. 25% calcite, 7% dolomite, and a large amount of total clay content with ca. 37%. The violet marl samples show strongly varying calcite and clay mineral contents, which makes their clear separation often difficult, in particular when values lie within 5-10% difference. Among the Geo-02 samples, the -82 sample contains the most quartz, while -114 contains the least with ca. 29% and ca. 26%, respectively, while always containing the highest amounts of calcareous minerals (calcite and dolomite) with at least 30%. Sample G6-01 depicts a violet marl with slightly different mineralogical distributions compared to the typical G4-47. Its quartz content lies at ca. 21%, while K-feldspar and Na-plagioclase contents are similar to G4-47 at ca. 2%. Calcite content depicts similar values with ca. 25% but G6-01 has an increased content of dolomite with ca. 14% for the sacrifice of a lower total clay content of ca. 28% compared to G4-47 (Fig. 5.6, 5.10). Sample G7-23 shows a similar mineralogical composition as G4-47 with the only difference having a higher Na-plagioclase content by ca. 4% compared to G6-01. The calcite content of G7-23 varies between G6-01 and G4-47 being at ca. 18%, and could potentially be associated to a clay-rich rock or the transition facies if it lacked the violet colour. The amount of dolomite is similar to both G4-47 and G6-01, while the total clay content is similar to rather G4-47 with ca. 38%. Sample Geo-02-228 shows increased amounts of dolomite compared to other samples of this category. Samples Pei-I-06 and Pei-I-11C depict further typical violet marl samples based on mineralogical patterns and their violet colour as inspected in the field. Pei-I-19C looks like the typical violet marl sample and contains the highest amount of calcite of all violet marls with a value of ca. 55%. The remaining minerals show a similar distribution. This brownish-violet (M3) marl lithotype is encountered e.g. in well Gex-CD-01 at a depth from 40.96–41.90 m (Fig. 5.5). The brownish

colour probably originates from Fe-hydroxides (weathering).

Fig. 5.10 refers to the calcareous-rich end-member of clay-rich samples as aforementioned. All violet marl samples are very fine-grained with their main percentage of quartz grain sizes ranging between 7.8 and 31 μm . While some of the violet marl contain high amounts of calcite, the transition to (Freshwater) limestone is only indicative by the absence of lamination in limestone comprising massive, compact rock samples with no plasticity or smeariness in the field. During the preparation of thin sections, the marly (and clay-rich) rocks tend to wash off easily (Fig. 5.9, 5.10). This adhesive behaviour predominantly depends on the amount of clay minerals present in general, as the smeariness tends to increase the adhesion on the glass plate. This is a similar behaviour encountered during the preparation of a textured XRD sample.

All analysed marl samples depict small flow zone indicator (FZI) values below the slope of 0.1 (e.g. Pei-I-19C), and show similar, low pore diameter results ranging between 4 and 60 nm (Pei-I-11C, Pei-I-19C), with even smaller pore diameters for sample G4-47 ranging only up to 40 nm (Fig. 5.15). Both rock quality indices and normalised porosity values range at the very low end with 0.001 μm and between 0.01 and 0.1.

Sand-rich rock (sandstone)

The sand-rich rock category is classified based on samples C1-02D (46.35 m), C1-08C (67.82 m), C1-17C (85.38 m), C1-19B (35.92 m), G1-19 (188.60 m), G4-07 (138.65 m), G4-08 (143.85 m), G4-16 (164.85 m), G4-18 (167.40 m), G5-10 (370.78 m), G5-11 (379.74 m), G5-20 (360.50 m), G7-06 (138.15 m), G7-07 (138.40 m), G7-09 (151.50 m), G7-11 (193.50 m), G7-12 (194.40 m), G7-18 (225.60 m), G7-19 (226.80 m), Sarzin-real (outcrop, 0 m) and Verney-left (outcrop, 0 m). Samples C1-08C, C1-17C, C1-19B, C2-03A, Pei-I-08C and Pei-I-17B are classified as very sand-rich rocks with more than 30% quartz, more than 30% total clay, ca. 10% calcite, 2-3% dolomite, ca. 3% K-feldspar, and ca. 13% Na-plagioclase (Fig. 5.6). Pei-I-08C contains slightly less quartz with ca. 27% compared to C1-08C, and feels more coarse-grained in the field when compared to e.g. sample Pei-I-17B, which shows similar mineralogical patterns but has large (>1 mm) grains incorporated into the matrix. Sample C1-02A contains ca. 10% more

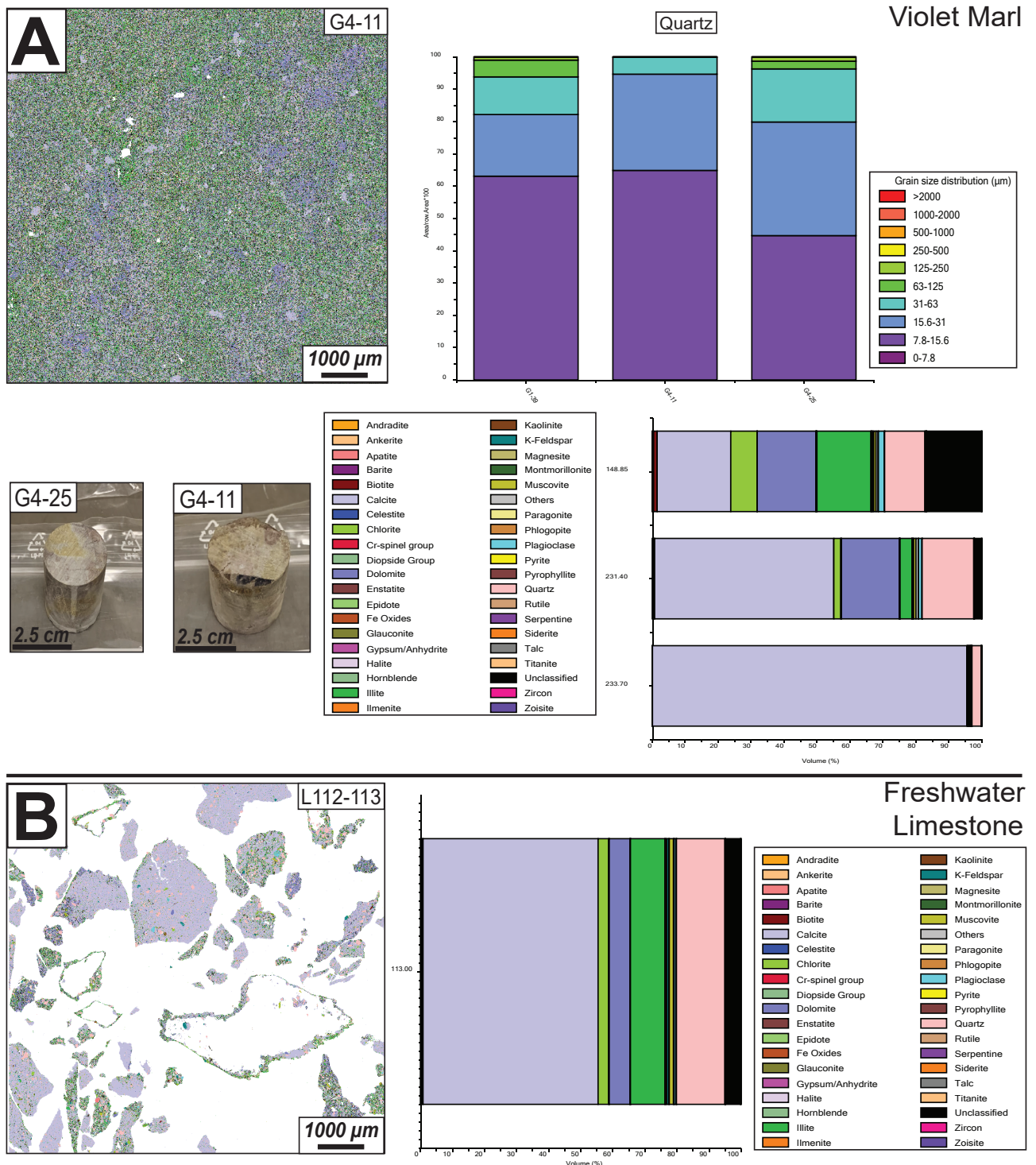


Fig. 5.10: Image analyses and quartz grain-size distribution via QEMSCAN for the violet marl (A) and freshwater limestone (B) with associated modal mineralogy of the Molasse Rouge formation.

calcite compared to sample C1-17C. This suggests carbonate cementation and a reason why C1-02A feels more fine-grained in the field compared to C1-17C. However, the remaining mineral contents of quartz, feldspar and total clay are similar (Fig. 5.6). These samples tend to be sand-richer in quartz values of ca. 30%, but comprise more calcite of ca. 10% compared to samples C1-08C, C1-17C, C1-19B, C2-03A, and Pei-I-08C. Sample G2-10 contains the highest content of dolomite with ca. 55%, marginal traces of calcite with ca. 1%, only ca. 12% of quartz, and ca. 25% of total clay, making this sample a transition from sand-rich to (Freshwater) limestone (dolomitic?) at a depth of ca. 249 m in Gex-CD-02. G4-07 is a sand-rich sample with >35% quartz, and the highest amount of K-feldspar with ca. 5%, the largest amount of Na-plagioclase with ca. 19% among all XRD samples, and ca. 10% calcite, <2% dolomite and ca. 25% total phyllosilicates.

Based on its low calcite content, there is predominantly clay mineral cementation and hardly any calcite cementation. Samples G5-18 and G6-10 show similar mineralogical patterns with the only difference of an increased calcite content by a difference of 5% in the G6-10 sample for the sacrifice of a 5% decrease of Na-plagioclase. G7-08 shows similar patterns but double the calcite amount of 22% for a decreased Na-plagioclase content at ca. 12%. Sample Pei-I-20C feels very coarse-grained in the field and depicts small (<1 mm) grains compared to aforementioned samples. However, it is more cemented given by the highest calcite content of all the samples in this category with a value of ca. 35%. G4-08 is similar to G4-07 but G4-08 contains 12% more calcite, which makes it appear greyer in colour and ca. 7% less quartz. This extra calcite gives it a higher grade of cementation. In comparison to C1-18C, G4-08 contains a similar amount of calcite but C1-18C is more clay-rich with ca. 33%, and contains ca. 6% of Na-plagioclase. G5-10 and G5-11 show similar mineralogical patterns compared to G4-08. Sample G5-13 is mineralogically similar to G4-08, G4-18, G5-10, G5-11, G5-20 and G7-06 but with two predominant differences: one being the increased amount of smectite with ca. 12%, and the other being the increased amount of serpentine with ca. 9%, depicting the highest amount among all XRD samples. G7-12 depicts the sample with the highest quartz content of ca. 73% in the Molasse Rouge formation. This defines the upper quartz-range limit, while completely lacking any carbonate minerals. With respect to clay content and clay

mineral distribution, the highest amount of kaolinite occurs in this sample with ca. 20% with only ca. 2% of chlorite, smectite, mica and Na-plagioclase.

Fig. 5.11 allows conclusions on the type of encountered minerals to be correlated with a sample's texture for the sand-rich rock category. The amount of serpentine seems to be distinctively correlated to coarse-grained (porous), sand-rich rock (sandstone). This deems necessary to further investigate the rock texture in QEMSCAN image analyses, as well as pore diameter distributions, porosity and permeability. In case they are less porous, the amount of smectite is increased as depicted in sample G5-13 while still being rich in quartz (sand-rich). Based on QEMSCAN image analyses (Fig. 5.11) as well as pore size distributions (Fig. 5.13, 5.14, 5.15), the sand-rich samples could be classified into three sub-categories yielding fine-grained, medium-grained and coarse-grained textures of sand-rich (sandstone) rock samples. Sample C1-02D comprises a fine-grained sample with pore diameters between 50-100 nm while the coarse-grained, hydrocarbon-bearing Pei-I-05B sample shows pore sizes between 4'000 and up to 60'000 nm, and Pei-I-16D even up to ca. 100'000 nm (Fig. 5.14).

Pei-I-05B is polluted by hydrocarbons as is sample G1-HC, which is easily recognizable in the field due to its hydrocarbon smell and coarse-grained (porous) texture. Sample G1-HC depicts a typical HC-bearing sandstone at a depth of 176.40 m in well Gex-CD-01 explicitly investigated in QEMSCAN (Fig. 5.11). It contains ca. 33% quartz, 3% K-feldspar, 10% Na-plagioclase, 15% calcite, 2% dolomite and 33% total clay minerals. The G1-HC sample shows the largest quartz grains with up to 1'000 μm , followed by a decreased percentage of quartz grain sizes between 125-250 μm in sample C1-19B, and up to 250-500 μm in sample G7-19 (Fig. 5.11). Pei-I-09D shows a similar mineralogical pattern with slightly higher amounts of Na-plagioclase, while sacrificing the additional content by less smectite compared to Pei-I-05B. Pei-I-16D and Pei-I-18B show similar mineralogical patterns compared to Pei-I-05B and -09D, whereas hydrocarbon amounts are lower, even questionable, based on their decreased hydrocarbon smell when inspected in the field. The well report, however, indicates traces of hydrocarbons. The hydrocarbon-polluted sandstone shows porosity values of 16-22% but at varying permeability values of ca. 46 mD (Pei-I-05B) to ca. 370 mD (Pei-I-16D), and up to 1087 mD (G4-17). The grain

size distribution of quartz is a good indicator among all sub-types for their texture (Fig. 5.11).

Fine-grained samples comprise the most percentage of 7.9-15.6 μm quartz grain-size distribution (green box), while increasing quartz grain sizes are apparently attributed to increasingly coarse-grained samples. The porous texture seems to be a characteristic feature for both serpentine- and hydrocarbon-bearing sandstones in the Molasse Rouge formation, exemplified by various porous sandstone bearing hydrocarbons such as the G1-HC sample in well Gex-CD-01 (Fig. 5.11). There is a direct correlation among increased grain sizes of quartz with their coarser-grained texture, which is also partly reflected in the high-pressure mercury injection measurements and the calculation of the flow zone indicator values (FZI, Fig. 5.39). The pore size distributions substantiate these findings by yielding pore diameter results at maximum values between 3'000 and 60'000 nm (red curve, Pei-I-05B), and a more porous, sand-rich rock (blue curve, Pei-I-16D), which goes along with increasing porosity and permeability yielding 20-30% and 1-1'000 mD, respectively. It should be mentioned that the MIP measures effective porosity, i.e. connected pores, which contribute to flow, and could be associated to absolute (single fluid) permeability in the presence of only hydrocarbons (Pei-I-05B). Hence, the sand-rich rocks that tend to have a high porosity, also show high permeability values, which is indicated by the pressure, as well as dedicated porosity and permeability analyses via gas flow (Fig. 5.38) and the respective calculations of flow zone indicators (Fig. 5.39) based on their low grade of cementation. From the measured samples, the coarse-grained Pei-I-05B sample shows a high value at an FZI slope of ca. 0.3 (Fig. 5.39) together with an even larger FZI slope of sample Pei-I-16D at ca. 0.5, also correlated with larger pore diameters. In a similar trend, fine-grained, sand-rich rocks (e.g. sample C1-02D) range at an FZI slope of ca. 0.006, depicting both a bad flow behaviour and low porosity. This suggests that the pores reflect effective porosity, i.e. interconnected pores. There also seems to be a shift from fine- to medium- to coarse-grained samples depending on the type and grade of cementation.

Fine-grained textured samples contain the highest amount of clay mineral illite, with small concentrations of smectite (illite-smectite transition). Both the medium- and coarse-grained samples shift towards higher content of smectite as well as chlorite, while simultaneously depicting increased

quartz grain sizes. Another distinct feature is the presence of serpentine in medium- to coarse-grained samples including hydrocarbon-bearing samples. Encountering serpentine, in particular, in sand-rich, coarse-grained (porous) intervals facilitates its recognition in the field, as this characteristic texture of rock could be identified in the field, which supports its practical identification and first qualitative estimate on-site. S1-S4 lithotypes show these sand-rich rocks, partly hydrocarbon-impregnated (S1), at a depth between 100.69 and 101.51 m, fine-laminated silty sandstone (S2), massive, compact sandstone (S3) at a depth between 58.95 and 59.90 m, and porous, fine-grained sandstone (S4), all cored along well Peissy-I. HC depicts the hydrocarbon-impregnated sandstone lithotype in Gex-CD-01 at a depth of 188.10 m, and very fine-grained, laminated sandstone (S5) is encountered in well Gex-CD-04 at 120.22 m (Fig. 5.5).

While the aforementioned samples all refer to the Molasse Rouge formation, another sand-rich rock (sandstone) type is depicted as part of the Siderolithic Formation. It is represented by sample Sarzin-real and contains ca. 73% quartz and ca. 26% kaolinite, which is the highest content of kaolinite together with the G7-12 sample across all investigated Cenozoic formations. It is not part of the three-class texture classification introduced for the sand-rich rocks (sandstone) of the Molasse Rouge formation, though. The second Siderolithic sandstone sample shows a different mineralogical pattern, most probably associated to the various smaller grains <1 mm embedded (cemented) in a mixture of calcite and clay mineral matrix. This suggests a heterogeneous pattern for this sandstone lithotype, although not statistically representative. It contains ca. 23% quartz with Na-plagioclase, calcite, dolomite, kaolinite at respective values of ca. 7%, 13%, 4%, and 5%. Among all samples, Sarzin-zufall shows the highest content of mica with ca. 28%. A distinct feature of the Siderolithic sandstone is its bright, ocker colour (Fig. 5.12), which makes it easy to recognize in the field and distinguish it from the Molasse Rouge sand-rich rock (sandstone). Samples from the Siderolithic Formation show the highest contents of kaolinite in sand-rich rock with minor occurrences of chlorite. These sandstones are predominantly cemented by kaolinite as the pore diameters depict a very low (fine-grained) population between 4 and up to ca. 90 nm, and a second population ranging between ca. 300 and 3'000 nm (Fig. 5.15). Lithotype S6

(Fig. 4.1) represents the Siderolithic Formation outcropping near Sarzin in the field, similar to the Sarzin-real and Sarzin-zufall samples, close to an abandoned, quartz-rich mine used for glass manufacturing (Fig. 4.1). Apart from the ocker colour, the Siderolithic sandstone is well distinguishable from the Molasse Rouge formation based on their apparent absence of stratification. Exception to this are the Siderolithic, quartz-rich sandstone outcropping at the *Rochers de Faverges* at the top of the Salève Mountain. This rock shows faint, well-sorted cross-bedding, which might suggest an aeolian origin (see chapter 4).

Gravel and conglomerate

C6-01D is sampled from 5 m depth at well C6, and is classified as a sandy to silty gravel lithotype as part of the glaciogenic deposits (Fig. 5.12). It contains ca. 26% quartz, 2% K-feldspar, 8% Na-plagioclase, ca. 30% calcite, ca. 2% dolomite and ca. 30% of total clay content. Similar samples A1 and A2 are part of the same gravel and conglomerate lithotype (Fig. 5.5). A1 represents Quaternary unconsolidated deposits at a depth between 4 to 5 m in C5 well, while A2 is comprised of gravelly, glaciogenic deposits at a depth from 32.25 to 39.25 m in well Montfleury-2. Illite, calcite and quartz are distributed in almost equal portions, and their loose, not-hardened consistency in the field makes them easily recognisable, despite their shallow depths commonly within the first 10 m. Fig. 5.12 shows moderate, equally distributed quartz grain sizes between 7.8-63 μm , depicting a more coarse-grained texture of these glaciogenic deposit samples compared with clay-rich and violet marl samples, but less than the coarse-grained sand-rich category.

Conglomeratic, low sphericity grains in a clayey matrix of siltstone (M5) are located at a depth between 124.12 and 125.12 m in well Peissy-I (Fig. 5.5). These C1 and C2 depict conglomeratic lithotypes in the Molasse Rouge formation and are differentiated by colour and grain size at depth levels 233.20 m and 188.70 m in Gex-CD-01, respectively. No mineralogical analyses are available at these deeper depth intervals.

Freshwater limestone

Samples G4-27 (240.45 m), G7-22 (244.4), L112-01A (124.10 m), -113 (113.00 m), -116 (116.00 m) and -129 (129.00 m) in wells Gex-CD-04, -07 and L112 represent the Freshwater limestone lithotype as part of the Molasse

Rouge formation. Sample G4-27 contains 100% calcite, with no other minerals encountered. Sample G7-22 contains slightly less calcite (98.6%) and the remaining percentages are shared among traces of clay minerals and quartz (Fig. 5.6, 5.10). Mornex outcrop samples depict Freshwater limestone rock, whereas their mineralogical distribution only differs for the "single rock" sample containing a total clay content of ca. 24% and a dolomite content of 4-6%. The "single rock" sample is considered an outlier because it has been taken next to the road from a single, smaller rock. No smectite contents are observed in neither of the Mornex samples.

Sample Pei-I-07C looks slightly different compared to the Mornex samples but contains ca. 89% of calcite and 11% of quartz. In fact, this makes the sample rather comparable to sample G7-22 despite its traces of clay minerals. Pei-I-07C, though, is similar to the Mornex samples in the sense that both contain large grains (<1 mm). However, this could bias the result towards a carbonate sample, since the larger grains consist of calcite. The description of sample Pei-I-07C also accounts for sample Pei-I-19B. The L lithotype depicts another Molasse Rouge freshwater limestone sample encountered in Gex-CD-07 at a depth of 234.7 m (Fig. 5.5).

Comparison with FTIR analyses

In XRD analyses, amorphous substances are not identifiable. This fact together with the intention of identifying organic matter led to conducting Fourier Transform Infrared (FTIR) spectroscopy analyses, which offer a qualitative mineral and organic content identification (Fig. 5.16). The combination of FTIR, ICP-MS and XRD further allows for correlations with respect to the chemical composition, alteration paths and encountered mineral phases. The measured spectra patterns are discussed based on the previously derived sand-rich, clay-rich, marl, limestone and gravel lithotypes.

The clay-rich and sand-rich rock types differ by the sharper peak at ca. $3'600\text{ cm}^{-1}$, which is probably related to the increased kaolinite content in the clay-rich samples. Sand-rich rock types contain slightly more organic matter based on the wider valley depicted in the spectra. This could suggest more free water in the coarse-grained, i.e. more porous sand-rich rock category. Water is an issue during

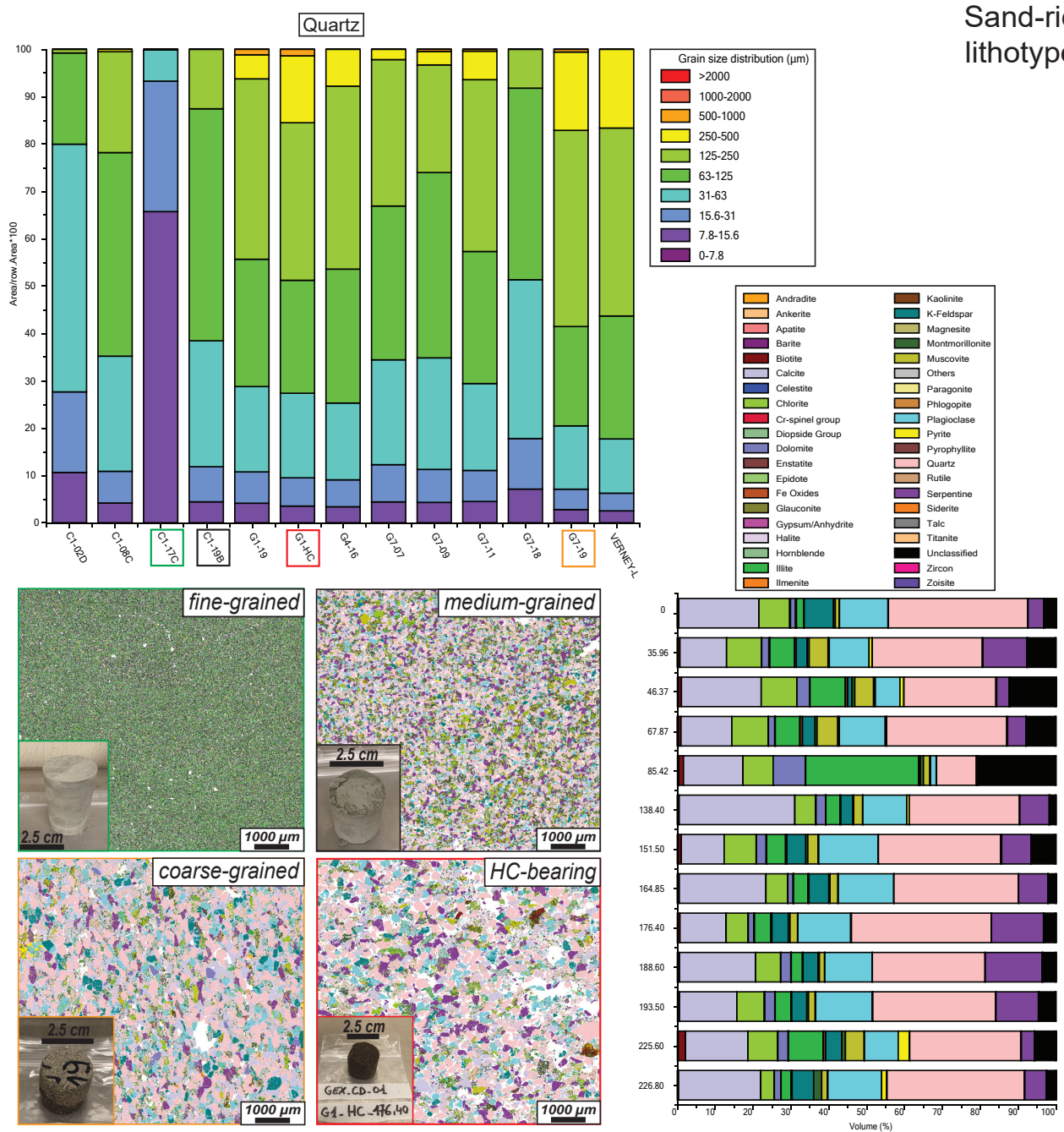
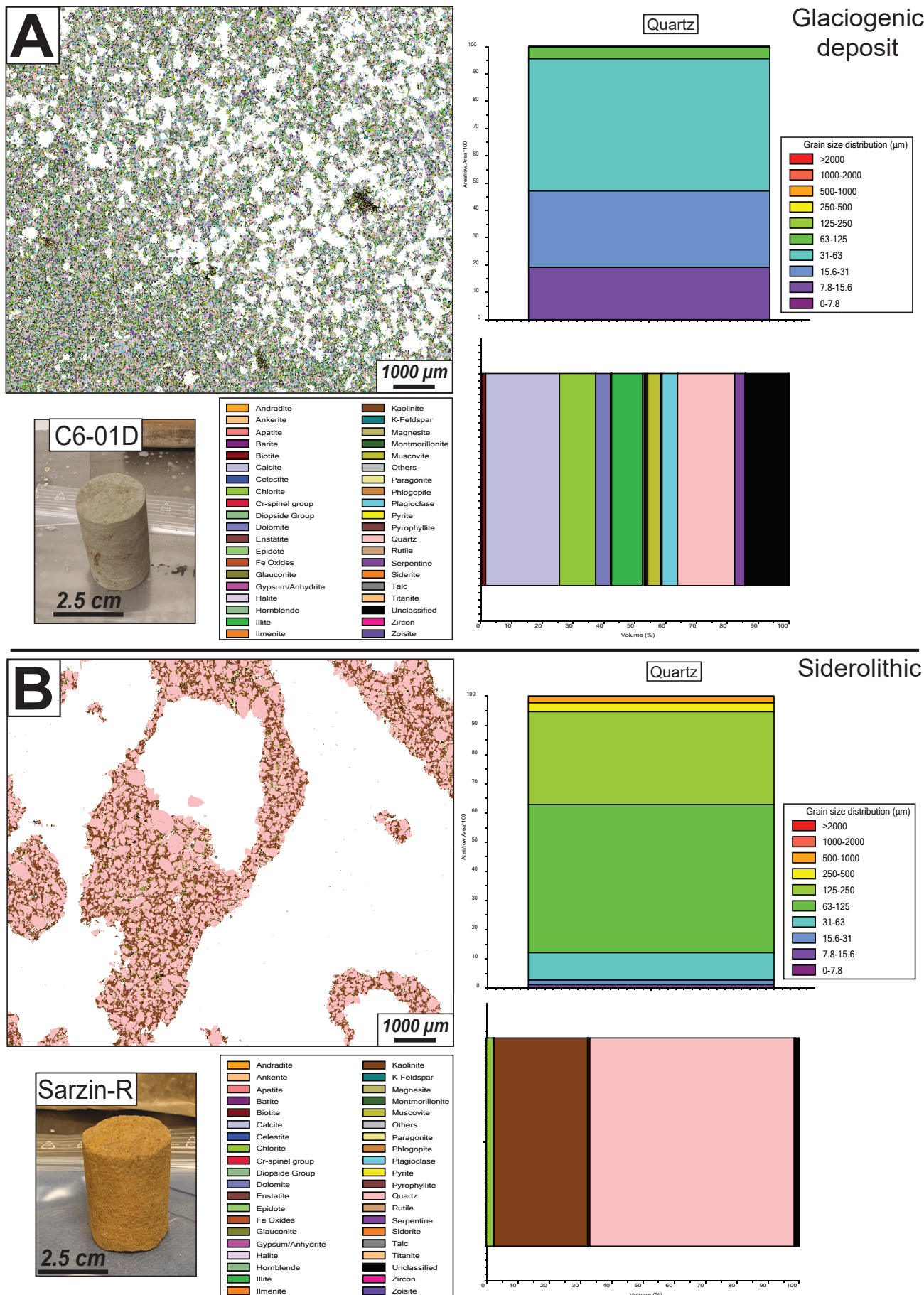


Fig. 5.11: Frame-colour-coded image analyses and quartz grain-size distribution via QEMSCAN with associated modal mineralogy of various sand-rich samples in the Molasse Rouge formation. HC=hydrocarbon.



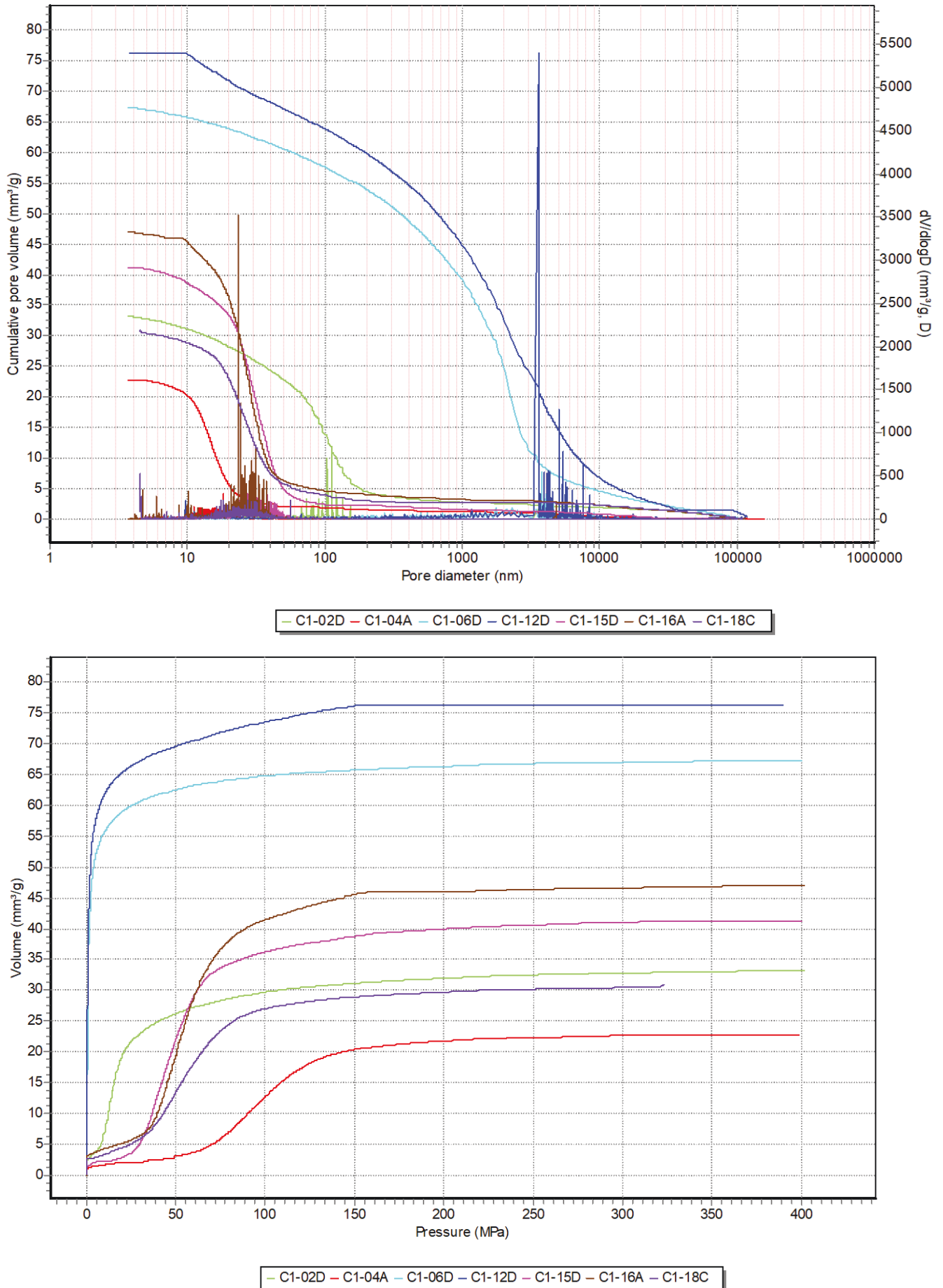


Fig. 5.13: Pore size distribution curves (left) and injected mercury volume versus pressure curves (right) measured on selected samples at the C-wells.

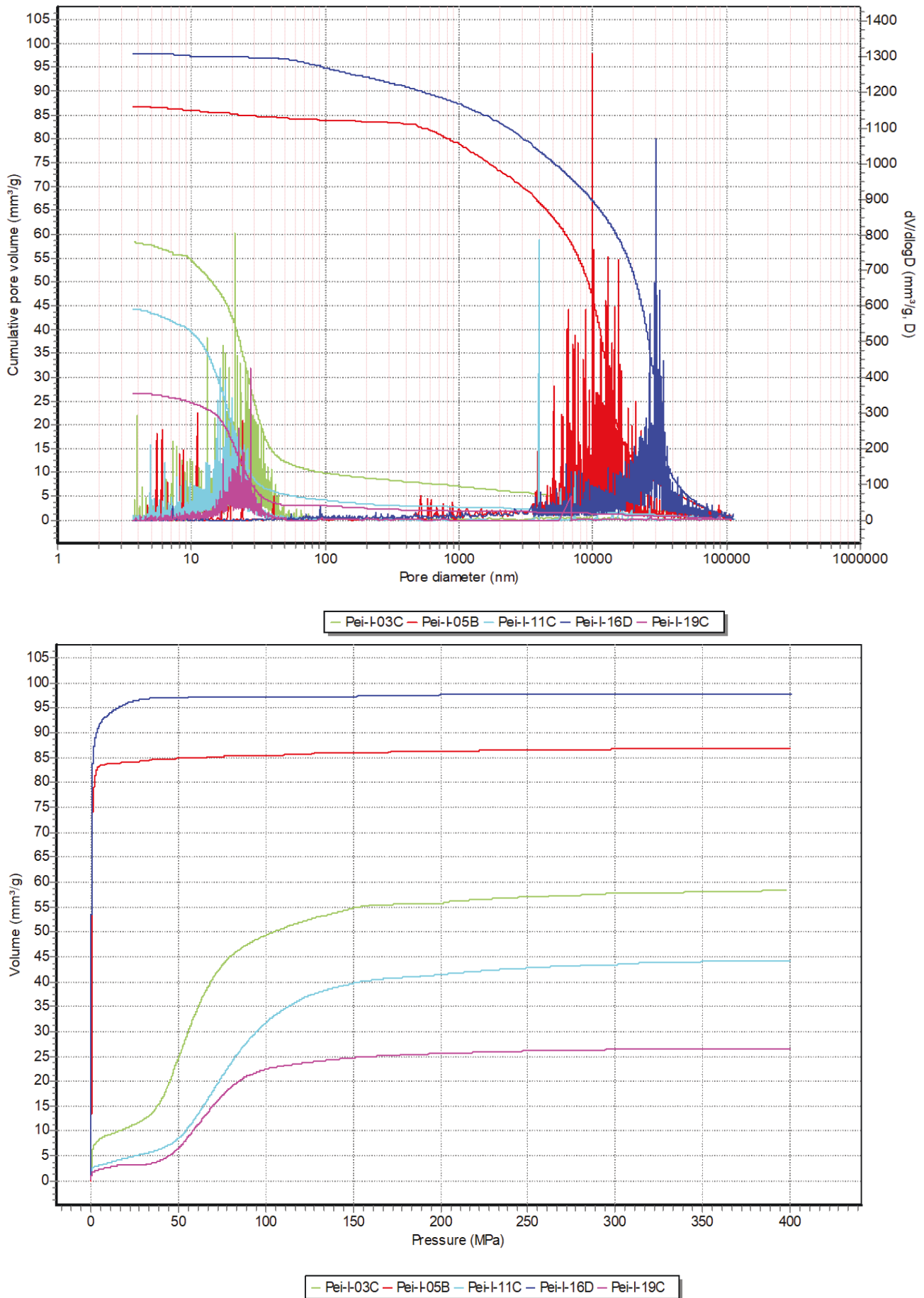


Fig. 5.14: Pore size distribution curves (left) and injected mercury volume versus pressure curves (right) measured on selected samples at well Peissy-I.

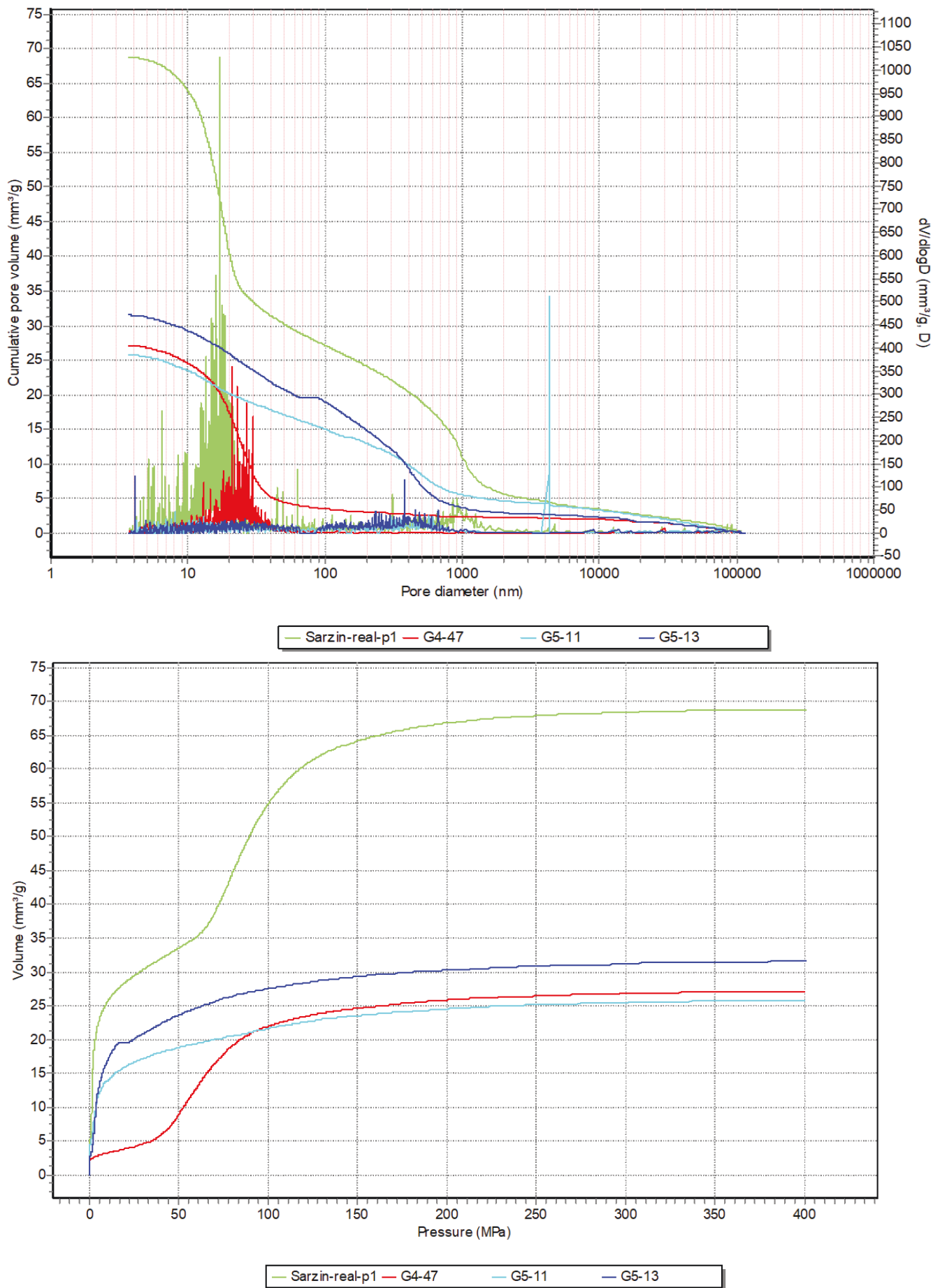


Fig. 5.15: Pore size distribution curves (left) and injected mercury volume versus pressure curves (right) measured on selected samples at wells Gex-CD-04, -05 and outcrops.

Table 5.2: Mercury intrusion porosimetry results for samples at well C1.

	C1-15D	C1-16A	C1-04A	C1-02D	C1-06D	C1-12D	C1-18C
Rock type	siltstone	siltstone	siltstone	sandstone	sandstone	sandstone	sandstone
Approximate borehole depth (m)	27	31	50	46	59	74	83
Total intruded volume (mm ³ /g)	41.26	47.03	22.77	33.14	67.31	76.43	31.01
Bulk density (g/cm ³)	2.4541	2.3773	2.5421	2.4669	2.2754	2.1897	2.5112
Envelope density (g/cm ³)	2.4541	2.3779	2.5424	2.4674	2.2763	2.1933	2.512
Apparent density (g/cm ³)	2.7306	2.6765	2.6983	2.6866	2.6869	2.6298	2.7232
Accessible porosity (%)	10.13	11.18	5.79	8.18	15.32	16.74	7.79
Total pore volume (mm ³ /g)	41.26	47.03	22.77	33.14	67.31	76.43	31.01
Total pore surf. area (m ² /g)	6.853	7.916	6.064	3.552	2.4	2.522	5.479
Average pore diameter (nm)	24.08	23.76	15.02	37.32	112.2	121.24	22.64
Modal pore diameter (nm)	30.78	23.27	18.26	113.29	3747.85	3567.49	4.56
Median pore diameter (nm)	30.41	27.09	15.41	88.62	1375.66	1507.59	27.07

Table 5.3: Mercury intrusion porosimetry results for samples of Gex-CD-04 and -05 wells and Sarzin outcrop.

	G4-47	Sarzin-real-p1	G5-11	G5-13
Rock type	siltstone	sandstone	sandstone	sandstone
Approximate depth (m)	205		380	395
Total intruded volume (mm ³ /g)	27.04	68.82	25.78	31.54
Bulk density (g/cm ³)	2.5403	2.2516	2.4961	2.458
Envelope density (g/cm ³)	2.5405	2.2535	2.4967	2.4585
Apparent density (g/cm ³)	2.7277	2.6646	2.6678	2.6646
Accessible porosity (%)	6.87	15.5	6.43	7.75
Total pore volume (mm ³ /g)	27.04	68.82	25.78	31.54
Total pore surf. area (m ² /g)	5.322	10.969	2.996	3.367
Average pore diameter (nm)	20.33	25.1	34.42	37.47
Modal pore diameter (nm)	20.72	17.11	4293.19	4.17
Median pore diameter (nm)	23.84	26.34	205.58	173.33

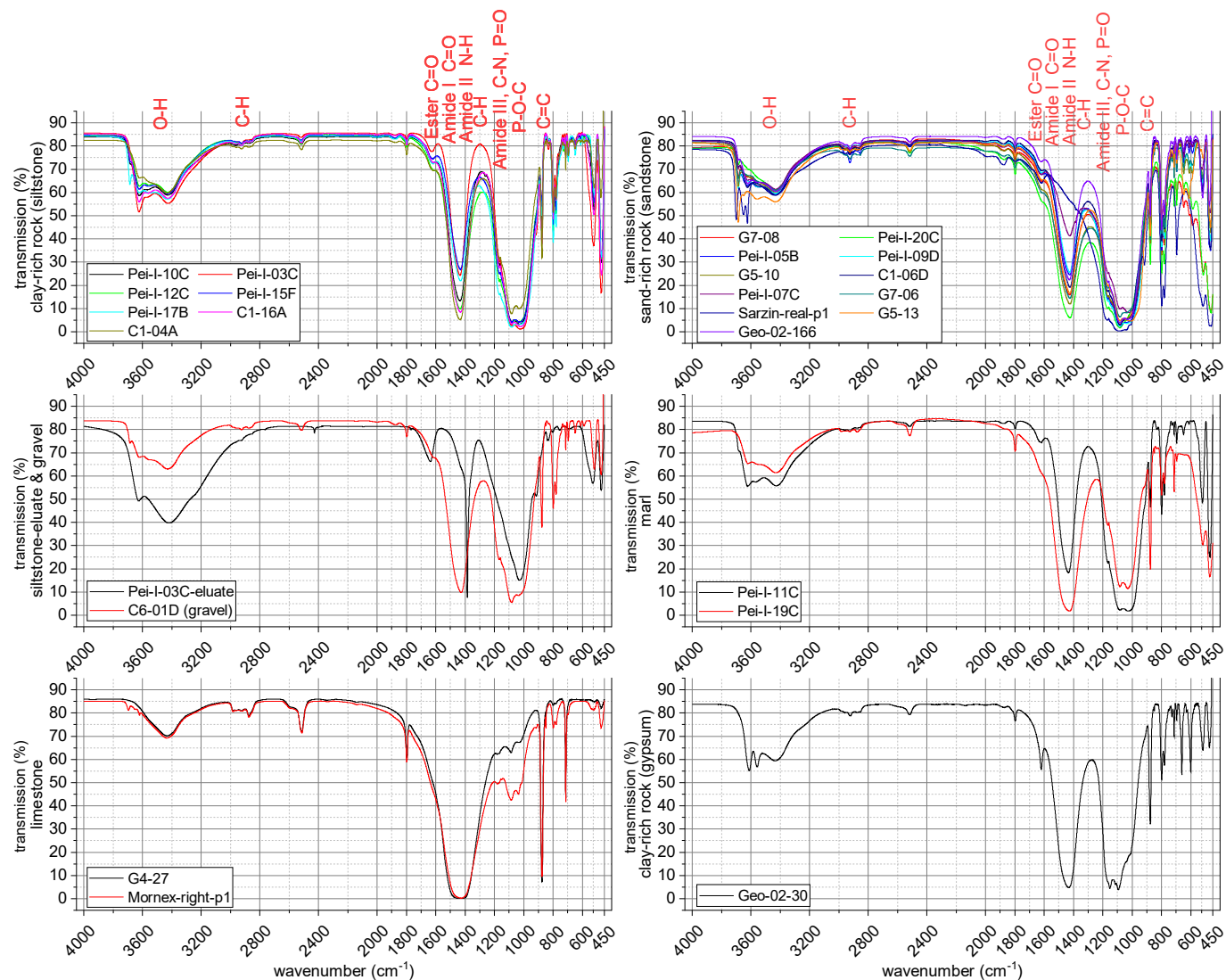


Fig. 5.16: FTIR spectra for sandstone, siltstone, marl and freshwater limestone lithotypes of the Molasse Rouge, and gravel lithotype of the glaciogenic deposits formation. Samples are taken from wells Peissy-I, C1, Gex-CD-04, -05, -07, Geo-02 as well as outcrops Sarzin and Mornex. Absorption bands (after Bertaux et al. (1998), Marel & Beutelspacher (1976), and Sauer & Wuthier (1988)) attributed to organic compounds occur at 3'600-3'200 (O-H), 2'950-2'850 (C-H), 1'750 (C=O) ester, 1'655 (C=O) amide, 1'550 (N-H, C-N), 1'460 (CH₂), 1'400-1'250 (P=O), 1'380 (CH₃), 1'240 (C-N, N-H), 1'060 (P-O-C), and 925 (C=C) cm⁻¹.

Table 5.4: Mercury intrusion porosimetry results for samples at well Peissy-I.

	Pei-I-03C	Pei-I-19C	Pei-I-11C	Pei-I-05B	Pei-I-16D
Rock type	siltstone	siltstone	marl	HC-sandstone	sandstone
Approximate borehole depth (m)	42	220	85	60	161
Total intruded volume (mm ³ /g)	58.32	26.57	44.3	86.74	97.93
Bulk density (g/cm ³)	2.2953	2.5195	2.3745	2.1501	2.0589
Envelope density (g/cm ³)	2.2957	2.5201	2.3754	2.1508	2.0605
Apparent density (g/cm ³)	2.65	2.7002	2.6536	2.643	2.5788
Accessible porosity (%)	13.39	6.69	10.52	18.65	20.16
Total pore volume (mm ³ /g)	58.32	26.57	44.3	86.74	97.93
Total pore surf. area (m ² /g)	10.168	5.286	10.589	0.898	0.665
Average pore diameter (nm)	22.94	20.11	16.73	386.49	589.2
Modal pore diameter (nm)	21.06	27.5	3955.9	9894.42	29755.32
Median pore diameter (nm)	26.94	22.45	19.07	10637.17	21539.64

FTIR analyses because the O-H groups produce a significant steep curve (free water H_2O between 1'756 to 1'600 cm^{-1}). The Siderolithic sandstone (Sarzin-real sample) shows little organic matter and main peaks in the quartz region. This is confirmed by XRD and QEMSCAN analyses making the Siderolithic sandstone the purest sand-rich rock with SiO_2 contents $>70\%$. The siltstone-eluate sample was tested due to the fact that a certain portion of the sample during ICP-OES measurement for exchangeable cations in acid precipitated. The extracted precipitation substance was analysed indicating distinct peaks in the 600-450 cm^{-1} region potentially attributed to gibbsite (hydrargillite?), which contains Al- and Fe-hydroxides (e.g. goethite) causing the precipitation and rusty (reddish) colour. The limestone samples depict a broad peak at ca. 1'400 cm^{-1} , which is attributed to carbonate content (calcite), together with a distinct peak close to 900 cm^{-1} . The latter is related to other carbonates containing Li^+ , K^+ and Na^+ elements, also located in the 895-831 cm^{-1} region. Peaks in the same spectra region are observed in carbonate-rich samples Pei-I-19C (clay-rich) or calcite-cemented sand-rich samples such as C1-06D. The marl lithotype contains a distinct curve drop from 3'600 cm^{-1} upward, which is related to increased kaolinite content. A slightly narrower peak at 1'100-1'000 cm^{-1} is associated to silicate minerals given by the Si-O molecule

vibrations. The latter is also distinctive in the sand-rich, clay-rich and gravel samples, while absent in the limestone. Peaks from 700 to 450 cm^{-1} are related to overlapping bands in all samples. The occurrence of the mineral lizardite (serpentine sub-group) in clay-rich samples (G7-08) at 3'685 cm^{-1} cannot be excluded.

5.3.2 Elemental distributions and alteration paths

ICP-MS and portable XRF analyses are used to cross-correlate elements via principal component analysis (PCA). The pXRF measurements enable a practical and cost-efficient detection of elemental composition of rocks and soils in the field whose reliability in combination with ICP-MS data is investigated to empirically correlate elemental concentrations via linear regression. Fig. 5.17 exemplifies the procedure for the Ca element. Eventually, environmental pollutants and qualitative alteration paths are discussed in this section.

$$Ca_{pXRF} = 1.288 \cdot Ca_{ICP} (Pearson's R = 0.93) \quad (5.1)$$

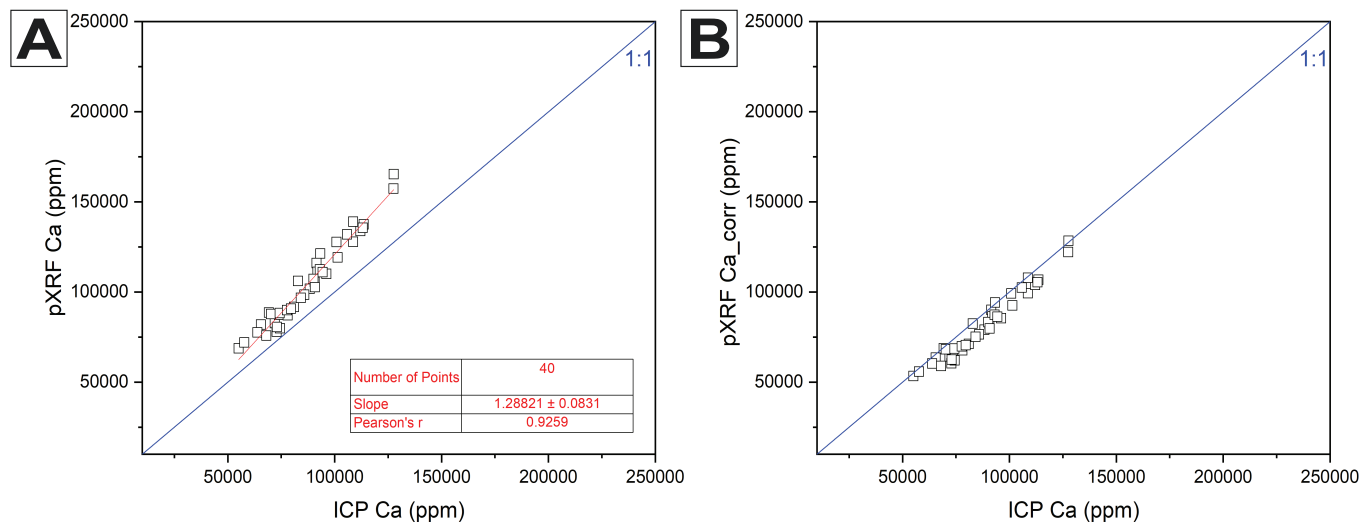


Fig. 5.17: Calculated correction coefficient on Ca element measured with pXRF and ICP-OES/-MS based on 40 Molasse Rouge samples in the Geo-02 well. (A) Ca content (ppm) before the correction. The slope yields a correction factor of 1.288. (B) Ca content (ppm) after the correction, showing a very good Pearson's correlation coefficient of 0.93 along the 1:1 line.

Linear regressions are calculated for elements Mg, Al, Ca, Ti, V, Cr, Fe and Ni as they form the main elements for the evaluation of application scenarios and environmental pollutants (see chapter 6). They yield positive elemental correlations among increasing atomic number and related increasing correction factors of elements Mg, Al, Ca, Ti, Fe, V, Cr, and Ni (Fig. 5.18) for the Molasse Rouge formation.

This contradicts studies that used the proposed method for both XRF field and XRF laboratory analyses (Roman Alday et al. 2018) in comparison to ICP-MS data instead (Fig. 5.19). Fig. 5.18 shows the larger correction factors correlated to ICP-MS laboratory measurements for Cr and Ni, representing driving elements for the classification into disposal classes. It seems that pXRF tends to both under- and overestimate some elements when compared to ICP-MS. Along the 1:1 lines except for Ni, elements represent good correlations among the two measurement techniques. Scattering is observed for elements Cr, Mg, Ti and Ni as the larger (heavier) elements. A rather low-confident correlation for element Ni is observed as one of the heaviest elements causing quantification issues with the pXRF technique. Except for element Ni, correlation factors exceed Pearson's correlation coefficients of 0.8 demonstrating very good correlations among the two analyses based on the derived empirical calibration and

corresponding correction factors.

The derived correction factors are suggested to be applied on the FCC's future data acquisitions in the field for first on-site (field) estimates, whereas concentrations of Ni would have to be treated with caution and are underestimated by pXRF. The vast majority of rock samples in the Molasse Rouge do not show concentrations >1.5% of elements Na or P (Fig. 5.21, 5.20). The element Na is not measured by pXRF and element Mg delivers a low level of confidence.

Rock alteration characterisation based on elemental composition

The pXRF measurements are used to derive clay mineral associations based on molar elemental ratios for an elemental rock characterisation. Fig. 5.21 predicts clay minerals chlorite, muscovite, biotite, and K-feldspar for 42 samples along well Geo-02. The vast majority of samples plot along the muscovite-chlorite line for both pXRF and ICP-MS data. This coincides well with mineral analyses by XRD and QEMSCAN (Fig. 5.6). Small amounts of biotite are detected $\leq 1\%$ in QEMSCAN and in the elemental analyses. The same explanation would apply for K-feldspar, often detected $\leq 1\%$ and not by pXRF-calculated molar ratios.

Despite the difference of the two statistical sample populations (42 pXRF versus 378 ICP samples), the alteration

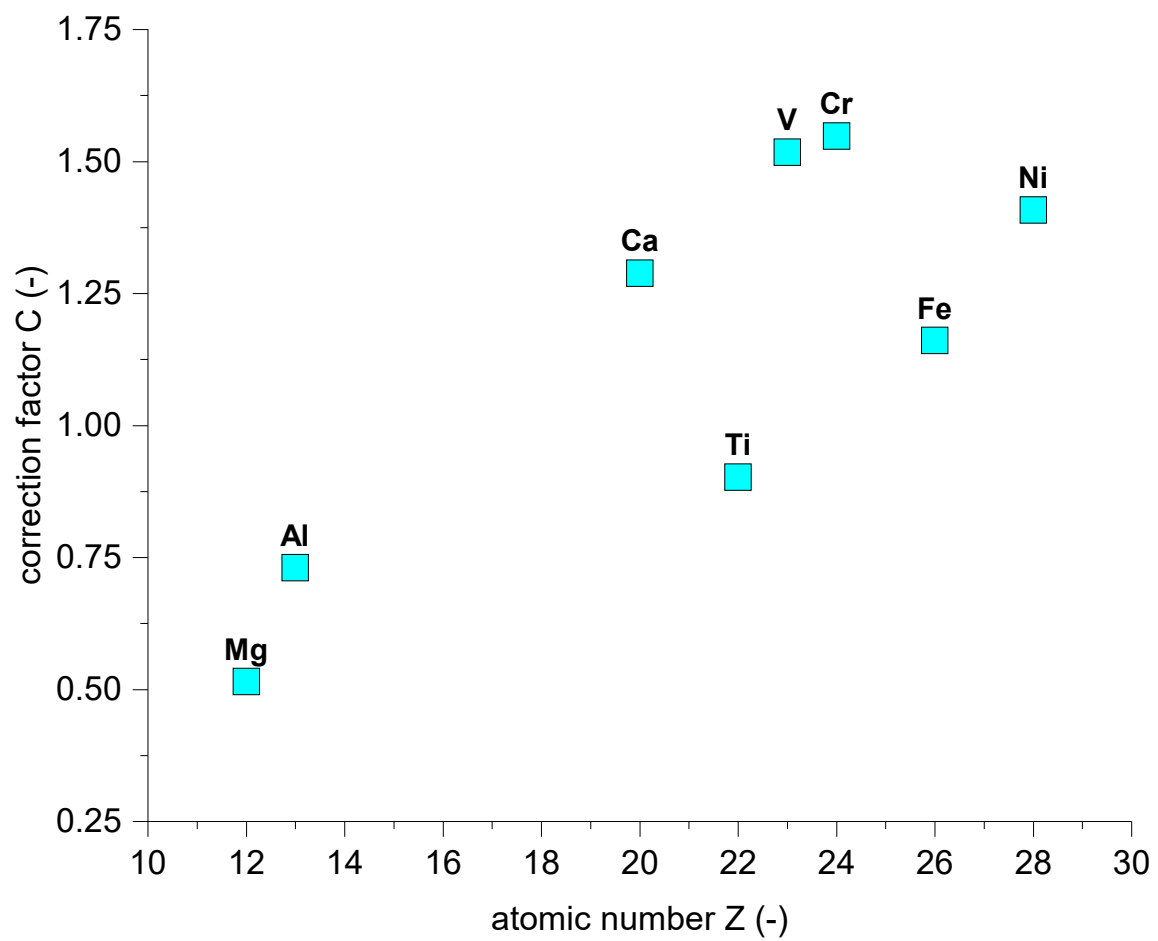


Fig. 5.18: Calculated correction factors for elements Mg, Al, Ca, Ti, Fe, V, Cr, and Ni as a function of atomic number (Z).

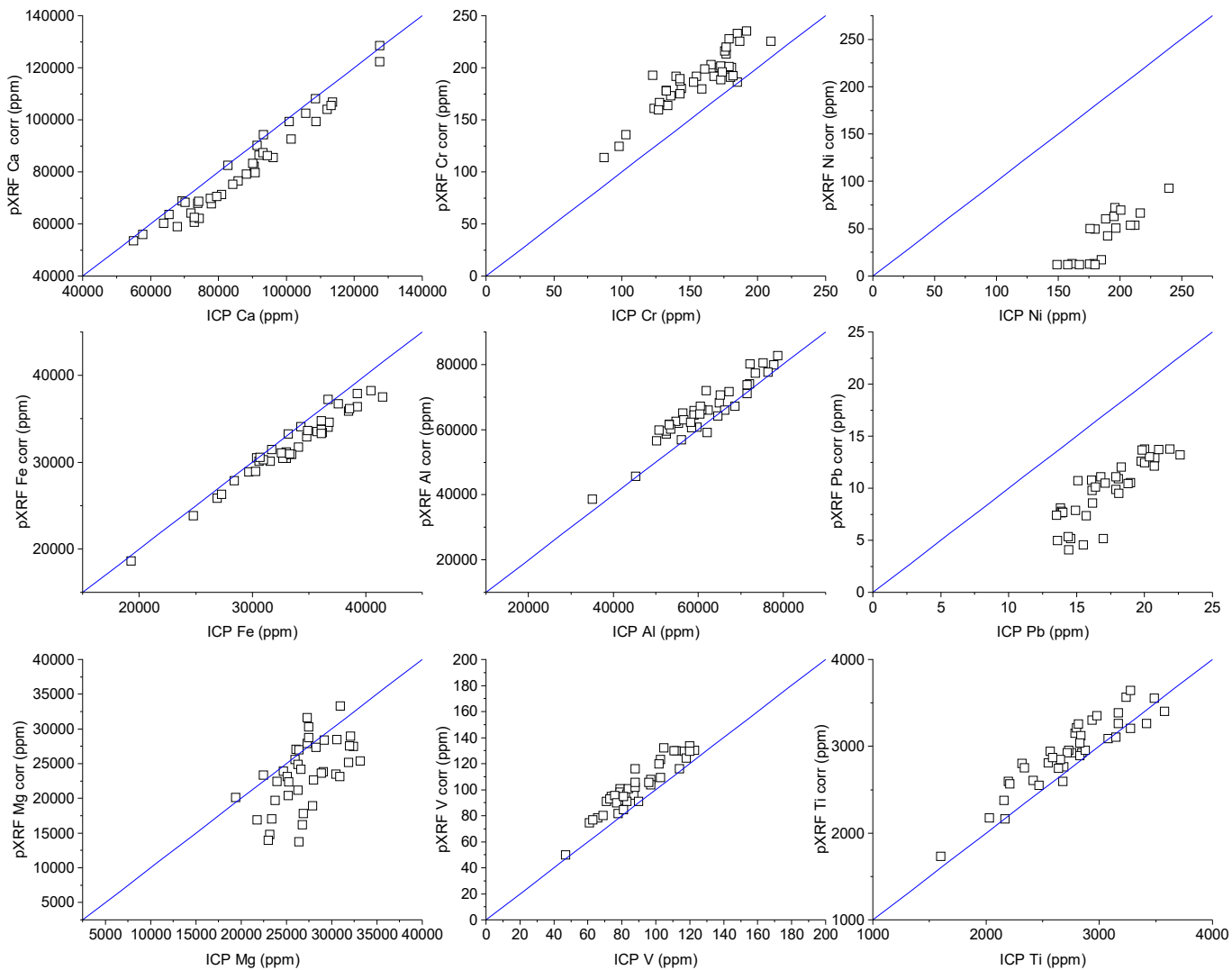


Fig. 5.19: Correction coefficient calculations applied for various elements essential for the identification of application scenarios and disposal classes.

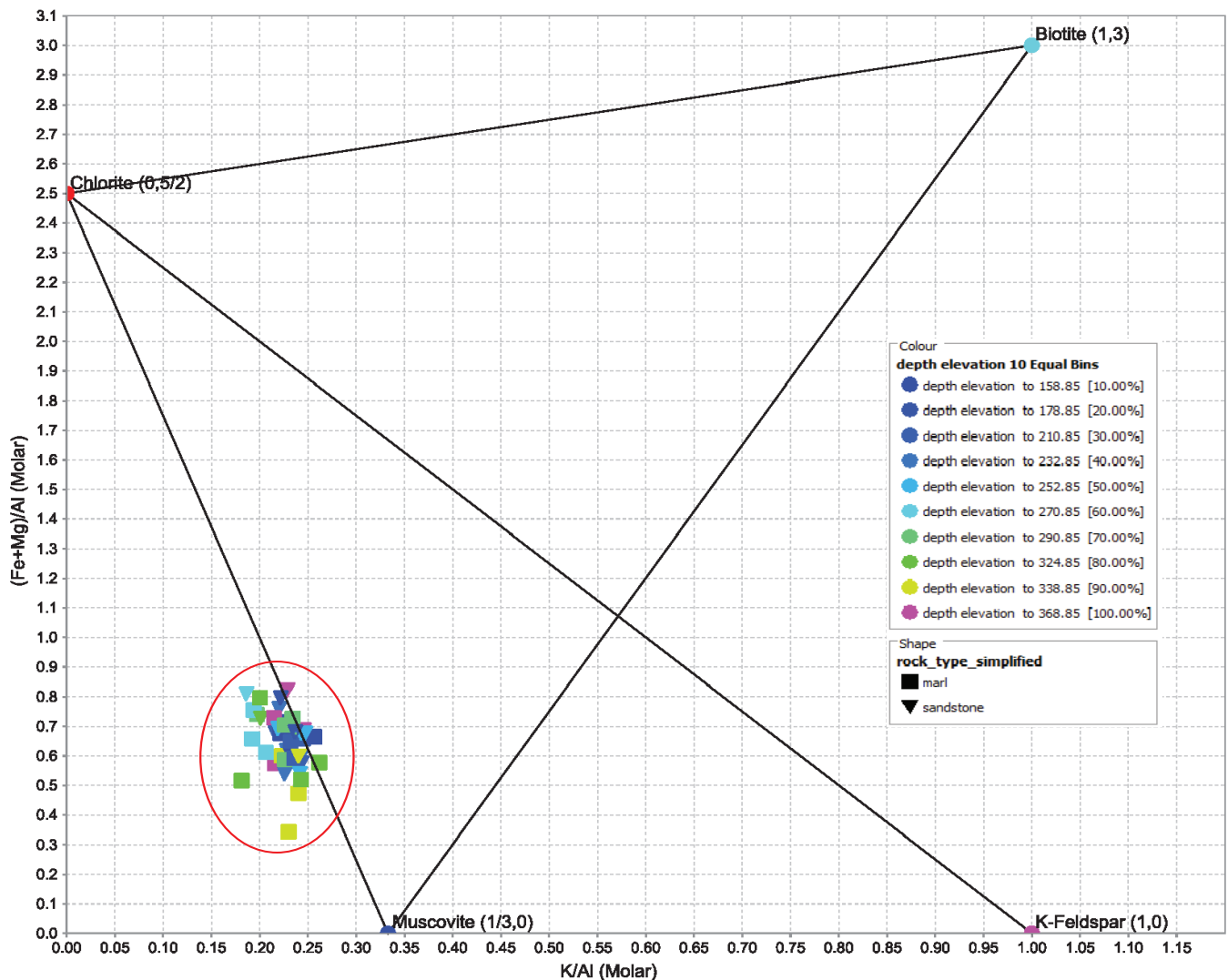


Fig. 5.20: Elemental molar ratios of 42 pXRF samples in well Geo-02 for the qualitative prediction of muscovite, K-feldspar, chlorite and biotite minerals based on Fe, Mg, K and Al in the Molasse Rouge formation, color-coded by depth intervals. No Na concentrations are required for this plot, as they are not measured by pXRF. Borehole Geo-02 represents predominantly sand-rich, clay-rich and marl samples. Numbers in brackets denote X and Y plot locations.

diagram paths show that pXRF analyses yield reasonable results for the qualitative prediction of K, Al, Fe and Mg-bearing clay minerals such as muscovite and chlorite.

Fig. 5.22 depicts the three chemical parameters SiO_2/Al_2O_3 ratio, Fe_2O_3/K_2O ratio and Ca content for the calculation of different (terrigenous) shale and sandstone lithotypes as initially proposed by Herron (1988). The idea of this method of characterisation is to check dependencies of the total iron content $Fe_2O_3_{(total)}$ because it is dependent on respective calculations for the prediction of application scenarios.

The vast amounts of samples plot in the shale, wacke and litharenite fields with only few exceptions inside the Fe-dominated sand region. The latter are associated to an increased content of Fe, they show a similar behaviour like the ocker (reddish) Siderolithic sandstone lithotype from the Siderolithic formation, which varies in terms of colour based on their Fe and Mg content. These sandstones are easily distinguishable in the field due to their red/orange colour and in the shale-sand rock classification diagram. The diagram is commonly referred to illustrate the geometrical relationship among sedimentary (and plutonic) composition trends, but works well for the present samples as part of the glaciogenic deposits, Grès et Marnes Gris à gypse, Molasse Rouge and Siderolithic formations.

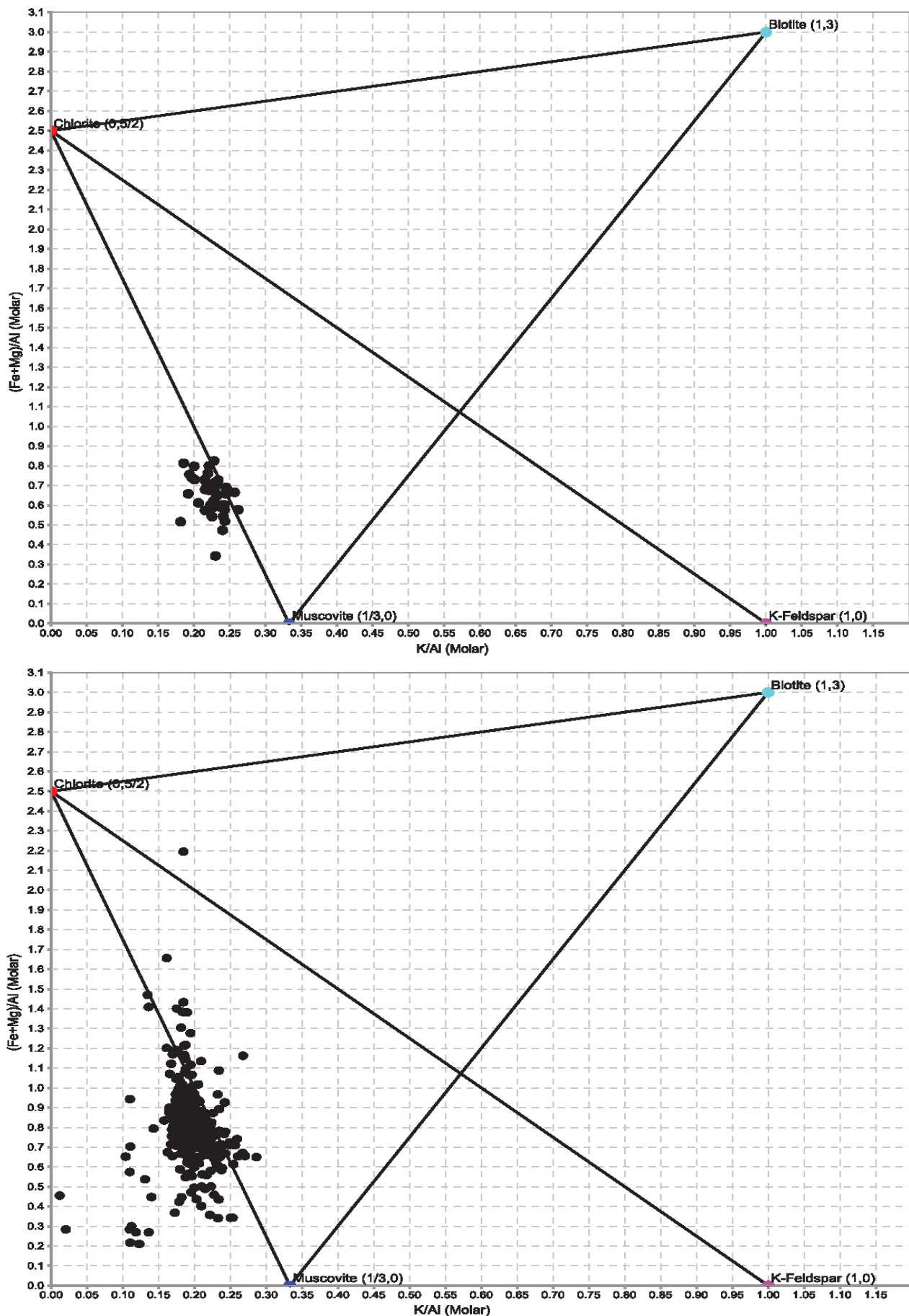


Fig. 5.21: Comparison of elemental molar ratios of 42 pXRF samples in the Geo-02 well (top) and 378 ICP samples across multiple wells (bottom) for the prediction of muscovite, K-feldspar, chlorite and biotite minerals based on Fe, Mg, K and Al elemental distributions in the Molasse Rouge formation. No Na concentrations are required for this plot, as they are not measured by pXRF.

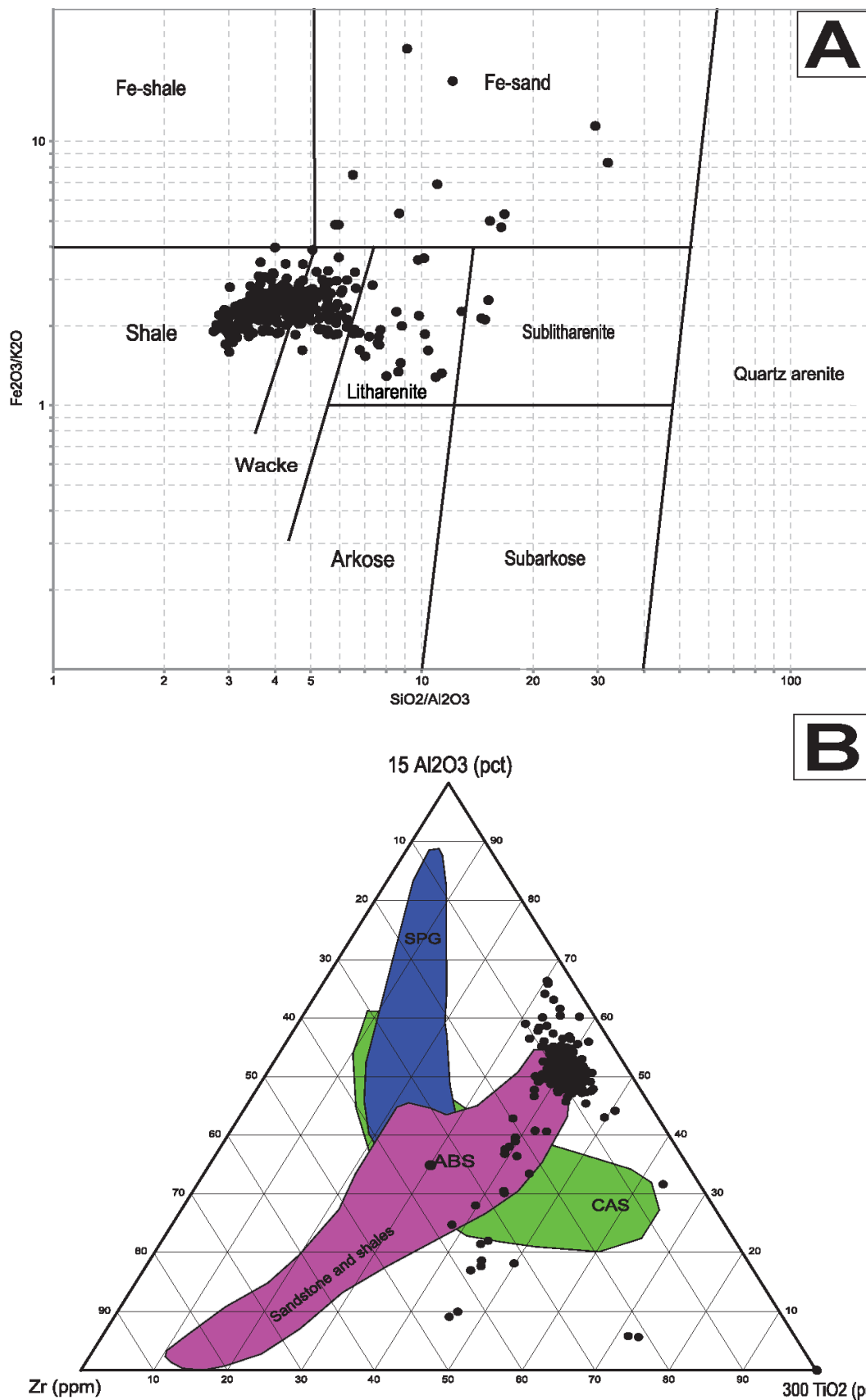


Fig. 5.22: Characterisation of alteration diagrams based on ICP data for 378 samples. (A) Rock characterisation of shale and sandstone based on major elements as proposed by Herron (1988). (B) Zr-Al₂O₃-TiO₂ weathered rock type characterisation after Garcia et al. (1994), valid for clastic sediments. ABS=average bulk sediment, CAS=calc-alkaline suite, SPG=strongly peraluminous granite.

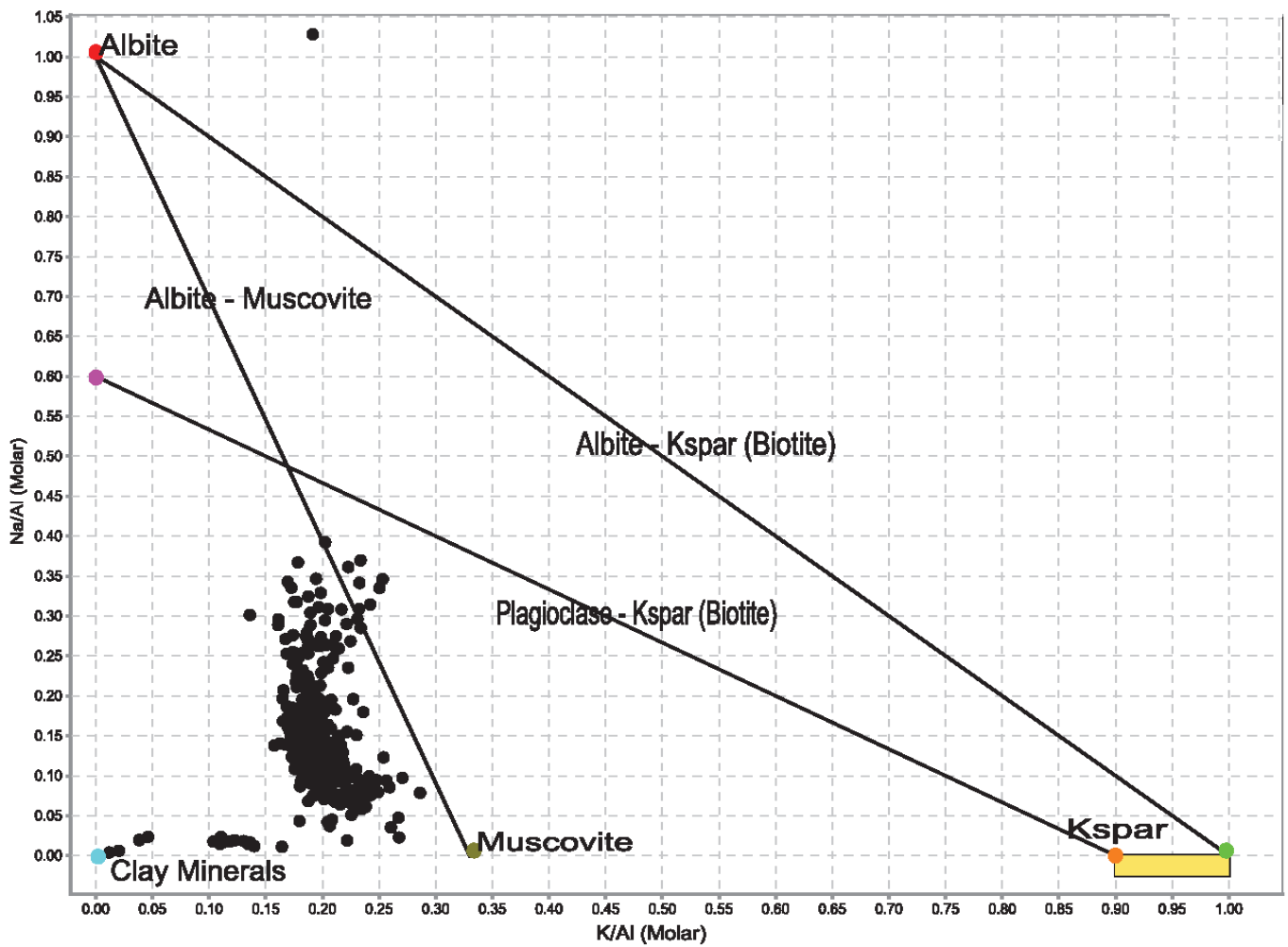


Fig. 5.23: Characterisation of alteration diagrams based on ICP data for 378 samples deriving alkali-alumina (K/Al and Na/Al) molar ratios after Davies & Whitehead (2006).

Compared with Fig. 5.22, which uses Zr and Ti concentrations to follow a proposed characterisation after Garcia et al. (1994), a similar behaviour is observed with the majority of samples located in the sandstone and shale region (violet). The few samples are either attributed to conglomerates and do not fulfill the classification's conditions, or contain less Al and Zr.

Fig. 5.23 provides alkali-alumina molar ratios of feldspars, mica and clay minerals. Albite plots along the line as muscovite; clay minerals and other aluminous non-alkali-bearing minerals such as chlorite, epidote and topaz lie at the origin. The resulting points lie within the muscovite, clay minerals and intersection point of plagioclase/K-feldspar (biotite) and albite-muscovite triangle, with no occurrences of albite.

Clay minerals are not well quantifiable as most of the samples contain larger amounts of chlorite plotting at the origin of this plot. On one hand, this gives the impression of mainly muscovite and biotite, while on the other hand, the samples contain a large portion of clay minerals, which plot close or at the origin of the plot. Hence, this plot might not be ideal for the derivation of clay minerals, but is indicative for their presence and could be considered a qualitative rather than a quantitative first estimate. Fig. 5.22 give a solid prediction of the lithotypes, and are based on cheaper ICP measurements than, for instance, mineralogical analyses such as XRD or QEMSCAN.

Fig. 5.24 depicts alteration paths based on elemental molar ratios of Fe, Mg, Na, K, and Si. For the vast amount of samples, the alteration from AF has already occurred, and they plot between muscovite and chlorite, with a strong tendency towards muscovite. When compared to Fig. 5.22, which in addition accounts for the Si content in the form of quartz, and hence separates the former red arrow into a violet followed by either black (quartz) or red (chlorite) arrows, an improved and more realistic prediction is observed when compared to XRD measurements that show particularly higher amounts of chlorite than muscovite.

Both diagrams show increased amount of muscovite over chlorite. However, as these diagrams refer to alteration process and progress, pure chlorite potentially detected in mineralogical analyses might not mirror elemental molar ratios in case the alteration process has not yet fully terminated. The samples plot rather at the beginning of

the respective alteration paths, which suggests that the analysed samples contain a significant lower amount of either Si content or Fe and Mg. A low Fe content would comply with the observations in Fig. 5.22 and refers to the low-Fe content sandstone of the Siderolithic formation and Molasse Rouge samples.

The highly cemented sand-rich (sandstone) rocks plot in the region towards muscovite, while the clay-rich (siltstone) rocks with high contents of chlorite plot towards the chlorite region. Fig. 5.25 depicts the Ishikawa Alteration Index (AI) versus the Advanced Argillic Alteration Index (AAAI) after Williams & Davidson (2004) and. An increase in AAAI represents a strong SiO_2 enrichment and, hence, the consecutive removal of chlorite, carbonate and feldspar. The arrow indicates the trend from unaltered rock (unaltered box) towards pyrophyllite alteration zones. The box for unaltered samples is defined in the advanced argillic alteration index by the spread of least altered (propylitic) samples as proposed by Large et al. (2001) and Williams & Davidson (2004), and in the AI by the least altered box of the alteration box plot.

Despite the majority of the samples being located in the unaltered box, the plot shows a reasonable trend towards calcite (no epidote), with samples along the trend line towards pyrophyllite. Possible causes are associated to incomplete clay diagenesis or differences in the depositional environment (marine/shallow water versus continental settings, see chapter 4). Fig. 5.22, 5.23, Fig. 5.24 and 5.25 depict a reasonable qualitative prediction of occurring mineral phases based on geochemical ICP data. These diagrams are indicative of the alteration of samples. Their grades of cementation in sandstone makes it possible to distinguish fine-, medium- and coarse-grained sub-types. In the Thônex-1 at ca. 408 m depth, as well as at various other boreholes, serpentinite is observed in coarse-grained sections with up to 12% of Cr. In contrast, occurring Cr-spinel show values up to 40% Cr. These medium- and coarse-grained, sand-rich samples are prone to serpentinite and a lower grade of cementation, while the fine-grained sand-rich rocks are influenced by cementation (either calcite or clay minerals, i.e. chlorite). The cementation is qualitatively captured in these alteration path diagrams. As the measurement of geochemical data is more cost-efficient compared to mineralogical analyses, these approaches are a valid method for the calculation of oxides and molar ratios and to some limited extent for

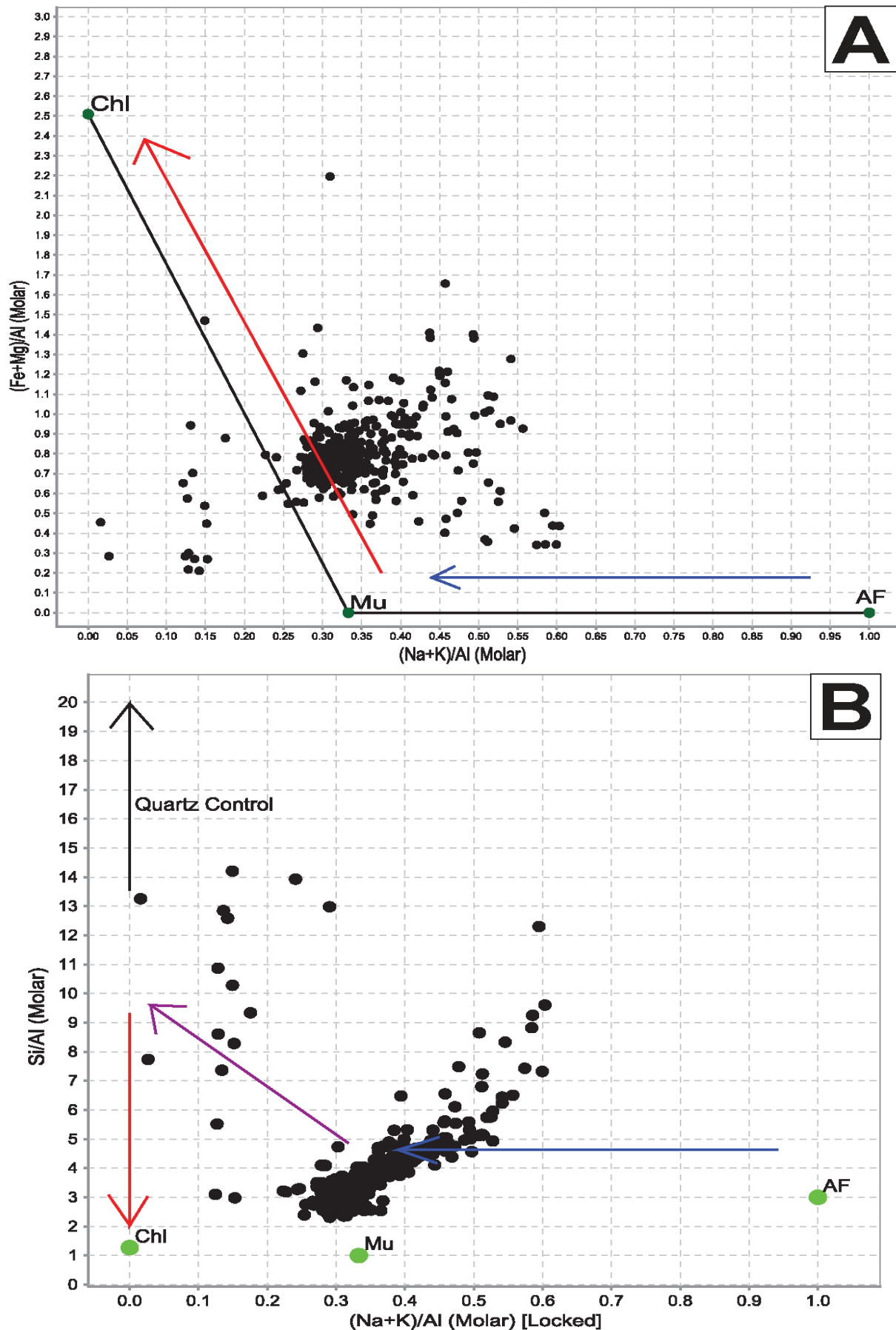


Fig. 5.24: Alteration paths based on ICP data for 378 samples in the Quaternary glaciogenic deposits, Molasse Rouge and Siderolithic formations. (A) Alkali-feldspar alteration with respect to Fe, Mg, Na and K content, showing the alteration paths of AF to muscovite (blue arrow) and chlorite (red arrow). (B) Alkali-feldspar alteration with additional respect to Si, Na and K content. Chl=chlorite, Mu=muscovite, AF=alkali feldspar.

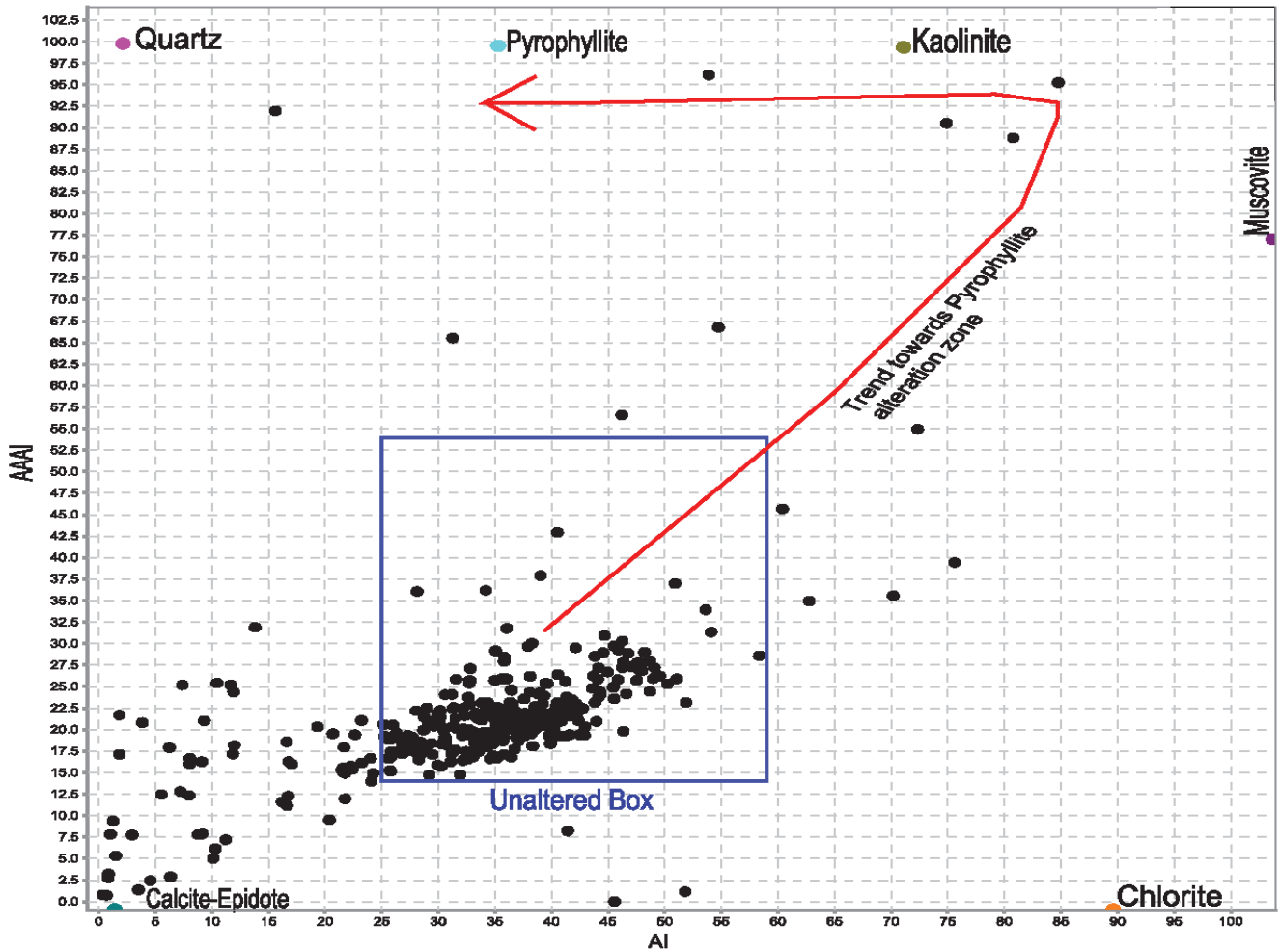


Fig. 5.25: Alteration paths based on ICP data for 378 samples in the Quaternary glaciogenic deposits, Molasse Rouge and Siderolithic formations depicting the Ishikawa alteration index (AI) versus advanced argillic alteration index (AAAI) after Stanley (2017). Chl=chlorite, Mu=muscovite, AF=alkali feldspar.

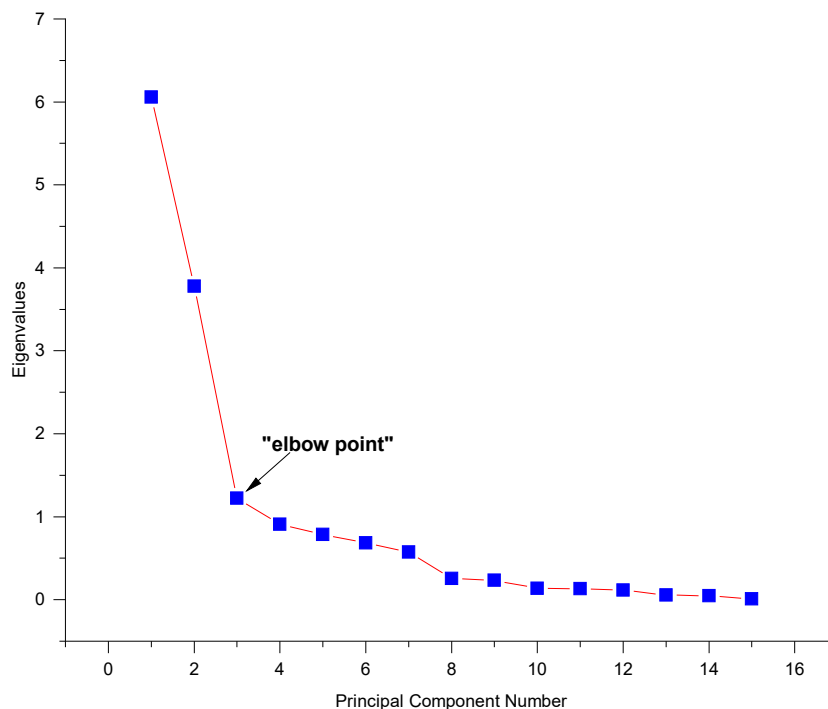


Fig. 5.26: Screeplot used for the determination of the optimal number of principal components comprising at least 80% of the total elemental ICP data variation. 3 PCs are chosen based on eigenvalues ≥ 1 depicted by the optimal "elbow point".

the qualitative derivation of clay mineral occurrences. However, they should be substantiated by quantitative mineralogical analyses. For proper both qualitative and quantitative clay mineral analyses, no measurement technique could replace the high reliability of XRD analyses.

Statistical analysis of elemental data

To substantiate the statistical representativity, a principal component analysis (PCA) is conducted following the Kaiser-Guttman rule. This rule is based on the cumulative percentage $\geq 80\%$ of eigenvalues $\leq 1\%$ representing a PC above the mean value (Fig. 5.26) and drives the number of principal components included.

The PCA biplot (Fig. 5.27) shows a high positive correlation of the polluting elements Cr and Ni, which play a crucial role as environmental pollutants. Cr and Ni are separated by small vector angles and depict similar vector orientation for the sand-rich (sandstone) rock type, substantiated by the direction and length of the SiO_2 vector denoting quartz content (amongst others). This implies that Cr and Ni contents are predominantly contained in

sand-rich (sandstone) rocks and would suggest their occurrence in e.g. the Cr-spinel and serpentine minerals in coarse-grained (medium-grained?) sand-rich samples (Fig. 5.11, 6.11). The amount of Fe-bearing minerals such as e.g. pyrite shows no correlation with polluting elements Ni and Cr. Ni and Cr show a high variability as indicated by their vector lengths. This means that their well-established correlation is not limited to sand-rich rocks but also to clay-rich and marly rocks.

Pb and Cd show a similar behaviour compared with Ni/Cr, while As values show less variation. A strong negative correlation among the limestone and sand-rich (sandstone) lithotypes is represented by the ca. 160° angle between the Ca and SiO_2 vectors, making the Freshwater limestone, sand-rich rocks and respective elements Pb, Cr and Ni clearly associated. This also suggests that Ni and Cr pollution is not encountered in the limestone lithotype. Polluting elements Cd, Sb, As and Pb are correlated with clay-rich (siltstone) and (violet) marl rocks with low variations. Element Ca refers to the limestone lithotype as well as to calcite-rich conglomerate and calcareous-rich (siltstone) outliers compared to siltstone samples closer to the average, indicated by their location closer to the origin of the plot. Ca is supposed to refer predominantly to calcite

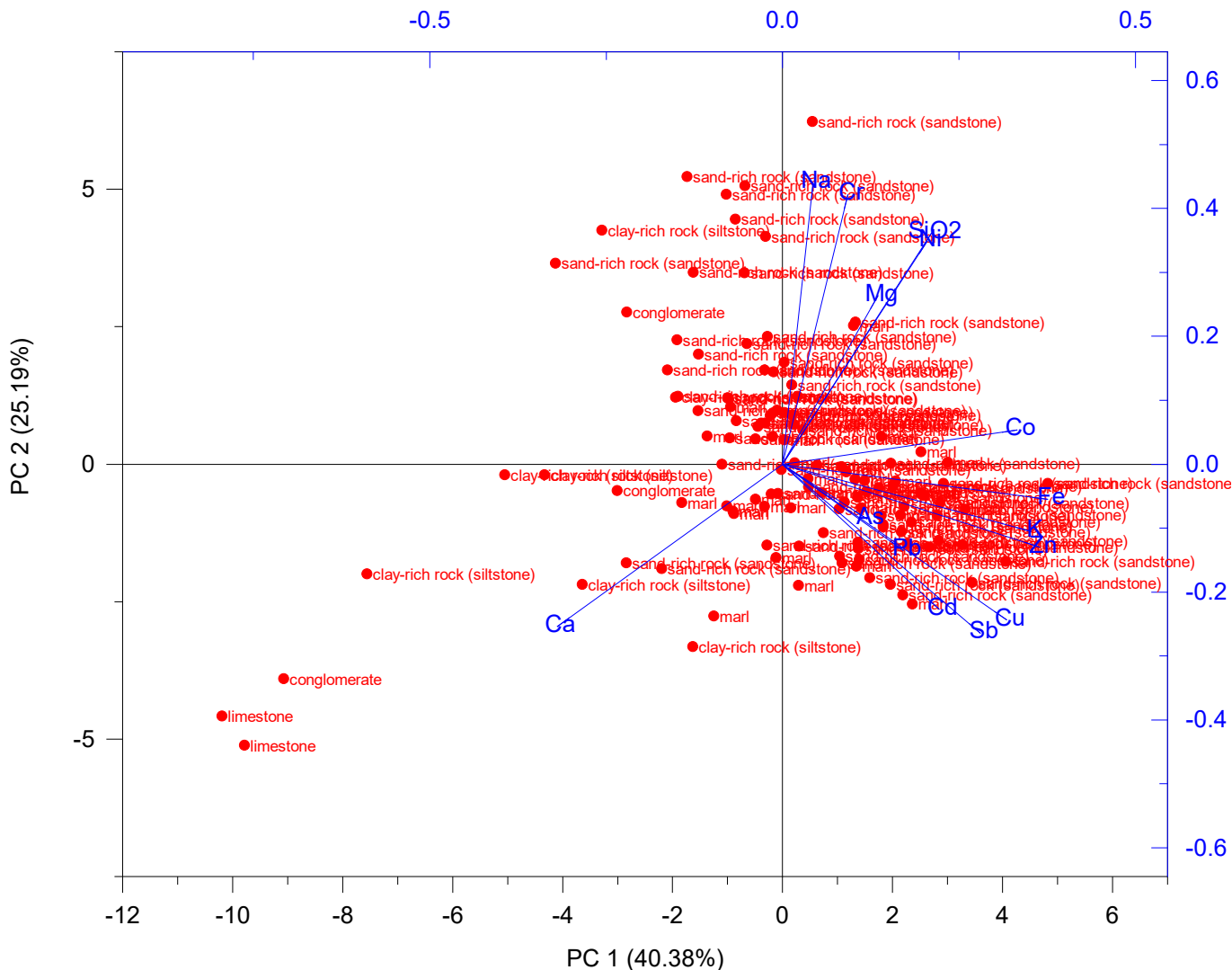


Fig. 5.27: Pairwise PCA biplot for cross-correlation of polluting elements and those relevant for application scenarios, combining vector loadings and scores of 342 Molasse Rouge samples labelled according to their classified category at the FCC depth interval between 100 and 300 m ASL based on ICP data. The PC1 & PC2 axes denote 40.38% and 25.19% of the variance of the data set, respectively.

with some of these samples containing also higher amounts of smectite in the form of Ca-montmorillonite. The Ca-montmorillonite directs the Ca vector towards clay-rich samples.

5.3.3 Plasticity modelling and physico-chemical correlations

Plasticity behaviour and temporal water absorption

Plasticity behaviour is an essential property for the prediction of application scenarios of clay-rich sedimentary raw material and is closely linked to swelling potential (Anagnostou 1993; Einstein 1996; Kovari et al. 1981b; Madsen

& Kahr 1985; Madsen & Nüesch 1991; Wanninger-Huber 2019). The plasticity is described by the three Atterberg limits that depict different water contents at the transition of the plasticity from liquid to plastic to shrinkage water contents.

The liquid limit, w_{LL} , represents the first Atterberg limit and critical water content at which a fine-grained soil no longer flows like a liquid. Research has shown that values between 26-30% are sufficient to transform soil into a mud that flows uncontrollably, whereas the addition of 2% lime could make the soil more rigid (Oggeri et al. 2014). The plastic limit, w_{PL} , depicts the second Atterberg limit and critical water content at which fine-grained soil can no longer be remolded without cracking. The shrinkage limit,

w_{SL} , comprises the third Atterberg limit and critical water content at which fine-grained soil no longer changes its volume upon drying. Any loss of moisture is compensated by the entry of air into the pores. For the measurement of liquid limits, the analysis after Casagrande (1932) is commonly used.

For this study, no analyses of Atterberg limits have been conducted and only digitisation of former values as measured during the LHC construction are considered. Yet, the Enslin-Neff, surface area (BET) and mineralogical analyses (XRD) are used to model respective liquid limits and plasticity indices, which depict decisive parameters for the evaluation of application scenarios discussed in chapter 6. Extrapolating the digitised Atterberg limits from Molasse Rouge samples measured during LHC construction at depths of ca. 30-150 m in the Molasse Rouge implies a risk because the present values depict very low water contents ($\leq 5\%$). This is due to their storage over a longer period of time when compared to the digitised but fresh samples of water contents averaged of 10% (Table 5.1, or Géotechnique Appliquée Dériaz & SA (GADZ) (1982b, 1993b, 2015a)).

The model approach proposed by Dieng (2005) is tested for conclusions on plasticity behaviour, liquid and plastic limits as well as plasticity indices. Their model relies on the temporal water absorption behaviour (Fig. 5.30) at distinct time intervals given by the criteria $w_A + 0.3 \leq 210\%$, whereas $w_{Ai} = w_{A100} - w_{A5}$ represents water absorption values after 5 and 100 minutes, respectively, in conjunction with the maximum identified water absorption during the full 24 h measurement duration. The liquid limit, w_{LL} and plasticity index, I_P are calculated according to (Dieng 2005):

$$w_{LL} = 0.61 \cdot (w_A + 0.3 \cdot w_{Ai}) \quad (5.2)$$

and

$$I_P = 0.51 \cdot (w_A + 0.3 \cdot w_{Ai}) - 13 \quad (5.3)$$

Among the digitised LHC site investigation data, the majority of samples show a liquid limit at around 20%, which plots in the low plasticity region (Fig. 5.28). Statistical outliers above the U-line are removed and showed values up to medium plasticity. Liquid limits show a distinct scattering with values from ca. 20% (low plasticity) up to 53% (high plasticity).

The calculation of I_P according to the model is valid for all soils if $w_A > 40\%$. The condition applies for the present samples, excluding only the ones containing hydrocarbons (e.g. Pei-I-05B) with low water absorption temporal behaviour (Fig. 5.30) yielding values of ca. 3%. Besides the successful usage of the Enslin-Neff analysis via the approach after Dieng (2005), further models are investigated using the inputs of BET specific surface area, A_S , proposed by Farrar & Coleman (1967) and basal spacing d-values inferred from XRD analyses according to Dolinar et al. (2007). Liquid limits after Farrar & Coleman (1967) using BET surface area are modelled according to (Farrar & Coleman 1967):

$$w_{LL} = 19 + 0.56 \cdot A_S \quad (5.4)$$

The model after Farrar & Coleman (1967) proves to be a good method for the derivation of liquid limits for Molasse Rouge samples, despite requiring elaborate and time-consuming BET laboratory measurements. Fig. 5.31 shows the derived linear correlation of total phyllosilicates from XRD analyses on 27 Molasse Rouge samples with a good correlation coefficient of ca. 0.7:

$$V_{phyllo} = w_{LL, modelled} \cdot 2.39 + 25.88 \quad (5.5)$$

The approach after Farrar & Coleman (1967) follows liquid limit calculations according to $w_L = 19 + 0.56 \cdot A_S$. The model after Dolinar & Trauner (2004) uses a linear relationship between the external surface area and the liquid limit, and differentiates among equations tailored for expanding and non-expanding minerals, i.e. montmorillonite and quartz. For non-expanding minerals, the intergrain water content is equal to the liquid limit. However, for samples including expanding minerals such as the Molasse Rouge or glaciogenic deposit samples, the quantity of water at liquid limit is equal to both the intergrain and interlayer water contents. Besides only yielding the liquid limits when using these models and, thus, relying on either plasticity limit measurements or respective correlations as applied after Dieng (2005), they either under- or overestimate liquidity limits when compared to actual measurements (Fig. 5.29). Liquid limits after Kahr & Madsen (1995) overestimate realistic,

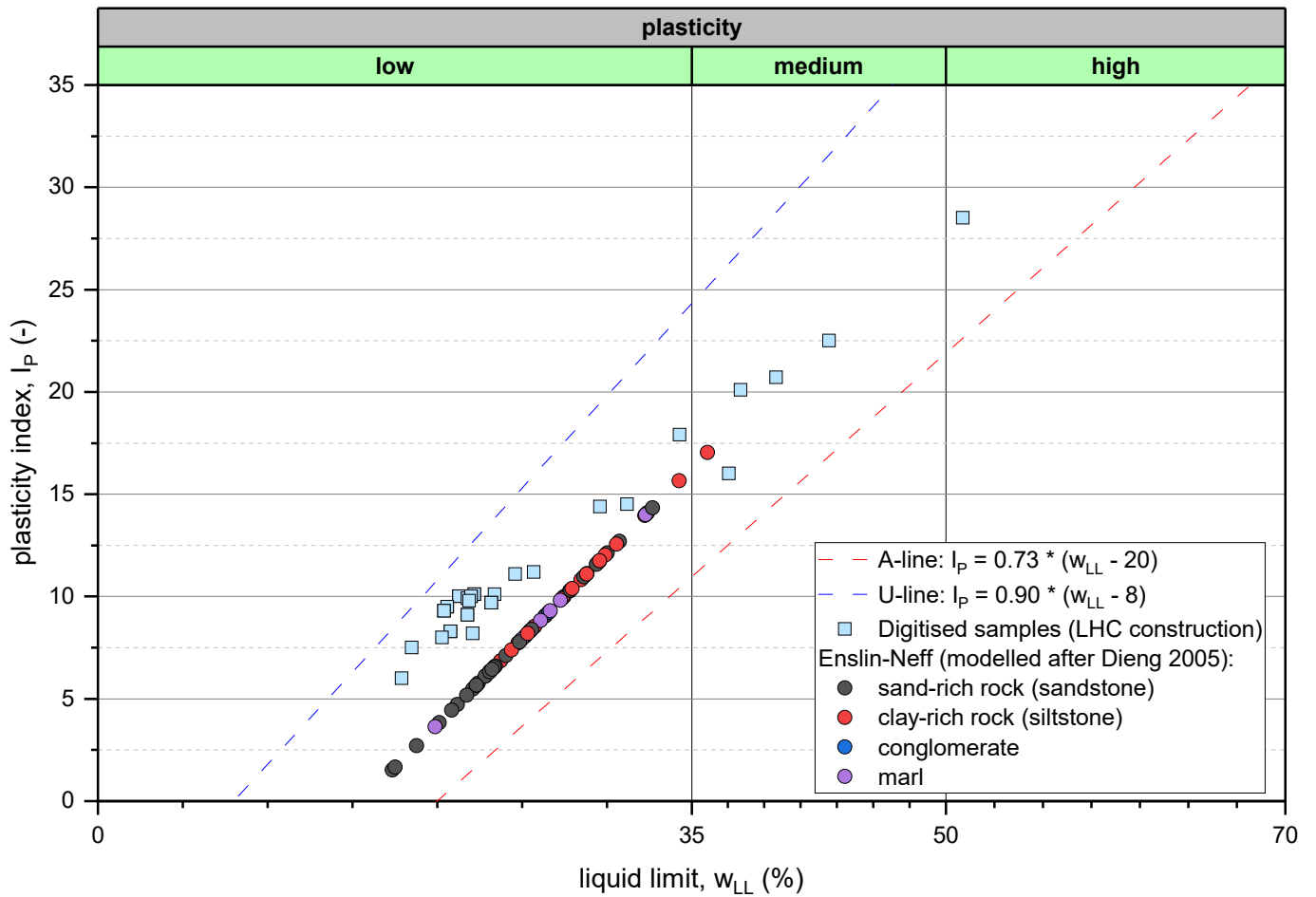


Fig. 5.28: Plasticity diagram grouped into low, medium and high plasticity for Molasse Rouge and Siderolithic rock samples comparing measured and modelled liquid limits via Enslin-Neff analyses, following the approach after Dieng (2005). The U-line defines the upper limit for natural soil. The A-line depicts the border between silt and clay.

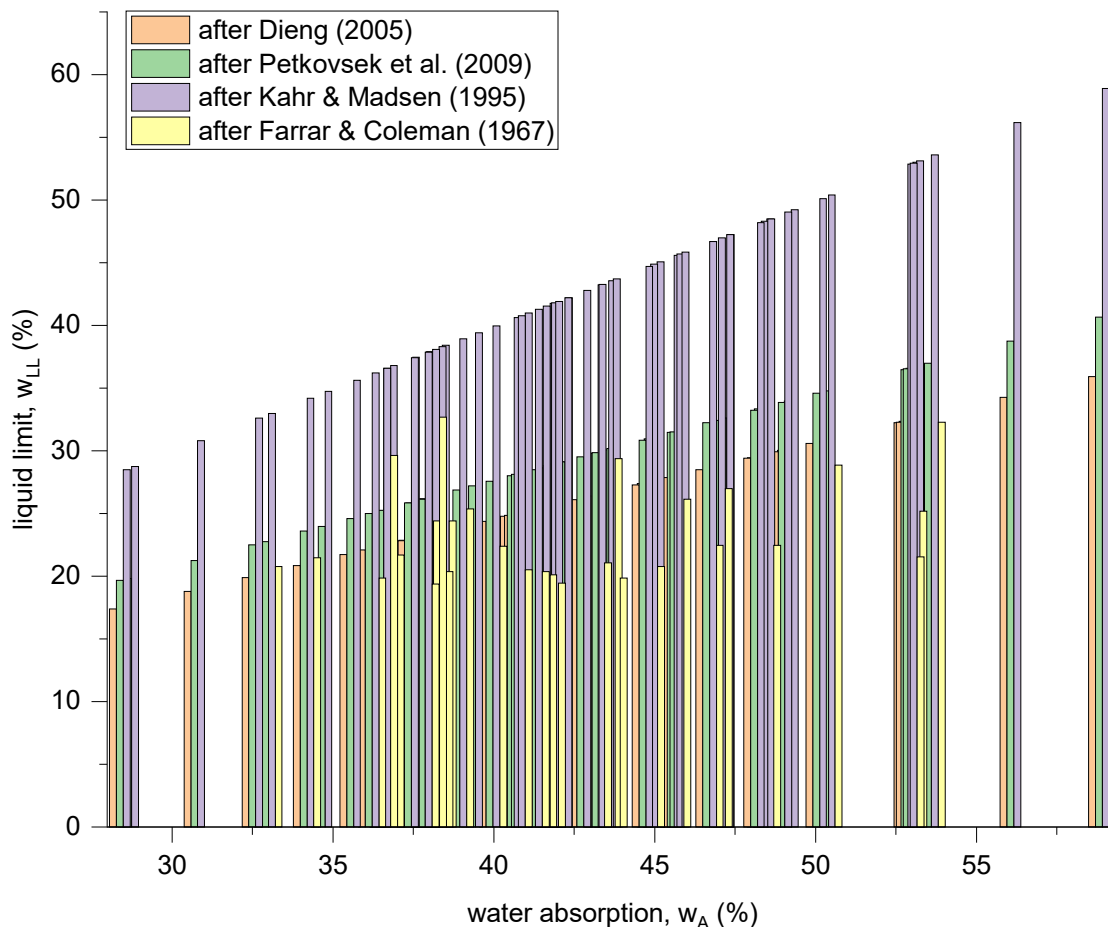


Fig. 5.29: Comparison of four modelled liquid limits. Note the overestimation of values after Kahr & Madsen (1995) as compared with digitised values.

i.e. digitised values, and would depict higher outcomes of plasticity indices for application scenarios such as brick production, shifting it to not feasible (too liquid) application and potential disposal.

It is concluded that the approach after Dieng (2005) is both the most reliable and conservative model for the present Molasse Rouge samples, and allows for direct calculations of plasticity indices using the Enslin-Neff temporal measurements. In addition, potential installation of Enslin-Neff on-site measurements favours the model after Dieng (2005) over the one after Farrar & Coleman (1967). The latter provides robust water absorption values but is dependant on time-expensive and complex specific surface area (BET) measurements. An issue with the approach after Dolinar et al. (2007) is the presence of expanding (swelling) clay minerals, as encountered in the Molasse Rouge formations represented by montmorillonite, and the required inputs. These inputs require specific surface

area, interlayer water quantity using calculations e.g., after Fink & Nakayama (1972), basal spacing values of montmorillonite at a relative humidity of 80% as well as exchangeable cations (Grim 1962), water adsorption (e.g. after Keeling et al. (1980)), and the total percentage of montmorillonite per sample (Dolinar & Trauner 2004). This approach is unpractical when compared to the models introduced by (Dieng 2005) and (Farrar & Coleman 1967).

Measurements of Atterberg limits after Casagrande (1932) are extensive and yield inconsistent, scattered results (Nagaraj et al. 2012; Wasti & Bezirci 1986). The approach after Dieng (2005) allows for a solid correlation while only performing the Enslin-Neff analysis, which could be terminated upon receipt of water absorption after 100 minutes if observing a steady water absorption behaviour with no further absorption after that time step. Except for the model after Dieng (2005), all other models require additional inputs for plasticity indices.

The temporal water absorption behaviour is the basis for the derivation of these plasticity indices after Dieng (2005). Fig. 5.30 depicts respective temporal Enslin-Neff measurements for sand-rich (Molasse Rouge and Siderolithic), clay-rich, marl and limestone samples. Water uptake over a longer period of time within hours implies that H_2O diffuses into the intermediate layers. If water uptake takes place within a short period of time of the first couple of minutes, this refers predominantly to capillary H_2O absorption. Maximum values peak for the clay-rich and marl samples with 0.58 and 0.46 ml, respectively. Marl and clay-rich samples show an immediate water absorption (e.g. Pei-I-03C), while others (e.g. C1-04A) do not show such a steep increase during the first minutes. Some samples persist to increase their water absorption over a longer period of time (e.g. C1-16A). The temporal water absorption behaviour depicts a distinct feature for hydrocarbon-bearing samples, also when subjected to (rain) water in the field as occurred during rock sampling (Fig. 5.30). Sample Pei-I-05B bears hydrocarbons and behaves very hydrophobically reaching maximum water absorption values of only 0.02 ml. Non-hydrocarbon-bearing sandstone reaches values up to 0.42 ml in the Molasse Rouge and 0.36 ml in the Siderolithic formations. Sand-rich samples show no temporal, consecutive water absorption over time. While this is explained best due to pores occupied by hydrocarbon, it is also caused by the decreased amount or complete lack of swelling clay minerals, i.e. smectite (Fig. 5.6).

The established correlation herein shows liquid limits and specific surface areas increasing linearly with increasing clay content (Fig. 5.32). Linear correlations with very good Pearson correlation coefficients of 0.8 for the water absorption to total phyllosilicate relationship, and ca. 0.9 for the water absorption to specific surface area correlation are derived. The amount of clay minerals, in particular, smectite predominantly influences the water absorption behaviour as well as specific surface area in this linear, positive correlation (Fig. 5.31). Previous studies (e.g. Farrar, Coleman 1967; Grim 1962; Muhunthan 1991; Seed et al. 1964; White 1949) have correlated these parameters and included also Atterberg limits, clay content, grain size, specific surface

area and cation exchange capacity. These linear correlation results, however, varied considerably, which is the reason for testing a reasonable (successful) polynomial fit as part of this study (Fig. 5.32) among surface area and water absorption. The linear correlation seems to work better for marl and clay-rich rocks, while a rather polynomial (exponential?) trend for sand-rich samples is observed, in particular at low surface areas and low water absorption values. Hence, the polynomial second-order trend through the full data for the surface area suggests a good convex quadratic relationship fit.

The confidence band shows the limits of all possible fitted lines for the given data. There is a 95% confidence that the best-fit line lies within the red band. The width of the confidence band is proportional to the standard error of the predicted y value. This means that the band becomes narrower when the standard error decreases, and gives the typical flared outward shape towards the end of the data range. For the case of zero error, the confidence band collapses into one single line.

Natural water content

For wells SLHC20 to -25 close to the FCC alignment in the northern construction area, digitised values of water contents of fresh Molasse Rouge samples are strongly varying, and show no distinct correlating trend with depth (Fig. 5.33). The water content is slightly decreasing with increasing depth as observed for the SPL wells further away from the FCC alignment. The transition between the Quaternary glaciogenic deposits and the Molasse Rouge formation extends approximately between depths of 25 to 40 m on average at well locations in the north. No groundwater aquifer zones are identified by increased water contents. Measured (non-digitised) samples as part of this study contain water contents between 0.1 to ca. 5% as they have been stored for a longer period of time (>1 year) but required water content measurements refer to dry-wet weight corrections.

Cation exchange capacity and exchangeable cations

Besides the exploitation of modal mineralogy, QEMSCAN image analyses, elemental distributions, and modelled plasticity behaviour for the characterisation of sampled

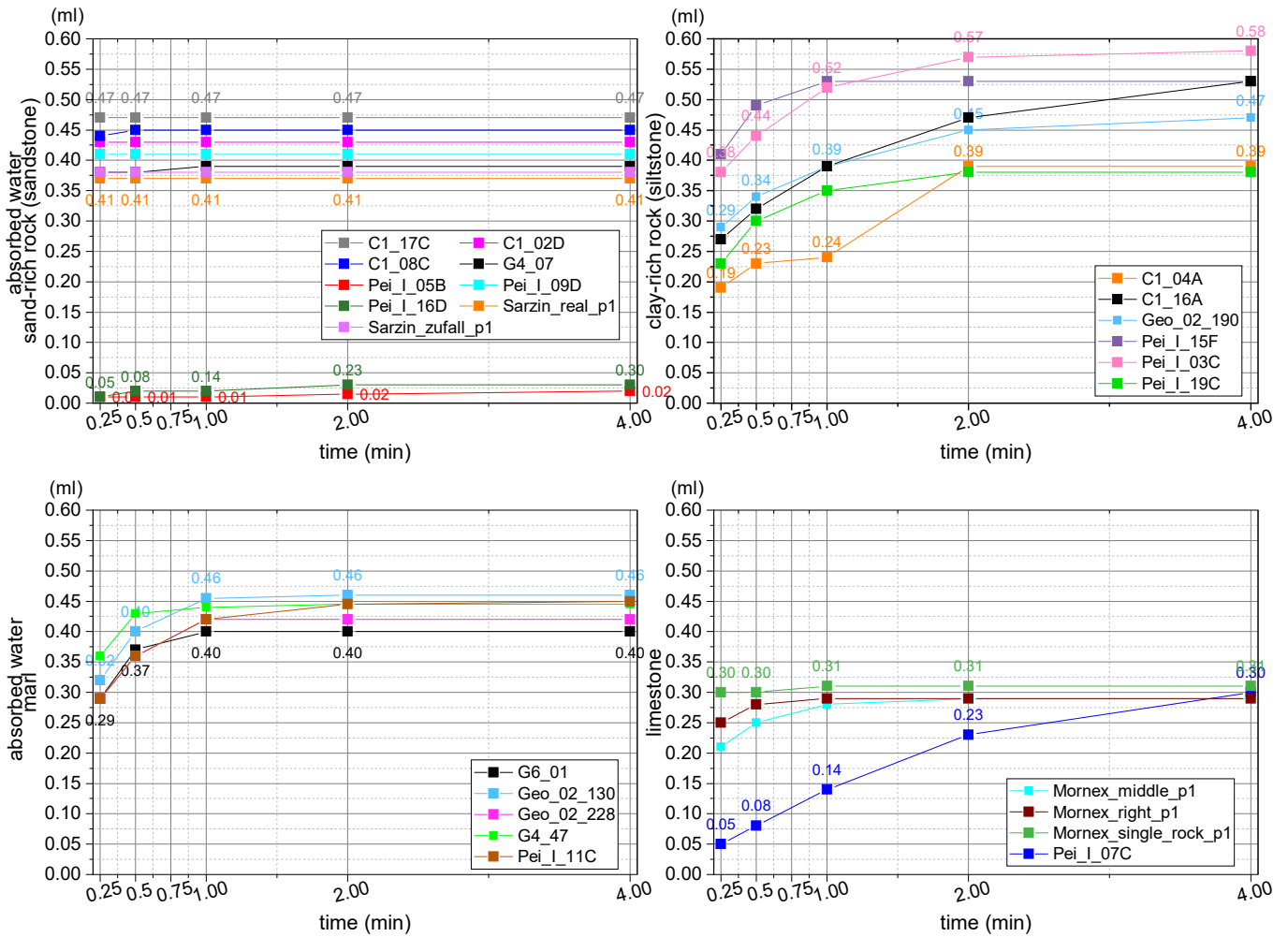


Fig. 5.30: Temporal water absorption behaviour of sand-rich, clay-rich, marl and limestone samples in the Molasse Rouge, and sand-rich rock (sandstone) of the Siderolithic formation measured via Enslin-Neff. Analyses lasted for 24 h per sample for the derivation of plasticity indices after Dieng (2005). The depicted samples show no significant increase of water absorption after 4 minutes, while after 30 minutes most of the behaviour is associated to evaporation.

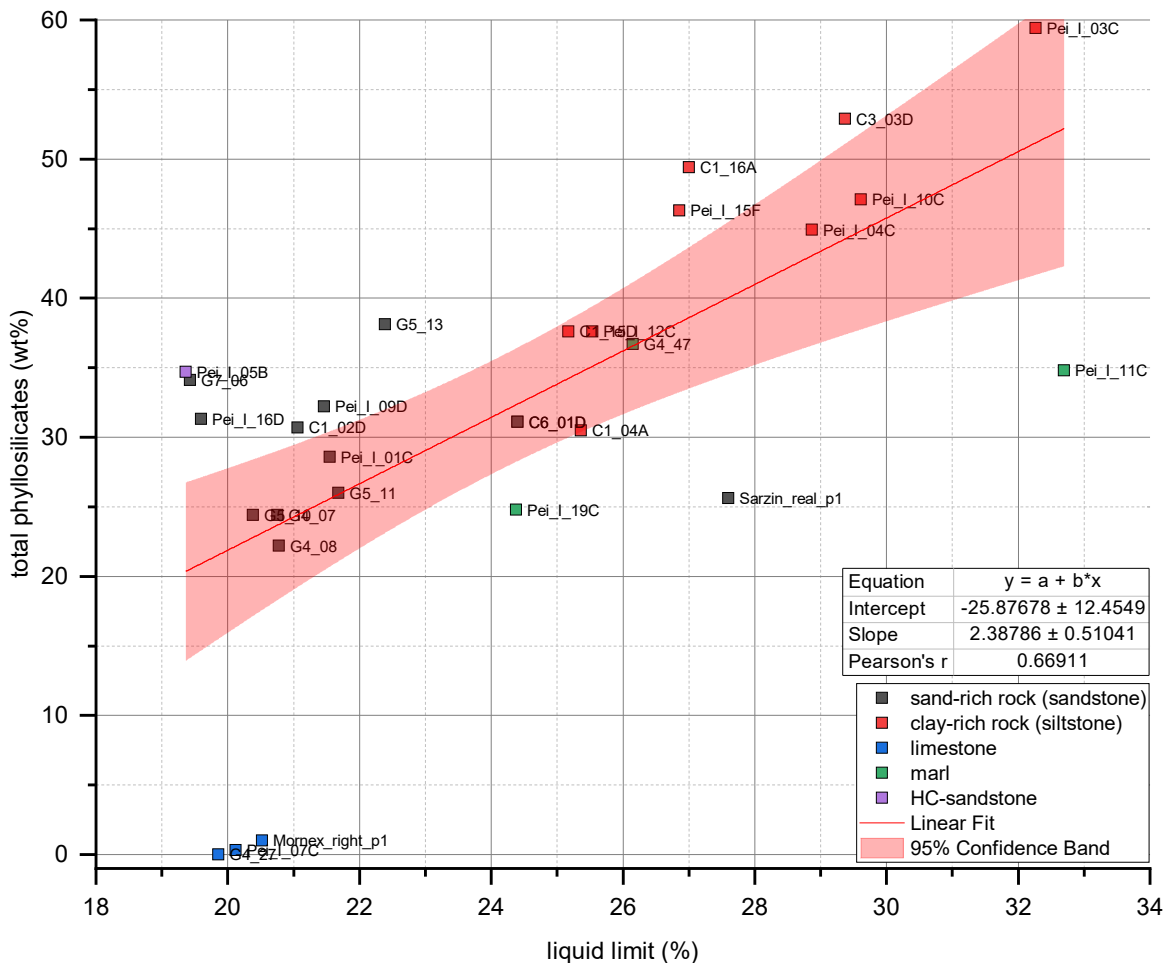


Fig. 5.31: Correlated linear relationship for 27 Molasse Rouge samples based on total phyllosilicate content from XRD analyses and modelled liquid limits using BET surface areas, A_S . Limestone outliers (Mornex samples) are excluded from the linear fit. All samples contain a TOC $\leq 1\%$.

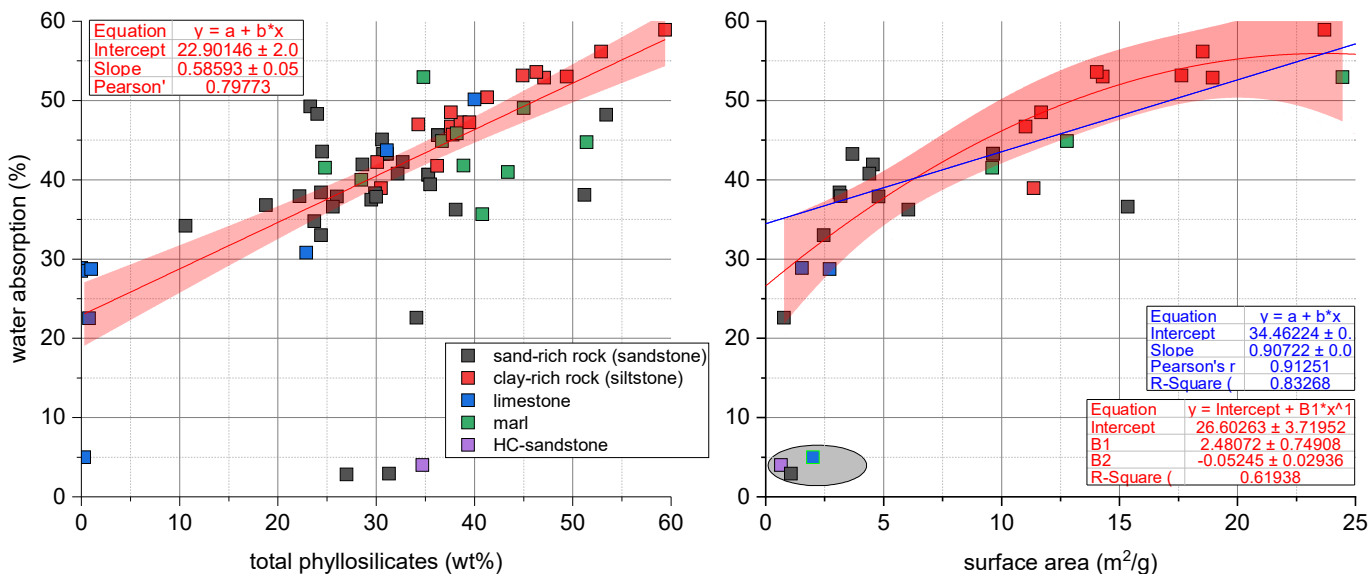


Fig. 5.32: Water absorption dependencies on total phyllosilicates based on 70 Molasse Rouge samples (left) and BET surface areas on 27 Molasse Rouge samples (right) with both linear (blue) and polynomial (red) correlations. Limestone outliers depicted in grey ellipses are excluded from fitting curves. The red area depicts the 95% confidence band ($y = \pm t_{\alpha/2}$) estimated standard error of prediction. All samples contain a TOC $\leq 1\%$.

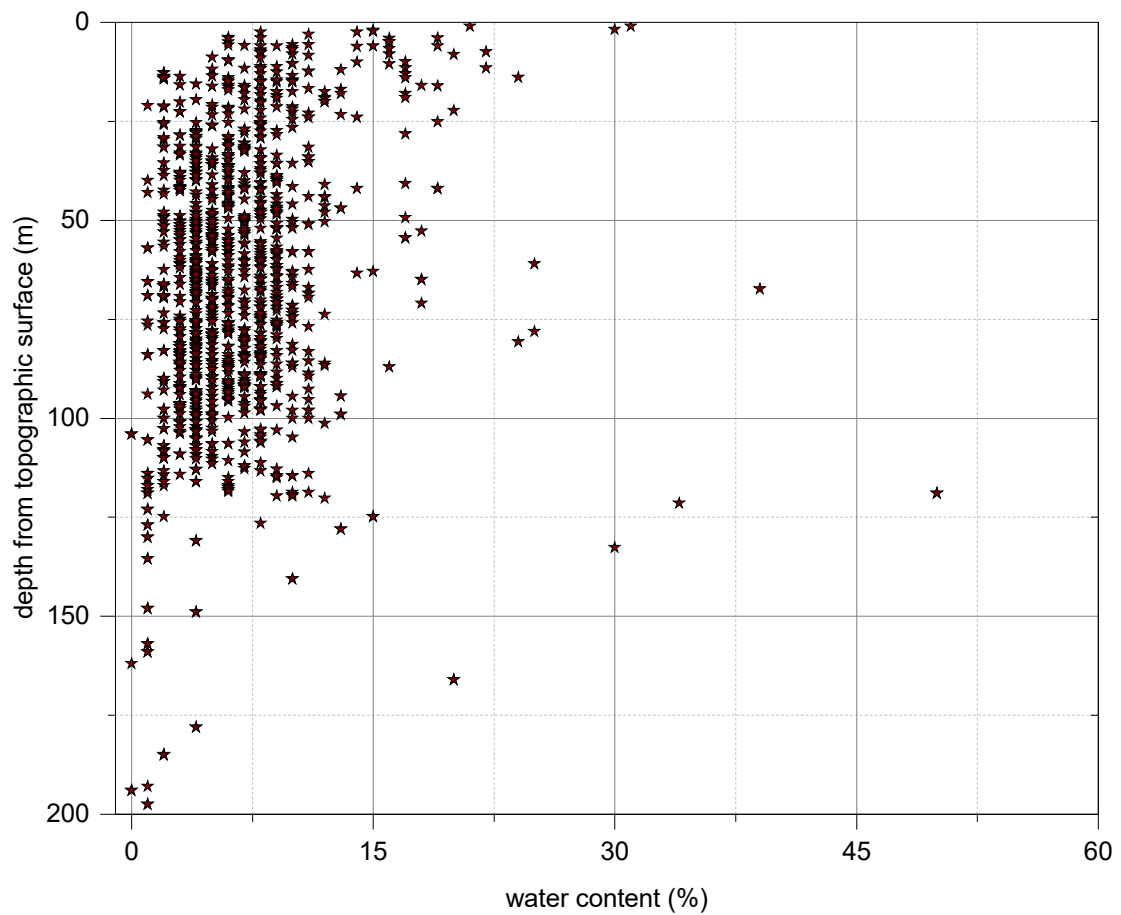


Fig. 5.33: Water content from 1'168 digitised Molasse Rouge samples taken during the LEP and LHC site investigations from boreholes SPLx.xx, SLHCxx, SPMxx, and Lxxx, with x denoting consecutive well numbers.

raw materials, further physico-chemical rock properties are now incorporated into the rock classification scheme. These include the cation exchange capacity (CEC), type of exchangeable cations, the amount of organic matter (TOC), solubility (eluate), water vapour adsorption and grain size distributions. All samples from the glaciogenic deposits, the Molasse Rouge, the Grès et Marnes Gris à gypse and Siderolithic formations show values $\leq 1\%$ of total organic carbon content.

As previously investigated, the complex matrix of various rock properties results from alteration paths of the parent rock (Fig. 5.24, 5.25). Two distinct proxies for these alterations are CEC values and exchangeable cations including the base cations K^+ , Ca^{2+} , Mg^{2+} , and Na^+ , the acidic cation Al^{3+} as well as trace metals Li^+ and Sr^{2+} . The latter two play a minor role compared to the base cations. The CEC value and exchangeable cations are the most sensitive parameters when it comes to changes of mineral properties (Dohrmann et al. 2012), and further play a crucial role in the prediction of application scenarios. The CEC value is required to understand nutrient availability for agricultural problems and plants, and is linked to essential cations such as K^+ and NH_4^+ as well as cations of non-acidic soils such as Na^+ , Mg^{2+} , and Ca^{2+} , which are fully reversibly adsorbed.

Differences of exchangeable cations could also be insightful in understanding transport processes in barrier materials. The most important property of CEC is its reversibility (Johnson 1859). The CEC is a good indicator for swelling behaviour and illitization (Kaufhold & Dohrmann 2010a,b). In the context of application scenarios, it is common to refer to the methylene blue value (MBV), which has been used successfully to derive both CEC and specific surface area values on bentonites assuming a monomolecular methylene blue covering (e.g. Kahr, Madsen 1995), which yielded reasonable correlations (Boust 1984; Brindley & Thompson 1970).

For the present study the CEC values derived by the copper-complex and exchangeable cations analyses are treated as the methylene blue value (MBV). The MBV analysis is an overestimation of CEC for sedimentary rock, and not a reliable analysis method despite its rapid application (Chiappone et al. 2004; Kahr & Madsen 1995; Yariv et al. 1990). Major drawbacks of the methylene blue test originate from the type of exchangeable cations of the

clay mineral, e.g., the fixed clay-to-water ratio, the observation of a constant pH, which is rare given the dissolution processes, and knowing the exact concentration of methylene blue in order to achieve reproducible results. Changes of pH are induced by differences in the soil-to-water extraction ratio, the electrolyte concentration of the soil suspension (Robertson et al. 1999). The MBV is suitable for quality control checks of a certain clay but due to its pH-dependent edge charge nature of clay minerals, yields too low CEC values in sulphuric acid solution (positive edge charge), and too high CEC values in alkaline (Na) pyrophosphate solutions (negative edge charge) (Kahr & Madsen 1995). This is the case in non-calcite (high pH) bearing Molasse Rouge samples. Hence, the Cu-trien complex is preferred and the CEC results presented herein depict the conservative end for clay minerals. During the methylene blue test, the methylene blue cation is exchanged (adsorbed) for the exchangeable cations of the respective clay minerals (Hofmann & Dammler 1969). Consequently, the methylene blue adsorption is strongly dependent on the dispersion, the pH value and the type of cation. Adsorption is complete explicitly in the Li^+ - and Na^+ -exchanged form, and incomplete methylene blue adsorption of exchangeable cations with higher charged and exchanged cations Ca^{2+} , Mg^{2+} and Al^{3+} . The methylene blue method is explained e.g., in (Hofmann & Dammler 1969) and Brindley & Thompson (1970).

Many authors have studied the influence, reliability and correctness of various CEC analysis techniques, including the Cu-trien method as conducted herein and the methylene blue value test. The term "correctness" was thereby often referred to properly functioning methods without any systematic errors, or at least knowing their sources (Dohrmann et al. 2012). The fixation of cations strongly depends on the clay mineral structure. A review study by Sawhney (1972) concluded that K^+ fixation differs among di- and trioctahedral 2:1 clay minerals, attributed to the fact that vertically oriented OH-dipoles of hydroxyls in trioctahedral layer silicates results in a weaker bonding of the K^+ than the inclined OH-dipole in the dioctahedral layer silicates. Given the smaller size of the octahedral sheet in dioctahedral minerals this produces shorter K-O bonds and causes the K^+ to be held more tightly in dioctahedral minerals. The selectivity of edge interlayer sites of illite for K^+ is about 500 times greater than for Ca^{2+} . Hence,

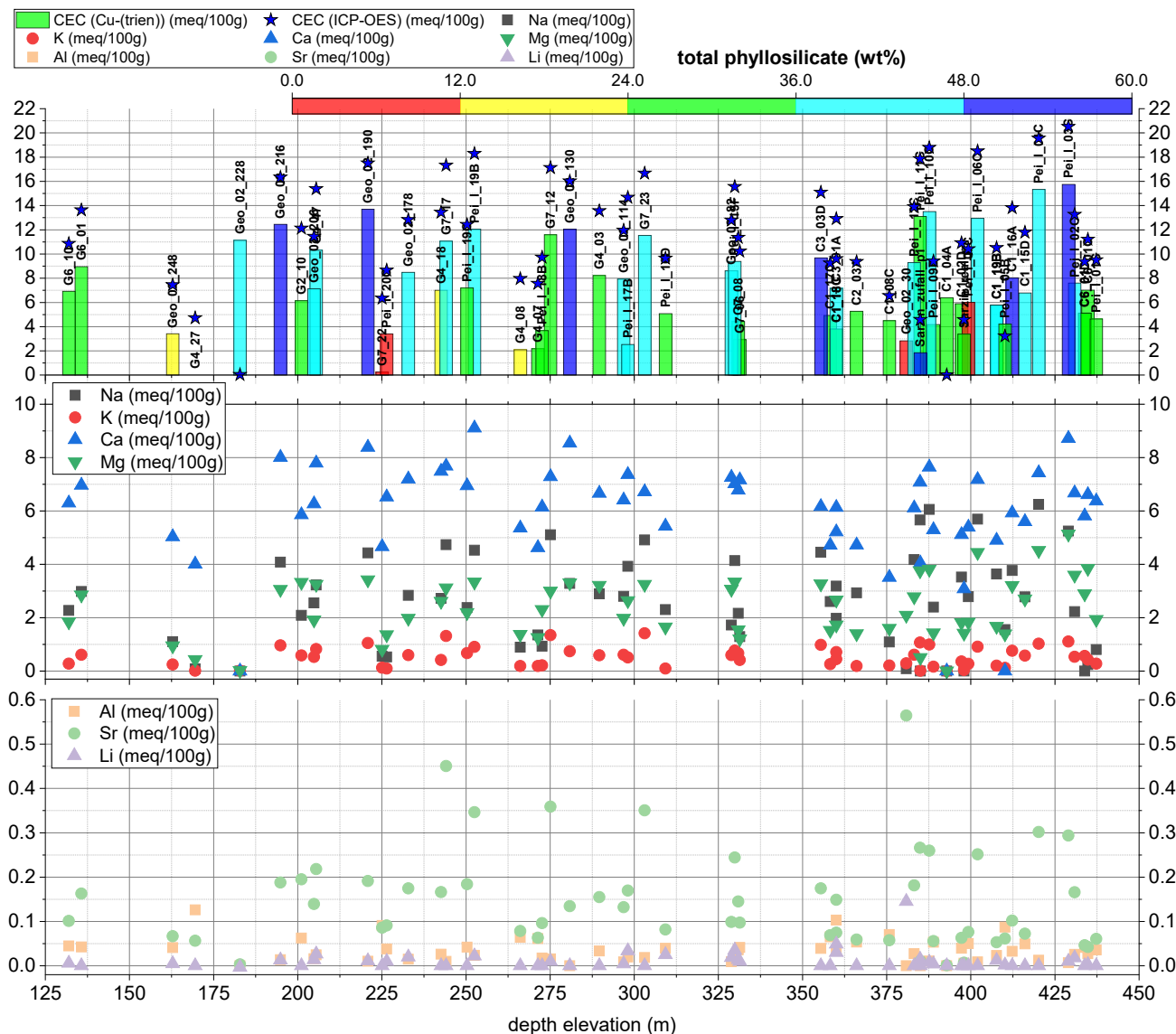


Fig. 5.34: (Top) Effective CEC from Cu-trien complex and sum of CEC ICP-OES analyses with respect to total phyllosilicate content. (Middle) Exchangeable cations Na, K, Ca and Mg. (Bottom) Exchangeable cations Al, Sr and Li. All at respective depth elevation levels relevant for the FCC range measured on 70 Molasse Rouge samples.

CEC analyses yield different results if samples contain substantial amounts of illite (M. L. Jackson 1962). This is the case for the samples studied herein.

While it is not the goal of the present study to predominantly investigate on the CEC and exchangeable behaviour of Molasse Rouge samples, it should be noted that most critical reactions are associated with carbonates and phosphates. Whether all cation-exchange processes should be characterized by the term "CEC" is not yet fully defined and the term should be used to explicitly describe reversible cation exchange processes even though former research misleadingly also used the CEC term for any replacements of cations when these exchanges were not reversible (see e.g., Dohrmann et al. 2012).

Fig. 5.34 shows the measured CEC values of both the Cu-trien complex and ICP-OES measurements (top), as well as the exchangeable cations Na, K, Ca, Mg (middle) and Al, Sr and Li (bottom) across the FCC's intersected depth interval. Shallower depth values (at 400-450 m) are relevant for shaft construction but main focus is spent on the 100-300 m ASL construction interval. The analyses reveal that all samples show little to no significant Li and Al exchangeable cations ranging between 0 and 0.12 meq/100g. Sr cations of range between values of 0.05 and up to 0.55 meq/100g. Correlations of XRD results (Fig. 5.6) with CEC values (Fig. 5.34) of Sr values up to ca. 0.2 meq/100g seem to correspond predominantly to samples G4-27, G4-07 or Pei-I-16D containing no gypsum or clay minerals (G4-27) but mainly quartz and calcite. This suggests that Sr cations are associated to calcite and predominantly to gypsum because the highest Sr values are measured in the sample with the highest gypsum content (Geo-02-30). At the same time, this sample contains total phyllosilicates below 12%, substantiating the argument of Sr being primarily associated with gypsum, calcite as well as quartz. The exchangeable Ca cation shows higher values associated with samples containing a higher content of calcite, and less data scattering in shallow depth intervals between ca. 450 and 350 m compared to deeper depths below 320 m.

Besides sample Geo-02-228 yielding no effective CEC, sample Geo-02-248 shows similar (high) Ca cation values despite a low phyllosilicate content. This substantiates the argument for calcite dissolution dissolving Ca cations. Besides calcite, the Ca cation could originate from the Ca-form of montmorillonite, which is predominant in the clay

mineral distribution. The data show that higher total phyllosilicate content correlates well with higher values of both Cu-trien CEC and exchangeable cation values. For sample Geo-02-30 containing the highest amounts of gypsum (Fig. 5.6), the question remains if more gypsum than calcite was dissolved and measured as exchangeable cation (Fig. 5.34).

Ideally, the sum of exchangeable cations coincides with the Cu-trien effective CEC values. Hence, the question is legitimate why 100% was not attained in any sample. Most of the samples contain cations in excess of the CEC, which could be explained by an excess of electrolyte. Furthermore, a larger anion concentration (e.g. from Cl^-) could explain the higher CEC values. The same would apply for an excess of sulphates, or varying pH regimes during the measurements. The chloride and sulphate anions could also form free salts that have not compensated the negatively-charged sites on clay minerals. Calcareous and saline soil exchangeable cations also overestimate CEC because measured cations include those solubilized from minerals (see e.g., (Robertson et al. 1999)). A final explanation refers to the adsorption on organic matter but can be excluded based on the low (<1%) TOC values.

The chloride and sulfate anions as well as dolomite inflate the exchangeable Na^+ , Mg^{2+} , and Ca^{2+} values. The soluble minerals gypsum, calcite, and dolomite are known to dissolve during experiments in order to exchange cations. Calcite dissolution during the analysis buffers the pH influenced by parameters such as reaction time and carbonate content. In carbonate minerals, according to the literature, it is assumed that the calcite and dolomite surfaces consist of three major ion exchanger sites, which include surface Ca, surface Mg, and surface carbonate (Mahani et al. 2016; Shabani & Zivar 2020). Zou et al. (2021) state that the ion exchanger absorbs the ions from the aqueous phase that causes a disturbance of the brine-rock equilibrium; in order to compensate that, the minerals precipitation-dissolution occurs to achieve the equilibrium in the aqueous phase. More calcite dissolution occurs in the brine-rock interaction leading to the compensation for the lack of cations in the aqueous phase, and hence to higher exchangeable Ca cation values. Dissolution of these minerals causes an excess of exchangeable Ca^{2+} with gypsum producing the highest excess, followed by calcite and dolomite, which is well depicted by e.g., samples Geo-02-30 (high

gypsum). The dissolution of dolomite also causes an excess of Mg^{2+} , although Mg cation values occur in moderate ranges between 1 and 5 meq/100g. Samples containing no dolomite or calcite (Sarzin-real) show low values of Mg cations. Even though the problem of inflated Ca^{2+} values caused by dissolution of calcite and dolomite could be minimized if calcite-saturated exchange solutions are used, this was not specifically targeted herein because the main goal was to derive basic CEC and exchangeable cation values. For the dissolution of Mg^{2+} , dolomite is the predominant dissolved mineral inferring the Mg^{2+} exchangeable cation. With reference to clay minerals, sample Pei-I-03C shows the highest Mg cation values. Its Mg cation values could be associated to samples that contain substantial amounts of mica and smectite as does the Pei-I-03C ranging at maximum Mg cation values across all samples.

High Ca and Mg cation values correspond to samples that contain more carbonate minerals, i.e. Freshwater limestone or the violet marl. K or Na cations correlate well with high amounts of kaolinite and illite. There seems to be a tendency that clay-rich rocks containing smectite tend to attract double positively-charged cations (Mg, Ca). The results depict that CEC originates predominantly from the exchangeable Ca cation.

Exchangeable cations Li, Sr and Al play a minor role. High exchangeable cation values correspond to samples containing above ca. 12% total phyllosilicate, i.e. clay mineral (smectite) content. Ca is mainly associated to calcite dissolution. Low total phyllosilicate content refers predominantly to low exchangeable K, Na, Mg (in that order) and low exchangeable Li, Al and Sr (in that order) cations, clearly associated to clay minerals, i.e. smectite (montmorillonite), while exchangeable Ca cations remain relatively high at values ranging between 5.5 and 9 meq/100g when encountering calcite (or dolomite) values above ca. 15-17% per sample (e.g. Geo-02-248, G7-22). The highest exchangeable Na and Mg cation values correspond to increased K values, with a total phyllosilicate content of $\geq 24\%$.

The data does not show a trend for the type or amount of exchangeable cations and CEC values with respect to depth. This underlines the heterogeneity of the Molasse Rouge not only by its stratigraphic levels and associated lithotypes but also its chemical rock behaviour.

Grain size distribution

For the evaluation of grain size distributions (GSD), respective data of 19 boreholes with a total of 53 sieve analyses have been digitised and categorised per formation (Fig. 5.35). The GSD curves extend from depths of 3 to 205.5 m.

In the glaciogenic deposit formation, two trends are observed, whereas below 50 m no pattern is distinguished (dark green) as summarised as one trend. From 50 to 100 m, clayey gravel and sandy gravel patterns are identified (light green). These two trends make the glaciogenic deposits a widely-graded material for the dark-green and closely-graded material for the light-green trends.

Two widely-graded and one closely-graded predominant patterns are identified in the Molasse Rouge formation. The first pattern (orange) is associated with sandy gravel at shallow depth below ca. 50 m. Clayey gravel is analysed in an interval from 50 to 75 m depicting the second trend (grey), with the third pattern attributed to silty sand in depths from 75 to 100 m (yellow). The first trend in the Molasse Rouge depicts a poorly graded rock ranging from clay up to fine to medium sand. The second trend is a widely graded rock with a high content of fine-grained, clay and silt with a small portion of sand and gravel. The first and second trend correlate with a mean permeability of about $5 * 10^{-8}$ m/s depicting impermeable rock. The third trend shows a widely graded rock mass with a low content of fine-grained clay, silt and sand with a high content of gravels and cobbles. For the third trend, the mean permeability results to ca. $4 * 10^{-3}$ m/s, classified as permeable. The less permeable rock is located at a deeper depth compared to the highly permeable rock. With respect to permeability behaviour, three similar trends are observed. The first one reflects a poorly-graded rock ranging from clay up to medium-to coarse-grained sand with a mean permeability of $1.5 * 10^{-6}$ m/s, classified as slightly permeable. The second trend depicts a widely-graded rock with low content of fine-grained grain sizes but a high content of gravel and cobbles having a mean permeability of $5.9 * 10^{-6}$ m/s, also slightly permeable. The third trend is a widely graded rock with a high content of fine-grained grain sizes and a mean permeability of $5.6 * 10^{-8}$ m/s, classified as poorly permeable. This behaviour is observed also visually in the field as well as by the mercury injection measurements that show hydrocarbon-sandstone as the

most coarse-grained, followed by respective populations of fine- and medium-grained sand-rich as well as clay-rich and marl samples (Table 5.2, 5.3, 5.4). They depict a large variability of pore diameter classified into the respective rock types introduced above, and show also a higher variability of grain sizes and respective (quartz) grain size distributions as depicted in QEMSCAN image analyses.

The Freshwater limestone allows only limited conclusions based on three grain size distribution curves that show a middle-graduated trend (blue).

Statistical analysis of physico-chemical data

A principal component analysis (PCA) has been performed for the physico-chemical data. Fig. 5.36 depicts the three principal components (PCs). Fig. 5.37 depicts the overlay of PCA loadings and scores. The investigated parameters are total phyllosilicates, smectite, quartz dolomite/ankerite and calcite contents, water absorption and water adsorption, CEC from ICP-OES analyses, as well as TIC and TC.

Sand-rich samples lie along the SiO_2 vector. They depict outliers being located farther away from the origin of the plot. The same accounts for the limestone sample. These three samples are located in the PC1-PC2 plane as well as one sand-rich sample in the top of the depicted plot. Smectite and total phyllosilicate vectors correspond well with the clay-rich and marl samples as do the calcite and dolomite vectors for the latter one. TC and TIC values lie in the PC1-PC2 plane and are associated with sand-rich, clay-rich and marl samples but not with the limestone lithotype. This means that organic matter is predominantly contaminated in sand-rich to clay-rich samples. TIC and TC parameters are not correlated with any water absorption or adsorption behavior depicted by the 90° angle among these vectors.

A relationship between the smectite, total phyllosilicate contents, water absorption and water adsorption is observed with an angle difference of ca. 50° . These physico-chemical properties correlate well with the presence of clay minerals. The longest vector length is depicted by the CEC parameter, which shows a very large variability. The CEC values from the Cu-trien complex analyses yield low eigenvalues when included in the PC analysis. There seems to

be no correlation for water absorption or water adsorption, smectite as well as total phyllosilicates and organic matter (TC and TIC) parameters for the limestone lithotype. However, this is due to the insignificant number of limestone samples.

5.3.4 Petrophysical and geomechanical correlations

Petrophysical and rock mechanical properties are further implemented into the rock classification scheme. These include porosity and permeability to conclude on flow zone indicator values, rock quality indices, ultrasonic wave velocities as well as rock strength properties such as uniaxial compressive strength, Brazilian tensile strength and abrasivity properties such as CAI, LAC and LBC indices.

Flow zone indicator, rock quality indices and ultrasonic wave velocities

Permeability and porosity values of the Molasse Rouge formation range predominantly between 0.001 to 10 mD and 0 to 19%, respectively. Their permeable properties depend on their grade and type of cementation, i.e. clay mineral content for sand-rich, clay-rich and marl rock types and carbonate content for marl limestone rock types (Fig. 5.38). The medium- and coarse-grained, sand-rich samples imply a secondary permeability, which establishes a continuous network path for an increase of permeability. These samples show a low grade of cementation and depict higher permeability and porosity values between 10 to 1'000 mD and 20 to 30%, respectively. During the well review process, Lugeon borehole test results in borehole SLHC21 and SLHC23 show permeability values ranging between 0 to 0.5 Lugeon Units in the Molasse Rouge, whereas 1 Lugeon Unit is equal to 10^{-7} m/s in a homogeneous, isotropic medium. The highest permeability values reach $5 \cdot 10^{-8}$ m/s. Based on these tests, no groundwater inflow has been observed in SLHC20-25 (Géotechnique Appliquée Dériaz & SA (GADZ) 1996a). These low permeability values obtained from the Lugeon tests coincide with respective permeability and porosity values acquired in boreholes farther to the south.

Fig. 5.38 shows no clear trend based on the total clay and carbonate contents. As a result, the fluid flow behaviour is

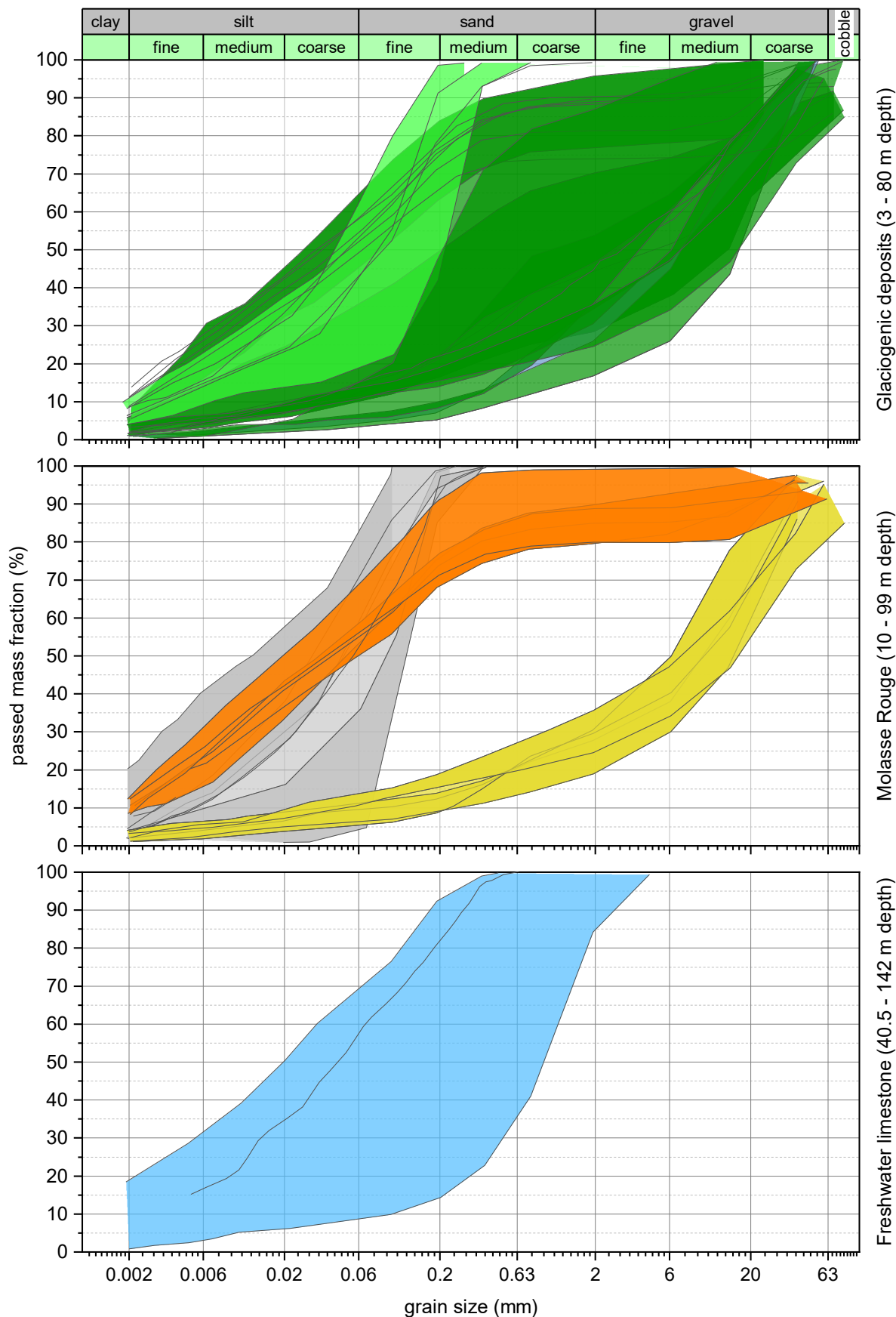


Fig. 5.35: Digitised grain size distribution curves as measured on samples taken during LEP and LHC site investigations from the following borehole locations: SPLx.xx, SLHCxx, SPMxx, and Lxxx, with xx denoting the consecutive well numbers. Colours depict different trends depending on curve uniformity. Data compiled from Géotechnique Appliquée Dériaz & SA (GADZ) (1981a,b, 1982a,b, 1992, 1993a,b, 1996a,b).

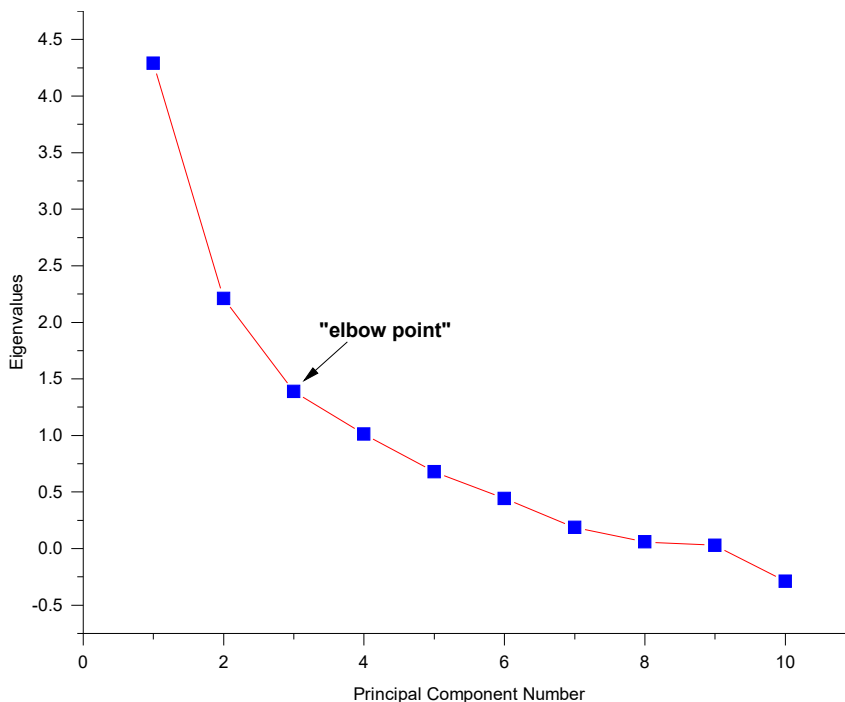


Fig. 5.36: PCA screeplot of clay data depicting the ideal number of principal components (3) based on the "elbow point". The three PC together make up ca. 79% of the total variation in the data sets comprising all physico-chemical, FTIR and XRD analyses.

investigated in more detail for these clay- and carbonate-rich samples and compared with marl and medium- to coarse-grained sand-rich samples in the Molasse Rouge formation. A useful parameter in order to assess fluid flow has been found by means of their rock quality index (RQI³) and flow zone indicator (FZI) as proposed by Amaefule et al. (1988). The FZI considers texture and mineralogy and is also more sensitive to pore geometry and hydraulic behaviour compared to permeability and porosity values. The FZI is a common parameter in the oil and gas industry to evaluate reservoir properties. Usually, these FZI values lie between 5 to 20 μm (e.g., for North Sea reservoirs), whereas the Molasse Rouge samples show lower FZI values between 0.001 and 1 μm and allow for further characterisation of respective sub-categories of clay-rich, sand-rich and marl samples. The FZI (μm) is calculated according to (McPhee et al. 2015):

$$RQI = 0.0314 \sqrt{\frac{k}{\phi}} \quad (5.6)$$

$$\phi_Z = \frac{\phi_e}{1 - \phi_e} \quad (5.7)$$

³Note that the RQI value should not be confused with the geomechanical rock quality designation index (RQD).

$$FZI = \frac{RQI}{\phi_Z} \quad (5.8)$$

where k is the Klinkenberg-corrected permeability (mD), ϕ_e depicts the core helium porosity and RQI is the rock quality index (μm), sometimes also referred to as *reservoir* quality index. In a *log-log* plot of RQI versus normalised porosity (Fig. 5.39), core samples with similar hydraulic characteristics and hence similar petrophysical properties lie along the FZI line depicting values from 0.001 to 5 μm . The intercept of the slope with the y-axis at normalised porosity is defined as the FZI for that group of samples. The majority of the data fall within a narrow range of FZI values from 0.001, 0.01 and 0.1 μm . Medium- to coarse-grained samples are located between FZI values of 0.1 to 1 μm . The plot also shows that clay-rich rock samples are less permeable (FZI value below 0.01 μm) compared to carbonate-rich(er) samples.

The fluid flow behaviour is influenced by grade and type of cementation and makes it prone to mineralogy and texture variations. A similar behaviour is found for compressional and shear-wave velocity values, which prove to be reasonable indicators for compaction trends. An excellent,

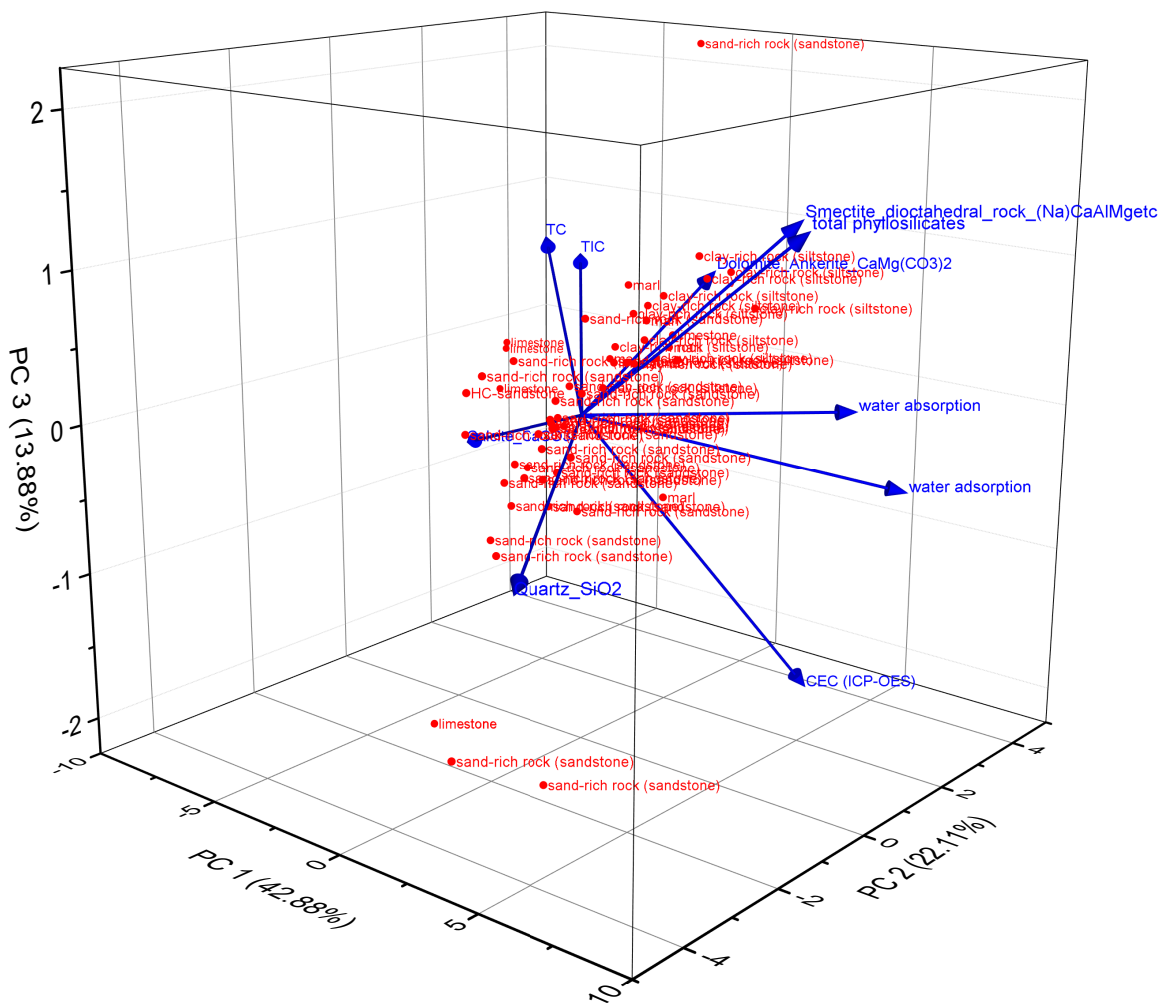


Fig. 5.37: Pairwise PCA 3D biplot of clay data for cross-correlations among total phyllosilicate, smectite, quartz, calcite, dolomite content with water absorption (Enslin-Neff), water adsorption (Keeling), CEC from Cu-(trien) and ICP-OES, TIC and TOC values. PC1, PC2 and PC3 denote 42.88%, 22.11% and 13.88% of the total variation along the components, respectively.

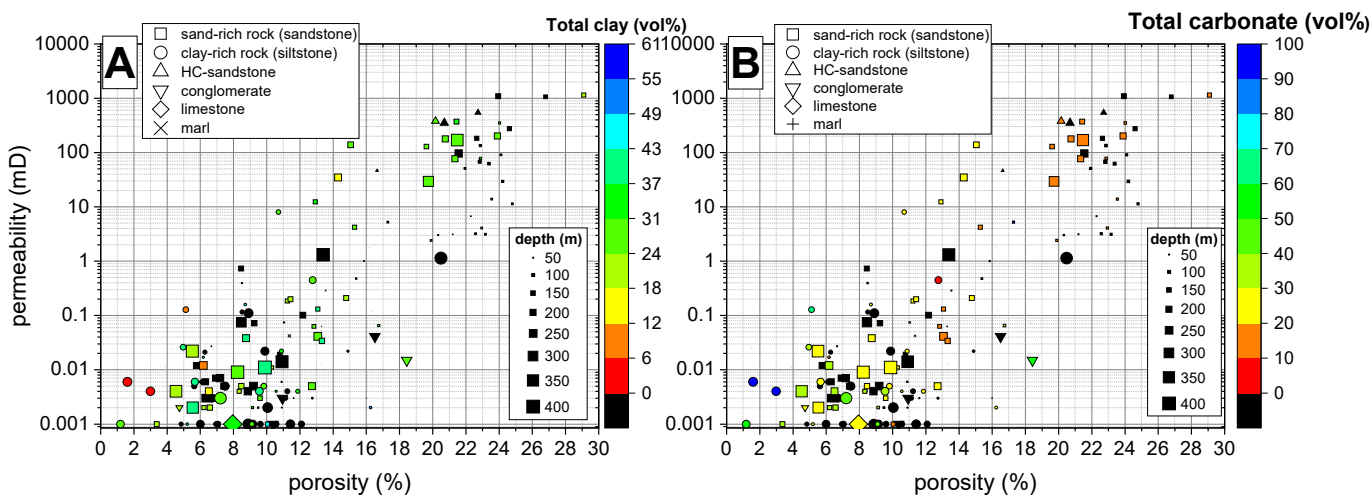


Fig. 5.38: Porosity and permeability results measured on 170 plug samples with respect to their total clay and total carbonate contents. 93 samples comprise the sum of mineralogical data (XRD and/or QEMSCAN). Samples without mineralogical information are depicted in black colour. Symbol size represents increasing sample (borehole) depths (m).

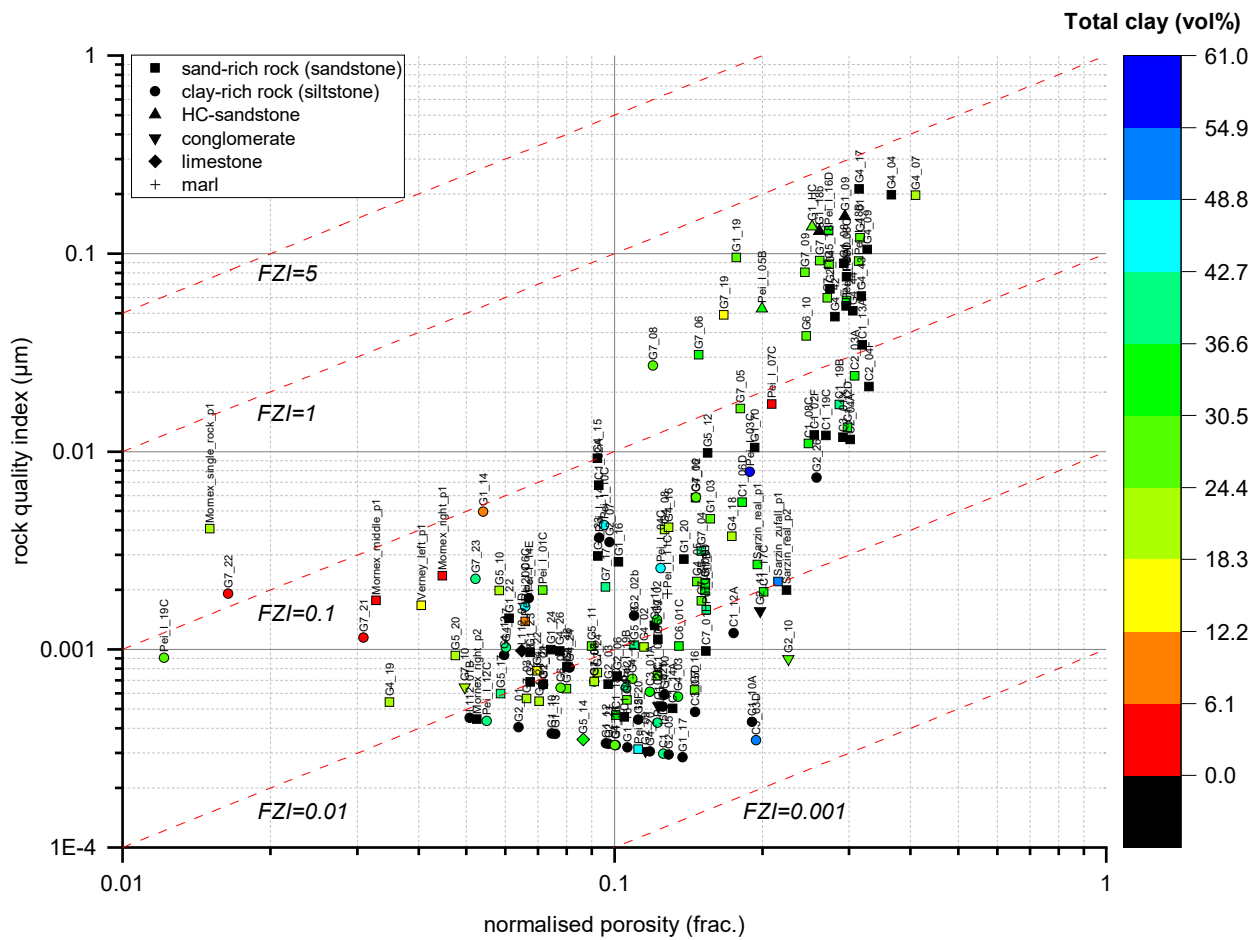


Fig. 5.39: Porosity versus rock quality index based on FZI calculations on 170 plug samples. 93 samples comprise summarised mineralogical data from XRD and QEMSCAN analyses, and respective total clay contents are colour-coded. Samples without mineralogical analysis are depicted in black colour.

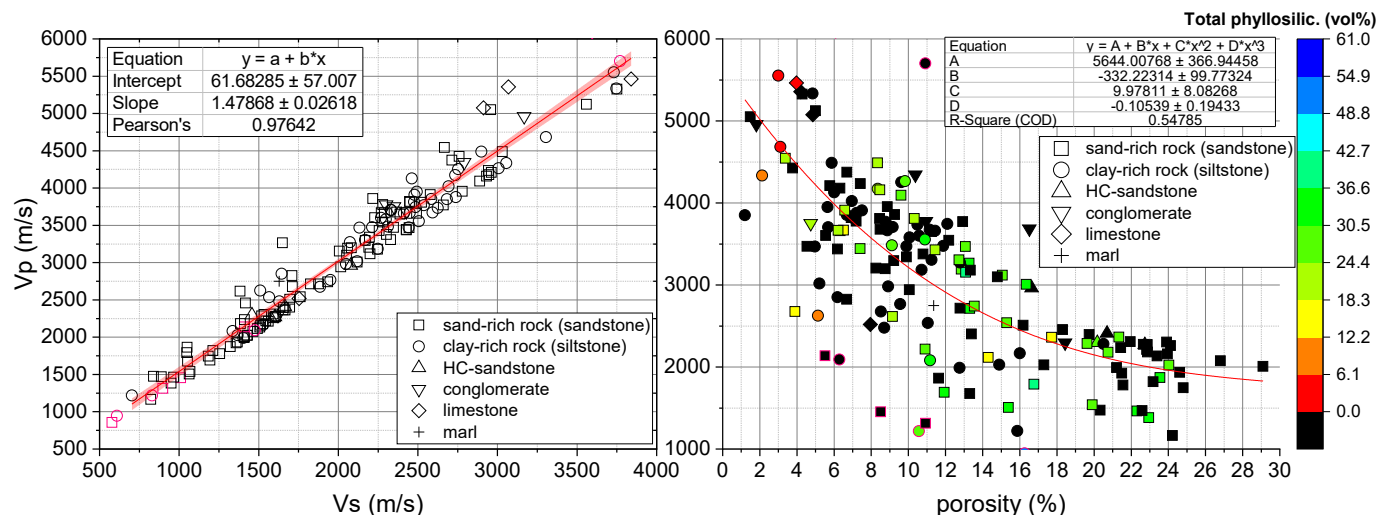


Fig. 5.40: Compressional (V_P) versus transversal (V_S) velocity and porosity with respect to total phyllosilic content. Outliers are circled in pink colour and excluded from statistical fitting analyses.

empirical correlation between V_P and V_S with a Pearson's correlation coefficient of 0.97 is derived for the Molasse Rouge samples (Fig. 5.40) yielding:

$$V_P = V_S \cdot 1.48 + 61.68 \quad (5.9)$$

An exponentially decreasing relationship among V_P and porosity is depicted (Fig. 5.40) showing compact, cemented, non-porous clay-rich rock samples at mid- to low porosity values of 1 to 15%. Compressional wave velocities depict 2'500 up to 4'500 m/s (then limestone), while the porous, sand-rich rocks show compressional wave velocities below 2'500 m/s.

Statistical analysis of combined petrophysical, physico-chemical and mineralogical properties

Fig. 5.42 and Fig. 5.43 show 170 Molasse Rouge, glaciogenic deposits, and Siderolithic samples with petrophysical parameters such as porosity, permeability, V_P , V_S and grain density with combined mineralogical measurements from both XRD and QEMSCAN analyses. The PCA is based on calculated eigenvalues to choose the proper number of three principal components (Fig. 5.41). Total phyllosilicate, quartz and carbonate contents are added up, respectively, and transformed into vol% for all samples via averaged mineral densities, since XRD results were initially acquired in wt%. In case both QEMSCAN and XRD analyses were measured, XRD results were

preferred⁴. 93 out of 170 samples contain these combined mineralogical data sets. The three principal components are split into two different PCA biplots (Fig. 5.42 and 5.43) incorporating the aforementioned properties.

The sand-rich rocks are not correlated to calcite nor total carbonate content but do so for clay-rich (partially marl) and limestone rock types. Vice-versa, quartz content is attributed to predominantly sand-rich rock. Grain density and porosity strongly correlates with permeability shown by low angle distances among their vectors. This associates lower grain density values (sand-rich) to higher porosity values. The permeability vector is shorter compared to all other ones, which depicts low data variation but improved representation along a different (third) PC. V_P and V_S properties are anti-correlated with porosity and permeability for sand-rich and clay-rich rock samples given their high grades of cementation from clay minerals or calcite. Total carbonate and total clay contents are prone to a (more) positive correlation with V_P and V_S properties compared to porosity and permeability showing a negative correlation for at least the total clay content, which is depicted by the tilt of vectors away or to respective parameters. Quartz content is not correlated to any of the aforementioned properties denoted by the ca. 90° angle among the respective vectors.

Based on 170 samples for all 5 parameters depicting V_P , V_S , porosity, permeability and grain density, there exists

⁴See discussion in chapter 6 on the comparison of mineralogical analyses).

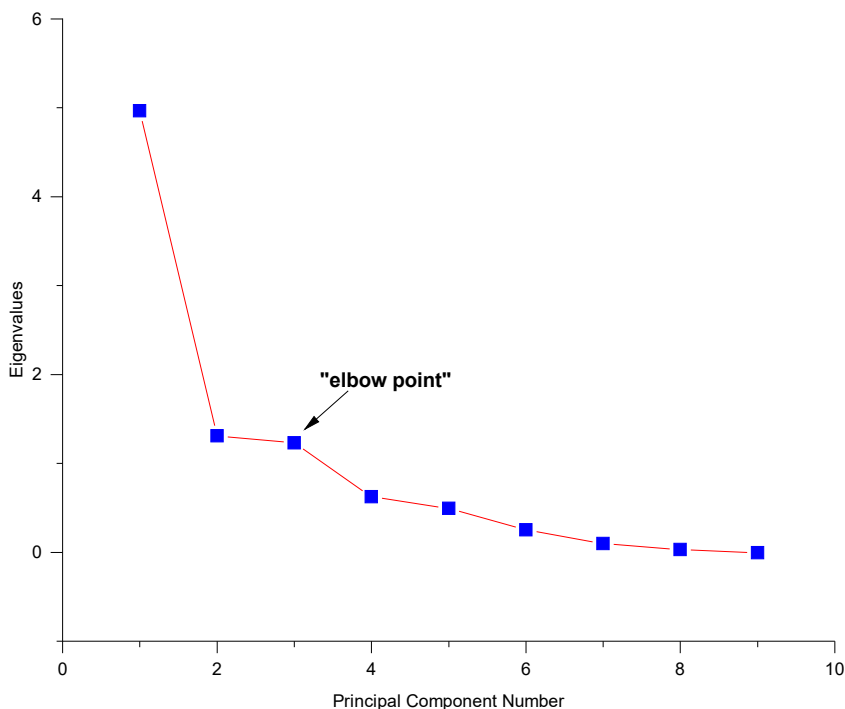


Fig. 5.41: PCA screeplot from petrophysics data on 170 Molasse Rouge samples for the identification of optimal principal components considering at least 80% of data variation.

a large data variation in the ultrasonic velocities and in the grain density. This becomes clear when checking the greater length of the porosity and permeability vectors. The behaviour for grain density is explained by the high heterogeneity of the Molasse Rouge. The slightly lower variation of V_S could be due to fewer sample measurements.

The biplots suggest that it is reasonable to classify the identified rock types based on calculated FZI and ultrasonic wave velocities. This serves as the basis to distinguish the three sub-types of sand-rich rocks and the clay-rich rock. The differentiation among clay-rich and marl rocks might not be distinct.

Rock strength and abrasivity behaviour

Uniaxial compressive strength (UCS) results allow for the Molasse Rouge to be classified as a soft formation. Fig. 5.44 shows stress-strain curves for sand-rich, clay-rich and marl samples. While both the sand-rich and marl samples reach UCS values up to 60 MPa, the clay-rich samples do not exceed 50 MPa before rock failure. The axial stress-strain curves are an indicator for the grade of cementation, as well-cemented (calcite), matrix-supported sand-rich rocks tend to reach higher UCS values compared to non-cemented samples. A similar argument is sufficient

for the explanation of higher UCS values for marl samples, which are cemented by calcite. The vast amount of rock samples lies within the UCS range of the very weak, weak and medium-weak marl between 2.2-5.1, 5.1-10.1 and 10.1-19.9 MPa (Fig. 5.45, 5.46, 5.47).

Based on boreholes SPL8.1, SPL8.2, SPL8.7, and SPL8.14 (see chapter 3 in Table 3.1 and database file in appendix C.2), the distribution of UCS values in the glaciogenic deposits formation are quite uniform and low. The total number of digitised samples amounts to 29. The Molasse Rouge formation depicts a median value of 18.35 MPa with a larger variation to higher strength values. 75% of the UCS measurements show values higher than 12.83 MPa. Digitised Young's moduli of the Molasse Rouge show a median value of 2.15 GPa. Data on Freshwater limestone depicts the highest variation with a median UCS of 57.5 MPa and median Young's modulus of 18.4 GPa.

For the Mesozoic limestone formations, UCS values are scattered with a lower boundary of 3.7 MPa and an upper boundary of 13 MPa. Young's modulus values in the Molasse Rouge formation depict a lower boundary of 30 MPa and an upper boundary of 1'700 MPa. The lower boundary in the upper Mesozoic limestone formation is ca. 500 MPa with the upper boundary at 4'000 MPa showing

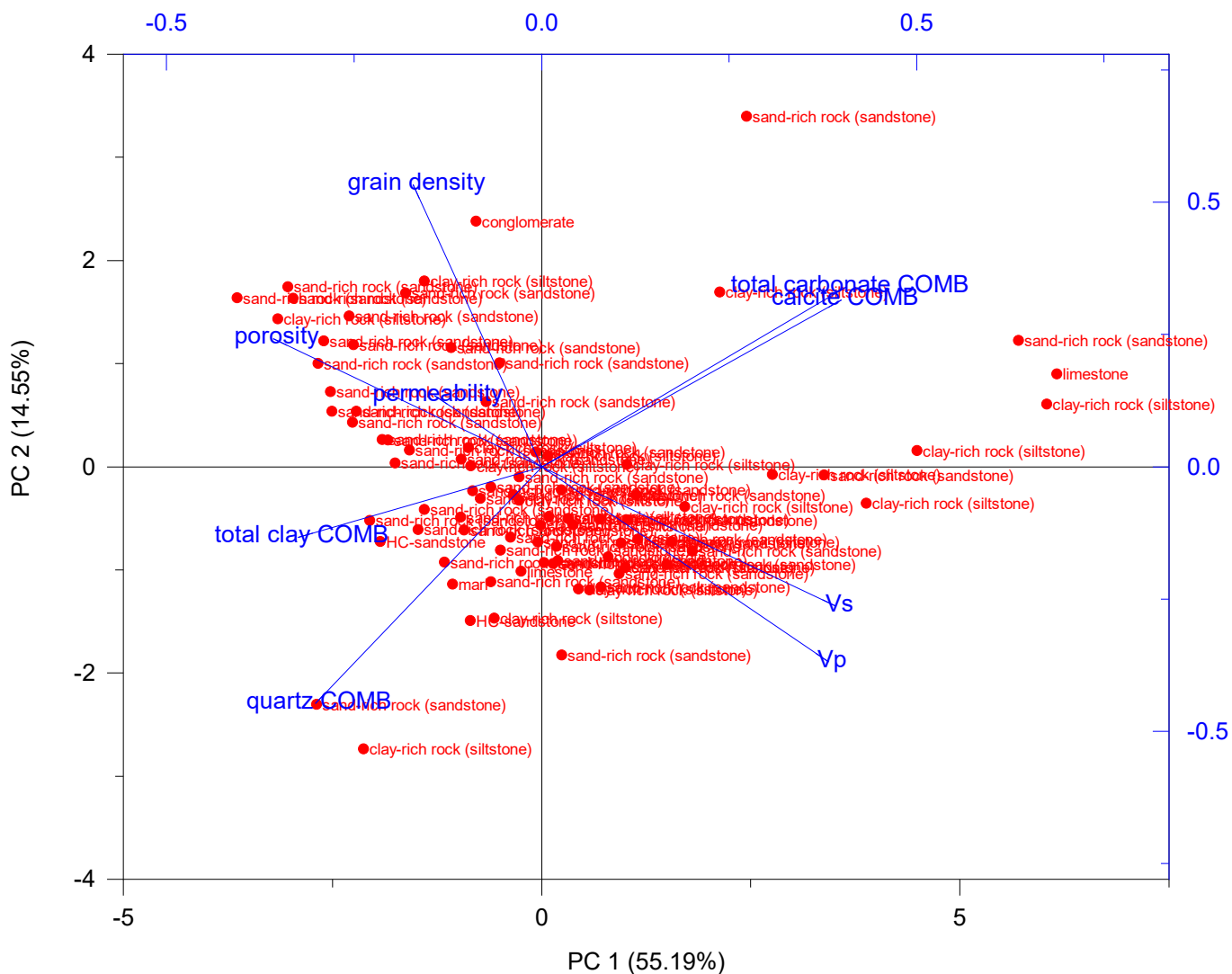


Fig. 5.42: PCA biplot of PC1 depicting 55.19% and PC2 with 14.55% of the total data variation from 170 Molasse Rouge samples for cross-correlation among petrophysical and mineralogical data. *COMB* refers to properties combining the results from both XRD and QEMSCAN.

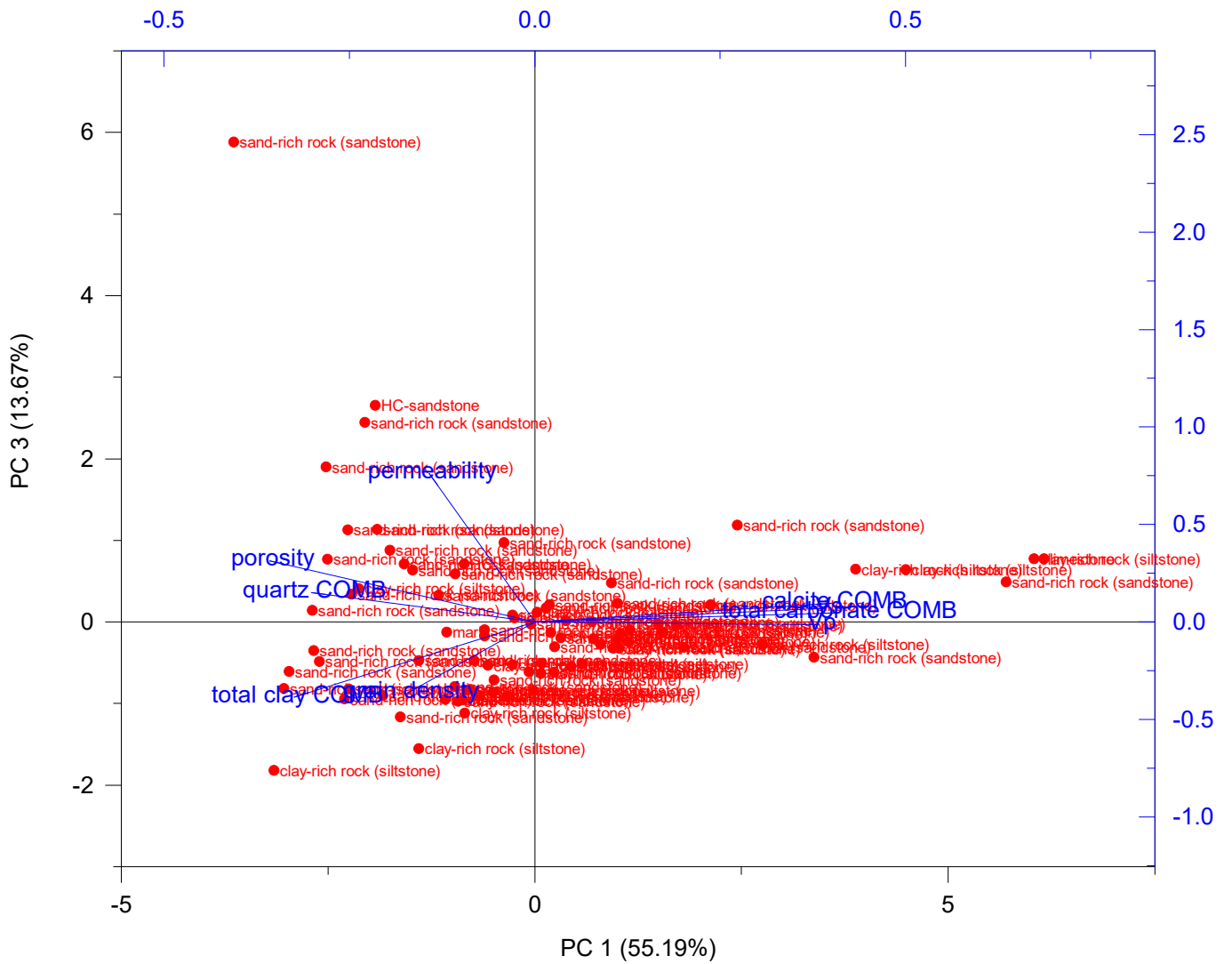


Fig. 5.43: Biplot of PC1 and PC3 with 13.67% of total data variation the same 170 Molasse Rouge samples.

variations up to 1'600 MPa. No distinct trends for both UCS and Young's Modulus are observed with increasing depth (Fig. 5.47) per formation. As a consequence, the scattered Young's modulus values were not further considered for the rock characterisation because they did not provide additional useful information to sub-divide the rock within a given formation. Young's modulus values are affected by drainage conditions and by effective stress. Undrained values are higher than drained values and higher effective stress values generally give higher modulus values within the same loading range. Regarding deformation moduli, confusion and uncertainties arise from lack of definitions, lack of explanation about data origin and differences in classification of rock types in the previous geotechnical reports provided by CERN.

The results depict weak, medium-strong and strong sandstone at 7.6-17.2, 17.2-31.9 and 31.9+ MPa regions, respectively, following the geotechnical classification by Fern et al. (2018). The grade and type of cementation, i.e. matrix composition (calcite or clay minerals), bounding of solid components, anisotropy, and fractures yield reasonable correlations with the petrophysical analyses such as V_P , V_S , porosity and permeability. This heterogeneous and anisotropic behaviour is represented in abrasivity properties.

The Cerchar Abrasivity Index (CAI) and LCPC abrasivity values (LAC) are dependant on the quartz content as well as on the rock's grain size distribution leading to a linear correlation of increasing quartz content with increasing abrasivity. The abrasivity is affected by the grain size distribution leading to less abrasion the more fine-grained the rock matrix (Fig. 5.35). A predominant difference between the CERCHAR and LCPC test is the fact that LCPC is independent of foliation and anisotropy. During CAI analysis, great caution must be spent on where the pin scratches the surface of a sample during the CERCHAR test and a low CAI value does not necessarily allow for conclusions on predominant fine-grained material.

The underlying measurement is taken from grain size distribution curves. QEMSCAN offers mineral (quartz) grain size distribution curves (Fig. 5.11, 5.9, 5.12, 5.10) but effort should be spent on actual (wet) sieving analyses.

Statistical analysis of geomechanical, petrophysical and mineralogical data

A principal component analyses is conducted for geomechanical, petrophysical and mineralogical data along four principal components based on the associated screeplot (Fig. 5.48). The four PCs compare the linear relationship of various properties (Fig. 5.49, 5.50, 5.51).

The results show that CAI and LAC values are positively correlated and do not infer any influence by the quartz content, i.e. abrasivity. Grain size plays a crucial role for the CAI value. The PCA shows that both CAI and LAC values are not highly influenced by mineral contents, i.e. also smectite, total phyllosilicates or calcite. Rock strength parameters such as the Brazilian tensile strength, point load index and UCS are positively correlated, denoted by ca. 35° angles among their vectors. The same is valid for the compressional wave velocities but at a wider angle of ca. 45°. The LBC value depicting rock breakability shows no influence on the aforementioned parameters. However, the LCPC analysis denotes an insignificant parameter for sedimentary rock compared to quantifying the breakability of e.g., metamorphic or magmatic hard rocks yielding UCS values above 150 MPa.

An anti-correlation among calcite and CAI is identified and seems reasonable because an increased calcite content (marl rock type) is associated to lower quartz content (sand-rich rock type). A similar trend is observed for the correlation of LAC and LBC vectors in particular for marl samples that also show a lower CAI abrasivity compared to sand-rich rocks. In the PC2-PC3 plane, the petrophysical ultrasonic velocities play an insignificant role denoted by the very short vector lengths (low data variation) and these short vectors are better represented in different PC plain (Fig. 5.49 and 5.50).

Rock quality designation index

Based on reviewed well reports and own field investigations, the rock quality designation index (RQD) is used to address the rock strength of intact rock mass. It is a common first estimate of rock quality during drilling and coring and used for the computation of rock mass indices of geotechnical design calculations of temporary support systems via empirical equations. The RQD is an index that provides a quantitative description of the discontinuities such as the number of cracks, joints and fractures in

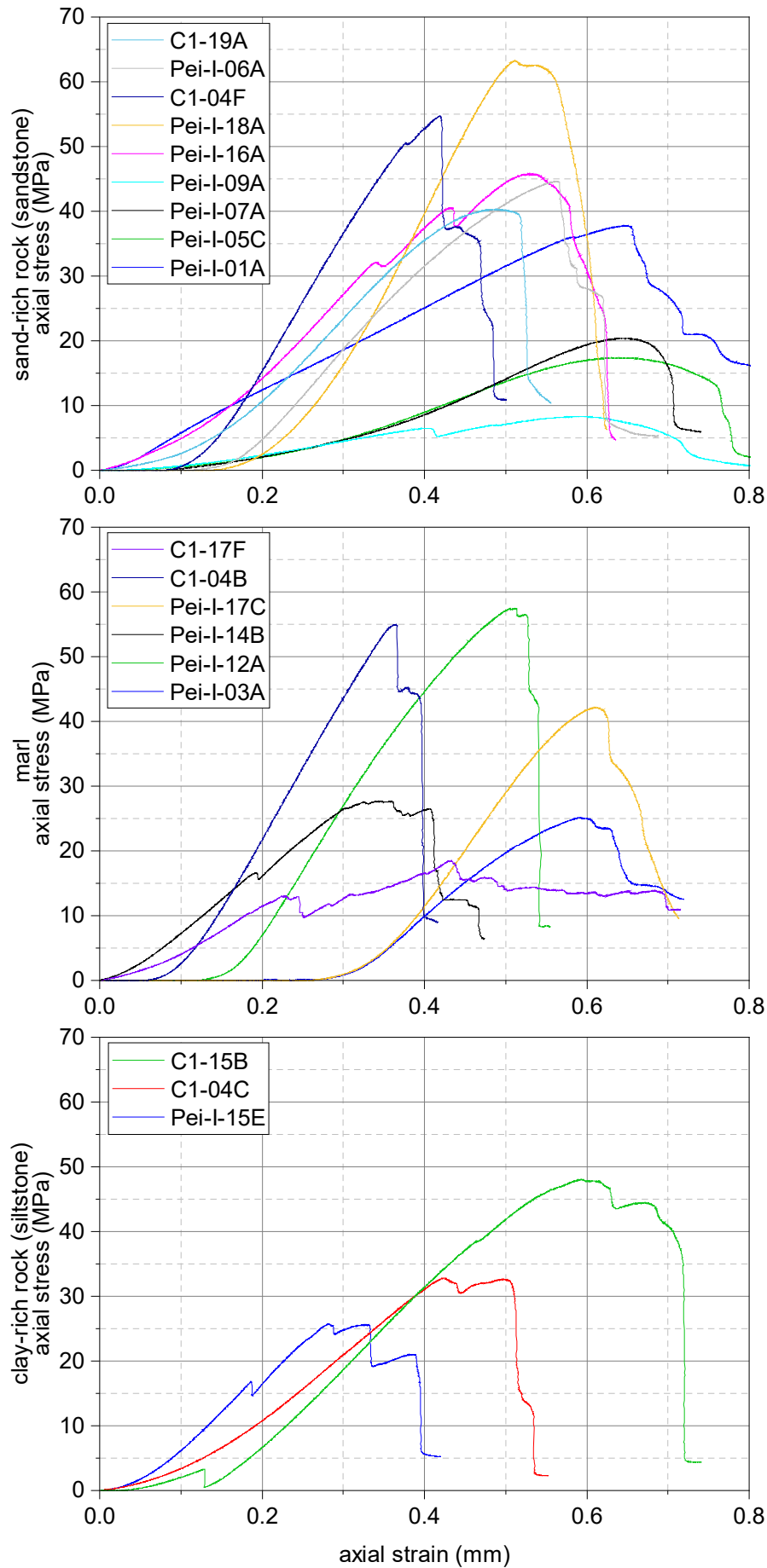


Fig. 5.44: Axial stress versus axial strain depicting the rock strength behaviour of clay-rich, sand-rich and marl rocks.

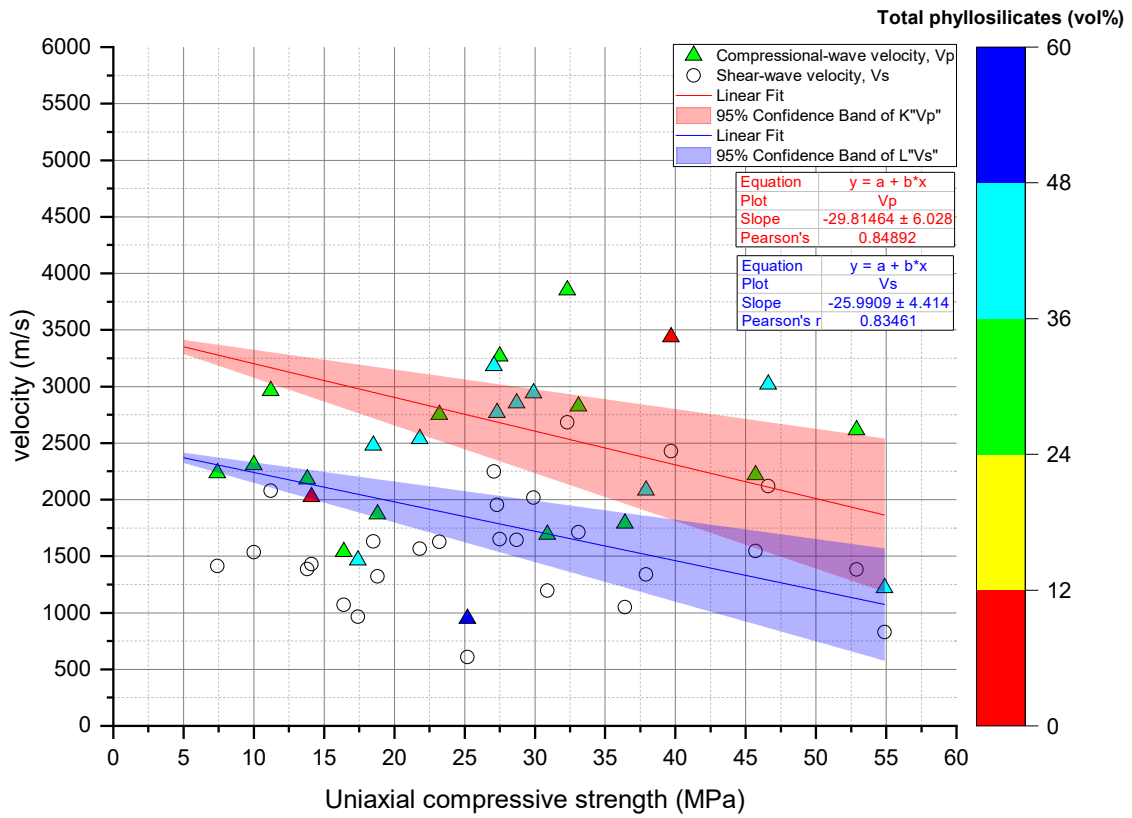


Fig. 5.45: Uniaxial compressive strength (UCS) correlated with both compressional (triangle) and shear-wave (circle) velocities from 27 Molasse Rouge samples, together with correlated fitting lines.

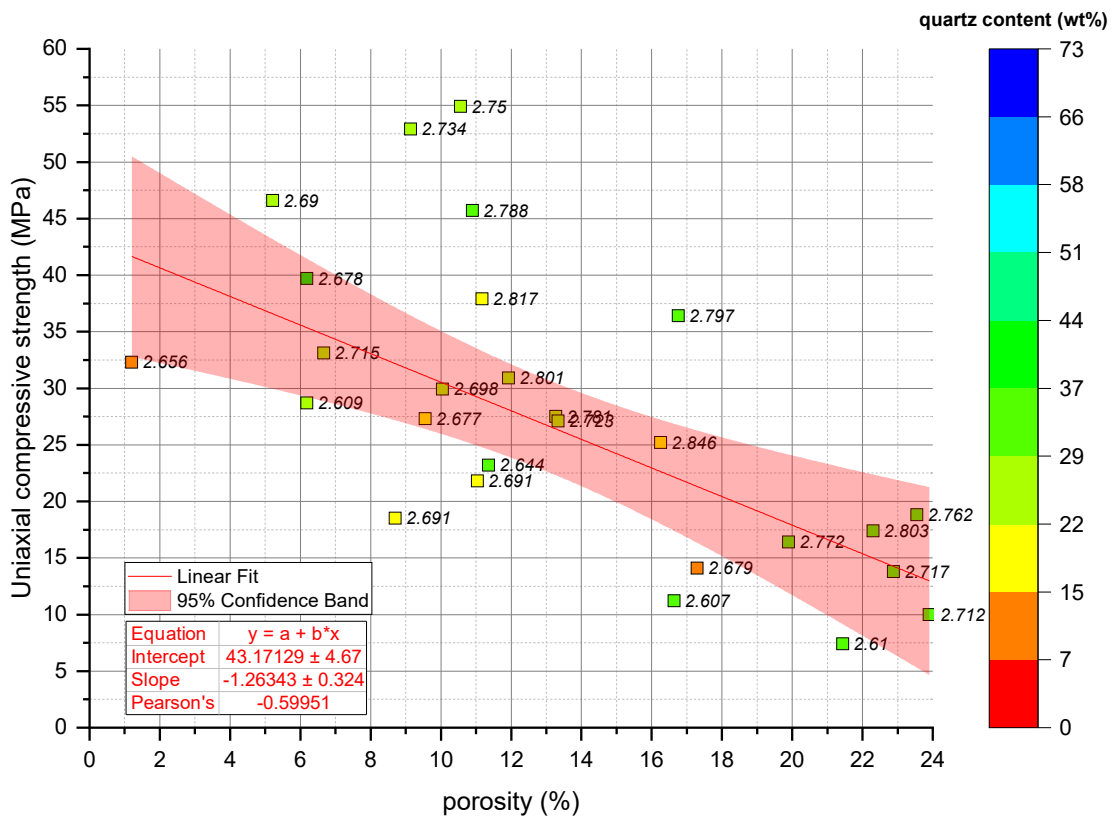


Fig. 5.46: Porosity correlated with uniaxial compressive strength (UCS), quartz content and respective grain densities (g/cm^3) from 27 Molasse Rouge samples.

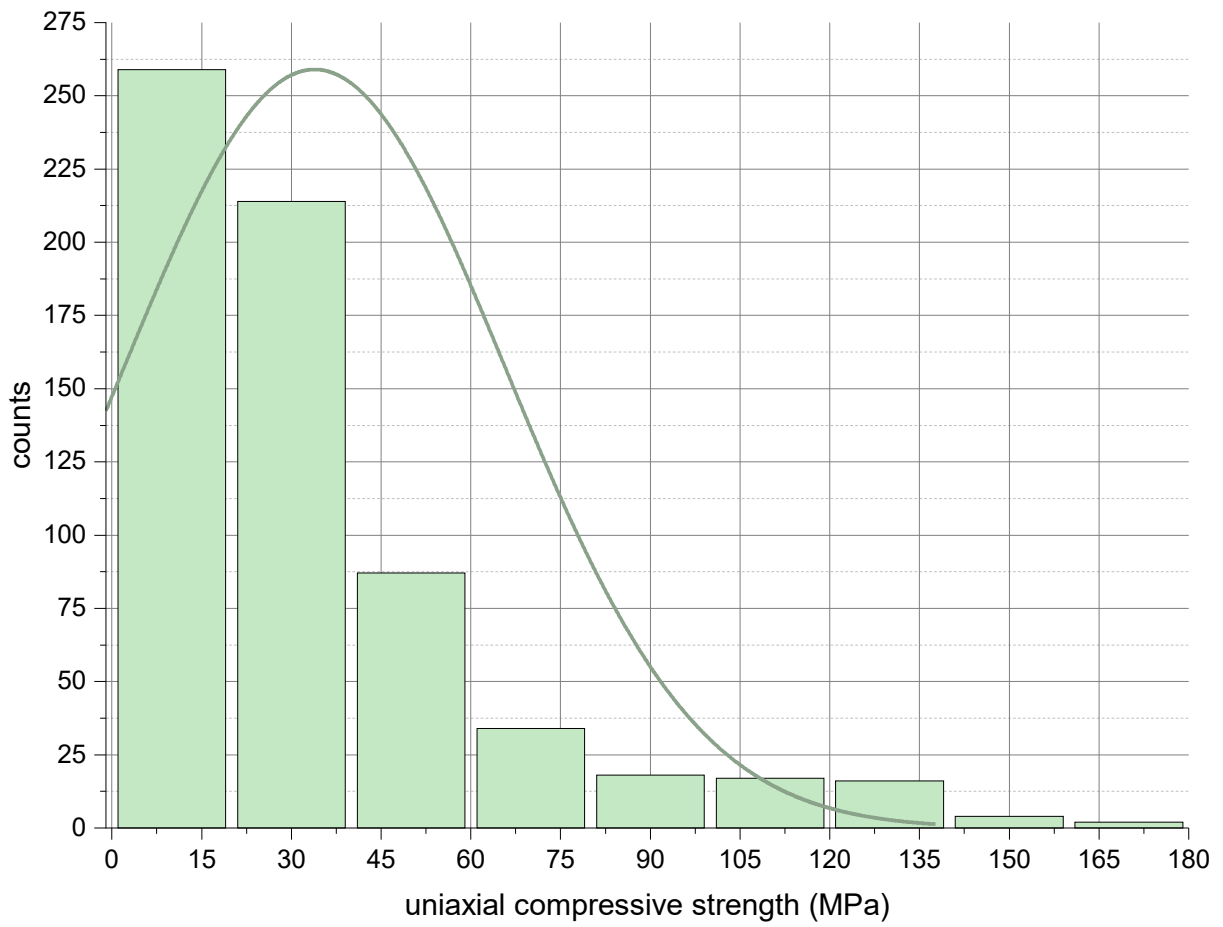


Fig. 5.47: Histogram of 152 measured and 499 digitised samples from the Molasse Rouge formation. For data sources see [Table 3.1](#).

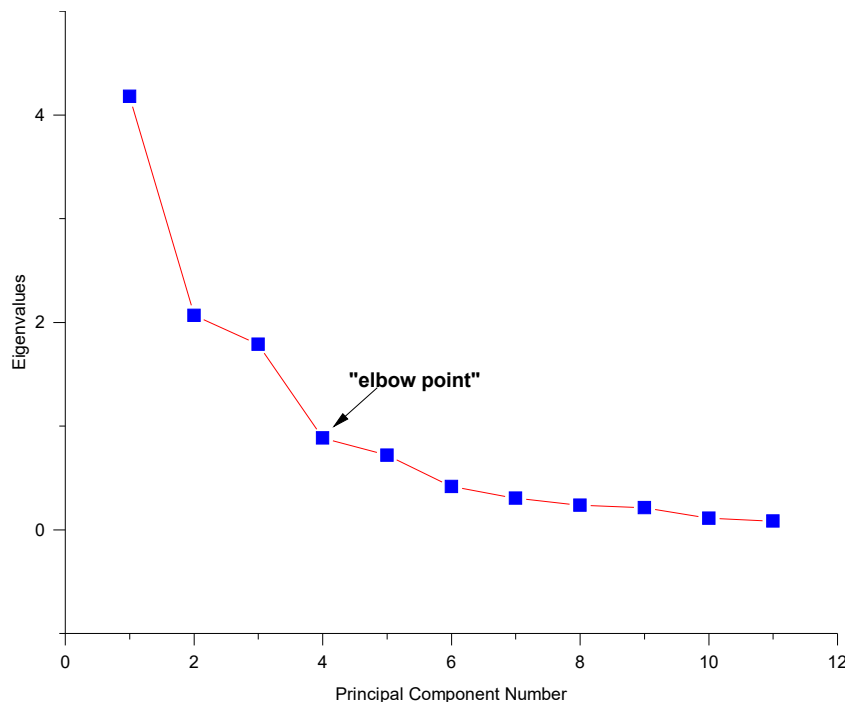


Fig. 5.48: PCA screeplot based on 33 Molasse Rouge samples featuring quartz, calcite and total clay content correlated with petrophysical data V_P , V_S , and geomechanical data CAI, LAC, LBC, point load indices, and UCS with reference to quartz, calcite, total phyllosilicate and smectite contents. The screeplot depicts the optimum number of PCs as 4 based on the "elbow point" as the last point of eigenvalues ≥ 1 , and a total variation across the data set of $\geq 80\%$. These 4 PCs are depicted and discussed below. All samples contain a TOC $\leq 1\%$.

a drill core, and is calculated according to:

$$RQD = \frac{\sum l_i}{l_{total}} \cdot 100 \quad (5.10)$$

where l_i is the length of a core piece longer than 10 cm, and l_{total} is the total length of the full core run. RQD values range from 40 to 100% measured along digitised boreholes in the northern part at the Swiss HL-LHC construction Point 1 in the glaciogenic deposits and Molasse Rouge formations. No trend with increasing depth is observed. RQD values are stated in each well report for wells C1, C2, C3, C4, SLHC 20, and SLHC21 (see chapter 3 in Table 3.1).

Marls in the Molasse Rouge formation are highly fractured or crushed. They occur in sub-horizontal layers with a thickness ranging between 10 to 60 cm but rarely less than 1 m. The sandstone is intact, though it occurs partly disturbed. According to the C1 log (see also Fig. 5.5, A1-A2 core images), the first 5 m of the bedrock are highly fractured. This could be associated with the drilling progress.

The Molasse Rouge depicts heterogeneous RQD values,

ranging from poor, weak marl to good, strong sandstone. In addition, the well reports show a decrease of RQD with depth, which is consistent across all boreholes (e.g. SLHC20 to -25), and would suggest a weakening rock towards deeper depths. For the investigated RQD values, the maximum depth from site investigation wells is located at ca. 120 m borehole depth (SLHCxx wells). Numerous horizontal, oblique or vertical joints are observed in intervals of 10 m. The number of oblique and vertical joints is less, compared to horizontal ones. It appears that sub-horizontal joints are much more numerous, up to 47 per 10 m (e.g. in well SLHC25 at 60–70 m). This could be related to stress relief after the glacier loss of ice cover (see chapter 4). There is a slight tendency for the joint numbers to increase with depth as observed in SLHC23 and SLHC25. These joints are closely linked to the general rock layering of the Molasse Rouge formation observed across various site investigation wells as part of LHC and HL-LHC site investigations. Various reports (e.g. Varley et al. 1996) refer to wells SLHC20-25 and respective depth interval between 50 to 60 m at which the rock consists predominantly of soft, sand-rich rock with fine beds of marls with a few meters in thickness.

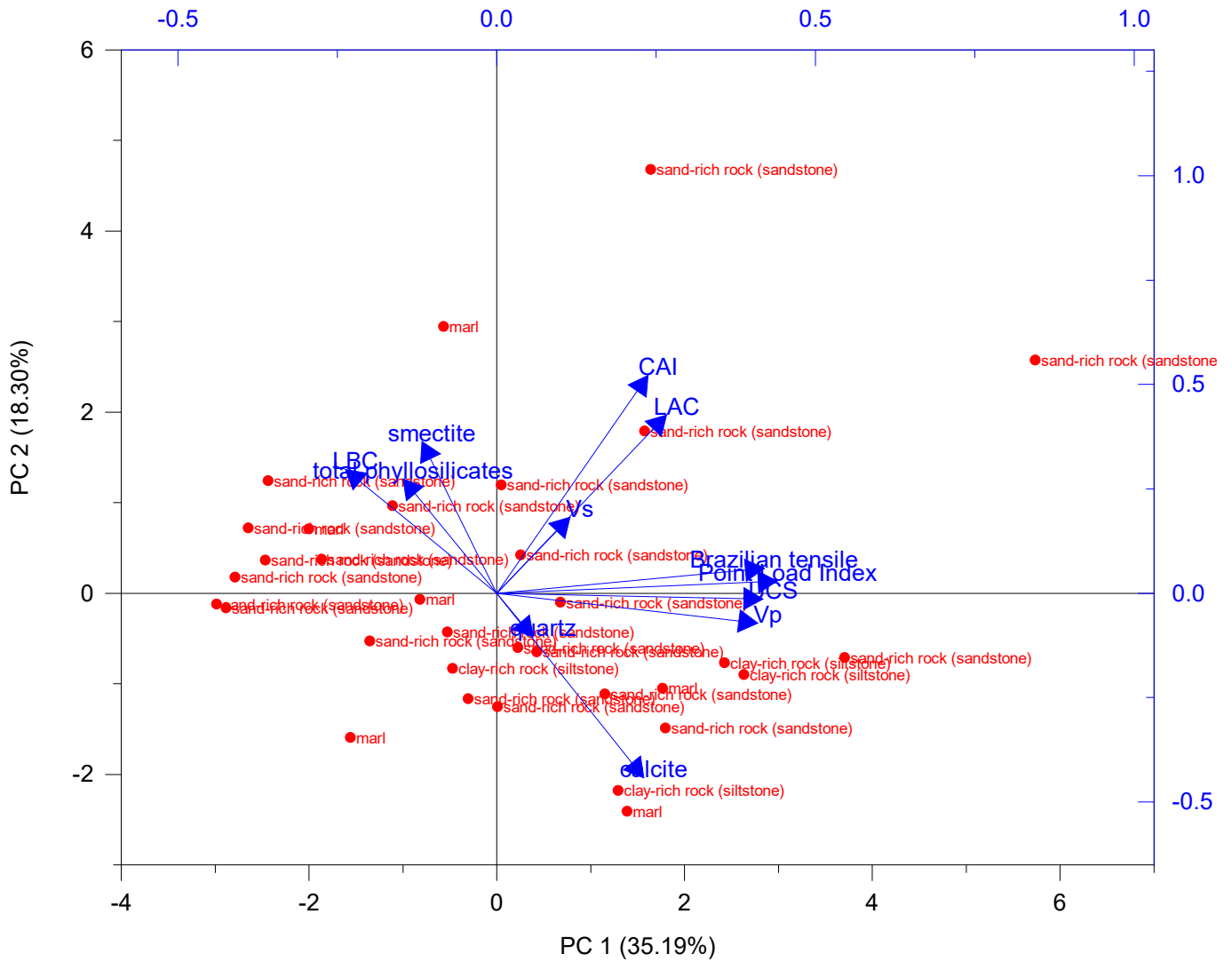


Fig. 5.49: Resulting PCA biplot for PC1 and PC2, based on 33 Molasse Rouge samples (Fig. 5.48) using the same input parameters. PC1 shows the largest total variation with 35.19%, and PC2 of 18.30%.

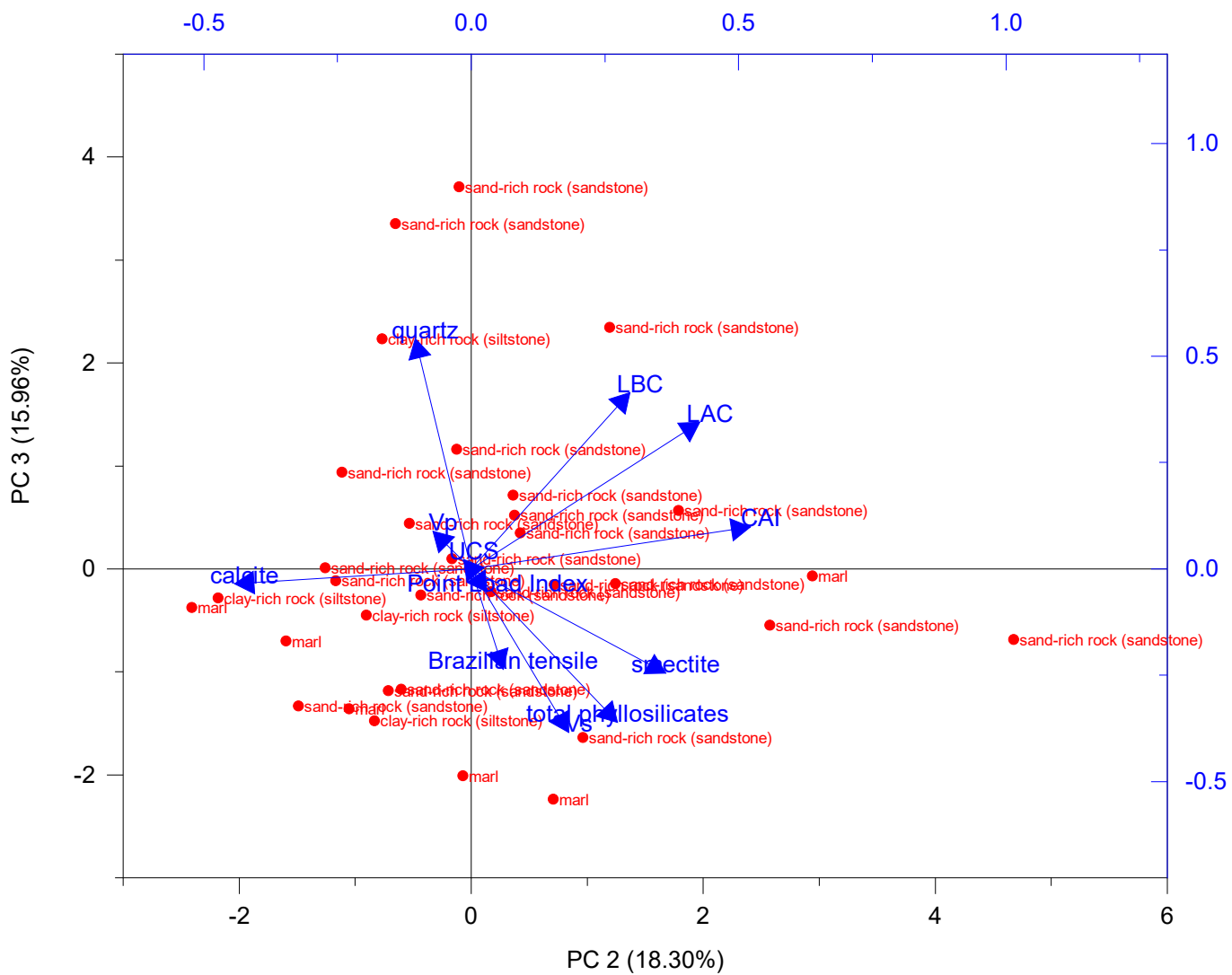


Fig. 5.50: Short vectors in Fig. 5.49 are better represented in different PC domains, plotting PC2 together with PC3 yields 18.30% and 15.96%, respectively based on 33 Molasse Rouge samples (Fig. 5.48) using the same input parameters but having an increased representation of e.g. the total phyllosilicate content, LAC, LBC, and calcite vectors.

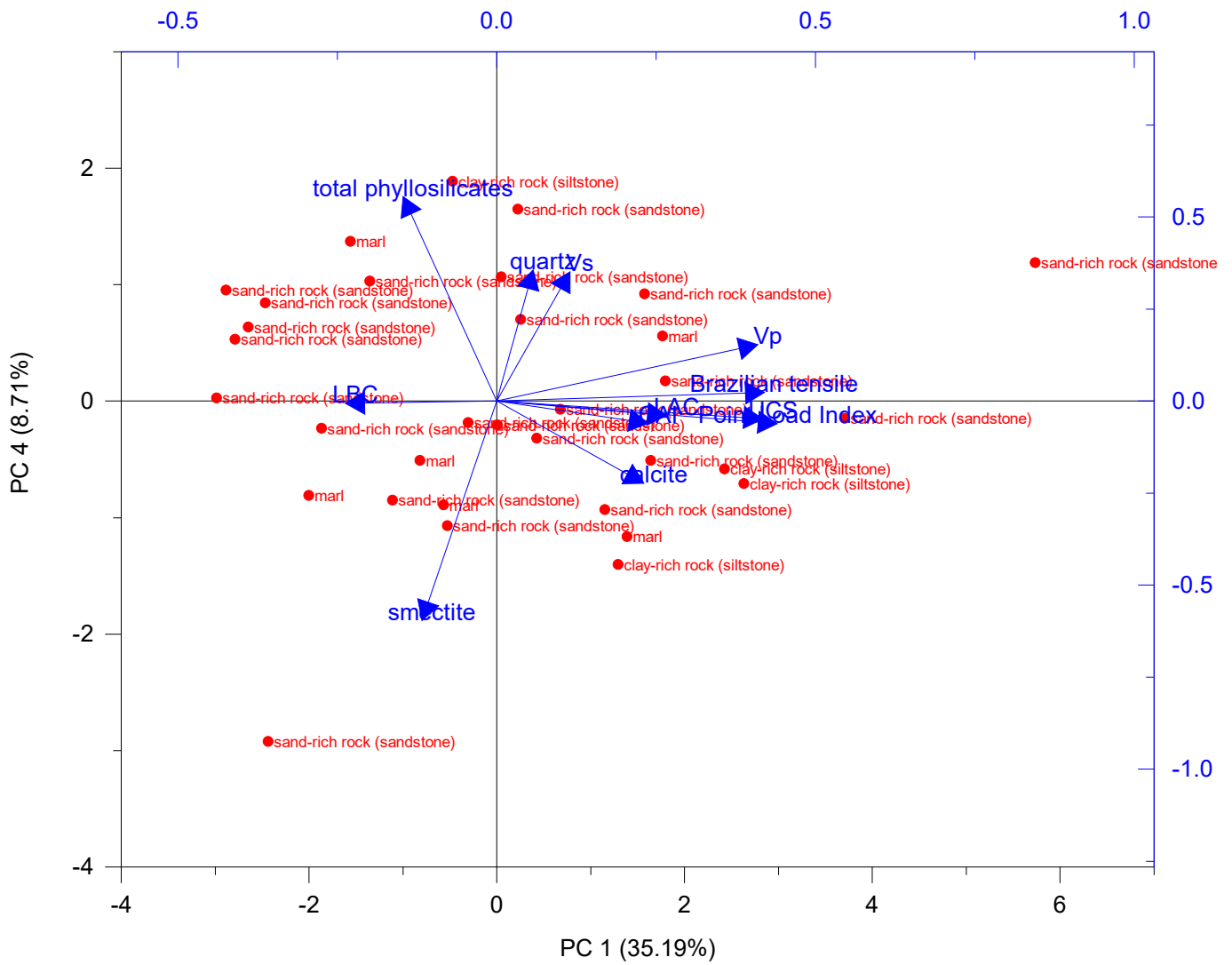


Fig. 5.51: PC1 and PC4 with 35.19% and 8.71%, respectively based on 33 Molasse Rouge samples (Fig. 5.48) using the same input parameters but having an increased representation of e.g. the total phyllosilicate content, LAC, LBC, and calcite vectors.

However, this changes at deeper depths between 50 to 60 m. At these depths, the percentage of marl is higher with thinner beds and, in particular, thin sandstone layers below 1 m in thickness. The Molasse Rouge rock is interpreted to be comprised of successive layers of good to excellent rock mass with RQD values ≥ 75 , but separated by layers of fair rock mass with a RQD ranging between 50 to 75% with occasional thin, poor to weak marl layers depicting RQD values ≤ 50 . The latter is predominantly associated to the weak (violet) marl.

These weak (violet) marl layers are potentially associated with descriptions as "lumpy" (Table 5.1), and are hereby additionally described as tectonised (crushed?) but generally soft and weathered in the field. The RQD values for the violet marl lies at ca. 75% on average. This is also reflected in an increased percentage of jointing as seen in the caliper logs indicating caving and washout zones (see chapter 4 for Geo-01, Geo-02 and Gex-CD-01 well, and Fern et al. (2018) for C1-C3 wells).

The following list states a summary of the average RQD values for each of the marl, clay-rich and sand-rich rock. Respective labels stated according to the geotechnical classification by Fern et al. (2018) are given in parenthesis, and contemplated by terms introduced in this study.

- (Weak) violet marl: RQD=40,
- (Soft marl), clay-rich and calcite-rich rock: RQD=75,
- (Medium marl), predominantly clay rich rock: RQD=87,
- (Soft sandstone), coarse-grained sand-rich rock: RQD=85,
- (Hard sandstone), medium-grained sand-rich rock: RQD=93, and
- (Very hard sandstone), fine- to medium-grained, sand-rich rock: RQD=96.

LHC site investigations reported an increase of the occurrence of weak layers with increasing depth (Varley et al. 1996), and future FCC site investigations will shed more light on respective tectonic and rock strength behaviour investigated on in-situ rock during drilling. It is explicitly noted that the discussion and interpretation on geological

discontinuities is just touched briefly, but should be elaborated in a separate future study together with new drilling data acquired during site investigations.

Various rock mechanics correlations among intact rock parameters have been investigated. The literature suggests that the compressive strength should be comprised between 20 to 27 times the point load index, following:

$$20 \cdot I_{S50} < UCS < 27 \cdot I_{S50} \quad (5.11)$$

It is observed that the interval calculated based on the point load index corresponds to the lower bounds of the UCS interval as defined by the classification based on UCS (Table 5.1). A linear relation between the point load test and the uniaxial compressive strength is derived (Fig. 5.53). This is well in line with strength predictions and allow for a direct and easily-applicable rock strength identification in the field based on quick point load index tests.

A number of Brazilian tensile strength tests have been performed during the LHC site investigation as well as part of this study. Ratios between UCS and tensile strength vary for the respective mean values (Fig. 5.53). Tensile strength values remain similar for all marl, clay-rich and sand-rich rock types. This brings up the question of reliability and sample representativity, as well as correctness of the classification for this parameter. Both point load and Brazilian tensile strength tests hardly show a direct correlation to distinguish clay-rich from marl rock samples. The distribution of the values of tensile strength for sand-rich rocks, on the other hand, from LHC Point 1 is representative.

Fig. 5.54 shows the established, linear correlations among CAI, LAC, LBC, UCS, PL and BRA geomechanical properties. Except for the LAC-LBC correlation, which shows large data scattering, linear trends are derived, yielding the following equations under the assumption that $y(x) = 0$ corresponds to $x = 0$ values, which is reasonable for the indication of rock strength:

$$CAI = LAC \cdot 3.26 \quad (5.12)$$

$$PL = UCS \cdot 0.05 \quad (5.13)$$

$$UCS = BRA \cdot 7.98 \quad (5.14)$$

Cerchar Abrasivity Indices (CAI) in the Molasse Rouge formation as well as LCPC abrasivity (LAC) and LCPC breakability (LBC) values indicate low abrasivity (Fig. 5.54). CAI values range between 0.1 to 0.8 and are classified as not very abrasive to slightly abrasive. These values seem low, in particular for what is normally a rather abrasive rock such as (pure) sandstone, whose CAI values would then range between 2 to 4. Digitised data from well L135 depicts a CAI values between 0.5 to 0.8, which is depicted as slightly abrasive but clearly not a (pure) Freshwater limestone as part of the Molasse Rouge, but potentially rather referring to a (marly) limestone sample (Table 4.1).

The low abrasiveness and hardness parameters stated by the LAC and LBC parameters are substantiated on lithological classifications (Fig. 5.54). No distinct patterns could be identified with the CERCHAR hardness data. According to various data reports (Table 3.1) along with the new data measured as part of this study, the limestone rock types depicts a CAI mean value of 0.74. The Molasse Rouge formation shows a CAI mean value of 0.38 classifying this formation as not very abrasive. The Mesozoic limestone formation is slightly abrasive.

Fig. 5.52 depicts decreasing bulk density as the samples become more fine-grained in texture, and weaker in terms of rock strength represented by point load indices and UCS values in the Molasse Rouge formation. There exists a correlation among grain size, texture and rock strength, depicting higher values for coarse-grained rock samples. There is a general trend towards a weak rock strength, with the majority of samples depicting values below a 1.2 point load index. Digitised samples did not contain explicit information on rock type or bulk density (black color).

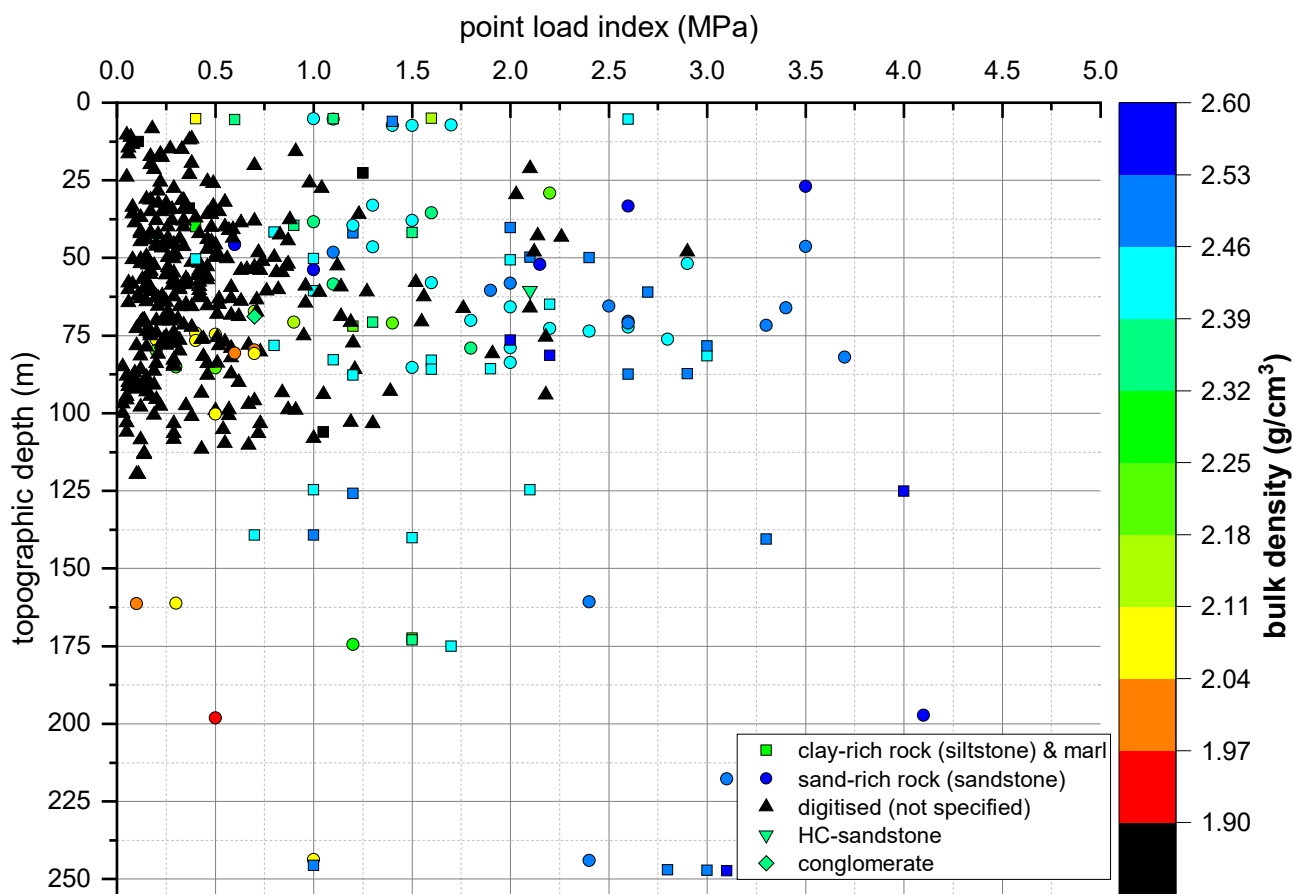


Fig. 5.52: 428 Molasse Rouge from both measured and digitised analyses results of point load indices versus borehole (topographic) depth at various locations, color-coded by bulk density. Data compiled from reviewed well reports, originating from the LEP, LHC and HL-LHC site investigations, see [Table 3.1](#).

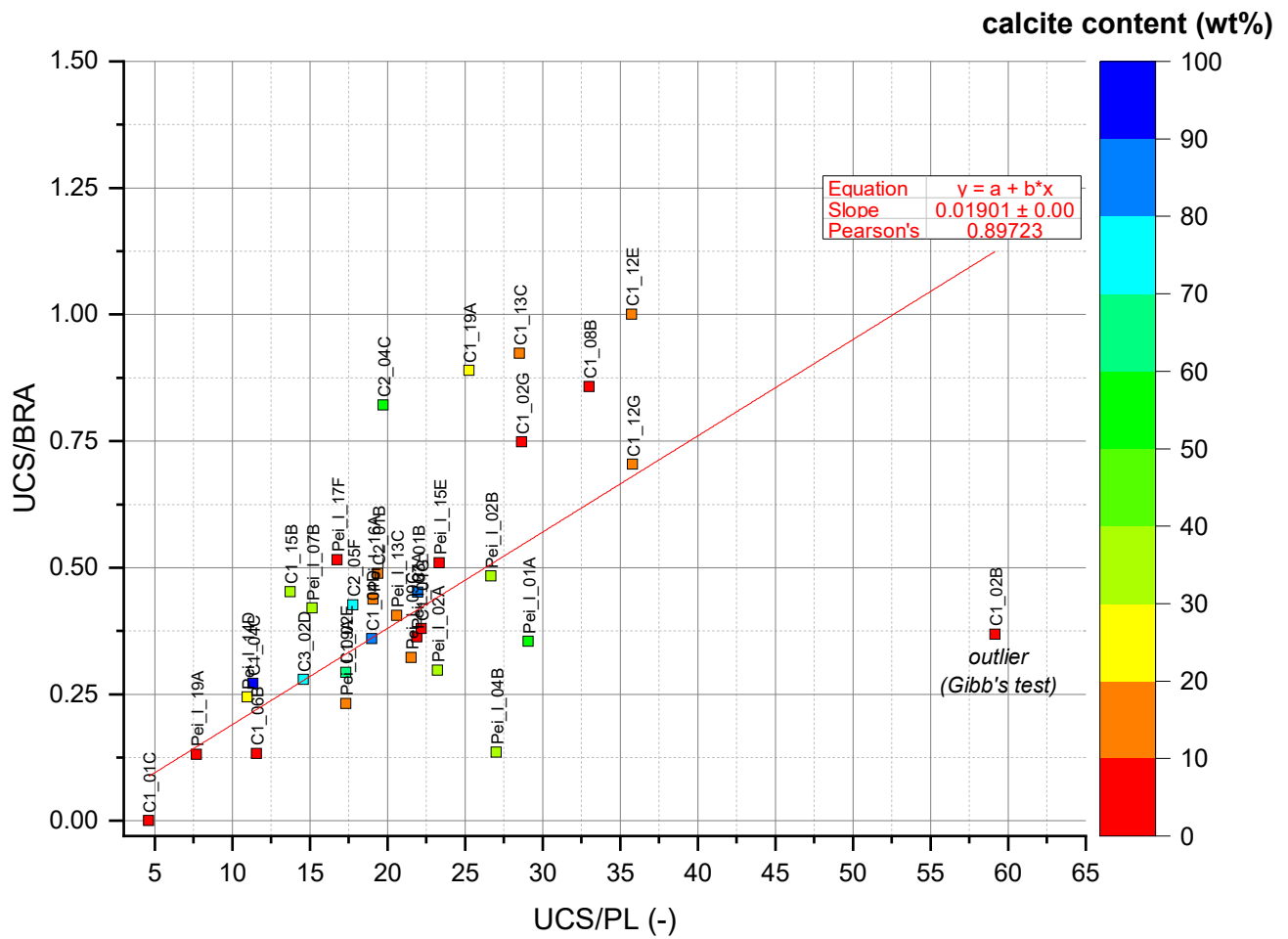


Fig. 5.53: Ratio of uniaxial compressive strength (UCS) and Brazilian tensile strength (BRA) to ratio of uniaxial compressive strength (UCS) and point load index (PL) with respective calcite content, calculated linear regression fit and outlier detection for the same 30 Molasse Rouge samples.

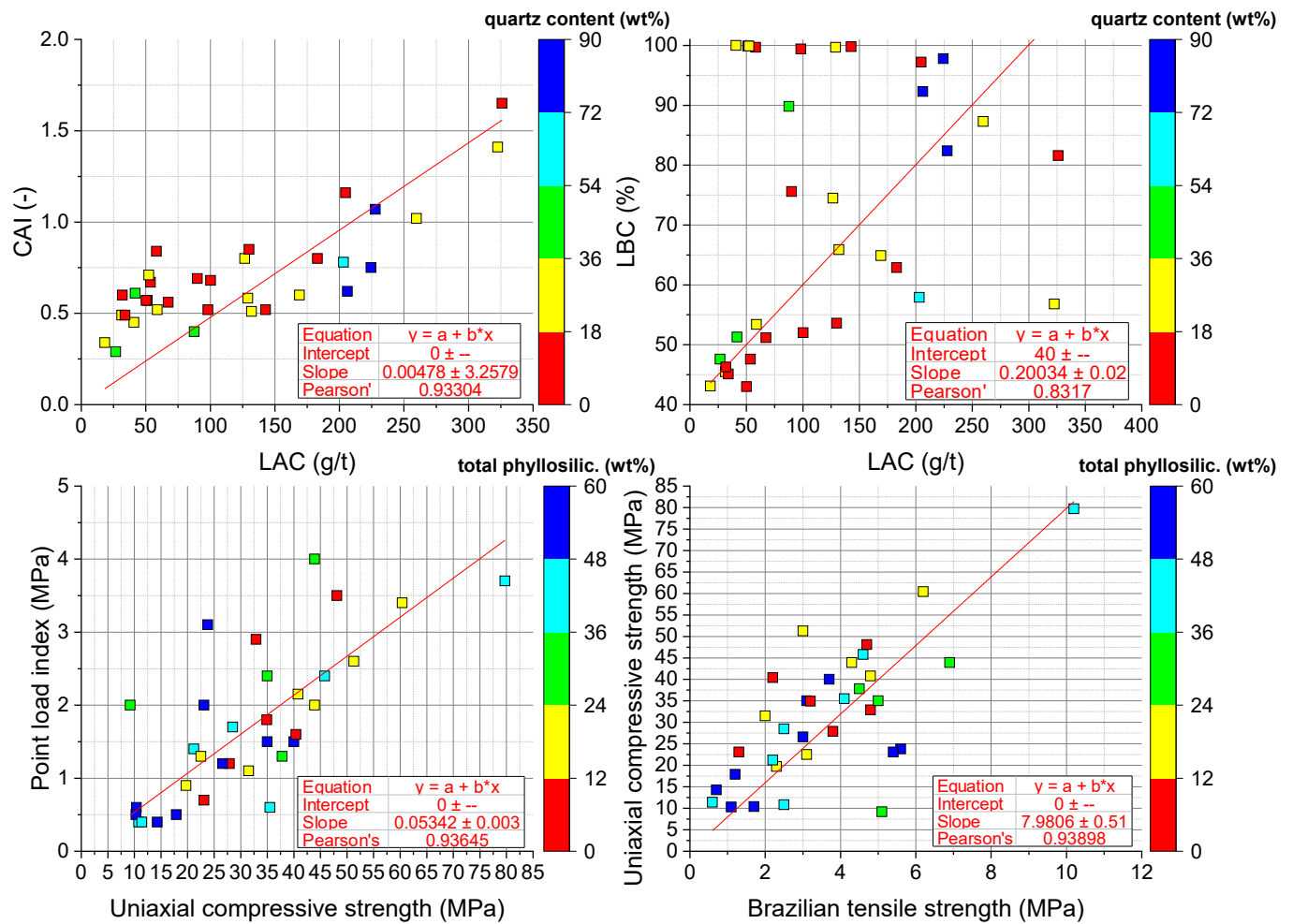


Fig. 5.54: Correlation of UCS, Brazilian tensile strength, CAI, LAC, and LBC values for the same 30 Molasse Rouge samples with colour-coded total clay and quartz contents.

6 Predictability of application scenarios for clay-rich sedimentary rock

6.1 Introduction

How to use excavated rock and soil in a resource-efficient manner has become integral to competitive tendering for construction approval of past and ongoing subsurface tunnelling projects across Europe (AlpTransit Gotthard 2017; Büchi & Thalmann 1995; Bufalini et al. 2017; Bundesamt für Umwelt Wald und Landschaft (BUWAL) 1999; Burdin & Monin 2009; Burdin et al. 2017; European Norm (EN) 2003a; Haas, Mongeard, et al. 2021; Keily 2020; Kwan & Jardine 1999; Magnusson et al. 2015; Thalmann 1996; Voiron et al. 2020; Voit & Zimmermann 2015; Voit & Kuschel 2020; Ziegler & Isler 2013). Large quantities of natural primary resources are extracted each year at international surface and subsurface civil engineering constructions (Haas, Mongeard, et al. 2021). About 60% of the raw material extracted from the lithosphere is used for civil engineering works and the building construction industry (Simion, Fortuna, et al. 2013). Tunnelling projects use ca. 30% of excavated material for beneficial purposes. In Europe, the estimated mineral extraction for the building industry is ca. 4.8 tons per inhabitant per year (Simion, Ghinea, et al. 2013; Zabalza Bribián et al. 2011).

A legal review by Haas, Galler, et al. (2020) on various application scenarios has raised concerns about a unilateral bias across the European countries including the United Kingdom, Switzerland, Austria, Germany, France and Italy towards specific, on-site application scenarios and considering excavated materials to be waste. The study has revealed a hampering heterogeneity of national legislation that still addresses excavated material as waste. The waste status and application scenarios are crucially linked to national and European legislation stating chemical (environmental) pollutants by their respective thresholds (Haas, Galler, et al. 2020; Voiron et al. 2020).

Haas, Mongeard, et al. (2021) reviewed and suggested that excavated metamorphic and igneous rock could be used

beneficially for road construction or concrete aggregates. They suggested that clay-rich sedimentary rocks could be used in cement, tile and brick production. However, these sedimentary-rock applications have been as additive or substitution material rather than as raw material.

Further previous research studies have elaborated on the incorporation of residue (waste) of raw materials and additives. They have argued successful substitutions providing values of up to 50% by reducing the consumption of natural clay resources for various products in the building construction industry (Alonso-Santurde et al. 2011; Bories et al. 2014; Monteiro & Vieira 2014; Zhang 2013). Applications range from a wide source of raw material using, for instance, granite sludge (Menezes et al. 2005), marble (Montero et al. 2009), limestone (Turgut & Murat Algin 2007) or slate (Campos et al. 2004) to process industrial waste into a valuable resource such as paper pulp (Asquini et al. 2008; Furlani et al. 2011) for magmatic and metamorphic excavated rocks. For excavated sedimentary materials, beneficial uses include aggregates for high-quality concrete and shotcrete (Thalmann et al. 2003), soil conditioning and improvement (Duarte 2007; Galli 2016; Minder et al. 2016; Oggeri & Vinai 2012; Peila 2014; Wu & Qu 2009; Zumsteg et al. 2012, 2013b; Zumsteg & Puzrin 2012) including glaciogenic deposits (Zumsteg & Langmaack 2017), lime addition in weak geological formations (Oggeri et al. 2014; Voit & Kuschel 2020) and dredged sediments from canals and harbours for sintering (El Fgaier et al. 2013; Frar et al. 2014; Romero et al. 2008, 2009). Research studies have been consecutively applied as suitable solutions within a mineralogical framework scheme for raw materials (Haurine 2015; Haurine et al. 2016).

Besides these valorisation attempts, the vast amount of excavated material on tunnelling excavation sites is disposed of as waste. Waste generation and disposal are indicators of inefficient processes and unsustainable uses

of natural resources leading to economic and environmental issues of excessive landfilling or quarry backfilling (Adler et al. 2016; Şchiopu et al. 2012). Landfilling and quarry backfilling nowadays rank at the bottom of beneficial uses in terms of environmental sustainability and (re)-conveyance into production chains (Haas, Galler, et al. 2020; Haas, Mongeard, et al. 2021).

The aforementioned studies on beneficial uses have been preceded by many field and laboratory analyses, including geochemistry, mineralogy, petrophysics and rock mechanics. However, these studies took predominantly one set of analyses into account. In contrast, the present study is superior because it is a new multi-disciplinary, analytical approach rather than one type of data. In addition, another difference is that this study for the FCC relies on pre-construction data that has not experienced soil or rock conditioning. Analyses of the raw material allowed for the derivation of empirical relations between rock strength and physical properties (see chapter 5).

For the case of potential disposal, threshold values or ranges are considered safe for beneficial uses based on national legislation (République Française 2003; Schweizerischer Bundesrat 2015), personal communication with experts, extensive reviews of manufacturers, as well as literature research extracted from Anger et al. (2015), BRGM (2009), Faure (2017), Fourvel (2018), Frar et al. (2014), Furlani et al. (2011), Garbarino et al. (2018), Haurine (2015), Haurine et al. (2016), Schorcht et al. (2013), Setec-Lerm (2020), Swiss Confederation (2021), and Wimmer-Frey & Schwaighofer (2002).

Results of the literature review in combination with the data analysis of the investigated rock materials discuss each application category for the identified clay-rich sedimentary raw material in the sections below. Having in mind a *zero-waste* policy that maximizes the outcome of beneficially usable excavated raw materials without any additives, two questions are answered: 1) whether there exists a minimum set of rock properties, which is sufficient for the prediction of application scenarios and can be applied in a generalized rock classification scheme; and based on these rock properties, 2) which application scenarios of raw materials based on cross-correlations of various data deem feasible. The following application scenarios address the technical compatibility of raw material for the usage of aggregates for bricks, tiles, concrete aggregates and lime production and selected

material for embankments, land reclamation (landfilling and backfilling) and agricultural use. Some text passages have been taken partly or in entirety from Haas, Galler, et al. (2020) and Haas, Mongeard, et al. (2021).

6.2 Bricks and tiles production

Tiles and bricks productions classify as potential application scenarios predominantly for the investigated Molasse Rouge formation. The evaluation of these beneficial uses depends on the chemical composition, type and amount of phyllosilicates, organic matter and the plasticity behaviour of the raw materials.

For both products, essential clay minerals are kaolinite, smectites (montmorillonite), chlorite, mica (muscovite, illite, sericite) as well as interstratifications of clay minerals such as illite-smectite. The kaolin minerals (kaolinite, fireclay) are important components of brick raw material. Kaolinite is preferred due to its plasticity behaviour. It causes a high plasticity behaviour, good shaping, approx. 3-10% drying shrinkage as well as 2-17% volume shrinkage during sintering. Illite is favoured for its plasticity and melting properties. Commonly, kaolinite and illite represent more than 2/3 of the total argillaceous minerals. Smectites are not desired since they induce swelling effects when in contact with water (Haurine 2015). Swelling clay minerals should be avoided and smectite (montmorillonite) values are tolerated up to approx. 10%, as they have a high mixing water requirement and react thixotropically (pressing problems). Low smectite occurrences favours the plasticity of the clay. The linear firing shrinkage reaches up to approx. 20% and a higher shear strength would be achieved with e.g., calcite admixture. Illite and muscovite have a predominant influence on the plasticity behaviour. They are characterised by a high content of K, which depicts a good fluxing agent and causes early melt formation (950-1050 °C), and a shorter sintering interval with a firing shrinkage of approx. 9-15%. Chlorite behaves similarly to mica, in particular with increased Mg and Fe content yielding increased viscosity of the melt. The Fe content (hematite formation at approx. 550 °C) are important parameters, and are qualitatively recognizable in the field due to the rock's reddish colour. This increased Fe content also reflects on the colour of the brick product. Firing shrinkage of up to

15% could be assumed.

For brick production, mineral phases quartz, feldspars, carbonates (calcite, dolomite and siderite), Fe-oxides such as siderite, Fe-hydroxides, sulphates (gypsum), sulphides (pyrite), amorphous phases (allophanes) as well as organic phases are important. Quartz is also present in raw brick material and treated as a stabiliser of the system. At 573 °C, the "quartz jump" yields the transformation from beta to alpha quartz and corresponds to a change in volume. Feldspars act as inert-reactive fillers at the brick firing temperatures. Sulphates (gypsum and anhydrite) as well as sulphides (pyrite) are generally undesirable inert constituents because efflorescence might occur, and SO_3^{2-} and SO_4^{2-} containing waste gases could pollute the final products. The content of phyllosilicates should ideally lie above 25 wt% and among all silicate minerals, phyllosilicate content should be greater than 35 wt%. Chlorite content should be lower than 20 wt%. Total organic carbon content should be as low as possible, with a maximum threshold of 5 wt%. Carbonate minerals should be kept between 15 to 20 wt%. Carbonates as well as lime silicates are present in the Molasse Rouge (Fig. 6.4). The presence of carbonates in the raw materials plays a crucial role. Calcite, dolomite and siderite impact porosity and water absorption, the firing colour, the firing shrinkage, particularly influenced by dolomite, and the strength. During brick firing a considerable amount of CO_2 is released and carbonates together with CaO and MgO react as fluxes with the silicates to form lime silicates. Coarse-grained carbonate fractions are undesirable, as they could later lead to harmful chipping of lime by hydration and carbonation. Iron oxides/hydroxides (e.g. haematite and goethite) are important parameters for the colour of the brick product if they are distributed equally in combination with carbonates.

For tile production, phyllosilicate content should ideally be greater than 30 wt%, whereas among all silicate minerals, values above 40 wt% are preferred. The carbonate content should not exceed 5 wt%. Raw mixes for tile production are sensitive to the clay mineral composition, which is reflected in terms of different sediment sources as input material (Haas et al. 2022; Haurine et al. 2016). Smectites have less adverse impacts on bricks compared to tiles production. Chlorite may alter the quality of the raw mix and a suggested threshold lower than 20 wt% should be maintained. The total organic carbon content should

be lower than 5 wt%, ideally 3 wt%, with plasticity values ranging between 15-50. Sulphides in the form of pyrite may be harmful. Organic fractions are also not desired because they are considered pollutants and interfere with further processing of the raw materials. In case they occur, small grain sizes and uniform distribution in the raw material is favoured. Here, FTIR analyses provided useful information on the organic matter contents.

The plasticity behaviour controlled by the amount of clay minerals is essential for brick and tile production. Atterberg limits, i.e. liquid and plastic limits should yield a plasticity index between 15 and 50 (Fig. 5.28, 5.28). The Enslin-Neff analysis of the Molasse Rouge samples proves to be a reasonable alternative to quickly and economically derive plasticity behaviour and predict the feasibility of brick or tile production.

The derived Augustinik diagram (Fig. 6.1) comprises the elemental composition of the raw materials and provides a robust approach for a first identification between the two beneficial use scenarios. Sandy, i.e. sand-rich lithotypes (see chapter 5) contain more hydrocarbons, Cr and Ni than clay-rich lithotypes in the Molasse formations (Fig. 5.11). These samples are not directly applicable for neither bricks nor tiles productions.

6.3 Cement, concrete and lime production

It has become an integrated procedure in tunnelling projects to investigate excavated material for concrete production (e.g., the Gotthard Base or Lötschberg tunnels) and an ancillary, elaborated discussion is found in Haas, Mongeard, et al. (2021).

Even though the terms cement and concrete are mistakenly used interchangeably, cement depicts an ingredient of concrete. Concrete is the main building material in today's construction industry. It comprises a mixture of aggregates and paste. The aggregates represent sand, gravel or crushed stone, while the paste constitutes water and portland cement. Cement commonly is made up of 10 to 15 vol% of the concrete mix. Through hydration, the cement and water harden and bind the aggregates into a mass. This hardening process pursues over time and implies that concrete becomes stronger the older it becomes.

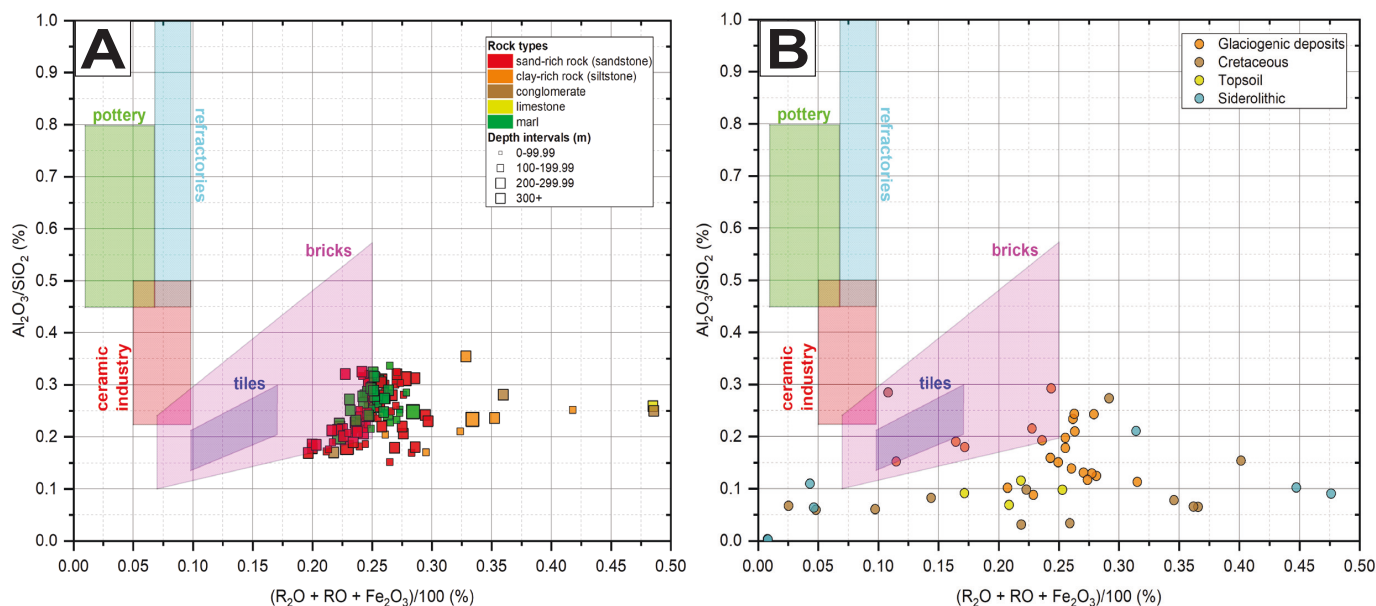


Fig. 6.1: Augustinik diagrams based on ICP-MS/OES measurements. (A) 322 Molasse Rouge samples grouped by lithotypes at respective depths, predominantly located in the bricks and tiles windows for direct application. Note that if mixed with pollutants no direct usage is possible and requires further processing. (B) 51 samples from the Cretaceous, glaciogenic deposits, Siderolithic and topsoil formations, with glaciogenic and clay-rich limestone samples depicting the predominant potential to be further used as bricks or tiles. Note that areas outside of applicability scenarios imply further processing or disposal of the sedimentary raw material. $R_2O = K_2O + Na_2O$, $RO = CaO + MgO + MnO$.

The portland cement is produced by cement manufacturers, which mine, for instance limestone, shale, iron ore, and clay. These materials are further crushed, screened, and placed in a cement kiln. After being heated to high temperatures, these materials form a mass called “clinker”, which is further finely grounded to receive portland cement. There exist various modifications of the portland cement, for instance the portland-limestone cement, which contains between 5% to 15% of limestone. In fact, five main cement types exist according to the DIN EN 197-1 standard ranging from portland cement to portland composite cement, blast furnace cement, pozzolanic cement and composite cement (Haas, Mongeard, et al. 2021). The cement nomenclature follows letters "A, B, C" that define the different number of main components. A maximum of 5 wt% minor components may be added. These minor components include inorganic, natural or synthetic mineral substances or processed fillers. The grain distribution of these fillers essentially influences the water retention capacity as well as the processability. The solidification is handled by calcium sulphate in additives such as anhydrite, gypsum or hemihydrate, which should be kept low in general. This could be of high importance for the FCC, since tunnelling through the Grès et Marnes Gris à gypse

formation will be exposed to anhydrite/gypsum.

The cement and aggregates give the final concrete product its essential specification required for its purposes. These relate, for instance, to water and humidity resistance or chemical weathering resistance. There are some misunderstandings when it comes to the term additives or additional components among the English, German and French language. The term additives means all sorts of extra components that are added to the TCS. However, in German and French there are clear distinctions, and the term is further subdivided into “Zuschlagstoffe/additifs” and “Zusatzmittel/adjuvants”. The “Zuschlagstoffe/additifs” contain a high percentage of the concrete’s volume in the end and are taken into account for chemical calculations. This does not count for the smaller amounts of “Zusatzmittel/adjuvants” that are not allowed to affect the final concrete’s strength or corrosion protection of the reinforcement. Despite the great amount of concrete types, the essential ingredients are split into basic component systems (Röhling et al. 2012):

- The Three-Component-System (TCS): This is the basic mixture for concrete and consists of cement being the binder using e.g., fly ash or silica fume, the aggregates (granulates) and tempering water. In order

to receive the certain mechanical and chemical properties, additives are poured into the TCS to create a five-component-system (FCS).

- The Five-Component-System (FCS): This mixture contains additional components (additives) that enhance, for instance, the concrete's strength, corrosion behaviour, amount of fine/coarse grains or chemical behaviour in warm or humid conditions.

The basic TSC mixture consists of cement, aggregates and tempering water. Aggregates are added to the cement mixture. These components define the concrete's final strength, stress behaviour and makes up between 65 and 80% of the main component's volume. In special cases, aggregates are replaced by organic, mostly processed substances or metal. A single concrete product should contain only one type of aggregate that fulfils the requirements of a very dense grain strength and a compact connection of the grain's surface to cement ratio. Furthermore, it should not adversely affect the concrete's solidification process nor its resistance against external forces. Under environmental conditions such as rain, snow or wind, the aggregate should also not dissolve, decompose or soften. Standardised descriptions accountable for concrete aggregates are found in EN 12620:2008-07 (aggregates) and EN 13055-1:2008 (light aggregates) (Röhling et al. 2012). For concrete production, a petrographic description (European Norm (EN) 2020a) and a series of qualification tests are required. These include breakability tests such as the Los Angeles (LA) test (Association française de normalisation (AFNOR) 2018), rock strength tests such as the unconfined compressive strength (UCS) or related indices like a point load (PL) test (International Society for Rock Mechanics (ISRM) 1972b), and indications of abrasivity tested via LCPC (Association française de normalisation (AFNOR) 2013) and CERCHAR tests. LA tests are used for both rock and concrete material.

According to Swiss standards, concrete aggregates need to have the following characteristics for concrete production: minimum rock strength, low chemical contamination, low AAR potential, mean grain size distribution according to EN 12620 and an optimal grain shape. These properties further include grain form, grain size, grain distribution, inherent strength and a full lack of harmful substances, which include clay and adhesive clay, chemical impurities i.e. sulphur compounds, and organic substances such as

soil remnants. These harmful substances (elements) are further discussed below.

Environmental cases demand frost-thaw and wear resistance. According to the geological rock classification (magmatic, metamorphic and sedimentary rocks), different usability and applicability is derived. Even though metamorphic and magmatic rocks qualify best as concrete aggregates (e.g., AlpTransit Gotthard 2017), sediment rocks gain more attention nowadays due to improved processing technologies and a general lack of natural resources that demand for raw materials, as this would be the case for the FCC. Due to the FCC's geological heterogeneity, the approach to use the Molasse Rouge materials for concrete aggregate production seems challenging since it contains fine-grained and clay minerals that would make the final product at least non-frost sensitive. The Molasse Rouge material would need to be tested against frost resistance in further studies. If the Molasse Rouge rock is properly processed and the final material lacks clay minerals, the material might become frost resistant. This would allow the Molasse Rouge materials to be used for concrete aggregate production upon testing using the standardised basic tests as suggested and listed in Haas, Mongeard, et al. (2021). Realistically, the excavated material will be transported to a concrete company site, sorted, crushed, sifted, stored in the weather and then mixed as aggregate with cement in batches of concrete.

The production of cement highly depends on the chemical composition (Fig. 6.2) of the raw material in the form of CaO , SiO_2 , Al_2O_3 , Fe_2O_3 and heavy-metal concentrations (Schorcht et al. 2013). The latter should ideally be above 80 wt%. White cement clinker is an option for the unpolluted portion of clay-rich raw material with little or no smectite content within the Grès et Marnes Gris à gypse and Molasse Rouge formations. Minor elements should not exceed concentrations of 10 ppm for Hg or 100 ppm for the sum of Hg, Cd and Ti. The sum of As, Ni, Co, Se, Te, Cr, Pb, Sb and V should and does not exceed 10'000 ppm, respectively. Total hydrocarbon content is required to be below 5'000 ppm, which is the case for the non-polluted samples in the glaciogenic deposits and Molasse Rouge formations.

The sum of Hg, Cd and Ti should not exceed 10, 100 and 10'000 ppm, respectively, and the Cl content should be below 0.1 wt%. In case the rock material is not polluted and not part of the Grès et Marnes Gris à gypse formation

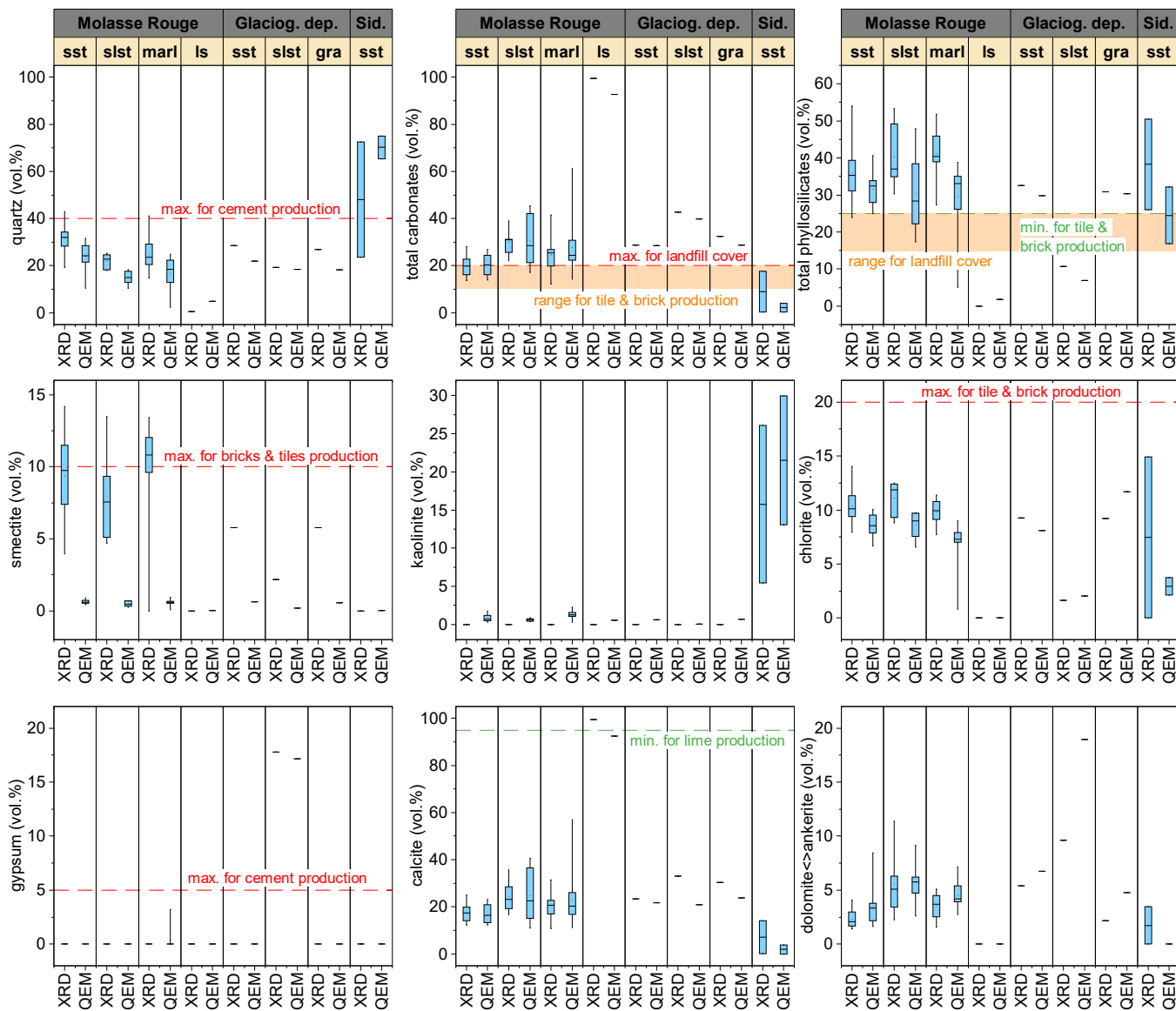


Fig. 6.2: Box plots with thresholds of mineralogical parameters for selected application scenarios based on a comparison of XRD and QEMSCAN measurements. Applicability threshold limits compiled from BRGM (2009), Garbarino et al. (2018), Schorcht et al. (2013), and Setec-Lerm (2020). Glaciog. dep.=glaciogenic deposits, Sid=Siderolithic Formation; sst=sandstone, slst=siltstone, ls=limestone, cgl=conglomerate, gra=gravel.

because it would be associated with exceeding gypsum contents, the investigated sedimentary rock ranges in the feasible application window for cement production. While the grain size distribution depends on the final mixture, the presented values as featured in Schorcht et al. (2013) comply well for cement production.

Fig. 6.2) provides the mineral content of the analysed samples. Mineral phases are predominated by the carbonate minerals calcite, dolomite and ankerite. Non-carbonate minerals include feldspar, quartz, total phyllosilicates and gypsum. Quartz content should range between 30 to 40 wt%, maximum amounts of gypsum should range between 2 to 5 wt%. Clay minerals without Mg are preferred because dolomite and magnesium carbonates generate MgO in the burning process. This process commonly causes an expansive effect when hydrated in clinker. The limit values given for MgO in the raw materials should range between 2 to 3 wt%. The feasibility of cement production further depends on the sum of CaO, SiO_2 , Al_2O_3 and Fe_2O_3 with at least 80 wt%. The SiO_2 content should ideally range between 30–40 wt% with gypsum contents not exceed 2–5 wt%. Clay minerals without Mg are preferred.

The main physical parameters depend on the desired concrete quality when mixing the cement with water. Two important parameters are the raw material's initial water content and its grain size distribution. The precise water content depends on the processing procedure and environmental conditions (e.g., summer heat, winter cold, sun, snow or rain), the required final product and final use. The Molasse Rouge samples show water contents between 0.4 to 5.15 wt%. This accounts for the analysed samples that have been stored for a >1 year time period in unsealed containers. For fresh samples, water contents vary between 3 to 8.6 % (Table 5.1) but reach up 50% (Fig. 5.33).

The fresh raw material should not *feel* muddy but rather solid. In terms of plasticity, this would range between plasticity indices of 10-20, and could be qualitatively estimated on-site by a registered, professional engineer and further analysed on-site by the Enslin-Neff method.

The prediction of lime production requires the identification of major oxides of Ca, Mg, Si, Al, and Fe and calcite.

Thresholds are of qualitative nature and target the highest CaO and lowest MgO contents. The calcium carbonate purity is of uttermost importance and requires a thorough quantitative representation of $CaCO_3$ (calcite, aragonite and vaterite minerals, depending on crystal form) and $CaMg(CO_3)_2$ (dolomite mineral). The $CaCO_3$ content should be above 95 wt%, ideally 97 wt% coming from e.g., a pure limestone rock. MgO content is acceptable up to 40% and are summarised commonly termed *dolomitic lime*. MgO content is limited predominantly for calcite lime. Maximum $CaMg(CO_3)_2$ (dolomite) contents of 5 wt% are tolerated but should be avoided.

The purity of limestone is influenced by the sedimentation source and differentiates 2 main geological origins. These depict the biochemical deposition of organisms with calcareous skeletons or the inorganic/chemical crystallization from solution. Less impurities are expected in limestone originating from the chemical process. The purer the limestone, the higher the quality of the final lime product after the calcining process. Lime reactivity may vary according to the crystallization parameters of calcite, whereas calcite originating from chemical precipitation is preferred. A thorough approach for quality control of limestone is to study the geological data in the region or to conduct a full elemental analysis (e.g. ICP or XRF). This allows to check the amount of elements that are not Ca or Mg (Schorcht et al. 2013). Based on the Geneva Basin's geological history neither of these two processes infer a pure limestone deposition. The Molasse Rouge Freshwater limestone yields calcite (carbonate) values that are too low and make the raw material rather unlikely for lime production (Fig. 6.2). Besides producing lime out of excavated raw material, the addition of lime to the rock material during excavation seems likely for stabilization purposes. The alkaline properties of lime increase the pH value of soil. The addition of lime is often exploited to neutralize acid components of industrial emissions. This modifies the soil properties diminishing its feasibility for agricultural usage or land-filling. It should be noted here that the consideration of adding lime to the raw material exceeds the scope of the present study.

6.4 Insulation material and glass production

The production of insulation material (glasswool or rockwool) is difficult to evaluate and strongly dependant on the final industrial mixture recipe. The application as insulation material requires both chemical and mineralogical analyses for Si, Al, Ca, Mg, K and Na oxides and respective minerals that include these elements. Most formulas for industrial production are subject to confidentiality. Essential oxides are SiO_2 , Al_2O_3 , CaO, MgO, K_2O , and Na_2O . Oxides are required for glass wool and rock wool manufacturing. Knowledge of their exact content is dependant on the final chemical mixture. It must be noted that mineralogical composition is rather a recommended than a required parameter because it later supports the prediction of the melting behaviour of the material in the kiln. Chemical composition knowledge is sufficient.

The application for common packaging glass requires the analyses of major elements Si, Ca, Na, K and B oxides. Mineral phases identification include quartz, feldspar, carbonates and phyllosilicates. The production of common packaging glass is not possible due to the missing analysis of boron content, respectively B_2O_3 (boric oxide). However, similar to glasswool production, the main components are comprised by SiO_2 , Al_2O_3 , CaO, MgO, K_2O , and Na_2O . Quartz (SiO_2) content above 80 wt% is preferred. Feldspars, carbonates and phyllosilicates depict minor issues and may occur in low concentrations.

6.5 Topsoil construction (agricultural use)

Topsoil construction is closely linked with the term agricultural use. These application scenarios share the identification and quantification of clay minerals, type of phyllosilicates, carbonates, CEC, pH values and the elemental composition aiming for most essential plant nutrients. These include elements P, K, Ca, Mg, N and $NH_4 - N$ as well as B, Co, Cu, Fe, Mn, Mo and Zn (oligo-elements). The 1:1 clay minerals (kaolinite) are preferred for aggregate formation, as well as a high

carbonate content ($CaCO_3$ and $CaMg(CO_3)_2$) to keep a basic topsoil pH value. In case carbonates are present, the pH value ranges at ca. 8. Exact thresholds are difficult to define but for the pH a basic rather than an acid environment is favoured because the plants and microorganisms take up many adsorbed nutrients in ionic form from basic soil solutions. This is an important factor for the applicability of excavated material as agricultural substrate and include the major cations (NH_4^+ , K^+ , Mg^{2+} , Ca^{2+} , Al^{3+}) and anions NO_3^- , SO_4^{2-} . Samples should generally be extracted when taken freshly from the field, prior to drying, in particular when if ions are subject to microbial transformations during storage (e.g., NH_4^+ , NO_3^- , PO_4^{3-}), or undergo volatilising (e.g. NH_4^+ , PO_4^{3-}). If immediate extraction is not possible, the ion of interest is unlikely to undergo microbial transformation (low organic matter) or precipitation reaction.

Understanding the size and composition of the soil solution together with knowledge of nutrient turnover rates provides crucial insights into soil nutrient availability and other bio-geochemical processes including weathering or leaching losses (Robertson et al. 1999). The cation exchange capacity of clay minerals, in particular of smectites, influences the cation retention and diffusion processes of charged and uncharged molecules. These diffusion processes strongly have an impact on the migration of cations and molecules through clay-rich barriers in nature. Cu-trien copper effective CEC values range between 0 to 16 meq/100g, which is not ideal for topsoil construction. CEC values should be below 1 (Fig. 6.3), which is not the case for any samples to be used for topsoil construction. However, nutrient availability seems high for clay-rich samples at shallower depths ranging between 450 and 350 m, then slowly decreasing until ca. 190 m based on their types of exchangeable cations (Ca, Mg, Na) relevant as nutrients for agricultural usage (Fig. 5.34). Minerals sylvite (KCl) and carnallite ($KMgCl_3 \cdot 6(H_2O)$) are typically beneficial for agricultural use to create potash. However, neither XRD nor QEMSCAN results depict these minerals but a future study explicitly on the agricultural usage might lead to further insights.

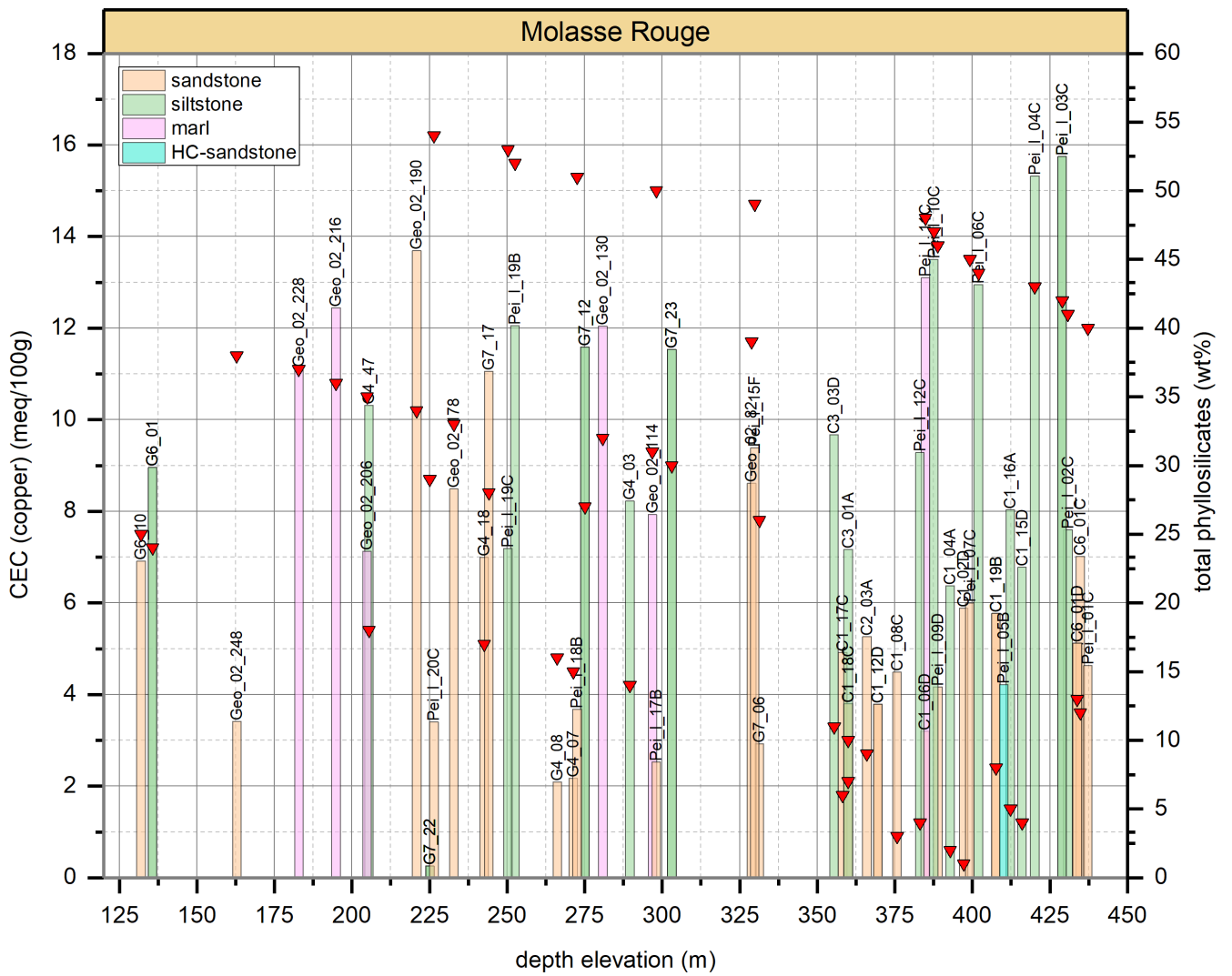


Fig. 6.3: CEC values derived from Cu-trien complex measurements with clay content from XRD analyses at respective depth elevation. All samples show CEC values ≥ 1 , relevant for the evaluation of application scenarios.

6.6 Landfilling and backfilling

Although landfilling and quarry backfilling are often referred to as proper application scenarios, these should be explicitly excluded from the terminology (Haas, Galler, et al. 2020; Haas, Mongeard, et al. 2021). As such, they provide the ultimate, non-sustainable solution for excavated raw material to be disposed under a non-legal waste status (Haas, Galler, et al. 2020). To some extent, agricultural use could be addressed as landfilling but strict legal requirements apply to avoid any kind of pollution.

Regardless of terminology, for landfilling the total clay mineral content should range between 15 to 25 wt%. Carbonate minerals should not exceed 20 wt%. The physico-chemical behavior is essential for leakage, seepage and subsidence. This requires the identification of the liquidity and plasticity limits with preferences of the former to be higher than 25 wt%. Both parameter threshold values are fulfilled for the investigated material. This depicts plasticity indices between 10 to 40, a permeability value of 10^{-9} m/s or lower, and a methylene blue value (MBV) above 6.

For quarry backfilling, grain size distribution defined for the maximum diameter depending on the geometry of the back-filled area is essential, as well as the geomechanical micro deval and Los Angeles values, both being below 40 in their respective units. For both landfilling and backfilling, national legislation for inert waste has to be fulfilled (see VVEA in Switzerland, Arrêté du 12/Dec/2014 in France) for pollutants and leaching behavior. These include As, Ba, Cd, Cr total, Cu, hg, Mo, Ni, Pb, Sb, Se, chlorides, fluorides, sulfates, phenol index, TOC, soluble fraction, aromatic hydrocarbons (BTEX), polycyclic aromatic hydrocarbons (PAH), aliphatic hydrocarbons (C_5 - C_{10} , C_{10} - C_{40}), volatile chlorinated hydrocarbons (LCKW), polychloride biphenyl (PCB), Benzo[a]pyrene (polycyclic aromatic hydrocarbon) and benzol. Leachate considerations apply for the use of mixed material for embankments and reclamation. Filling and mechanical parameters are less important than chemical issues, which are the driving environmental factor. The chemical components of any leachate must be below the respective national toxicity thresholds for safety.

The potential for disposing excavated materials in landfills makes it necessary to discuss techniques for rock purification. The routine technique used in Switzerland involves washing and then landfilling the polluted material, which

implies costly and harmful conditions for the environment upon disposal.

Economic and environmentally friendly cleaning techniques are still required to avoid polluting the environment (Kang et al. 2015; Laporte-Saumure et al. 2010; Lee & Kim 2010). Bio-remediation processes are cost-effective, eco-friendly and are highly efficient as compared to physico-chemical methods for remediation of metals from soil contaminated sites (Adler et al. 2016; Naik & Dubey 2013). Sparse information is available on the purification by microbial cells for soil bio-remediation (Diels et al. 1999). The phyto-remediation techniques seem to fit in-situ cleaning of heavy-metal polluted material as encountered in the Molasse Rouge and Siderolithic formations. The choice of a remediation method is crucial and this choice depends on several criteria such as the polluting elements, rock composition and presence of groundwater aquifers, which all should be meticulously evaluated (Degryse et al. 2009; Rooney et al. 1999; Scullion 2006). Bio-remediation techniques usually take more time than physico-chemical techniques and are affected by high metal contents that could impede the growth of organisms used for bio-remediation, particularly phyto-remediation (Adler et al. 2016). A possible approach would be bio-augmentation with a strain able to adsorb high amounts of heavy-metals. This approach could contribute to making heavy metals less available in the biosphere. Phyto-extraction seems to be an appropriate remediation method for the heavy metals encountered in the Molasse Rouge and Siderolithic formations. It is a low cost and environment-friendly cleanup application (Adler et al. 2016).

6.7 Identification of essential rock properties, environmental pollutants and disposal

For the evaluation of application scenarios of sedimentary raw materials, the physico-chemical behaviour of clay minerals plays a crucial role. So far, the previous sections have discussed potential application scenarios (Fig. 6.5) for clay-rich sedimentary raw material as encountered in the glaciogenic deposits, the Grès et Marnes Gris à gypse, the Molasse Rouge and the Siderolithic formations. These

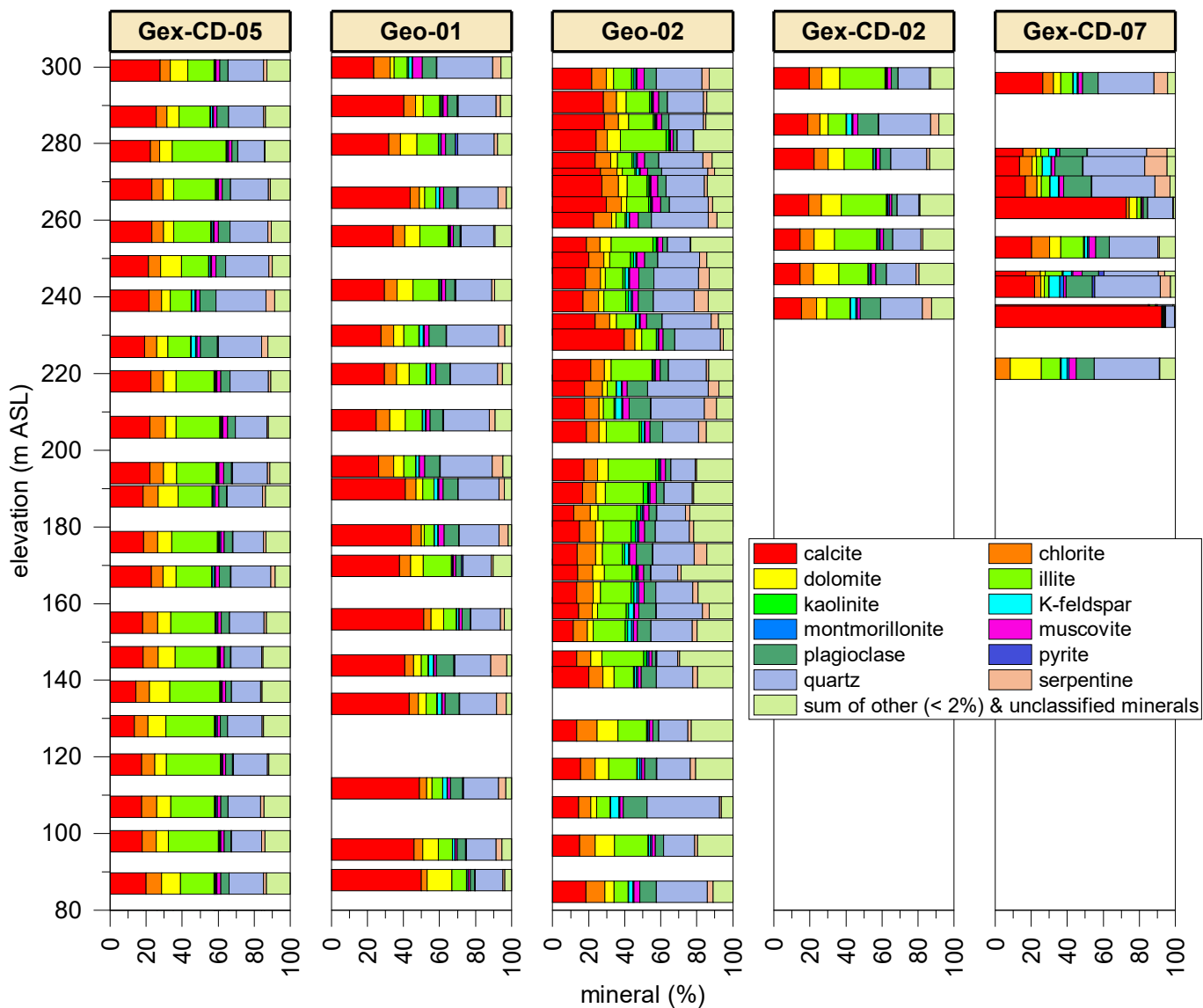


Fig. 6.4: QEMSCAN analyses of 5 wells extending across the north/northwestern area of the FCC construction ring at its current elevation depth between 100 and 300 m above sea level, highlighting the vertical (220 m) and lateral (100 m to 4 km) heterogeneity of the Molasse Rouge formation. Each bar represents one sample, whereas minor minerals with volume concentrations below 2% were summarised with unclassified minerals. For statistical mineral distribution see Fig. 6.6.

applications require the knowledge of 91 parameters for a sufficient identification and include the major (e.g. Ca, Si, Al, Fe) and minor (e.g. Na, K, P, Mg, Cl, Hg, Cd, Ti, As, Ni, Co, Se, Te, Cr, Pb, Sb, V) elements in their oxide, sulfide, sulfate and carbonate mineral states together with phyllosilicates, organic compounds (total organic carbon) and physico-chemical parameters describing grain size distributions, water content, liquid and plastic limits, methylene blue value (MBV), cation exchange capacity (CEC) and eluate (leachate). The last two play an important role for the derivation of environmental hazards, which include hydrocarbons and heavy-metal ions. The following paragraphs discuss the relevance of various rock properties in the context of environmental pollutants that require excavated raw materials to be treated and disposed as waste.

Essential rock properties

Out of the 91 identified parameters, 74 have been measured or correlated as part of this study and 13 parameters have been consulted from third-party data (see chapter 3, Table 3.1). This suggests the following analyses:

1. Elemental composition: portable XRF, ICP-OES/MS;
2. Mineralogical composition, mineral shape and distributions: XRD, QEMSCAN, FTIR;
3. Eluate: ICP-OES (leachate analysis), cuvette tests
4. Organic compounds: ion chromatography, gas chromatography and PetroFLAGTM test, FTIR;
5. CEC (as MBV), exchangeable cations, pore size distribution, porosity, permeability thermal treatment (loss of water mass), liquid and plastic limits, plasticity index (modelled), grain size distribution (third-party): Cu-trien complex, ICP-OES, MIP, Enslin-Neff, sieving.

Four (4) unknowns remain and depict the dissolved organic carbon (DOC) content, the boron trioxide (B_2O_3) content, the Los Angeles (LA) and Micro-Deval (MD) indices, and would imply future measurements. The DOC is measured by standard wet chemical and photo-chemical methods (Wangersky 1993), boron trioxide requires knowledge of the desired, final glass product (also measured on the glass product) (Aghili et al. 2018). The two geomechanical LA and MD indices are obtained via respective

testing apparatus.

All parameters are numeric data, except for the pH value and the crystallization process of calcite. The pH as a binary parameter indicating acid or base, and the calcite crystallization, a lime-production parameter, as binary for biogenic or chemical were treated qualitatively. The most important parameters are the minerals, elements, physico-chemical and geomechanical parameters. The mineral groups comprise carbonates, oxides, sulphates and sulfides. The phyllosilicate group is differentiated into the serpentinite group [antigorite, chrysotile, lizardite], the clay minerals group (1:1 halloysite, kaolinite; 2:1 pyrophyllite, talc, illite, montmorillonite, chlorite, [vermiculite], [sepiolite] and [palygorskite]), and the mica group (biotite, muscovite, glauconite, [fuchsite], phlogopite, [lepidolite], [margarite]). The term *total clay* refers to the phyllosilicate clay-mineral subgroup. Fig. 6.5 gives an overview of the parameters required for each evaluated application. In the case that standards or common procedures require further measurement procedures for reliable conclusions, see Haas, Mongeard, et al. (2021).

Sources of environmental pollutants and disposal evaluation

The beneficial use of excavated rock and soil is restricted by nationally legislated thresholds for environmental compatibility. Contaminants are present in rock and soil. The results of various analyses dictate the proper separation of excavated material into usable raw materials or waste. To be used, excavated rock and soil must be inert and non-polluted according to both Swiss and French national legislation. However, the previous chapters have shown that this is not the case. The excavated material contain various amounts of hydrocarbons and heavy-metal ions, which are predominantly associated with clay minerals and sulfides. These chemical levels define the type and severity of legislatively defined pollution. The materials represent environmental hazards when the contaminants exceed the national threshold limits. If true, the materials must undergo purification or disposal.

Robust laboratory analyses for environmental pollutants are pXRF and ICP-MS/OES measurements. For rare organic compounds, FTIR serves as a qualitative measurement but to identify specific organic pollutants it requires additional analyses such as ion and gas chromatography which were not performed as part of this study. Specific

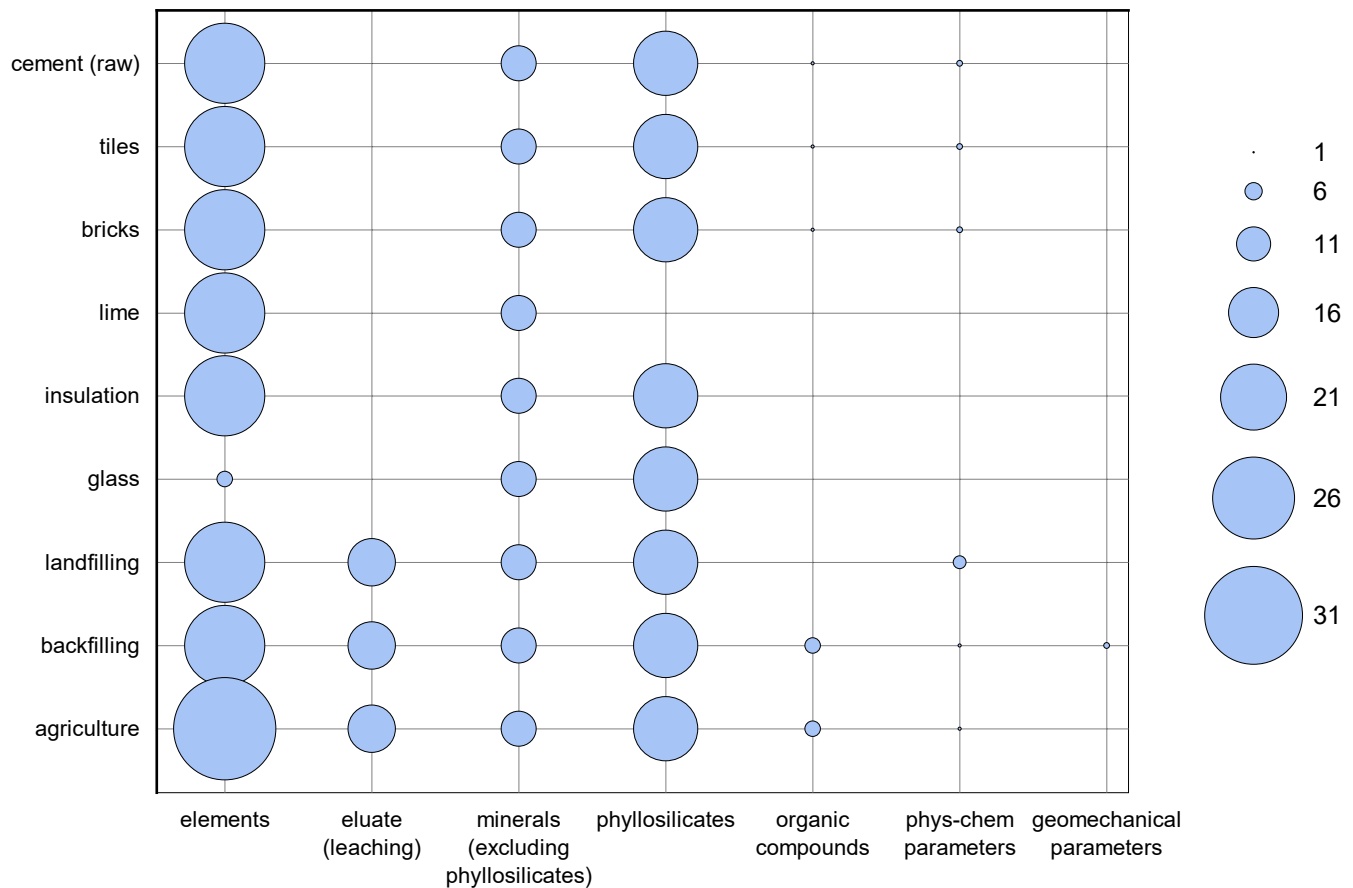


Fig. 6.5: Essential parameters for selected potential application scenarios. The bubble size and colour depict the number of parameters per category. Parameters are further elicited in the text, and based on national legislation (République Française 2003; Schweizerischer Bundesrat 2015), personal communication with experts and research of manufacturer’s thresholds, or taken from Anger et al. (2015), BRGM (2009), Faure (2017), Fourvel (2018), Frar et al. (2014), Furlani et al. (2011), Garbarino et al. (2018), Haurine (2015), Haurine et al. (2016), Schorcht et al. (2013), Setec-Lerm (2020), Swiss Confederation (2021), and Wimmer-Frey & Schwaighofer (2002).

organic compounds include PCBs, phenol, PAHs, BTEX (benzene, toluene, methylbenzene and xylene), PNAs (poly-nuclear aromatics), LCKW, and aliphatic hydrocarbons. Based on Fig. 6.6 and an extended extrapolation of the geological environment, calcite and quartz values show large variations both across and within wells when compared to the other minerals. This underlines the challenging task of predominantly identifying sandstone, marl and siltstone lithotypes and ultimately predicting polluted lithotypes. Serpentine occurs in larger quantities in Gex-CD-07. Since serpentine was identified as a carrier of polluting elements and hydrocarbons. This suggests that this well and the area towards the Northwest could be subjected to increased concentrations of the polluting elements Ni and Cr as well as hydrocarbons.

The detection of hydrocarbon plays a major role across the whole Geneva Basin. The PetroFLAGTM hydrocarbon

analysis yields the most economically efficient method for determining hydrocarbon contamination on-site. It yields reliable results as shown on HL-LHC Point 1’s construction site (Voiron et al. 2020). Unlike specific laboratory measurements, the PetroFLAGTM test does not target specific compounds such as BTEX or PNAs that could be part of hydrocarbon mixtures. Instead, the method is sensitive to heavier hydrocarbons such as oils and greases compared to lighter and more volatile hydrocarbons (ppm range). Brake fluid, phosphate ester based hydraulic oil and other soluble fluids are not detected by the PetroFLAGTM system (EQUIPCO 2022). Other laboratory hydrocarbon analyses are strongly dependant on the used extraction solvents. Typically, chlorinated solvents or freon are used with a high extraction efficiency of polar organic compounds, while yielding low extraction efficiency for hydrocarbons. However, the PetroFLAGTM test contains

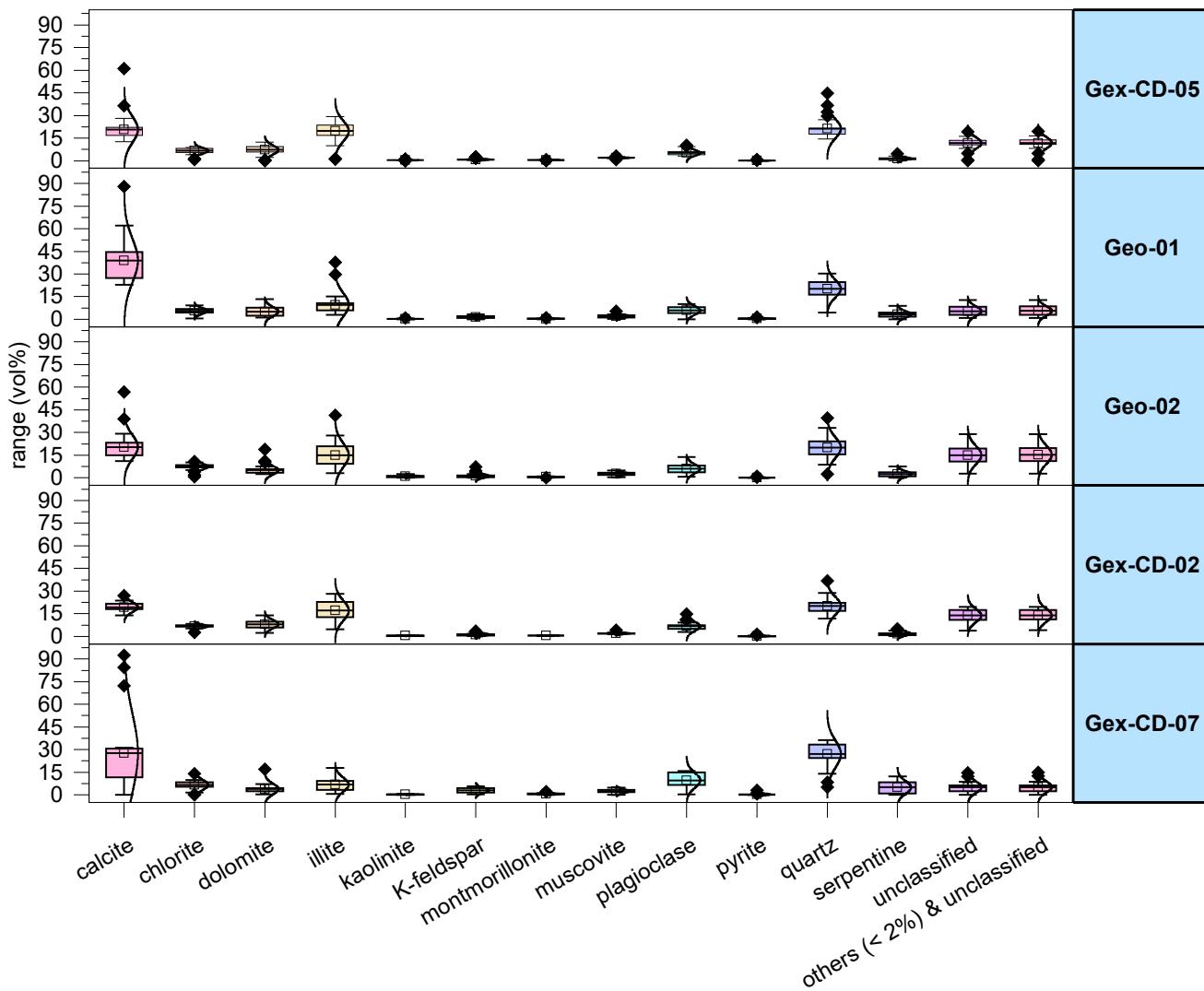


Fig. 6.6: Statistical distribution of essential minerals based on QEMSCAN measurements for Geo-01, Geo-02, Gex-CD-02, -05 and -07 wells. The middle line in the box denotes the mean value. Black curves indicate the normal distribution of the data. Diamond symbols represent extreme values (outliers). A wider trend of increased quartz value in the northern part of the basin (Geo-01, Geo-02, Gex-CD-07) is observed. The Geo-01 profile is enriched in dolomite but shows lower values of plagioclase compared to other wells. Values of "other" minerals do not represent a large portion of the data set as indicated by the marginal difference between the "unclassified" and the sum ("unclassified" and "others") with <2 vol%.

no chlorofluorocarbons or chlorinated solvents, which also makes the extraction efficiency unaffected by soil moisture (EQUIPCO 2022). In rare cases the PetroFLAG™ test indicates higher hydrocarbon concentrations than other methods, in particular when subjected to the dilution effect in the presence of water. This would then result in a significantly lower response, but this is compensated by the water content determination of the respective soil sample and correcting for the difference between wet and dry weights (Lee et al. 1993; USEPA 1992). That being said, hydrocarbon contamination should be characterised by a certified laboratory.

The PetroFLAG™ results correlated well with those from the literature for various hydrocarbon laboratory tests. The correlations were up to 92% and yielded no false-negative tests and only two false-positive tests (Pitard 1992; Wright 1995; Wright & Jermstad 1995). Hydrocarbon measurements at HL-LHC Swiss Point 1 yield average values of 0.25 mg/kg, which depicts the basin's northern part relevant for the FCC layout. In conjunction with eluate analyses as well as heavy-metals encountered in the Molasse Rouge formation, this leads to Swiss disposal classes B to E (Haas, Galler, et al. 2020; Haas, Mongeard, et al. 2021). In some cases also E+, which depicts the most hazardous class in Switzerland. Hydrocarbon accumulations was in the order of 30 to 35% in the case of HL-LHC Point 1 (Haas, Mongeard, et al. 2021). Hydrocarbon pollution should be considered as one of the main challenges during the excavation from a beneficial use perspective (Voiron et al. 2020). It is reasonable to apply the same value for the FCC excavation. But, it must be noted that increasing hydrocarbon pollution could be encountered towards the south of the basin as indicated in the cross-sections.

An increasing trend of large amounts of accumulated hydrocarbons is interpreted from south to north across the basin at the elevation of the FCC tunnel, which is likely to be drilled through hydrocarbon-rich rock. Well C1 at the Swiss HL-LHC Point 1 shows small amounts of hydrocarbon accumulations at the level of the tunnel, whereas boreholes C2 and C3 show complete absence of hydrocarbons at the same level. Thus the most critical pollution layer could possibly fall in a type B disposal site. The northern wells (Gex-CD-01, Gex-CD-07, Peissy-I, SLHC-wells, C-wells) contain most of the hydrocarbons within the studied area (see cross sections A & B in

chapter 4). An exception is marked by the Thônex-1 well encountering the highest thickness of Grès et Marnes Gris à gypse. This formation does not contain hydrocarbons in the investigated well but their distribution across the basin within this formation cannot be excluded. Apart from the Molasse Rouge, deeper carbonate formations in the former Urgonien facies (Lower Cretaceous), Muschelkalk (Middle Triassic) and Buntsandstein sandstone (Lower Triassic) show hydrocarbon accumulations in e.g., wells Chatillon-1 and Charmont-1 close to the Jura in the northwestern sector of the FCC's construction area. While these units are not primarily ranging within the projected FCC construction depths, adjacent faults might represent potential migration pathways for hydrocarbons toward the FCC depth intervals. The identification of these potential faults and associated, fractured migration paths should be addressed and examined in future.

The lateral and vertical distributions of hydrocarbons as encountered also at the HL-LHC Point 1 construction (Fig. 6.7) have been discussed from a stratigraphic point of view along the two cross sections (see chapter 4 in Fig. 4.10 and 4.11). Substantial amounts of bituminous and gaseous hydrocarbons are identified in the massive dolostones in the Goldberg and Twannbach formations encountered in all wells featuring these two formations, often also featuring karstic intervals in the Twannbach Formation. The Roches des Hirondelles Formation's Vallorbe Member presents a substantial hazard of hydrocarbons and karst, both extending over several tens of meters vertically at the FCC tunnel level. The Vions Formation shows indices of hydrocarbons which are shared with the Grand Essert Formation's Neuchâtel Member bearing a severe hazard of karstic intervals. This suggests that hydrocarbon accumulations as heavier oil and asphalt are associated with karstic intervals in the Mesozoic fractured limestone formations.

Even though hydrocarbons occur predominantly in bituminous form, well Geo-01-DAS located about 300 m next to the deeper Geo-01 well also shows the presence of gas in the Molasse Rouge (pers. comm. with Guglielmetti L., 2020). The area of Satigny is particularly well known for gas occurrences in the shallow wells (Do Couto et al. 2021). This suggests that gas-bearing (hydrocarbon) horizons are likely to be encountered in the northern part of the construction area and should be addressed during site investigations. With respect to their total well

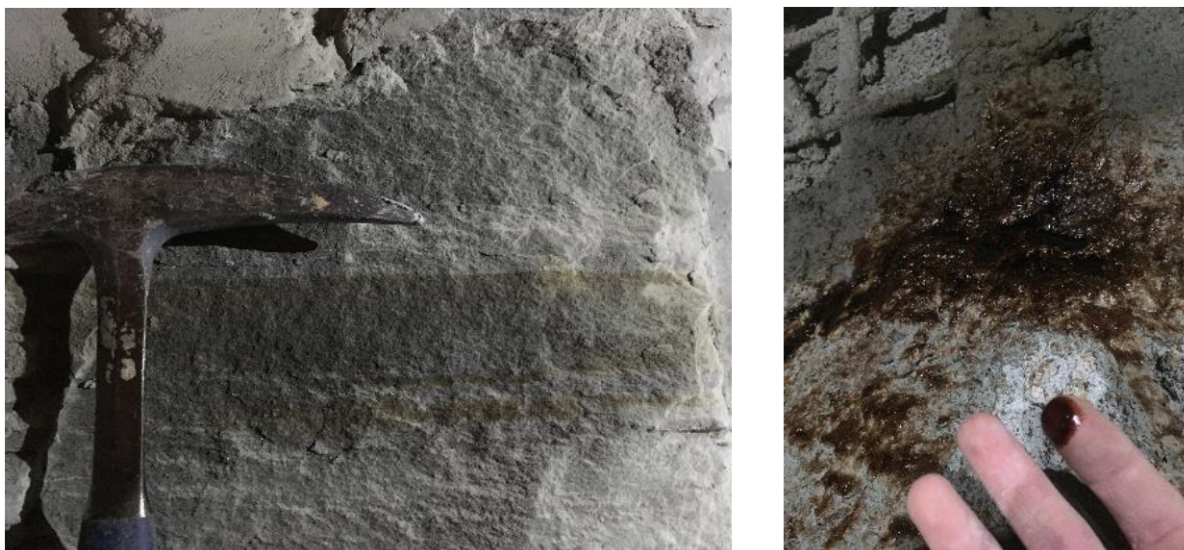


Fig. 6.7: Fresh hydrocarbons (oil) encountered on raw tunnel face at Swiss Point 1 during HL-LHC excavation analysed via the PetroFLAGTM test. Modified after Voiron et al. (2020).

depths, the Gex-CD-01 and its neighbouring Gex-CD-07 well show the highest hydrocarbon indices in medium to coarse-grained sandstones in the Molasse Rouge (HC lithotype, Fig. 5.5) and to some extent in the Mesozoic limestone formations (Fig. 4.10). In rare occurrences (e.g. well L134B), the Quaternary deposits also contain bituminous hydrocarbons.

Geochemical analyses (ICP-OES/MS, pXRF) are used for the identification of environmental pollutants. Fig. 6.8 shows the most abundant polluting elements in the Molasse Rouge formation based on pXRF measurements. Cr and Ni are the most polluting elements based on their frequencies and concentrations. Fig. 6.8 shows that 6 As values exceed the green line but not the orange line, no Pb values exceed the green line, 11 Ni values exceed the green line but not the orange line and all Cr values exceed the green but not the orange line. Hence, most of the samples fall at least into the Swiss disposal class B based on Cr concentrations. Ni values at 150-175, 200-240 and 265 m, exceed Swiss disposal class A because polluted thresholds lie above 15 ppm between 130 and 145 m and at ca. 200 m. Pb values have no influence on the status of pollution. No Pb pollution is measured in the Geo-02 samples by pXRF.

Based on ICP measurements, except for Biollay, Verney and Sarzin outcrop samples, all 378 samples are polluted

in Ni with values between 50 to 500 ppm. Respective threshold values are anchored in national legislation and summarised in Haas, Mongeard, et al. (2021). This makes all samples at least Swiss disposal class B polluted. Samples C1-15A, C3-04B, Geo-02-158, L112-121 and L112-130 are polluted in As with values greater than or equal to 15 ppm but less than 30 ppm (Swiss disposal A). C2-06B, G2-05, G3-C10, G5-22, L112-117, -118, -119 and -126 are polluted in As with values greater than or equal to 30 ppm (Swiss disposal B). L112-118 is highly polluted in As with a value of 90.1 ppm, which is greater than 50 ppm making it a Swiss disposal class E. The remaining samples have As values less than 15 ppm and, therefore, are not polluted in As. Out of the 378 measured ICP samples, only samples G1-27, G2-C25, Geo-02-30 would be polluted and also contain fluorine values of 1.04 mg/L, i.e. referring to ppm (mg/kg) in liquid form. Samples L112-01A, -116, -129, Montfleury-01, -03, -04, -10, Mornex, Nyoux and Sarzin are neither polluted by As, Cu, Pb nor Cr(total), Ni, Sb, Zn or Cd according to Swiss law. The rest of the samples (and respective borehole locations) are at least polluted in one of the elements. The highest and most frequent pollution originates from Ni and total Cr, followed by As, Pb, Sb, Cu and Pb. Cr^{VI} values lead to potential Swiss disposal class E or E+.

Fig. 6.9, 6.10 depicts measured cuvette samples. All samples are at least polluted in ammonium with values greater than 0 mg/L (disposal class A), and some samples exceeding threshold pollution values for class E (e.g.

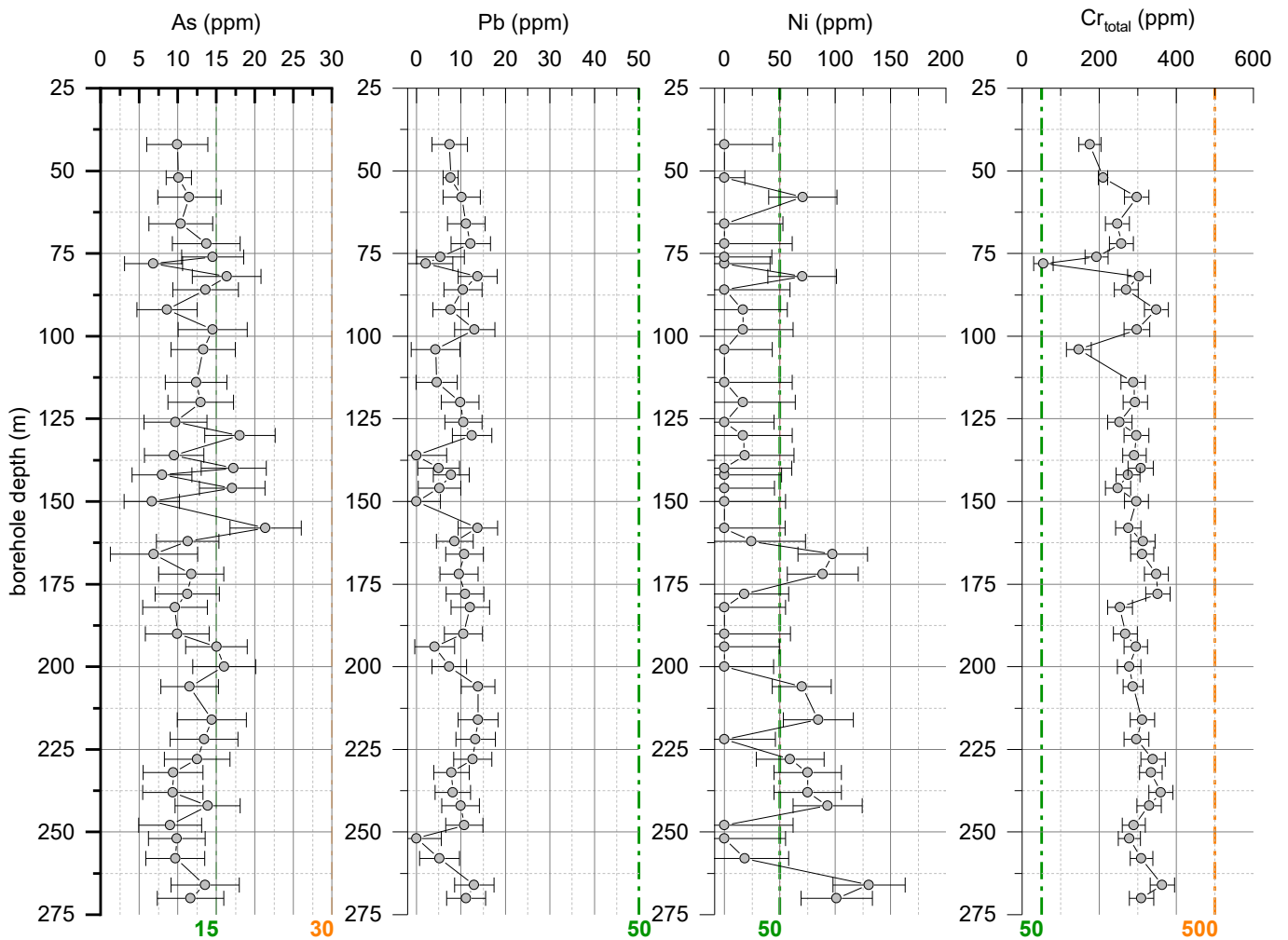


Fig. 6.8: Polluting elements As, Pb, Ni and Cr_{total} including error bars based on pXRF data along well Geo-02 depth in the Molasse Rouge with respective threshold limits for Swiss disposal classes. Class A=non-polluted (green line), class B=polluted (orange line), class E=highly polluted and hazardous (red line).

G4-18 with 0.582 mg/L, G5-17 with 0.667 mg/L or G5-14 with 0.686 mg/L). Except for Sarzin, all samples are polluted in F by class A with values between 0.1 to 1.71 mg/L. The maximum value is reached by sample G7-17 in Gex-CD-07 at a depth of 225.4 m. Measured samples are not class-B polluted in Nitrite greater than 1 mg/L but all show traces of nitrite, making the raw material fall into class A disposal. With respect to national disposal classes, elements As, Cd, Cr_{total} , Cu, Hg, Ni, Pb, Sb and Zn are relevant in addition to eluate analyses of $NH_4^+ - N$, F^- , CN^- , $NO_2^- - N$, Cr^{6+} , SO_4^{2-} , CN^- , dissolved organic carbon (DOC) and organic compounds such as PCBs, TOC, phenol, PAH, BTEX, LCKW, aliphatic hydrocarbons, benzo[a]pyrene, benzol and halogenated organic substances, and cuvette tests (6.9).

Fig. 6.9 shows leachate analyses measured in cuvette tests for polluting substances with respective limits of no disposal classes (below green line), mildly-polluted material (between green and orange lines) referred to as Swiss disposal class A, medium-polluted (between orange and red lines) often referred to as Swiss disposal class B and highly-polluted material (above red line), often referred to as Swiss disposal class E. French disposal classes refer to K3, K2 and K1, respectively. Ions $NO_2^- - N$ and CN^- mark no correlation with pollution across all samples, followed by mildly-polluted material by F^- ranging between 0 and 2 mg/L, in conjunction with $NH_4^+ - N$, most of the samples ranging less than the polluted class of 0.5 mg/L. Only one sand-rich sample shows NH_4^+ values greater than 0.5 mg/L. However, a main issue is the high Cr^{VI} values across all samples with values up to 0.9 mg/L particularly in the depth interval 425 to 240 m, which makes the material highly-polluted and hazardous. These maximum values are predominantly associated with clay-rich rock, and play only a minor role for some sand-rich rock, mostly in well Geo-02 of the Molasse Rouge formation. The Siderolithic sandstone is another highly-polluted sample but part of the underlying Siderolithic formation.

Fig. 6.10 depicts the correlations of occurring polluting ions among the measured samples in the Molasse Rouge formation based on cuvette tests. Values between -0.3 and +0.3 are generally considered non-robust, i.e. depicting a weak, linear correlation. This accounts for F and Cr^{VI} , F and NH_4^+ , F and Cr^{VI} , F and $NO_2^- - N$, Cr^{VI} and

NH_4^+ , $NO_2^- - N$ and NH_4^+ as well as CN^- and $NO_2^- - N$. There exists a strong positive correlation between Cr^{VI} and $NO_2^- - N$ as well as Cr^{VI} with CN^- of 0.7 and 0.8, respectively. A strong decreasing relationship between F and increasing CN^- is observed with a value of -0.7. A similar anti-correlation exists between NH_4^+ and CN^- . These anti-correlations suggest that none of these ions occur simultaneously in the same sample.

Besides having analysed the identified polluting substances, the next steps are to derive their origin and distribution along the FCC layout in a longitudinal cross-section. Fig. 6.11 shows the elemental source of elements Mg and Cr that contribute essentially to application and disposal scenarios. Mg concentrations are largely attributable to the minerals chlorite, dolomite, illite, serpentine and traces to biotite, montmorillonite and talc. Cr is associated to the Cr-spinel group. Ca is predominantly attributed to calcite and dolomite, with traces to montmorillonite, while Si is primarily dominant in quartz and silicate minerals. Na is associated with mainly plagioclase as well as traces to montmorillonite and paragonite. While Geo-02 exemplifies the elemental associations. Polluting element Ni was not analysed in QEMSCAN due to analysis limitations (see chapter 3). Elements As, Hg, and Cd are identified in wells C1-C6, Geo-02, Gex-CD-02, -04, -05, -07, Humilly-2, L112, Montfleury, Thônex-1 and Geo-01-DAS. No Pb could be identified in C1-C6, Geo-02, Gex-CD-04, -07, Humilly-2, L112, Montfleury, Thônex-1 and Geo-01-DAS but was identified in Gex-CD-01, -02 and -03. Outcrop samples Sarzin, Mornex, Biollay and Verney yielded no indications of Cr, Pb, Hg, As or Cd. Nyoux showed only concentrations of Cr but no Pb, Hg, As or Cd.

Portable XRF and ICP measurements allow the derivative of respective oxides such as SiO_2 , TiO_2 , Al_2O_3 , Fe_2O_3 , MnO , MgO , CaO , K_2O , Na_2O and P_2O_5 , which are crucial for the evaluation and predictability of application and disposal scenarios. Essential trace elements include fluorine [F], chlorine [Cl], sulphur [S], transition and heavy metals. Further methods such as wet chemical analysis and atomic absorption spectrometry (AAS) are possible but have not been conducted as part of this study. The alkali oxides K_2O and Na_2O belong to feldspars (potassium feldspar, albite), mica minerals (illite, muscovite) and, to a lesser extent, smectites

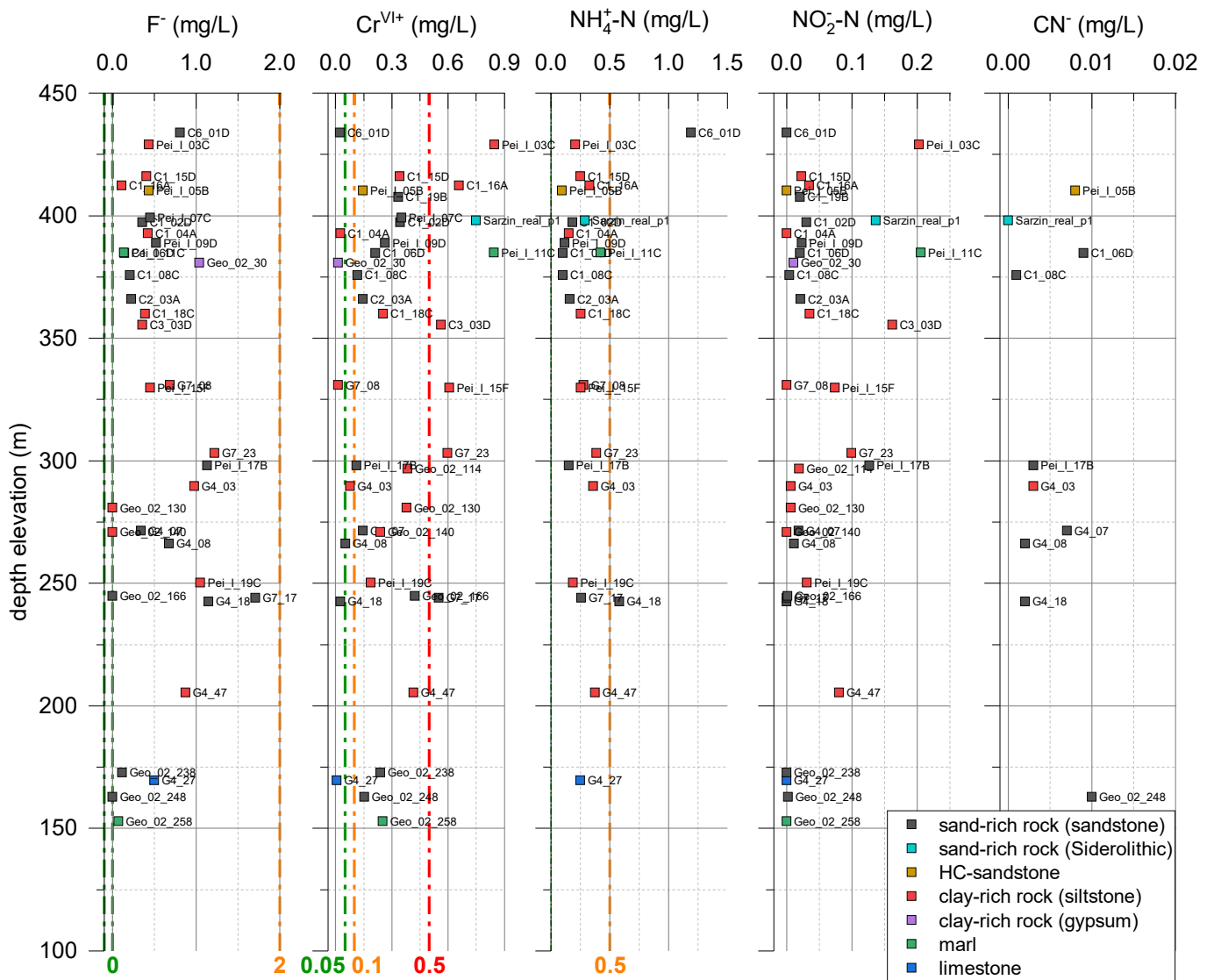


Fig. 6.9: Ion analyses based on cuvette tests across various boreholes, depicted in the proposed FCC depth range. In liquid form, mg/L is equivalent to mg/kg (ppm).

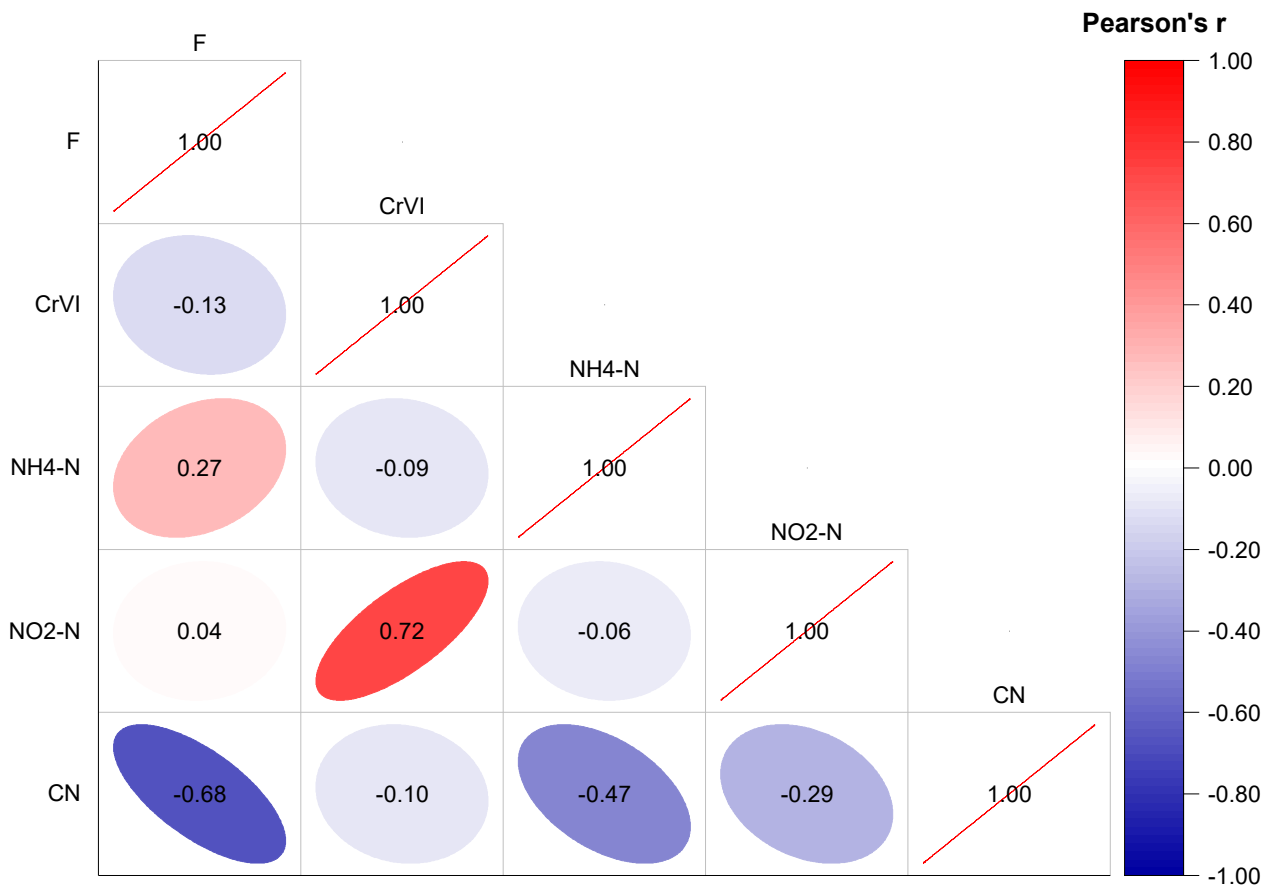


Fig. 6.10: Pairwise cross-correlation of cuvette analyses with respective dependencies for F, Cr-VI, NH4-N, NO2-N and CN using Pearson’s correlation coefficient for monotonic, linear relationships, and a significance level of 0.95.

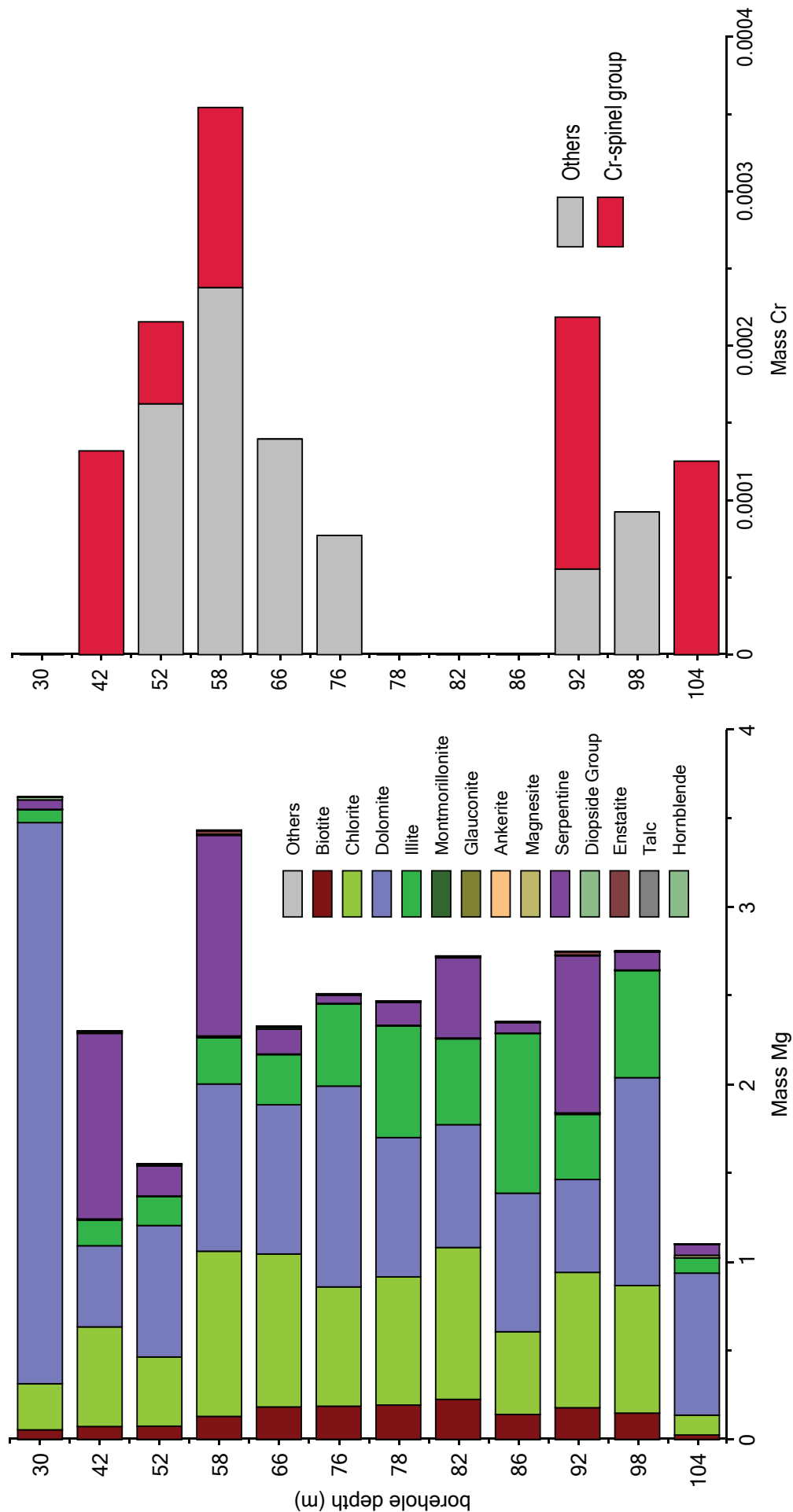


Fig. 6.11: Elemental department from QEMSCAN measurements for Mg and Cr exemplified by well Geo-02. Mass units in %.

(Ca-montmorillonite). The alkali oxides act as fluxing agents during brick firing and lead to a decrease of melting points. The Fe_2O_3 content is a decisive parameter for the degree of (red) colouration. K_2O and Na_2O are mainly found in feldspars (potassium feldspar, albite), in mica minerals (illite, sericite, muscovite) and, to a lesser extent, in smectites (montmorillonite). Elements such as F, Cl and S must be determined using for instance cuvette tests as described below. SiO_2 content should be clearly distinguished among all silicate components including quartz, clay minerals or feldspars, and does not individually represent a specific parameter for the identification of application scenarios (excluding glass production) or raw material control. Al_2O_3 and TiO_2 are attributed to clay. Feldspars (among other minerals) represent the Al_2O_3 content and values are limited up to 40% for the firing process and not encountered in any of the geological formations herein. CaO and MgO contents act as fluxes and react with silicates of the raw material during firing. CaO and MgO predominantly refer to carbonates but also to the plagioclase, smectites (Ca-montmorillonite) and chlorite. Trace elements, F, Cl, S and V are of particular importance because both the kiln atmosphere (environmental conditions) and the brick products (efflorescence) are strongly affected.

Fig. 6.12 depicts a longitudinal cross-section along the current FCC perimeter and predicts respective disposal scenarios based on the available data. Swiss thresholds and limits are taken into account for evaluating respective scenarios because they depict the lower thresholds when compared with France (see chapter 2). Results depict the occurrence of low- to highly-polluted rock in the main geological formation of the FCC depicted by the Molasse Rouge. Raw materials are predominantly falling into Swiss disposal classes A, B, E. Their French equivalents are disposal classes ISDN and ISDNI.

Based on the previous findings, it is suggested to adapt to the following rock-type classes with respect to application and disposal scenarios:

1. gravel (conglomerate): loose, fairly unconsolidated rock material that contains a grain size mixture between medium sand and clay (no direct application),
2. unpolluted sand-rich rock (future detailed investigations on concrete/cement applicability),
3. unpolluted clay-rich rock (brick and tile production),
4. unpolluted limestone (future detailed investigations on concrete/cement applicability),
5. polluted rock depicting any rock from 1-4 (no direct beneficial use; requires purification or disposal according to Swiss and French national disposal classes based on grades of hydrocarbon pollution or chemical pollutants) and

6.8 Analytical limitations and recommendations for minimum sets of analyses

Initial geological and geotechnical site investigations for subsurface projects are usually conducted 5 to 10 years in advance and preceded by selected field and laboratory analyses to investigate the underlying geology. Laboratory analyses build the foundation to derive a rock characterisation, which will be up-scaled for potential usage during tunnel construction (Skuk & Schierl 2017). Rock material tests can easily last for several months (Galler et al. 2012) and the development of new concepts can take up to 10 years (DRAGON 2014; Erben & Galler 2014; Resch et al. 2009; Vollprecht et al. 2019). While these results have served as bases for geotechnical design calculations for past European tunnelling projects, the question remains on how to predict the encountered geology efficiently and successfully. Within the context of this study, focus is spent on the prediction of beneficial uses based on an aforementioned understanding of the depositional environment as well as on cross-correlations among mineralogical, geochemical, petrophysical and rock mechanics laboratory data. The hope is that this study will lead to future standard procedures to evaluate excavated rock and soil for beneficial uses.

Suggestions for a minimum set of field and laboratory analyses are targeted herein. The predicted beneficial uses of the materials are based on a rock mass classification anchored in a comprehensive set of field and laboratory analyses across various geoscientific disciplines. The data set includes mechanical strength and petrophysical properties, elemental, mineral and leachate concentrations, as well as physico-chemical parameters such as water absorption, adsorption, and cation exchange capacity

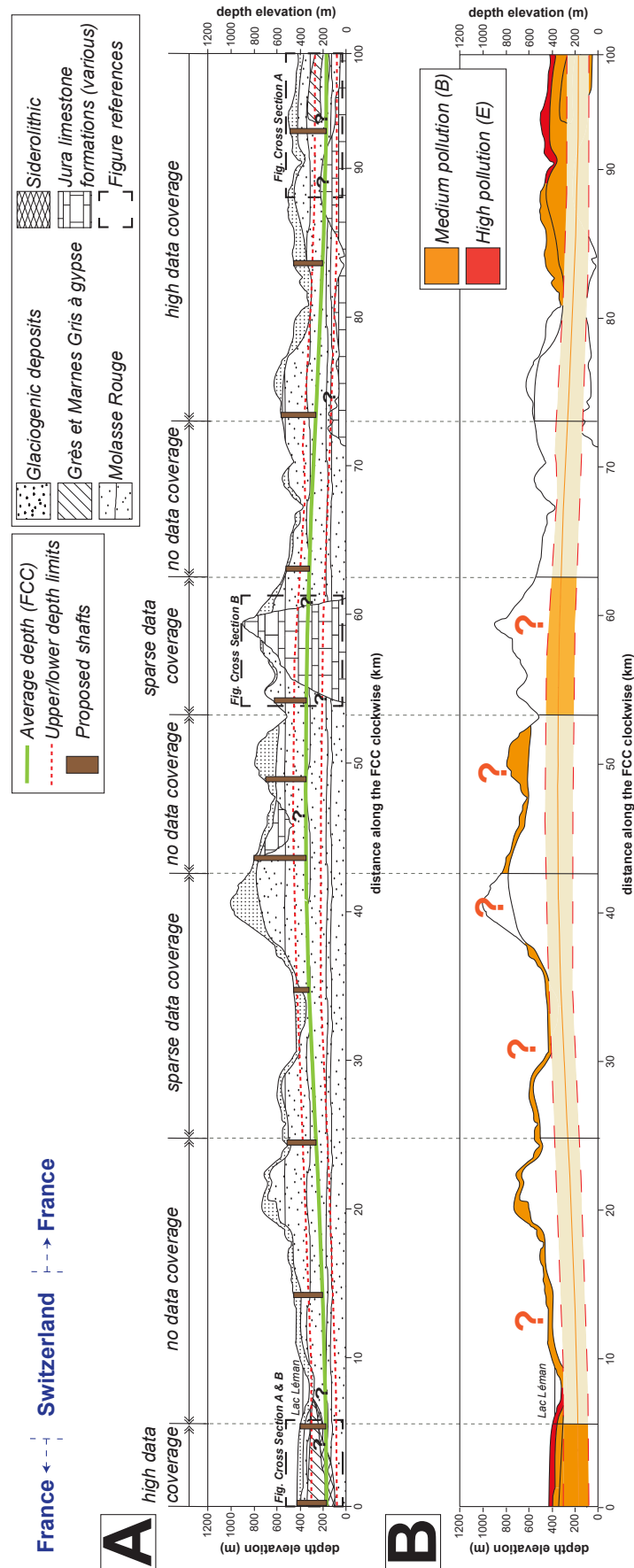


Fig. 6.12: (A) Longitudinal tunnel section along the FCC in clockwise direction based on identified geology, laboratory and field data. (B) Longitudinal tunnel section showing proposed grade of pollution with respect to disposal of the excavated raw material. Extrapolations in areas with no data coverage yield predictions of grades of pollution, also marked as "?". For zoomed-in areas see cross sections A and B in chapter 4. The pollution follows the trend identified in geochemical and cuvette analyses. Faults are excluded for increased readability. FCC layout after (Abada et al. 2019a).

predominantly influenced by natural clay minerals. From these data, correlations and extrapolations to any number of parameters are possible and successful (Adams 2005; Salehin 2017; Yan 2002). The goal is to address a common applicability rock classification scheme (ARCS) that would target the usage of excavated material for international tunnelling projects rather than fitted to individual projects.

Discussion of analytical limitations

Laboratory analyses are crucial for the characterisation of excavated material. Their strength and weaknesses are discussed among mandatory and optional laboratory methods with respect to application scenarios and environmental pollutants.

The cation exchange capacity (CEC) test is a first plausibility test for occurrences of smectite and an indicator of swelling potential caused by freely-dissolved elements in pore water and adsorbed ions in pores. Swelling potential correlates directly with the CEC, that is, the amount of swelling increases with increasing CEC values. The amount of acid affects the CEC. The more acid in leachate solution, the less adsorption (lower CEC) because the cations (e.g. Na, K) are replaced by H^+ of the acid. TOC content determination works for calcite, ankerite, dolomite, aragonite. Aragonite is commonly formed under predicted marine conditions, which allow predictions of higher ankerite values in the suggested marine depositional environment towards the south in the basin. CEC could be further measured according to e.g. French standard NF X31-130. For the Cu-trien copper complex measurement, it is recommended to determine the extinction at a wavelength of 577 nm, as this is the copper triethylenetetramine complex' adsorption maximum in order to achieve a maximum accuracy. Meier & Kahr (1999) potentially confused the adsorption maximum of $[Cu(\text{trien})]^{2+}$ with the methylene blue at 620 nm (Ammann 2003). The CEC value can well replace the MBV value on a 1:1 basis.

Scanning electron microscope analyses (SEM) should be used to resolve clays and their crystal structure. Semi-quantitative analysis in QEMSCAN is possible but it shows only a statistical distribution (for elemental mapping function) rather than real quantitative values. A back-scattered image in QEMSCAN is possible but not

optimal. In QEMSCAN only resolution up to 10 micrometer occur for the sacrifice of analysing heavier elements. The QEMSCAN's main limitations include to distinguish between phases of similar chemical composition, to differentiate lithic fragments and to identify diagenetic overgrowths and small-scale interstratified clays. Identification of minerals is increased when analysing the thin sections under the optical polarizing microscopy. These limitations lead to unclassified minerals of up to 17% (Haas, De Haller, Moscariello, et al. 2020)). Detection of these unclassified minerals relies on the database and cannot be fully avoided due to physical mixtures of clay minerals and overlaps of grains (especially at the boundary). Most of these unknowns are associated with the boundary of serpentine with other minerals. In QEMSCAN, the grain density of each mineral is actually the grain density of the whole sample but the algorithm identifies each chemical composition, defines the mineral, associates the grain density of that mineral, and calculates the average of all encountered minerals in a sample. An advantage of QEMSCAN is also the direct derivation of two types of densities: (1) the grain density and (2) the bulk density does, whereas only the former includes porosity. Similar to portable XRF, Ni is not measured in QEMSCAN elemental mapping because analyses here they were measured with 15 kV when Ni would require a voltage of 25 kV. This limitation is accepted for the sake of increased resolution for the fine-grained particles (clay minerals). It is based on the lower radius of ca. 3 μm of the excited sphere by the beam using 15 keV instead of 25 keV. A voltage of 25 kV is commonly chosen for heavy elements such as Ni or Cr, which increases the sampled area by sacrificing the degree of resolution. Usually, a sample size of 2-3 μm is used for 15 kV, and 4-5 μm at 25 kV. Hence, it is a trade-off between identifying fine-grained (clay) material and heavy-metals.

FTIR shows the identification of kaolinite, type of bounded cations (Al, Mg or Fe; also in carbonates with Li^+ , K^+ and Na^+), and for the identification of tri- or dioctahedral clay minerals (Gordon & Sephton 2016; Josh et al. 2019; Schroeder 2002; Zviagina et al. 2020). FTIR limitations imply the differentiation of elements with a similar amount of electrons due to their activation energy. FTIR should be considered a qualitative, complementary measure particularly related to anion detection (e.g. SO_3 , OH^- , SO_4^{2-} , H_2O).

XRD allows a reasonable representativity of bulk rock samples. This is unlikely the case for QEMSCAN because grains for subsequent thin section preparation might be biased and need to be carefully selected to capture the rock's main geochemical and mineralogical components. Here, FTIR offers to complementarily verify the results given by the former two methods but should not be used as a single mineralogical analysis. The quantification of carbonate content is feasible via both XRD and QEMSCAN measurements. During XRD, calcite, dolomite/ankerite and siderite are analysed, while for QEMSCAN it is calcite, dolomite, ankerite, siderite and magnesite. The difference is that magnesite is measured in QEMSCAN. Ankerite and dolomite are distinguishable in QEMSCAN. Hydrotalcite is not identified with QEMSCAN analysis. For XRD, everything below 5% is not detected. The sum of unclassified minerals and clay minerals in QEMSCAN analyses compared with clay minerals in XRD analyses show similar results but still contain up to 10% of difference and yet the unclassified mineral portion (Fig. 6.6). Si:Al ratio and geochemical analysis using QEMSCAN should not be used to identify clay minerals, since they provide only qualitative measures (Fig. 5.20, 5.21, 5.24, 5.25). Some clay minerals show quite similar chemical composition, and their quantitative identification is best achieved by preparing textured samples succeeded by proper treatment in ethylene glycol atmosphere for XRD analysis (Fig. 5.8). This problem arises if the clay mineral is not of pure quality. Even minor interstratifications alter the result, and, for instance, QEMSCAN breaks down for the identification of interstratified clay minerals. Thus, it is recommended to use XRD for identification of clay minerals and then add the QEMSCAN analysis as supporting evidences.

Experimental methods for the chemical composition suggest ICP-MS/OES for laboratory analyses, and portable XRF (pXRF) for analyses on-site. The pXRF device allows for a cost-effective field measurement that yields both qualification and quantification of the most important major and minor elements. Consecutive calculation and plotting in an Augustinik diagram elucidates on the specific applications (Fig. 6.1). Portable XRF allows estimates of major elements but fails for alkali metals. ICP is well suited for the latter and, in addition, also measures trace elements. Portable XRF well predicts potential application scenarios (Fig. 6.13).

Portable XRF does overestimate the heavier elements compared to ICP. This could be explained by the fact that elements are dissolved in acid for ICP measurements, while pXRF measures the surface of a rock specimen with no chemical acid treatment. Regardless, the fact of a conservative estimate rather than one that is too low, is generally preferred for further disposal and application scenario planning. pXRF fails for alkali-metal analysis in reliable concentration measurements. The derived 1:1 ratio plots give a calibration of pXRF to ICP, so that not all samples would have to be measured with ICP but pXRF. The pXRF analyses correlate well with ICP analyses. Advantages of pXRF stem from the fact that any kind of sample type (cores, rock chips or rock powder) leads to quick results. Portable XRF devices have been commonly used on mining sites for production and exploration as well as in the construction industry (Hall et al. 2014). Potential deployment at the tunnel face makes it an efficient device for a first estimate of excavated rock material for its elemental composition. The pXRF measurement is mainly affected by erroneous sampling preparation, grain size, nugget effects, surface irregularities, sample thickness, weathering effects and depth of penetrating X-rays. The latter is usually in the range of sub-millimetres and depends on the element's atomic weight. The larger sample quantity, its portable flexibility and the fact that reasonable geochemical results are retrieved in a very cost-efficient manner, could make the pXRF device a preferred (standardised?) method in tunnelling for geochemical analyses prior to the classification of excavated material. Reasonable pXRF results are achieved for heavier elements starting at Mg. Lighter elements such as Na have lower energy levels that prevent them from being absorbed and lack a detectable quantification with enough significance. pXRF good for first estimations but for ppm concentrations ICP is preferred. Na_2O content is missing when based on pXRF analyses in an Augustinik diagram. However, pXRF still yields good predictions for application scenarios because according to ICP analyses the maximum Na value of 3.4% (average value of ca. 1%) does not affect the results tremendously. The pXRF serves as a practical tool for a first, quick and quantitative estimate of beneficial uses and polluted substances on-site. For the analysis of trace elements, ICP needs to be performed.

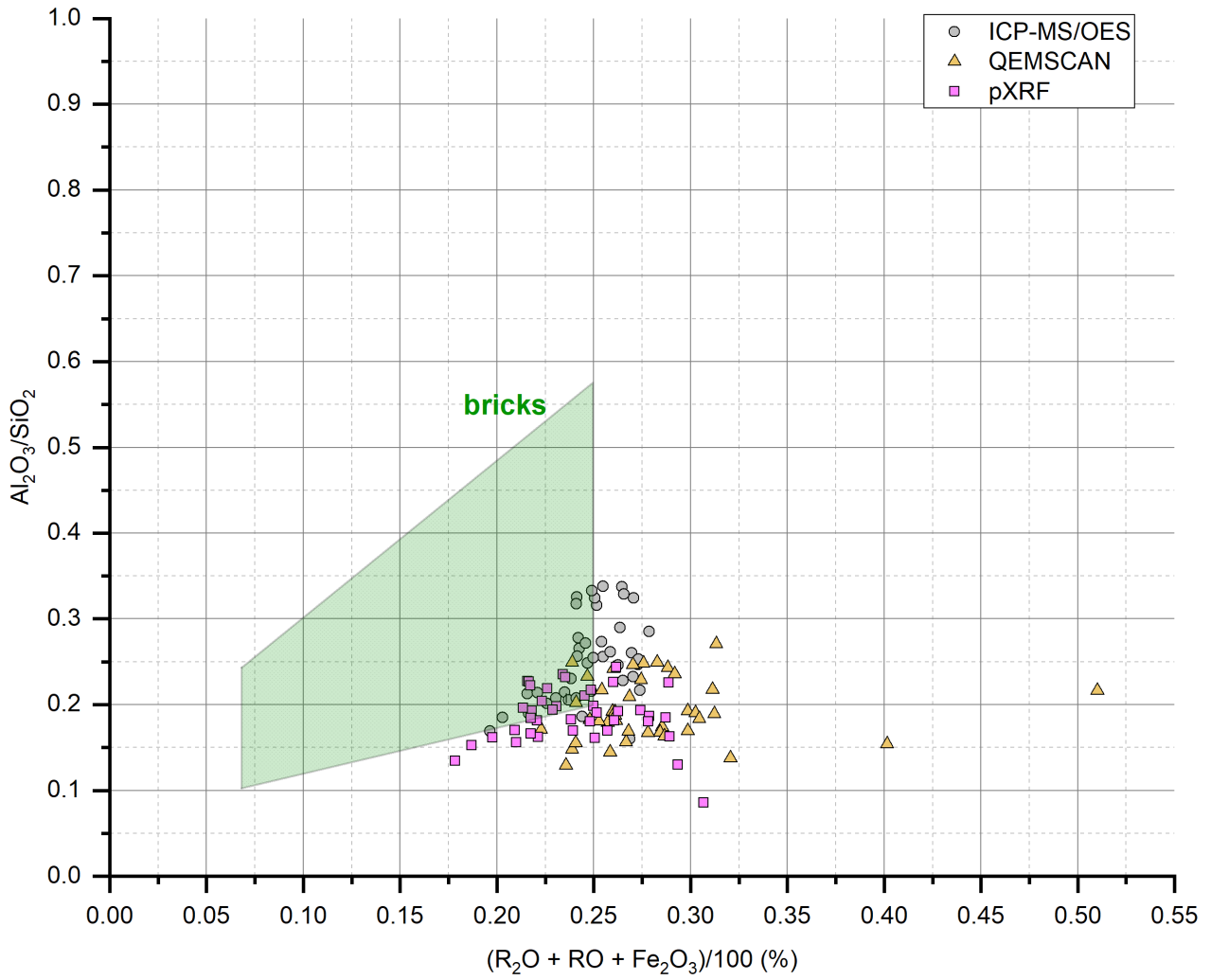


Fig. 6.13: Augustinik diagram comparison of elemental data from QEMSCAN, pXRF and ICP measurements, plotted in application scenarios.

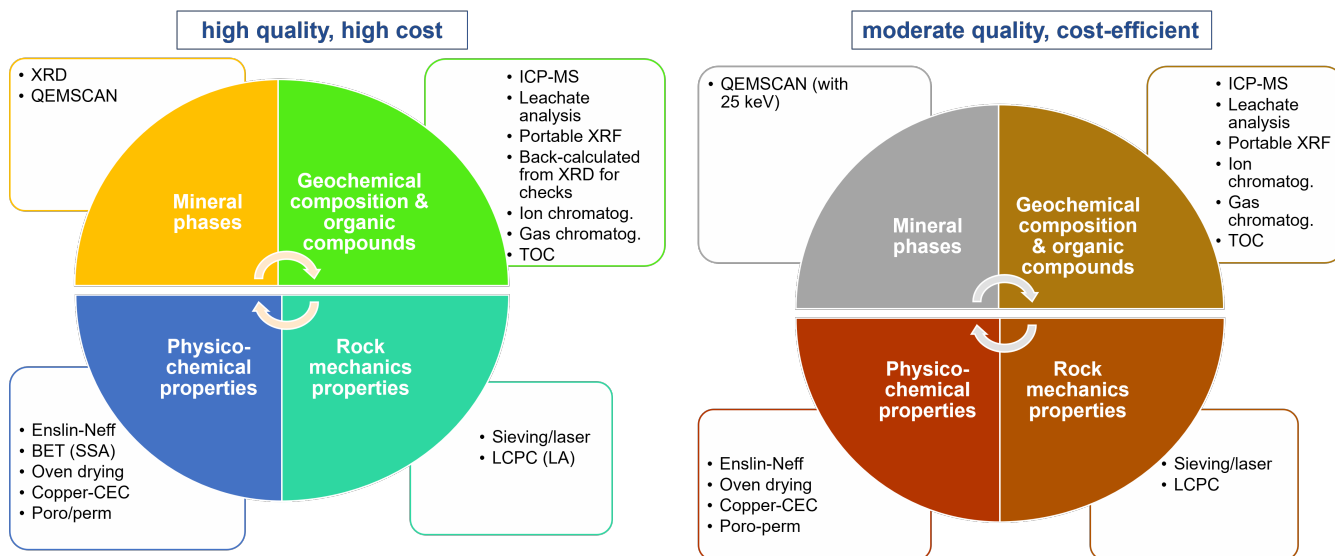


Fig. 6.14: Suggestions of minimum sets of easily-applicable and cost-efficient analyses streams for a successful prediction of application scenarios or disposal.

Minimum sets of analyses

The applicability of excavated rock and soil is dependent on its rock properties, the industrial need for mineral resources in the nearby-area, transport infrastructure for managing the excavated material, CO_2 emissions and economic considerations. The suggestion of a minimum set of analyses considers five important factors: (1) the quality and (2) level of confidence of a measurement, (3) its time duration and (4) practical applicability preferably on-site and (5) its economic efficiency. These terms aim, in particular, also for a simplified identification in the field that make it practical during future excavation to sort the material. As derived in the aforementioned chapters, the potential solution for Molasse Rouge and glaciogenic deposit samples is predominantly brick production (Fig. 6.1).

When considering economic efficiency of measurements, mineralogical laboratory analyses are more expensive compared to geochemical analyses. Depending on the number of analysed elements, geochemical analyses are quite inexpensive. Rock mechanics tests commonly range between the two with a tendency to higher costs for e.g., UCS tests. Lower prices apply for CERCHAR or LCPC tests, which are similar to pXRF or ICP measurements. The pXRF is an ideal field analysis tool, which is cheap and allows for quick and robust results with respect to main pollutants of the Molasse Rouge and glaciogenic deposits as well as quick first-estimates of application scenarios. A comparable tool

for the measurement of $C_5 - C_{10}$ and $C_{10} - C_{40}$ (hydrocarbons) is given by the PetroFLAGTM test as shown in Voiron et al. (2020).

Grain size distributions in the ranges of $<2 \mu\text{m}$, $2-20 \mu\text{m}$ and $>20 \mu\text{m}$ form an integral part of the evaluation of application scenarios based on a various set of possible laboratory analyses. These are commonly retrieved from the following two methods: (1) the sedimentation method and/or laser granulometry for the fine-grained particles in the clay fraction and (2) grain size mesh towers for larger fractions up to the cobble fraction. While the sedimentation methods takes at least 24 h, laser granulometry takes the optical refractive index of the material into account, and is thus quick to perform. A drawback originates from extensive preparation of the sample material using ultrasound to avoid clay amalgamation, which could destroy the layer packets, and hence alter the grain size distribution curve. The sedimentation methods are further divided into the following procedures: sieve analysis for the coarse-grained particles, hydrometer method (DIN 18123), a sedi-graph, sedimentation balance, pipette analysis ($<63 \mu\text{m}$), Atterberg method ($2-63 \mu\text{m}$) and the centrifuge method ($<2 \mu\text{m}$). The sieve analysis, pipette analysis, Atterberg method and centrifuge method offer the advantage to obtain different fractions of the sample and thus yield an effective grain size separation available for further investigations (e.g. mineral phases). This is of high importance for the fine-grained fractions ($<2 \mu\text{m}$). It is crucial to determine the types of minerals occurring in different particle

size fractions, particularly for the clay fraction $<2 \mu\text{m}$, and the proportions among them to evaluate reaction mechanisms during the firing process.

Mercury intrusion porosimetry (MIP) analysis is useful for the detailed study of physico-chemical behaviour of Molasse Rouge samples. It is not deemed necessary for concluding on mutual parameters such as porosity or permeability and is considered a supplementary method.

Various measurements exist to derive the cation exchange capacity. They range from the exchange of inorganic cations by cationic species such as ammonium, K, Na, methylene blue, Co(III) hexamine complex, Ba, Ag thiourea complex, to the Cu(II) ethylenetetramine complex, or organic cations such as alkylammonium (Meier & Kahr 1999; Rémy & Orsini 1976). The highly-anticipated methylene blue test and its associated methylene blue value (MBV) result in a slight overestimation of the CEC (e.g. Kahr, Madsen 1995; Yariv et al. 1990). For the present study this implies a *worst-case* scenario when equating the CEC value from the copper complex measurement and the methylene blue test for the evaluation of application options requiring higher CEC values. CEC measurements are to be used as a plausibility test for occurrences of smectite.

The Enslin-Neff method provides robust results to conclude on the plasticity behaviour of raw material. Its installation on-site is easily-applicable and measurements require only a full day without any extensive laboratory preparations. It is highly suggested to implement these analyses for prediction of application scenarios.

The identified analyses must be cost-efficient and fast for tunnelling advancement in the subsurface. Fig. 6.14 summarises the potential sets of analyses in the following two analyses branches:

1. for rock strength (physico-mechanical properties like porosity, permeability, grain size distribution, rock tests, smectite identification via XRD), followed by
2. 2) geochemical/mineralogical data set (type of clays, its distribution, also grain size distribution for EPB-tunnelling, usage scenarios). For EPB, the clay type and distribution is important, for slurry-machine the grain size distribution is essential.

An on-site expert is suggested for a first evaluation of application scenarios along tunnel advancement, who extracts the macroscopic information on freshly excavated

material. This aligns with on-site tests such as the PetroFLAGTM test or pXRF analyses for hydrocarbon occurrences and chemical pollutants, respectively. These procedures then follow elaborated laboratory analyses. The expert then decides on further transport and processing of the raw material or input for temporary storage. Caution is advised, in general, on the sandier intervals since they are prone to hydrocarbon pollution and chemical pollutants such as increased Cr contents.

The suggested drilling program (well-logging) based on location of well sites and actual geophysical logging methods are GR, RHOB including the photoelectric factor log, DT, ILD and NEUT. Analyses should comprise what is typically called a *core routine analysis* and *core special analysis* as these terms summarise the petrophysical and mineralogical analyses presented herein. These tests are to be linked with the Enslin-Neff, portable pXRF, ICP and PetroFLAGTM analyses as part of future site investigations.

7 Summary

The aim of this study was to characterise the rock units encountered by the future subsurface infrastructure built for the next-generation CERN Future Circular Collider (FCC) particle accelerator within the Geneva Basin to assess potential applications of the excavated materials. The added scientific values comprise the vast amount of data sets and samples across the Geneva Basin, the identification of encountered geological units and the geological hazards by the FCC. Empirical cross-correlations allowed for the prediction of application scenarios and the identification of the quickest, and most time-efficient analyses. In realisation of this study, the legal and technical findings, results, correlations and predictions are summarised:

- European Union initiatives encourage and support using excavated material across Europe. Austria, Switzerland and France are leaders and role models in this effort and provide solid legislation and national guidelines. Italy lacks such support and guidance. Legislation for environmental protection such as land-fill is completely absent in Italy.
- Alpine countries and the EU still consider excavated rock and soil as waste. This view discourages and limits legislation and guidance for using this potentially valuable resource for the benefit of society. Existing Austrian, Swiss and French laws and guidelines could serve as a template for legislation to encourage beneficial uses of excavated material. Limitations for the definition of relevant consumers contain the physical and chemical characterisation of excavated rock and soil as well as their positioning in relation to inert waste thresholds, in particular (geo)-chemical pollutants. An adaption and homogenisation of these thresholds is highly recommended among Alpine countries and could lead to a mutual European legislation by standardising technical measurements and legal approaches.
- A material-flow sequence is suggested to be installed on a tunnel boring machine for on-line analyses, conditioning, separating and transporting excavated material to consumers within a European legal framework. A dedicated European authority should be responsible for managing, monitoring and safeguarding the material.
- Metadata of existing stratigraphic information was reviewed from 661 boreholes, outcrops and excavation sites. These data were from well reports across the Geneva Basin, geophysical well-logs and digitised laboratory analyses. The results of digitised and newly acquired petrophysical, geomechanical, geochemical and mineralogical field and laboratory analyses of in total 2'461 rock samples have been compiled in a database that is accessible using the Microsoft Access database management system.
- The data review revealed a distinct lack of data in the western to south-western subsurface parts of the FCC's proposed subsurface construction area. These areas should be the focus of future site investigations.
- The cross-correlation of more than 70 parameters yielded new (predominantly) linear, empirical, material-property relationships for the glaciogenic deposits, Molasse Rouge and Siderolithic formations.
- The FCC's stratigraphic evaluation revealed 25 lithotypes across 13 geological formations. Intersected with the geographically defined Geneva Basin, the FCC intersects in reverse chronostratigraphic order (top-to-bottom):
 - Holocene topsoil,
 - Quaternary post-glacial deposits and Last Glacial Maximum (LGM) moraines, inter-gacial and pre-glacial sediments,
 - Oligocene Molasse Rouge and Grés et Marnes Gris à gypse (LFM),
 - Eocene Siderolithic Formation and the Eocene(?) Transition zone (Perte-du-Rhône Formation?)

marking the Cenozoic-Mesozoic stratigraphic boundary(?), followed by

- the Jura units represented by the Cretaceous Vallorbe Formation, the Hauterive and Neuchâtel Members of the Grand Essert Formation and the Gorges de l'Orbe Formation (former Urgonien, Early Cretaceous) as well as the Vuache, Chambotte, Vions, Pierre-Châtel and Goldberg formations, with
 - the Twannbach, Etiollets and currently debated Balsthal and Vellerat formations completing the Jurassic units of the Jura.
- Potential geological hazards for tunnelling feature karstic intervals, fractured limestones, clayey sandstones, hydrocarbon zones and swelling clays. Karstic intervals are hazards to increased water ingress during tunnelling excavation and occur in fractured limestones of the Grand Essert Formation's Neuchâtel Member, Roches des Hirondelles Vallorbe Member and Vuache Formation. In addition, karstic intervals are associated with the sandstone-bearing Transition zone and Siderolithic Formation. Swelling potential is a hazard to tunnelling construction because of the volume increase of rock leading to e.g., stuck tunnel boring machine (TBM). Swelling is associated with up to 17.2% of smectite and anhydrite and occurs in Molasse Rouge and Grès et Marnes Gris à gypse formations. The Grès et Marnes Gris à gypse formation with highest amounts of anhydrite/gypsum are absent in the north-western part of the basin, and occur only locally at e.g., geothermal wells Geo-02 and Thônex-1.
 - Hydrocarbons and chemical pollutants (e.g., Ni, Cr) are environmental hazards to the direct usage of excavated material and require purification. Hydrocarbons occur in both gaseous and bituminous forms across all wells in the Molasse Rouge and Mesozoic fractured limestones. Within the Molasse Rouge, hydrocarbons are associated with the upper sandstone succession. Hydrocarbon-polluted sandstones show porosity values of 16 to 22% at strongly varying permeability values of ca. 46 mD to ca. 370 mD (both in well Peissy-I), and up to 1087 mD (Gex-CD-04) depending on type and grade of cementation. Ni and Cr pollution is not encountered in the limestone lithotype but restricted to predominantly the sand-rich and sandier, clay-rich rock types.
 - The calculated sand-silt-clay model is based on available well-logs and calibrated petrophysical and geochemical laboratory data from well Geo-01. It estimates volumes of sand, silt, (dry) clay, clay-bound water and formation water showing predominantly silt across the full borehole interval and a sand-rich trend from 350 to 230 m ASL, which changes to a trend in increased amounts of (dry) clay in the lower 200 to 100 m ASL. The results allowed for conclusions on clay types, for predominantly dispersed and structural clay in the Molasse Rouge formation. The data indicate high amounts of clay-bound water at depth intervals from 130 to 140 m ASL and 150 to 200 m ASL, associated with moderate amounts of sand. Clay-bound water decreases upwards towards surface topography level. Water content (formation water) remains constant from 375 to 80 m ASL but shows increased values between 70 and 20 m ASL, together with higher sand and reduced silt and clay content.
 - The Molasse Rouge tends to contain both dispersed and structural shale. A few samples show clean (sand-rich) zones, which are mostly related to non-cemented, porous sandstones.
 - The Molasse Rouge formation shows a heterogeneous matrix density distribution between 2.55 and 3.13 g/cm^3 and volumetric photoelectric factors (PEFs) of 4 up to 16 b/cm^3 . Muscovite occurs in log lithotypes. Mineral variations agree qualitatively well with QEM-SCAN and XRD mineralogical analyses. Calcareous intervals predominantly contain dolomite and calcite, which show up in the PEF log.
 - The glaciogenic deposits contain similar mineralogy to the Molasse Rouge, with less variability in matrix density ranging up to 2.95 g/cm^3 and less abundance in muscovite. Overlaps of neutron and density logs underline the impermeable Molasse Rouge formation. These low-permeability intervals contain high amounts of silt.
 - The photoelectric factor (PEF) log allows a first, qualitative characterisation of lithotypes together with gamma ray, neutron, density and sonic logs. Gamma

ray logs alone are not sufficient and hamper the identification of the shale-/sand-dominated Molasse Rouge without amended mineralogical analyses. Neutron and density logs allow the differentiation among permeable (glaciogenic deposits) and impermeable formations (anhydrite-rich Grès et Marnes Gris à gypse; clay-rich Molasse Rouge).

- The PEF log is the optimum tool for an initial rock-type determination. Nevertheless, laboratory analyses were required to discriminate between the Molasse Rouge and the Grès et Marnes Gris à gypse formations. The significant difference among these two formations is the higher gypsum/anhydrite content in the Grès et Marnes Gris à gypse formation. The Mesozoic clayey limestone shows lesser content in clay minerals. The GR log alone is not sufficient to properly distinguish between sand- and shale-dominated intervals because of the heterogeneity of the Molasse Rouge formation.
- Based on analytical field and laboratory analyses, the Molasse Rouge is a heterogeneous formation whose rocks are characterised on a micro-scale into nine (9) lithotypes based on their grain size distribution, texture, mineralogy, physico-chemical, petrophysical and geomechanical rock behaviour: three sand-rich (sandstone), three clay-rich (siltstone), a marl, a conglomerate and a gravel lithotypes.
 - Quartz-feldspathic, sand-rich rocks (sandstone) are often micaceous, and cemented by either calcite or clay minerals (predominantly illite, rarely chlorite) precipitation. These sand-rich rock samples are characterised into fine-grained, medium-grained and coarse-grained textures, based on their pore-size distribution and on image analyses of their quartz grain-size distributions. These sand-rich rocks appear blue-greyish to (green)-grey in color in the field and possess mineral fractions of quartz (40-70%), feldspar (5-10%), calcite (20-45%) and clay minerals/mica (5-20%). The coarse-grained sandstones contain hydrocarbons and the highest contents of serpentine and have variable porosity of 16-22% and varying permeability of 46 mD to 370 mD up to 1087 mD depending on cementation and texture. The Siderolithic sandstones typically contain ca. 72% quartz and 28% kaolinite. When the quartz content ranges at ca. 22%, the Siderolithic sandstones, the mica, chlorite, smectite and traces of dolomite replace the kaolinite.
- Clay-rich rocks, i.e. (violet) marl, are typically laminated or plated. The (beige) siltstones contain micro-crystalline quartz (15-30%), feldspar (0-5%), calcite (20-30%) and clay minerals including mica (45-60%). The clay fraction is further subdivided into illite/mica (20-35%), chlorite (15-18%), and swelling montmorillonitic clay (10-18%). Clay-rich rocks have low porosity and permeability values of 1-15% and below 1 mD, respectively. As a result, their flow zone indicator (FZI) slope values are below 0.01, probably because of their high grade of cementation by illite or calcite.
- Sandy marl is the transition, or intermediate, facies between sandstone and marl. Its mineralogy includes quartz (20-40%), feldspar (5%), calcite (20-30%) and clay minerals/mica (20-45%). Its clay fraction includes illite including mica (12-18%), chlorite (10-14%) and montmorillonitic clay (8-13%).
- Rock mechanics tests based on uniaxial compressive strength values predominantly range from 3-41 MPa across all clay-rich, marl and sand-rich samples with the highest, extreme values occurring in the coarse-grained, sand-rich rocks up to ca. 85 MPa. The weak and medium-strong sandstones are associated to sand-rich, porous and medium- to coarse-grained rocks. The strong sandstone are fine-grained, sand-rich rock that is cemented by either calcite or clay minerals. It was difficult to find strong correlations between the geomechanical and petrophysical properties (e.g. UCS versus porosity, V_P , V_S). These weak linear trends are attributed to the high heterogeneity of the Molasse Rouge formation. Initial descriptions by Fern et al. (2018) are contemplated herein by various analyses amongst mineralogical analyses for tunnelling and beneficial uses and show (Table 5.1):
 - Weak, medium-strong and strong sandstone with ca. 40-70% quartz, 5-20% total clay, 5-45% calcareous minerals, 5-10% feldspar

- Medium-weak marl with 20-40% quartz, 45-60% total clay, calcareous minerals 20-30%
- Weak marl with 15-30% quartz, 45-60% total clay, and calcareous minerals of 20-30%.
- The coarse-grained, sand-rich rocks are associated with bituminous hydrocarbons, the highest contents of serpentinite, as well as Cr_{total} and Ni pollution of up to 380 ppm and 130 ppm, respectively. Hydrocarbon-polluted sandstone shows porosity values of 16 to 22% at strongly varying permeability values of ca. 46 mD to 370 mD, and up to 1087 mD, depending on type and grade of cementation. Leachate results show clay-rich samples being highly polluted by Cr^{-VI} with values up to 0.9 mg/L in the Molasse Rouge formation. The Siderolithic sandstone is another highly-polluted rock type but part of the underlying Siderolithic formation. These results would allow no direct application of the coarse-grained sand-rich rock but force purification or hazardous disposal. Clay-rich rocks, i.e. (violet) marl, commonly laminated or plated and then hereby classified as beige siltstone, yield average values of micro-crystalline quartz (15-30 wt.%), feldspar (0-5 wt.%), calcite (20-30 wt.%), phyllosilicates (45-60 wt.%). Further analyses as part of the phyllosilicates yield illite and mica (20-35 wt.%), chlorite (15-18 wt.%), and swelling clay of Ca-montmorillonite type (10-17 wt.%). Results of clay-rich rocks (siltstone) yield two different cementation processes implying either calcite or clay minerals (predominantly illite, rarely chlorite) precipitation in the pore space. Clay-rich rocks including the beige siltstone show low porosity and permeability values of 1 to 15% and below 1 mD, respectively, resulting in calculated flow zone indicator (FZI) slopes below 0.01 due to their high grade of cementation by illite or calcite. Sandy marl, classified as the transition (intermediate facies) between sandstone and marl yield average values of quartz (20-40 wt.%), feldspar (5 wt.%), calcite (20-30 wt.%) and phyllosilicates (20-45 wt.%). Clay mineral analyses yield illite including mica (12-18 wt.%), chlorite (10-14 wt.%), and swelling clay of Ca-montmorillonite type (8-13 wt.%).
- Quartz-feldspathic sand-rich rock (sandstone), often micaceous and either cemented by calcite or clay minerals (e.g. illite or chlorite) are categorized into three classes depicting fine-grained, medium-grained and coarse-grained textures, based on their investigated pore size and quartz grain-size distributions. These sand-rich rocks appear blue-greyish to (green)-grey in color in the field, and yield average values of quartz (40-70%), feldspar (5-10%), calcite (20-45%) and clay minerals/mica (5-20%). The coarse-grained sandstone is subject to hydrocarbon pollution and highest contents of serpentinite. The Siderolithic sandstone depicts values of ca. 72% quartz, with the remaining percentage consisting of kaolinite. When quartz content ranges at lower values of ca. 22%, the Siderolithic sandstone then allocates its high kaolinite value to mica, chlorite, smectite and traces of dolomite. Clay-rich rocks, i.e. (violet) marl, commonly laminated or plated and then depicted as (beige) siltstone, yield average values of micro-crystalline (Fig. 5.11) quartz (15-30%), feldspar (0-5%), calcite (20-30%) and clay minerals including mica (45-60%). The clay fraction is further subdivided into illite/mica (20-35%), chlorite (15-18%), and swelling clay of montmorillonite type (10-18%). Sandier marl, classified as the transition (intermediate facies?) between sandstone and marl yield average values of quartz (20-40%), feldspar (5%), calcite (20-30%) and clay minerals/mica (20-45%). Further subdivision of the clay mineral analyses yield illite including mica (12-18%), chlorite (10-14%), and again swelling clay of montmorillonite type (8-13%). An extensive discussion on the predictability of application scenarios is stated in chapter 6.
- Analyses to characterise the rock and predict beneficial uses or disposal are the portable XRF analysis and the Enslin-Neff water-absorption method to be applied on-line or on-site. XRD and QEMSCAN are reliable analyses for the quantitative determination of mineral composition for the identification of application scenarios. In addition, FTIR and optical microscopy offer a qualitative mineral identification, and QEMSCAN image analyses allow for the investigation of rock texture, together with grain size distributions of quartz. The combination of XRD and FTIR enables to identify the modal composition of the sedimentary raw material with sufficient accuracy and allows for

their respective correlations with respect to the chemical composition, alteration paths, and encountered mineral phases. Brick production requires natural raw materials that contain clay minerals, which are identifiable using the XRD, QEMSCAN, pXRF and ICP methods. However, FTIR should be considered as a complementary method but mounted on a conveyor belt and using near-IR it could also serve as a solid method for a quick and cost-efficient identification of minerals. Portable XRF measurements allow for an easy and cost-efficient detection of elemental composition of rocks and soils in the field. The PetroFLAG test is a reliable field analysis, too. The test follows similar sample handling and field measurement techniques as do the performed cuvette tests.

- The model approach after Dieng (2005) using the input data from Enslin-Neff water-absorption analyses enables precise predictions of the Atterberg liquid and plastic limits as well as other essential plasticity indices for evaluating uses for excavated material. The Enslin-Neff measurement could replace the Casagrande methods for determining the liquid and plastic limits of soil Casagrande (1932). Hence, Enslin-Neff analyses (modelled after Dieng (2005)) are recommended; cuvette tests and PetroFLAG tests should be integrated in a systematic sampling program as part of future tunnelling sites including the FCC site. These tests require similar sample amounts, are easy to conduct, cost effective and time efficient.
- First on-site investigations are suggested to be conducted by a geologist. GR, SP and DT logs, water adsorption, specific surface area and exchangeable ion analyses, UCS, Point Load, CERCHAR, LCPC and Brazilian tensile tests are linked with the previously mentioned ones in the following.
- The RQD values of sand-rich rocks suggest a poorly fractured rock mass and the conditions of the joints assumed to be fair, rarely good. The RQD of violet marl samples suggests a fractured rock mass and the conditions of the joints are poor (slickensided) as encountered with in some violet marl layers.
- The vast amount of more than 400 samples from the Molasse Rouge formation falls outside any direct application window. Based on samples falling into the direct application of bricks production, hydrocarbon-bearing sand-rich samples are not directly usable. These sand-rich, coarse-grained rocks are predominantly associated with bituminous hydrocarbon or coal as well as Cr and Ni pollution. In some samples they contain high grades of Cr-VI pollution with up to ca. 0.9 mg/L, allowing no direct application but forcing purification or disposal, falling within the most hazardous disposal class for both France and Switzerland.
- Modelled liquid limits and plasticity indices based on Enslin-Neff analyses yield robust results supporting the applicability window of bricks production, and could replace the liquid limit tests after Casagrande on future tunnelling sites for the evaluation of application scenarios. Suggested applications for the encountered sedimentary raw material from the Molasse Rouge and, to a certain extent, from the glaciogenic deposits formations are the production of brick and, with some limitations, for tile production. Dedicated future research is recommended for raw material conditioned with additives on the agricultural usage and cement mixtures.
- All samples from the glaciogenic deposits, the Molasse Rouge, the Grès et Marnes Gris à gypse and Siderolithic formations show values $\leq 1\%$ of total organic carbon content.
- A major environmental issue for the direct application of the FCC's excavated materials originates from hydrocarbon occurrences in both gaseous and bituminous form and are predominantly associated with the Molasse Rouge and limestone fractured Mesozoic formations encountered across more than two thirds of the 661 investigated wells.
- Remaining Molasse Rouge samples comprising clay-rich (siltstone) and violet marl rocks suitable for direct application are associated with bricks production. These samples commonly range at a depth of 200+ m measured from topographic surface. However, tile production is negligible and was only identified in two samples. The topsoil and Siderolithic formations indicate no direct application possibilities, similar to the Cretaceous formations, which only yield one sample suitable for bricks production.

- For the prediction of direct beneficial application uses, empirical correlations are established for the first time for the glaciogenic deposits and the Molasse Rouge formations as part of the Geneva Basin for all measured rock properties. Clay-rich (siltstone) and marl rock samples are suitable for direct application as bricks production. Tile production as another potential application is negligible and has been identified only in two clay-rich rock samples. The topsoil and Siderolithic formations indicate no direct application windows, similar to the Cretaceous formations that yield only one sample suitable for bricks production. However, the majority of the Molasse Rouge samples fall outside any direct application window. Some of the glaciogenic deposits samples fall into the direct application of the brick production window. Suggested applications for the FCC's sedimentary raw material from the Molasse Rouge and, to a certain extent, from the glaciogenic deposits formations are the production of brick and, with some limitations, tile production. Future research is recommended for raw material conditioned with additives on the agricultural usage and cement mixtures.
- It is suggested that the on-site geologist should first extract the macroscopic information on freshly excavated material. This geologist inspects the material for visual pollution (e.g. hydrocarbons), then performs PetroFlag tests on it, and decides on which (temporary) storage the excavated material should be stored before detailed laboratory results decide on any further application scenarios, purification or disposal. Simultaneously, the geologist performs pXRF tests (at least three times) on the material to check for elemental composition and major chemical pollutants.

The findings stipulate a robust predictive approach for large-scale subsurface construction and lithotyping, aimed at establishing a knowledge base for potential application scenarios of excavated material and engineering rock classifications. This makes the FCC not only a European exhibit in terms of dimensional extent but also a worldwide feasibility study, paving the way to predictive rock classification schemes for potential applicability scenarios.

8 Conclusions

The European Organization for Nuclear Research (CERN) initiated the Future Circular Collider (FCC) feasibility study in 2013 to evaluate the construction of tunnels to host a next-generation particle accelerator. The tunnel facility will comprise 90-100 km in circumference in the Geneva Basin located in eastern France and western Switzerland. This thesis reports subsurface conditions expected during tunnel excavation and predicts potential beneficial uses for the excavated rock and soil, which implies a status of waste according to national and European legislation. A multidisciplinary rock classification has been developed to correlate field and laboratory analyses. These include petrophysical (well-logs), geomechanical, mineralogical and geochemical parameters from available rock sample material to predict on potential application scenarios.

A detailed stratigraphic evaluation of the shallow subsurface across the Geneva Basin is based on a review of existing well report and geophysical well-log data from former research and industrial activities preceded by their digitization and analysis as well as sedimentological and petrographical descriptions of lithotypes from sampled rock material. The FCC's stratigraphic evaluation revealed 25 lithotypes across 13 geological formations. Intersected with the geographically defined Geneva Basin, the FCC intersects in reverse chronostratigraphic order (top-to-bottom) of Holocene topsoil, Quaternary post-glacial deposits and Last Glacial Maximum (LGM) moraines, inter-glacial and pre-glacial sediments, which overlie the Oligocene Molasse Rouge and Grès et Marnes Gris à gypse (LFM) followed by the Eocene Siderolithic Formation. The Transition zone (Perte-du-Rhône Formation?) marks Cenozoic-Mesozoic stratigraphic boundary, before encountering the Jura units represented by the Cretaceous Vallorbe Formation, the Hauterive and Neuchâtel Members of the Grand Essert Formation and the Gorges de l'Orbe Formation (former Urgonien, Early Cretaceous) as well as the Vuache, Chambotte, Vions, Pierre-Châtel and Goldberg formations.

Geological hazards feature karstic intervals, fractured limestones, clayey sandstones, hydrocarbon zones and swelling

clays. Karstic intervals are hazards because of increased water ingress during tunnelling excavation and occur in fractured limestones of the Grand Essert Formation's Neuchâtel Member, Roches des Hirondelles Vallorbe Member and Vuache Formation. Karstic intervals may be associated with the sandstone-bearing Transition zone and Siderolithic Formation.

Swelling potential is a hazard to tunnelling construction because of the volume increase of rock leading to e.g., stuck tunnel boring machine (TBM). The geological hazard of swelling is associated with up to 17.2% of smectite and anhydrite and occurs in the Molasse Rouge and Grès et Marnes Gris à gypse formations. The Grès et Marnes Gris à gypse formation with highest amounts of anhydrite/gypsum are absent in the north-western part of the basin.

In total, 91 parameters are found relevant for the prediction of application scenarios. These properties include mineralogical and elemental compositions, grain size distribution and plasticity behaviour. Augustinik diagrams predict tiles and bricks productions for the encountered clay-rich rock of the glaciogenic deposits and Molasse Rouge formations. The Molasse Rouge Freshwater limestone does not fall in any direct application windows. No direct beneficial use are predicted for rock material that contains hydrocarbons or chemical (heavy metal) pollutants. Hydrocarbon and Ni/Cr polluted raw material is predominantly associated with sand-rich, medium- to coarse-grained rock. Experimental analyses for the prediction of application scenarios suggest XRD, ICP-MS/OES for laboratory analyses, and portable XRF for a first on-site prediction. The pXRF device allows for a robust and cost-effective field measurement, which yields qualification and quantification of the essential elements and pollutants. Enslin-Neff measurements support the rock characterisation and allow for plasticity behaviour predictions relevant for bricks and tiles productions.

The present study marks a crucial step towards increased beneficial use cases of both international and national tunnelling projects in similar geological conditions.

9 Outlook

The present study provides a solid basis for future research. It entailed the analysis of hundreds of wells, digitised geophysical well-logs and 2'461 rock samples. It amounted to more than 100 km of cumulative length from 47 well locations and a vast set of geoscientific analyses from across the Geneva Basin. The following paragraphs provide future directions for the extensive data sets acquired during this study. Every new sample provides an opportunity to improve on the knowledge acquired to date and guides future plans along the next phases of the FCC and its construction.

Geological and tectonic research

To better understand the karstic intervals associated with Mesozoic limestones, the Siderolithic Formation and Transition zone, further geological investigations should be conducted. The Siderolithic Formation and Transition zones are considered karstic infills, whose quartz content originated from Alpine erosion (Haas et al. 2022). Future scientific studies could enlighten on the Transition zone, which is still subject to current research and yet undefined according to official Swiss stratigraphic terminology. The geochemical, mineralogical and descriptive data on outcrops and samples could aim to substantiate ongoing research and potentially link it with the overlying Siderolithic formation. These stratigraphic investigations could be further extended to the base of the Tabalcon subunit, which is encountered in close vicinity to the Salève (Haas et al. 2022). Little knowledge has been gathered on this limestone unit but a detailed analyses of well reports and potentially the digitisation of well tests might lead to a better understanding of the geological history and lateral extension across the Geneva Basin.

The basin's source rock for the generation of hydrocarbons is located at Carboniferous and Triassic depth levels (Fig. 4.1) intersecting the Cretaceous(?) and Oligocene(?) sections, and potentially the Molasse Rouge, and therefore, the FCC tunnel perimeter.

The identification of structural faults and their seismic

activity is of predominant importance for the FCC construction and future physics experiments. This should be further investigated and would impose both geological and environmental hazards for engineering construction based on the fact that besides the challenging fault structure itself for tunnelling. Existing seismic studies could be linked with analysed geophysical well-logs (seismic-to-well-tie), and further integrated with both academic and publicly available data on natural fractures (e.g. GEOMOL project) as well as newly acquired surveys. This would satisfy the identification of yet undefined stratigraphic units as well as the overarching aim of implementing all measured data as part of this study into various models that would combine fault and fracture as well as facies and property modelling incorporating parameters relevant for the FCC site investigations across the whole Geneva Basin. These resulting models of the basin's architecture could lead to hydrocarbon distribution maps, in particular, for the SE region of the Salève and at the Bornes Plateau, which both show missing data as shown in Haas et al. (2022). This would also allow to test the hypothesis of a separated continental/marine environment in combination with aforementioned investigations on the stratigraphy. Furthermore, a petrophysical study on the presented data set could be conducted in greater detail, starting from the evaluation of cementation exponent ("shape factor") in Archie's equation by incorporating HPMI tortuosity (Carniglia 1986), specific surface area, cation exchange capacity, porosity and permeability values in conjunction with (modelled) geophysical well-logs (Salem & Chilingarian 1999; Shahi et al. 2018). Upscaling effects of lab and well-log results should then be considered thoroughly.

Besides using the laboratory results as calibration data for various scientific undertakings, the geochemical analyses could be used to outline a thorough sediment provenance analysis study across the Geneva Basin, linked with the hypothesis of a marine/continental environment. FTIR analyses might impose the derivation of a study on the geological origin of Molasse Rouge sediments. Leachate analyses should be extended by analyses using CO_2 saturated samples. These should simulate leaching behaviour when

in contact with rain water. Tests of asbestos (silicate minerals) should be conducted under a transmission electron microscope, since certain samples require the identification of asbestos type and its effect on applicability and/or disposal of excavated material.

A comparison of laboratory with geophysical well-log data could be conducted. This would strengthen the rock mass classification and mechanical earth model, which are the basis for our predictions of natural-fracture networks, karstic intervals and tunnel-stability problems. Large-scale (3D) modelling, the geophysical well-logs offer an opportunity to model elastic and rock strength properties locally (1D). Rock mechanics tests performed here could be used for calibration. A 1D mechanical earth model (MEM) could be constructed. As more data become available, the 1D MEM could be extended to two and three dimensions for natural-fracture prediction across the basin and wellbore-stability predictions at future drilling sites for upcoming FCC site investigations.

As conducted by a former study (Kaelin et al. 1992), estimated sonic and density logs could be used for the calculation of deposition, uplift and erosion rates in the Swiss Molasse Basin. A similar approach could be performed using the DT and RHOB well-logs digitized and provided herein.

Permeability estimations would be possible from nuclear magnetic resonance (NMR) logs but none are available. However, the modified Kozeny-Carman equation allows to derive permeability from specific surface area, porosity and mercury injection.

At the Geo-01 well, there is a deep aquifer causing artesian flow, which caused water ingress problems during drilling. However, their geological trend is suggested to be studied with more accuracy, since it would allow better prediction of the Grès et Marnes Gris à gypse lateral and vertical distribution, a formation prone to swelling, as well as the distribution of unconsolidated glaciogenic deposits that are captured in between syn- and anticlines and that presently host important groundwater reservoirs.

Further site investigations should aim at these conditions and identifying the spacing of joints during drilling, in order to better characterise the rock mass and depict the GSI, i.e. joint condition and spacing. Since the FCC's current layout runs at several depth intervals through the

Transition zone, geophysical seismic surveys should be conducted targeting these formation as part of future site investigations.

Missing data coverage and additional analyses for tunnelling construction

Based on the thorough evaluation of the current data situation, new data surveys should aim first for regions with missing data as indicated in Haas et al. (2022). This includes, in particular, geophysical measurements such as 2D or 3D seismic surveys and borehole logging for new wells. Re-logging of older wells, or those that were originally not logged could be beneficial. Although not investigated herein, further analyses could include differential thermal analysis (DTA) and thermogravimetry analysis (TGA), which would deem necessary as part of national standards and disposal legislation.

Dedicated studies on (pure) clay minerals of the Molasse Rouge formation are of interest for removing the pollutants that are associated with clay minerals. This requires purification and it is suggested to follow the procedure by Tributh & Lagaly (1986). Impurities such as carbonates, Fe-oxides, and organic matter are removed and further processed by sedimentation to obtain a $<2 \mu\text{m}$ fraction. Finally, the clay should be subjected to dialysis until salt-free, dry-frozen and grinded to a powder for further analyses. Dedicated swelling tests, as proposed e.g. by Pimentel (2015), would deem feasible and reasonable for further geotechnical design calculations since the Molasse Rouge formation has been identified for showing swelling. Swelling consists of two mechanisms depicted by the mechanical and physico-chemical swelling. On one hand, mechanical swelling is a product of the elastic and time-dependent recovery of the compressed mineral framework on stress unloading, in fact more prone to stress relief than mineralogy. On the other hand, physico-chemical swelling is dependent on mineralogy, cementation, electrolyte concentration and the nature of cations. Hence, presence of clay minerals with a high swelling potential does not imply that swelling might occur upon stress relief. Axial Huder-Amberg swelling tests, i.e. deformations were digitised parallel and normal to the recovered core axis as well as the maximum related swelling pressures on two samples from boreholes C1 and C3 and also for samples from

SLHC20 to -25. The two fundamental parameters in tunnelling design are depicted by the maximal swelling pressure and the rate of swelling. In conjunction with mineralogical results, cation exchange capacity and electrolyte concentrations, swelling behaviour could be further investigated for future design calculations using the digitised data as well as the new, upcoming FCC site investigation data. Similar studies could be performed on the permeability of rock in-situ using the Lugeon tests. However, Lugeon permeability is not a direct value for permeability per se but rather a quantitative comparison of in-situ permeability.

Exemplified by the Lyon-Turin project, prompt-gamma neutron activation analyses (PGNAA) would allow the identification of many elements simultaneously in samples of varying grain sizes. Such a study could also be linked to its installation on a conveyor belt together with portable XRF analyses for on-line, real-time analyses during future excavation. A similar approach could be foreseen for near-infrared and far-infrared spectroscopy measurements that contemplate the mid-infrared analyses conducted in the present study. These hyper-spectral image analysis (near-IR) could be applied for the identification of clays.

The micro deval test might be required for certain application scenarios in future such as concrete applicability based on national legislation. An extensive list of requirements for concrete production has been elaborated in Haas, Mongeard, et al. (2021). According to the European standard, the MD test uses 1 kg of sample material of a 10-40 mm sample fraction averaging the result of two runs for each sample. Hence, 2 kg of rock material are required for each sample.

The data scatter of measured values (e.g. CEC or exchangeable cations, see Dohrmann et al. (2012)) is typically larger if various laboratories and research teams from different countries are involved. Hence, it is recommended to stick to one laboratory per type of analysis, in order to have comparable values and laboratory technique procedures.

Extended deterministic and stochastic data analysis

The acquisition of new laboratory measurements and its combination with existing ones presented herein would allow the exploration of machine learning (ML) algorithms

and an extended statistical evaluation including e.g. analysis of variance (ANOVA) or factor analysis (FA) in order to find further correlations potentially linked with new data acquired during upcoming site investigations as part of the FCC in a geological context. With increasing data sets, the application of stochastic rather than deterministic approaches is suggested for data analyses. Although ML approaches are commonly taken with large data sets (100'000+ data entries), supervised ML could aim for the applicability predictions in particular for regions with missing data. The existing descriptions of rock cores in the field based on the results presented herein should be further integrated into the supervised ML approach and direct both the training and validation data sets. Unsupervised ML might imply a greater challenge since the data sets are too small but K-means clustering based on all parameters measured across the fields of geomechanics, petrophysics and mineralogy might bear further potential for both an updated rock characterisation. Thus, establishing and testing the robustness among ML and various empirical relationships of laboratory and geophysical well-log data is worth exploring, naming a few former research studies with a specific emphasis on specific surface area, porosity and permeability (e.g. Basbug, Karpyn 2007; Brooks, Purcell 1952; Chilingarian et al. 1990; Donaldson et al. 1975; Kumar, Fatt 1970; Lee, Lee 2013; Li, Engler 2001; Mohammadi et al. 2020; Mortensen et al. 1998).

Database maintenance and software development

The database created as part of the present study, often referred to as the "Geo" database, would suggest the implementation into existing CERN-wide databases relevant for future decisions of the FCC. In particular, this would refer to e.g. the GIS database hosted by CERN, and would allow a direct connection via an SQL (PostgreSQL) interface with ArcGIS. The increased database with the investigated geological formations, geophysical well-logs, extracted well reports as well as field and laboratory data should be used not only for the FCC construction but also for national Swiss and French databases hosted by regional authorities or geological state surveys such as the BRGM or Swisstopo. This would extend and cover the westernmost part of Switzerland and easternmost region in France, creating comparable data coverage

to the eastern Swiss Molasse Basin as well as the southern German and eastern Austrian Molasse basins. Potentially constituting the foundation of the FCC construction with respect to using the measured rock mechanics data for tunnelling design calculations, a logical step would be to create a graphical user interface (GUI) in e.g. Python or MATLAB and link it with the database environment, e.g. keeping the Microsoft Access data structure. Together with the merged CERN GIS database, this would ease the process to generate valuable and reliable future decisions for the FCC project, and would suggest the development of a database tool similar to the tunnel optimisation tool (TOT), in order to quickly respond to upcoming technical or environmental challenges, sharing data with companies for design calculations or offering simple data access for various public and private entities. For the sake of data type storage and respective maintenance, lower-case and underscores should be avoided to reduce issues with linking and exporting to third-party software packages. Except for sample-ID, location-ID and sample type, text should be kept in longstring-format, while double format is recommended for numeric comma values as well as date and integer for respective formats to optimize database storage. It is recommended to use an input mask wizard to make sure that a predefined format is suggested when entering new data. Validation rules should be linked with these input masks to guarantee a consistent data format in case non-technical users add new data. Examples for such validation rules would infer the names of geological formations or data ranges of laboratory analyses, in order to avoid transposed or dimensional errors. Microsoft's Access software offers these validation and input mask tools.

Application scenarios for conditioned and processed soil

While the present study successfully dealt with research questions designed for the direct applicability of sedimentary raw material, further studies should be implemented to process the sampled material (ca. 500 kg of rock and soil) herein for e.g. cement production, agricultural usage or 3D printing for bricks. The latter might offer the applicability to be used for parts of buildings or individual houses. The next step would be to test the proposed application scenarios on rock mixtures of the respective rock samples, and test the production of cement, tiles,

and bricks with various additives. A study in more detail could aim for the production of bricks or tiles in 3D-printing, with the target to produce these on the tunnelling construction site. For the evaluation of 3D-printing, the remaining rock samples would have to be investigated for their extrusion and viscosity behaviour in different mixtures. Further usage of artificial rock samples could be used for exhibitions, e.g. at CERN's Science Gateway or during its "Open Days", taking home a souvenir of the largest subsurface infrastructure currently in planning by humankind. CERN's school programs could aim for in-class activities and educational demonstrations by producing cement or small bricks. In particular, the geomechanical tests with UCS values leading the way could be of high significance for the evaluation of excavated rock as aggregates for cement mixtures as well as on conditioned, processed rock material. Apparently, this also includes the performance of respective UCS tests on final products.

The mineral composition, physico-chemical properties and grain size distributions make the investigated raw material potentially feasible for concrete aggregate production. Despite the accumulation of a large data set for this study, laboratory testing for the raw materials' applicability as cement or concrete aggregate production as well as tests on final concrete products should be the focus of future studies. The petrographical study presented herein is a solid and reliable starting point to further account for freeze-thaw resistance tests on the raw material, alkali-aggregate reactions, and the investigation of relevant pollutants outlined in national guidelines and regulations (e.g. Schorcht et al. 2013). This includes additives and aggregates for the production of cement and concrete, as outlined in Swiss guidelines and regulations (e.g. Swiss Confederation 2016), and should be further extended on a set of yet-to-define concrete product types and their physico-chemical behaviour once processed with applicable material. The final concrete product's characteristics are highly dependant on grain size distribution and grain shape, which are both influenced by the type of excavation method when investigating the direct application of raw material. The same is suggested for the excavated material's requirement to be used as combustible. This also includes the review of national and European standards as mentioned in Haas, Mongeard, et al. (2021). For concrete production, grain size distribution and grain shape constitute the largest impact on concrete applicability. Both properties

are strongly dependant on the type of excavation method, which would suggest thorough research studies on the optimum type of excavation technique, with respect to both technical and economic feasibility. While the latter could be related to socio-economic impact studies and therefore left out for detailed descriptions, the former is closely linked to environmental issues and the applicability of the excavated raw material. Similarly, agricultural soil to admix with artificial material would have to be tailored to additional geochemical and leachate analyses, since heavy-metals are the driving factors influencing the application outcome in a sustainable context.

There exists a certain potential of producing bricks by using 3D printing. It is suggested to set up a dedicated study to investigate its feasibility performing additional laboratory tests such as viscosity, plasticity and physico-chemical behaviour analyses that result in parameters relevant for 3D printing.

A future study should investigate whether asbestos might be encountered in some of the Molasse Rouge rocks. These could be analysed e.g., via QEMSCAN (electron microscope) image analyses.

Hyper-spectral image analysis (near-IR) could be applied for the further investigation of clays, also as part of analyses on a conveyor belt at the construction site.

The discussion on the rock classification scheme for applicability scenarios in conjunction with geotechnical design calculations aiming explicitly at the chemical, hydro-mechanical and physical rock behaviour as proposed by various researchers (e.g. Chang et al. 2006b; Kahlouche et al. 2021) is also worth considering.

With respect to processed rock material, the flotation technique should be explicitly mentioned, and the characteristic processing material to be added to generate a final product. Important parameters would include magnetic susceptibility, surface wettability and more grain size distribution analyses. The latter should also include the fraction $<63 \mu\text{m}$, to be analysed by laser diffraction. In addition, computer tomography measurements generate 3D images from 2D back-projected scans that allow conclusions on grain size distribution, grain form, interstratifications and micro-fractures. Hence, these could be performed on existing rock samples collected as part of this study to investigate grain size distributions by ML image analyses. Further required parameters such as colour and

texture descriptions as well as density measurements conducted as part of this study should be incorporated to set up a generalized plan of attribute feature classes (German: "*Merkmalsklassenanalyse*"), which is commonly performed on excavated material as part of a processing plan. Regardless of the ultimate chosen application scenario, it is suggested to derive a quality control procedure not only in a site-specific, industrial framework but in a scientific, generalized matter that would allow its application for similar rock worldwide.

The type of excavation method for the FCC will have a crucial impact on feasible application scenarios as elaborated in Haas, Mongeard, et al. (2021). Further studies should be conducted simulating different excavation methods and their influence on the excavated rock. This could involve the shape of excavated rock being either blocky (drill and blast) or in chip format of different length (TBM), which highly depends on the disc spacing (Entacher et al. 2014). The grain size distribution varies extensively among conventional and mechanized tunnelling. Ranges of 0-150 mm are typical for TBMs and 0-900 mm for drill and blast advancement (Fachgruppe für Untertagebau (FGU) 2016). TBM cutter spacing between 80-90 mm are common and research has shown spacings of up to 130 mm for hard rock such as granodiorite (Büchi & Thalmann 1995). The platy shape of chips during TBM favours geomechanical analyses as well as processing for further use. Chemical admixtures during face stabilization for slurry- and EPB-TBMs contaminate the material in a way that makes it impossible to properly process the material posteriori. Swiss legislation does not imply solutions for surfactants being incorporated into excavation material due to the use of an EPB machine. Nitrites and nitrates during drill and blast are common contaminates. For concrete production, this would mean that an additional washing processing removing the nitrates and nitrites would need to be installed. Sequential blasting produces 0-600 mm grains. Excavated material from mechanized tunnelling must be cleaned more accurately when compared to conventional methods in particular for subsequent, potential concrete production. This will likely require a high supply of dewatering presses and voluminous washing drums to remove fine-grained particles ($< 0.063 \text{ mm}$). Portions of up to 12% of fine-grained particles are possible when excavating with a TBM (Thalmann-Suter 2015; Thalmann et al. 2003; Thalmann 1996). Dedicated vertical impact crushers need

to be tuned for breaking TBM rock fragments efficiently without producing excessive sand surplus. As shown in previous sections, excavated material above 8 mm of grain size must be crushed to fulfil concrete aggregate specifications. Chemical and biochemical treatment of FCC's excavated material including chromium, nickel and hydrocarbon contamination further hamper the cleaning process. This fact emphasises a thorough FCC geological investigation since environmental considerations depend on it.

Excavation techniques for the FCC and clay clogging phenomenon

The final tunnelling excavation technique to be used for the FCC construction is still subject to current technical evaluation. The main sections of the FCC tunnel will predominantly be excavated by tunnel boring machines (TBM) in the Cenozoic glaciogenic deposits and Molasse Rouge formation. In the Mesozoic limestone formations, drill and blast is the most likely option due to the karstified intervals and the potential water ingress as encountered during former underground works. For sedimentary rock, plausible options are slurry and earth pressure balanced (EPB) shield machines for the tunnel excavation. The grain size distribution is one of the most crucial criteria to decide on either an earth pressure balanced (EPB) or a slurry shield machine. Due to the fact that the FCC tunnel has a construction depth located at ca. 100 to 300 m, the grain size distributions gained from digitised data is too shallow. These samples show grain size distributions, which are depicted in the main window and transition area of EPB shield machines. Besides the grain size distribution, the full data should be used for future decisions on the type of excavation method used for the FCC's main tunnel, galleries and alcoves. The application of a slurry shield machine considering values of permeability, abrasivity (CERCHAR), UCS and RQD seems feasible (DAUB-Arbeitskreis 2021). However, based on the fact that the grain size distributions are not depicted in the main applicable window, its successful application remains questionable. The FCC's site investigation mark an essential step towards this decision, in particular for its relevant construction depths, rather than extrapolating digitised shallower data. However, the content of grains smaller than 0.06 mm is about 35-70% with a rather low permeability of ca. $5 \cdot 10^{-8}$ m/s, and low CAI values of 0.1 to

0.8. The rather high RQD values of ca. 90% encountered in the Molasse Rouge formation are critical when using an EPB shield machine. Additional measures might require soil conditioning (DAUB-Arbeitskreis 2021). Based on these input parameters, this would suggest the selection of an EPB machine but further investigations should be performed for more robust data in the FCC's depth intervals.

With respect to tunnelling hazards, swelling potential caused by clay minerals such as smectite (Haas et al. 2022), further studies on the swelling behaviour of Molasse clays and natural clay minerals should be investigated. This could infer swelling pressure tests under confined and unconfined conditions and their correlations with the results presented herein. This also includes the assessment of clay clogging and the disintegration of fine-grained, clay-rich rock material during mechanised tunnelling. The ability of clay to stick on mechanised steel parts of a tunnelling boring machine that results in clogging depends on a number of factors such as the soil's grain-size distribution, type of clay minerals, plasticity behaviour, water content, and availability of (free) water (Hollmann & Thewes 2013; Thewes & Hollmann 2016). According to Thewes (1999), clay clogging occurs in particular when swelling clays are present with more than 10%, as analysed as part of this study. Both osmotic (illite) and intracrystalline (montmorillonite) swelling play a crucial role. Besides the adhesive behaviour of illite, even kaolinite can lead to clogging, which could be investigated further. Oliveira et al. (2019) proposed a soil characterisation scheme for the evaluation and testing of clogging phenomena responsible of various soil types, with some of the tests performed herein. A future study could discuss the phenomenon in the context of the different types of mechanised tunnelling foreseen for the FCC, building upon derived clogging diagrams (Hollmann & Thewes 2013) of soil conditions during excavation (raw material), performed slump tests and explicit plasticity (consistency) laboratory analyses potentially mixed with additives for stabilization purposes during excavation. Such additives for soil conditioning of the raw material could include but are not limited to surfactant agent (foam) for the reduction of internal friction, polymers commonly utilised in the presence of excess of water in the ground, bentonite slurry changing the initial rheology of the soil and other additives like anti-abrasion chemicals, tail sealing greases, backfilling mortars, anti-clogging

agents, non-ionic defoaming agents for post-conditioning treatment, lime and calcareous filler. Chemical degradation of some of these additives as well as their potential leakage into the ground will play a crucial role and should be included in future investigations. Extensive research has been conducted over the past years on the clogging phenomenon or leaching characteristics from conditioned tunnel muck (e.g. Zumsteg et al. 2013a,b, 2018) and would allow the verification and evaluation of these findings applied to the Molasse Rouge formation and the FCC tunnel. The application of face stabilization foam and geopolymers bear potential especially for fine-grained, clay-rich rock material as this is the case for the FCC's geological units (Minder et al. 2016; Zumsteg et al. 2013b).

Economic considerations

While the presented analyses stream well addresses the rock properties decisive for the successful characterisation of excavated raw material for its direct application, further factors will play a crucial role. These include the economic demand for mineral resources in the region, the transport infrastructure to either directly use the raw material or set up processing plants, which also require space for temporary storage, and a CO_2 balance on the associated environmental conditions. Ultimately, it is necessary to identify and collaborate with local companies that are able to process the excavated material on behalf of the FCC. In case backfilling is chosen for a certain percentage of the excavated material, local or regional quarries would have to be identified. These implications could be summarised in future (economic) studies.

References

- Abada, A., Abbrescia, M., AbdusSalam, S. S., Abdyyukhanov, I., & et al. (June 2019a). FCC Physics Opportunities. *The European Physical Journal C* 79.6, p. 474. ISSN: 1434-6052. DOI: [10.1140/epjc/s10052-019-6904-3](https://doi.org/10.1140/epjc/s10052-019-6904-3).
- (June 2019b). FCC-ee: The Lepton Collider. *The European Physical Journal Special Topics* 228.2, pp. 261–623. ISSN: 1951-6401. DOI: [10.1140/epjst/e2019-900045-4](https://doi.org/10.1140/epjst/e2019-900045-4).
- (July 2019c). FCC-hh: The Hadron Collider. *The European Physical Journal Special Topics* 228.4, pp. 755–1107. ISSN: 1951-6401. DOI: [10.1140/epjst/e2019-900087-0](https://doi.org/10.1140/epjst/e2019-900087-0).
- (July 2019d). HE-LHC: The High-Energy Large Hadron Collider. *The European Physical Journal Special Topics* 228.5, pp. 1109–1382. ISSN: 1951-6401. DOI: [10.1140/epjst/e2019-900088-6](https://doi.org/10.1140/epjst/e2019-900088-6).
- Abonazel, M. R., Gamal Ghallab, M., Reda Abonazel, M., & Gamal Ibrahim, M. (2018). On Estimation Methods for Binary Logistic Regression Model with Missing Values New estimations in dynamic panel models View project Simulation Using R View project On Estimation Methods for Binary Logistic Regression Model with Missing Values. *International Journal of Mathematics and Computational Science* 4.3, pp. 79–85. ISSN: 2381-7011.
- Abreu, V. & Anderson, J. (July 1998). Glacial Eustasy During the Cenozoic: Sequence Stratigraphic Implications. *AAPG Bulletin* 82, pp. 1385–1400. DOI: [10.1306/1D9BCA89-172D-11D7-8645000102C1865D](https://doi.org/10.1306/1D9BCA89-172D-11D7-8645000102C1865D).
- Adams, S. J. (2005). Core-to-Log Comparison - What's A Good Match? *SPE Journal* 97013. DOI: [10.2118/97013-MS](https://doi.org/10.2118/97013-MS).
- Adler, A., Devarajan, N., Wildi, W., & Poté, J. (2016). Metal Distribution and Characterization of Cultivable Lead-Resistant Bacteria in Shooting Range Soils. *Soil and Sediment Contamination* 25.4, pp. 378–394. ISSN: 15497887. DOI: [10.1080/15320383.2016.1138929](https://doi.org/10.1080/15320383.2016.1138929).
- Aghili, S., Panjepour, M., & Meratian, M. (2018). Kinetic analysis of formation of boron trioxide from thermal decomposition of boric acid under non-isothermal conditions. *Journal of Thermal Analysis and Calorimetry* 131.3, pp. 2443–2455. ISSN: 1588-2926. DOI: [10.1007/s10973-017-6740-3](https://doi.org/10.1007/s10973-017-6740-3).
- Alber, M., Yarali, O., Dahl, F., Bruland, A., Kasling, H., Michalakopoulos, T. N., Cardu, M., Hagan, P., Aydin, H., & Ozarslan, A. (2014). ISRM suggested method for determining the abrasivity of rock by the cerchar abrasivity test. *Rock Mechanics and Rock Engineering* 47.1, pp. 261–266. ISSN: 07232632. DOI: [10.1007/s00603-013-0518-0](https://doi.org/10.1007/s00603-013-0518-0).
- Alhawari, O., Awan, U., Bhutta, M. K. S., & Ali Ülkü, M. (2021). Insights from circular economy literature: A review of extant definitions and unravelling paths to future research. *Sustainability (Switzerland)* 13.2, pp. 1–22. ISSN: 20711050. DOI: [10.3390/su13020859](https://doi.org/10.3390/su13020859).
- Alija, S., Torrijo, F. J., & Quinta-Ferreira, M. (2013). Geological engineering problems associated with tunnel construction in karst rock masses: The case of Gavarres tunnel (Spain). *Engineering Geology* 157, pp. 103–111. ISSN: 00137952. DOI: [10.1016/j.enggeo.2013.02.010](https://doi.org/10.1016/j.enggeo.2013.02.010).
- Allen, P. A., Crampton, S. L., & Sinclair, H. D. (Sept. 1991). The inception and early evolution of the North Alpine Foreland Basin, Switzerland. *Basin Research* 3.3, pp. 143–163. ISSN: 0950-091X. DOI: [10.1111/j.1365-2117.1991.tb00124.x](https://doi.org/10.1111/j.1365-2117.1991.tb00124.x).
- Allen, T. (1990). Particle Size Measurement. 4th. London/New York/Tokyo/Melbourne/Madras: Springer, Dordrecht. ISBN: 978-0-412-35070-2. DOI: [10.1007/978-94-009-0417-0](https://doi.org/10.1007/978-94-009-0417-0).
- Alonso-Santurde, R., Andrés, A., Viguri, J. R., Raimondo, M., Guarini, G., Zanelli, C., & Dondi, M. (2011). Technological behaviour and recycling potential of spent foundry sands in clay bricks. *Journal of Environmental Management* 92.3, pp. 994–1002. ISSN: 03014797. DOI: [10.1016/j.jenvman.2010.11.004](https://doi.org/10.1016/j.jenvman.2010.11.004).
- Alonso, E. & Olivella, S. (Jan. 2008). Modelling Tunnel Performance in Expansive Gypsum Claystone. *12th International Conference on Computer Methods and Advances in Geomechanics 2008* 2.

- AlpTransit Gotthard (2017). AlpTransit Gotthard and Ceneri base tunnel - the logical continuation in the south. Lucerne, Switzerland: AlpTransit Gotthard Ltd.
- Altamura, P. (2013). Gestione eco-efficace dei materiali da costruzione nel ciclo di vita dell'edificio. Strumenti per la prevenzione, il riuso e il riciclo dei rifiuti da C&D. PhD thesis. Sapienza University, Rome, Italy.
- Amaefule, J., Kersey, D., Marschall, D., Powell, J., Valencia, L., & Keelan, D. (1988). Reservoir Description: a Practical Synergistic Engineering and Geological Approach Based on Analysis of Core Data. *Society of Petroleum Engineers* 18167, p. 30. DOI: [10.2523/18167](https://doi.org/10.2523/18167).
- Amir, K., Philippe, S., Philippe-Hervé, L., Vincenzo, S., Bastien, H., Albert, G., Jean-Loup, R., & Bernard, P. (2020). Changes in hydrodynamic process dominance (wave, tide or river) in foreland sequences: The subalpine Miocene Molasse revisited (France). *Sedimentology* 67.5, pp. 2455–2501. ISSN: 13653091. DOI: [10.1111/sed.12708](https://doi.org/10.1111/sed.12708).
- Ammann, L. (2003). Cation exchange and adsorption on clays and clay minerals. PhD thesis. Christian-Albrechts-Universität zu Kiel, p. 119.
- Anagnostou, G. (1993). A model for swelling rock in tunnelling. *Rock Mechanics and Rock Engineering* 26.4, pp. 307–331. ISSN: 07232632. DOI: [10.1007/BF01027115](https://doi.org/10.1007/BF01027115).
- (2007). Design uncertainties in tunnelling through anhydritic swelling rocks. *Felsbau* 25.4, pp. 48–54. ISSN: 01746979.
- Anagnostou, G., Pimentel, E., & Serafeimidis, K. (2010). Swelling of sulphatic claystones - some fundamental questions and their practical relevance / . Quellen von sulfatführenden Tonsteinen - Themen der Grundlagenforschung und ihre praktische Bedeutung. *Geomechanics and Tunnelling* 3.5, pp. 567–572. ISSN: 1865-7362. DOI: [10.1002/geot.201000033](https://doi.org/10.1002/geot.201000033).
- Andrews, D. (Apr. 2015). The circular economy, design thinking and education for sustainability. *Local Economy* 30, pp. 305–315. DOI: [10.1177/0269094215578226](https://doi.org/10.1177/0269094215578226).
- Anger, B., They, F., & Levacher, D. (2015). Caractérisation des sédiments fins des retenues hydroélectriques en vue d'une pré-orientation vers des filières de valorisation matière. *Conférence Méditerranéenne Côtière et Maritime, Edition 3, Ferrara, Italia*, pp. 97–102. DOI: [10.5150/cmcm.2015.020](https://doi.org/10.5150/cmcm.2015.020).
- Ariza, L. & Dallapiazza, W. (2018). Cost and schedule study - phase 3 report - final issue FCC-CIV-CSS RPT 006. Tech. rep., p. 142.
- Arn, R. (1984). Contribution à l'étude stratigraphique du Pléistocène de la région lémanique. PhD thesis. University of Lausanne, p. 307.
- Asquini, L., Furlani, E., Bruckner, S., & Maschio, S. (2008). Production and characterization of sintered ceramics from paper mill sludge and glass cullet. *Chemosphere* 71.1, pp. 83–89. ISSN: 00456535. DOI: [10.1016/j.chemosphere.2007.10.037](https://doi.org/10.1016/j.chemosphere.2007.10.037).
- Asquith, G., Krygowski, D., Henderson, S., & Hurley, N. (Jan. 2004). Basic well log analysis. American Association of Petroleum Geologists. ISBN: 9781629810492. DOI: [10.1306/Mth16823](https://doi.org/10.1306/Mth16823).
- Augustinik, A. (1957). Ceramic Leningrad. *Ceramic Leningrad*.
- Ayres, R. & Talens Peiró, L. (Mar. 2013). Material efficiency: Rare and critical metals. *Philosophical transactions. Series A, Mathematical, physical, and engineering sciences* 371, p. 20110563. DOI: [10.1098/rsta.2011.0563](https://doi.org/10.1098/rsta.2011.0563).
- Bachmann, G. H., Dohr, G., & Muller, M. (1982). Exploration in a classic thrust belt and its foreland: Bavarian Alps, Germany. *American Association of Petroleum Geologists Bulletin* 66.12, pp. 2529–2542. ISSN: 01491423. DOI: [10.1306/03b5ac69-16d1-11d7-8645000102c1865d](https://doi.org/10.1306/03b5ac69-16d1-11d7-8645000102c1865d).
- Bachmann, G. H. & Müller, M. (1991). The Molasse Basin, Germany: evolution of a classic petroliferous foreland basin. Ed. by Spencer (AM). European A. Oxford: University Press. Chap. Generation, pp. 263–276.
- (1992). Sedimentary and structural evolution of the German Molasse Basin. *Eclogae Geol Helv. Eclogae Geol Helv* 85, pp. 519–530.
- Bachmann, G. H., Müller, M., & Weggen, K. (1987). Evolution of the Molasse Basin (Germany, Switzerland). *Tectonophysics* 137.1-4, pp. 77–92. ISSN: 00401951. DOI: [10.1016/0040-1951\(87\)90315-5](https://doi.org/10.1016/0040-1951(87)90315-5).
- Barra Caracciolo, A., Cardoni, M., Pescatore, T., & Patrocco, L. (July 2017). Characteristics and environmental fate of the anionic surfactant sodium lauryl ether sulphate (SLES) used as the main component in foaming agents for mechanized tunnelling. *Environmental Pollution* 226, pp. 94–103. ISSN: 0269-7491. DOI: [10.1016/J.ENVPOL.2017.04.008](https://doi.org/10.1016/J.ENVPOL.2017.04.008).

- Bartenstein, H. (1978). Erdolvorkommen im Molassebecken. *Erdol und Kohle - Erdgas Petrochemie vereinigt mit Brennstoff-Chemie* 31, pp. 393–394.
- Bartsch, H. J. & Sachs, M. (2018). Taschenbuch mathematischer Formeln für Ingenieure und Naturwissenschaftler. Carl Hanser Verlag GmbH & Company KG. ISBN: 9783446457072.
- Basbug, B. & Karpyn, Z. (2007). Estimation of permeability from porosity, specific surface area, and irreducible water saturation using an artificial neural network. *Proceedings of the SPE Latin American and Caribbean Petroleum Engineering Conference* 3, pp. 1244–1253. DOI: [10.2118/107909-ms](https://doi.org/10.2118/107909-ms).
- Becker, A. (2000). The Jura Mountains - an active foreland fold-and-thrust belt? *Tectonophysics*. ISSN: 00401951. DOI: [10.1016/S0040-1951\(00\)00089-5](https://doi.org/10.1016/S0040-1951(00)00089-5).
- Beer, A. (1852). Bestimmung der Absorption des rothen Lichts in farbigen Flüssigkeiten. *Annalen der Physik und Chemie* 86.1, pp. 78–88. DOI: [10.1002/andp.18521620505](https://doi.org/10.1002/andp.18521620505).
- Bellopede, R. (Apr. 2011). Main Aspects of Tunnel Muck Recycling. *American Journal of Environmental Sciences* 7, pp. 338–347. DOI: [10.3844/ajessp.2011.338.347](https://doi.org/10.3844/ajessp.2011.338.347).
- Benedikt, M., Blondel, A., Janot, P., Mangano, M., & Zimmermann, F. (2020). Future Circular Colliders succeeding the LHC. *Nature Physics* 16.4, pp. 402–407. ISSN: 17452481. DOI: [10.1038/s41567-020-0856-2](https://doi.org/10.1038/s41567-020-0856-2).
- Berdugo, I., Alonso, E., Romero, E., & Gens, A. (June 2009). Tunnelling and swelling in Triassic sulphate-bearing rocks. Part II-case studies from Jura Mountains. *Revista Épsilon* 12, pp. 39–53.
- Bergaya, F. & Lagaly, G., eds. (2013). Handbook of Clay Science. Vol. 5. Developments in Clay Science. Elsevier, pp. 1–813. DOI: [10.1016/B978-0-08-098258-8.09992-2](https://doi.org/10.1016/B978-0-08-098258-8.09992-2).
- Berger, J.-P. (1996). Cartes paléogéographiques-palinspastiques du bassin molassique suisse (Oligocène inférieur–Miocène moyen). *Neues Jahrb. Geol. Palaeontol.* Abh. 202, pp. 1–44.
- Bertaux, J., Fröhlich, F., & Ildefonse, P. (1998). Multi-component analysis of FTIR spectra: Quantification of amorphous and crystallized mineral phases in synthetic and natural sediments. *Journal of Sedimentary Research* 68.3, pp. 440–447. ISSN: 15271404. DOI: [10.2110/jsr.68.440](https://doi.org/10.2110/jsr.68.440).
- Bigham, J. M., Dixon, J. B., Milford, M. H., Roth, S. B., Weed, S. B., & Kissel, D. E., eds. (1989). Minerals in Soil Environments. Second edi. SSSA Book Series 5. Soil Science Society of America, p. 1244. ISBN: 9780891187875. DOI: [10.2136/sssabookser1.2ed](https://doi.org/10.2136/sssabookser1.2ed).
- Blengini, G. & Garbarino, E. (July 2010). Resources and waste management in Turin (Italy): The role of recycled aggregates in the sustainable supply mix. *Journal of Cleaner Production* 18, pp. 1021–1030. DOI: [10.1016/j.jclepro.2010.01.027](https://doi.org/10.1016/j.jclepro.2010.01.027).
- Bories, C., Borredon, M. E., Vedrenne, E., & Vilarem, G. (2014). Development of eco-friendly porous fired clay bricks using pore-forming agents: A review. *Journal of Environmental Management* 143, pp. 186–196. ISSN: 10958630. DOI: [10.1016/j.jenvman.2014.05.006](https://doi.org/10.1016/j.jenvman.2014.05.006).
- Bouguer, P. (1729). Essai d’optique: Sur la gradation de la lumière. Claude Jombert, 164 pp. DOI: [ark:/12148/bpt6k10405749](https://doi.org/ark:/12148/bpt6k10405749).
- Boust, D. (1984). Mesures des surfaces spécifiques de sédiment. *Marine Bulletin Liaison LCPC* 134, p. 60.
- Brenchley, P. J. (Apr. 1992). A geologic time scale 1989. Ed. by W. Harland, R. L. Armstrong, A. Cox, L. E. Craig, A. G. Smith, & D. G. Smith. Vol. 27. John Wiley & Sons Ltd, p. 263. ISBN: 0521383617. DOI: [10.1002/gj.3350270220](https://doi.org/10.1002/gj.3350270220).
- Brentini, M. (2018). Impact d’une donnée géologique hétérogène dans la gestion des geo-ressources: analyse intégrée et valorisation de la stratigraphie à travers le bassin genevois (Suisse, France). PhD thesis. Université de Genève, p. 236. DOI: [10.13097/archive-ouverte/unige:103409](https://doi.org/10.13097/archive-ouverte/unige:103409).
- BRGM (2009). Réactualisation du Guide Equivalence pour l’étanchéité passive des installations de stockage de déchets, RP-57081-FR.
- (2021). Online Infoterre Webpage.
- Brindley, G. W. & Brown, G. (1980). Crystal Structures of Clay Minerals and their X-Ray Identification. Mineralogical Society of Great Britain & Ireland. ISBN: 9780903056083. DOI: [10.1180/mono-5](https://doi.org/10.1180/mono-5).
- Brindley, G. W. & Thompson, T. D. (1970). Methylene Blue Absorption by Montmorillonites. Determinations of Surface Areas and Exchange Capacities with Different Initial Cation Saturations (Clay-Organic Studies XIX). *Israel Journal of Chemistry* 8.3, pp. 409–415. DOI: <https://doi.org/10.1002/ijch.197000047>.

- Brindley, G. & Pedro, G. (1972). Report of the AIPEA Nomenclature Committee. *AIPEA Newsletter* 7, pp. 8–13.
- Brink, H. J., Burri, P., Lunde, A., & Winhard, H. (1992). Hydrocarbon habitat and potential of Swiss and German Molasse Basin: a comparison. *Ecologiae Geologicae Helvetiae*. ISSN: 00129402.
- Brombal, D., Wang, H., Pizzol, L., Critto, A., Giubilato, E., & Guo, G. (Nov. 2015). Soil environmental management systems for contaminated sites in China and the EU. Common challenges and perspectives for lesson drawing. *Land Use Policy* 48, pp. 286–298. ISSN: 0264-8377. DOI: [10.1016/J.LANDUSEPOL.2015.05.015](https://doi.org/10.1016/J.LANDUSEPOL.2015.05.015).
- Brooks, C. & Purcell, W. (1952). Surface area measurements on sedimentary rocks. *SPE Fall Meeting of the Petroleum Branch of AIME, Texas*.
- Brunauer, S., Emmett, P. H., & Teller, E. (Feb. 1938). Adsorption of Gases in Multimolecular Layers. *Journal of the American Chemical Society* 60.2, pp. 309–319. ISSN: 15205126. DOI: [10.1021/ja01269a023](https://doi.org/10.1021/ja01269a023).
- Bruning, O., Klein, M., Myers, S., Osborne, J., Rossi, L., Waaijer, C., & Zimmermann, F. (2013). Civil engineering feasibility studies for future ring colliders at cern. *IPAC 2013: Proceedings of the 4th International Particle Accelerator Conference*, pp. 969–971.
- Büchi, E. & Thalmann, C. (1995). Wiederverwertung von TBM-Ausbruchmaterial. Einfluss des Schneidrollenabstands. TBM Know-how zum Projekt NEAT. *Atlas Copco-Robbins Symposium, 16. März*. Lucerne, Switzerland, p. 9.
- Buafalini, M., Dati, G., Rocca, M., & Scevaroli, R. (2017). The Mont Cenis Base Tunnel. *Geomechanik und Tunnelbau* 10.3, pp. 246–255. ISSN: 18657389. DOI: [10.1002/geot.201700009](https://doi.org/10.1002/geot.201700009).
- Burdin, J. & Monin, N. (2009). The management of excavated materials from the Lyon-Turin rail link project. *Geomechanik und Tunnelbau* 2.5, pp. 652–662. ISSN: 18657362. DOI: [10.1002/geot.200900048](https://doi.org/10.1002/geot.200900048).
- Burdin, J., Monin, N., & Thalmann, C. (2017). L'utilisation des matériaux extraits des ouvrages souterrains. *Entrepren. DOSSIER - MATEX*, p. 13.
- Burkhard, M. (1990). Aspects of the large-scale Miocene deformation in the most external part of the Swiss Alps (Subalpine Molasse to Jura fold belt). *Eclogae Geol. Helv.* Vol. 83. 3. Basel: Birkhäuser Verlag, pp. 559–583.
- Burkhard, M. & Sommaruga, A. (Jan. 1998). Evolution of the western Swiss Molasse basin: structural relations with the Alps and the Jura belt. *Geological Society, London, Special Publications* 134.1, 279 LP –298. DOI: [10.1144/GSL.SP.1998.134.01.13](https://doi.org/10.1144/GSL.SP.1998.134.01.13).
- Burri, M. (1981). Les terrasses lémaniques: géologie. *Arch. Sui. Anthropol. Gén.* 45.2, pp. 107–115.
- Butscher, C., Huggenberger, P., & Zechner, E. (2011). Impact of tunneling on regional groundwater flow and implications for swelling of clay-sulfate rocks. *Engineering Geology* 117.3, pp. 198–206. ISSN: 0013-7952. DOI: <https://doi.org/10.1016/j.enggeo.2010.10.018>.
- Butscher, C., Mutschler, T., & Blum, P. (2016). Swelling of clay-sulfate rocks: A review of processes and controls. *Rock Mechanics and Rock Engineering* 49.4, pp. 1533–1549. ISSN: 07232632. DOI: [10.1007/s00603-015-0827-6](https://doi.org/10.1007/s00603-015-0827-6).
- Buxtorf, A. (1916). Prognosen und Befunde beim Hauensteinbasis- und Grenchenbergtunnel und die Bedeutung der Letzteren für die Geologie des Juragebirges. *Verh. Naturforsch. Ges. Basel* 27, pp. 185–254.
- Cabello Eras, J., Sagastume, A., Capote, D., Hens, L., & Vandecasteele, C. (May 2013). Improving the environmental performance of an earthwork project using cleaner production strategies. *Journal of Cleaner Production* 47, pp. 368–376. DOI: [10.1016/j.jclepro.2012.11.026](https://doi.org/10.1016/j.jclepro.2012.11.026).
- Campos, M., Velasco, F., Martínez, M. A., & Torralba, J. M. (2004). Recovered slate waste as raw material for manufacturing sintered structural tiles. *Journal of the European Ceramic Society* 24.5, pp. 811–819. ISSN: 09552219. DOI: [10.1016/S0955-2219\(03\)00325-X](https://doi.org/10.1016/S0955-2219(03)00325-X).
- Carniglia, S. C. (1986). Construction of the tortuosity factor from porosimetry. *Journal of Catalysis* 102.2, pp. 401–418. ISSN: 10902694. DOI: [10.1016/0021-9517\(86\)90176-4](https://doi.org/10.1016/0021-9517(86)90176-4).
- Casagrande, A. (1932). Research on the Atterberg limits of soils. *Public Roads* 13, pp. 121–136.
- Offset-dependent reflectivity - Theory and practice of AVO analysis: (1993). *Investigations in Geophysics Series No. 8 (SEG)*. Ed. by J. Castagna & M. Backus. ISBN: 1-56080-059-3. DOI: [10.1190/1.9781560802624.fm](https://doi.org/10.1190/1.9781560802624.fm).
- Cederbom, C., Schlunegger, F., Sinclair, H. D., & Beek, P. van der (2008). Late Neogene climatic, tectonic and geodynamic(?) forcing on the European Alps recorded by

- the erosion history of the North Alpine Foreland Basin. *Geophys. Res. Abstr.* 10, EGU2008-A-01147.
- Cederbom, C., Sinclair, H. D., Schlunegger, F., & Rahn, M. K. (2004). Climate-induced rebound and exhumation of the European Alps. *Geology* 32, pp. 709–712.
- Centre d'Etudes et Recherches de Charbonnages de France (CERCHAR) (1986). The Cerchar Abrasiveness Index. Verneuil, France.
- Chang, C., Zoback, M. D., & Khaksar, A. (2006a). Empirical relations between rock strength and physical properties in sedimentary rocks. *Journal of Petroleum Science and Engineering* 51.3-4, pp. 223–237. ISSN: 09204105. DOI: [10.1016/j.petrol.2006.01.003](https://doi.org/10.1016/j.petrol.2006.01.003).
- (2006b). Empirical relations between rock strength and physical properties in sedimentary rocks. *Journal of Petroleum Science and Engineering* 51.3-4, pp. 223–237. ISSN: 09204105. DOI: [10.1016/j.petrol.2006.01.003](https://doi.org/10.1016/j.petrol.2006.01.003).
- Chapman, D., Metje, N., & Stärk, A. (2017). Introduction to tunnel construction. Second edi. Boca Raton: CRC Press, p. 425. ISBN: 978-1-4987-6639-5. DOI: [10.1201/9781315120164](https://doi.org/10.1201/9781315120164).
- Charollais, J. & Badoux, H. (1990). Suisse Lemanique pays de Geneve et Chamblais: Guides Geologiques Regionaux. Paris: Masson. ISBN: 9782225821080.
- Charollais, J., Weidmann, M., Berger, J.-P., Engesser, B., Hotellier, J.-F., Gorin, G., Reichenbacher, B., & Schäfer, P. (Nov. 2007). La Molasse du bassin franco-genevois et son substratum. *Archives des Sciences* 60, pp. 59–174.
- Charollais, J., Wernli, R., Mastrangelo, B., Metzger, J., Busnardo, R., Clavel, B., Conrad, M., Davaud, E., Granier, B., Martin, M. S., & Weipmann, M. (2013). Présentation d'une nouvelle carte géologique du Vuache et du Mont de Musièges (Haute-Savoie, France) stratigraphie et tectonique. *Archives des Sciences* 66.1, pp. 1–63. ISSN: 1661464X.
- Chau, K. T. (1997). Young's Modulus Interpreted from Compression Tests with End Friction. *Journal of Engineering Mechanics* 123, pp. 1–7. ISSN: 0733-9399. DOI: [10.1061/\(asce\)0733-9399\(1998\)124:10\(1171\)](https://doi.org/10.1061/(asce)0733-9399(1998)124:10(1171)).
- Chave, A. (2017). Computational Statistics in the Earth Sciences: With Applications in MATLAB. Cambridge University Press, p. 464. ISBN: 978-1107096004.
- Chelle-Michou, C., Do Couto, D., Moscariello, A., Renard, P., & Rusillon, E. (May 2017). Geothermal state of the deep Western Alpine Molasse Basin, France-Switzerland. *Geothermics* 67.2017, pp. 48–65. ISSN: 03756505. DOI: [10.1016/j.geothermics.2017.01.004](https://doi.org/10.1016/j.geothermics.2017.01.004).
- Cheng, K. (1962). EDTA as Masking Agent in Selective Spectrophotometric Determination of Copper with Triethylenetetramine. An Interpretation of Masking. *Analytical Chemistry* 34.11, pp. 1392–1396. DOI: [10.1021/ac60191a013](https://doi.org/10.1021/ac60191a013).
- Chester, R. & Elderfield, H. (1967). The application of infra-red absorption spectroscopy to carbonate mineralogy. *Sedimentology* 9, pp. 5–21. DOI: [10.1111/j.1365-3091.1967.tb01903.x](https://doi.org/10.1111/j.1365-3091.1967.tb01903.x).
- (1968). The infrared determination of opal in siliceous deep-sea sediments. *Geochimica et Cosmochimica Acta* 32, pp. 1128–1140. DOI: [10.1016/0016-7037\(68\)90113-0](https://doi.org/10.1016/0016-7037(68)90113-0).
- Chiappone, A., Marello, S., Scavia, C., & Setti, M. (2004). Clay mineral characterization through the methylene blue test: Comparison with other experimental techniques and applications of the method. *Canadian Geotechnical Journal* 41.6, pp. 1168–1178. ISSN: 00083674. DOI: [10.1139/T04-060](https://doi.org/10.1139/T04-060).
- Chilingarian, G. V., Chang, J., & Bagrintseva, K. I. (1990). Empirical expression of permeability in terms of porosity, specific surface area, and residual water saturation of carbonate rocks. *Journal of Petroleum Science and Engineering* 4.4, pp. 317–322. ISSN: 09204105. DOI: [10.1016/0920-4105\(90\)90029-3](https://doi.org/10.1016/0920-4105(90)90029-3).
- Chittoori, B., Puppala, A., Reddy, R., & Marshall, D. (Mar. 2012). Sustainable Reutilization of Excavated Trench Material, pp. 4280–4289. ISBN: 978-0-7844-1212-1. DOI: [10.1061/9780784412121.440](https://doi.org/10.1061/9780784412121.440).
- Claesson, J. & Bohlooli, B. (2002). Brazilian test: Stress field and tensile strength of anisotropic rocks using an analytical solution. *International Journal of Rock Mechanics and Mining Sciences* 39.8, pp. 991–1004. ISSN: 13651609. DOI: [10.1016/S1365-1609\(02\)00099-0](https://doi.org/10.1016/S1365-1609(02)00099-0).
- Clausi, M., Fernández-Jiménez, A., Palomo, A., Tarantino, S., & Zema, M. (May 2018). Reuse of waste sandstone sludge via alkali activation in matrices of fly ash and metakaolin. *Construction and Building Materials* 172, pp. 212–223. DOI: [10.1016/j.conbuildmat.2018.03.221](https://doi.org/10.1016/j.conbuildmat.2018.03.221).
- Clerc, N. & Moscariello, A. (2020). A revised structural framework for the Geneva Basin and the neighboring

- France region as revealed from 2D seismic data: implications for geothermal exploration. *Swiss Bulletin for Applied Geology* 25.1+2, pp. 109–131.
- Clerc, N., Rusillon, E., Moscariello, A., Renard, P., Paolacci, S., & Meyer, M. (2015). Detailed Structural and Reservoir Rock Typing Characterisation of the Greater Geneva Basin, Switzerland, for Geothermal Resource Assessment. Tech. rep. April, p. 11. DOI: [10.1002/2017EF000724](https://doi.org/10.1002/2017EF000724).
- Cochran, K., Townsend, T., Reinhart, D., & Heck, H. (2007). Estimation of regional building-related C&D debris generation and composition: Case study for Florida, US. *Waste Management* 27.7, pp. 921–931. ISSN: 0956-053X. DOI: <https://doi.org/10.1016/j.wasman.2006.03.023>.
- Conrad, M.-A. & Ducloz, C. (1977). Nouvelles observations sur l'Urgonien et le Sidérolithique du Salève. *Eclogae Geologicae Helvetiae* 70.1-3.
- Courboux, F., Deichmann, N., & Gariel, J. C. (1999). Rupture complexity of a moderate intraplate earthquake in the Alps: The 1996 M5 Epagny-Annecy earthquake. *Geophysical Journal International*. ISSN: 0956540X. DOI: [10.1046/j.1365-246X.1999.00931.x](https://doi.org/10.1046/j.1365-246X.1999.00931.x).
- Crain, E. (2021). Crain's Petrophysical Handbook. English. Rocky Mountain House.
- Cunningham, R. & Williams, R. (1980). Diffusion in Gases and Porous Media. New York: Springer Science & Business Media. ISBN: 978-1-4757-4985-4. DOI: [10.1007/978-1-4757-4983-0](https://doi.org/10.1007/978-1-4757-4983-0).
- Dahlbo, H., Bacher, J., Lähtinen, K., Jouttijärvi, T., Suoheimo, P., Mattila, T., Sironen, S., Myllymaa, T., & Saramäki, K. (Mar. 2015). Construction and demolition waste management - A holistic evaluation of environmental performance. *Journal of Cleaner Production* 107. DOI: [10.1016/j.jclepro.2015.02.073](https://doi.org/10.1016/j.jclepro.2015.02.073).
- Daintith, J. (2014). A dictionary of physics. Sixth edit. Oxford University Press, p. 616. ISBN: 9780199233991. DOI: [10.1093/acref/9780199233991.001.0001](https://doi.org/10.1093/acref/9780199233991.001.0001).
- Darling, T. (2005). Well Logging and Formation Evaluation. First edit. Gulf Professional Publishing, p. 336. ISBN: 9780080457956. DOI: [10.1016/B978-0-7506-7883-4.X5000-1](https://doi.org/10.1016/B978-0-7506-7883-4.X5000-1).
- DAUB-Arbeitskreis (2021). Empfehlungen zur Auswahl von Tunnelvortriebsmaschinen. Köln: Deutscher Ausschuss für unterirdisches Bauen e. V. (DAUB), p. 48.
- Davies, J. F. & Whitehead, R. E. (2006). Alkali-alumina and MgO-alumina molar ratios of altered and unaltered rhyolites. *Exploration and Mining Geology* 15.1-2, pp. 75–88. ISSN: 09641823. DOI: [10.2113/gsemg.15.1-2.75](https://doi.org/10.2113/gsemg.15.1-2.75).
- Degryse, F., Smolders, E., & Parker, D. R. (Aug. 2009). Partitioning of metals (Cd, Co, Cu, Ni, Pb, Zn) in soils: concepts, methodologies, prediction and applications – a review. *European Journal of Soil Science* 60.4, pp. 590–612. ISSN: 1351-0754. DOI: <https://doi.org/10.1111/j.1365-2389.2009.01142.x>.
- Deville, E., Blanc, E., Tardy, M., Beck, C., Cousin, M., & Ménard, G. (1994). Thrust Propagation and Syntectonic Sedimentation in the Savoy Tertiary Molasse Basin (Alpine Foreland). *Hydrocarbon and Petroleum Geology of France*, pp. 269–280. DOI: [10.1007/978-3-642-78849-9_{1}19](https://doi.org/10.1007/978-3-642-78849-9_{1}19).
- Diamantaras, K. & Kung, S. (1996). Principal component neural networks: theory and applications. New York, NY: Wiley.
- Diels, L., De Smet, M., Hooyberghs, L., & Corbisier, P. (1999). Heavy metals bioremediation of soil. *Molecular Biotechnology* 12.2, pp. 149–158. ISSN: 1559-0305. DOI: [10.1385/MB:12:2:149](https://doi.org/10.1385/MB:12:2:149).
- Diem, B. (1986). Die Untere Meeresmolasse zwischen der Saane (Westschweiz) und der Ammer (Oberbayern). PhD thesis. Universität Bern.
- Dieng, M. A. (2005). Der Wasseraufnahmeversuch nach Din 18132 in einem neu entwickelten Gerät. *Bautechnik* 82.1, pp. 28–32. ISSN: 09328351. DOI: [10.1002/bate.200590024](https://doi.org/10.1002/bate.200590024).
- Dinnebier, R. E. & Billinge, S. J. L., eds. (2008). Powder Diffraction - Theory and Practice. The Royal Society of Chemistry, p. 582. ISBN: 978-0-85404-231-9. DOI: [10.1039/9781847558237](https://doi.org/10.1039/9781847558237).
- Do Couto, D., Garel, S., Moscariello, A., Bou Daher, S., Littke, R., & Weniger, P. (2021). Origins of hydrocarbons in the Geneva Basin: insights from oil, gas and source rock organic geochemistry. *Swiss Journal of Geosciences* 114.1. ISSN: 16618734. DOI: [10.1186/s00015-021-00388-4](https://doi.org/10.1186/s00015-021-00388-4).
- Doebelin, N. & Kleeberg, R. (2015). Profex: A graphical user interface for the Rietveld refinement program BGMN. *Journal of Applied Crystallography* 48, pp. 1573–1580. ISSN: 16005767. DOI: [10.1107/S1600576715014685](https://doi.org/10.1107/S1600576715014685).

- Dohrmann, R., Genske, D., Karnland, O., Kaufhold, S., Kiviranta, L., Olsson, S., Plötze, M., Sandén, T., Sellin, P., Svensson, D., & Valter, M. (2012). Interlaboratory CEC and exchangeable cation study of bentonite buffer materials: II. Alternative methods. *Clays and Clay Minerals* 60.2, pp. 176–185. ISSN: 00098604. DOI: [10.1346/CCMN.2012.0600206](https://doi.org/10.1346/CCMN.2012.0600206).
- Dolinar, B., Mišič, M., & Trauner, L. (2007). Correlation between surface area and Atterberg limits of fine-grained soils. *Clays and Clay Minerals* 55.5, pp. 519–523. ISSN: 00098604. DOI: [10.1346/CCMN.2007.0550506](https://doi.org/10.1346/CCMN.2007.0550506).
- Dolinar, B. & Trauner, L. (2004). Liquid limit and specific surface of clay particles. *Geotechnical Testing Journal* 27, pp. 580–584.
- Donaldson, E. C., Kendall, R. F., Baker, B. A., & Manning, F. S. (1975). Surface-Area Measurement of Geologic Materials. *Society of Petroleum Engineers Journal* 15.2, pp. 111–116. ISSN: 0197-7520. DOI: [10.2118/4987-pa](https://doi.org/10.2118/4987-pa).
- Donzeau, M., Wernli, R., Charollais, J., & Monjuvent, G. (1997). Saint-Julien-en-Genevois Carte géologique de la France au 1:50 000, feuille 653 et notice explicative. BRGM, Orléans.
- Doppler, G. (1989). Zur Stratigraphie der nördlichen Vorlandmolasse in Bayrisch-Schwaben. *Geol. Bavarica* 94, pp. 83–133.
- Dosal, E., Coronado, M., Muñoz, I., Viguri, J. R., & Andrés, A. (2012). Application of Multi-Criteria decision-making tool to locate construction and demolition waste (C&DW) recycling facilities in a northern Spanish region. *Environmental Engineering and Management Journal* 11.3, pp. 545–556. ISSN: 15829596. DOI: [10.30638/eemj.2012.067](https://doi.org/10.30638/eemj.2012.067).
- Duarte, M. Á. P. (2007). Foam as a soil conditioner in tunnelling: physical and mechanical properties of conditioned sands. PhD thesis. University of Oxford, p. 385.
- Dunkl, I. & Demény, A. (1997). Exhumation of the Rechnitz Window at the border of the Eastern Alps and the Pannonian basin during Neogene extension. *Tectonophysics* 272, pp. 197–211.
- Dupuis, D. (2009). Etude des sédiments quaternaires, de la Molasse et sa tectonique, dans le Grand Lac (Leman) a partir de données sismiques 2D et 3D. PhD thesis. Université de Genève, p. 238.
- Duyckaerts, G. (1959). The infrared analysis of solid substances. *Analyst* 84, pp. 201–214. DOI: [10.1039/AN9598400201](https://doi.org/10.1039/AN9598400201).
- Edelman, F. (1949). On the compression of a short cylinder between rough end-blocks. *Quarterly of Applied Mathematics* 7.3, pp. 334–337. DOI: <http://www.jstor.org/stable/43633728>.
- Einfalt, H.-C., Fecker, E., & Götz, H.-P. (1979). Das Dreiphasensystem Ton, Anhydrit, Gips und dessen zeitabhängiges Verhalten bei Zugabe von wässrigen Lösungen. 4. *Internationaler Felsmechanik-Kongress, Montreux*.
- Einstein, H. H. (1996). Tunnelling in difficult ground - Swelling behaviour and identification of swelling rocks. *Rock Mechanics and Rock Engineering* 29.3, pp. 113–124. ISSN: 07232632. DOI: [10.1007/BF01032649](https://doi.org/10.1007/BF01032649).
- El Fgaier, F., Lafhaj, Z., & Chapiseau, C. (2013). Use of clay bricks incorporating treated river sediments in a demonstrative building: Case study. *Construction and Building Materials* 48, pp. 160–165. ISSN: 09500618. DOI: [10.1016/j.conbuildmat.2013.06.030](https://doi.org/10.1016/j.conbuildmat.2013.06.030).
- Ellis, D. V. & Singer, J. (2007). Well Logging for Earth Scientists. Second ed. Springer, p. 698. ISBN: 978-1-4020-3738-2. DOI: [10.1007/978-1-4020-4602-5](https://doi.org/10.1007/978-1-4020-4602-5).
- Entacher, M., Lorenz, S., & Galler, R. (Sept. 2014). Tunnel boring machine performance prediction with scaled rock cutting tests. *International Journal of Rock Mechanics and Mining Sciences* 70, pp. 450–459. ISSN: 1365-1609. DOI: <https://doi.org/10.1016/j.ijrmms.2014.04.021>.
- EQUIPCO (2022). Manual for the PetroFLAG analysis (English). Tech. rep., p. 22.
- Erben, H. & Galler, R. (2014). Tunnel spoil – New technologies on the way from waste to raw material / Tunnelausbruch – Neue Technologien für den Weg vom Abfall zum Rohstoff. *Geomechanics and Tunnelling* 7.5, pp. 402–410. DOI: [10.1002/geot.201400043](https://doi.org/10.1002/geot.201400043).
- Erdős, Z., Huismans, R. S., & Beek, P. van der (2019). Control of increased sedimentation on orogenic fold-and-thrust belt structure – insights into the evolution of the Western Alps. *Solid Earth* 10.2, pp. 391–404. DOI: [10.5194/se-10-391-2019](https://doi.org/10.5194/se-10-391-2019).
- Etat de Genève (1994). Forage géothermique de Thônex - Rapport final. Tech. rep.

- Evans, L. (2016). Particle accelerators at CERN: From the early days to the LHC and beyond. *Technological Forecasting and Social Change* 112, pp. 4–12. ISSN: 0040-1625. DOI: [10.1016/j.techfore.2016.07.028](https://doi.org/10.1016/j.techfore.2016.07.028).
- Evans, R. (1967). The atomic nucleus. New York, NY: McGraw-Hill.
- F.R.S., K. P. (1901). LIII. On lines and planes of closest fit to systems of points in space. *The London, Edinburgh, and Dublin Philosophical Magazine and Journal of Science* 2.11, pp. 559–572. DOI: [10.1080/14786440109462720](https://doi.org/10.1080/14786440109462720).
- Farmer, V. C. (Jan. 1974). The Infrared Spectra of Minerals. DOI: [10.1180/mono-4](https://doi.org/10.1180/mono-4).
- Farrar, D. & Coleman, J. (1967). The Correlation of Surface Area With Other Properties of Nineteen British Clay Soils. *Journal of Soil Science* 18.1, pp. 118–124. ISSN: 13652389. DOI: [10.1111/j.1365-2389.1967.tb01493.x](https://doi.org/10.1111/j.1365-2389.1967.tb01493.x).
- Faure, A. (2017). Capacité d'un sédiment à se substituer à la fraction argileuse de la matière première de l'industrie des liants hydrauliques - Thèse de doctorat. PhD thesis. Université de Limoges, p. 337.
- Federal Office of Topography (swisstopo) (2016). Approximate formulas for the transformation between Swiss projection coordinates and WGS84.
- Fern, E. J., Di Murro, V., Soga, K., Li, Z., Scibile, L., & Osborne, J. A. (July 2018). Geotechnical characterisation of a weak sedimentary rock mass at CERN, Geneva. *Tunnelling and Underground Space Technology* 77, pp. 249–260. ISSN: 0886-7798. DOI: [10.1016/J.TUST.2018.04.003](https://doi.org/10.1016/J.TUST.2018.04.003).
- Filon, L. N. G. & Ewing, J. A. (1901). On the elastic equilibrium of circular cylinders under certain practical systems of load. *Proceedings of the Royal Society of London* 68.442-450, pp. 353–358. DOI: [10.1098/rsp1.1901.0056](https://doi.org/10.1098/rsp1.1901.0056).
- Fink, D. & Nakayama, F. (1972). Equation for describing the free swelling of montmorillonite in water. *Soil Science* 114, pp. 355–358.
- Fiore, J. (2007). Quaternary subglacial processes in Switzerland: Geomorphology of the Plateau and seismic stratigraphy of Western Lake Geneva. PhD thesis. University of Geneva, p. 169.
- Fiore, J., Pugin, A., & Beres, M. (Jan. 2002). Sedimentological and GPR Studies of Subglacial Deposits in the Joux Valley (Vaud, Switzerland): Backset Accretion in an Esker Followed by an Erosive Jökulhlaup. *Géographie physique et Quaternaire* 56, p. 19. DOI: [10.7202/008602ar](https://doi.org/10.7202/008602ar).
- Fiore, S., Cuadros, J., & Huertas, F., eds. (2013). Interstratified Clay Minerals - Origin, Characterization and Geochemical Significance. Bari, Italy: Digilabs. ISBN: 978-88-7522-046-4. DOI: [10.13140/RG.2.1.3084.2721](https://doi.org/10.13140/RG.2.1.3084.2721).
- Fjaer, E., Holt, R., Horsrud, P., Raaen, A., & Risnes, R. (2008). Petroleum related rock mechanics. 2nd editio. Elsevier, p. 491. ISBN: 978-0-444-50260-5.
- Flury, B. (1988). Common principal components and related models. New York, NY: Wiley.
- Forchheimer, P. (1901). Wasserbewegung durch Boden. *Zeitschrift des Vereins deutscher Ingenieure* 45, p. 1731.
- Foth, H. (1991). Fundamentals of Soil Science. 8th. New York/Chichester/Brisbane/Toronto/Singapore: John Wiley & Sons, p. 384. ISBN: 978-0-471-52279-9.
- Fourvel, G. (2018). Valorisation agronomique des sédiments fins de retenues hydroélectriques en construction d'Anthrosols fertiles. PhD thesis. Université Bretagne Loire, p. 397.
- Franklin, J. A. (1985). Suggested method for determining point load strength. *International Journal of Rock Mechanics and Mining Sciences & Geomechanics Abstracts* 22.2, pp. 51–60. ISSN: 0148-9062. DOI: [10.1016/0148-9062\(85\)92327-7](https://doi.org/10.1016/0148-9062(85)92327-7).
- Frar, I., Ben Allal, L., Ammari, M., & Lamrani, S. (2014). Intégration des matériaux en terre cuite dans la valorisation des sédiments marins. *MATEC Web of Conferences* 11, pp. 1–4. ISSN: 2261236X. DOI: [10.1051/mateconf/20141101025](https://doi.org/10.1051/mateconf/20141101025).
- Frisch, W., Kuhle, J., Dunkl, I., & Brügel, A. (1998). Palinspastic reconstruction and topographic evolution of the Eastern Alps during late Tertiary tectonic extrusion. *Tectonophysics*. ISSN: 00401951. DOI: [10.1016/S0040-1951\(98\)00160-7](https://doi.org/10.1016/S0040-1951(98)00160-7).
- Fröhlich, F. (May 1989). Deep-sea biogenic silica: new structural and analytical data from infrared analysis - geological implications. *Terra Nova* 1.3, pp. 267–273. ISSN: 0954-4879. DOI: <https://doi.org/10.1111/j.1365-3121.1989.tb00368.x>.
- Füchtbauer, H. (1959). Die Schüttungen im Chatt und Aquitan der deutschen Alpenvorlandsmolasse. *Eclogae Geol. Helv.* 73, pp. 173–203.

- Fuller, C. W., Willett, S. D., & Brandon, M. T. (2006). Formation of forearc basins and their influence on subduction zone earthquakes. *Geology*. ISSN: 00917613. DOI: [10.1130/G21828.1](https://doi.org/10.1130/G21828.1).
- Furlani, E., Tonello, G., Maschio, S., Aneggi, E., Minichelli, D., Bruckner, S., & Lucchini, E. (2011). Sintering and characterisation of ceramics containing paper sludge, glass cullet and different types of clayey materials. *Ceramics International* 37.4, pp. 1293–1299. ISSN: 02728842. DOI: [10.1016/j.ceramint.2010.12.005](https://doi.org/10.1016/j.ceramint.2010.12.005).
- Gaines, G. & Thomas, H. (1953). Adsorption Studies on Clay Minerals. II. A Formulation of the Thermodynamics of Exchange Adsorption. *J. Chem. Phys.* 21.714. DOI: [10.1063/1.1698996](https://doi.org/10.1063/1.1698996).
- Galler, R., Biermeier, F., & Lassnig, K. (2012). Prognose von Tunnelausbruchsmaterial.
- Galler, R. & Voit, K. (2014). Tunnelausbruch – wertvoller mineralischer Rohstoff. *Betonkalender 2014, 103. Jahrgang*, pp. 423–468.
- Galli, M. (2016). Rheological characterisation of Earth-Pressure-Balance (EPB) support medium composed of non-cohesive soils and foam. PhD thesis, pp. 1–383.
- Gangoells, M., Casals, M., Forcada, N., & Macarulla, M. (Dec. 2014). Analysis of the implementation of effective waste management practices in construction projects and sites. *Resources, Conservation and Recycling* 93, pp. 99–111. ISSN: 0921-3449. DOI: [10.1016/J.RESCONREC.2014.10.006](https://doi.org/10.1016/J.RESCONREC.2014.10.006).
- Garcia, D., Fontelles, M., & Moutte, J. (1994). Sedimentary Fractionations between Al, Ti, and Zr and the Genesis of Strongly Peraluminous Granites. *The Journal of Geology* 102.4, pp. 411–422. DOI: [10.1086/629683](https://doi.org/10.1086/629683).
- Garefalakis, P. & Schlunegger, F. (2019). Tectonic processes, variations in sediment flux, and eustatic sea level recorded by the 20 Myr old Burdigalian transgression in the Swiss Molasse basin. *Solid Earth* 10.6, pp. 2045–2072. ISSN: 18699529. DOI: [10.5194/se-10-2045-2019](https://doi.org/10.5194/se-10-2045-2019).
- Gegenhuber, N. (2015). Application of Gassmann's equation for laboratory data from carbonates from Austria. *Austrian Journal of Earth Sciences* 108.2, pp. 239–244. DOI: [10.17738/ajes.2015.0024](https://doi.org/10.17738/ajes.2015.0024).
- Geissdoerfer, M., Savaget, P., Bocken, N., & Hultink, E. (Feb. 2017). The Circular Economy – A new sustainability paradigm? *Journal of Cleaner Production* 143, pp. 757–768. DOI: [10.1016/j.jclepro.2016.12.048](https://doi.org/10.1016/j.jclepro.2016.12.048).
- Gertsch, L., Fjeld, A., Nilsen, B., & Gertsch, R. (Oct. 2000). Use of TBM muck as construction material. *Tunnelling and Underground Space Technology* 15.4, pp. 379–402. ISSN: 0886-7798. DOI: [10.1016/S0886-7798\(01\)00007-4](https://doi.org/10.1016/S0886-7798(01)00007-4).
- Gervaise, J. (1972). Études géologiques et géotechniques effectuées sur le site du synchrotron européen de 300 GeV - CERN/MC/61/Rev. Tech. rep. Geneva.
- Ghisellini, P., Ripa, M., & Ulgiati, S. (Mar. 2018). Exploring environmental and economic costs and benefits of a circular economy approach to the construction and demolition sector. A literature review. *Journal of Cleaner Production* 178, pp. 618–643. ISSN: 0959-6526. DOI: [10.1016/J.JCLEPRO.2017.11.207](https://doi.org/10.1016/J.JCLEPRO.2017.11.207).
- Goodall, W. R., Scales, P. J., & Butcher, A. R. (2005). The use of QEMSCAN and diagnostic leaching in the characterisation of visible gold in complex ores. *Minerals Engineering* 18.8, pp. 877–886. ISSN: 08926875. DOI: [10.1016/j.mineng.2005.01.018](https://doi.org/10.1016/j.mineng.2005.01.018).
- Gordon, P. R. & Sephton, M. A. (2016). Rapid habitability assessment of Mars samples by pyrolysis-FTIR. *Planetary and Space Science* 121, pp. 60–75. ISSN: 00320633. DOI: [10.1016/j.pss.2015.11.019](https://doi.org/10.1016/j.pss.2015.11.019).
- Gorin, G., Morend, D., & Pugin, A. (2003). Bedrock, Quaternary sediment and recent fault activity in central Lake Neuchâtel, as derived from high-resolution reflection seismics. *Eclogae Geologicae Helvetiae*. ISSN: 00129402. DOI: [10.1007/978-3-0348-7992-7{_}2](https://doi.org/10.1007/978-3-0348-7992-7{_}2).
- Gorin, G., Signer, C., & Amberger, G. (Jan. 1993). Structural configuration of the western Swiss Molasse Basin as defined by reflection seismic data. *Eclogae Geologicae Helvetiae* 86, pp. 693–716.
- Gottlieb, P., Wilkie, G., Sutherland, D., Suthers, S., Perera, K., Jenkins, B., Spencer, S., Butcher, A., & Rayner, J. (2000). Using Quantitative Electron Microscopy for Process Mineralogy Applications. *Journal of The Minerals, Metals & Materials Society* 52.April, pp. 24–25. DOI: [10.1007/s11837-000-0126-9](https://doi.org/10.1007/s11837-000-0126-9).
- Gradstein, F., Ogg, J., & Smith, A., eds. (2004). Chronostratigraphy: Linking time and rock - A Geologic Time Scale. Cambridge University Press, p. 45. ISBN: 978-0-521-78142-8. DOI: [10.1017/CB09780511536045](https://doi.org/10.1017/CB09780511536045).
- Graf, H. R. & Burkhalter, R. (2016). Quaternary deposits: concept for a stratigraphic classification and nomenclature—an example from northern Switzerland.

- Swiss Journal of Geosciences* 109.2, pp. 137–147. ISSN: 16618734. DOI: [10.1007/s00015-016-0222-7](https://doi.org/10.1007/s00015-016-0222-7).
- Grim, R. (1962). *Applied Clay Mineralogy*. McGraw-Hill Company, p. 422.
- Gross, D., Sachsenhofer, R. F., Bechtel, A., Gratzner, R., Grundtner, M. L., Linzer, H. G., Misch, D., Pytlak, L., & Scheucher, L. (2018). Petroleum Systems in the Austrian Sector of the North Alpine Foreland Basin: An Overview. *Journal of Petroleum Geology*. ISSN: 17475457. DOI: [10.1111/jpg.12704](https://doi.org/10.1111/jpg.12704).
- Grubbs, F. E. (1969). Procedures for Detecting Outlying Observations in Samples. *Technometrics* 11.1, pp. 1–21. ISSN: 15372723. DOI: [10.1080/00401706.1969.10490657](https://doi.org/10.1080/00401706.1969.10490657).
- Guggenheim, S., Adams, J. M., Bain, D. C., Bergaya, F., Brigatti, M. F., Drits, V. A., Formoso, M. L., Galán, E., Kogure, T., & Stanjek, H. (2006). Summary of recommendations of nomenclature committees relevant to clay mineralogy: Report of the Association Internationale pour l'Etude des Argiles (AIPEA) nomenclature committee for 2006. *Clays and Clay Minerals* 54.6, pp. 761–772. ISSN: 00098604. DOI: [10.1346/CCMN.2006.0540610](https://doi.org/10.1346/CCMN.2006.0540610).
- Guggenheim, S. & Martin, R. (1996). Reply to the comment by D.M. Moore on Definition of clay and clay mineral: Joint report of the AIPEA and CMS Nomenclature Committees. *Clays and Clay Minerals* 44, pp. 713–715.
- Guggenheim, S. & Martin, R. T. (1995). Definition of Clay and Clay Mineral: Joint Report of the Aipea Nomenclature and CMS Nomenclature Committees. *Clays and Clay Minerals* 43.2, pp. 255–256. ISSN: 1552-8367. DOI: [10.1346/CCMN.1995.0430213](https://doi.org/10.1346/CCMN.1995.0430213).
- Gusterhuber, J., Hinsch, R., & Sachsenhofer, R. F. (2014). Evaluation of hydrocarbon generation and migration in the Molasse fold and thrust belt (Central Eastern Alps, Austria) using structural and thermal basin models. *AAPG Bulletin*. ISSN: 01491423. DOI: [10.1306/06061312206](https://doi.org/10.1306/06061312206).
- Haas, M., Carraro, D., Ventra, D., Plötze, M., De Haller, A., & Moscariello, A. (2022). Integrated stratigraphic, sedimentological and petrographical evaluation for CERN's Future Circular Collider subsurface infrastructure (Geneva Basin, Switzerland-France). *Swiss Journal of Geosciences*.
- Haas, M., De Haller, A., Moscariello, A., Scibile, L., Benedikt, M., Gengenhuber, N., & Galler, R. (2020). A mineralogical re-use classification model of molasse rock mass in the Geneva Basin. *ISRM International Symposium - EUROCK2020, June 14-19, 2020, physical event not held*. Trondheim.
- Haas, M., Galler, R., Scibile, L., & Benedikt, M. (2020). Waste or valuable resource – a critical European review on re-using and managing tunnel excavation material. *Resources, Conservation and Recycling* 162, p. 105048. ISSN: 18790658. DOI: [10.1016/j.resconrec.2020.105048](https://doi.org/10.1016/j.resconrec.2020.105048).
- Haas, M., Mongeard, L., Ulrici, L., D'Aloia, L., Cherrey, A., Galler, R., & Benedikt, M. (2021). Applicability of excavated rock material: a European technical review implying opportunities for future tunnelling projects. *Journal of Cleaner Production* 315, p. 128049. DOI: [10.1016/j.jclepro.2021.128049](https://doi.org/10.1016/j.jclepro.2021.128049).
- Hall, G. E., Bonham-Carter, G. F., & Buchar, A. (2014). Evaluation of portable X-ray fluorescence (pXRF) in exploration and mining: Phase 1, control reference materials. *Geochemistry: Exploration, Environment, Analysis* 14.2, pp. 99–123. ISSN: 14677873. DOI: [10.1144/geochem2013-241](https://doi.org/10.1144/geochem2013-241).
- Haq, B. U. (2014). Cretaceous eustasy revisited. *Global and Planetary Change and Planetary Change* 113, pp. 44–58.
- Haq, B. U., Hardenbol, J., & Vail, P. R. (1987). Chronology of Fluctuating Sea Levels Since the Triassic. *Science* 235.4793, pp. 1156–1167. DOI: [10.1126/science.235.4793.1156](https://doi.org/10.1126/science.235.4793.1156).
- Hasegawa, M., Usui, M., & Gotoh, K. (1993). Geological prognosis ahead of a tunnel face. *Engineering Geology* 35.3, pp. 229–235. ISSN: 0013-7952. DOI: [https://doi.org/10.1016/0013-7952\(93\)90011-Z](https://doi.org/10.1016/0013-7952(93)90011-Z).
- Haurine, F. (2015). Caractérisation d'atterrissements d'argiles récents sur le territoire français, en vue de leur valorisation dans l'industrie des matériaux de construction en terre cuite. PhD thesis. Mines ParisTech.
- Haurine, F., Cojan, I., & Bruneaux, M. A. (2016). Development of an industrial mineralogical framework to evaluate mixtures from reservoir sediments for recovery by the heavy clay industry: Application of the Durance system (France). *Applied Clay Science* 132-133, pp. 508–517. ISSN: 01691317. DOI: [10.1016/j.clay.2016.07.022](https://doi.org/10.1016/j.clay.2016.07.022).
- Herb, R. (1988). Eocaene Paläogeographie und Paläotektonik des Helvetikums. *Eclogae Geol Helv* 81, pp. 611–657.

- Herron, M. M. (1988). Geochemical classification of terrigenous sands and shales from core or log data. *Journal of Sedimentary Research* 58.5, pp. 820–829. ISSN: 1527-1404. DOI: [10.1306/212F8E77-2B24-11D7-8648000102C1865D](https://doi.org/10.1306/212F8E77-2B24-11D7-8648000102C1865D).
- Herwanger, J., Bottrill, A., & Popov, P. (May 2016). One 4D geomechanical model and its many applications. *78th EAGE Conference and Exhibition 2016: Efficient Use of Technology - Unlocking Potential* 2016.1, pp. 1–5. DOI: [10.3997/2214-4609.201601368/CITE/REFWORKS](https://doi.org/10.3997/2214-4609.201601368/CITE/REFWORKS).
- Herwanger, J. (2011). Seismic Geomechanics: How to Build and Calibrate Geomechanical Models using 3D and 4D Seismic Data. ISBN: 9789073834101. DOI: [10.3997/9789073834101](https://doi.org/10.3997/9789073834101).
- Herwanger, J. & Horne, S. A. (2009). Linking reservoir geomechanics and time-lapse seismics: Predicting anisotropic velocity changes and seismic attributes. *Geophysics* 74.4, W13–W33. ISSN: 00168033. DOI: [10.1190/1.3122407](https://doi.org/10.1190/1.3122407).
- Higgs, P. W. (1964). Broken Symmetries and the Masses of Gauge Bosons. *Phys. Rev. Lett.* 13.16, pp. 508–509. DOI: [10.1103/PhysRevLett.13.508](https://doi.org/10.1103/PhysRevLett.13.508).
- Hilda, L., Olu, S., Ajay, K., Lafebre, H., Songonuga, O., & Kathuria, A. (July 1998). Contaminated Soil Management at Construction Sites. *Practice Periodical of Hazardous, Toxic, and Radioactive Waste Management* 2.3, pp. 115–119. DOI: [10.1061/\(ASCE\)1090-025X\(1998\)2:3\(115\)](https://doi.org/10.1061/(ASCE)1090-025X(1998)2:3(115)).
- Hill, H. J. & Milburn, J. D. (Dec. 1956). Effect of Clay and Water Salinity on Electrochemical Behavior of Reservoir Rocks. *Transactions of the AIME* 207.01, pp. 65–72. ISSN: 0081-1696. DOI: [10.2118/532-G](https://doi.org/10.2118/532-G).
- Hinsch, R. (2013). Laterally varying structure and kinematics of the Molasse fold and thrust belt of the Central Eastern Alps: Implications for exploration. *AAPG Bulletin*. ISSN: 01491423. DOI: [10.1306/04081312129](https://doi.org/10.1306/04081312129).
- Hofmann, U. & Dammler, I. (1969). Methylenblanadsorption an Montmorillonit. *Chimia* 23, pp. 476–480.
- Hollmann, F. S. & Thewes, M. (2013). Assessment method for clay clogging and disintegration of fines in mechanised tunnelling. *Tunnelling and Underground Space Technology* 37.20 13, pp. 96–106. ISSN: 08867798. DOI: [10.1016/j.tust.2013.03.010](https://doi.org/10.1016/j.tust.2013.03.010).
- Homewood, P., Allen, P. A., & Williams, G. D. (Dec. 1986). Dynamics of the Molasse Basin of Western Switzerland. *Foreland Basins*. Wiley Online Books, pp. 199–217. DOI: [doi:10.1002/9781444303810.ch10](https://doi.org/10.1002/9781444303810.ch10).
- Hotelling, H. (1933). Analysis of a complex of statistical variables into principal components. *Journal of Educational Psychology* 24.6, pp. 417–441. ISSN: 1939-2176(Electronic),0022-0663(Print). DOI: [10.1037/h0071325](https://doi.org/10.1037/h0071325).
- Huang, L., Bohne, R. A., Bruland, A., Jakobsen, P. D., & Lohne, J. (2015). Environmental impact of drill and blast tunnelling: life cycle assessment. *Journal of Cleaner Production* 86, pp. 110–117. ISSN: 0959-6526. DOI: <https://doi.org/10.1016/j.jclepro.2014.08.083>.
- Iacoboaia, C., Aldea, M., & Petrescu, F. (2019). Construction and demolition waste - A challenge for the European Union? *Theoretical and Empirical Researches in Urban Management* 14.1, pp. 30–52.
- Ibarrola, N. & Jones, M. (2016). Analysis and Evaluation of the CERN Reference Systems. *International Workshop on Accelerator Alignment, Grenoble, October 3-7, 2016*, p. 4.
- Ibele, T. (2011). Tectonics of the western Swiss Molasse Basin during Cenozoic times. PhD thesis.
- International Centre for Diffraction Data (ICDD) (1998). PDF2 XRD Database (version 1998).
- International Society for Rock Mechanics (ISRM) (1972a). Suggested method for determining the point load strength index, International Society for Rock Mechanics.
- (1972b). Suggested methods for determining the uniaxial compressive strength on rock materials and the point load strength index. Tech. rep. International Society of Rock Mechanics (ISRM).
- (1978). Suggested methods for determining sound velocity.
- (1979). Suggested Method for Determining the Uniaxial Compressive Strength and Deformability of Rock Materials, International Society for Rock Mechanics.
- Jackson, J. (1991). A user's guide to principal components. New York, NY: Wiley.
- Jackson, M. L. (1962). Interlayering of Expansible Layer Silicates in Soils by Chemical Weathering. *Clays and Clay Minerals* 11.1, pp. 29–46. ISSN: 1552-8367. DOI: [10.1346/CCMN.1962.0110104](https://doi.org/10.1346/CCMN.1962.0110104).

- Jaeger, J. C., Cook, N. G. W., & Zimmerman, R. (2007). *Fundamentals of Rock Mechanics*. 4th editio. Wiley-Blackwell, p. 488. ISBN: 978-0-632-05759-7.
- Jasmund, K. & Lagaly, G. (1993). *Tonminerale und Tone - Struktur, Eigenschaften, Anwendung und Einsatz in Industrie und Umwelt*. Darmstadt: Steinkopff Verlag. ISBN: 978-3-7985-0923-8. DOI: [10.1007/978-3-642-72488-6](https://doi.org/10.1007/978-3-642-72488-6).
- Jaynes, W. F. & Bigham, J. M. (1986). Multiple Cation-Exchange Capacity Measurements on Standard Clays Using a Commercial Mechanical Extractor. *Clays and Clay Minerals* 34.1, pp. 93–98. ISSN: 1552-8367. DOI: [10.1346/CCMN.1986.0340112](https://doi.org/10.1346/CCMN.1986.0340112).
- Jenny, J., Burri, J.-P., Muralt, R., Pugin, A., Schegg, R., Ungemach, P., Vuataz, F.-D., & Wernli, R. (1995). Le forage géothermique de Thônex (Canton de Genève): Aspects stratigraphiques, tectoniques, diagénétiques, géophysiques et hydrogéologiques. *Eclogae Geologicae Helvetiae* 88.2, pp. 365–396.
- Johnson, S. (1859). On some points of agricultural science. *American Journal of Science and Arts Series* 2.28, pp. 71–85.
- Joint Venture MARTI AG (2018). Plan de gestion des matériaux d'excavation. Tech. rep., p. 6.
- Jolliffe, I. (2002). *Principal component analysis*. 2nd edn. New York, NY: Springer.
- Jones, S. (1972). A rapid accurate unsteady-state Klinkenberg permeameter. *Society of Petroleum Engineers Journal* 12.5, pp. 383–397. DOI: [10.2118/3535-PA](https://doi.org/10.2118/3535-PA).
- (1997). A technique for faster pulse-decay permeability measurements in tight rocks. *Journal of SPE Formation Evaluation* 12, pp. 19–26. DOI: [10.2118/28450-PA](https://doi.org/10.2118/28450-PA).
- Josh, M., Delle Piane, C., Esteban, L., Bourdet, J., Mayo, S., Pejčić, B., Burgar, I., Luzin, V., Clennell, M. B., & Dewhurst, D. N. (2019). Advanced laboratory techniques characterising solids, fluids and pores in shales. *Journal of Petroleum Science and Engineering* 180. April, pp. 932–949. ISSN: 09204105. DOI: [10.1016/j.petrol.2019.06.002](https://doi.org/10.1016/j.petrol.2019.06.002).
- Kaelin, D. (1997). Litho- und Biostratigraphie der mittel- bis obermiozänen Bois de Raube-Formation (Nordwestschweiz). *Eclogae Geologicae Helvetiae*. ISSN: 00129402.
- Kaelin, D. & Kempf, O. (2009). High-resolution stratigraphy from the continental record of the Middle Miocene Northern Alpine Foreland Basin of Switzerland. *Neues Jahrbuch für Geologie und Paläontologie - Abhandlungen* 254.1-2, pp. 177–235. ISSN: 00777749. DOI: [10.1127/0077-7749/2009/0010](https://doi.org/10.1127/0077-7749/2009/0010).
- Kaelin, D., Rybach, L., Kempter, E., Kaelin, B., Rybach, L., & Kempter, E. (1992). Rates of deposition, uplift and erosion in the Swiss Molasse basin, estimated from sonic- and density-logs. *Bull. Swiss. Assoc. Petroleum Geol. and Eng.* 58, pp. 9–22.
- Kahlouche, H., Gheris, A., & Guenfoud, M. (2021). Characterisation of the chemo-mechanical behaviour of clays polluted by BTEX: a case study of benzene. *International Journal of Geo-Engineering* 12.1. ISSN: 2092-9196. DOI: [10.1186/s40703-021-00157-0](https://doi.org/10.1186/s40703-021-00157-0).
- Kahr, G. & Madsen, F. (1995). Determination of the cation exchange capacity and the surface area of bentonite, illite and kaolinite by methylene blue adsorption. *Applied Clay Science* 9.5, pp. 327–336. ISSN: 01691317. DOI: [10.1016/0169-1317\(94\)00028-0](https://doi.org/10.1016/0169-1317(94)00028-0).
- Kang, C.-H., Oh, S. J., Shin, Y., Han, S.-H., Nam, I.-H., & So, J.-S. (2015). Bioremediation of lead by ureolytic bacteria isolated from soil at abandoned metal mines in South Korea. *Ecological Engineering* 74, pp. 402–407. ISSN: 0925-8574. DOI: <https://doi.org/10.1016/j.ecoleng.2014.10.009>.
- Karner, G. D. & Watts, A. B. (Dec. 1983). Gravity anomalies and flexure of the lithosphere at mountain ranges. *Journal of Geophysical Research: Solid Earth* 88.B12, pp. 10449–10477. ISSN: 0148-0227. DOI: [10.1029/JB088iB12p10449](https://doi.org/10.1029/JB088iB12p10449).
- Käsling, H., Thiele, I., & Thuro, K. (2007). Abrasivitätsuntersuchungen mit dem Cerchar-Test - Eine Evaluierung der Versuchsbedingungen. *16. Tagung für Ingenieurgeologie und Forum Junge Ingenieurgeologen*. Bochum, pp. 229–235.
- Kaufhold, S. & Dohrmann, R. (2010a). Effect of extensive drying on the cation exchange capacity of bentonites. *Clay Minerals* 45.4, pp. 441–448. ISSN: 0009-8558. DOI: [10.1180/claymin.2010.045.4.441](https://doi.org/10.1180/claymin.2010.045.4.441).
- (2010b). Stability of bentonites in salt solutions: II. Potassium chloride solution — Initial step of illitization? *Applied Clay Science* 49.3, pp. 98–107. ISSN: 0169-1317. DOI: <https://doi.org/10.1016/j.clay.2010.04.009>.
- Keeling, P., Kirby, E., & Robertson, R. (1980). Moisture adsorption and specific surface area. *J. Brit. Ceram. Soc.* 79, pp. 36–40.

- Keily, J. (2020). Excavating Tunnel: The Archaeology of Crossrail.
- Keller, B. (1989). Fazies und Stratigraphie der Oberen Meeressmolasse (unteres Miozän) zwischen Napf und Bodensee. ger. PhD thesis. Bern: Universität Bern.
- (Jan. 1992). Hydrogeology of the Swiss Molasse Basin: A review of current knowledge and considerations for the future. *Eclogae Geol Helv. Eclogae Geologicae Helvetiae* 85, pp. 611–651.
- Kempf, O. & Matter, A. (Jan. 1999). Magnetostratigraphy and depositional history of the Upper Freshwater Molasse (OSM) of eastern Switzerland. *Eclogae Geologicae Helvetiae* 92, pp. 97–103.
- Kempf, O. & Pross, J. (2005). The lower marine to lower freshwater Molasse transition in the northern Alpine foreland basin (Oligocene; central Switzerland-south Germany): Age and geodynamic implications. *International Journal of Earth Sciences* 94.1, pp. 160–171. ISSN: 14373254. DOI: [10.1007/s00531-004-0437-0](https://doi.org/10.1007/s00531-004-0437-0).
- Kenley, R. & Harfield, T. (Jan. 2011). Greening procurement: a research agenda for optimizing mass-haul during linear infrastructure construction. *Sixth International Conference on Construction in the 21st Century (CITC-VI)*, pp. 235–240.
- Kissling, D. (1974). L'Oligocène de l'extrémité occidentale du bassin molassique suisse: stratigraphie et aperçu sédimentologique. PhD thesis. Université de Genève.
- Klimchouk, A. (1996). The dissolution and conversion of gypsum and anhydrite. *International Journal of Speleology* 25.3/4, pp. 21–36. ISSN: 0392-6672. DOI: [10.5038/1827-806x.25.3.2](https://doi.org/10.5038/1827-806x.25.3.2).
- Klinkenberg, L. (1941). The permeability of Porous media to liquids and gases. *API Drilling and Productions Practices* Vol. API-41-200. New York, pp. 200–213.
- Kovári, K., Amstad, C., & Anagnostou, G. (1987). Tunnelbau in quellfähigem Gebirge.pdf. *Mitteilungen der Schweizerischen Gesellschaft für Boden- und Felsmechanik, Frühjahrstagung 7. Mai, Biel*, pp. 1–8.
- Kovári, K., Madsen, F. T., & Amstad, C. (1981a). Tunneling with yielding support in swelling rocks. *ISRM International Symposium, IS 1981* September, pp. 1019–1026.
- (1981b). Tunneling with yielding support in swelling rocks.
- Kovári, K. & Vogelhuber, M. (2014). Empirical Basis for the Design of Tunnel Linings in Swelling Rock containing Anhydrite. *Proceedings of the World Tunnel Congress 2014 - Tunnels for a better Life*. Foz do Iguaçu, Brazil, pp. 1–9.
- Kovári, K., Amberg, F., & Ehrbar, H. (2002). Mastering of Squeezing Rock in the Gotthard Base. *World Tunneling*, pp. 234–238.
- Kugler, H., Schwaighofer, B., & Gruber, S. (2002). Die Modifizierung des Wasseraufnahmeversuches nach Enslin-Neff. *Beiträge zur Jahrestagung Wien, Berichte der DTTG, Band 9*. Ed. by F. Ottner & S. Gier, p. 9.
- Kuhlemann, J. (2000). Post-collisional sediment budget of circum-Alpine basins (Central Europe). *Mem Sci Geol Padova* 52, pp. 1–91.
- Kuhlemann, J., Frisch, W., Székely, B., Dunkl, I., Kázmér, M., & Kazmer, M. (Oct. 2002). Post-collisional sediment budget history of the Alps: Tectonic versus climatic control. *International Journal of Earth Sciences* 91, pp. 818–837. ISSN: 14373254. DOI: [10.1007/s00531-002-0266-y](https://doi.org/10.1007/s00531-002-0266-y).
- Kuhlemann, J. & Kempf, O. (2002). Post-Eocene evolution of the North Alpine Foreland Basin and its response to Alpine tectonics. *Sedimentary Geology* 152.1-2, pp. 45–78. ISSN: 00370738. DOI: [10.1016/S0037-0738\(01\)00285-8](https://doi.org/10.1016/S0037-0738(01)00285-8).
- Kumar, J. & Fatt, I. (1970). Nuclear Magnetic Resonance Study of Porosity, Permeability and Surface Area of Unconsolidated Porous Materials. *The Log Analyst* 11.01.
- Kumar, S., Thomas, B., Gupta, V., Basu, P., & Shrivastava, S. (Jan. 2018). Sandstone wastes as aggregate and its usefulness in cement concrete – A comprehensive review. *Renewable and Sustainable Energy Reviews* 81. DOI: [10.1016/j.rser.2017.08.044](https://doi.org/10.1016/j.rser.2017.08.044).
- Kwan, J. & Jardine, F. (June 1999). Ground engineering spoil: practices of disposal and reuse. *Engineering Geology* 53.2, pp. 161–166. ISSN: 0013-7952. DOI: [10.1016/S0013-7952\(99\)00029-0](https://doi.org/10.1016/S0013-7952(99)00029-0).
- La Vigne, J., Herron, M., & Hertzog, R. (1994). Density-Neutron Interpretation In Shaly Sands. *SPWLA 35th Annual Logging Symposium*. Vol. All Days. SPWLA Annual Logging Symposium. Tulsa, Oklahoma.
- Ladd, M. (1998). Introduction to physical chemistry. Cambridge University Press. DOI: [10.1017/CB09781139170925](https://doi.org/10.1017/CB09781139170925).

- Lagotala, H. (1945). Travaux de forage de Peissy: rapport final (Société d'Études pour la mise en valeur des gisements métallifères suisses) - swisstopo Bericht no. 1050. Tech. rep.
- Lal, M. (1999). Shale stability: drilling fluid interaction and shale strength. *SPE Latin American and Caribbean Petroleum Engineering Conference*. Caracas, Venezuela. DOI: [10.2118/54356-MS](https://doi.org/10.2118/54356-MS).
- Lambert, J. H. (1760). Photometria sive de mensura et gradibus luminis, colorum et umbrae (Photometry: On the measure and gradations of light, colors, and shade). Augsburg ("Augusta Vindelicorum"), Germany: Eberhardt Klett, p. 391.
- Laporte-Saumure, M., Martel, R., & Mercier, G. (2010). Evaluation of Physicochemical Methods for Treatment of Cu, Pb, Sb, and Zn in Canadian Small Arm Firing Ranges Backstop Soils. *Water, Air, & Soil Pollution* 213.1, pp. 171–189. ISSN: 1573-2932. DOI: [10.1007/s11270-010-0376-2](https://doi.org/10.1007/s11270-010-0376-2).
- Large, R. R., Gemell, J. B., Paulick, H., & Huston, D. L. (2001). The Alteration Box Plot: A Simple Approach to Understanding the Relationship between Alteration Mineralogy and Litho geochemistry Associated with Volcanic-Hosted Massive Sulfide Deposits. *Economic Geology* 96.5, pp. 957–971.
- Laubscher, H. (1961). Die Fernschubhypothese der Jurafaltung. *Eclog. Geol. Helvet.* 54, pp. 221–281.
- Lee, B. H. & Lee, S. K. (2013). Effects of specific surface area and porosity on cube counting fractal dimension, lacunarity, configurational entropy, and permeability of model porous networks: Random packing simulations and NMR micro-imaging study. *Journal of Hydrology* 496, pp. 122–141. ISSN: 00221694. DOI: [10.1016/j.jhydrol.2013.05.014](https://doi.org/10.1016/j.jhydrol.2013.05.014).
- Lee, K.-Y. & Kim, K.-W. (Dec. 2010). Heavy Metal Removal from Shooting Range Soil by Hybrid Electrokinetics with Bacteria and Enhancing Agents. *Environmental Science & Technology* 44.24, pp. 9482–9487. ISSN: 0013-936X. DOI: [10.1021/es102615a](https://doi.org/10.1021/es102615a).
- Leemann, A., Thalmann, C., & Studer, W. (2005). Alkali-aggregate reaction in Swiss tunnels. *Materials and Structures* 38.3, pp. 381–386. ISSN: 1871-6873. DOI: [10.1007/BF02479305](https://doi.org/10.1007/BF02479305).
- Lemcke, K. (1967). Zwölf Jahre Öl- und Gasförderung im süddeutschen Alpenvorland: ein Überblick. *Bulletin der Vereinigung Schweiz. Petroleum-Geologen und -Ingenieure* 33, pp. 23–31.
- (1984). Geologische Vorgänge in den Alpen ab Obereozän im Spiegel vor allem der deutschen Molasse. *Geologische Rundschau* 73.1, pp. 371–397. ISSN: 1432-1149. DOI: [10.1007/BF01820376](https://doi.org/10.1007/BF01820376).
- (1988). Geologie von Bayern.—I. Teil: Das bayerische Alpenvorland vor der Eiszeit. Ed. by E. Schweizerbart. Stuttgart, p. 175.
- Lemcke, K., Engelhardt, W., & Füchtbauer, H. (1953). Geologische und sedimentpetrographische Untersuchungen im Westteil der ungefalteten Molasse des deutschen Alpenvorlandes. *Beih. Geol. Jahrb.* 11, pp. 1–182.
- Li, D. & Engler, T. (2001). Development of a New equation and an Algorithm To Estimate Permeabilities for Clean Formations From Resistivity Logs. *Society of Petroleum Engineers, SPE-68820 2*, pp. 1–9. DOI: [10.2523/68820-ms](https://doi.org/10.2523/68820-ms).
- Li, J., Hong, A., Yuan, D., Jiang, Y., Deng, S., Cao, C., & Liu, J. (Oct. 2020). A new distributed karst-tunnel hydrological model and tunnel hydrological effect simulations. *Journal of Hydrology*, p. 125639. ISSN: 00221694. DOI: [10.1016/j.jhydrol.2020.125639](https://doi.org/10.1016/j.jhydrol.2020.125639).
- Little, R. J. A. (1992). Regression With Missing X's: A Review. *Journal of the American Statistical Association* 87.420, pp. 1227–1237. ISSN: 01621459.
- Lunardi, P. (2014). The underground as a resource and reserve for new spaces: ADECO-RS as an effective tool to be able to realize them. *Proceedings of the World Tunnel Congress 2014*.
- Lv, Y., Jiang, Y., Hu, W., Cao, M., & Mao, Y. (July 2020). A review of the effects of tunnel excavation on the hydrology, ecology, and environment in karst areas: Current status, challenges, and perspectives. DOI: [10.1016/j.jhydrol.2020.124891](https://doi.org/10.1016/j.jhydrol.2020.124891).
- Ma, Y. Z. (2019). Quantitative Geosciences: Data Analytics, Geostatistics, Reservoir Characterization and Modeling. ISBN: 9783030178598. DOI: [10.1007/978-3-030-17860-4](https://doi.org/10.1007/978-3-030-17860-4).
- Madritsch, H., Preusser, F., Fabbri, O., Bichet, V., Schlunegger, F., & Schmid, S. M. (2010). Late Quaternary folding in the Jura Mountains: Evidence from syn-erosional deformation of fluvial meanders. *Terra Nova*. ISSN: 09544879. DOI: [10.1111/j.1365-3121.2010.00928.x](https://doi.org/10.1111/j.1365-3121.2010.00928.x).

- Madsen, F. & Kahr, G. (1985). Quellende Gesteine Als Ursache Von Problemen Im Untertagebau. *Mitteilungen des Institutes fuer Grundbau und Bodenmechanik, Eidgenoessische Technische Hochschule Zurich* 125, pp. 50–51.
- Madsen, F. & Kahr, G. (1993). Wasserdampfadsorption und spezifische Oberfläche von Tonen. *Berichte der Deutschen Ton- und Tonmineralgesellschaft DTTG, Beiträge zur Jahrestagung in Hannover, 9.-11. September 1992*. Hannover, pp. 165–181.
- Madsen, F. & Nüesch, R. (1991). The swelling behaviour of clay-sulfate rocks. *7th ISRM Congress*. Vol. 4, pp. 285–288. DOI: [10.1016/0148-9062\(92\)93858-h](https://doi.org/10.1016/0148-9062(92)93858-h).
- Magnusson, S., Lundberg, K., Svedberg, B., & Knutsson, S. (Apr. 2015). Sustainable management of excavated soil and rock in urban areas – A literature review. *Journal of Cleaner Production* 93, pp. 18–25. ISSN: 0959-6526. DOI: [10.1016/J.JCLEPRO.2015.01.010](https://doi.org/10.1016/J.JCLEPRO.2015.01.010).
- Mahani, H., Keya, A. L., Berg, S., & Nasralla, R. (2016). Electrokinetics of Carbonate/Brine Interface in Low-Salinity Waterflooding: Effect of Brine Salinity, Composition, Rock Type, and pH on ζ -Potential and a Surface-Complexation Model. *SPE Journal* 22.01, pp. 53–68. ISSN: 1086-055X. DOI: [10.2118/181745-PA](https://doi.org/10.2118/181745-PA).
- Makhloufi, Y., Rusillon, E., Brentini, M., Moscarillo, A., Meyer, M., & Samankassou, E. (2018). Dolomitization of the Upper Jurassic carbonate rocks in the Geneva Basin, Switzerland and France. *Swiss Journal of Geosciences* 111.3, pp. 475–500. ISSN: 1661-8734. DOI: [10.1007/s00015-018-0311-x](https://doi.org/10.1007/s00015-018-0311-x).
- Marel, H. W. v. d. & Beutelspacher, H. (1976). Atlas of infrared spectroscopy of clay minerals and their admixtures / H. W. van der Marel and H. Beutelspacher, in collaboration with E. Reitz and P. Krohmer. Amsterdam ; New York: Elsevier Scientific Pub. Co. ISBN: 0444411879.
- Marsh, H. W. (1998). Pairwise deletion for missing data in structural equation models: Nonpositive definite matrices, parameter estimates, goodness of fit, and adjusted sample sizes. *Structural Equation Modeling: A Multidisciplinary Journal* 5.1, pp. 22–36. DOI: [10.1080/10705519809540087](https://doi.org/10.1080/10705519809540087).
- Marzouk, M. & Azab, S. (Jan. 2014). Environmental and economic impact assessment of construction and demolition waste disposal using system dynamics. *Resources, Conservation and Recycling* 82, pp. 41–49. DOI: [10.1016/j.resconrec.2013.10.015](https://doi.org/10.1016/j.resconrec.2013.10.015).
- Mattelaer, P. (2019). High-Luminosity LHC Project at CERN. *Swiss Tunnel Congress 2019*, pp. 38–47.
- Matter, A. (Jan. 1980). Flysch and Molasse of Western and Central Switzerland. *Geology of Switzerland: A Guide Book. Part B Geological Excursions*. Ed. by P. Home-wood & R. Trümpy. Basel: Wepf & Co., pp. 261–293. ISBN: 3-85977-063-2.
- Mauriohooho, K., Barker, S. L., & Rae, A. (2016). Mapping lithology and hydrothermal alteration in geothermal systems using portable X-ray fluorescence (pXRF): A case study from the Tauhara geothermal system, Taupo Volcanic Zone. *Geothermics* 64, pp. 125–134. ISSN: 03756505. DOI: [10.1016/j.geothermics.2016.03.005](https://doi.org/10.1016/j.geothermics.2016.03.005).
- Mavko, G., Mukerji, T., & Dvorkin, J. (2009). The rock physics handbook. 2nd editio. New York: Cambridge University Press. DOI: [10.1017/CB09780511626753](https://doi.org/10.1017/CB09780511626753).
- Mazurek, M., Hurford, A. J., & Leu, W. (2006). Unravelling the multi-stage burial history of the Swiss Molasse Basin: Integration of apatite fission track, vitrinite reflectance and biomarker isomerisation analysis. *Basin Research* 18.1, pp. 27–50. ISSN: 0950091X. DOI: [10.1111/j.1365-2117.2006.00286.x](https://doi.org/10.1111/j.1365-2117.2006.00286.x).
- McPhee, C., Reed, J., & Zubizarreta, I. (2015). Core Analysis: A Best Practice Guide. Ed. by J. Cubitt & H. Wales. 1st editio. Amsterdam: Elsevier B.V. ISBN: 978-0-444-63533-4.
- Meier, L. & Kahr, G. (1999). Determination of the cation exchange capacity (CEC) of clay minerals using the complexes of copper(II) ion with triethylenetetramine and tetraethylenepentamine. *Clays and Clay Minerals*, 47, pp. 386–388. DOI: [10.1346/CCMN.1999.0470315](https://doi.org/10.1346/CCMN.1999.0470315).
- Melcher, C., Schweitzer, J., Manente, R., & Peterson, C. (1991). Applicability of GSO scintillators for well logging. *IEEE Transactions on Nuclear Science* 38.2, pp. 506–509. DOI: [10.1109/23.289349](https://doi.org/10.1109/23.289349).
- Menezes, R. R., Ferreira, H. S., Neves, G. A., Lira, H. d. L., & Ferreira, H. C. (2005). Use of granite sawing wastes in the production of ceramic bricks and tiles. *Journal of the European Ceramic Society* 25.7, pp. 1149–1158. ISSN: 09552219. DOI: [10.1016/j.jeurceramsoc.2004.04.020](https://doi.org/10.1016/j.jeurceramsoc.2004.04.020).
- Miller, P., Reid, A., & Zuiderwyk, M. (1982). QEM*SEM image analysis in the determination of modal assays,

- mineral associations and mineral liberation. *Proceedings of the 14th International Mineral Processing Congress, October 17-23*. Toronto.
- Minder, P., Puzrin, A. M., & Plötze, M. (2016). Enhanced delivery of chemical agents in soil improvement applications. *Geotechnique* 66.6, pp. 469–480. ISSN: 17517656. DOI: [10.1680/jgeot.15.P.127](https://doi.org/10.1680/jgeot.15.P.127).
- Mishra, S. & Datta-Gupta, A. (2017). *Applied Statistical Modeling and Data Analytics*. Elsevier B.V., p. 250. ISBN: 9780128032800. DOI: [10.1016/C2014-0-03954-8](https://doi.org/10.1016/C2014-0-03954-8).
- Mittal, V. K. & Sangwan, K. S. (2014). Prioritizing barriers to green manufacturing: Environmental, social and economic perspectives. *Procedia CIRP* 17, pp. 559–564. ISSN: 22128271. DOI: [10.1016/j.procir.2014.01.075](https://doi.org/10.1016/j.procir.2014.01.075).
- Mock, S. & Herwegh, M. (2017). Tectonics of the central Swiss Molasse Basin: Post-Miocene transition to incipient thick-skinned tectonics? *Tectonics* 36.9, pp. 1699–1723. ISSN: 19449194. DOI: [10.1002/2017TC004584](https://doi.org/10.1002/2017TC004584).
- Mock, S., Von Hagke, C., Schlunegger, F., Dunkl, I., & Herwegh, M. (2020). Long-wavelength late-Miocene thrusting in the north Alpine foreland: Implications for late orogenic processes. *Solid Earth*. ISSN: 18699529. DOI: [10.5194/se-11-1823-2020](https://doi.org/10.5194/se-11-1823-2020).
- Mohammadi, M., Shadizadeh, S. R., Manshad, A. K., & Mohammadi, A. H. (2020). Experimental study of the relationship between porosity and surface area of carbonate reservoir rocks. *Journal of Petroleum Exploration and Production Technology* 10.5, pp. 1817–1834. ISSN: 21900566. DOI: [10.1007/s13202-020-00838-z](https://doi.org/10.1007/s13202-020-00838-z).
- Monnier, F. (Feb. 1982). Thermal diagenesis in the Swiss Molasse Basin: implications for oil generation. *Canadian Journal of Earth Sciences* 19.2, pp. 328–342. DOI: [10.1139/e82-025](https://doi.org/10.1139/e82-025).
- Monteiro, S. N. & Vieira, C. M. F. (2014). On the production of fired clay bricks from waste materials: A critical update. *Construction and Building Materials* 68, pp. 599–610. ISSN: 09500618. DOI: [10.1016/j.conbuildmat.2014.07.006](https://doi.org/10.1016/j.conbuildmat.2014.07.006).
- Montero, M. A., Jordán, M. M., Hernández-Crespo, M. S., & Sanfeliu, T. (2009). The use of sewage sludge and marble residues in the manufacture of ceramic tile bodies. *Applied Clay Science* 46.4, pp. 404–408. ISSN: 01691317. DOI: [10.1016/j.clay.2009.10.013](https://doi.org/10.1016/j.clay.2009.10.013).
- Moore, D. & Reynolds, R. (1989). *X-ray Diffraction and the Identification and Analysis of Clay Minerals*. Vol. 38. Oxford University Press, p. 448. DOI: [10.1346/CCMN.1990.0380416](https://doi.org/10.1346/CCMN.1990.0380416).
- Moreno, B. & García-Álvarez, M. T. (2018). Measuring the progress towards a resource-efficient European Union under the Europe 2020 strategy. *Journal of Cleaner Production* 170.2018, pp. 991–1005. ISSN: 09596526. DOI: [10.1016/j.jclepro.2017.09.149](https://doi.org/10.1016/j.jclepro.2017.09.149).
- Mortensen, J., Engstrøm, F., & Lind, I. (1998). The Relation Among Porosity, Permeability, and Specific Surface of Chalk From the Gorm Field, Danish North Sea. *SPE Reservoir Engineering (Society of Petroleum Engineers)* 1.3, pp. 245–250. ISSN: 08859248. DOI: [10.2118/31062-pa](https://doi.org/10.2118/31062-pa).
- Mosar, J. (1999). Present-day and future tectonic underplating in the western Swiss Alps: Reconciliation of basement/wrench-faulting and decollement folding of the Jura and Molasse basin in the Alpine foreland. *Earth and Planetary Science Letters* 173.3, pp. 143–155. ISSN: 0012821X. DOI: [10.1016/S0012-821X\(99\)00238-1](https://doi.org/10.1016/S0012-821X(99)00238-1).
- Moscariello, A. (1996). Quaternary geology of the Geneva Bay: sedimentary record, palaeoclimatic and palaeoenvironmental reconstruction since the Last Glacial Cycle. PhD thesis. University of Geneva, p. 230.
- (2018a). Alluvial fans and fluvial fans at the margins of continental sedimentary basins: Geomorphic and sedimentological distinction for geo-energy exploration and development. *Geological Society Special Publication* 440.1, pp. 215–243. ISSN: 03058719. DOI: [10.1144/SP440.11](https://doi.org/10.1144/SP440.11).
- (Jan. 2018b). The geomorphological landscapes in the Geneva Basin. *Landscapes and Landforms of Switzerland (WGLC)*. Ed. by E. Reinard. Springer, Cham, pp. 83–96. ISBN: 978-3-030-43201-0. DOI: [10.1007/978-3-030-43203-4_6](https://doi.org/10.1007/978-3-030-43203-4_6).
- (2019). Exploring for geo-energy resources in the Geneva Basin (Western Switzerland): Opportunities and challenges. *Swiss Bulletin for Applied Geology* 24.2, pp. 105–124. ISSN: 16641884.
- Moscariello, A., Gorin, G., Rusillon, E., & Charollais, J. (2014). Geology of Western Switzerland and nearby France in a Geo-Energy perspective - Field Trip B1 Guide Book. *19th International Sedimentological Congress Geneva, 18-22 August*, p. 27.
- Moscariello, A., Guglielmetti, L., Omodeo-Salé, S., De Haller, A., Eruteya, O., Lo, H., Clerc, N., Makloufhi,

- Y., Do Couto, D., Ferreira De Oliveira, G., Perozzi, L., DeOliveira, F., Hollmuller, P., Quiquerez, L., Nawratil De Bono, C., Martin, F., & Meyer, M. (2020). Heat production and storage in Western Switzerland: advances and challenges of intense multidisciplinary geothermal exploration activities, an 8 years progress report. *Proceedings World Geothermal Congress 2020, April 26 - May 2*. Reykjavik.
- Moscariello, A., Pugin, A., Wildi, W., Beck, C., Chapron, E., De Batist, M., Girardclos, S., Ivy Ochs, S., Rachoud-Schneider, A., Signer, C., & Van Clauwenberghe, T. (1998). Déglaciation würmienne dans des conditions lacustres à la terminaison occidentale du bassin lémanique (Suisse occidentale et France). *Eclogae Geologicae Helveticae* 91, pp. 185–201.
- Muhunthan, B. (1991). Liquid limit and surface area of clays. *Géotechnique* 41.1, pp. 135–138. ISSN: 17517656. DOI: [10.1680/geot.1991.41.1.135](https://doi.org/10.1680/geot.1991.41.1.135).
- Nagaraj, H., Sridharan, A., & Madhu, B. (2012). Comparative study of determination of liquid limit by Percussion cup method, Cone Penetration method and ko-Stress method. *International Symposium on Lowland Technology*. Bali, Indonesia.
- Naik, M. M. & Dubey, S. K. (2013). Lead resistant bacteria: Lead resistance mechanisms, their applications in lead bioremediation and biomonitoring. *Ecotoxicology and Environmental Safety* 98, pp. 1–7. ISSN: 0147-6513. DOI: <https://doi.org/10.1016/j.ecoenv.2013.09.039>.
- Neff, H. (2005). Der Wasseraufnahmeversuch nach Enslin-Neff in der erd- und grundbautechnischen Praxis. 5. *Österreichische Geotechniktagung*. 21.02. & 22.02.2005, Vienna, p. 27.
- Neff, H. (1959). Über die Messung der Wasseraufnahme ungleichförmiger bindiger anorganischer Bodenarten in einer neuen Ausführung des Enslingerätes. *Die Bautechnik* 11, p. 10.
- Oggeri, C., Fenoglio, T. M., & Vinai, R. (2014). Tunnel spoil classification and applicability of lime addition in weak formations for muck reuse. DOI: [10.1016/j.tust.2014.07.013](https://doi.org/10.1016/j.tust.2014.07.013).
- Oggeri, C. & Vinai, R. (2012). Soil Conditioning and Ground Monitoring for Shield Tunnelling. *Revista Minelor* 18.4, pp. 2–14.
- Oliveira, D. G., Thewes, M., & Diederichs, M. S. (Dec. 2019). Clogging and flow assessment of cohesive soils for EPB tunnelling: Proposed laboratory tests for soil characterisation. *Tunnelling and Underground Space Technology* 94, p. 103110. ISSN: 08867798. DOI: [10.1016/j.tust.2019.103110](https://doi.org/10.1016/j.tust.2019.103110).
- Ortner, H., Aichholzer, S., Zerlauth, M., Pilser, R., & Fügenschuh, B. (2015). Geometry, amount, and sequence of thrusting in the Subalpine Molasse of western Austria and southern Germany, European Alps. *Tectonics*. ISSN: 19449194. DOI: [10.1002/2014TC003550](https://doi.org/10.1002/2014TC003550).
- Oxburgh, E. (1981). Geology of Switzerland: A Guide-Book. Part A: An Outline of the Geology of Switzerland. *Mineralogical Magazine* 44, pp. 366–366. ISSN: 0026-461X. DOI: doi.org/10.1180/minmag.1981.044.335.28.
- Pacheco-Torgal, F. (Jan. 2020). Introduction to advances in construction and demolition waste, pp. 1–10. ISBN: 9780128190555. DOI: [10.1016/B978-0-12-819055-5.00001-2](https://doi.org/10.1016/B978-0-12-819055-5.00001-2).
- Panagos, P., Van Liedekerke, M., Jones, A., & Montanarella, L. (Apr. 2012). European Soil Data Centre: Response to European Policy Support and Public Data Requirements. *Land Use Policy* 29, pp. 329–338. DOI: [10.1016/j.landusepol.2011.07.003](https://doi.org/10.1016/j.landusepol.2011.07.003).
- Paolacci, S. (2012). Seismic facies and structural configuration of the Western Alpine Molasse basin and its substratum (France and Switzerland). PhD thesis. Université de Genève.
- Pecharsky, V. & Zavalij, P. (2009). Fundamentals of Powder Diffraction and Structural Characterization of Materials. 2nd editio. Boston: Springer US, p. 744. ISBN: 978-0-387-09578-3. DOI: [10.1007/978-0-387-09579-0](https://doi.org/10.1007/978-0-387-09579-0).
- Peila, D. (2014). Soil conditioning for EPB shield tunnelling. *KSCE Journal of Civil Engineering* 18.3, pp. 831–836. ISSN: 19763808. DOI: [10.1007/s12205-014-0023-3](https://doi.org/10.1007/s12205-014-0023-3).
- Petkovšek, A., Maček, M., & Majes, B. (2009). A laboratory characterization of soils and clay-bearing rocks using the Enslin-Neff water-adsorption test. *Acta Geotechnica Slovenica* 6.2, pp. 5–13. ISSN: 18540171.
- Peugh, J. L. & Enders, C. K. (2004). Missing Data in Educational Research: A Review of Reporting Practices and Suggestions for Improvement. *Review of Educational Research* 74.4, pp. 525–556. DOI: [10.3102/00346543074004525](https://doi.org/10.3102/00346543074004525).

- Pfiffner, O.-A. (Dec. 1986). Evolution of the North Alpine Foreland Basin in the Central Alps. DOI: [doi:10.1002/9781444303810.ch11](https://doi.org/10.1002/9781444303810.ch11).
- (2020). The Geology of Switzerland. *Landscapes and Landforms of Switzerland. World Geomorphological Landscapes Book Series (WGLC)*. Ed. by E. Reynard. Springer, Cham. ISBN: 978-3-030-43203-4. DOI: [10.1007/978-3-030-43203-4](https://doi.org/10.1007/978-3-030-43203-4).
- (Jan. 2021). The Geology of Switzerland, pp. 7–30. ISBN: 978-3-030-43201-0. DOI: [10.1007/978-3-030-43203-4](https://doi.org/10.1007/978-3-030-43203-4).
- Pichard, C. & Fröhlich, F. (Nov. 1986). Analyses IR quantitatives des sédiments. Exemple du dosage du quartz et de la calcite. *Oil & Gas Science and Technology* 41.6, pp. 809–819. DOI: [10.2516/ogst:1986048](https://doi.org/10.2516/ogst:1986048).
- Pickell, J., Swanson, B., & Hickman, W. (1966). Application of Air-Mercury and Oil-Air Capillary Pressure Data In the Study of Pore Structure and Fluid Distribution. *Society of Petroleum Engineers Journal* 6.01, pp. 55–61. ISSN: 0197-7520. DOI: [10.2118/1227-pa](https://doi.org/10.2118/1227-pa).
- Pickett, G. (1944). Application of the Fourier Method to the Solution of Certain Boundary Problems in the Theory of Elasticity. *Journal of Applied Mechanics* 11.3, A176–A182. ISSN: 0021-8936. DOI: [10.1115/1.4009381](https://doi.org/10.1115/1.4009381).
- (1974). Formation evaluation - unpublished lecture notes.
- Pierdona, L. (2018). Chemical stratigraphy and petrography of the Molasse in the Geneva Basin (Master thesis). Université de Genève, p. 131.
- Pimentel, E. (2015). Existing Methods for Swelling Tests - A Critical Review. *Energy Procedia* 76, pp. 96–105. ISSN: 18766102. DOI: [10.1016/j.egypro.2015.07.857](https://doi.org/10.1016/j.egypro.2015.07.857).
- Pirrie, D., Butcher, A. R., Power, M. R., Gottlieb, P., & Miller, G. L. (Jan. 2004). Rapid quantitative mineral and phase analysis using automated scanning electron microscopy (QemSCAN); potential applications in forensic geoscience. *Geological Society, London, Special Publications* 232.1, 123 LP –136. DOI: [10.1144/GSL.SP.2004.232.01.12](https://doi.org/10.1144/GSL.SP.2004.232.01.12).
- Pitard, F. (1992). Pierre Gy's Sampling Theory and Sampling Practice, Volumes 1 and 2. Boca Raton, FL: CRC Press.
- Plinninger, R. & Thuro, K. (2004). Wear Prediction in Hardrock Excavation Using the CERCHAR Abrasiveness Index (CAI). *International Symposium EUROCK 2004* 1, pp. 1–6.
- Prieto, L. A. (2012). The Cerchar Abrasivity Index's applicability to dredging rock. *Proceedings of the Western Dredging Association (WEDA XXXII) Technical Conference and Texas A&M University (TAMU 43) Dredging Seminar, June 10-13*. San Antonio.
- Priyadharshini, P., Ramamurthy, K., & Robinson, R. (Sept. 2017). Excavated soil waste as fine aggregate in fly ash based geopolymer mortar. *Applied Clay Science* 146, pp. 81–91. ISSN: 0169-1317. DOI: [10.1016/J.CLAY.2017.05.038](https://doi.org/10.1016/J.CLAY.2017.05.038).
- Rahimzadeh, A., Sher, W., Davis, P., & Tang, W. (Jan. 2018). Management of Excavated Material in Infrastructure Construction-A Critical Review of Literature. *Conference: International Conference on Architecture and Civil Engineering*. Sydney, Australia.
- Rehbock-Sander, M. & Jesel, T. (2018). Fault induced rock bursts and micro-tremors – Experiences from the Gotthard Base Tunnel. *Tunnelling and Underground Space Technology* 81.October 2017, pp. 358–366. ISSN: 08867798. DOI: [10.1016/j.tust.2018.07.003](https://doi.org/10.1016/j.tust.2018.07.003).
- Reid, A., Gottlieb, P., Macdonald, K. J., & Miller, P. (Jan. 1984). QEM*SEM Image Analysis of Ore Minerals: Volume Fraction, Liberation and Observational Variances, pp. 191–204.
- Rémy, J. & Orsini, L. (1976). Utilisation du chlorure de cobalthexamine pour la détermination simultanée de la capacité d'échange et des bases échangeables dans les sols. *Sciences de Sol* 4, pp. 269–275.
- Renli, L., Helstrup, O. A., Ke, G., & Thompson, N. (2019). Fast 4D geomechanical modeling with multiple applications. *Society of Petroleum Engineers - SPE Norway One Day Seminar 2019*, SPE-195606–MS. DOI: [10.2118/195606-ms](https://doi.org/10.2118/195606-ms).
- Resch, D., Lassnig, K., Galler, R., & Ebner, F. (2009). Tunnel excavation material - high value raw material. *Geomechanik und Tunnelbau* 2.5, pp. 612–618. ISSN: 18657362. DOI: [10.1002/geot.200900047](https://doi.org/10.1002/geot.200900047).
- Revil, A. & Leroy, P. (2004). Constitutive equations for ionic transport in porous shales. *Journal of Geophysical Research* 109.B3, B03208. DOI: [10.1029/2003JB002755](https://doi.org/10.1029/2003JB002755).
- Rios, F. C. (Aug. 2018). Beyond Recycling: Design for Disassembly, Reuse, and Circular Economy in the Built Environment. PhD thesis.
- Ritter, H. L. & Drake, L. C. (Dec. 1945). Pressure Porosimeter and Determination of Complete Macropore-Size Distributions. *Industrial & Engineering Chemistry*

- Analytical Edition* 17.12, pp. 782–786. ISSN: 0096-4484. DOI: [10.1021/i560148a013](https://doi.org/10.1021/i560148a013).
- Ritter, S., Einstein, H., & Galler, R. (Jan. 2013). Planning the handling of tunnel excavation material – A process of decision making under uncertainty. *Tunnelling and Underground Space Technology* 33, pp. 193–201. DOI: [10.1016/j.tust.2012.08.009](https://doi.org/10.1016/j.tust.2012.08.009).
- Ritzén, S. & Sandström, G. Ö. (Jan. 2017). Barriers to the Circular Economy – Integration of Perspectives and Domains. *Procedia CIRP* 64, pp. 7–12. ISSN: 2212-8271. DOI: [10.1016/J.PROCIR.2017.03.005](https://doi.org/10.1016/J.PROCIR.2017.03.005).
- Robben, C. & Wotruba, H. (Aug. 2019). Sensor-Based Ore Sorting Technology in Mining—Past, Present and Future. *Minerals* 9, p. 523. DOI: [10.3390/min9090523](https://doi.org/10.3390/min9090523).
- Robertson, G., Sollins, P., Ellis, B., & Lajtha, K. (1999). Exchangeable Ions, pH, and Cation Exchange Capacity. *Standard Soil Methods for Long-Term Ecological Research*. Ed. by G. P. Robertson, D. C. Coleman, C. S. Bledsoe, & P. Sollins. Oxford University Press. Chap. Chapter 6, pp. 106–114.
- Rodríguez, G., Alegre, F. J., & Martínez, G. (May 2007). The contribution of environmental management systems to the management of construction and demolition waste: The case of the Autonomous Community of Madrid (Spain). *Resources, Conservation and Recycling* 50.3, pp. 334–349. ISSN: 0921-3449. DOI: [10.1016/J.RESCONREC.2006.06.008](https://doi.org/10.1016/J.RESCONREC.2006.06.008).
- Röhling, S., Eifert, H., & Jablinski, M. (2012). Betonbau - Band 1: Zusammensetzung, Dauerhaftigkeit, Frischbeton. Fraunhofer IRB Verlag, p. 446.
- Rolnick, L. S. (1954). The stability of gypsum and anhydrite in the geologic environment. PhD thesis. Massachusetts Institute of Technology (MIT), p. 156.
- Roman Alday, M., Kouzmanov, K., Harlaux, M., & Stefanova, E. (2018). Comparative study of XRF and portable XRF analysis and application in hydrothermal alteration geochemistry: The Elatsite porphyry Cu-Au-PGE deposit, Bulgaria. *16th Swiss Geoscience Meeting*, p. 2.
- Romero, M., Andrés, A., Alonso, R., Viguri, J., & Rincón, J. M. (2008). Sintering behaviour of ceramic bodies from contaminated marine sediments. *Ceramics International* 34.8, pp. 1917–1924. ISSN: 02728842. DOI: [10.1016/j.ceramint.2007.07.002](https://doi.org/10.1016/j.ceramint.2007.07.002).
- (2009). Phase evolution and microstructural characterization of sintered ceramic bodies from contaminated marine sediments. *Journal of the European Ceramic Society* 29.1, pp. 15–22. ISSN: 09552219. DOI: [10.1016/j.jeurceramsoc.2008.04.038](https://doi.org/10.1016/j.jeurceramsoc.2008.04.038).
- Rooney, C. P., McLaren, R. G., & Cresswell, R. J. (1999). Distribution and Phytoavailability of Lead in a Soil Contaminated with Lead Shot. *Water, Air, and Soil Pollution* 116.3, pp. 535–548. ISSN: 1573-2932. DOI: [10.1023/A:1005181303843](https://doi.org/10.1023/A:1005181303843).
- Rusillon, E. (2018). Characterisation and rock typing of deep geothermal reservoirs in the Greater Geneva Basin (Switzerland & France). PhD thesis. Université de Genève, p. 257. DOI: [10.13097/archive-ouverte/unige:105286](https://doi.org/10.13097/archive-ouverte/unige:105286).
- Sachsenhofer, R. F., Leitner, B., Linzer, H. G., Bechtel, A., Ćorić, S., Gratzner, R., Reischenbacher, D., & Soliman, A. (2010). Deposition, erosion and hydrocarbon source potential of the Oligocene Eggerding Formation (Molasse Basin, Austria). *Austrian Journal of Earth Sciences*. ISSN: 20727151.
- Salehin, S. (2017). Investigation into engineering parameters of marls from Seydoon dam in Iran. *Journal of Rock Mechanics and Geotechnical Engineering* 9.5, pp. 912–923. ISSN: 16747755. DOI: [10.1016/j.jrmge.2017.05.002](https://doi.org/10.1016/j.jrmge.2017.05.002).
- Salem, H. & Chilingarian, G. (1999). The Cementation Factor of Archie's Equation for Shaly Sandstone Reservoirs. *Journal of Petroleum Science and Engineering* 23, pp. 83–93. DOI: [10.1016/S0920-4105\(99](https://doi.org/10.1016/S0920-4105(99).
- Salisbury, J. (1993). Mid-infrared spectroscopy: Laboratory data. *Remote Geochemical Analysis: Elemental and Mineralogical Composition*. Ed. by C. Pieters & P. Englert. Cambridge University Press, pp. 79–98.
- Sauer, G. & Wuthier, R. (1988). Fourier Transform Infrared Characterization of Mineral Phases Formed during Induction of Mineralization by Collagenase-released Matrix Vesicles in Vitro. *Journal of Biological Chemistry* 263.27, pp. 13718–13724.
- Savage, G. M., Golueke, C. G., & Stein, E. L. v. (1994). Landfill mining: past and present. English.
- Sawhney, B. L. (1972). Selective Sorption and Fixation of Cations by Clay Minerals: A Review. *Clays and Clay Minerals* 20.2, pp. 93–100. ISSN: 1552-8367. DOI: [10.1346/CCMN.1972.0200208](https://doi.org/10.1346/CCMN.1972.0200208).

- Schegg, R. (1993). Thermal maturity and history of sediments in the North Alpine Foreland Basin (Switzerland, France). PhD thesis. Université de Genève, p. 193. DOI: [10.13097/archive-ouverte/unige:110443](https://doi.org/10.13097/archive-ouverte/unige:110443).
- Schegg, R. (1992). Coalification, shale diagenesis and thermal modelling in the Alpine Foreland basin: the Western Molasse basin (Switzerland/France). *Organic Geochemistry* 18.3, pp. 289–300. ISSN: 01466380. DOI: [10.1016/0146-6380\(92\)90070-E](https://doi.org/10.1016/0146-6380(92)90070-E).
- Schegg, R. & Leu, W. (1996). Clay mineral diagenesis and thermal history of the Thonex well, Western Swiss Molasse Basin. *Clays and Clay Minerals* 44.5, pp. 693–705.
- Șchiopu, A. M., Piuleac, G. C., Cojocaru, C., Apostol, I., Mămăligă, I., & Gavrilăscu, M. (2012). Reducing environmental risk of landfills: Leachate treatment by reverse Osmosis. *Environmental Engineering and Management Journal* 11.12, pp. 2319–2331. ISSN: 15829596. DOI: [10.30638/eemj.2012.286](https://doi.org/10.30638/eemj.2012.286).
- Schlumberger (2006). Oilfield technologies in space, sonic advances, acoustic waves and high-resolution core visualization. *Oilfield Review*, pp. 1–68. ISSN: 09231730.
- (2021). Schlumberger oilfield glossary - edition 2021.
- Schlunegger, F. (1999). Controls of surface erosion on the evolution of the Alps: Constraints from the stratigraphies of the adjacent foreland basins. *International Journal of Earth Sciences*. ISSN: 14373254. DOI: [10.1007/s005310050265](https://doi.org/10.1007/s005310050265).
- Schlunegger, F., Matter, A., Burbank, D. W., & Klaper, E. M. (1997). Magnetostratigraphic constraints on relationships between evolution of the central Swiss Molasse basin and Alpine orogenic events. *Bulletin of the Geological Society of America*. ISSN: 00167606. DOI: [10.1130/0016-7606\(1997\)109<0225:MCORBE>2.3.CO;2](https://doi.org/10.1130/0016-7606(1997)109<0225:MCORBE>2.3.CO;2).
- Schlunegger, F., Melzer, J., & Tucker, G. (2001). Climate, exposed source-rock lithologies, crustal uplift and surface erosion: a theoretical analysis calibrated with data from the Alps/North Alpine Foreland Basin system. *International Journal of Earth Sciences* 90.3, pp. 484–499. ISSN: 1437-3262. DOI: [10.1007/s005310100174](https://doi.org/10.1007/s005310100174).
- Schlunegger, F. & Castelltort, S. (2016). Immediate and delayed signal of slab breakoff in Oligo/Miocene Molasse deposits from the European Alps. *Scientific Reports* 6.August. ISSN: 20452322. DOI: [10.1038/srep31010](https://doi.org/10.1038/srep31010).
- Schlunegger, F. & Hinderer, M. (Dec. 2001). Crustal uplift in the Alps: why the drainage pattern matters. *Terra Nova* 13.6, pp. 425–432. ISSN: 0954-4879. DOI: [10.1046/j.1365-3121.2001.00374.x](https://doi.org/10.1046/j.1365-3121.2001.00374.x).
- Schlunegger, F. & Kissling, E. (2015). Slab rollback orogeny in the Alps and evolution of the Swiss Molasse basin. *Nature Communications* 6.1, p. 8605. ISSN: 2041-1723. DOI: [10.1038/ncomms9605](https://doi.org/10.1038/ncomms9605).
- Schlunegger, F. & Mosar, J. (2011). The last erosional stage of the Molasse Basin and the Alps. *International Journal of Earth Sciences* 100.5, pp. 1147–1162. ISSN: 14373254. DOI: [10.1007/s00531-010-0607-1](https://doi.org/10.1007/s00531-010-0607-1).
- Schmid, S. M., Pfiffner, O.-A., Froitzheim, N., Schönborn, G., & Kissling, E. (Oct. 1996). Geophysical-geological transect and tectonic evolution of the Swiss-Italian Alp. *Tectonics* 15.5, pp. 1036–1064. ISSN: 02787407. DOI: [10.1029/96TC00433](https://doi.org/10.1029/96TC00433).
- Schön, J. H. (2015). Physical Properties of Rocks - Fundamentals and Principles of Petrophysics. Ed. by J. Cubitt & H. Wales. 2nd editio. Leoben: Elsevier B.V., p. 59. ISBN: 978-0-08-100404-3.
- Schopper, H. F. (2009). LEP: the lord of the collider rings at CERN 1980-2000: the making, operation and legacy of the world's largest scientific instrument. English. Berlin: Springer. ISBN: 978-3-540-89300-4.
- Schroeder, P. (2002). Infrared spectroscopy in clay science. *Teaching clay science* 11.January 2002, pp. 181–206.
- Schulz, H. M., Sachsenhofer, R. F., Bechtel, A., Polesny, H., & Wagner, L. (June 2002). The origin of hydrocarbon source rocks in the Austrian Molasse Basin (Eocene-Oligocene transition). *Marine and Petroleum Geology* 19.6, pp. 683–709. ISSN: 02648172. DOI: [10.1016/S0264-8172\(02\)00054-5](https://doi.org/10.1016/S0264-8172(02)00054-5).
- Schweizerischer Bundesrat (2015). Verordnung über die Vermeidung und die Entsorgung von Abfällen (Abfallverordnung, VVEA). 2015.April 2020, pp. 1–46.
- Scullion, J. (Feb. 2006). Remediating polluted soils. eng. *Die Naturwissenschaften* 93.2, pp. 51–65. ISSN: 0028-1042 (Print). DOI: [10.1007/s00114-005-0079-5](https://doi.org/10.1007/s00114-005-0079-5).
- Seed, H. B., Woodward, R. J., & Lundgren, R. (1964). Clay Mineralogical Aspects of the Atterberg Limits. *Journal of the Soil Mechanics and Foundations Division* 90.4, pp. 107–131. DOI: [10.1061/JSFEAQ.0000628](https://doi.org/10.1061/JSFEAQ.0000628).
- Shabani, A. & Zivar, D. (2020). Detailed analysis of the brine-rock interactions during low salinity water injection by a coupled geochemical-transport model. *Chemical Geology* 537, p. 119484. ISSN: 0009-2541. DOI: <https://doi.org/10.1016/j.chemgeo.2020.119484>.

- Shahi, M., Salehi, M. M., & Kamari, M. (2018). New correlation for estimation of cementation factor in Asmari carbonate rock reservoirs. *Egyptian Journal of Petroleum* 27.4, pp. 663–669. ISSN: 1110-0621. DOI: <https://doi.org/10.1016/j.ejpe.2017.10.002>.
- Silva, R. V., Brito, J., & Dhir, R. (Dec. 2016). Availability and processing of recycled aggregates within the construction and demolition supply chain: A review. *Journal of Cleaner Production* 143. DOI: [10.1016/j.jclepro.2016.12.070](https://doi.org/10.1016/j.jclepro.2016.12.070).
- Simion, I. M., Fortuna, M. E., Bonoli, A., & Gavrilescu, M. (2013). Comparing environmental impacts of natural inert and recycled construction and demolition waste processing using LCA. *Journal of Environmental Engineering and Landscape Management* 21.4, pp. 273–287. ISSN: 16486897. DOI: [10.3846/16486897.2013.852558](https://doi.org/10.3846/16486897.2013.852558).
- Simion, I. M., Ghinea, C., Maxineasa, S. G., Taranu, N., Bonoli, A., & Gavrilescu, M. (2013). Ecological footprint applied in the assessment of construction and demolition waste integrated management. *Environmental Engineering and Management Journal* 12.4, pp. 779–788. ISSN: 15829596. DOI: [10.30638/eemj.2013.097](https://doi.org/10.30638/eemj.2013.097).
- Sinclair, H. D. & Allen, P. A. (Sept. 1992). Vertical versus horizontal motions in the Alpine orogenic wedge: stratigraphic response in the foreland basin. *Basin Research* 4.3-4, pp. 215–232. ISSN: 0950-091X. DOI: [10.1111/j.1365-2117.1992.tb00046.x](https://doi.org/10.1111/j.1365-2117.1992.tb00046.x).
- Sinclair, H. D., Coakley, B. J., Allen, P. A., & Watts, A. B. (June 1991). Simulation of Foreland Basin Stratigraphy using a diffusion model of mountain belt uplift and erosion: An example from the central Alps, Switzerland. *Tectonics* 10.3, pp. 599–620. ISSN: 0278-7407. DOI: [10.1029/90TC02507](https://doi.org/10.1029/90TC02507).
- Singh, B. & Goel, R. (1999). Rock Mass Classification - A practical approach in Civil Engineering. Elsevier Ltd., p. 267. ISBN: 978-0-08-043013-3. DOI: [10.1016/B978-0-08-043013-3.X5000-7](https://doi.org/10.1016/B978-0-08-043013-3.X5000-7).
- Skuk, S. & Schierl, H. (2017). Brenner Base Tunnel: First results of the exploratory tunnels from a geological and geomechanical point of view: Case studies of four fault zones. *Geomechanik und Tunnelbau* 10.3, pp. 275–290. ISSN: 18657389. DOI: [10.1002/geot.201700012](https://doi.org/10.1002/geot.201700012).
- Solbakk, T. (2020). Different aspects of detecting karst with geophysical methods – Tales from the underworld. PhD thesis. Norwegian University of Science and Technology NTNU. ISBN: 9788247194669.
- Sommaruga, A. (1997). Geology of the Central Jura and the Molasse Basin: new insight into an evaporite-based foreland fold and thrust belt. PhD thesis. Université de Neuchâtel, p. 176.
- (1999). Décollement tectonics in the Jura foreland fold-and-thrust belt. *Marine and Petroleum Geology*. ISSN: 02648172. DOI: [10.1016/S0264-8172\(98\)00068-3](https://doi.org/10.1016/S0264-8172(98)00068-3).
- (2011). From the central Jura Mountains to the Molasse Basin (France and Switzerland). *Bulletin für Angewandte Geologie* 16.2, pp. 63–75. ISSN: 14206846. DOI: [10.5169/seals-327746](https://doi.org/10.5169/seals-327746).
- Sommaruga, A., Eichenberger, U., & Marillier, F. (2012). Seismic Atlas of the Molasse Basin. *Beiträge zur Geologie der Schweiz - Geophysik*, 64 pp. DOI: [PNR61](https://doi.org/10.2590/14206846).
- Sommaruga, A., Mosar, J., Schori, M., & Gruber, M. (2017). The Role of the Triassic Evaporites Underneath the North Alpine Foreland. *Permo-Triassic Salt Provinces of Europe, North Africa and the Atlantic Margins*. DOI: [10.1016/b978-0-12-809417-4.00021-5](https://doi.org/10.1016/b978-0-12-809417-4.00021-5).
- Sparks, D. L., Page, A. L., Helmke, P. A., Loeppert, R. H., Soltanpour, P. N., Tabatabai, M. A., Johnston, C. T., & Sumner, M. E., eds. (1996). Methods of Soil Analysis Part 3 - Chemical Methods. SSSA Book Series 5. Soil Science Society of America, p. 1424. ISBN: 9780891188254. DOI: [10.2136/sssabookser5.3](https://doi.org/10.2136/sssabookser5.3).
- Spiegel, C., Kuhlemann, J., Dunkl, I., & Frisch, W. (2001). Paleogeography and catchment evolution in a mobile orogenic belt: The Central Alps in Oligo-Miocene times. *Tectonophysics*. ISSN: 00401951. DOI: [10.1016/S0040-1951\(01\)00187-1](https://doi.org/10.1016/S0040-1951(01)00187-1).
- Spooner, P. (2014). Lifting the Fog of Confusion Surrounding Clay and Shale in Petrophysics. *SPWLA 55th Annual Logging Symposium, May 18-22*, pp. 1–14.
- Stanley, C. (2017). Molar Element Ratio Analysis of Litho-geochemical Data: A Toolbox for Use in Mineral Exploration and Mining. *Geochemistry: Exploration, Environment, Analysis* 20.2, p. 233. DOI: [10.1144/geochem2019-033](https://doi.org/10.1144/geochem2019-033).
- Stauble, M. & Pfiffner, O.-A. (1991). Processing, interpretation and modeling of seismic reflection data in the Molasse Basin of eastern Switzerland. *Eclogae Geologicae Helveticae*. DOI: [10.5169/seals-166767](https://doi.org/10.5169/seals-166767).
- Stefansky, W. (1972). Rejecting Outliers in Factorial Designs. *Technometrics* 14.2, pp. 469–479. ISSN: 15372723. DOI: [10.1080/00401706.1972.10488930](https://doi.org/10.1080/00401706.1972.10488930).

- Steiner, W. (1993). Swelling rock in tunnels: Rock characterization, effect of horizontal stresses and construction procedures. *International Journal of Rock Mechanics and Mining Sciences and* 30.4, pp. 361–380. ISSN: 01489062. DOI: [10.1016/0148-9062\(93\)91720-4](https://doi.org/10.1016/0148-9062(93)91720-4).
- Strasser, A., Charollais, J., Conrad, M. A., Clavel, B., Pictet, A., & Mastrangelo, B. (2016). The Cretaceous of the Swiss Jura Mountains: an improved lithostratigraphic scheme. *Swiss Journal of Geosciences* 109.2, pp. 201–220. ISSN: 16618734. DOI: [10.1007/s00015-016-0215-6](https://doi.org/10.1007/s00015-016-0215-6).
- Strunck, P. & Matter, A. (Jan. 2002). Depositional evolution of the western Swiss molasse. *Eclogae Geol. Helv.* 95, pp. 197–222.
- Su, M., Liu, Y., Xue, Y., Cheng, K., Ning, Z., Li, G., & Zhang, K. (2021). Detection method of karst features around tunnel construction by multi-resistivity data-fusion pseudo-3D-imaging based on the PCA approach. *Engineering Geology* 288.March. ISSN: 00137952. DOI: [10.1016/j.enggeo.2021.106127](https://doi.org/10.1016/j.enggeo.2021.106127).
- Sumner, M. E. & Miller, W. P. (1996). Cation Exchange Capacity and Exchange Coefficients. *Methods of Soil Analysis*. John Wiley & Sons, Ltd. Chap. 40, pp. 1201–1229. ISBN: 9780891188667. DOI: <https://doi.org/10.2136/sssabookser5.3.c40>.
- Swanson, B. F. (1979). Visualizing Pores and Nonwetting Phase in Porous Rock. *Journal of Petroleum Technology* 31.1, pp. 10–18. ISSN: 01492136. DOI: [10.2118/6857-PA](https://doi.org/10.2118/6857-PA).
- Tang, W., Liu, X.-P., Hu, X.-X., Zhang, X.-L., & Wang, S.-X. (2013). The Correlation of Neutron and Density Logs and its Application in Tight Gas Reservoirs Identification. *SPE Unconventional Gas Conference and Exhibition, January 2013*. Muscat. DOI: [10.2118/163951-MS](https://doi.org/10.2118/163951-MS).
- Tanikawa, W. & Shimamoto, T. (2006). Klinkenberg effect for gas permeability and its comparison to water permeability for porous sedimentary rocks. *Hydrology and Earth System Sciences Discussions* 3, pp. 1315–1338. ISSN: 1027-5606. DOI: [10.5194/hessd-3-1315-2006](https://doi.org/10.5194/hessd-3-1315-2006).
- Teuscher, P., Thalmann, C., Fetzner, A., & Carron, C. (Jan. 2007). Alpenquerende Tunnel: Materialbewirtschaftung und Betontechnologie beim Lötschberg-Basistunnel. *Beton- und Stahlbetonbau* 102.1, pp. 2–10. ISSN: 0005-9900. DOI: [10.1002/best.200600526](https://doi.org/10.1002/best.200600526).
- Thalmann-Suter, C. N. (2015). Concrete aggregate production with TBM muck explained on the alptransit tunnel projects. *Utilizing Ready Mix Concrete and Mortar*, pp. 131–144. DOI: [10.1680/urcam.28234.0013](https://doi.org/10.1680/urcam.28234.0013).
- Thalmann, C., Schindler, C., Kruse, M., & Basler, E. (2003). Aggregates for High Quality Concrete and Shotcrete Made Out of Excavated Rock Material – Experiences Gained on the Alptransit Tunnel Projects. *Proceedings of Industrial Minerals and Buildings Stones Figure 1*, pp. 1–12.
- Thalmann, C. (1996). Beurteilung und Möglichkeiten der Wiederverwertung von Ausbruchmaterial aus dem maschinellen Tunnelvortrieb zu Betonzuschlagstoffen. PhD thesis. PhD thesis, Eidgenössische Technische Hochschule (ETH), Zurich, p. 115.
- The Nobel Prize Committee (2013). The Nobel Prize in Physics 2013 for the theoretical discovery of a mechanism that contributes to our understanding of the origin of mass of subatomic particles, and which recently was confirmed through the discovery of the predicted fundamental particle.
- Thewes, M. (1999). Adhäsion von Tonböden beim Tunnelvortrieb mit Flüssigkeitsschilden / Adhesion of Clays During Tunnelling with Slurry Shields. PhD thesis. Vol. 21.: Berichte aus Bodenmechanik und Grundbau der Bergischen University Wuppertal.
- Thewes, M. & Hollmann, F. (2016). Assessment of clay soils and clay-rich rock for clogging of TBMs. *Tunnelling and Underground Space Technology* 57, pp. 122–128. ISSN: 08867798. DOI: [10.1016/j.tust.2016.01.010](https://doi.org/10.1016/j.tust.2016.01.010).
- Thouvenot, F., Frechet, J., Tapponnier, P., Thomas, J. C., Le Brun, B., Menard, G., Lacassin, R., Jenatton, L., Grasso, J. R., Coutant, O., Paul, A., & Hatzfeld, D. (1998). The M(L) 5.3 Epagny (French Alps) earthquake of 1996 July 15: A long-awaited event on the Vuache Fault. *Geophysical Journal International*. ISSN: 0956540X. DOI: [10.1046/j.1365-246X.1998.00662.x](https://doi.org/10.1046/j.1365-246X.1998.00662.x).
- Thuro, K. & Plinninger, R. (2001). Scale effects in rock strength properties. Part 2. Point load test and point load strength index. *ISRM Regional Symposium Eurock 2001, June 3-7, 2001*. Espoo, pp. 175–180. ISBN: 90-2651-821-8.
- Thuro, K., Singer, J., Käsling, H., & Bauer, M. (2007). Determining abrasivity with the LCPC test. *1st Canada - U.S. Rock Mechanics Symposium, May 2007*. Vancouver, pp. 827–834. ISBN: 0415444012.
- Tittman, J. (1987). Geophysical well logging. Orlando, FL: Academic Press. ISBN: 9780323160551.

- Tokgöz, N. (Feb. 2013). Use of TBM excavated materials as rock filling material in an abandoned quarry pit designed for water storage. *Engineering Geology* 153, pp. 152–162. ISSN: 0013-7952. DOI: [10.1016/J.ENGGE0.2012.11.007](https://doi.org/10.1016/J.ENGGE0.2012.11.007).
- Tributh, H. & Lagaly, G. (1986). Aufbereitung und Identifizierung von Boden- und Lagerstättentonen. *GIT Fachz. Lab* 30, pp. 524–529.
- Trümpy, R. (1973). The timing of orogenic events in the Central Alps. *Gravity and Tectonics*. Ed. by K. DeJong & R. Scholten. London: Wiley, pp. 229–251.
- Trümpy, R. & Schweizerische Geologische Kommission (1980). *Geology of Switzerland - a guide-book. Part B: Geological excursions*. Basel; New York: Wepf & Co., p. 334. ISBN: 9783859770621.
- Turgut, P. & Murat Algin, H. (2007). Limestone dust and wood sawdust as brick material. *Building and Environment* 42.9, pp. 3399–3403. ISSN: 03601323. DOI: [10.1016/j.buildenv.2006.08.012](https://doi.org/10.1016/j.buildenv.2006.08.012).
- Ulery, A. & Drees, L., eds. (2008). *Methods of Soil Analysis Part 5 - Mineralogical methods*. SSSA Book Series 5. Soil Science Society of America, p. 521. ISBN: 9780891188469. DOI: [10.2136/sssabookser5.5](https://doi.org/10.2136/sssabookser5.5).
- Ulusay, R., ed. (2015). *The ISRM Suggested Methods for Rock Characterization, Testing and Monitoring: 2007-2014*. Springer, Cham. ISBN: 978-3-319-36132-1. DOI: [10.1007/978-3-319-07713-0](https://doi.org/10.1007/978-3-319-07713-0).
- Valantin, A. (1974). Examen des differents procedes classiques de determination de la nocivite des roches vis-à-vis de l'abattage mecanique. *Industr. Miner.* 3, pp. 133–140.
- Van der Marel, H. & Beutelspacher, H. (1976). *Atlas of Infrared Spectroscopy of Clay Minerals and their Admixtures*. Amsterdam: Elsevier, 396 pp. DOI: [10.1180/claymin.1977.012.3.11](https://doi.org/10.1180/claymin.1977.012.3.11).
- Van der Vegt, P., Janszen, A., & Moscariello, A. (2012). Tunnel valleys: current knowledge and future perspectives. *Glaciogenic reservoirs and hydrocarbon systems*. Ed. by M. Huuse, J. Redfern, D. Le Heron, R. Dixon, A. Moscariello, & J. Craig. *Geol Soc Spec Publ*, pp. 75–97.
- Vázquez, E. (2013). Overview Regarding Construction and Demolition Waste in Several Countries. *Progress of Recycling in the Built Environment: Final report of the RILEM Technical Committee 217-PRE*. Ed. by E. Vázquez. Dordrecht: Springer Netherlands, pp. 37–173. ISBN: 978-94-007-4908-5. DOI: [10.1007/978-94-007-4908-5_{_}3](https://doi.org/10.1007/978-94-007-4908-5_{_}3).
- Velis, C. A. & Brunner, P. H. (2013). Recycling and resource efficiency: It is time for a change from quantity to quality. *Waste Management and Research* 31.6, pp. 539–540. ISSN: 10963669. DOI: [10.1177/0734242X13489782](https://doi.org/10.1177/0734242X13489782).
- Vernet, J.-P. (1958). Études sédimentologiques et pétrographiques des Formations Tertiaires et Quaternaires de la partie occidentale du Plateau Suisse. *Eclogae Geol. Helv.* 51.3, pp. 1115–1152.
- Vieira, C. S. & Pereira, P. M. (Oct. 2015). Use of recycled construction and demolition materials in geotechnical applications: A review. *Resources Conservation and Recycling* 103, pp. 192–204. ISSN: 18790658. DOI: [10.1016/j.resconrec.2015.07.023](https://doi.org/10.1016/j.resconrec.2015.07.023).
- Voiron, J., Haas, M., & Amiot, J.-B. (2020). CERN HL-LHC POINT 1, Gestion des matériaux d'excavation potentiellement pollués aux hydrocarbures. *AFTES congress Paris 2020, September 6-8, 2021*.
- Voit, K. & Zimmermann, T. (2015). Characteristics of selected concrete with tunnel excavation material. DOI: [10.1016/j.conbuildmat.2015.10.016](https://doi.org/10.1016/j.conbuildmat.2015.10.016).
- Voit, K. (2013). *Einsatz und Optimierung von Tunnelausbruchmaterial des Brenner Basistunnels*, PhD thesis. Ed. by W. Universität für Bodenkultur. Verlag Guthmann-Peterson, p. 320. ISBN: 978-3-900782-78-8.
- Voit, K. & Kuschel, E. (2020). Rock material recycling in tunnel engineering. *Applied Sciences (Switzerland)* 10.8. ISSN: 20763417. DOI: [10.3390/APP10082722](https://doi.org/10.3390/APP10082722).
- Vollprecht, D., Sattler, T. M., Doschek-Held, K., Galler, R., Schimek, J., Kasper, T., Daul, J., & Pomberger, R. (2019). Innovative Deponierung sowie Recycling von Mineralwolleabfällen im Bergversatz, in der Zementindustrie und in der Mineralwolleindustrie – das Projekt RecyMin. *Berliner Konferenz Mineralische Nebenprodukte und Abfälle*. Vol. 6, p. 480. ISBN: 978-3-944310-47-3.
- Von Hagke, C., Cederbom, C. E., Oncken, O., Steckli, D. F., Rahn, M. K., & Schlunegger, F. (2012). Linking the northern Alps with their foreland: The latest exhumation history resolved by low-temperature thermochronology. *Tectonics*. ISSN: 02787407. DOI: [10.1029/2011TC003078](https://doi.org/10.1029/2011TC003078).
- Vrakas, A. & Anagnostou, G. (2016). Ground Response to Tunnel Re-profiling Under Heavily Squeezing Conditions. *Rock Mechanics and Rock Engineering* 49.7,

- pp. 2753–2762. ISSN: 07232632. DOI: [10.1007/s00603-016-0931-2](https://doi.org/10.1007/s00603-016-0931-2).
- Wangersky, P. J. (1993). Dissolved organic carbon methods: a critical review. *Marine Chemistry* 41.1, pp. 61–74. ISSN: 0304-4203. DOI: [https://doi.org/10.1016/0304-4203\(93\)90106-X](https://doi.org/10.1016/0304-4203(93)90106-X).
- Wanninger-Huber, T. (2019). Experimental investigations for the modelling of anhydritic swelling claystones. PhD thesis. ETH Zurich. DOI: [10.3929/ethz-b-000369625](https://doi.org/10.3929/ethz-b-000369625).
- Washburn, E. W. (1921). The Dynamics of Capillary Flow. *Phys. Rev.* 17.3, pp. 273–283. DOI: [10.1103/PhysRev.17.273](https://doi.org/10.1103/PhysRev.17.273).
- Wasti, Y. & Bezirci, M. H. (May 1986). Determination of the consistency limits of soils by the fall cone test. *Canadian Geotechnical Journal* 23.2, pp. 241–246. ISSN: 0008-3674. DOI: [10.1139/t86-033](https://doi.org/10.1139/t86-033).
- Waxman, M. & Smits, L. (1968). Electrical conductivities in oil-bearing shaly sands. *SPE Journal* 8.02, pp. 107–122. DOI: [10.2118/1863-A](https://doi.org/10.2118/1863-A).
- Wegmüller, S., Amberger, G., & Vernet, J.-P. (1995). La formation de Montfleury près de Genève: Etude palynologique et sédimentologique d'une séquence du Pleistocène moyen. *Eclogae Geologicae Helvetiae* 88.3, pp. 595–614. DOI: [10.5169/seals-167689](https://doi.org/10.5169/seals-167689).
- Wehner, H., Hufnagel, H., Kuckelkorn, K., Schoell, M., & Teschner, M. (1983). On the genesis of hydrocarbons in the German Alpine foreland.
- Wenighofer, R. & Galler, R. (2017). Digitale Ortsbrustbilder mittels Kamerabefahrung eines TBM-Bohrkopfs Digital Imaging of the Tunnel Face Through the Cutter Head Using Cameras. *BHM Berg- und Hüttenmännische Monatshefte* 162.12, pp. 568–572. ISSN: 0005-8912. DOI: [10.1007/s00501-017-0684-6](https://doi.org/10.1007/s00501-017-0684-6).
- Wetzel, A., Allenbach, R., & Allia, V. (2003). Reactivated basement structures affecting the sedimentary facies in a tectonically “quiescent” epicontinental basin: An example from NW Switzerland. *Sedimentary Geology*. ISSN: 00370738. DOI: [10.1016/S0037-0738\(02\)00230-0](https://doi.org/10.1016/S0037-0738(02)00230-0).
- Whitaker, S. (1986). Flow in porous media I: A theoretical derivation of Darcy's law. *Transport in Porous Media* 1, pp. 3–25. DOI: [10.1007/BF01036523](https://doi.org/10.1007/BF01036523).
- White, W. (1949). Atterberg plastic limits of clay minerals. *American Mineralogist* 34.7-8, pp. 508–512. ISSN: 0003-004X.
- Wildi, W. (1997). Le site naturel de Genève. *Les monuments d'art et d'histoire du Canton de Genève. Tome 1: La Genève sur l'eau*. Ed. by P. Broillet. Basel. ISBN: 3-909164-61-7.
- Wildi, W., Corboud, P., & Gorin, G. (2017). Guide : géologie et archéologie de Genève Guidebook : geology and archaeology of Geneva. *Société de physique et d'histoire naturelle de Genève*, p. 93.
- Willett, S. D. & Schlunegger, F. (2010). The last phase of deposition in the Swiss Molasse Basin: From foredeep to negative-alpha basin. *Basin Research* 22.5, pp. 623–639. ISSN: 0950091X. DOI: [10.1111/j.1365-2117.2009.00435.x](https://doi.org/10.1111/j.1365-2117.2009.00435.x).
- Williams, N. & Davidson, G. (2004). Possible submarine advanced argillic alteration at the Basin Lake prospect, Western Tasmania, Australia. *Economic Geology* 99.5, pp. 987–1002. DOI: [10.2113/99.5.987](https://doi.org/10.2113/99.5.987).
- Wimmer-Frey, I. & Schwaighofer, B. (2002). Österreichische Ziegelrohstoffe. *DTTG Deutsche Ton- und Tonmineralgruppe e.V.* Ed. by F. Ottner & S. Gier, pp. 257–268.
- Winkler-Hermaden, A. (1958). Geologisches Kräftespiel und Landformung. *GFF*. ISSN: 20000863. DOI: [10.1080/11035895809447260](https://doi.org/10.1080/11035895809447260).
- Wothke, W. (1993). Nonpositive definite matrices in structural modeling. *Testing structural equation models*. Ed. by K. Bollen & J. Long. Newbury Park, CA: Sage, pp. 256–293.
- Wright, K. (1995). Evaluation of a New Field Test Kit for Determining Total Petroleum Hydrocarbon Concentrations in Soil at a Site Contaminated by Diesel Fuel. *AEHS Conference on Hydrocarbon Contaminated Soils, January 11-13*. New Orleans.
- Wright, K. & Jermstad, D. (1995). Evaluation of a Rapid Field Analytical Test Kit for Assessing Hydrocarbon Soil Contamination. *Third International Conference On-Site Analysis, January 22-25*. Houston, TX.
- Wu, L. & Qu, F.-z. (2009). Discrete element simulation of mechanical characteristic of conditioned sands in EPB shield tunneling. *J. Cent. South Univ. Technol.* 16, pp. 1028–1033. DOI: [10.1007/s11771](https://doi.org/10.1007/s11771).
- Wyllie, M. R. J., Gregory, A. R., & Gardner, L. W. (1956). Elastic wave velocities in heterogeneous and porous media. *Geophysics* 21.1, pp. 41–70. DOI: [10.1190/1.1438217](https://doi.org/10.1190/1.1438217).
- Yan, J. (2002). Reservoir parameters estimation from well log and core data: A case study from the North Sea.

- Petroleum Geoscience* 8.1, pp. 63–69. ISSN: 13540793. DOI: [10.1144/petgeo.8.1.63](https://doi.org/10.1144/petgeo.8.1.63).
- Yariv, S., Nasser, A., & Bar-on, P. (1990). Metachromasy in clay minerals spectroscopic study of the adsorption of crystal violet by laponite. *Journal of Chemical Society, Faraday Transactions* 86.9, pp. 1593–1598. DOI: [10.1039/FT9908601593](https://doi.org/10.1039/FT9908601593).
- Yilmaz, I. (2001). Gypsum/anhydrite: Some engineering problems. *Bulletin of Engineering Geology and the Environment* 60.3, pp. 227–230. ISSN: 14359529. DOI: [10.1007/s100640000071](https://doi.org/10.1007/s100640000071).
- Zabalza Bribián, I., Valero Capilla, A., & Aranda Usón, A. (2011). Life cycle assessment of building materials: Comparative analysis of energy and environmental impacts and evaluation of the eco-efficiency improvement potential. *Building and Environment* 46.5, pp. 1133–1140. ISSN: 0360-1323. DOI: <https://doi.org/10.1016/j.buildenv.2010.12.002>.
- Zhang, G., Germaine, J. T., Martin, R. T., & Whittle, A. J. (2003). A simple sample-mounting method for random powder X-ray diffraction. *Clays and Clay Minerals* 51.2, pp. 218–225. ISSN: 00098604. DOI: [10.1346/CCMN.2003.0510212](https://doi.org/10.1346/CCMN.2003.0510212).
- Zhang, L. (2013). Production of bricks from waste materials - A review. *Construction and Building Materials* 47, pp. 643–655. ISSN: 09500618. DOI: [10.1016/j.conbuildmat.2013.05.043](https://doi.org/10.1016/j.conbuildmat.2013.05.043).
- Zhang, N., Duan, H., Sun, P., Li, J., Zuo, J., Mao, R., Liu, G., & Niu, Y. (Mar. 2020). Characterizing the generation and environmental impacts of subway-related excavated soil and rock in China. *Journal of Cleaner Production* 248, p. 119242. ISSN: 0959-6526. DOI: [10.1016/J.JCLEPRO.2019.119242](https://doi.org/10.1016/J.JCLEPRO.2019.119242).
- Ziegler, H.-J. & Isler, A. (2013). Zusammenfassender geologischer Schlussbericht Lötschberg-Basistunnel. Wabern, Switzerland: Landesgeologie (Bundesamt für Landestopografie swisstopo), p. 93. ISBN: 9783302400853.
- Ziegler, P. (1990). Geological Atlas of Western and Central Europe. Geological Atlas of Western and Central Europe Band 1. Shell Internationale Petroleum Maatschappij B.V. ISBN: 9789066441255.
- Ziegler, P. & Fraefel, M. (May 2009). Response of drainage systems to Neogene evolution of the Jura fold-thrust belt and Upper Rhine Graben. *Swiss Journal of Geosciences* 102. DOI: [10.1007/s00015-009-1306-4](https://doi.org/10.1007/s00015-009-1306-4).
- Zoback, M. (2007). Reservoir Geomechanics. Cambridge University Press, p. 449. ISBN: 978-0-521-77069-9. DOI: [10.1017/CB09780511586477](https://doi.org/10.1017/CB09780511586477).
- Zou, Y., Zheng, C., & Sheikhi, S. (2021). Role of ion exchange in the brine-rock interaction systems: A detailed geochemical modeling study. *Chemical Geology* 559. November 2020, p. 119992. ISSN: 00092541. DOI: [10.1016/j.chemgeo.2020.119992](https://doi.org/10.1016/j.chemgeo.2020.119992).
- Zumsteg, R., Plötze, M., & Puzrin, A. (2013a). Reduction of the clogging potential of clays: New chemical applications and novel quantification approaches. *Bio- and Chemo- Mechanical Processes in Geotechnical Engineering - Geotechnique Symposium in Print 2013* 4, pp. 44–54. DOI: [10.1680/bcmgpe.60531.004](https://doi.org/10.1680/bcmgpe.60531.004).
- Zumsteg, R., Plötze, M., & Puzrin, A. M. (2012). Effect of Soil Conditioners on the Pressure and Rate-Dependent Shear Strength of Different Clays. *Journal of Geotechnical and Geoenvironmental Engineering* 138.9, pp. 1138–1146. ISSN: 1090-0241. DOI: [10.1061/\(asce\)gt.1943-5606.0000681](https://doi.org/10.1061/(asce)gt.1943-5606.0000681).
- (2013b). Effects of dispersing foams and polymers on the mechanical behaviour of clay pastes. *Géotechnique* 63.11, pp. 920–933. DOI: [10.1680/geot.12.P.044](https://doi.org/10.1680/geot.12.P.044).
- (2018). Leaching Characteristics of Chemicals from Conditioned Tunnel Muck. *Journal of Geotechnical and Geoenvironmental Engineering* 144.2, p. 06017016. ISSN: 1090-0241. DOI: [10.1061/\(asce\)gt.1943-5606.0001790](https://doi.org/10.1061/(asce)gt.1943-5606.0001790).
- Zumsteg, R. & Puzrin, A. M. (2012). Stickiness and adhesion of conditioned clay pastes. *Tunnelling and Underground Space Technology* 31, pp. 86–96. ISSN: 08867798. DOI: [10.1016/j.tust.2012.04.010](https://doi.org/10.1016/j.tust.2012.04.010).
- Zumsteg, R. & Langmaack, L. (2017). Mechanized Tunneling in Soft Soils: Choice of Excavation Mode and Application of Soil-Conditioning Additives in Glacial Deposits. *Engineering* 3.6, pp. 863–870. ISSN: 20958099. DOI: [10.1016/j.eng.2017.11.006](https://doi.org/10.1016/j.eng.2017.11.006).
- Zviagina, B. B., Drits, V. A., & Dorzhieva, O. V. (2020). Distinguishing features and identification criteria for K-dioctahedral 1M micas (Illite-aluminoceladonite and illite-glaucoune-celadonite series) from middle-infrared spectroscopy data. *Minerals* 10.2. ISSN: 2075163X. DOI: [10.3390/min10020153](https://doi.org/10.3390/min10020153).
- Zweigel, J., Aigner, T., & Luterbacher, H. (Jan. 1998). Eustatic versus tectonic controls on Alpine foreland basin fill: sequence stratigraphy and subsidence analysis in the

SE German Molasse. *Geological Society, London, Special Publications* 134.1, 299 LP –323. DOI: [10.1144/GSL.SP.1998.134.01.14](https://doi.org/10.1144/GSL.SP.1998.134.01.14).

Technical reports

- Agostini, C., Loo, Y., & ARUP (2016). Technical Note from 25 February 2016: Geological uncertainties investigation along FCC tunnel alignment (n° 216967-05). Tech. rep., pp. 1–4.
- Amberg Engineering (2015). FCC Risk Assessment - report 10G00049-FCC-01_v01, 02 November 2015. Tech. rep., pp. 1–42.
- Bureau Veritas (2015). SO-19, Internal Reference Material for Whole Rock Analysis (LF300-Si), Revision 2015.3. Tech. rep.
- (2018a). Dolomite-3 internal Reference Material for LOI determination, Revision 2018.1, May 16. Tech. rep.
 - (2018b). OREAS 45h, Ore Research & Exploration P/L, Lateritic Soil Litho geochem., Certified Reference Material, Document-No. COA-1343-OREAS45h-R2. Tech. rep.
 - (2019a). Metals, Minerals & Environmental, Schedule of Services & Fees. Tech. rep.
 - (2019b). OREAS 25A-4A, Reference Material for Multi Acid Digestion, Revision 2019.2. Tech. rep.
- Canzoneri, A., Amiot, J.-B., Rozemberg, F., Merlini, D., Gianelli, F., Como, G., De Salvo, F., Helou, C., Lopez, L., & Mattelaer, P. (2018). CERN (HL-LHC): New underground & surface structures at Point 1 & Point 5. Tech. rep., pp. 1–10.
- CEREMA (2020). Préfaisabilité géologique et géotechnique, Rapport d'étude FCC. Tech. rep., p. 10.
- CERN (1982). Étude d'impact du projet LEP sur l'environnement. Tech. rep., p. 174.
- (1989). CERN archives: document CERN/FC/3061. Tech. rep.
 - (2012). A Multi-TeV Linear Collider based on CLIC Technology: CLIC Conceptual Design Report. Ed. by M. Aicheler, P. Burrows, M. Draper, T. Garvey, P. Lebrun, K. Peach, N. Phinney, H. Schmickler, D. Schulte, & N. Toge, p. 841. ISBN: 978-92-9083-379-6.
 - (2014). FCC - Determination of the geological survey area. Tech. rep.
- Chablais, J. & Moscariello, A. (2012). Coretest Systems Inc., AP-608 Automated Permeameter-Porosimeter, Operator's Quick Manual, GE-RGBA Report 2012001. Tech. rep. University of Geneva.
- Chablais, J. & Rusillon, E. (2018). Fiche Forage - Géo-01. Tech. rep.
- Chablais, J. & Savoy, L. (2019). Géo-02 (SIG) - Litholog de forage - Litholog (LLR). Tech. rep.
- Coretest Systems Inc. (2008). Coretest Systems Inc., Grain Volume Measurement System, Operator's Manual, Supplement to Operator's Manual for AP-608 Automated Permeameter-Porosimeter. Tech. rep.
- (2011). AP-608 Automated Permeameter-Porosimeter, Operator's Manual, V6g1. Tech. rep.
- Doumer, P. & British Petrol (France) (1983a). Société Française des Pétroles BP - Rapport 16.1213 de fin de sondages: Gex-CD-01 (géologie). Tech. rep.
- (1983b). Société Française des Pétroles BP - Rapport 16.1214 de fin de sondages: Gex-CD-02 (géologie). Tech. rep.
 - (1983c). Société Française des Pétroles BP - Rapport 16.1215 de fin de sondages: Gex-CD-03 (géologie). Tech. rep.
 - (1983d). Société Française des Pétroles BP - Rapport 16.1216 de fin de sondages: Gex-CD-04 (géologie). Tech. rep.
 - (1983e). Société Française des Pétroles BP - Rapport 16.1217 de fin de sondages: Gex-CD-05 (géologie). Tech. rep.
 - (1983f). Société Française des Pétroles BP - Rapport 16.1218 de fin de sondages: Gex-CD-06 (géologie). Tech. rep.
 - (1983g). Société Française des Pétroles BP - Rapport 16.1219 de fin de sondages: Gex-CD-07 (géologie). Tech. rep.
- DRAGON (2014). DRAGON: Development of resource-efficient and advanced underground technologies. Tech. rep.
- Fachgruppe für Untertagebau (FGU) (2016). Bewirtschaftung und Wiederverwertung von Ausbruchmaterial - Inventar Schweizer Großprojekte. Ed. by P. Michel, F.

- Bertholet, M. Neuenschwander, & C. Carron. Esslingen: Fachgruppe für Untertagebau, p. 53.
- Geostats PTY LTD Mining Industry Consultants (2020a). Reference Material Manufacture and Sales, Certified Ore Grade Base Metal Reference Material, GBM309-15.
- (2020b). Reference Material Manufacture and Sales, Certified Pulp Graphite Reference Material, GGC-10.
 - (2020c). Reference Material Manufacture and Sales, Certified Sulphur and Carbon Reference Material, GS311-1.
 - (2020d). Reference Material Manufacture and Sales, Certified Sulphur and Carbon Reference Material, GS910-4.
- Géotechnique Appliquée Dériaz & SA (GADZ) (1981a). Obturation des forages L133, L134, L134 BIS. Tech. rep.
- (1981b). Sondage SPM1; Sondage SPM2 (includes SPM3 et SPM4); Sondages SPL 2.1 et 2.2; Sondage SPM5. Tech. rep.
 - (1982a). Sondage L135. Tech. rep.
 - (1982b). Sondage SPL7.2; Sondage SPL8.1; Sondage SPL8.2; Sondage SPL8.7; Sondages SPL8.5 et 8.8, Sondages SPL8.9 et 8.13; Sondages SPL 8.10 et 8.12; Sondages SPL 8.14 et 8.15; Sondage SPM11; Sondage SPM15; Sondage SPM16. Tech. rep.
 - (1992). Sondage de reconnaissance SPL1.02. Tech. rep.
 - (1993a). Projet LHC - Synthèse géologique et géotechnique. Tech. rep. Geneva, Switzerland.
 - (1993b). Projet LHC (SLHC12). Tech. rep.
 - (1996a). Projet LHC - LOT 1 (SLHC 20, SLHC 21, SLHC 22, SLHC 23, SLHC 24, SLHC 25). Tech. rep.
 - (1996b). Projet LHC - LOT 3 (SLHC10, SLHC11, SLHC 42, SLHC 43, SLHC 44, SLHC 49, SLHC 50). Tech. rep.
 - (1997). Statistique molasse (globale) - marnes standards, marnes altérées, marnes gruméleuses, marnes gréseuses, grès tendres, grès durs, grès très durs et marno-calcaires - synthèse LHC 1995-1997 (annexe 4g). Tech. rep.
 - (2015a). High Luminosity LHC Point 1 - Sondage C1, 7222.101. Tech. rep.
 - (2015b). High Luminosity LHC Point 1 - Sondage C2, 7222.102. Tech. rep.
 - (2015c). High Luminosity LHC Point 1 - Sondage C3, 7222.103. Tech. rep.
 - (2015d). High Luminosity LHC Point 1 - Sondage C4, 7222.104. Tech. rep.
 - (2016a). High Luminosity LHC Point 1 - Sondage C5, 7222.105. Tech. rep.
 - (2016b). High Luminosity LHC Point 1 - Sondage C6, 7222.106. Tech. rep.
 - (2016c). High Luminosity LHC Point 1 - Sondage C7, 7222.107. Tech. rep.
- Haas, M., De Haller, A., Le Cottonnec, A., & Moscardiello, A. (Apr. 2021a). A large-scale geochemical and petrophysical data set measured across the Geneva Basin as part of CERN's FCCIS Mining-The-Future competition. DOI: [10.5281/zenodo.4725558](https://doi.org/10.5281/zenodo.4725558).
- (2021b). Description of laboratory analyses performed at Université de Genève (UNIGE) in Geneva, Switzerland. Tech. rep. DOI: [10.5281/zenodo.4727054](https://doi.org/10.5281/zenodo.4727054).
- Haas, M., Gegenhuber, N., & Galler, R. (2021). Description of laboratory analyses performed at Montanuniversität Leoben (MUL) in Leoben, Austria. Tech. rep. DOI: [10.5281/zenodo.4727074](https://doi.org/10.5281/zenodo.4727074).
- Haas, M., Krainz, J., Villeneuve, M., Gegenhuber, N., & Galler, R. (Apr. 2021). A large-scale geomechanical and petrophysical data set measured across the Geneva Basin as part of CERN's FCCIS Mining-The-Future competition. DOI: [10.5281/ZENODO.4725585](https://doi.org/10.5281/ZENODO.4725585).
- Haas, M. & Plötze, M. (Apr. 2021a). A large-scale geochemical, mineralogical and clay analyses data set measured across the Geneva Basin as part of CERN's FCCIS Mining-The-Future competition. DOI: [10.5281/zenodo.4725517](https://doi.org/10.5281/zenodo.4725517).
- (2021b). Description of laboratory analyses performed at the Swiss Federal Institute of Technology (ETH) in Zurich, Switzerland. Tech. rep., pp. 1–15. DOI: [10.5281/zenodo.4727039](https://doi.org/10.5281/zenodo.4727039).
- Hach Lange GmbH (2021). Hach LCK Cuvette Test System, Reference Guide. Tech. rep.
- Lanterno, E., Kunzle, A., Gervaise, J., & Bruderlein, J. (1981). Projet LEP - Sondages de reconnaissance: CERN SPS-SU-81-2. Tech. rep.
- Leco (2007). Leco CS230 Carbon/Sulfur Series, Technical Data Sheet, R2.511-REV1. Tech. rep.
- Lee, W., Houchin, C., & Albergo, N. (1993). TRPH Discrimination of Petroleum and Non-petroleum Organic Materials. Tech. rep.
- Lunardi, P. (2008). Design and Construction of Tunnels: analysis of controlled deformation in rocks and soils (ADECO-RS). Berlin: Springer Berlin Heidelberg. ISBN: 9783540738756. DOI: [10.1007/978-3-540-73875-6](https://doi.org/10.1007/978-3-540-73875-6).
- Lunardi, P., Cassani, G., & Bindi, R. (2007). From the Adeco-RS Approach to the Tunneling Industrialisation.

- Madinier, B., Voiron, J., & Amiot, J.-B. (2017). High-Luminosity LHC Project: Geotechnical Baseline Report. Tech. rep., p. 59.
- Mathieux, F., Ardente, F., Bobba, S., Nuss, P., Blengini, G. A., Dias, P. A., Blagoeva, D., Torres De Matos, C., Wittmer, D., Pavel, C., Hamor, T., Saveyn, H., Gawlik, B., Orveillon, G., Huygens, D., Garbarino, E., Tzimas, E., Bouraoui, F., & Solar, S. (2017). Critical Raw Materials and the Circular Economy. Background report. December. ISBN: 9789279742828. DOI: [10.2760/378123](https://doi.org/10.2760/378123).
- ORIGIN (2020). High-Luminosity Large Hadron Collider (HL-LHC) Report: Spoil classification record. Tech. rep.
- Perkin Elmer SCIEX Instruments (2020). ELAN 9000 ICP-MS, Optimized for routine Ultra-trace Analysis, Technical Data Sheet. Tech. rep.
- POROTEC GmbH (now Microtrac) (2021). Bedienungsanleitung Porosimeter Pascal-140/240/440. Tech. rep.
- Quorum Technologies (n.d.). Quorum Technologies Q150T S/E/ES Sample Preparation System, Instruction Manual.
- Services Industriels de Genève (SIG) (2019). Projet Géothermie 2020 - Sondage de Satigny - Géo-1-DAS. *Well report Géo-01-DAS*.
- Setec-Lerm (2020). Study report: Survey of regional opportunities for the management of FCC spoil - accompanying guidance note, CERN report n° 48393.001.01.A. Tech. rep., p. 19.
- Spectro Ciros Vision (2004). High-Performance second-generation ICP-OES-CCD spectrometer, Technical Data Sheet. Tech. rep.
- USEPA (1992). SW846 Method 3550A ultrasonic Extraction, Revision 1, November 1992. Tech. rep.
- Varley, P., Lang, A., Guitton, C., & Package, L. C. E. C. S. (1996). Geological and Geotechnical Interpretive Review - Doc.Ref. S067-ST. Tech. rep.
- Vernus, E., Bonnet, J., Gonzalez, L., Roche, L., & Serpeau, J. (2017). Etude n°15-0159/1A: Gestion et réutilisation des matériaux excavés - comment favoriser l'économie circulaire?

Legislation, norms and guidelines

- American Society for Testing and Materials (ASTM) (1976). Standard Test Method for Laboratory Determination of Pulse Velocities and Ultrasonic Elastic Constants of Rock. <http://www.astm.org/cgi-bin/resolver.cgi?D2845-08>.
- Association française de normalisation (AFNOR) (2000). Gestein - Bestimmung der Schleifbarkeit für Gestein - Teil 1: Ritzprobe mittels Spitzhacke, NFP 94-430-1.
- (2013). P18-579:2013-02-09 Granulats - Détermination des coefficients d'abrasivité et de broyabilité.
 - (2018). EN 1097-2: Prüfverfahren für mechanische und physikalische Eigenschaften von Gesteinskörnungen - Teil 2: Verfahren zur Bestimmung des Widerstandes gegen Zertrümmerung; Deutsche und Englische Fassung prEN 1097-2:2018.
- Association Française des Tunnels Et De L'Espace Souterrain (AFTES) (2019). Recommendations of AFTES GT35RIA2: Management and use of excavated materials, p. 60. ISBN: 9782901148029.
- Bundesamt für Umwelt Wald und Landschaft (BUWAL) (1999). Richtlinie für die Verwertung, Behandlung und Ablagerung von Aushub-, Abraum- und Ausbruchmaterial (Aushubrichtlinie).
- Deutsches Institut für Normung (DIN) (1983). Deutsche Einheitsverfahren zur Wasser-, Abwasser- und Schlammmuntersuchung - Kationen (Gruppe E) - Bestimmung des Ammonium Stickstoffs (E5) - DIN 38406-5.
- (1987). Deutsche Einheitsverfahren zur Wasser-, Abwasser- und Schiammmuntersuchung Anionen (Gruppe D) - Photometrische Bestimmung von Chrom(VI) mittels 1,5-Diphenylcarbazid (D 24) - DIN 38405-24.
 - (1998). Untersuchung von Bodenproben - Wassergehalt - Teil 1: Bestimmung durch Ofentrocknung - DIN 18121-1.
 - (2012). Soil, testing procedures and testing equipment - Determination of water absorption - DIN 18132.
 - (2014). Bestimmung der spezifischen Oberfläche von Festkörpern mittels Gasadsorption - BET-Verfahren (ISO 9277:2010).
 - (2019). Evaluation of pore size distribution and porosity of solid materials by mercury porosimetry and gas adsorption - Part 1: Mercury porosimetry (ISO 15901-1:2016).
- European Commission (2005). Trans-European Transport Network - TEN-T priority axes and projects.
- (2008a). Directive 2008/98/EC on waste (Waste Framework Directive). <https://ec.europa.eu/environment/waste/framework/>.
 - (2008b). Sustainable Consumption and Production and Sustainable Industrial Policy Action Plan.
 - (2010). Europe 2020 - A European strategy for smart, sustainable and inclusive growth.
 - (2011). Roadmap to a Resource Efficient Europe.
 - (2012). A stronger European industry for growth and economic recovery.
 - (2016a). EU Construction & Demolition Waste Management Protocol. *Official Journal of the European Union* June, pp. 1–22. ISSN: 20711050. DOI: [10.3390/su11133638](https://doi.org/10.3390/su11133638).
 - (2016b). Sustainable Use of Natural Resources.
 - (2018). TEN-T evaluation roadmap.
 - (2020). Construction and Demolition Waste.
- European Environment Agency (2009). Diverting waste from landfill. <https://www.eea.europa.eu/publications/diverting-waste-from-landfill-effectiveness-of-waste-management-policies-in-the-european-union>.
- European Norm (EN) (1993). Wasserbeschaffenheit - Bestimmung von Nitrit - Spektrometrisches Verfahren (ISO 6777:1984), Deutsche Fassung EN 26777:19.
- (2001). Characterization of sludges – Determination of dry residue and water content; German version EN 12880:2000.
 - (2003a). Characterization of waste - Leaching - Compliance test for leaching of granular waste materials and sludges - Part 2: One stage batch test at a liquid to solid ratio of 10 l/kg for materials with particle size below 4 mm (without or with size reduction).
 - (2003b). Non-destructive testing - X-ray diffraction from polycrystalline and amorphous material - Part 1: General principles; German version EN 13925-1:2003.

- European Norm (EN) (2003c). Non-destructive testing - X-ray diffraction from polycrystalline and amorphous material - Part 2: Procedures; German version EN 13925-2:2003.
- (2015). Geotechnical investigation and testing - Laboratory testing of soil - Part 1: Determination of water content (ISO 17892-1:2014); German version EN ISO 17892-1:2014.
 - (2020a). prEN 932-3 - Prüfverfahren für allgemeine Eigenschaften von Gesteinskörnungen - Teil 3: Durchführung und Terminologie einer vereinfachten petrographischen Beschreibung.
 - (2020b). Sludge, treated biowaste, soil and waste - Determination of total organic carbon (TOC) by dry combustion; German and English version EN 15936:2020.
- Garbarino, E., Orveillon, G., Saveyn, H., Barthe, P., & Eder, P. (2018). Best Available Technique (BAT) Reference Document for the Management of Waste from Extractive Industries (in accordance with Directive 2006/21/EC), EUR 28963 EN. *European Commission, Joint Research Centre Reference Reports*.
- LawInsider (2022). The definition of waste. <https://www.lawinsider.com/dictionary/excavation-waste>.
- République et Canton de Genève (2016). Guide pour la réutilisation des matériaux d'excavation non pollués. 1ère édit. Service de géologie, sols et déchets (GESDEC), République et Canton de Genève.
- République Française (2003). Code de l'environnement.
- (2014a). Arrêté du 12 décembre 2014 relatif aux conditions d'admission des déchets inertes dans les installations relevant des rubriques 2515, 2516, 2517 et dans les installations de stockage de déchets inertes relevant de la rubrique 2760.
 - (2014b). JORF n° 0289 du 14 décembre 2014. <https://www.legifrance.gouv.fr/jorf/2014/12/14/0289>.
 - (2015). La loi de transition énergétique.
 - (2016). Arrêté du 15 février 2016 relatif aux installations de stockage de déchets non dangereux, JORF n°0069, texte n°3.
- Schorcht, F., Kourti, I., Scalet, B., Roudier, S., & Sancho, L. (2013). Best Available Techniques (BAT) Reference Document for the Production of Cement, Lime and Magnesium Oxide, EUR 26129 EN. *European Commission, Joint Research Centre Reference Reports*, p. 506. DOI: [10.2788/12850](https://doi.org/10.2788/12850).
- Swiss Confederation (1983). Federal Act on the Protection of the Environment.
- (1989). Convention de Bâle sur le contrôle des mouvements transfrontières de déchets dangereux et de leur élimination.
 - (1998). Ordinance on the Remediation of Polluted Sites. <https://www.admin.ch/opc/en/classified-compilation/19983151/201705010000/814.680.pdf>.
 - (2005). Ordonnance sur les mouvements de déchets.
 - (2016). Ordonnance sur la limitation et l'élimination des déchets (Ordonnance sur les déchets, OLED). <https://www.fedlex.admin.ch/eli/oc/2015/891/fr>.
 - (2021). Verwertung von Aushub- und Ausbruchmaterial - Teil des Moduls Bauabfälle der Vollzugshilfe zur Verordnung über die Vermeidung und die Entsorgung von Abfällen (Abfallverordnung, VVEA).

A Peer-reviewed journal articles

A.1 Waste or valuable resource – a critical European review on re-using and managing tunnel excavation material

Table A.1: Overview of authorship and metadata of the presented publication.

Title	Waste or valuable resource – a critical European review on re-using and managing tunnel excavation material
Author names	Maximilian Haas, Robert Galler, Luigi Scibile, Michael Benedikt
First author	Maximilian Haas
First author's contributions	Conceptualization; literature review; formal analysis; visualizations; writing (original draft); writing (review & editing)
Scientific value	Conclusions on heterogeneous legislature based on a legal state-of-the-art review for managing excavated tunnel material across Europe, with an emphasis on the countries France, Switzerland, Austria, Germany, Italy and the United Kingdom.
Status	Published in <i>Resources, Conservation & Recycling</i>
Peer-reviewed journal	Yes
Full citation	Haas M., Galler R., Scibile L., Benedikt M., Waste or valuable resource – a critical European review on re-using and managing tunnel excavation material, <i>Resources, Conservation and Recycling</i> , Volume 162 (2020), ISSN 0921-3449, https://doi.org/10.1016/j.resconrec.2020.105048 .



Contents lists available at ScienceDirect

Resources, Conservation & Recycling

journal homepage: www.elsevier.com/locate/resconrec

Review

Waste or valuable resource – a critical European review on re-using and managing tunnel excavation material

Maximilian Haas^{a,b,*}, Robert Galler^b, Luigi Scibile^a, Michael Benedikt^a^a European Organization for Nuclear Research (CERN), Esplanade Des Particules 1, Meyrin 1211, Switzerland^b Chair of Subsurface Engineering, Montanuniversität, Erzerzog-Johann-Strasse 3, Leoben 8700, Austria

ARTICLE INFO

Keywords:

Re-use
Excavation
Tunnelling
Waste
Legislation
Europe

ABSTRACT

Re-use of excavated rock and soil from subsurface tunnelling has become an essential legal and technical factor in underground construction projects. European Union initiatives have caused an emergence of legal documents and technical guidelines for re-using excavated material. An improving situation towards a homogeneous European legislation is missing and site-specific re-use solutions are still favoured within the framework of national legislation. In this paper, we present a detailed review of legislation and technical concepts within the scope of re-using excavated rock and soil across Europe focusing on the Alpine countries. Austria, Switzerland and France prove to be role models in re-using excavated material whereas Italy is providing a limited amount of national solutions. Excavated rock and soil are still considered waste, which hampers legislation procedures and efficient technical re-use as a potential resource. National guidelines and recommendations bear huge potential to serve as a basis for a homogenisation of European legislation. Technical limitations imply physical and chemical characterisation of excavated rock and soil as well as their positioning in relation to inert waste thresholds, which requires a sophisticated material flow analysis. We introduce a material flow analysis concept installed on a tunnel boring machine managing on-line analyses, conditioning, separation and transport to consumers of excavated material resource-efficiently within a mutual European legal framework. A dedicated European authority is suggested to undertake responsibility for the material management and governing a technical database obliged to aim for maximum, efficient re-use and public awareness.

1. Introduction

Construction and demolition (C&D) waste makes up about one third of total waste produced in the European Union (EU) with a re-use rate of 46% on average (European Commission, 2016a; Poulidakos et al., 2017). Hence, the question of resource-efficiency in the context of re-use is quickly raised, yet vaguely answered. Excavated rock and soil originating from underground tunnelling projects make up an essential part of the total amount of C&D waste but are sparsely addressed nor described in an independent framework (Whittaker et al., 2019). It is required to highlight this sub-category of C&D waste whose expectations range at more than 700 million tonnes within the next years due to an increasing rate of projects currently under construction or at feasibility check. We discovered a distinct lack of research articles within a both legal and technical scope of re-using excavated rock and soil from subsurface construction projects treated substantively from C&D waste. Therefore, this paper aims to review and compare national

and EU re-use legislation and suggests a technical re-use material flow concept on a tunnel boring machine (TBM) applied across a mutual European re-use legislation framework, focusing on the Alpine countries Austria, Switzerland, France and Italy. The on-line material flow analysis aims to evaluate potential re-usability of excavated rock and soil from subsurface tunnelling projects emphasising material management and stating technical limitations.

The paper addresses the following research questions:

- What is the current legal state-of-the-art regarding European Union, Austrian, French, Swiss and Italian legislation within the scope of re-using excavated rock and soil?
- What are the thresholds and limitations of current legal frameworks?
- How can material management and material flow analysis be improved in terms of re-using excavated rock and soil from a mutual European legal and technical point of view?

* Corresponding author.

E-mail address: maximilian.mathias.haas@cern.ch (M. Haas).<https://doi.org/10.1016/j.resconrec.2020.105048>

Received 31 March 2020; Received in revised form 8 June 2020; Accepted 9 July 2020

0921-3449/ © 2020 Elsevier B.V. All rights reserved.

1.1. Initial re-use of excavated rock and soil

First re-use concepts were proposed in 1953 with landfilling as the ultimate solution, which soon turned out to have a negative impact on the environment (Savage et al., 1994) ranking at the bottom of valuable re-use scenarios. Environmental pollution since the 1970's caused European countries to develop institutional and technical tools to deal with soil contamination related to landfilling, industrial or mining activities (Brombal et al., 2015). The European Commission and the European Environmental Agency (EEA) were founded and developed a European Soil Data center (ESDAC) to survey European-wide soil contaminations (Panagos et al., 2012) as most severe problems stem from contaminated construction sites (Rahimzadeh et al., 2018). First innovative re-use ideas of tunnel excavation material apart from landfill date back to the 1990's when a lack of natural aggregates occurred on top of environmental issues (Gertsch et al., 2000; Kwan and Jardine, 1999).

Starting in the 2000's, new constructions and extensions of Europe's tunnel network (TEN-T) beard potential for excavated material to be re-used in a sustainable, circular economy (European Commission, 2005) since supply of natural resources from underground constructions results in millions of cubic meters of excavated material and were considered potential resources (DRAGON, 2014). Environmental regulations as part of the environmental impact assessment, and a general shift towards a more sustainable construction industry gave increased recognition to re-use of excavated rock and soil within the past 30 years. Up to now, research studies focused rather on a comparison of environmental impacts and treatment of C&D waste as a whole than separating each type of waste individually and highlighting discussions with legal background (Ghisellini et al., 2018). Even though limiting factors such as legislation and management issues are well-known and hamper recycled products in the construction industry (Gangolells et al., 2014; Silva et al., 2016), a clear and precise review on how to describe, treat and track excavated material from a legal point of view has neither been addressed nor requested in a European framework. However, the idea of a continuous material loop thrived within a circular economy and landfill mining emerged as a useful source (Altamura, 2013; Andrews, 2015), whereas illegal landfill disposal has been present from the start (Marzouk and Azab, 2014; Pacheco-Torgal, 2020).

1.2. Recent re-use of excavated rock and soil

Input material for re-use purposes stems from C&D waste, i.e. excavated rock and soil, which experiences recycling in a vast variety across Europe (Dahlbo et al., 2015; European Commission, 2020). Today, the question why excavated material needs to be processed originates from two reasons: a) due to legal regulations, which force the removal of waste status, and b) due to a proper preparation (pre-processing) of resources further used as e.g. concrete additives. Several European construction sites have successfully re-used excavated material in various scenarios, while concrete and geopolymer applications rank amongst the most applicable and recent re-use solutions

(Blengini and Garbarino, 2010). Their examples imply projects requiring non-sophisticated pre-processing since raw excavated material already comprises good re-use quality (Galler and Voit, 2014; Resch et al., 2009). However, more sophisticated yet site-specific re-use solutions due to complex geology led to several technical approaches for classification.

Ritter et al. (2013) derived a computer-based tool named Decision Aids for Tunnelling (DAT) enabling uncertainty calculations for excavation material handling (Ritter et al., 2013). On top of that, valuable re-use of excavated rock and soil depicts efficient ways of resource exploitation with advanced GIS applications, concrete aggregate production, construction of road sections, handling of contaminated soil, sensor-based sorting, aerobic landfilling and a general improvement of environmental performance (Cabello Eras et al., 2013; Lafebre et al., 1998; Read et al., 2001; Robben and Wotruba, 2019; Robinson and Kapo, 2004; Rodríguez et al., 2007). Moreno and García-Álvarez (2018) developed a Resource-Efficiency Capacity Index based on 29 indicators in the *Roadmap to a Resource Efficient Europe* document, which results in Austria being amongst the top performers (Moreno and García-Álvarez, 2018).

With more than 700 million tons of C&D waste produced each year in the EU (Iacoboaia et al., 2019) and predictions of more than 800 million tonnes of excavated rock and soil within the next years (DRAGON, 2014), European initiatives drew the construction sector's attention continuously to fostering resource efficiency as the guiding principle for EU policies. The Alpine countries Austria, Switzerland, France and Italy make up a big part of the proposed excavated material due to their tunnel infrastructure applied in a vast variety of complex tunnelling conditions. These conditions have justified a general trend towards site-specific re-use scenarios (Ghisellini et al., 2018), which is still the current case. For each construction site, material is analysed and specifically prepared for processing in factories on-site or at dedicated sites in the near vicinity aiming for minor environmental impacts.

On one hand, several researchers revealed environmental advantages when re-using excavated rock and soil on-site (Cabello Eras et al., 2013; Chittoori et al., 2012; Lafebre et al., 1998). The reduction of transport ways, the diminution of pollutants as well as the recycling of the excavation material bear large environmental protection potential. On the other hand, the presence of polluted material plays a major factor during excavation, which impacts landfill prices depending on regulatory national thresholds and integration of risk in the mechanism for adjusting execution time. Polluted material always involves purification and pre-processing. Research has shown that economic benefits result in costs tending to be lower than investing in new material or disposing excavated material (Ritter et al., 2013) leading to a reduction of material management costs by up to 85% (Chittoori et al., 2012). Depending on the geological composition of the material, it is possible to re-use up to 100% of excavated material. In fact, re-use of excavated material was set to a certain percentage level across Europe (Vieira and Pereira, 2015), whereas limited data is available for re-using merely excavated rock and soil in the EU (Magnusson et al., 2015).

Table 1

Europe's approach to resource-efficiency within the scope of EU initiatives and directives encouraging re-use of excavated rock and soil in Europe. EU member states are obliged to transpose EU law in national law.

Name of document	Date of publication	Legal entity
EU construction and demolition waste management protocol	18.09.2018	European Commission
A Stronger European Industry for Growth and Economic Recovery	10.10.2012	European Commission
Roadmap to a Resource Efficient Europe	20.09.2011	European Commission
A European strategy for smart, sustainable and inclusive growth	03.03.2010	European Commission
Directive 2008/98/EC on waste (Waste Framework Directive)	19.11.2008	European Commission
The Raw Materials Initiative - Meeting our Critical Needs for Growth and Jobs in Europe	04.11.2008	European Commission
Sustainable Consumption and Production and Sustainable Industrial Policy Action Plan	16.07.2008	European Commission

1.3. Europe's initiatives impacting re-use of excavated rock and soil

Between 2000 and 2010 European initiatives as indicated in Table 1 proposed a clear direction to efficient re-use of resources causing increased commencements of national legislation and guidelines. Legal considerations were thriving, however, its resulting heterogeneity and bad communication of future legislation are still one of today's key issues (Mittal and Sangwan, 2014).

The definition of C&D waste, respectively excavated rock and soil (Blengini and Garbarino, 2010; Coronado et al., 2011; Hiete et al., 2011; Simion et al., 2013) is not treated homogeneously from a legal perspective, even though all countries favour a transformation of waste into a resource. European initiatives culminated in different researchers' opinions stating that e.g. full implementation of European waste legislation will increase micro-pollutant recycling (Knapp et al., 2017; Lee et al., 2014). These results conclude that regulations are required to guarantee adequate quality control measures, whereas Arm et al., 2017 state that European Directives are very sensitive to legal definitions interpreted amongst the member states. The EU waste framework directive does not distinguish between various recovery processes and refers to a weight-based approach, which favours large and heavy waste streams (Arm et al., 2017). Gálvez-Martos et al. (2018) criticise the use of weight percentages in several law texts as it results in a focus on dense mineral fractions rather than on fractions with higher potential environmental impact (Gálvez-Martos et al., 2018). All authors indicate the argument of separation of type of fraction in the directive, substantiated by our research. While national and European legislations have increased since the year 1990 (Fischer and Werge, 2009) and achieved reasonable results in comparison with e.g. China (Brombal et al., 2015), it appears that the current legal framework is not sufficient and an urge for mutual technical guidelines.

Mutuality and homogenisation come with several limitations and issues. The responsibility of monitoring and enforcing re-use is scattered across many authorities at national, regional and provincial or cantonal levels across Europe. Landfill is still commonly chosen for re-using excavated rock and soil, which requires a transparent legislation for landfill mining. Quality and quantity of deposited resources transformed into marketable recyclables are partially addressed including how environmental legislation and subsidies apply to landfill mining (Krook et al., 2011). The EU deals with an increasing shortage of land, hence landfill reduction is preferential (Magnusson et al., 2015).

European strategies include the reduction and closure of landfills for excavated rock and soil to foster on-site re-use, as this was the case for total C&D waste in 2009 (European Environment Agency, 2009).

The EU's ten-year strategy invested great efforts in smart, sustainable and inclusive growth (European Commission, 2010) for a transition towards a resource-efficient, low-carbon economy to achieve sustainable growth by 2020 (European Commission, 2012). It is mentioned that treatment and excavation of natural resources should be in accordance with a protecting environment and circular economy. The *Roadmap to a Resource-efficient Europe* visualises that "...by 2050 the EU's economy has grown in a way that respects resource constraints and planetary boundaries, thus contributing to global economic transformation" (European Commission, 2011). It connects resource policies to initiatives such as the *Raw Materials Initiative* and suggests to provide excavated material as raw material input for construction (European Commission, 2008a). The EU *Thematic Strategy on the Sustainable Use of Natural Resources* outlined decoupling resource usage and economic growth (European Commission, 2016b). In the *Sustainable Consumption and Production and Sustainable Industrial Policy* the European Commission aimed to give further impetus to resource-efficiency and eco-innovative production processes, to reduce dependency on raw materials and to encourage optimal, high-quality re-use (European Commission, 2008b; Velis and Brunner, 2013). The European goal has been set to recycle at least 70% of excavated material, whereas an actual 50% missed the target already for 2019

(European Commission, 2018a). France has implemented this plan into national legislation and constituted that 70% of excavated rock and soil material must be re-used per region (République Française, 2015).

Within the next years, global population will grow to estimated 9 billion whereas 3 billion people are expected to reach the middle class having a huge impact on the demand of resources and space (Rios, 2018). Resource potential is proposedly lying in current and future subsurface projects. Within the scope of the *Trans-European Transport Network (TEN-T) Initiative* considerable input material is available for re-use within the upcoming years (European Commission, 2018b, 2005). However, these numbers underline the urgency of first, a legal homogenisation for excavated rock and soil across Europe and second, a review of potential technical re-use concepts to stem increasing excavation volumes (Brombal et al., 2015). There are plenty of resources available from the construction sector, whereas key issue will be how to re-use them in the most efficient way in both legal and technical terms (Allwood et al., 2011; Pacheco-Torgal and Labrincha, 2013).

2. Re-use legislation for excavated rock and soil across Europe

The European Union waste concept is defined in the Waste Framework Directive 2008 and sets out measures to protect the environment by reducing the overall European impacts on resources (European Commission, 2008c). Excavated rock and soil are part of the waste regime and thus under the validity of the Waste Management Act. The objective definition of waste is not fulfilled for tunnel excavation material recycled on construction sites according to EU directives. To re-use excavation material from tunnelling construction sites, it is necessary to reach the end of waste status. Waste can be recycled if the same requirements as for primary raw material is fulfilled. The fact that most excavated material is not available in a form for instant re-use and that possibilities for recycling must be carefully measured, satisfies the objective's definition of waste. Legal waste terminology is regulated by federal governments and EU directives that must be transposed into national law of each member state. A comprehensive list of legislation, guidelines and recommendations for Austria, Switzerland, France and Italy within the scope of re-using excavated rock and soil from subsurface tunnelling sites is summarised in Table 2.

In Austria all 9 counties are obliged to follow national laws and regional guidelines are not common. The Federal Act on Sustainable Waste Management (AWG) contains the definition of waste, its life-cycle, methodological order of avoidance and elimination as well as rights and obligations of the waste owner, transport regulations, cross-border transport and limit thresholds for each waste category (Bundesministerium Landwirtschaft Regionen und Tourismus, 2002). The Federal Waste Management Plan is published every six years and initiates objectives of the AWG 2002 (Bundesministerium Klimaschutz Umwelt Energie Mobilität Innovation und Technologie, 2017). The recycling building materials regulation (Bundesministers für Land- und Forstwirtschaft Umwelt und Wasserwirtschaft, 2015) standardises requirements and unifies designations and technical assessments of recycled construction material. The Austrian trend of recognizing material flow analyses to increase re-use has been introduced by many researchers at an early stage (e.g. Allesch and Brunner, 2017) making Austria a European role model in re-using excavated rock and soil.

France is structured in a decentralised hierarchy and distributes legal power in descending order from national legal entity in Paris (*l'état*) to its 13 *régions* and 101 *départements, pays* and *communes*. French waste law is in accordance with EU law and Article L541–1–1 of the French Environment Code, which has partly incorporated EU directives (République Française, 2003).

Switzerland is subdivided into 26 cantons, which have autonomous legal power for re-use legislation. This implies that each canton can derive their own cantonal recommendations and guidelines. The re-use case must be credible and detailed in a specific document to meet the requirements of Federal Ordinance on Waste Limitation and

Table 2
Chronological overview for re-use legislation of excavated rock and soil material from underground tunnelling constructions across Europe.

Country	Original name of legislation*	Date of commencement	Date of latest version	Authority or publisher
Austria	Recycling-Baustoffverordnung	29.06.2015	27.10.2016	Bundesministerium für Land- und Forstwirtschaft, Umwelt und Wasserwirtschaft
	Deponieverordnung	30.01.2008	27.10.2016	Bundesministerium für Land- und Forstwirtschaft, Umwelt und Wasserwirtschaft
	Abfallverzeichnisverordnung	23.12.2003	23.12.2008	Bundesministerium für Land- und Forstwirtschaft, Umwelt und Wasserwirtschaft
	Abfallwirtschaftsgesetz	16.07.2002	25.05.2020	Bundesministerium für Land- und Forstwirtschaft, Umwelt und Wasserwirtschaft
	Bundes-Abfallwirtschaftsplan	1992	2018**	Bundesministerium Klimaschutz, Umwelt, Energie, Mobilität, Innovation und Technologie
	Altlastensanierungsgesetz	07.06.1989	29.10.2019	Bundesministerium für Land- und Forstwirtschaft, Umwelt und Wasserwirtschaft
Switzerland	ÖBV-Richtlinie zur Verwendung von Tunnelausbruchmaterial	-	01.10.2015	Österreichische Bautechnik Vereinigung
	Verordnung über die Vermeidung und Entsorgung von Abfällen	01.01.2016	01.04.2020	Bundesamt für Umwelt
	Verordnung des UVEK über Listen zum Verkehr mit Abfällen	01.01.2006	01.01.2018	Bundesamt für Umwelt
	Verordnung über den Verkehr mit Abfällen	01.01.2006	01.01.2020	Bundesamt für Umwelt
canton Geneva	Loi sur la gestion des déchets	05.08.1999	21.03.2015	Le Conseil d'état de la République et canton de Genève
canton Geneva	Règlement d'application de la loi sur la gestion des déchets	05.08.1999	12.09.2018	Le Conseil d'état de la République et canton de Genève
	Basler Übereinkommen über die Kontrolle der grenzüberschreitenden Verbringung gefährlicher Abfälle und ihrer Entsorgung	05.05.1992	06.05.2020	Several contracting parties
	Verordnung über den Verkehr mit Sonderabfällen	07.10.1983	12.07.2005	Bundesamt für Umwelt
	Bundesgesetz über den Umweltschutz	07.10.1983	01.03.2020	Bundesversammlung der Schweizerischen Eidgenossenschaft
	Verordnung über die Sanierung von belasteten Standorten	01.10.1998	01.05.2017	Bundesamt für Umwelt
	Grenzüberschreitender Verkehr mit Abfällen (gilt für das Fürstentum Liechtenstein und die Schweiz)	-	05.05.2020	Bundesamt für Umwelt
	Messmethoden im Abfall- und Altlastenbereich	-	08.12.2017	Bundesamt für Umwelt
canton Geneva	Déchets - Diagnostic de Pollution - Gestion des Terrains Pollués	-	01.11.2017	République et Canton de Genève & service de géologie, sols et déchets
canton Geneva	Plan de gestion des déchets de chantier	-	01.09.2017	République et Canton de Genève & service de géologie, sols et déchets
	Baustellen-Entsorgungskonzept	-	01.07.2017	Swiss cantons, Bundesamt für Umwelt, ARV-Verband, VBSA-Verband
	Grenzüberschreitender Verkehr mit Abfällen	-	05.05.2017	Bundesamt für Umwelt
	Klassierung von abgetragenem Ober- und Unterboden	-	01.04.2017	Bundesamt für Umwelt
canton Geneva	Guide pour la réutilisation des matériaux d'excavation non pollués, 1ère édition	-	01.04.2016	République et Canton de Genève & Service de géologie, sols et déchets
	Bewirtschaftung und Wiederverwertung von Ausbruchmaterial (Gestion et valorisation des matériaux d'excavation)	-	2016	Fachgruppe für Untertagebau
	Herleitung von Konzentrationswerten und Feststoff-Grenzwerten	-	29.01.2014	Bundesamt für Umwelt
	Richtlinie für die Verwertung mineralischer Bauabfälle	-	25.05.2010	Bundesamt für Umwelt
	Abfall- und Materialbewirtschaftung bei UVP-pflichtigen und nicht UVP-pflichtigen Projekten	-	20.11.2006	Bundesamt für Umwelt
	Richtlinie für die Verwertung, Behandlung und Ablagerung von Aushub-, Abraum- und Ausbruchmaterial:	-	01.06.1999	Bundesamt für Umwelt
	Aushubrichtlinie	-	17.08.2015	La République Française
France	La loi du transition énergétique	07.08.2015	27.12.2019	La République Française
	La loi NOTRE et la nouvelle organisation territoriale	2007 (1807)	16.11.2018	La République Française
	Code de commerce	28.02.2002	07.11.2018	La République Française
	Code de l'environnement	-	15.05.2020	La République Française
	Recommendations of AFTES (GT35RIA2): Management and use of excavated materials	-	2019	Association Française des Tunnels Et De L'Espace Souterrain
	Guide méthodologique de comblement de cavités à l'aide de matériaux alternatifs	-	12.2016	Bureau de recherches géologiques et minières
	Natural Geological Materials Excavated during Underground Works	-	2016	Le Centre D'Études des Tunnels

(continued on next page)

Table 2 (continued)

Country	Original name of legislation*	Date of commencement	Date of latest version	Authority or publisher
Italy	Misure urgenti per l'apertura dei cantieri, la realizzazione delle opere pubbliche, la digitalizzazione del Paese, la semplificazione burocratica, l'emergenza del dissesto idrogeologico e per la ripresa delle attività produttive	13.09.2014	11.11.2014	Repubblica Italiana
	Misure per la crescita economica	21.06.2013	-	Repubblica Italiana
	Regolamento recante la disciplina dell'utilizzazione delle terre e rocce da scavo	12.04.2006	21.09.2012	Repubblica Italiana
	Norme in materia ambientale	06.04.2006	14.04.2006	Repubblica Italiana
	Criteri di ammissibilità dei rifiuti in discarica	03.08.2005	-	Repubblica Italiana
	Norme affinché gli uffici pubblici e le società a prevalente capitale pubblico coprano il fabbisogno annuale di manufatti e beni con una quota di prodotti ottenuti da materiale riciclato nella misura non inferiore al 30% del fabbisogno medesimo	08.03.2003	05.08.2003	Repubblica Italiana
	Regolamento recante norme concernenti le modalità di prestazione della garanzia finanziaria per il trasporto transfrontaliero di rifiuti	10.11.1998	-	Repubblica Italiana

No date of commencement implies concepts, recommendations or guidelines. Swiss legislation is available in French, German, Italian and English language.

* Official languages of each country have been chosen for labelling legislation.

** Austrian waste plan revised each six years at random dates.

Elimination. Agricultural re-use may not be legally eligible except under certain conditions if evidence for benefits can be clearly demonstrated.

The Italian Republic consists of 20 regions divided into autonomous provinces regulated in the Third Book of the Italian Civil Code (*Costituzione della Repubblica, 1942*). The definition of waste is specified in the Italian law in Article 183 of *decreto legislativo nr. 152/2006 (norme in materia di ambiente (Codice ambiente) (Repubblica Italiana, 2006a)*. It serves as the main document of C&D waste regulations, including excavated rock and soil and sets the rules for regional plans for waste management and addresses responsibility to regions for waste management planning, whereas provinces are responsible for controlling waste management activities.

2.1. Heterogeneity and limitations of European national and trans-national re-use legislation

Re-use potential is strongly associated to waste status. National governments focus on regulations dealing with the definition of waste but use different approaches for its removal. In Austria, excavated rock and soil recycled in plants is sorted by different quality classes for unrestricted usability, restricted usability and limited usability. Based on chemical and mineralogical investigations, a substance must be addressable to waste according to the Waste Catalogue Ordinance (*Bundesministerium Landwirtschaft Regionen und Tourismus, 2008a*). Production of recycled material is eligible based on chemical composition and associated threshold values stated in the Landfill Ordinance (*Bundesministerium Landwirtschaft Regionen und Tourismus, 2008b*). The Landfill Ordinance provides procedures to prevent negative effects of waste landfill on the environment and human health. The Austrian Contaminated Site Remediation Act passes laws on how to secure and remediate contaminated sites (*Bundesministerium Landwirtschaft Regionen und Tourismus, 1989*). According to Austrian law, contaminated sites are old deposits or abandoned sites containing a significant risk to human health or the environment. Old deposits contain waste owned by authorised or unauthorised persons, whereas old sites host plants in which environmentally hazardous substances are treated. Unless an ordinance pursuant to the European Waste Framework Directive on Waste provides otherwise, existing substances are treated as waste until they or the substances derived from them are used directly as substitutes for raw materials or for products manufactured from primary raw materials. This results in the end of the waste status when recovery processes are completed.

In France, a similar situation applies for dangerous waste containing toxic or dangerous elements that represent risks for human health or the environment. Waste is classified as hazardous if it contains pollutants specified in Article R541-8 of the Environment Code, whereas non-hazardous waste is defined by excluding hazardous waste. These pollutants include polychlorinated biphenyls, polycyclic aromatic hydrocarbons, lead or asbestos and are specified in most national texts. Disposal is divided into three disposal classes based on pollutant thresholds including classes for inert, non-polluted waste (ISDI), non-dangerous and non-inert waste (ISDNDNI) and dangerous waste (ISDD). Ultimate waste is considered for no further re-use or recovery under current technical and economic conditions by extraction or reduction of its pollutants according to Article L541-2-1 of the Environment Code (*République Française, 2003*). Producers or holders of waste may dispose waste in predefined waste storage facilities. This is similar to Austrian or Swiss disposal classes based on grade of pollution of excavated material, which is re-used if similar contaminated thresholds are not exceeded (*Swiss Confederation, 2016*). According to the Federal Act on the Protection of the Environment, the obligation for remediation resides with the cantons, whereas costs are borne by the polluter (*Swiss Confederation, 1983*). If the polluter cannot be identified, the costs are allocated by the responsible communities.

Despite similar disposal classes compared amongst France, Austria

and Switzerland, French legislation distinguishes between *re-use* and *valorisation*. *Déchets* (waste) aims for *valorisation* or *élimination*, while *matériaux*, i.e. excavated rock and soil material, refer to re-use as a secondary raw material. Hence, valorisation should be used only when implying a preceding waste status. In fact, the status *matériaux* is assigned to any kind of material on-site. A French project owner is entitled to re-use the excavated material as part of the construction, for a construction site being part of the same operation or applying no re-use. This is in compliance with many French guidelines, too and is similar to Swiss project owners who must provide the quality and the quantity of the forecasted waste and disposal chain. In case waste exceeds a quantity of 200 m³ likely to contain hazardous polluting elements, tracking and evidence of waste elimination must be provided before the end of construction phase in France, Austria as well as in Switzerland. From a legal point of view, excavated rock and soil on French territory is not considered waste if the project owner re-uses the material on-site. This also includes spatially distributed locations contractually bounded to the same project owner. Thus, the material loses its waste status when temporarily stored on the construction site. For on-site re-use, the *préfet* issues authorization to the project owner filing an *installation classée pour la protection de l'environnement (ICPE)*. For treatment on a dedicated site, a third party may perform processing (grinding, crushing, sorting) on behalf of the project owner. After processing, the project owner retrieves the treated material and discard is excluded. In case of no re-use, the material is assigned with waste status and the "... project owner remains responsible for these materials until their disposal or final recovery unless the materials come out of an ICPE classified facility or an IOTA classified facility in the conditions laid down by the end of waste order" according to Article L.541-2 and L.541-4.3 of the Environmental Code (*République Française, 2003*). It is upon the French project owner's initiative in the context of an inert waste storage facility to verify the facility by the *service de la prévention des risques et des nuisances (DRIEE)* and the associated acceptance procedures will have to be recorded by the *préfet* in an additional decree. It must be disposed in a landfill site in accordance with Decision 2003/33/EC of 19 December 2002. Landfilling cavities (excluding active quarries) as ISDI former quarries that have received discharge under the mining code or that have been the subject of a report on the end of work are not subject to ICPE regulations. It is then possible to store waste under the status of a development subject to meeting the conditions of the following section or ISDI. This is unexceptionally applied in France. The ISDI regulations apply, except in the case of storage in underground caverns and water caverns. Storage in natural or artificial underground cavities or below the water table are excluded by Article 3 and 4 of the Decree (*République Française, 2003*). In case of damage caused by improper use of waste for recovery, the developer is responsible according to Article 1242 of the French Civil Code (*République Française, 2016*), which is also in accordance with Austrian and Swiss law. The use of excavated material for rehabilitation of quarries is considered as recovery when the operations carried out are consistent with the operation of the quarry or during its rehabilitation, also considering future use of the construction site.

In comparison to EU member states, Swiss legal hierarchy differs in terms of federal and cantonal empowering legislation. Each canton is eligible to pass own guidelines or recommendations published by cantonal authorities. Switzerland offers a suitable framework for the implementation of disposal facilities including legislation, regulatory guidance and a dedicated selection process defined in e.g. the Sectoral Plan Geological Repositories (*Zuidema, 2015*). Basic definitions of waste types include excavated rock and soil, its avoidance, mixture with other waste, legal obligation to recycle waste and re-use excavated material on-site or in various disposal classes as mentioned in the Ordinance on the Avoidance and the Disposal of Waste (*Swiss Confederation, 2016*). The *Swiss Convention de Bâle sur le contrôle des mouvements transfrontières de déchets dangereux et de leur élimination* (*Swiss Confederation, 1989*) (not available in English; commonly

translated as *Basel Convention*) is exceptional among the Alpine countries and describes control of transborder waste transport and its associated elimination as well as the definition of waste acceptance from other countries whereas only non-polluted material is valid for export. According to the Basel Convention, exported material must be re-used and cannot be disposed in dumps, except when special exemption is granted by the Federal Environmental Office. Trans-national projects require a dedicated exportation and notification procedure including tracking and in case the excavated material remains in Switzerland, Federal Ordinance on Waste Limitation and Elimination applies. Further detailed explanations on international waste transfer are available in the document *Transboundary Movements of Waste, Communication from the Federal Environmental Office* and on the website of the confederation. The *Ordonnance sur les mouvements de déchets, OLED* (*Swiss Confederation, 2005*) (not available in English) assures that waste is treated on proper, non-environmental protected sites, regulates national and trans-national waste transport and gives definitions of transborder waste and demands waste reporting obligation. The threshold values therein allow for a material classification into polluted and non-polluted categories similar to Austria and France including requirements of a tracking system and regulatory thresholds for e.g. heavy metals such as lead, nickel, chrome or copper, aliphatic and aromatic hydrocarbons or polychlorinated biphenyl concentrations. Swiss responsibility of excavated material is attributed to the project owner, unless otherwise indicated in construction contracts. The issue of land ownership is handled in Switzerland in the sense that "...the ownership of land extends upwards and downwards to the airspace and the ground, insofar as there is an interest in the exercise of the ownership." (*Swiss Confederation, 1907*). Since 2019, Swiss law enables the re-use of polluted material on-site. This avoids transportation, carbon dioxide emissions and noise. Depending on the destination, material exceeding the thresholds depicted as non-polluted material can still be classified as such. The Swiss canton Geneva serves as a good example of recommended guidelines being incorporated into cantonal legislation. Following a convention between the Swiss Confederation and the canton Geneva on the delegation of execution tasks, the Swiss competent authority for the exportation of non-polluted excavated material coming from construction sites of canton Geneva is entitled by the *service de géologie, sols et déchets, GESDEC* (*Swiss Confederation, 1999, 1998*). This constitutes that construction site A and construction site B cannot collect their waste in a single transport. The guideline for recycling, treatment and disposal of excavated, overburdened and waste material regulates quality requirements and restrictions for excavated rock and soil to be re-used in Switzerland (*Bundesamt für Umwelt, 1999*).

In Switzerland, the project owner is responsible for disposal. This provision creates homogeneity so that disposal planning and execution responsibilities are attached to the client like in Austria and France. A quarry authorization is granted for the exploitation of a given material. The re-use of excavated material for rehabilitation of quarries is considered as recovery when the operations are consistent with the operation of the quarry or during its rehabilitation.

In contrast to Austria, France and Switzerland, Italy does not provide pollution threshold values. They are set by the authorities on specific cases, e.g. the Lyon-Turino project. Italian waste laws and directives are mainly adopted from EU legislation (Directive 2008/98/EC) and were implemented by the *decreto nr. 205/2010* amending Part IV of the *decreto legislativo nr. 152/06*. Article 184-ter describes technical criteria to end waste status as well as material flow and priority modes of procedure for implementing regulations. Within the past years, legislation for excavated rock and soil has evolved steadily resulting in the *decreto ministeriale nr. 161* of 10 August in 2012 and Article 41 of the *BIS DL 69/2013* (*Repubblica Italiana, 2013, 2012*). The former regulates the re-use of excavated material (*regolamento materiali da scavo, piani di utilizzo*). Article 41 c. 2 and Article 41-bis c.1e5 of the *decreto legislativo 69/2013 convertito L. 98/2013* set the rules for the

piani di utilizzo, a re-use plan for excavated rock and soil. The *decreto ministeriale nr. 203 del 8/5/2003* sets a quota of 30% for recycled material and products in public procurement including construction material (Repubblica Italiana, 2003a). Article 185 of *decreto legislativo nr. 152/2006* excludes uncontaminated soil and other naturally occurring material from the definition of waste during construction activities. The material must be used in its natural state on-site (Repubblica Italiana, 2006a, 2006b), whereas strategies are set rather at regional and provincial levels (Repubblica Italiana, 2006b). Article 34 of the *decreto legislativo 12–9–2014 nr. 133* from 13 September 2014 allow the re-use in-situ of excavated material (Repubblica Italiana, 2014). The *decreto ministeriale 5/2/98* deals with dangerous and non-dangerous waste and contains criteria for construction waste considered as a secondary raw material (*materie prime secondarie*). The Italian Institute for the Protection of the Environment (ISPRA) is entitled to record regional and provincial data related to C&D waste, whereas no specific data is available for excavated rock and soil. In Italy soil is not implemented in C&D waste statistics (DELOITTE, 2015) even though definition of waste corresponds to EU legislation and waste management plans.

An explicit lack of landfilling policies results in Italy's target to flexibly control landfilling by a specific tax. Landfilling is allowed for inert waste at specific sites without prior characterization according to Article 2 of *decreto ministeriale 13 marzo 2003* (Repubblica Italiana, 2003b). Waste may be temporarily stored for one year before disposal and three years before recovery. Exceptions are made for natural background contamination or the provincial government can approve exceptions in individual cases. If the polluter cannot be identified, or if the damage is the responsibility of the general public, the remediation costs are paid by the general public. Backfilling is a recovery option, which is suitable for waste used for reclamation in excavated areas or for landscaping and where waste replaces non-waste material. For transborder shipments of waste, EC Regulation 1013/2006 and the *decreto ministeriale* of 3 September 1998 nr. 370 apply (Repubblica Italiana, 1998).

Italy's approach to inherit EU legislation is a step in the right direction for a future homogenisation but still lacks sophisticated development compared to Austria, France or Switzerland. It is worth mentioning that specific uses for excavated material are mentioned for which the by-product regulation is applicable: excavated material that originates from a production process but is not directly aim of production processes is considered a by-product, unless it is used as a substitute for raw materials or landfilling. Like in the Austrian Minerals Plan, European Commission proposes a platform for member states to exchange best practices in the area of land use planning. This should be emphasised by all member states and unified.

Both Switzerland and Austria constitute pioneering examples on how to deal with re-use of excavated material in both legal and technical matters. Responsibility for disposal is held by the project owner and cantonal and federal guidelines have been developed to characterise and valorise excavated rock and soil. This provision further creates uniformity for disposal planning, contamination thresholds and responsibilities attached to the client that are similar amongst Austria, France and Switzerland.

2.2. Requirements and limitations for a mutual European re-use legislation

Removing waste status makes it imperative to treat excavated rock and soil. Legislation plays a decisive role in the excavation of underground material and should be considered a helpful trend-setter rather than an enforced obligation. Site-specific negotiations years before actual start of construction are based on technical and legal questions from a client's and contractor's perspective and result in time-consuming and extensive procedures. The current heterogenic approach is not in compliance with increasing re-use efficiency. The goal of a mutual European legal framework includes overcoming cultural,

technical and legal discrepancies as well as economic interests of industrial companies. Once a homogeneous EU legislation is derived, Europe can serve as role model in world-wide re-use economy of excavated rock and soil as it is already shown by some Alpine countries. Extension of such a mutual legislation to the whole world might be feasible whereas national power and different governmental structures might be limiting factors. A first approach to a mutual legislation requires one single authority that deals with the re-use of excavated rock and soil across Europe instead of expelling site-specific re-use scenarios to each national government that further complies with EU legislation. This would also force construction companies to quantify excavated material and increase available statistical data of excavated rock and soil.

To avoid landfilling a standardised framework that forces evaluation of economic, environmental as well as technical performance should be incorporated into formal legislation leading to prohibition of illegal disposal. Austria, France and Switzerland developed guidelines on how to analyse and re-use excavated rock and soil during underground works emphasising avoidance of illegal disposal. A summary of these documents would bear potential as a mutual legal basis for Europe. These recommendations comprise similar scenarios for the management of excavated material from a project owner's perspective, indicate main uses, consider transport routes for excavated material or evaluate influence of the type of excavation method on final re-use via descriptions and analyses of physical and chemical properties. Such guidelines are published by associated authorities or industrial companies such as the *Österreichische Bautechnik Vereinigung, ÖBV* in Austria, (*Österreichische Bautechnik Vereinigung, 2015*), the *Française des Tunnels Et De L'Espace Souterrain, AFTES (Association Française des Tunnels Et De L'Espace Souterrain, 2019)*, the *Guide méthodologique de comblement de cavités à l'aide de matériaux alternatifs* published by the *Bureau de recherches géologiques et minières, BRGM (Bureau de recherches géologiques et minières, 2016)* and *Le Centre D'Etudes des Tunnels, CETU (Le Centre D'Etudes des Tunnels, 2016)* in France as well as the *service de géologie, sols et déchets, GESDEC (République et Canton de Genève, 2016)* for the canton Geneva and the *Sectoral Plan Geological Repositories (Zuidema, 2015)* in Switzerland. The mutual legislation should facilitate construction companies to receive organisational resources and avoid inconsistencies in governmental management, which have been a key factor in restricting a common European legislation underlined by several researchers (Korhonen et al., 2018; Mangla et al., 2017; Ritzén and Sandström, 2017).

In current legislation, polluted and non-polluted excavated material takes on the status of waste. Chemical thresholds for contamination exist but strongly vary in each country. This is treated differently in the mining industry. Opinions of mining companies being more efficient and higher in quality compared to tunnel construction sites do no longer hold its ground as research has shown that for each ton of mined material more than 85% became waste, whereas this number increases to 99% for some materials (Pacheco-Torgal and Jalali, 2011). It does not make sense to give tunnel excavation material the status of waste since incorporated blasting substances such as nitrites and nitrates are similar for mining activities. Consequently, it must be favoured to combine re-use legislation and mining law. Since geological resources are detached from political borders, types of excavation, e.g. tunnel boring machine versus mining activities and the framed legal empowering system, mining and tunnel excavation limitations need to be overcome to guarantee a resource-efficient and sustainable re-use on a mutual scale. This incorporates reconsidering material flow analyses and material management concepts.

A future goal must be the establishment of close relationships with representatives of national environmental authorities, standardisation bodies and governmental organizations forming working groups to homogenise European re-use. Approaches could be applied to the whole world if guideline and recommendation documents would be adapted

from Alpine countries once enough data was available to prove its efficiency. Excavated material being less feasible for high-quality applications might be used for landscaping on-site instead of landfilling. The intention of re-use should not be competition to local raw materials companies but to make the material available at reasonable prices to save raw material deposits and increase environmental benefits. Excavation close to consumers is essential as it reduces transport costs, fossil fuel consumption and strengthens regional industries. It requires visionary thinking making these re-used resources available on a regional and global scale, demanding also advanced technical concepts.

3. Material flow concept in mechanized tunnelling in a mutual legal re-use framework

Re-use applicability depends on geotechnical, petrophysical, mineralogical and geochemical properties of excavated rock and soil, and its underlying material management boundary conditions as indicated in Fig. 1.

Excavated material has a strategic impact on sustainable management of limited mineral resources, higher resource-efficiency and a sustainable environment. A material flow analysis concept with expected masses of excavated material should be prepared during feasibility phase of any underground project. Within the scope of an underground project, the constructor measures data of the subsurface via geophysical and/or geotechnical tests during site investigations and actual construction. Drilling samples or geophysical loggings should be analysed to obtain essential information regarding complex geological situation incorporated before construction. Based on the resulting geological profile, volume and properties of the future excavated material can be estimated in advance and fine-tuned as construction progresses. The concept is based on an on-line database derived by continuous analyses on a conveyer belt attached to a TBM as indicated in Fig. 2, and considers an environmental and sustainable storage of oversupply in excavated material to cover future demands and the usage of less quality material. Transport routes, material specific processing, intermediate storage and landfilling should be taken into consideration in terms of CO₂ emission but are neglectable for on-line analyses. The material management concept is a basis to prepare delivery contracts with potential industrial consumers.

The proposed on-line database contains a matrix with integrated specific requirement lists for relevant and possible re-use parameters at

local and global level linked to economic and environmental transport routes. Processing of raw material could distinguish between hard, soft and mixed rock as well as different mineral phases and would combine its transport to eligible industrial consumers. The individual re-use scenarios could be derived from a requirement matrix like a risk mitigation matrix. Using the database, the constructor can thus immediately determine the re-use potential of the subsurface. Technical data would be continuously updated and linked to mutual legal contamination thresholds or trans-national transport legislation registered in the database. Intermediate purchasers and material processing companies were eligible to access the database and specifically store their demands and requirements such as material properties, time of demand, volume or maximum transport distances. Excavated material would be classified by real-time comparison with the required specifications in the on-line database as seen in Fig. 3 and framed by one European authority described in the previous section. It could be argued that legislation drives the requirements of technical concepts, whereas it must be considered that natural resources need to be pre-processed for construction material anyway. Economic re-use benefits would result from earnings by selling certain material quality and from savings, first from the substitution of purchased aggregates for the internal needs of the site with the excavated material and second, through reduced landfill costs.

Technical re-use concepts have become a mandatory part of environmental impact assessment procedures to receive construction approval.

Thus, sorting excavated material is possible before start of construction and during site investigations. In case properties of excavated material do not comply with quality requirements or industrial standards for application on-site, the material should be used for embankments (landfilling). However, this should be overcome by iterating the processes in the red dashed square in Fig. 3. On-line analyses ease the process of waste avoidance due to characterising the material on a conveyer belt without touching the surface leading to avoidance of waste status and tracking material flows. This would also give improved statistical insights into rare and critical metals (Ayres and Talens Peiró, 2013) also linking it to construction information models (BIM) and mining. A dedicated European authority should be responsible for the material management, which emphasises the development of a material management concept and governs the legal and technical database to publish reports on resource status similar to Austrian reports such as

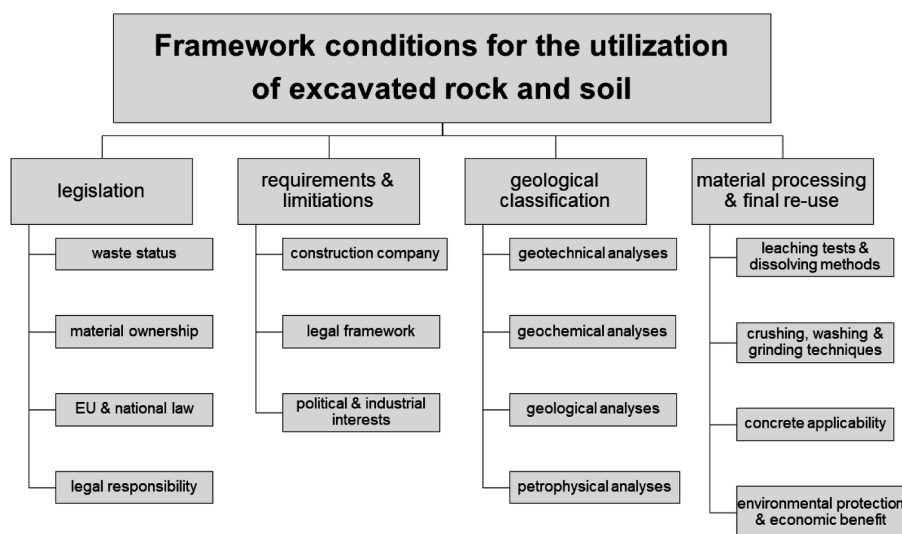


Fig. 1. Re-use organigram for excavated rock and soil specifying geology, processing techniques and laws. Mutual legislation must be the framing element for engineering re-use purposes.

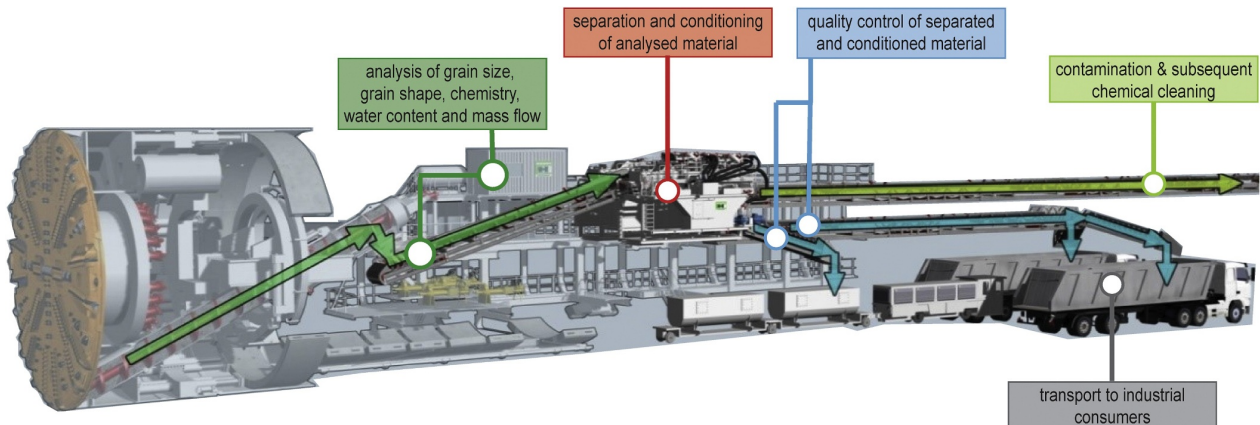


Fig. 2. Schematic on-line analysis of excavated rock and soil material shown on a tunnel boring machine (TBM) for mechanical excavation.

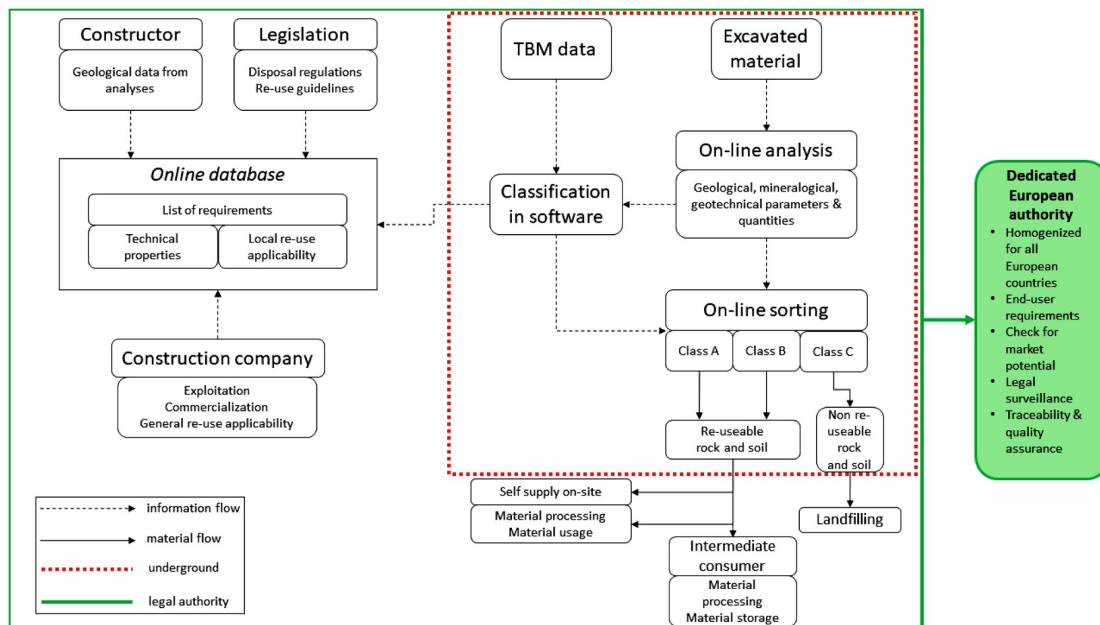


Fig. 3. Conceptual management and caption of re-use potential for excavated rock and soil framed by a legal European authority (green line). The red square indicates tasks to be conducted on-site, respectively underground.

Kritische Rohstoffe für die Hochtechnologieanwendung in Österreich (Luidold, 2013). Industries must be incorporated by the European re-use authority and support classification models including geotechnical, petrophysical, geological, mineralogical and geochemical parameters in their laws. The new authority should be responsible for the material usage and waste management emphasising the development of a material flow analysis and operating the technical database. Excavated material from subsurface construction sites would increasingly conquer European land masses. It should be the goal to maximise valorisation for final products to avoid landfilling. Re-use goals set to 90% or beyond should be outlined as a European standard and are likely achievable within a mutual legal and technical framework. The new and innovative technologies should be used for an on-line analysis of excavated material on tunnel boring machines. Such a concept has not been suggested before and bears potential for resource-efficient and sophisticated re-use collected in a single process. The concept of on-line analyses on the TBM, respectively conveyer belt additionally saves time by avoiding sending samples to laboratories.

4. Conclusions

In this paper, we elaborated a review of European Union and Alpine country legislation for the re-use of excavated rock and soil, which gained significance due to an increasing demand for subsurface tunnelling projects. An improving situation towards a homogeneous European legislation is present yet site-specific re-use solutions are still favoured within the framework of national legislation. However, EU initiatives have caused an emergence of re-using excavated material across Europe. Austria, Switzerland and France prove to be role models in re-using excavating material substantiated by solid legislation and national guidelines. Italy is lacking dedicated national solutions. Legislation for environmental protection such as landfill is completely absent. Alpine countries and the EU still consider excavated rock and soil as waste. This is a limiting factor and hampers legislation procedures and efficient technical re-use as a potential resource. Comparison and incorporation of mining laws might seem useful in a mutual legal context. Existing Austrian, Swiss and French laws and guidelines could

serve as a first European legal template published by a single authority with legal power. Especially national guidelines and recommendations bear huge potential to serve as a basis for homogenisation. Further limitations for the definition of relevant consumers contain the geo-physical, mineralogical and geochemical characterisation of excavated rock and soil as well as their positioning in relation to inert waste thresholds as defined amongst different national legislations. An adaption and homogenisation of these thresholds is highly recommended amongst Alpine countries and could lead to a mutual European legislation by standardising technical measurements and legal approaches.

An advanced material flow analysis concept should be installed on a tunnel boring machine efficiently managing on-line analyses, conditioning, separation and transport to consumers of excavated material within a mutual European legal framework. A dedicated European authority is suggested to be responsible for the material management and a legal and technical database obliged to publish reports and data on resource status. The main goal must range at 90% re-use or beyond subsequent to aiming at avoidance of landfilling. These targets should be outlined in a mutual European standard document.

From a legal point of view, the focus within the next decade should be put on a strict convergence of national laws to one strong European legislation published by a single European authority in legal charge. Technical future work should be spent on finding analyses easily and efficiently applied on a tunnel boring machine. Furthermore, a comparison of on-line and laboratory results in terms of accuracy and type of excavation method, respectively mechanized versus conventional tunnelling is suggested as well as detailed analyses of contaminated excavation material originating from subsurface tunnelling and mining sites.

Declaration of Competing Interest

The authors declare that they have no known competing financial interests or personal relationships that could have appeared to influence the work reported in this paper.

References

- Allesch, A., Brunner, P.H., 2017. Material flow analysis as a tool to improve waste management systems: the case of Austria. *Environ. Sci. Technol.* 51, 540–551. <https://doi.org/10.1021/acs.est.6b04204>.
- Allwood, J., Ashby, M., Gutowski, T., Worrell, E., 2011. Material efficiency: a white paper. *Resour. Conserv. Recycl.* 55, 362–381. <https://doi.org/10.1016/j.resconrec.2010.11.002>.
- Altamura, P., 2013. Gestione eco-efficace dei materiali da costruzione nel ciclo di vita dell'edificio. Strumenti per la prevenzione, il riuso e il riciclo dei rifiuti da C&D, PhD thesis. Sapienza University, Rome, Italy.
- Andrews, D., 2015. The circular economy, design thinking and education for sustainability. *Local Econ* 30, 305–315. <https://doi.org/10.1177/0269094215578226>.
- Arm, M., Wik, O., Engelsen, C.J., Erlandsson, M., Hjelmar, O., Wahlström, M., et al., 2017. How Does the European Recovery Target for Construction & Demolition Waste Affect Resource Management? *Waste and Biomass Valorization* 8, 1491–1504. <https://doi.org/10.1007/s12649-016-9661-7>.
- Association Française des Tunnels Et De L'Espace Souterrain, A., 2019. Recommendations of AFTES GT35RIA2: Management and Use of Excavated Materials. FFE - Advertising agency, Paris, France 15 rue des sablons, 75116.
- Ayres, R., Talens Peiró, L., 2013. Material efficiency: rare and critical metals. *Philos. Trans. A. Math. Phys. Eng. Sci.* 371, 20110563. <https://doi.org/10.1098/rsta.2011.0563>.
- Blengini, G., Garbarino, E., 2010. Resources and waste management in Turin (Italy): the role of recycled aggregates in the sustainable supply mix. *J. Clean. Prod.* 18, 1021–1030. <https://doi.org/10.1016/j.jclepro.2010.01.027>.
- Brombal, D., Wang, H., Pizzol, L., Critto, A., Giubilato, E., Guo, G., 2015. Soil environmental management systems for contaminated sites in China and the EU. Common challenges and perspectives for lesson drawing. *Land use policy* 48, 286–298. <https://doi.org/10.1016/j.landusepol.2015.05.015>.
- Bundesamt für Umwelt, W. und L. (BUWAL), 1999. Aushubrichtlinie [WWW Document]. URL https://www.abfall.ch/pages/info/pdf/CH40_Aushubrichtlinie.pdf (accessed 2.19.20).
- Bundesministerium Klimaschutz Umwelt Energie Mobilität Innovation und Technologie, 2017. Bundes-Abfallwirtschaftsplan [WWW Document]. URL <https://www.bmlrt.gv.at/umwelt/abfall-ressourcen/bundes-abfallwirtschaftsplan/BAWP2017-Final.html> (accessed 6.5.20).
- Bundesministerium Landwirtschaft Regionen und Tourismus, 2008a. Abfallverzeichnisverordnung [WWW Document]. URL <https://www.ris.bka.gv.at/GeltendeFassung/Bundesnormen/20003077/Abfallverzeichnisverordnung%2CFassungvom19.02.2020.pdf> (accessed 2.19.20).
- Bundesministerium Landwirtschaft Regionen und Tourismus, 2008b. Deponieverordnung 2008 [WWW Document]. URL <https://www.ris.bka.gv.at/GeltendeFassung/Bundesnormen/20005653/DVO2008%2CFassungvom19.02.2020.pdf> (accessed 2.19.20).
- Bundesministerium Landwirtschaft Regionen und Tourismus, 2002. Abfallwirtschaftsgesetz [WWW Document]. URL <https://www.ris.bka.gv.at/GeltendeFassung/Bundesnormen/20002086/AWG2002%2CFassungvom19.02.2020.pdf> (accessed 2.19.20).
- Bundesministerium Landwirtschaft Regionen und Tourismus, 1989. Altlastensanierungsgesetz [WWW Document]. URL <https://www.ris.bka.gv.at/GeltendeFassung.wxe?Abfrage=Bundesnormen&Gesetzesnummer=10010583> (accessed 2.19.20).
- Bundesministers für Land- und Forstwirtschaft Umwelt und Wasserwirtschaft, 2015. Recycling-Baustoffverordnung [WWW Document]. URL <https://www.ris.bka.gv.at/GeltendeFassung.wxe?Abfrage=Bundesnormen&Gesetzesnummer=20009212> (accessed 6.5.20).
- Bureau de recherches géologiques et minières, 2016. Guide méthodologique de comblement de cavités à l'aide de matériaux alternatifs.
- Cabello Eras, J., Sagastume, A., Capote, D., Hens, L., Vandecasteele, C., 2013. Improving the environmental performance of an earthwork project using cleaner production strategies. *J. Clean. Prod.* 47, 368–376. <https://doi.org/10.1016/j.jclepro.2012.11.026>.
- Chittoori, B., Puppala, A., Reddy, R., Marshall, D., 2012. Sustainable Reutilization of Excavated Trench Material. *Geotechnical Special Publication*. <https://doi.org/10.1061/9780784412121.440>.
- Coronado, M., Dosal, E., Coz, A., Viguri, J., Andrés, A., 2011. Estimation of construction and demolition waste (C&DW) generation and multicriteria analysis of C&DW management alternatives: a case study in Spain. *Waste and Biomass Valorizat.* 2, 209–225. <https://doi.org/10.1007/s12649-011-9064-8>.
- Costituzione della Repubblica, 1942. Il Codice Civile Italiano [WWW Document]. URL http://www.jus.unitn.it/cardoza/Obiter_Dictum/codciv/Codciv.htm (accessed 2.27.20).
- Dahlbo, H., Bacher, J., Lähntinen, K., Jouttijärvi, T., Suoheimo, P., Mattila, T., Sironen, S., Myllymaa, T., Saramäki, K., 2015. Construction and demolition waste management - A holistic evaluation of environmental performance. *J. Clean. Prod.* 107. <https://doi.org/10.1016/j.jclepro.2015.02.073>.
- DELOITTE, 2015. Screening template for construction and demolition waste management in Italy [WWW Document]. URL https://ec.europa.eu/environment/waste/studies/deliverables/CDW_Italy_Factsheet_Final.pdf (accessed 3.24.20).
- DRAGON, 2014. DRAGON: development of resource-efficient and advanced underground technologies [WWW Document]. URL http://www.dragonproject.eu/_pdf/5301e37519b4c.pdf (accessed 2.14.20).
- European Commission, 2020. Construction and demolition waste [WWW Document]. URL https://ec.europa.eu/environment/waste/construction_demolition.htm (accessed 2.27.20).
- European Commission, 2018a. EU construction and demolition waste management protocol [WWW Document]. URL https://ec.europa.eu/growth/content/eu-construction-and-demolition-waste-protocol-0_pt (accessed 2.14.20).
- European Commission, 2018b. TEN-T evaluation roadmap [WWW Document]. URL https://ec.europa.eu/info/law/better-regulation/initiatives/ares-2018-4706847_en (accessed 6.5.20).
- European Commission, 2016. EU construction & demolition waste management protocol. *Off. J. Eur. Union* 1–22. <https://doi.org/10.3390/su11133638>.
- European Commission, 2016b. Sustainable use of natural resources [WWW Document]. URL https://ec.europa.eu/environment/archives/natres/titles1_2.htm (accessed 3.16.20).
- European Commission, 2012. A stronger European industry for growth and economic recovery [WWW Document]. URL <https://eur-lex.europa.eu/LexUriServ/LexUriServ.do?uri=COM:2012:0582:FIN:EN:PDF> (accessed 2.14.20).
- European Commission, 2011. Roadmap to a resource efficient Europe [WWW Document]. URL <https://eur-lex.europa.eu/legal-content/EN/TXT/PDF/?uri=CELEX:52011DC0571&from=EN> (accessed 2.14.20).
- European Commission, 2010. Europe 2020 - A European strategy for smart, sustainable and inclusive growth [WWW Document]. URL <https://ec.europa.eu/eu2020/pdf/COMPLETENBARROSO007-Europe2020-ENversion.pdf> (accessed 2.14.20).
- European Commission, 2008a. The raw materials initiative - meeting our critical needs for growth and jobs in Europe [WWW Document]. URL <https://eur-lex.europa.eu/LexUriServ/LexUriServ.do?uri=COM:2008:0699:FIN:en:PDF> (accessed 2.14.20).
- European Commission, 2008b. Sustainable consumption and production and sustainable industrial policy action plan [WWW Document]. URL <https://eur-lex.europa.eu/legal-content/EN/TXT/PDF/?uri=CELEX:52008DC0397&from=EN> (accessed 3.16.20).
- European Commission, 2008c. Directive 2008/98/EC on waste (waste framework directive) [WWW Document]. URL <https://ec.europa.eu/environment/waste/framework/> (accessed 2.27.20).
- European Commission, 2005. Trans-European transport network - TEN-T priority axes and projects [WWW Document]. URL https://ec.europa.eu/ten/transport/projects/doc/2005_ten_t_en.pdf (accessed 2.14.20).
- European Environment Agency, 2009. Diverting waste from landfill [WWW Document]. URL <https://www.eea.europa.eu/publications/diverting-waste-from-landfill-effectiveness-of-waste-management-policies-in-the-european-union> (accessed 3.11.20).
- Fischer, C., Werge, M., 2009. EU As a Recycling Society. Present recycling Levels of Municipal Waste and Construction & Demolition Waste in the EU. *European Topic Centre on Resource and Waste Management*, Copenhagen, Denmark.
- Galler, R., Voit, K., 2014. Tunnelausbruch - wertvoller mineralischer Rohstoff. In: *Betonkalender 2014. Jahrgang*. 103. pp. 423–468.

- Gálvez-Martos, J.-L., Styles, D., Schoenberger, H., Zeschmar-Lahl, B., 2018. Construction and demolition waste best management practice in Europe. *Resour. Conserv. Recycl.* 136, 166–178. <https://doi.org/10.1016/J.RESCONREC.2018.04.016>.
- Gangolelli, M., Casals, M., Forcada, N., Macarulla, M., 2014. Analysis of the implementation of effective waste management practices in construction projects and sites. *Resour. Conserv. Recycl.* 93, 99–111. <https://doi.org/10.1016/J.RESCONREC.2014.10.006>.
- Gertsch, L., Fjeld, A., Nilsen, B., Gertsch, R., 2000. Use of TBM muck as construction material. *Tunn. Undergr. Sp. Technol.* 15, 379–402. [https://doi.org/10.1016/S0886-7798\(01\)00007-4](https://doi.org/10.1016/S0886-7798(01)00007-4).
- Ghisellini, P., Ripa, M., Ulgiati, S., 2018. Exploring environmental and economic costs and benefits of a circular economy approach to the construction and demolition sector. A literature review. *J. Clean. Prod.* 178, 618–643. <https://doi.org/10.1016/J.JCLEPRO.2017.11.207>.
- Hiete, M., Stengel, J., Ludwig, J., Schultmann, F., 2011. Matching construction and demolition waste supply to recycling demand: a regional management chain model. *Build. Res. Inf.* 39, 333–351. <https://doi.org/10.1080/09613218.2011.576849>.
- Iacoboaia, C., Aldea, M., Petrescu, F., 2019. Construction and demolition waste - A challenge for the European union? *Theor. Empir. Res. Urban Manag.* 14, 30–52.
- Knapp, J., Allesch, A., Müller, W., Bockreis, A., 2017. Methods to estimate the transfer of contaminants into recycling products – A case study from Austria. *Waste Manag.* 69. <https://doi.org/10.1016/j.wasman.2017.08.035>.
- Korhonen, J., Honkasalo, A., Seppälä, J., 2018. Circular economy: the concept and its limitations. *Ecol. Econ.* 143, 37–46. <https://doi.org/10.1016/j.ecolecon.2017.06.041>.
- Krook, J., Svensson, N., Eklund, M., 2011. Landfill mining: a critical review of two decades of research. *Waste Manag.* 32, 513–520. <https://doi.org/10.1016/j.wasman.2011.10.015>.
- Kwan, J.C., Jardine, F., 1999. Ground engineering spoil: practices of disposal and reuse. *Eng. Geol.* 53, 161–166. [https://doi.org/10.1016/S0013-7952\(99\)00029-0](https://doi.org/10.1016/S0013-7952(99)00029-0).
- Lafebre, H., Songonuga, O., Kathuria, A., 1998. Contaminated soil management at construction sites. *Pract. Period. Hazardous, Toxic, Radioact. Waste Manag.* 2, 115–119. [https://doi.org/10.1061/\(ASCE\)1090-025X\(1998\)2:3\(115\)](https://doi.org/10.1061/(ASCE)1090-025X(1998)2:3(115)).
- Le Centre D'Etudes des Tunnels, C., 2016. Natural geological materials excavated during underground works.
- Lee, J., Pedersen, A., Thomsen, M., 2014. Are the resource strategies for sustainable development sustainable? Downside of a zero waste society with circular resource flows. *Environ. Technol. Innov.* 1. <https://doi.org/10.1016/j.eti.2014.10.002>.
- Luidold, S., et al., 2013. Kritische Rohstoffe für die Hochtechnologieanwendung. In: *Österreich, Berichte aus Energie- und Umweltschutz (Bundesministerium für Verkehr, Innovation und Technologie)*. Vienna.
- Magnusson, S., Lundberg, K., Svedberg, B., Knutsson, S., 2015. Sustainable management of excavated soil and rock in urban areas – A literature review. *J. Clean. Prod.* 93, 18–25. <https://doi.org/10.1016/J.JCLEPRO.2015.01.010>.
- Mangla, S.K., Govindan, K., Luthra, S., 2017. Prioritizing the barriers to achieve sustainable consumption and production trends in supply chains using fuzzy analytical hierarchy process. *J. Clean. Prod.* 151, 509–525. <https://doi.org/10.1016/J.JCLEPRO.2017.02.099>.
- Marzouk, M., Azab, S., 2014. Environmental and economic impact assessment of construction and demolition waste disposal using system dynamics. *Resour. Conserv. Recycl.* 82, 41–49. <https://doi.org/10.1016/j.resconrec.2013.10.015>.
- Mittal, V.K., Sangwan, K.S., 2014. Prioritizing barriers to green manufacturing: environmental, social and economic perspectives. *Procedia CIRP* 17, 559–564. <https://doi.org/10.1016/j.procir.2014.01.075>.
- Moreno, B., García-Álvarez, M.T., 2018. Measuring the progress towards a resource-efficient European union under the Europe 2020 strategy. *J. Clean. Prod.* 170, 991–1005. <https://doi.org/10.1016/j.jclepro.2017.09.149>.
- Österreichische Bautechnik Vereinigung, 2015. Richtlinie “Verwendung Von Tunnelausbruchmaterial. Österreichische Bautechnik Vereinigung ÖBV.
- Pacheco-Torgal, F., 2020. Introduction to advances in construction and demolition waste. pp. 1–10. <https://doi.org/10.1016/B978-0-12-819055-5.00001-2>.
- Pacheco-Torgal, F., Jalali, S., 2011. *Eco-efficient Construction and Building Materials*. Springer Verlag, London.
- Pacheco-Torgal, F., Labrincha, J.A., 2013. The future of construction materials research and the seventh millennium development goal: a few insights. *Constr. Build. Mater.* 40, 729–737. <https://doi.org/10.1016/j.conbuildmat.2012.11.007>.
- Panagos, P., Van Liedekerke, M., Jones, A., Montanarella, L., 2012. European soil data centre: response to European policy support and public data requirements. *Land use policy* 29, 329–338. <https://doi.org/10.1016/j.landusepol.2011.07.003>.
- Poulikakos, L.D., Papadaskalopoulou, C., Hofko, B., Gschösser, F., Cannone Falchetto, A., Bueno, M., Arraigada, M., Sousa, J., Ruiz, R., Petit, C., Loizidou, M., Partl, M.N., 2017. Harvesting the unexplored potential of European waste materials for road construction. *Resour. Conserv. Recycl.* 116, 32–44. <https://doi.org/10.1016/j.resconrec.2016.09.008>.
- Rahimzadeh, A., Sher, W., Davis, P., Tang, W., 2018. Management of excavated material in infrastructure construction—a critical review of literature. In: *Conference: International Conference on Architecture and Civil Engineering*. Sydney, Australia.
- Read, A., Hudgins, M., Harper, S., Phillips, P., Morris, J., 2001. The successful demonstration of aerobic landfilling: the potential for a more sustainable solid waste management approach? *Resour. Conserv. Recycl.* 115–146.
- Repubblica Italiana, 2013. DL 69/2013 convertito L. 98/2013 [WWW Document]. URL <https://www.gazzettaufficiale.it/eli/id/2013/08/20/13A07086/sg>.
- Repubblica Italiana, 2012. Decreto del Ministero dell'Ambiente e della tutela del Territorio e del Mare 10 agosto 2012, n. 161 Regolamento recante la disciplina dell'utilizzazione delle terre e rocce da scavo [WWW Document]. URL https://www.bosettiegatti.eu/info/norme/statali/2012_0161.htm (accessed 3.25.20).
- Repubblica Italiana, 2006a. Norme in materia ambientale [WWW Document]. URL <https://www.camera.it/parlam/leggi/deleghe/06152dl.htm> (accessed 3.24.20).
- Repubblica Italiana, 2006b. Decreto Legislativo 3 aprile 2006, n. 152 “Norme in materia ambientale” [WWW Document]. URL <https://www.camera.it/parlam/leggi/deleghe/06152dl3.htm> (accessed 3.25.20).
- Repubblica Italiana, 2003a. Decreto ministeriale (Ambiente) 8 maggio 2003, n. 203 [WWW Document]. URL https://www.bosettiegatti.eu/info/norme/statali/2003_0203.htm (accessed 3.24.20).
- Repubblica Italiana, 2003b. Decreto Ministeriale del 13/03/2003 Criteri di ammissibilità dei rifiuti in discarica [WWW Document]. URL http://www.ati4umbria.it/normativa/dm13_03_03.pdf (accessed 3.25.20).
- Repubblica Italiana, 1998. Decreto ministeriale di 3 September 1998 n°370 [WWW Document]. URL <https://www.gazzettaufficiale.it/eli/id/1998/10/26/098G0420/sg> (accessed 3.25.20).
- République et Canton de Genève, 2016. Guide pour la réutilisation des matériaux d'excavation non pollués. Service De géologie, Sols Et Déchets (GESDEC), 1ère édit. ed. République et Canton de Genève.
- République Française, 2016. Code Civil Français [WWW Document]. URL https://www.legifrance.gouv.fr/affichCode.do?cidTexte=LEGITEXT000006070721&dateTexte=20080225#.
- République Française, 2015. La loi du transition énergétique [WWW Document]. URL <https://www.legifrance.gouv.fr/affichTexte.do?cidTexte=JORFTEXT000031044385> (accessed 2.24.20).
- République Française, 2003. Code de l'environnement [WWW Document]. URL <https://www.legifrance.gouv.fr/affichCode.do?cidTexte=LEGITEXT000006074220>.
- Resch, D., Lassnig, K., Galler, R., Ebner, F., 2009. Tunnel excavation material - high value raw material. *Geomech. und Tunnelbau* 2, 612–618. <https://doi.org/10.1002/geot.200900047>.
- Rios, F.C., 2018. Beyond recycling: design for disassembly, reuse, and circular economy in the built environment.
- Ritter, S., Einstein, H., Galler, R., 2013. Planning the handling of tunnel excavation material – A process of decision making under uncertainty. *Tunn. Undergr. Sp. Technol.* 33, 193–201. <https://doi.org/10.1016/j.tust.2012.08.009>.
- Ritzén, S., Sandström, G.Ö., 2017. Barriers to the circular economy – integration of perspectives and domains. *Procedia CIRP* 64, 7–12. <https://doi.org/10.1016/J.PROCIR.2017.03.005>.
- Robben, C., Wotruba, H., 2019. Sensor-based ore sorting technology in mining—past, present and future. *Minerals* 9, 523. <https://doi.org/10.3390/min9090523>.
- Robinson, G., Kapo, K., 2004. A GIS analysis of suitability for construction aggregate recycling sites using regional transportation network and population density features. *Resour. Conserv. Recycl.* 42, 351–365. <https://doi.org/10.1016/j.resconrec.2004.04.009>.
- Rodríguez, G., Alegre, F.J., Martínez, G., 2007. The contribution of environmental management systems to the management of construction and demolition waste: the case of the autonomous community of Madrid (Spain). *Resour. Conserv. Recycl.* 50, 334–349. <https://doi.org/10.1016/J.RESCONREC.2006.06.008>.
- Savage, G.M., Golueke, C.G., von Stein, E.L., 1994. Landfill mining: past and present. *BioCycle* (USA).
- Silva, R.V., Brito, J., Dhir, R., 2016. Availability and processing of recycled aggregates within the construction and demolition supply chain: a review. *J. Clean. Prod.* 143. <https://doi.org/10.1016/j.jclepro.2016.12.070>.
- Simion, I., Fortuna, M., Bonoli, A., Gavrilescu, M., 2013. Comparing environmental impacts of natural inert and recycled construction and demolition waste processing using LCA. *J. Environ. Eng. Landsc. Manag.* 21, 273–287. <https://doi.org/10.3846/16486897.2013.852558>.
- Swiss Confederation, 2016. Ordinance on the avoidance and the disposal of waste [WWW Document]. URL <https://www.admin.ch/opc/en/classified-compilation/20141858/201901010000/814.600.pdf> (accessed 2.19.20).
- Swiss Confederation, 2005. Ordonnance sur les mouvements de déchets [WWW Document]. URL <https://www.admin.ch/opc/fr/classified-compilation/20021080/index.html> (accessed 2.19.20).
- Swiss Confederation, 1999. Bundesverfassung der Schweizerischen Eidgenossenschaft [WWW Document]. URL <https://www.admin.ch/opc/de/classified-compilation/19995395/202001010000/101.pdf> (accessed 2.24.20).
- Swiss Confederation, 1998. Ordinance on the remediation of polluted sites (Contaminated Sites Ordinance, CSO) [WWW Document]. URL <https://www.admin.ch/opc/en/classified-compilation/19983151/201705010000/814.680.pdf> (accessed 2.24.20).
- Swiss Confederation, 1983. Federal act on the protection of the environment [WWW Document]. URL <https://www.admin.ch/opc/en/classified-compilation/19830267/201801010000/814.01.pdf> (accessed 2.24.20).
- Swiss Confederation, 1907. Schweizerisches Zivilgesetzbuch [WWW Document]. URL <https://www.admin.ch/opc/de/classified-compilation/19070042/202001010000/210.pdf> (accessed 2.24.20).
- Velis, C.A., Brunner, P.H., 2013. Recycling and resource efficiency: it is time for a change from quantity to quality. *Waste Manag. Res.* 31, 539–540. <https://doi.org/10.1177/0734242X13489782>.
- Vieira, C., Pereira, P., 2015. Use of recycled construction and demolition materials in geotechnical applications: a review. *Resour. Conserv. Recycl.* 103, 192–2014. <https://doi.org/10.1016/j.resconrec.2015.07.023>.
- Whittaker, M.J., Grigoriadis, K., Soutsos, M., Sha, W., Klinge, A., Paganoni, S., Casado, M., Brander, L., Mousavi, M., Scullin, M., Correia, R., Zerbi, T., Staiano, G., Merli, I., Ingrassio, I., Attanasio, A., Largo, A., 2019. Novel construction and demolition waste (CDW) treatment and uses to maximize reuse and recycling. *Adv. Build. Energy Res.* 1–17. 0. <https://doi.org/10.1080/17512549.2019.1702586>.
- Zuidema, P., 2015. The Swiss waste management program. *Prog. Nucl. Energy* 84. <https://doi.org/10.1016/j.pnucene.2015.02.002>.

A.2 Applicability of excavated rock material: A European technical review implying opportunities for future tunnelling projects

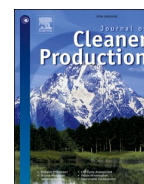
Table A.2: Overview of authorship and metadata of the presented publication.

Title	Applicability of excavated rock material: A European technical review implying opportunities for future tunnelling projects
Author names	Maximilian Haas, Laëtitia Mongeard, Luisa Ulrici, Laetitia D'Aloïa, Agnès Cherrey, Robert Galler, Michael Benedikt
First author	Maximilian Haas
First author's contributions	Conceptualization; literature review; formal analysis; visualizations; writing (original draft); writing (review & editing)
Scientific value	Introduction of a new terminology within the framework of excavated tunnel material, as well as a state-of-the-art review of European subsurface construction projects and applied technical usage scenarios.
Status	Published in <i>Journal of Cleaner Production</i>
Peer-reviewed journal	Yes
Full citation	Haas M., Mongeard L., Ulrici L., D'Aloïa L., Cherrey A., Galler R., Benedikt M., Applicability of excavated rock material: A European technical review implying opportunities for future tunnelling projects, <i>Journal of Cleaner Production</i> , Volume 315 (2021), ISSN 0959-6526, https://doi.org/10.1016/j.jclepro.2021.128049 .



Contents lists available at ScienceDirect

Journal of Cleaner Production

journal homepage: www.elsevier.com/locate/jclepro

Applicability of excavated rock material: A European technical review implying opportunities for future tunnelling projects

Maximilian Haas^{a,b,*}, Laëtitia Mongeard^c, Luisa Ulrici^a, Laetitia D'Aloia^d, Agnès Cherrey^d, Robert Galler^b, Michael Benedikt^a

^a European Organization for Nuclear Research (CERN), Esplanade Des Particules 1, 1211, Meyrin, Switzerland

^b Subsurface Engineering, Montanuniversität, Erzherzog-Johann-Strasse 3, 8700, Leoben, Austria

^c ENS de Lyon, 15 Parvis René Descartes, 69007, Lyon, France

^d Centre d'Études des Tunnels (CETU), 25 Avenue François Mitterrand, 69500, Bron, France

ARTICLE INFO

Handling editor: Cecilia Maria Villas Bôas de Almeida

Keywords:

Future circular collider (FCC)
Excavated tunnel material
Subsurface
Tunnelling

ABSTRACT

The European Organization for Nuclear Research (CERN) is a world-wide leading organisation in the field of particle physics and operation of high-class particle accelerators. Since 2013, CERN has undertaken feasibility investigations for a particle accelerator, named Future Circular Collider (FCC) to be installed within a 90–100 km subsurface infrastructure likely to enter construction phase after 2030. An important aspect of its construction and environmental impact assessment is the management of approximately 9.1 million m³ of excavated rock and soil. The aim of this paper is to thoroughly review the applications of excavated material across European subsurface construction projects from a technical point of view and set them into context with studies currently ongoing for FCC. We propose a conceptual flow model for rock characterisation with respect to both applicability of excavated material and tunnelling excavation techniques for future international subsurface construction projects.

The review has revealed a vast and encouraging potential across different European construction sites efficiently using excavated rock and soil over the past decade ranging from concrete production, geopolymer production, embankment and landfilling. Examples of reviewed subsurface tunnelling projects are likely to be applied for FCC including concrete production, clay-sealing for embankments, geopolymer face stabilization, re-cultivation or agricultural usage as mixed soil material or sustainable waste disposal.

1. Introduction

The utilisation of excavated rock and soil has gained worldwide significance in a circular economy based on the principle “Reduce, Re-Use and Recycle” (Esa et al., 2016; Geissdoerfer et al., 2017; Ghisellini et al., 2018; Huang et al., 2018; Korhonen et al., 2018). More than 200 international tunnels longer than 3000 m are currently under construction representing about 600 million tons of excavation material (EXMAT) (Burdin et al., 2017), whereas infrastructure projects forecast about 800 million tons within the next 50 years urging a thorough review of subsurface construction projects and associated industrial applications for excavated material (Burdin, 2015; DRAGON, 2014; Iacoboaia et al., 2019).

During the past twenty years, large subsurface infrastructure projects produced a vast amount of excavated material (Galler, 2016, 2019,

2016; Resch et al., 2009), adapted associated legislation (Haas et al., 2020b; Resch, 2012) and endeavoured sustainable waste reduction (Cabello Eras et al., 2013; Magnusson et al., 2015). Environmental considerations are an inevitable keystone for the construction approval and hence, require to demonstrate potential scenarios or disposal as well as management concepts of using excavated material (Erben, 2016; Galler, 2015; Voit and Kuschel, 2020). Although finding utilisations of excavated material are compulsory, recurring technical challenges remain and originate from geological complexity and underlying processing techniques (Lassnig, 2012). This complexity is anchored in the interdisciplinarity across all fields of geosciences, including mineralogy, geochemistry, petrophysics and rock mechanics. Strategies demand thorough pre-investigations, years before the start of drilling campaigns, to analyse a representative amount of encountered rock during construction. Then, proposed laboratory analyses build the foundation to derive a rock characterisation upscaled for potential usage of the

* Corresponding author. Esplanade Des Particules 1, 1211, Meyrin, Switzerland.

E-mail address: maximilian.mathias.haas@cern.ch (M. Haas).

<https://doi.org/10.1016/j.jclepro.2021.128049>

Received 12 January 2021; Received in revised form 17 June 2021; Accepted 19 June 2021

Available online 25 June 2021

0959-6526/© 2021 Elsevier Ltd. All rights reserved.

List of abbreviations

AFTES	Association Française des Tunnels et de l'Espace Souterrain	EU	European Union
AUT	Austria	FCC	Future Circular Collider
BBT	Brenner Base Tunnel	FR	France
CBT	Ceneri Base Tunnel	GBT	Gotthard Base Tunnel
CERN	European Organization for Nuclear Research	GER	Germany
CETU	Le Centre d'Etudes des Tunnels	GPE	Grand Paris Express tunnel system
CEVA	Tunnel de Champel	HL-LHC	High-Luminosity Large Hadron Collider
CH	Switzerland	KAT	Koralalm Tunnel
DIN	Deutsches Institut für Normung	LBT	Lötschberg Base Tunnel
DRAGON	Development of Resource-efficient and Advanced Underground Technologies	LHC	Large Hadron Collider
EN	European Norm	ÖBB	Österreichische Bundesbahnen (Austrian Rail Network)
EPB	Earth Pressure Balanced tunnel boring machine	SBT	Semmering Base Tunnel
		TBM	Tunnel Boring Machine
		TELT	Tunnel Euralpin Lyon Turin SAS
		UK	United Kingdom

underlying excavated geology (Skuk and Schierl, 2017). Several tunnelling projects started rock investigations focusing explicitly on one potential application scenario due to either technical feasibility, geological conditions or time-savings. This, in most cases, inferred concrete aggregate applicability (Burdin et al., 2017). However, rock material tests can last for several months (Galler et al., 2012) and the development of new concepts can take up to one decade (DRAGON, 2014; Erben and Galler, 2014; Resch et al., 2009; Vollprecht et al., 2019).

For this reason, the Future Circular Collider (FCC) study at the European Organization for Nuclear Research (CERN) started its geological analyses in 2018. Upon project realisation, the FCC underground infrastructure would rank at the topmost ambitious subsurface projects across Europe within the next 20 years and will host particle colliders as successors of the Large Hadron Collider (LHC) at CERN.

In this paper, state-of-the-art utilisation of excavated material is discussed by a thorough review of referenced European subsurface projects and case studies. Based on these examples, their excavated material is set into context with excavation methods (conventional versus mechanised tunnelling), and potential applications for FCC are outlined in an engineering context deriving a general procedure for rock characterisation approaches and raw material management. In accordance with environmental and legal considerations, first characterisation and management concepts are stated and introduce the utilisation of excavated material as part of the FCC study to favour successful project approval and construction of a 90–100 km quasi-circular subsurface infrastructure (Abada et al., 2019; Benedikt et al., 2020; Bruning et al., 2013).

2. Applications and challenges of excavated rock material

2.1. Former applications

Landfilling was one of the first concepts in 1953, which used excavated tunnel material (Savage et al., 1994). Until the 1980's, the utilisation of excavated material as part of subsurface construction sites was neglected due to a simple reason: tunnel boring machine (TBM) cutterheads mainly consisted of bits that produced fine-grained excavated material, which hampered applications drastically (Thalmann et al., 2003). An increasing shift towards reduction of landfills due to recent regulations encourages its usage and underlines its environmental and technical requirement in a sustainable resource economy across Europe (European Commission, 2008, 2010, 2011, 2012, 2011, 2008; Krook et al., 2011). Former research has derived legal implications of using and managing excavated material from subsurface tunnelling projects (Haas et al., 2020b), as well as indicated that the use

of excavated rock and soil are efficiently reducing climate impact, transportation, the amount of landfilled material and the need of quarry material (Blengini and Garbarino, 2010; CL:AIRE, 2013; Magnusson et al., 2015; Simion et al., 2013; Zuo et al., 2013). The transition of waste to a resource is the premise to reduce environmental impacts in closest vicinity to the construction site and increase sustainability on both regional and national scales. Crucial decisions for feasibility concepts require large surface or subsurface storage facilities to treat – or in case of waste – dispose excavated material. Potentially large areas for interim disposal and timing of disposed material foresee a well-planned schedule, which is strongly associated to geological risks encountered during excavation.

Concrete aggregate production from tunnelling projects currently ranks at the highest quality of application scenarios (Akhtar and Sar-mah, 2018). Its usage on construction site is targeted for installations of tunnel inner lining elements or invert construction as the concrete material provides a vast amount of different characteristics applicable to several installation steps during construction (Voit and Zimmermann, 2015). Former prognoses estimated about 6% of excavated material to be used as concrete aggregates and 15% suitable as filling material implying that 79% had to be deposited (Becker et al., 1997; Saathof and Ketelaars, 1999), whereas it must be noted that these percentage values are highly dependent on underlying geological conditions.

In the past ten years, a general trend towards advanced resource-efficient strategies in the European Union, in line with the European initiative (European Commission, 2011, 2012), has been observed based on former research focusing on utilising excavated tunnel material in various scenarios (Moreno and García-Álvarez, 2018). The DRAGON project aimed for new developments of a prototype for automated bypass analyses, on-line classifications and in-stream sorting of excavated material mounted on TBMs (DRAGON, 2014). In addition, valuable excavated rock and soil were identified via advanced analysing techniques specifically adapted for excavated material in geographical information system (GIS) applications. Successful utilisation of excavated rock caused a general trend towards improved environmental performance, which finally led to an increased public awareness and has continuously forced engineers to come up with innovative solutions of using excavated material (Cabello Eras et al., 2013; Lafebre et al., 1998; Read et al., 2001; Robben and Wotruba, 2019; Robinson and Kapo, 2004; Rodríguez et al., 2007).

2.2. Technical challenges

During construction, the inspection of excavated material is usually conducted by a geologist in conventional tunnelling or by different camera types and sensors at the tunnel face in mechanised tunnelling

Table 1
Overview of compared European subsurface construction projects with geological units and main usage scenarios. *Scheduled date.

Country	Construction project	Type	Length (km)	Start of construction	Opening	Client	Encountered rock type	Main use	References
Switzerland	Gotthard Base tunnel	rail	51.1	1999	2016	AlpTransit Gotthard AG	granite, fragmented sediments	concrete aggregates, backfilling, embankment, disposal	AlpTransit Gotthard (2017), Ehrbar (2008), Fabbri (2004), Fachgruppe für Untertagebau, FGU (2016)
Switzerland	Löschberg Base tunnel	rail	34.6	1999	2007	BLS AlpTransit AG	sandstone, limestone, granodiorite, gneiss, granite, amphibolite	concrete aggregates, embankment, landfill, disposal	AlpTransit Gotthard (2017), Burdin et al. (2017), Ernst Basler and Partner (2012), Teuscher et al. (2007), Ziegler and Isler (2013), Fachgruppe für Untertagebau, FGU (2016)
Germany	Katzenberg tunnel	rail	9.4	2003	2012	Deutsche Bahn	sandstone, conglomerate, anhydrite/gypsum	concrete aggregates, embankment, landfill, disposal	Burdin et al. (2017), Haid and Hammer (2009)
Switzerland	Nant de Drance hydropower plant	hydropower plant	n/a	2008	2014	Nant de Drance SA	mylonite, granite, gneiss, grauwacke	concrete aggregates, landfill	Burdin et al. (2017), International Tunneling and Underground Space Association(2019), Fachgruppe für Untertagebau, FGU (2016)
Austria	Semmering Base tunnel	rail	27.3	2012	2027*	ÖBB Infrastruktur AG	albite-gneiss, amphibolite, dolomite, marble, mica-shale, phyllitic material	disposal	Daltler (2017), Elkici et al. (2011)
Austria	Koralpin tunnel	rail	38.9	2009	2026*	ÖBB Infrastruktur AG	gneiss, amphibolite, marble, mica-shale, sandstone, siltstone	concrete aggregates	(Posch et al. (2014, 2015b), Schubel and Schaffer (2020)
Austria/Italy	Brenner Base tunnel	rail	64.0	2015	2027*	Brenner Basisstunnel BBT SE	Bündnerschiefer, quartz phyllite, gneiss, granite	concrete aggregates, drainage gravel, embankment, landfill, disposal	Bergmeister (2013, 2007), Gattinoni et al. (2016), Skuk and Schierl (2017), Tamparopoulos (2012), Voit (2013), Voit and Kuschel (2020), Wenighofer and Galler (2017)
France/Switzerland	High-Luminosity Large Hadron Collider	laboratory	-	2018	2020	CERN	sandstone, marl, conglomerate, anhydrite/gypsum	industrial consumers for concrete, embankment, disposal	Voiron et al. (2020)
France	Grand Paris Express	rail	205	2015	2030*	Société du Grand Paris (SGP)	sandstone, marl, conglomerate, anhydrite/gypsum	embankments	Le Centre D'Etudes des Tunnels (2019, 2017, 2016), Vernus et al. (2017)
France/Italy	Lyon-Turin	rail	53.7	2011	2030*	TELT, SNCF Réseau & RFI	quartzite, limestone, gneiss, mica-shale, sandstone, anhydrite/gypsum, shale, carbon, gneiss	concrete aggregates, embankment, landfill	Bufalini et al. (2017), Burdin and Monin (2009), Stephen (2020), T.E.L.T. consortium (2020), T.E.L.T. consortium (2018)
United Kingdom	Crossrail	rail	118	2009	2023*	UK Network Rail	clayey material (London clay)	island construction	Kelly (2020), Wood and Agency (2017)
Switzerland	CEVA	rail	1.62	2012	2017	canton Geneva	glacial, unconsolidated sediments	concrete aggregates	Fachgruppe für Untertagebau, FGU (2016)

(Robben and Wotruba, 2019; Wenighofer and Galler, 2017). This allows for a separation of excavated rock into technical application classes. Subsequently, the material is sorted, processed, and, if required, temporarily stored. Suitable systems of dry or wet processing is costly. Hence, the operation of processing plants under different conditions as well as high demands upon quality control require a sophisticated material management plan (Burdin et al., 2017; Voit, 2013).

Environmental impact assessments and related regulations force an increased recognition of the utilisation of excavated material upon successful project approval (Marzouk and Azab, 2014; Thalmann, 1996). Excavated material is analysed chemically, mineralogically and geomechanically in advance and prepared for processing on a small-scale in laboratories followed by large-scale analyses on construction sites. These analyses characterise the material for engineering purposes into subsequent application classes. Reconciliation of these analyses with national and European legislation classify excavated material as waste if they leave the construction site, requiring technical procedures such as processing (washing, crushing, sieving) and treating (chemically and/or physio-mechanically) conducive to removal of waste status in favour of environmental sustainability (Blengini and Garbarino, 2010; Dahlbo et al., 2015). The definition of excavated material as *waste* per se does not hamper its potential applications but rather leads to rigorous engineering procedures and laboratory analyses aiming for compliance with legal thresholds and regulations upon removal of polluting substances (Rios, 2018; Ritter et al., 2013; Ritzén and Sandström, 2017; Rodríguez et al., 2007).

3. Methodology

Within the next two decades, upgraded infrastructure is built through the Western and Eastern Alps for goods transportation. The New Railway Through the Alps (NRLA) route (AlpTransit Gotthard, 2017) including the Ceneri and Gotthard Base tunnel and the Trans-European Transport Network (TEN-T) represent major upgrades of several tunnels creating and connecting high-speed routes such as the south-west Europe Salamanca-Porto-Lisboa-Madrid-Paris-Lyon or Lyon-Torino-Trieste-Ljubljana-Budapest axes (European Commission, 2005, 2018). In total, this will comprise additionally 4800 km of roads and 12500 km of rails resulting in million tons of excavated material. This deems an evaluation necessary for past and current construction projects.

For this study, subsurface infrastructure projects stated in Table 1 across France, Switzerland, Austria, Italy and the United Kingdom have been thoroughly investigated on a site-specific and state-of-the-art basis by analysing project related data, visiting dedicated construction sites, talking to project engineers, international experts and governmental entities and reviewing scientific literature. Findings are presented in tables compiled from construction reports, final project reports and the literature. National and European legislation about using and managing excavated rock and soil is used to frame discussions, whereas the reader is referred to Haas et al. (2020b) for a detailed legal derivation across European countries. Case studies listed in Table 1 provide a variety of technical scenarios to use excavated material considering heterogeneous geological conditions, technical challenges for processing raw material and environmental issues such as heavy metal ion concentrations, natural radioactivity or hydrocarbon contaminations.

During the review process, legal and contractual documents as well as site-specific reports and scientific literature used different terminology with respect to using and handling excavated material. These terms often implied a legal status in case the excavated material is referred to as waste. For consistency purposes in this study, the terms *applicability*, *application*, *use*, *usage* and *utilisation* are concurrently used and imply a neutral handling of excavated material with no further legal implications. Although very common, the term *re-use* is strictly avoided as it implies misleading information, since raw excavated material has not been used before and should not be confused with the term *recycling*. In

case excavated material is inferred from a legal point of view, this is explicitly mentioned.

It must be noted that exact values for excavated and utilised material varied substantially depending on advancement of construction, continuous improvement of material flow analyses, different techniques in real-world projects and scientific literature. Associated discussions on implications for the FCC underground infrastructure and potential applications are further compared with reviewed case studies.

4. Applicability of tunnel excavation material across Europe

This section provides a technical in-depth review of each European subsurface project listed in Table 1. National and cross-border issues are highlighted and build the technical foundation for comparisons of engineering demands and technical applications scenarios for FCC mentioned in succeeding sections.

4.1. Austria

4.1.1. Koralm tunnel (KAT)

The Koralm tunnel delivers a faster connection between the counties Styria and Carinthia. Contract KAT2 produced about 8.6 million tons of excavated rock and soil (Posch et al., 2015b), whereas about 50% of the suitable tunnel spoil was preliminarily screened, divided into four classes and used for concrete aggregate production including high-strength concrete with a main purpose of inner lining element casting (Posch et al., 2015b; Voit et al., 2015). Investigations on iron and aluminium eluate concentrations were performed and included tests of selected additives such as cement or resin foam (Posch et al., 2015a). According to Austrian legislation under the Federal Waste Management Plan (Bundesministerium Klimaschutz Umwelt Energie Mobilität Innovation und Technologie, 2017) and the Landfill Regulations (Bundesministerium Landwirtschaft Regionen und Tourismus, 2008), material excavated from tunnel is declared as waste. Adverse discrepancies with authorities resulted in delays with the client and contractor on conclusions about the excavated material, its chemical evaluation (threshold limits) and decisions for final usage (Posch et al., 2014).

4.1.2. Brenner Base tunnel (BBT)

The Brenner Base tunnel opens a faster connection along the Scandinavian-Mediterranean TEN-T railway axis from Helsinki, Finland to Valletta, Island of Malta through the southern Italian ports, extending from Innsbruck, Austria to Fortezza (Franzensfeste) in Italy. Predictions estimated about 43 million tons of excavated Buendner schist (Bündnerschiefer), quartz phyllite, gneiss and granite (Voit et al., 2015). Laboratory and on-site analyses were performed to check for potential applications of excavated material. These large-scale tests inferred about 55 tons of raw material from drilling and blasting excavation and were processed in several steps starting with the largest grain size of 700 mm. In a first iteration, processing started with crushing the material by a jaw crusher and impact mill under wet conditions to eliminate fine-grained particles with a bucket wheel. After certain processing improvements, a second optimized procedure included a separator grid, wet sieving equipment, a vertical mill and cyclone separation equipment that produced reasonable results and succeeded laboratory tests for concrete mixtures and durability (Voit et al., 2015). A geomechanical classification encountered main geological units and faults and paved the way towards potential use scenarios (Gattinoni et al., 2016). Chemical adjustments optimized concrete feasibility and were used for high-quality concrete and shotcrete. The outcome of extensive laboratory investigations summarized representative excavated material into four lithostratigraphic units (Voit, 2013), and differentiated among three application classes for high quality material for concrete aggregates (class A), medium-quality material for embankment and backfilling (class B) and non-useable material determined for disposal (Bergmeister, 2013).

4.2. Switzerland

In Switzerland, the Swiss Tunnelling Society (STS) currently aims for the development of a new excavation guideline as part of the *Schweizerischer Ingenieur-und Architektenverein* (Swiss Society of Engineers and Architects), SIA. This implies a mutual database starting with the largest tunnelling projects in Switzerland (Fachgruppe für Untertagebau (FGU), 2016). A similar approach has been suggested by Haas et al. (2020a) on a European scale. Each application category for using excavated material requires the analysis of different geomechanical, petrophysical, chemical and mineralogical parameters (e.g. grain size, grain shape, grain density, rock composition), which are regulated in Swiss SIA and Schweizerischen Verbands der Straßen-und Verkehrsfachleute (Swiss Association of Road and Transport Professionals), VSS standards.

4.2.1. Gotthard Base tunnel (GBT)

The two-tube railway Gotthard Base tunnel extends from the north portal at Erstfeld in canton Uri to the south portal at Bodio in canton Ticino. The main tunnel consists of a total length of 57 km making it currently the longest tunnel in the world, and an essential part of the TEN-T network (European Commission, 2005). The complete subsurface infrastructure consists of 153.3 km of access tunnels, shafts, railway tunnels, connecting galleries and auxiliary structures (Ehrbar, 2008). About 80% of excavation was performed by open hard-rock TBM (lots Bodio and Amsteg) and 20% by conventional drilling and blasting (lot Faido), excavating a total volume of 28.2 million tons of granite and highly fragmented sediments (AlpTransit Gotthard, 2017). Construction processing plants have been realised to recycle the muck and to produce concrete aggregates. Depending on the petrography and the properties of the excavated material, about 28% of the entire muck could be used. The expected recycling rate was approximately 85%, while the concrete aggregate production was estimated at about 22% of the entire muck. Parts of the excavated material were used as filling material and the remaining material was transported to final deposits or to an inert landfill. Three application classes were identified ranging from concrete aggregate production (A) to backfilling and embankment material (B) and contaminated or wet material (Z) (Fachgruppe für Untertagebau (FGU), 2016). At lot Bodio, about 65% were classified as class A material, while 75% were used for aggregates in concrete production and 2.15 million tons for embankment (Fachgruppe für Untertagebau (FGU), 2016). The muck contamination caused by loss of oil from TBMs, waste products from explosives, chemicals and heavy metals from rebounded shotcrete permitted to store this contaminated material in an inert landfill. The muck was transported with conveyor belt systems (Fabbri, 2004). External material from third-parties was bought from portal Bodio due to a supply gap between Bodio and Faido, geological fault systems and increasing excess of production (Fachgruppe für Untertagebau (FGU), 2016). Gravel processing plants were running for 10 years without interruptions. Lot Faido used 70% as class A material and provided another 10% to lot Bodio. About 0.7 million tons were used as embankment material in Biasca (ATG Ceneri). For Faido, no external material had to be bought from third parties. Lot Amsteg used 70% as class A material, of which 80% were used for concrete aggregates. Another 0.65 million tons were used for embankment in Altdorf, Rynächt and another 2.4 million tons for lake embankments in canton Uri. In total, 35% of excavated material at Amsteg were used and another 45% for lake embankments, whereas excess of press sludge turned out to be a significant problem. Concrete feasibility tests included geomechanical tests and crushing plants with integrated friction mill, powerful thickener installations and mica separation with flotation technique for adequate concrete quality (Thalmann et al., 2003).

4.2.2. Ceneri Base tunnel (CBT)

The twin-tube 15.4 km Ceneri Base tunnel marks together with the Gotthard and Lötschberg Base tunnels the main elements of the New Railway Links through the Alps (NRLA) route (Merlini et al., 2018). Its

underlying geology was subdivided into nine different geological formations ranging from gneiss to amphibolite, serpentinite, phyllonite and mylonite separated by major fault systems and entirely excavated by drill and blast with only a few metres of overlying rock (AlpTransit Gotthard, 2017; Merlini et al., 2018). Excavation started from Sigirino, as well as portals Vigana and Vezia. About 25% of 8.6 million tons of excavated material could be successfully used for concrete and shotcrete production. Remaining material was transported by conveyor belts to permanent deposits for the construction of a wild-animal corridor at Monte Ferrino (AlpTransit Gotthard, 2017).

4.2.3. Lötschberg Base tunnel (LBT)

Together with the Gotthard Base tunnel, the two-tube 34.6 km railway Lötschberg Base tunnel is part of the New Rail Link Through the Alps (NRLA) route and was constructed at north and south lots providing the first high-speed connection from Frutigen to Raron in Switzerland. Its opening in 2007 preceded the excavation of 16 million tons of rock and soil, whereas 10 million were associated to the south and 6 million to the north portal (Teuscher et al., 2007). The north tunnel was solely excavated by conventional methods (drill and blast), while the south tunnel portal was partly excavated by a hard-rock TBM as well as drill and blast in different geological units of sandstone, siliceous limestone, lithotamian limestone, granodiorite, gneiss, granite and amphibolite (Fachgruppe für Untertagebau (FGU), 2016; Teuscher et al., 2007). Excavated material was classified into three application classes ranging from concrete to sand-gravel production (K1), embankment and backfilling (K2) and disposal (K3). The excavated material was transported by conveyor belts to two silos. Additional conveyor belts connected the silos with two elevators mounted with cup ribbons and connected tubular conveyor belts for transporting the material to processing equipment. Transportation of excavated material was conducted by train on tipping gutters for industrial shipment. Dumpers, loaders, excavators and bulldozers supported the transport of excavated material among conveyor belts and trains on-site. Well-timed gravel processing at the north portal allowed production of concrete aggregates in compliance with the south portal to avoid any excess of material at the end of construction (Fachgruppe für Untertagebau (FGU), 2016). Pressed sludge had a significant impact on the processing as this material was not allowed to be disposed temporarily due to groundwater contamination. A high percentage of sludge was contaminated with hydrocarbons, which forced disposal as hazardous waste. In total, 40% of excavated material could be used, which covered the full demand for concrete aggregate production on-site. The most important element at Lötschberg was the gravel processing equipment for concrete production. Different crushing, washing and sieving equipment sorted the material to make it applicable for concrete production. The southern tunnel occupied about 20 ha of processing equipment for loading/unloading of trains, construction vehicles, interim disposal, concrete aggregate material storage and offices.

4.2.4. Nant de Drance pumped-storage hydro power plant

This case study represents a pumped-storage hydro power plant construction in canton Wallis. Open hard-rock TBM and drill and blast advancement were chosen to excavate a total of 4.2 million tons of mylonite, granite, migmatic gneiss, orthogneiss and grauwacke. The owner, Nant de Drance SA, was supported by a dedicated staff managing the characterisation of excavation material, its handling, storing and using as concrete aggregate material. Four application classes were chosen to properly manage material for concrete production (1a), limited concrete production due to amount of mica (1b), production of gravel-sand (2) or no specified usage (3).

The excavation material management plan was included in the main construction contract. On one hand, this allowed for a specialized company to find proper application scenarios; on the other hand, tendering of companies was limited to purely managing excavation material. Processing plant equipment was adjusted to gravel production

with 0–250 mm raw material. No third-party material needed to be acquired for this project and a full self-supply was granted. Natural radioactive material was encountered unexpectedly in the form of 10 tons of uranite, which was disposed as hazardous waste (Burdin et al., 2017). Analyses of heavy metal ions in mud and arsenic press sludge were subjected to special waste treatment and disposal in Vallon de Châteland, Switzerland.

4.2.5. High-Luminosity Large Hadron Collider (HL-LHC), Point 1

An emphasis is put on this project due to the proximity and implications for the FCC study at CERN. HL-LHC project involved the construction of complex underground infrastructures in the Geneva Basin on both sides of the French-Swiss border, adjacent to existing underground infrastructure of the Large Hadron Collider operated at CERN (Fern et al., 2018; Voiron et al., 2020). Swiss Point 1 site comprised the construction of a shaft with an internal diameter of about 12 m to a depth of ca. 60 m (PM17), a cavern of 18 m in diameter and 45–50 m in length (US/UW17) as well as a main gallery of 50 m² section and a length of 300 m, both connected to secondary galleries of 50–70 m in length (UA/UPR 13 & 17 and UL 13 & 17). Underlying geology comprised Molasse units, which were deposited as detrital formations during the alpine orogeny (Moscariello et al., 2020; Oxburgh, 1981). A geotechnical classification based on HL-LHC Point 1 data in Switzerland subdivided the Molasse formation into very weak marl, weak marl, medium-weak marl, weak sandstone, medium-strong sandstone and strong sandstone formations (Fern et al., 2018). These six categories were based on uniaxial compressive strength, Young's modulus and Atterberg limits and were used for first trends of application scenarios for excavated material. The Molasse formation contains natural hydrocarbons originating from natural degradation of organic material accumulated as lenses and layers of variable extent and thickness (Voiron et al., 2020). It should be noted that such lenses had already been encountered at CERN during the civil engineering work for excavation of the currently operational LHC, with hydrocarbon contents ranging from 700 to 2800 ppm. At Point 1, C₁₀ to C₄₀ hydrocarbons were detected in both solid and liquid state during excavation via a PetroFLAG® test. It comprised an inexpensive and environmental-friendly portable field device for determining a probable contamination of a 10 g material sample. Concentrations of hydrocarbons C₁₀ to C₄₀ were evaluated in laboratory according to the SN EN 14039 standard, with results available within 3–10 days. Concentrations of C₅ to C₁₀ hydrocarbons were also evaluated according to the measurement of purgeable organic compounds in water by gas chromatography. Within the Swiss legal framework, these results were considered to further decide on the quality of material to judge further applications or disposal. Any contaminations were assessed at the end of each excavation step by the geotechnical engineer in charge of geological monitoring of the project (personal communications with Jérémy Voiron). Excavated material was transported to the surface via a six cubic metre skip and dumped on the surface site in a weather-protected hall.

Excavated material at the HL-LHC project required a thorough purification linked to chemical pollutants such as nickel and chromium. For the HL-LHC Point 1 construction site in Switzerland, the total excavated material was about 50'000 m³. Original pollution was estimated at 25%, whereas an actual 35% were encountered (status February 2020, personal communication with Jérémy Voiron). Excavated material was sent to a local concrete producer for Point 1 material and local soil purification companies for HL-LHC's Point 5 in France. Based on Swiss and French legislation (République de Canton Genève, 2016; République Française, 2015, République Française, 2003; Confederation, 2016, 2005, 1998, 1989, 1983), the grade of pollution was significantly higher at LHC Point 5 compared to Point 1. Swiss disposal classes for Point 1 were applied as respectively A, (B-), B, E and E+ classified material. For Point 5 French acceptance thresholds classified as ISDI (inert waste), ISDND (non-inert non-hazardous waste) and ISDD (dangerous waste). This project marks a crucial local example, as

similar situations might occur for the FCC project.

Based on instructions given by the engineer to the contractor, final destinations of excavated material were specific disposal, or used on-site depending on the degree of pollution. Unpolluted but surplus material was disposed as unpolluted excavated material in accordance with Swiss legislation.

Particularly in the constructing tunnels, it was found that excavated material contained traces of pollution measured by laboratory tests that were not previously detectable. Hence, in accordance with the Swiss precautionary principle, all excavated material was considered potentially polluted and transported to sheltered temporary storage areas, thus causing increased space constraints. The management of potentially polluted excavation material required increased continuous monitoring during excavation until usage or final disposal were decided (personal communications with Pieter Mattelaer). The different stocks were defined according to the origin of the material (per excavated structure) and were spatially separated by modular concrete blocks.

Based on laboratory results and in accordance with the regulatory thresholds defined by Swiss authorities for hydrocarbons, four application classes were identified: grade A material used for backfilling on-site or disposal as unpolluted material; grade B⁻ material as very low-polluted material within the lower limit used for backfilling on the project site; grade B⁺ material as slightly polluted within the upper limits shipped to type B material and grade E material shipped to a cement factory. Class E material was integrated into the flour preparation mixture used in the homogenisation bed of the kilns, and composed of a fraction of 30–40% sandstones, marls and conglomerates (Molasse formation) from the project, and limestone and siliceous material delivered by other quarries (Voiron et al., 2020). The HL-LHC project was a good example for showing the legal and technical harmonization of stakeholders and authorities as implementations for appropriate use of excavated material was necessary. This development was conducted in close collaboration with associated Swiss authorities and governmental entities (Vernus et al., 2017; Voiron et al., 2020). The legal and technical reconciliation was an inevitable step towards a successful use of excavated material. Similar usages and management concepts of excavated material will be required for FCC.

4.2.6. Tunnel de Champel (CEVA)

The CEVA project comprises a railway tunnel with a length of 1.62 km in canton Geneva and is stated as a comparable example for both the High Luminosity LHC project and FCC at CERN. The concept for material management was included in the main construction contract and included full-face excavation of 30'000 tons of glacial, unconsolidated sediments in loose rock using face stabilization and pipe umbrellas. Excavated material was primarily used as concrete aggregates. Due to the populated area, limited space for disposal was given and processing plants were part of a local concrete producer to whom material was consecutively delivered after each excavation step. Processing included sieving and washing as well as cyclones for sand production. Transport was carried out with dumpers and trucks (Fachgruppe für Untertagebau (FGU), 2016).

4.3. Germany

4.3.1. Small- and mid-sized tunnel projects across southern Germany

In southern Germany 26 km of tunnels were constructed producing about 4.5 million tons of excavation material. A large amount of this material featured a high content of gypsum, salt, clay and sandstone. The goal was to use excavated material for dams, noise protection walls, concrete production, and diaphragm walls for landfilling structures. Certain excavated material was used in the ceramic industries as bricks and coarse ceramic products. The sandstones were used for several construction purposes. On one hand, early detection of chemical and morphological characteristics helped to increase the quantity of useable material and depicted a precondition for industrial application; on the

other hand, the detection and separation of some expected metals like nickel, chromium and cadmium led to an industrial utilisation and reduction of disposal areas required for hazardous waste. In both cases, it was mandatory to avoid mixing up excavation material containing these metals in higher concentrations due to dilution.

4.3.2. Katzenberg tunnel

Excavation of the Katzenberg tunnel as part of the new railway line from Karlsruhe, Germany to Basel, Switzerland included the use of about 2.3 million m³ of surfactant contaminated rock material via Earth Pressure Balance (EPB) excavation. 75% were driven in open and 25% in closed EPB mode dependant on face stabilization requirements. Recultivation of an abandoned limestone quarry was the ultimate and most sustainable usage. Since project and quarry owner as well as the contractor were responsible for management and treatment of excavated material, special contractual agreements were arranged. These included the storage handling for the quarry owner, geogene liability for the project owner and associated additives for final storage (Haid and Hammer, 2009). Prognosis for the prevention of seeping water was guaranteed in advance by adding lime to the pulpy excavated material in EPB advancement. EPB excavation turned out to be challenging in tertiary sediment rocks such as sandstone, conglomerate and anhydrite/gypsum.

High concentrations of heavy metal ions, arsenic, cadmium, dissolved organic carbon, sulphide and sulphate during pre-investigations implied an adapted contractual model, which was granted by national authorities under the condition of proving seeping water prevention. Seeping water prognosis included thorough analyses of both Katzenberg tunnel's excavated rock material as well as subsurface conditions at the limestone quarry. Conditions given by the authority to approve the tunnelling construction inferred a geogenic background contamination check, investigations against mobility for heavy metal ions, arsenic and sulphur components including permeability measures of excavated material, and the degradability of additives (surfactants). Excavated, pasty material was directly delivered to the quarry via conveyer belts from the south portal (Haid and Hammer, 2009). Unpredicted encounters of 6'000 m³ natural bitumen at the transition of limestone to tertiary sediment rocks led to delays in advancement and required special analyses and disposal in presence of national authorities due to impossible chemical separation from the natural rock composite (Haid and Hammer, 2009). Leakage proof was verified for the backfilled material in the quarry by drilling to the original quarry depth level before disposal and analysing the drilled material and flow characteristics. Higher sulphate concentrations were caused by chemical oxidation processes within the backfilled material but were still in accordance with national guidelines and chemical thresholds. Based on predictions from pre-investigations, no further implementations had to be recalled and guaranteed successful applications of excavated material.

4.4. France

4.4.1. Tunnel Euralpin Lyon-Turin (TELT)

Modernisation of existing axes and new routes incorporate the east-west Lyon-Turin axis and the north-south Brenner Base tunnel. The Euralpin Lyon-Turin (TELT) project currently under construction will connect France and Italy via new railway lines as part of the TEN-T Lissabon-Kiew axis and is split into a French part from Lyon to Saint-Jean-De-Maurienne, an international part from Saint-Jean-De-Maurienne to Bruzolo dedicated to TELT (Burdin and Monin, 2009), and an Italian section dedicated to the RFI, a sub-branch consortium of the project. The total length of the project consists of 300 km, whereas about 150 km are covered by 10 tunnels with a total excavated volume of 60 million tons (Burdin and Monin, 2009). Main French tunnels are the Chartreuse and Montcenis Base tunnel excavated in gneiss, granite, molasse, limestone and glacial moraine formations. French and Italian authorities intend to maximise the use of excavated material targeting a

quota of about 33%. Focus of application concepts is restricted to the Chartreuse tunnel (24.7 km) and the Montcenis Base tunnel (ca. 53 km). Three application classes have been derived ranging from no use, i.e. disposal (class 3) due to bad rock quality or political decisions forcing the owner to dump the excavated material, usage as embankments and bearing stratum (class 2) and concrete aggregate production (class 1) (written communications with Jacques Burdin). The use of excavated material is subject to the project owner's responsibility based on contractual negotiations (Burdin and Monin, 2009). For the TELT project, the same material requirements for concrete aggregate production apply as for the Gotthard and Lötschberg Base tunnels. Three aggregate classes with a grain size of 16 mm will be produced (Burdin and Monin, 2009). To guarantee high quality concrete, caution was spent on sand production requiring special crushers for processing. For the whole project, 140 site investigation drillings have been performed including two directed drillings. Core material was used to analyse and predict application potential along the tunnels for a period of six consecutive years (Burdin and Monin, 2009). For large-scale laboratory analyses, two processing plants have been installed on the French side to simulate potential application scenarios. Intensified research had to be spent on the analysis of SO₃-related geological formations such as anhydrite to increase potential application ratio, since sulphated material occurs in the main tunnel sections (Stephen, 2020). For two years, these analyses have been performed to improve EN 12620 standards dealing with concrete applicability of material with more than 0.2% SO₃. More than 50% of excavated rock material will be produced in order to produce concrete mixtures for segments, concrete lining and railway embankments in line with the latest regulatory framework on environmental and sustainable construction (T.E.L.T. consortium, 2020).

4.4.2. Grand Paris Express (GPE)

The Grand Paris Express project currently includes the construction of the metro underground system in and around Paris and depicts an efficient example of handling large quantities of excavated material, and quickly deriving methods to decrease temporary storage. GPE is using its excavated material on-site by creating a temporary platform to store and treat the spoil material. The material is then likely to be distributed to local consumers and quarries in future (Le Centre D'Etudes des Tunnels, 2019; 2017). The GPE is mainly excavated by an EPB machine and 50% of the excavated material is related to ancillary works.

4.5. United Kingdom

4.5.1. Crossrail tunnel

The London Crossrail project constructs a new express rail line to provide London and its suburbs with an extended metro system. In total, 21 km of tunnels (42 km of tubes) excavate clay, sand, gravel and marl as part of the London clay geological formation via an EPB machine. Environmental impact assessment concluded on the construction of an island in a protected natural area close to district Essex using about 4 million tons of excavated material as the optimal solution. Applications of excavated material were hampered in the beginning by the client, who initiated several studies to investigate clay material as swelling clay (Burdin et al., 2017), and archaeological artifacts encountered during construction (Keily, 2020). Usage of clay in industrial processes was not confirmed since the manufactured product experienced difficulties in sale numbers on the free market (Burdin et al., 2017).

5. Discussion

The Future Circular Collider study has been undertaking dedicated research since 2018 for finding environmental-friendly and sustainable application scenarios of excavated material in line with evaluated tunnelling excavation techniques. Finding proper applications is of utmost significance for subsequent project approval in the framework

Table 2

Compilation of geotechnical, petrophysical and geological rock parameters measured during site investigations in the Molasse formation for CERN's currently running Large Hadron Collider (GADZ, S.A., 1993). Laboratory analyses are currently extended along the full extent of the FCC tunnel alignment and contemplated by chemical, mineralogical, petrophysical, geomechanical and clay analyses for an advanced rock characterisation.

Parameter	Unit	compact fine-grained material			compact coarse-grained material		
		no. samples	average value	variation coefficient	no. samples	average value	variation coefficient
RQD	%	–	95–100	–	–	85–95	–
water content	%	244	4.7	17.0	62	8.2	15.0
bulk density	t/m ³	141	2.56	1.4	37	2.36	2.1
dry density	t/m ³	137	2.45	2.2	37	2.18	2.3
grain density	t/m ³	80	2.75	0.7	22	2.73	0.7
vacuum index	–	137	0.126	19	37	0.266	15.0
compressive strength	MPa	79	22.3	34	20	9.6	37.0
Young's modulus	MPa	76	2790	56	19	1260	49
Brazilian tensile strength	MPa	32	2.13	39	5	1.06	34
Cerchar hardness	–	59	9.6	25	12	5.6	18
Cerchar abrasivity	–	40	0.4	38	8	0.3	–
quartz content	%	6	40–66	–	2	69–70	–
water flow rate (from Lugeon)	l/min*m	53	<0.1	–	3	0.5	–

Parameter	Unit	gravelly marls			marls		
		no. samples	average value	variation coefficient	no. samples	average value	variation coefficient
RQD	%	–	80–95	–	–	70–78	–
Water content	%	146	6.8	11.0	147	9.8	11.7
Bulk density	t/m ³	92	2.50	1.2	85	2.40	2.3
Dry density	t/m ³	91	2.34	1.8	85	2.19	3.5
Grain density	t/m ³	48	2.77	0.8	47	2.79	0.5
Vacuum index	–	91	0.19	14.0	85	0.279	17.6
Liquidity limit (Atterberg)	%	6	37.4	13.6	19	55.1	11.6
Plasticity limit (Atterberg)	%	6	18.6	13.2	19	24.2	14.4
plasticity index	%	6	18.8	20.2	19	30.9	17.1
Compressive strength	MPa	31	9.4	46.0	19	3.3	58
Young's modulus	MPa	28	820	67.0	15	225	78
Brazilian tensile strength	MPa	10	1.52	30.7	2	0.5	–
Quartz content	%	–	20–40	–	–	15–30	–
Content of swelling clay	%	–	8–13	–	–	10–18	–
Inflation pressure	MPa	7	0.5–1.2	–	13	0.5–1.2	–
Swelling rate	%	7	1.14	35.0	13	3.4	76
Permeability (Lugeon)	l/min*m	53	<0.1	–	53	<0.1	–

Parameter	Unit	compact fine-grained material			compact coarse-grained material		
		no. samples	average value	variation coefficient	no. samples	average value	variation coefficient
RQD	%	–	95–100	–	–	85–95	–
water content	%	244	4.7	17.0	62	8.2	15.0
bulk density	t/m ³	141	2.56	1.4	37	2.36	2.1
dry density	t/m ³	137	2.45	2.2	37	2.18	2.3
grain density	t/m ³	80	2.75	0.7	22	2.73	0.7
vacuum index	–	137	0.126	19	37	0.266	15.0
compressive strength	MPa	79	22.3	34	20	9.6	37.0
Young's modulus	MPa	76	2790	56	19	1260	49
Brazilian tensile strength	MPa	32	2.13	39	5	1.06	34
Cerchar hardness	–	59	9.6	25	12	5.6	18
Cerchar abrasivity	–	40	0.4	38	8	0.3	–
quartz content	%	6	40–66	–	2	69–70	–
water flow rate (from Lugeon)	l/min*m	53	<0.1	–	3	0.5	–

Parameter	Unit	gravelly marls			marls		
		no. samples	average value	variation coefficient	no. samples	average value	variation coefficient
RQD	%	–	80–95	–	–	70–78	–
Water content	%	146	6.8	11.0	147	9.8	11.7
Bulk density	t/m ³	92	2.50	1.2	85	2.40	2.3
Dry density	t/m ³	91	2.34	1.8	85	2.19	3.5
Grain density	t/m ³	48	2.77	0.8	47	2.79	0.5
Vacuum index	–	91	0.19	14.0	85	0.279	17.6
Liquidity limit (Atterberg)	%	6	37.4	13.6	19	55.1	11.6
Plasticity limit (Atterberg)	%	6	18.6	13.2	19	24.2	14.4
plasticity index	%	6	18.8	20.2	19	30.9	17.1
Compressive strength	MPa	31	9.4	46.0	19	3.3	58
Young's modulus	MPa	28	820	67.0	15	225	78
Brazilian tensile strength	MPa	10	1.52	30.7	2	0.5	–
Quartz content	%	–	20–40	–	–	15–30	–
Content of swelling clay	%	–	8–13	–	–	10–18	–
Inflation pressure	MPa	7	0.5–1.2	–	13	0.5–1.2	–
Swelling rate	%	7	1.14	35.0	13	3.4	76
Permeability (Lugeon)	l/min*m	53	<0.1	–	53	<0.1	–

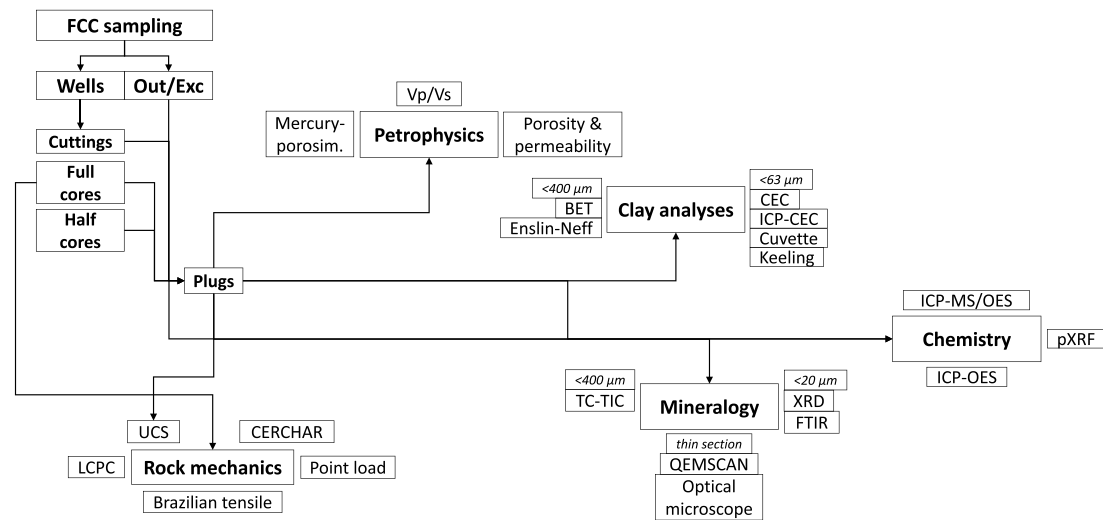


Fig. 1. Laboratory analyses of samples taken from wells, outcrops (Out) and excavation sites (Exc) along FCC's proposed tunnel alignment. Different types of samples (cuttings, full cores, half cores, plugs) and sample fractions ($<400\ \mu\text{m}$, $<63\ \mu\text{m}$, $<20\ \mu\text{m}$) have been used depending on analysis requirements. Its results are implemented into a conceptual flow model for identifying potential application scenarios of excavated material. V_p = compressional wave velocity, V_s = shear wave velocity, ICP-OES = Inductively Coupled Plasma Optical Emission Spectrometry, ICP-MS = Inductively Coupled Plasma Mass Spectrometry, pXRF = portable X-ray fluorescence, XRD = X-ray diffraction, FTIR = Fourier Transform Infrared spectroscopy, QEMSCAN = automated mineralogy (electron microscope), TC-TIC = carbon content determination, CEC = effective cation exchange capacity via $[\text{Cu}(\text{trien})_3]^{2+}$ complex, ICP-CEC = exchangeable cations via ICP-OES, Cuvette = anion analyses, Keeling = water vapour adsorption, EnslinNeff = water absorption, BET = specific surface, UCS = uniaxial compressive strength, LCPC = Laboratoire Central des Ponts et Chaussées (breakability), CERCHAR = abrasivity.

of the European Strategy Update for Particle Physics (ESUPP), which proposes visions in the field of particle physics in the future (Benedikt et al., 2020).

Based on existing data of FCC's underlying geology and previously discussed comparisons of subsurface projects, concepts of excavated material management and preliminary implications for potential applications of excavated material are discussed. These derivations are substantiated by an improved rock characterisation model in line with tunnelling excavation techniques and summarized in a conceptual flow model for quick on-site evaluation. The results of FCC's chemical, mineralogical, geomechanical and petrophysical laboratory analyses will be presented in more detail in separate upcoming studies.

5.1. FCC material management concept

A material management plan (German: *Marschplan*, French: *la gestion des matériaux excavés*) includes technical concepts of excavated rock and soil as useable material from construction sites to processing facilities. Two contractual types of implementations potentially exist for the management of FCC's excavated material. Either they are part of the main construction contract or they are treated as an individual contract as given for the Lötschberg, Gotthard or Lyon-Turin projects. An advantage of the former option is a reduction of involved people, therefore offering efficient coordination. However, the latter option might lead to technically more advanced results as it usually includes a specialized company in the field of using excavated material. Responsibility is always accounted to the client, i.e. in the case of FCC it would be CERN, which must deal with management of excavation material and final use or disposal. As described above, CERN has performed a vast amount of sample analyses along the current FCC layout. These results will be further used for planning an optimised use already before

construction.

Final and interim disposal locations must be implemented as well as its associated transport routes considering distances and relief conditions; furthermore, type of transport vehicles, e.g. conveyor belt or rail and their impacts on environment and project costs must be clearly stated. The decision process consists in a multi-factor analysis of several aspects related to environmental impact: for example, analyses of dust produced by trucks or conveyor belts, noise mitigation and re-cultivation of surrounding areas after the project's end must be accounted properly. These dedicated areas, which in the case of the Lötschberg Base tunnel covered up to 20 ha (Teuscher et al., 2007), might exceed FCC's required space due to its excavated quantities. Lötschberg, Gotthard, HL-LHC and TELT suggest a minimum of three use classes, e.g. F1, F2, F3 with sub-classes (a, b, c), specifying each use scenario in more detail, which might apply for FCC, too. Specific application classes for FCC's will be presented in a separate study. Former values of encountered Molasse formation restricted to the construction area of CERN's LHC are available in Table 2.

Besides the management of excavated material, the type of excavation, i.e. conventional or mechanised tunnelling, must be mentioned in the material management plan. The type of machines required for processing to transport the material and forecasting mean and maximum volumes of excavated material is closely associated. Potential applications of excavated material depend on a preceding rock characterisation based on mineralogical, chemical, petrophysical and geomechanical laboratory tests. For the development of a material management plan, data from existing boreholes (subsurface geology) and outcrops (surface geology) needs to be analysed. Regardless of whether the concept relies on data from site investigations or existing boreholes, it is continuously updated as new information is acquired, even during construction phase.

Since FCC will be based in two adjacent countries, transnational transport of waste should be discussed in the framework of the Basel convention (Swiss Confederation, 1989). As experiences with the HL-LHC project showed, a difference in predicted and experiences with the levels of hydrocarbon pollution and associated usage of excavated material (25% versus 35%) might be expected. Therefore, a sensitivity analysis proves to be an essential part of quantitative and qualitative risk assessment for contamination of FCC's proposed construction lots to avoid massive divergence between percentage of pollution and associated dumping costs. Such a risk study is currently ongoing and based on the outcome of geochemical and mineralogical laboratory analyses concluding on potential contaminations.

5.2. Laboratory analyses for rock characterisation of FCC's excavated material

So far, more than 600 existing boreholes were identified relevant for FCC's subsurface infrastructure originating from French and Swiss national or cantonal geothermal drillings, water wells, hydrocarbon exploration and site investigation wells across the Geneva Basin. Samples were taken at these well locations and contemplated by outcrop samples for surface geology correlations. An overview of currently performed laboratory tests and geophysical well logging analyses can be taken from Fig. 1. An advanced rock characterisation based on these analyses will be presented in a separate study. Here, focus is spent on the technical cause and logistical approach of these analyses. A thorough understanding of the underlying geological conditions is required to analyse, evaluate and interpret its geomechanical and petrophysical behaviour as well as its mineralogical and chemical composition. These small-scale laboratory analyses will be further upscaled by modelling chemical, mineralogical and geomechanical distributions. Within the next decade, large-scale (field) tests conducted before start of construction are planned. Site investigations will be needed to continuously update the models and fine-tune rock classification.

FCC's main geological formations primarily refer to Molasse deposits representing intercalations of sandstone, marl, conglomerate, anhydrite/gypsum and contaminating substances such as hydrocarbons or heavy metal ions similar to the HL-LHC and Grand Paris Express projects. On top of that, karstic formations, swelling rock and potential geological faults bear tunnelling risks that need to be overcome as much as the usage of further encountered formations like unconsolidated sediments and limestone.

There is still a significant amount of uncertainty as to the prediction of a distribution of polluted material, despite the implementation of a consequent geotechnical investigation campaign. Hydrocarbon pollution, respectively bitumen and/or gas, may be present in a large part of FCC's excavated Molasse formation. In fact, it was of the order of 35% in the case of HL-LHC Point 1. Therefore, this will be considered as one of the main environmental challenges during the construction for FCC.

The current highest-ranked usage value of excavated material is the production of concrete aggregates as showed in the Gotthard, Lötschberg, HL-LHC or TELT projects (AlpTransit Gotthard, 2017; Burdin and Monin, 2009; Teuscher et al., 2007; Voit et al., 2015). The application of face stabilization foam and geopolymers bear potential especially for fine-grained, clay-rich rock material as this is the case for FCC's Molasse formation (Minder et al., 2016; Zumsteg et al., 2013). Requirements and on-site demands must comply with industrial processing companies and consumers in the surrounding area to guarantee regional sustainability. A first proposed rock characterisation in FCC's conceptual design volumes (CDRs) differentiates between hard rock and soft rock (Abada et al., 2019) and is coordinated in accordance with expected masses of excavated material, the possibility of a self-supporting jobsite and a resource-efficient industrial utilisation at each FCC lot. It considers the ecological intermediate storage of oversupply in excavated material to cover future demands, and the usage, respectively disposal, of low-quality material. Transport routes, material

Table 3

Standard values for aggregates for concrete applicability of sandstone, quartzitic sandstone and quartzite/grauwacke, which covers FCC's Molasse formation. Quartzite/grauwacke values depict upper limits, sandstone values represent lower limits (Locher, 2000; Röhling et al., 2012)

parameter	unit	lower limit	upper limit
bulk density	kg/m ³	2.00	2.65
true density	kg/m ³	2.00	2.68
adsorption of water (after EN 52103)	%	0.2	0.9
compressive strength	N/mm ²	30	300
Young's modulus	N/mm ²	2	60
thermal expansion coefficient, 0–60 °C	10 ⁻⁶ /K	11	11.8

specific processing, intermediate storage and landfilling must also be taken into consideration in terms of CO₂ emissions.

In order to respond to FCC's excavation efficiency requirements (Haas et al., 2020b), an innovative material management concept might be introduced based on an on-line analysis (on conveyer belt) and associated database. This database, similar to the European soil data centre (Panagos et al., 2012) should contain a matrix with integrated specific requirements for the relevant usage and further processing of raw material from industrial companies. The individual utilisation scenarios can then be derived from this matrix. During both site investigations and construction, data of rock material is continuously gathered and, based on the resulting rock composition, distributed to adequate application classes and processing units. Using the database, the constructor can thus immediately determine the use application potential and match with local processing companies. Moreover, legal requirements and pollutant thresholds should be entered in this database and intermediate purchasers as well as processing companies could access this database and input their technical requirements, e.g. material properties, time of demand, excavated volumes and maximum transport distances for a successful application. Haas et al. (2020b) proposed an on-line analysis on a TBM conveyor belt that continuously transfers the measured results to the data control centre while excavated material is classified by direct comparison with the required specifications in the online database. This could be one of FCC's aims to apply such a concept and sort excavated material into different categories during TBM excavation. The extensive amount of various laboratory analyses is one of the reasons to provide optimized measuring devices to analyse the material in the subsurface. In parallel, the analysis data is used for the self-supply of the jobsite with excavated material. In case the properties of the excavated material do not comply with the quality requirements for direct applicability at the jobsite or in industry, then it could be used for embankments or landfilling, ultimately.

Environmental impacts like production of noise and dust will significantly be reduced by using excavated material on-site and underground. Mass flow analyses are performed following the concept first introduced in 1991 (Baccini and Brunner, 1991). The reason for applying these methods is to compare different application scenarios and disposal. Substitution effects caused by replacement of primary material with excavation material are identified and quantified. Considering these aspects, underground constructions in the future would substantially contribute to resource-efficient and CO₂-reduced emissions.

5.3. Discussion of FCC's processing plant infrastructure

Laboratory analyses are followed by processing plants using recycling units like crushers and sieves. Excavation material is used on-site as construction material or transported to industrial clients. FCC's goals are a maximum waste and disposal reduction. Proper processing equipment are the key factor for a successful usage for both on-site and industrial supply. The Brenner Base tunnel was one of the few examples to use a dynamic three-phase processing procedure that was optimized by large-scale tests of several thousands of tons. Based on the BBT

Table 4

Overview of parameters and associated standards to be checked for applicability as concrete aggregate for FCC's excavated rock material published by the European Norm committee.

name of parameter	standard
grain shape FI	DIN EN 933-3
flakiness index SI	DIN EN 933-3
largest grain	DIN EN 933-1
bulk density	DIN EN 1097-6
grain size distribution	DIN EN 933-2 / DIN EN 1097-3
fine proportion	DIN EN 933-1
sand equivalent value (SE)	DIN EN 933-8
methylene blue value (MB)	DIN EN 933-9
mussel shell content	DIN EN 933-7
resistance to fragmentation (LA coefficient)	DIN EN 1097-2
impact fragmentation value	DIN EN 1097-2
abrasion value (AAV)	DIN EN 1097-8
nordic abrasion coefficient (AN)	DIN EN 1097-9
polishing value (PSV)	DIN EN 1097-8
micro-deval coefficient (MDE)	DIN EN 1097-1
content of water-soluble chloride ions	DIN EN 1744-1
content of acid-soluble chloride ions	DIN EN 1744-5
acid-soluble sulphate content	DIN EN 1744-1
total sulphur content	DIN EN 1744-1
humus	DIN EN 1744-1
fulvic acid	DIN EN 1744-1
carbonate content of aggregates	DIN EN 196-21
shrinkage due to drying of aggregates	DIN EN 1367-4
water absorption	DIN EN 1097-6:2013
water absorption as preliminary test for frost-thaw cycle resistance	DIN EN 1097-6:2013
frost-thaw cycle resistance	DIN EN 1367-1
frost-thaw change with simultaneous exposure to salt	DIN EN 1367-6
magnesium sulphate value	DIN EN 1367-2
alkali silica reactivity	CEN/TR 16349
angularity of fine aggregates	DIN EN 933-6
flow coefficients ECS	DIN EN 933-6
percentage of partially/fully broken and rounded grains	DIN EN 933-5

example, this could imply train terminals and train stations, dedicated areas to load and unload trains, conveyor belts and buffer support required in conjunction with processing advancement. Conveyor belts offer reasonable flexibility to automate analyses, rock characterisation and processing of excavation material to ensure sustainable transport.

Measuring equipment for on-line-measurements needs to be installed directly onto the hauling installations (Müller et al., 2011). The main parameters of the material concerning its suitability as a resource, are chemical impurities, grain size distribution, water content, grain shape and mass flow. The main on-line chemical method currently used is prompt gamma neutron activation analysis (PGNAA) and grain size distribution analyses.

5.4. Potential applications for FCC's excavated material

As further application scenarios of excavated material will be progressively checked within the scope of chemical, mineralogical, petro-physical and geomechanical laboratory analyses, one promising option is the production of concrete aggregates based on existing data about sandstones, marls and conglomerates as part of the Molasse formation. Further scenarios are discussed below in more detail.

5.4.1. Concrete aggregate production

Certain standardised rock parameters as depicted in Table 4 must be fulfilled by FCC's excavated material before they are considered for concrete usage. These properties include grain form, grain size, grain distribution, inherent strength, lack of harmful substances such as (adhesive) clay, sulphur compounds and organic substances. FCC's

Table 5

Required parameters to test on fresh concrete according to European standards.

name of parameter	standard
shape, dimensions and other requirements of specimen and moulds	EN 12390-1
preparing and curing specimen for strength tests	EN 12390-2
compressive strength	EN 12390-3
largest grain	EN 12620
compaction measure	EN 12350-4
spreading	EN 12350-5
water leaching tendency	EN 480-4
heat generation during hardening	EN 12390-15
shrinkage	EN 12390-16
tensile splitting strength	EN 12390-6
determination of carbonation resistance at atmospheric levels of carbon dioxide	EN 12390-10
determination of chloride resistance, unidirectional diffusion	EN 12390-11
determination of carbonation resistance, accelerated carbonation method	EN 12390-12
depth of water penetration under pressure	EN 12390-8
bulk density (fresh and hardened concrete)	EN 12390-7
determination of creep of concrete in compression	EN 12390-17
determination of chloride migration coefficient	EN 12390-18

subsurface geology is split into three main geological formations, so far: moraine formation, Molasse formation and limestone formation. FCC's encountered sedimentary Molasse deposits consist of irregular layers and lenses of marls and sandstones that originate from alpine erosion (Piffner, 2014).

Petrographic descriptions (European Commission, 2020) and a series of qualification tests are required to test if excavated material can be applied as aggregates for concrete production. Whenever sediment rock is used for a potential concrete usage, its petrographic origin including its geological age and type of origin must be supplied according to DIN EN 932-3. In the case of FCC, concrete applicability description of its excavated material would be: Lower Marine Molasse (geological term), accumulated in the Geneva Basin (location) in Middle Oligocene (geological time) due to alpine orogeny (geological cause). Laboratory tests of rock include breakability tests such as the Los Angeles (LA) test (Association française de normalisation, 2018), rock strength tests such as the unconfined compressive strength (UCS) or related indices like a point load (PL) test (International Society for Rock Mechanics and Rock Engineering, 1972), indications of abrasivity tested via LCPC (Association française de normalisation, 2013) and Cerchar tests. LA tests are used for both rock and concrete material, whereas chips from TBM and rock fragments from drill and blast excavation are suitable. According to Swiss standards, concrete aggregates need to have the following characteristics to be feasible for further usage: minimum rock strength, low chemical contamination, low alkali aggregate reactions, mean grain size distribution and grain shape according to EN 12620. Often, a value of 100 N/mm² is mentioned (Dubuisson, 1995; Natursteineindustrie Bundesverband, 1993), whereas research at the Gotthard Base tunnel showed a sufficient value of 75 N/mm² (Kruse and Weber, 1995). However, for in-situ lining, the latter value is too high and could be applicable only for concrete segments. Mortar research has shown that the amount, grain size and type of free mica strongly influences concrete applicability (Swiss Federal Laboratories for Materials science and Technology, 1998). First mineralogical X-ray diffraction (XRD) results of FCC samples revealed a high content of up to 38% of clay. Due to the Molasse's heterogeneity, the approach for concrete production seems challenging since it contains fine-grained and clay minerals that would make the final product also frost sensitive. Further in-depth laboratory analyses to evaluate parameters of fresh concrete as depicted in Table 5 will be necessary in addition.

Experiences at the Lötschberg and Gotthard Base tunnels would

suggest that the contractor is responsible for concrete production while the owner would be responsible for the concrete mixture whose observed standard must be indicated. Hence, the project client is awarded with a double role: on one hand as the own supplier for raw material to the industrial consumers, who will accept the material for concrete production; and on the other hand, as the consumer, who might buy the final concrete product from these processing plants for construction purposes. In any case, however, concrete analyses must be undertaken by the project owner. Amongst many quality controls, concrete tests must include resistance against alkali-aggregate-reactions (AAR) and conclude in suggestions for the optimal concrete mixture for construction. AAR prevention is a typical Swiss and French approach originating from the French standards ([Association française de normalisation, 1990](#)), and could be applied to the three Swiss FCC lots foreseen in FCC's current tunnel layout. AAR prevention is given once it fulfils the requirements stated in AFNOR P18-454 ([Association française de normalisation, 2004](#)). Potential reactivity is analysed via microbar tests as described in AFNOR P18-594 document ([Association française de normalisation, 2015](#)). With respect to the three reaction types of AAR, Swiss legislation only contains alkali silicic acid reaction and alkali silicate reaction. The alkali carbonate reaction is subject of current legal developments. However, as certain amounts of carbonates are present in FCC's Molasse formation, this would imply trans-national passage. Triggers of these chemical reactions is caused by a high amount of humidity, high alkali concentrations in the pore fluid and reactive components in the rock material. Thresholds of alkali concentrations and fine-grained particles are treated in EN 450-1 ([European Commission, 2012](#)). Aggregates added to the concrete mixture define its final strength, stress behaviour and make up between 65 and 80% of the main component's volume. Under environmental conditions such as rain, snow or wind, the aggregate should not dissolve, decompose or soften. Environmental cases demand frost-thaw and wear resistance. Standardised descriptions accountable for concrete aggregates are found in European norms EN 12620:2008-07 (aggregates) and EN 13055-1:2008 (light aggregates) as well as in NF P 18-545 for France.

Besides existing procedures of common concrete mixtures, standard EN 206/CN has enabled the creation of engineering concretes and development of geopolymer binders from sedimentary rock powder ([Lahoti et al., 2017](#)). Further discussions should lead to the modification of standards and common practices since it is not yet clearly stated in NF EN 206/CN. The Swiss Alpine-NEAT crossings implying the Lötschberg and Gotthard tunnels were one of the first projects that particularly required a permit given on the compulsory condition of using excavation material. Under this impetus, the players in other major projects began to integrate this discipline into the preparation of contractual documents. AFTES provided a first *recommandation* (recommendation) on the subject to support project owners, engineering offices and contractors describing the legal procedure ([Association Française des Tunnels Et De L'Espace Souterrain, 2019](#)).

Once the raw rock material fulfils the required parameters, further analyses need to be performed on fresh and hardened concrete as listed in [Table 5](#). The *Deutscher Ausschuss für Stahlbeton* (*German Committee for Reinforced Concrete*) ([Deutscher Ausschuss für Stahlbeton DAFStb, 2001](#)) suggests preventions against harmful alkali reactions within the concrete in their guideline. Rock strength and elastic properties of final concrete highly depend on the source ingredients and its related physical parameters. Even though a high rock strength is intended as input material for concrete production, low elastic parameters such as Young's modulus does not necessarily impact the concrete. In fact, low elastic values are favoured for concrete as they minimize cracking and damage behaviour to punctual pressure ([Thalmann et al., 2003](#)). While it has become an integrated procedure in subsurface projects to use limestone as aggregates for concrete production or, in the cases of Gotthard and Lötschberg Base tunnels also as additives, a potential use of rocks encountered in the Molasse formation for concrete applicability in the FCC study has yet not been fully investigated. Both glacial,

unconsolidated sediments and limestone formation will be included in future studies as they make up about 10.3% of the total volume of excavated material in the current FCC subsurface layout. Depending on future alignment optimizations, this value might increase up to 15% and hence, is significant for the FCC study.

5.4.2. Further potential applications of FCC's excavated material

Parameters analysed in laboratories and stated in [Table 2](#) might imply further application scenarios beyond concrete production that are briefly discussed here, and are in line with parameters given for sedimentary rock in [Table 3](#). Agricultural use as soil mixture for the creation of vineyards is one feasible option similar to a study conducted in Lausanne, Switzerland ([Reynard and Estoppey, 2020](#)). Besides agricultural use, sealing of dumps might be given by the Molasse's clayey composition, as well as face support in the case of an EPB-TBM construction as geopolymers or different mixtures of bentonite for slurry-TBM pressure stabilizers ([Minder et al., 2016](#); [Zumsteg et al., 2013](#)) could all imply feasible application scenarios of excavated material. Recultivation using excavated material for soil replacements as proved by experiments at the Koralm tunnel ([Schubel and Schaffer, 2020](#)) or creating embankments and landfilling should also not be excluded at this early stage of pre-investigations.

5.5. Impact of excavation method

The type of excavation influences processing equipment, which further needs to be adapted a priori to different usages of excavated material. The shape of excavated rock can either be blocky (drill and blast) or in chip format of different length (TBM), which highly depends on the disc spacing ([Entacher et al., 2014](#)). The grain size distribution varies extensively among conventional and mechanised tunnelling. Ranges of 0–150 mm are typical for TBMs and 0–900 mm for drill and blast advancement ([Fachgruppe für Untertagebau \(FGU\), 2016](#)). TBM cutter spacing between 80 and 90 mm are common and research has shown spacings of up to 130 mm for hard rock such as granodiorite ([Büchi and Thalmann, 1995](#)). The platy shape of chips during TBM favours geomechanical analyses as well as processing for further use. Chemical admixtures during face stabilization for slurry- and EPB-TBMs contaminate the material in a way that makes it impossible to properly process the material posteriori. Swiss legislation does not yet imply solutions for surfactants being incorporated into excavation material as part of EPB excavation. Nitrites and nitrates during drill and blast are common contaminants. For concrete production, this would mean that an additional washing processing removing the nitrates and nitrites would need to be installed. Sequential blasting produces 0–600 mm grains.

Excavated material from mechanised tunnelling must be cleaned more accurately when compared to conventional methods in particular for subsequent, potential concrete production. This will likely require a high supply of dewatering presses and voluminous washing drums to remove fine-grained particles (<0.063 mm). Portions of up to 12% of fine-grained particles are possible when excavating with a TBM ([Thalmann et al., 2003](#)). Dedicated vertical impact crushers need to be tuned for breaking TBM rock fragments efficiently without producing excessive sand surplus. As shown in previous sections, excavated material above 8 mm of grain size must be crushed to fulfil concrete aggregate specifications. Chemical and biochemical treatment of FCC's excavated material including chromium, nickel and hydrocarbon contamination further hamper the cleaning process. This fact emphasises a thorough FCC geological investigation since environmental impact assessment drives construction approval.

A world-wide trend tends towards mechanised tunnelling for 80% of linear works; approximately 80% of these works are carried out in soft ground ([Burdin, 2015](#)) and foreseen for FCC's soft (Molasse) rock excavation. For FCC's mechanised tunnelling, TBM disk spacing is crucial to understand the impact on processing excavation material.

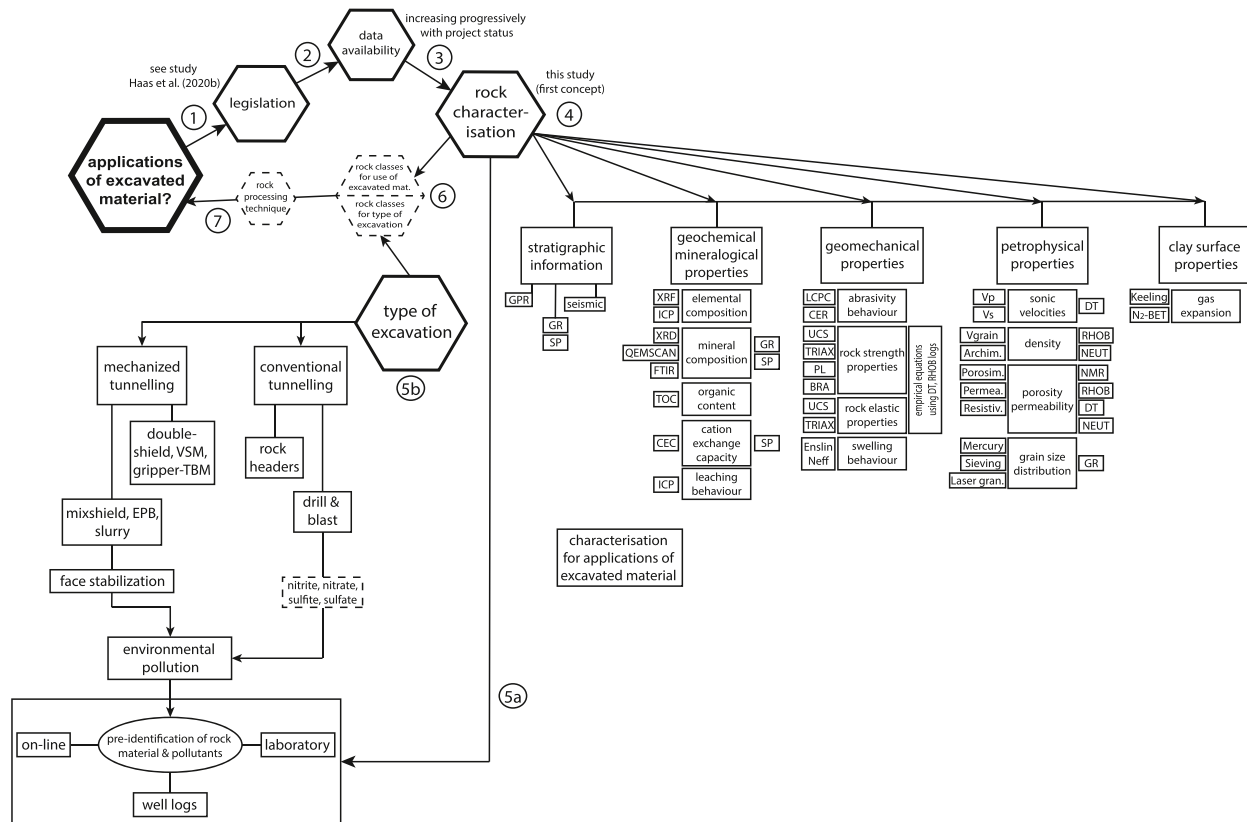


Fig. 2. Proposed conceptual flow model for subsurface infrastructure projects, including FCC, deriving and deciding on applications for excavated material based on legislation (1), data availability (2) and rock characterisation (3), which further influences laboratory and field tests (4) and implies tunnelling excavation techniques (5a). Simultaneously, potential excavation techniques based on experience from regional projects are evaluated (5b), leading to two distinguished rock classes with respect to excavation method and applicability of excavated material (6). Depending on excavation technique, excavated material is processed and scenarios for the application of excavated material (7) are derived. Essential rock parameters issue from geophysical wireline logs, petrophysical, geomechanical, mineralogical, chemical and clay analyses. Under (4), for each set of parameters, laboratory analyses are shown on the left-hand side, and well log equivalent parameters on the right-hand side, respectively. GPR = ground penetrating radar, GR = gamma ray log, SP = spontaneous potential log, DT = delta-time (sonic) log, RHOB = bulk density log, NEUT = neutron porosity log, NMR = nuclear magnetic resonance log, XRF = X-Ray fluorescence, ICP = inductively coupled plasma, XRD = X-Ray diffractometry, QEMSCAN = automated mineralogical & petrography detection (electron microscope), FTIR = Fourier Transform Infrared spectroscopy, TOC = total organic carbon, CEC = cation exchange capacity, LCPC = Laboratoire Central des Ponts et Chaussées abrasivity, UCS = uni-axial compressive strength, TRIAX = tri-axial compressive strength, PL = point load, BRA = Brazilian tensile strength, Vp = compressional wave velocity, Vs = shear wave velocity, Vgrain = grain volume, archim. = porosity measurement after Archimedes principle, porosim = porosity measurement after Boyle's law, permea. = permeability measurement with permeameter, mercury = mercury intrusion porosimetry, resistiv. = resistivity measurements, laser gran = laser granulometry for fine-grained material, N₂-BET = Brunauer-Emmett-Teller clay surface analysis, Keeling = water vapour adsorption after Keeling, Enslin-Neff = water absorption behaviour for water uptake capacity (swelling). All analyses have been conducted over the past 1.5 years and will provide a first rock characterisation for FCC's encountered geology.

Additionally, the type of TBM (e.g. EPB machine) has a huge impact on further use of excavated material since added conditioners to stabilize the face must be removed in further processing steps. Coarse-grained material should be preferred for later processing since fine-grained material is not suitable for e.g. concrete production. For conventional tunnelling, longer time-shifted blasting intervals are required to obtain coarse-grained material.

With respect to processing the material to useable material, crushing needs to be adapted for each application purpose. Local industries should be contacted to implement a classification model that includes geomechanical, petrophysical, mineralogical parameters in compliance with chemical and clay analyses of the material. Pre-investigation

results of FCC as currently conducted will play a significant role for first estimations before any site investigation campaigns have been started. These laboratory results will be presented in a separate study and comply well with the database concept introduced earlier.

The quality assurance on-site (e.g. via on-line monitoring) is a closing aspect to guarantee the implementation of a contractual model on the construction site. A conceptual flow model for FCC with respect to type of excavation and its associated rock classification based on different laboratory analyses and geophysical well logs is suggested in Fig. 2.

Table 6

Swiss and French disposal classes with associated chemical pollutant thresholds (status 2021). Hydrocarbon (HC) pollution substantially influenced the environmental impact assessment related to the HL-LHC project. ISDI = inert waste, ISDND = non-inert non-hazardous waste, ISDD = dangerous waste. *Approximate industry prices based on High-Luminosity LHC project as of year 2018. *E+ often treated individually for each construction site dependant on highest concentrations of pollutants. **Standardised leaching test to be applied after NF EN 12457-2. Values refer to dry substances only, according to the Ordinance on the Limitation and Disposal of Waste (OLED), RO 2015 5699 of December 4, 2015 as of January 1, 2019, the Order of February 15, 2016 on non-hazardous waste storage facilities, JORF n°0069 of March 22, 2016, text n°3 and Order of December 12, 2014 on the conditions of admission of inert waste in facilities falling under headings 2515, 2516, 2517 and in inert waste storage facilities falling under heading 2760 of the nomenclature of classified facilities, JORF n°0289 of December 14, 2014 page 21032, text n°11.

Country	Disposal class	Prices* per ton (CHF for CH, EUR for FR)	HC _{C5-C10} (mg/kg)	HC _{C10-C40} (mg/kg)	Cr _{total} (mg/kg)	Cr(VI) (mg/kg)	Ni (mg/kg)
Switzerland	A	25	<1	<50	<50	–	<50
	B	60	1–10	50–500	50–500	–	50–500
	E	150	10–100	500–5000	500–1000	<0.5	–
	E+	200*	>100	>5000	–	>0.5	–
			Total organic carbon mg/kg				
France	Aménagement (BRGM guideline 2000)				<90	–	<60
	ISDI	3	<500		<0.5**	–	<0.4
	ISDND	60	50000		10-70**	–	10–40
	ISDD	140	60000		>70**	–	>40

5.6. Potential disposal for FCC's excavated material

Having one of the highest construction and demolition waste (C&D) production of 246 mio. tons in 2012 (Akhtar and Sarmah, 2018), France aims for a maximum use of excavated tunnel material. Construction sites are subject to waste regulations resulting from the Waste Framework Directive 2008/98/EC and the legislative and regulatory provisions in the environment code.

The Euralpin Lyon-Turin tunnel, Grand Paris Express project, La Ligne Nouvelle Provence Côte d'Azur (LN PCA) and the CIGEO projects are currently France's most ambitious underground undertakings and might be superseded by FCC construction. In France, the status of *déchets* (waste) is not applied to excavated material used on construction site. Thus, excavated material leaving the defined construction area is considered waste although the *matériaux* (material) might be further used outside. France uses the legal empowering waste status to direct construction companies towards a more sustainable, environmental-friendly treatment of excavated material. This is treated mutually in Switzerland and anchored in both cantonal and federal legislation. Parallel, trans-national projects in the French *région* (region) of Auvergne-Rhône Alps would influence FCC (e.g. Lyon-Turin) significantly according to these governmental targets since subsurface projects are cumulatively summarized per region in terms of excavated volumes.

Legal authorities, public organisations, and administrations of the French Ministry of Ecological Transition push for waste valorisation and publish recommendations and guidelines for the usage of excavated material. The two major entities are the *Association Française des Tunnels et De L'Espace Souterrain (AFTES)* and the central technical service *Le Centre D'Etudes des Tunnels (CETU)* linked to the French ministry of environment and *Direction Générale des Infrastructures, des Transports et de la Mer* (Directorate General for Infrastructure, Transport and Oceans) providing technical support to national tunnelling projects, in conjunctions with e.g. Standard NFP11-300 Execution of earthworks, Classification of materials useable in the construction of embankments and road infrastructure form layers and the SETRA's technical guide (CEREMA, 2021). Legally binding regulations, in particular disposal classes as stated in Table 6 and its associated threshold limits for chemical pollutants will become significantly important as mineable resources get dramatically less in future. A thorough review of European legislation for excavated material can be taken from Haas et al. (2020b).

In France, waste can be classified implicitly under certain conditions, which allow the transformation of waste into a resource. Excavated material removed from a French or Swiss construction site, whether polluted or not, takes on the status of waste. In this case, the operator of the excavation is responsible for the excavated material. Then, legal

treatment methods apply in accordance with Article L. 541-1 of the Environment Code as follows: (1) reducing production and harmfulness, (2) use of excavated material on site, (3) material recovery (particularly in development or via the backfilling of quarries) and (4) elimination. This complies with chemical and mineralogical laboratory analyses and associated pollutants, which are currently identified for FCC as part of its extensive laboratory analyses.

6. Conclusions

Subsurface infrastructure projects pave the way to potential resources via sophisticated concepts on how to valorise, respectively use excavated material reaching an increasing level of environmental significance. A common goal of subsurface projects is to maximize the use of excavated material, produce sustainable products and minimize landfilling as one of the low-quality application scenarios. The status of waste is a tool to control environmental impacts, and valorisation is strongly encouraged.

Based on an extensive review of subsurface case studies, potential application scenarios of FCC's proposed excavated material were evaluated in this study. Apart from concrete production being one of the options, an improved rock characterisation and subsequent applications of excavated material are in line with on-line analyses mounted on TBMs and stored in a dedicated database. FCC aims towards the development of a material management concept succeeding an extensive sampling and testing procedure. Close collaborations with the authorities of the two countries impacted by the FCC construction, France and Switzerland, have been established with national and cantonal authorities to ensure adequate legislation review years before start of construction.

The management and remediation of excavated material from subsurface projects need to be further optimised in future. This is particularly crucial for a common database, which should summarize all relevant construction and excavation analyses. FCC's proposed 90-100 km subsurface infrastructure exhibits an example of early-stage investigations, an extensive set of performed laboratory analyses for rock characterisation, trans-national project management and communication among the project owner and its associated collaborating partners and governmental authorities. This paper has outlined both technical, i. e. geological and environmental limiting factors that might impact efficient application concepts.

The upcoming decade will be used to conduct geological site investigations to create a thorough material management plan in accordance with French and Swiss authorities and improve FCC's geological subsurface model, which will feature results from preceding laboratory

analyses. Potential application of excavated material might arise from gravel and sandy material and perhaps used for concrete production. It is important to analyse individual scenarios in more detail, i.e. to check concrete applicability and its associated problems with alkali aggregate reactions, frost resistance or high sulphate concentrations as well as the use of geopolymers.

Future research goals to be presented in separate studies consist of the derivation of a detailed stratigraphic understanding of FCC's geological formations in the Geneva Basin. This also includes evaluation and potential correlations among performed laboratory analyses. In addition, associated geophysical well-log data would enable the identification of sandy and shaly layers, calculations of rock strength parameters and elastic properties during site investigations, to be linked to potential application scenarios.

ORCID iD authorship contribution statement

Maximilian Haas: Conceptualization, Data curation, Formal analysis, Investigation, Methodology, Visualization, Writing – original draft, Writing – review & editing. **Laëtitia Mongeard:** Writing – review & editing. **Luisa Ulrici:** Writing – review & editing. **Laëtitia D'Aloia:** Writing – review & editing. **Agnès Cherrey:** Writing – review & editing. **Robert Galler:** Supervision. **Michael Benedikt:** FCC project leader, Supervision.

Acknowledgements

The authors would like to thank Dr. Jacques Burdin (Ingenieur Conseil) and Dr. Michael Plötze (ClayLab, Institute for Geotechnical Engineering, ETH Zurich) for their valuable input, which helped improving the manuscript. Pieter Mattelaer (project leader) and Jérémy Voiron (geotechnical engineer) are sincerely thanked for providing the data for CERN's HL-LHC construction project and for the fruitful discussions on-site.

This study has received funding from the European Union's Horizon 2020 research and innovation programme under grant No. 951754.

References

- CLAIRE, 2013. Remediation of four sites in Northwest England: a successfully completed multi-site, multi-consultant cluster project. *Case Study Bull. CSB* 11.
- Abada, A., Abbrescia, M., AbdusSalam, S.S., Abdylukhanov, I., Abelleira Fernandez, J., Abramov, A., Aburua, M., Acar, A.O., Adzic, P.R., Agrawal, P., Aguilar-Saavedra, J. A., Aguilera-Verdugo, J.J., Aiba, M., Aichinger, I., Aielli, G., Akay, A., Akhundov, A., Aksakal, H., Albacete, J.L., Albergro, S., Alekou, A., Aleksa, M., Aleksan, R., Alemany Fernandez, R.M., Alexahin, Y., Alía, R.G., Alioli, S., Alipour Tehrani, N., Allanach, B. C., Allport, P.P., Altinli, M., Altmannshofer, W., Ambrosio, G., Amorim, D., Amstutz, O., Anderlini, L., Andreazza, A., Andreini, M., Andriatis, A., Andris, C., Andronic, A., Angelucci, M., Antinori, F., Antipov, S.A., Antonelli, M., Antonello, M., Antonoli, P., Antusch, S., Anulli, F., Apollinario, L., Apollinari, G., Apollonio, A., Appeló, D., Appleby, R.B., Apyan, A., Apyan, A., Arbey, A., Arbuzov, A., Arduini, G., Ari, V., Arias, S., Armesto, N., Arnaldi, R., Arsenyev, S.A., Arzeo, M., Asai, S., Aslanides, E., Aßmann, R.W., Astapovych, D., Atanasov, M., Atieh, S., Attié, D., Auchmann, B., Audurier, A., Aull, S., Aumon, S., Aune, S., Avino, F., Avriilaud, G., Aydin, G., Azatov, A., Azuelos, G., Azzi, P., Azzolini, O., Azzurri, P., Bacchetta, N., Bacchiocchi, E., Bachacou, H., Baek, Y.W., Baglin, V., Bai, Y., Baird, S., Baker, M.J., Baldwin, M.J., Ball, A.H., Ballarino, A., Banerjee, S., Barber, D.P., Barducci, D., Barhroux, P., Barna, D., Barnaföldi, G.G., Barnes, M.J., Barr, A., Barranco García, J., da Costa, J., Bartmann, W., Baryshevsky, V., Barzi, E., Bass, S.A., Bastianin, A., Baudouy, B., Bauer, F., Bauer, M., Baumgartner, T., Bautista-Guzmán, I., Bayindir, C., Beaudette, F., Bedeschi, F., Béguin, M., Bellafont, I., Bellagamba, L., Bellegarde, N., Belli, E., Bellingeri, E., Bellini, F., Bellomo, G., Belomestnykh, S., Bencivinni, G., Benedikt, M., Bernardi, G., Bernardi, J., Bernet, C., Bernhardt, J.M., Bernini, C., Berriaud, C., Bertarelli, A., Bertolucci, S., Besana, M.I., Besançon, M., Beznosov, O., Bhat, P., Bhat, C., Biagini, M.E., Bissrotte, J.L., Bibet Chevalier, A., Bielert, E.R., Biglietti, M., Bilei, G.M., Bilki, B., Biscari, C., Bishara, F., Blanco-García, O.R., Blázquez, F.R., Blekman, F., Blondel, A., Blümlein, J., Boccali, T., Boels, R., Bogacz, S.A., Bogomyagkov, A., Boine-Frankenheim, O., Boland, M.J., Bologna, S., Bolukbasi, O., Bomben, M., Bondarenko, S., Bonvini, M., Boos, E., Bordieri, B., Bordry, F., Borghello, G., Borgonovi, L., Borowka, S., Bortoletto, D., Boschini, D., Boscolo, M., Boselli, S., Bosley, R.R., Bossu, F., Botta, C., Bottura, L., Bouchez, R., Boutin, D., Bovone, G., Božović Jelisavić, I., Bozbey, A., Bozzi, C., Bozzini, D., Braccini, V., Braibant-Giacomelli, S., Bramante, J., Braun-Munzinger, P., Briffa, J.A., Britzger, D., Brodsky, S.J., Brooke, J.J., Bruce, R., Brüchman De Renstrom, P., Bruna, E., Brüning, O., Brunner, O., Brunner, K., Bruzzone, P., Buffat, X., Bulyak, E., Burkart, F., Burkhart, H., Burnet, J.-P., Butin, F., Buttazzo, D., Butterworth, A., Caccia, M., Cai, Y., Caiffi, B., Cairo, V., Cakir, O., Calaga, R., Calatroni, S., Calderini, G., Calderola, G., Caliskan, A., Calvet, D., Calviani, M., Camalich, J.M., Camarri, P., Campanelli, M., Camporesi, T., Canbay, A.C., Canepa, A., Cantergiani, E., Cantore-Cavalli, D., Capeans, M., Cardarelli, R., Cardella, U., Cardini, A., Carloni Calame, C.M., Carra, F., Carra, S., Carvalho, A., Casalbuoni, S., Casas, J., Cascella, M., Castelnovo, P., Castorina, G., Catalano, G., Cavanini, V., Cazzato, E., Cennini, E., Cerri, A., Cerutti, F., Cervantes, J., Chaikovska, I., Chakraborty, J., Chala, M., Chamizo-Llatas, M., Chanal, H., Chanal, D., Chance, S., Chancé, A., Charitos, P., Charles, J., Charles, T.K., Chattopadhyay, S., Chehab, R., Chekanov, S.V., Chen, N., Chernoded, A., Chetvertkova, V., Chevalier, L., Chiarelli, G., Chiarello, G., Chiesa, M., Chiggiato, P., Childers, J.T., Chmieleńska, A., Cholokian, A., Chomaz, P., Chorowski, M., Chou, W., Chruszcz, M., Chyhyrnyets, E., Cibirnetto, G., Ciftci, A.K., Ciftci, R., Cimino, R., Ciuchini, M., Clark, P.J., Coadou, Y., Cobal, M., Coccaro, A., Cogan, J., Cogneras, E., Collamati, F., Colldelram, C., Collier, P., Collet, J., Contino, R., Conventi, F., Cook, C. T.A., 2019. FCC-ee: the Lepton collider. *Eur. Phys. J. Spec. Top.* 228, 261–623. <https://doi.org/10.1140/epjst/e2019-900045-4>.
- Akhtar, A., Sarmah, A.K., 2018. Construction and demolition waste generation and properties of recycled aggregate concrete: a global perspective. *J. Clean. Prod.* 186, 262–281. <https://doi.org/10.1016/j.jclepro.2018.03.085>.
- Association française de normalisation, et al., 1990. *Granulats: Essai d'abrasivité et de broyabilité* (P 18-579). AFNOR, Paris.
- Association française de normalisation, 2004. *Contrete - Reactivity of a Concrete Formula with Regard to the Alkali-Aggregate Reaction - Performance Test - Béton, NF. AFNOR*, Paris.
- Association française de normalisation, 2013. P18-579:2013-02-09 *Granulats - Détermination des coefficients d'abrasivité et de broyabilité*. AFNOR, Paris.
- Association française de normalisation, 2015. *Aggregates - Test Methods on Reactivity to Alkalies - Granulats*. AFNOR, Paris.
- Association française de normalisation, 2018. EN 1097-2: Prüfverfahren für mechanische und physikalische Eigenschaften von Gesteinskörnungen - Teil 2: Verfahren zur Bestimmung des Widerstandes gegen Zertrümmerung; Deutsche und Englische Fassung prEN 1097-2:2018. AFNOR, Paris.
- Association Française des Tunnels Et De L'Espace Souterrain, 2019. *Recommendations of AFTES GT35RIA2: Management and Use of Excavated Materials*. FFE - Advertising agency: 15 rue des sablons, Paris, France, p. 75116.
- Baccini, P., Brunner, P., 1991. *Metabolism of the Anthroposphere: Analysis, Evaluation, Design*. The MIT Press. <https://doi.org/10.7551/mitpress/8720.001.0001>.
- Basler, Ernst, Partner, 2012. *Verkehrliche und räumliche Auswirkungen des Lötschberg-Basistunnels*, pp. 43–50.
- Becker, L., Golsner, J., Kraiger, H., Stieber, B., 1997. Recycling and deposition of excavation material. *Felsbau* 15, 108–110.
- Benedikt, M., Blondel, A., Janot, P., Mangano, M., Zimmermann, F., 2020. Future circular colliders succeeding the LHC. *Nat. Phys.* 16, 402–407. <https://doi.org/10.1038/s41567-020-0856-2>.
- Bergmeister, K., 2007. Alpenquerende Tunnel Projektübersicht und Materialbewirtschaftung beim Brenner Basistunnel. *Beton- Stahlbetonbau* 102, 19–23. <https://doi.org/10.1002/best.200600529>.
- Bergmeister, K., 2013. Vorerkundung und Baufortschritt beim Brenner Basistunnel. *Beton- Stahlbetonbau* 108, 35–42. <https://doi.org/10.1002/best.201380006>.
- Blengini, G., Garbarino, E., 2010. Resources and waste management in Turin (Italy): the role of recycled aggregates in the sustainable supply mix. *J. Clean. Prod.* 18, 1021–1030. <https://doi.org/10.1016/j.jclepro.2010.01.027>.
- Bruning, O., Klein, M., Myers, S., Osborne, J., Rossi, L., Waajjer, C., Zimmermann, F., 2013. *Civil engineering feasibility studies for future ring colliders at cern*. IPAC 2013 Proc. 4th Int. Part. Accel. Conf. 969–971.
- Büchi, E., Thalman, C., 1995. Wiederverwertung von TBM-Ausbruchmaterial. Einfluss des Schneidrollenabstands. TBM Know-how zum Projekt NEAT. In: *Atlas Copco-Robbins Symposium*, 16. März. Lucerne, Switzerland, p. 9.
- Bufalini, M., Dati, G., Rocca, M., Scevaroli, R., 2017. The Mont cenis base tunnel. *Geomech. Tunnelbau* 10, 246–255. <https://doi.org/10.1002/geot.201700009>.
- Bundesministerium Klimaschutz Umwelt Energie Mobilität Innovation und Technologie, 2017. *Bundesabfallwirtschaftsplan. BMK [WWW document]*. <https://www.bmlrt.gv.at/umwelt/abfall-ressourcen/bundes-abfallwirtschaftsplan/BAWP2017-Final.html>. (Accessed 6 May 2020).
- Bundesministerium Landwirtschaft Regionen und Tourismus, 2008. *Deponieverordnung 2008 [WWW document]*. BMK. https://www.ris.bka.gv.at/GeltendeFassung/Bundesnormen/20005653/DVO_2008%2C_Fassung_vom_19.02.2020.pdf. (Accessed 19 February 2020).
- Bundesverband, Natursteineindustrie, 1993. *Bauen mit Splittbeton*. Bundesverband Naturstein-Industrie e.V., Bonn.
- Burdin, J., 2015. L'utilisation de granulats provenant de la transformation des matériaux d'excavation des tunnels pour la fabrication des bétons. *AFGC*, 18 et 19 Mars, p. 12.
- Burdin, J., Monin, N., 2009. The management of excavated materials from the Lyon-Turin rail link project. *Geomech. Tunnelbau* 2, 652–662. <https://doi.org/10.1002/geot.200900048>.
- Burdin, J., Monin, N., Thalman, C., 2017. *L'utilisation des matériaux extraits des ouvrages souterrains*, *Entrepr. ed. DOSSIER - MATEX*.
- Cabello Eras, J., Sagastume, A., Capote, D., Hens, L., Vandecasteele, C., 2013. Improving the environmental performance of an earthwork project using cleaner production strategies. *J. Clean. Prod.* 47, 368–376. <https://doi.org/10.1016/j.jclepro.2012.11.026>.
- CEREMA, 2021. *Technical guide [WWW document]*. <https://www.cerema.fr/fr/centre-ressources/boutique/technical-guide-pot-bearings>. (Accessed 1 July 2021).

M. Haas et al.

Journal of Cleaner Production 315 (2021) 128049

- Stephen, S.O.M., 2020. Presentation of the Project Lyon-Turin Ferroviaire. TELT. Swiss Confederation, 1983. Federal act on the protection of the environment [WWW document]. <https://www.admin.ch/opc/en/classified-compilation/19830267/201801010000/814.01.pdf>. (Accessed 24 February 2020).
- Swiss Confederation, 1989. Convention de Bâle sur le contrôle des mouvements transfrontières de déchets dangereux et de leur élimination [WWW document]. <https://www.admin.ch/opc/fr/classified-compilation/19890050/index.html>. (Accessed 19 February 2020).
- Swiss Confederation, 1998. Ordinance on the remediation of polluted sites (contaminated sites Ordinance, CSO) [WWW document]. <https://www.admin.ch/opc/en/classified-compilation/19983151/201705010000/814.680.pdf>. (Accessed 24 February 2020).
- Swiss Confederation, 2005. Ordonnance sur les mouvements de déchets [WWW document]. <https://www.admin.ch/opc/fr/classified-compilation/20021080/index.html>. (Accessed 19 February 2020).
- Swiss Confederation, 2016. Ordinance on the avoidance and the disposal of waste [WWW document]. <https://www.admin.ch/opc/en/classified-compilation/20141858/201901010000/814.600.pdf>. (Accessed 19 February 2020).
- Dahlbo, H., Bacher, J., Lähinen, K., Jouttijärvi, T., Suoheimo, P., Mattila, T., Sironen, S., Myllymaa, T., Saramäki, K., 2015. Construction and demolition waste management - a holistic evaluation of environmental performance. *J. Clean. Prod.* 107 <https://doi.org/10.1016/j.jclepro.2015.02.073>.
- Daller, J., 2017. Selection of construction methods in rock tunneling [WWW document]. https://ic-group.org/fileadmin/Magazines/ITA_2017_Slo/171128_DALLER_CO_NSTR_METHOD_ITA_LJUBLJANA.pdf.
- Deutscher Ausschuss für Stahlbeton (DAfStb), 2001. Vorbeugende Maßnahmen gegen schädigende Alkali-reaktion im Beton: Alkali-Richtlinie. DAfStb, Berlin.
- DRAGON, 2014. Development of resource-efficient and advanced underground technologies. DRAGON [WWW document]. <http://www.dragonproject.eu/pdf/5301e37519b4c.pdf>. (Accessed 14 February 2020).
- Dubuisson, B., 1995. Encyclopédie pratique de la construction et du bâtiment. Exécution de la construction traditionnelle Titre II-3e Partie, Paris.
- Ehrbar, H., 2008. Gotthard-Base-Tunnel - experiences with different tunnelling methods. In: 2^o Congresso Brasileiro de Túneis e Estruturas Subterrâneas Seminário Internacional "South American Tunnelling" - 2008 Estruturas Subterrâneas Seminário Internacional "South American Tunnelling" - 2008.
- Ekici, Z., Rüegg, C., Wilfinger, N., Wagner, O.K., Weigl, J., 2011. Auswahl der Vortriebsmethode beim Semmering-Basistunnel Neu. *Geomech. Tunnelbau* 4, 544–552. <https://doi.org/10.1002/geot.201100037>.
- Entacher, M., Lorenz, S., Galler, R., 2014. Tunnel boring machine performance prediction with scaled rock cutting tests. *Int. J. Rock Mech. Min. Sci.* 70, 450–459. <https://doi.org/10.1016/j.ijrmmms.2014.04.021>.
- Erben, H., 2016. Real-Time Material Analysis and Development of a Collaboration and Trading Platform for Mineral Resources from Underground Construction Projects. PhD thesis, 206 pages. Montanuniversität Leoben, Austria.
- Erben, H., Galler, R., 2014. Tunnel spoil – new technologies on the way from waste to raw material/Tunnelausbruch – Neue Technologien für den Weg vom Abfall zum Rohstoff. *Geomech. Tunn.* 7, 402–410. <https://doi.org/10.1002/geot.201400043>.
- Esa, M.R., Halog, A., Rigamonti, L., 2016. Developing strategies for managing construction and demolition wastes in Malaysia based on the concept of circular economy. *J. Mater. Cycles Waste Manag.* 19, 1144–1154. <https://doi.org/10.1007/s10163-016-0516-x>.
- European Commission, 2005. Trans-European transport network - TEN-T priority axes and projects [WWW document]. https://ec.europa.eu/ten/transport/projects/doc/2005_ten_t_en.pdf. (Accessed 14 February 2020).
- European Commission, 2008. The raw materials initiative - meeting our critical needs for growth and jobs in Europe [WWW document]. <https://eur-lex.europa.eu/LexUriServ/LexUriServ.do?uri=COM:2008:0699:FIN:en:PDF>. (Accessed 14 February 2020).
- European Commission, 2010. Europe 2020 - a European strategy for smart, sustainable and inclusive growth [WWW Document]. <https://ec.europa.eu/eu2020/pdf/COMPLETE%20EN%20BARROSO%2007%20-%20EN%20version.pdf>. (Accessed 14 February 2020).
- European Commission, 2011. Roadmap to a resource efficient Europe [WWW document]. <https://eur-lex.europa.eu/legal-content/EN/TXT/PDF/?uri=CELEX:52011DC0571&from=EN>. (Accessed 14 February 2020).
- European Commission, 2012. European Norm 450-1: Fly Ash for Concrete - Part 1: Definition, Specifications and Conformity Criteria. EC. German version EN 450-1: 2012.
- European Commission, 2012. A stronger European industry for growth and economic recovery [WWW document]. <https://eur-lex.europa.eu/LexUriServ/LexUriServ.do?uri=COM:2012:0582:FIN:EN:PDF>. (Accessed 14 February 2020).
- European Commission, 2018. TEN-T evaluation roadmap [WWW document]. https://ec.europa.eu/info/law/better-regulation/initiatives/ares-2018-4706847_en. (Accessed 6 May 2020).
- European Commission, 2020. European Norm: prEN 932-3 - Prüfverfahren für allgemeine Eigenschaften von Gesteinskörnungen - Teil 3: Durchführung und Terminologie einer vereinfachten petrographischen Beschreibung. EC.
- Fabbri, D., 2004. The Gotthard base tunnel: project overview [WWW document]. <https://www.lombardi.ch/de-de/SiteAssets/Publications/1214/Pub0394-L-The-Gotthard-Base-Tunnel-Project-overview.pdf>. (Accessed 14 February 2020).
- Fachgruppe für Untertagebau FGU, 2016. Bewirtschaftung und Wiederverwertung von Ausbruchmaterial - Inventar Schweizer Großprojekte. Fachgruppe für Untertagebau, Esslingen.
- Fern, E.J., Di Murro, V., Soga, K., Li, Z., Scibile, L., Osborne, J.A., 2018. Geotechnical characterisation of a weak sedimentary rock mass at CERN. *Tunn. Undergr. Sp. Technol.* 77, 249–260. <https://doi.org/10.1016/j.tust.2018.04.003>.
- GADZ, S.A., 1993. Projet LHC - Synthèse géologique et géotechnique. Geneva, Switzerland. GADZ reports, CERN LHC.
- Galler, R., 2015. Ressourceneffiziente Verwertung von Tunnelausbruchmaterial. *Tunnel* 7, 44–59.
- Galler, R., 2016. Verwendung von Tunnelausbruchmaterial - Verpflichtung zur Ressourcenschonung für künftige Generationen. *Österreichische Ingenieur- und Architekt. ÖIAZ* 161, 5–13.
- Galler, R., 2019. Tunnelausbruchmaterial - Abfall oder mineralischer Rohstoff? In: Thiel, S., Thomé-Kozmiensky, E., Pretz, T., Senk, D.G., Wotruba, H. (Eds.), *Mineralische Nebenprodukte Und Abfälle* 6, pp. 562–576.
- Galler, R., Biermeier, F., Lassnig, K., 2012. Prognose von Tunnelausbruchmaterial. Gattinoni, P., Pizzarotti, E.M., Scesi, L., 2016. Geomechanical characterisation of fault rocks in tunnelling: the Brenner base tunnel (northern Italy). *Tunn. Undergr. Space Technol.* 51, 250–257. <https://doi.org/10.1016/j.tust.2015.10.043>.
- Geissdoerfer, M., Savaget, P., Bocken, N., Hultink, E., 2017. The Circular Economy – a new sustainability paradigm? *J. Clean. Prod.* 143, 757–768. <https://doi.org/10.1016/j.jclepro.2016.12.048>.
- Ghisellini, P., Ripa, M., Ulgiati, S., 2018. Exploring environmental and economic costs and benefits of a circular economy approach to the construction and demolition sector. A literature review. *J. Clean. Prod.* 178, 618–643. <https://doi.org/10.1016/j.jclepro.2017.11.207>.
- AlpTransit Gotthard, 2017. AlpTransit Gotthard and Ceneri Base Tunnel - the Logical Continuation in the South. AlpTransit Gotthard Ltd., Lucerne, Switzerland.
- Haas, M., De Haller, A., Moscardello, A., Scibile, L., Benedikt, M., Gegenhuber, N., Galler, R., 2020a. A mineralogical re-use classification model of molasse rock mass in the Geneva Basin. *EUROCK2020 Conf. Proc.*, Trondheim, Norway. (in press).
- Haas, M., Galler, R., Scibile, L., Benedikt, M., 2020b. Waste or valuable resource – a critical European review on re-using and managing tunnel excavation material. *Resour. Conserv. Recycl.* 162, 105048. <https://doi.org/10.1016/j.resconrec.2020.105048>.
- Haid, H.G., Hammer, H., 2009. Katzenbergtunnel - Umwelttechnische und genehmigungsrechtliche Randbedingungen für die Verwertung von Tunnelausbruchmaterial. *Geomech. Tunnelbau* 2, 643–651. <https://doi.org/10.1002/geot.200900033>.
- Huang, B., Wang, X., Kua, H., Geng, Y., Bleischwitz, R., Ren, J., 2018. Construction and demolition waste management in China through the 3R principle. *Resour. Conserv. Recycl.* 129 <https://doi.org/10.1016/j.resconrec.2017.09.029>.
- Iacoboaia, C., Aldea, M., Petrescu, F., 2019. Construction and demolition waste - a challenge for the European Union? *Theor. Empir. Res. Urban Manag.* 14, 30–52.
- International Society for Rock Mechanics and Rock Engineering, 1972. Suggested Methods for Determining the Uniaxial Compressive Strength on Rock Materials and the Point Load Strength Index. ISRM.
- International Tunneling and Underground Space Association, 2019. Handling, Treatment and Disposal of Tunnel Spoil Materials. ITA.
- Keily, J., 2020. Excavating tunnel: the archaeology of Crossrail [WWW document]. <https://www.museumoflondon.org.uk/discover/tunnel-developmental-archaeology-crossrail-docklands>. (Accessed 11 February 2020).
- Korhonen, J., Honkasalo, A., Seppälä, J., 2018. Circular economy: the concept and its limitations. *Ecol. Econ.* 143, 37–46. <https://doi.org/10.1016/j.ecolecon.2017.06.041>.
- Krook, J., Svensson, N., Eklund, M., 2011. Landfill mining: a critical review of two decades of research. *Waste Manag.* 32, 513–520. <https://doi.org/10.1016/j.wasman.2011.10.015>.
- Kruse, M., Weber, R., 1995. Beton aus TBM-Ausbruchmaterial. *Schweizer Ing. Architekt.* 47.
- Lafebre, H., Songonuga, O., Kathuria, A., 1998. Contaminated soil management at construction sites. *Pract. Period. Hazard. Toxic. Radioact. Waste Manag.* 2, 115–119. [https://doi.org/10.1061/\(ASCE\)1090-025X\(1998\)2:3\(115\)](https://doi.org/10.1061/(ASCE)1090-025X(1998)2:3(115)).
- Lahoti, M., Wong, K.K., Tan, K.H., Yang, E.H., 2017. Use of alkali-silica reactive sedimentary rock powder as a resource to produce high strength geopolymer binder. *Construct. Build. Mater.* 155, 381–388. <https://doi.org/10.1016/j.conbuildmat.2017.08.109>.
- Lassnig, K., 2012. Verwendung von Tunnelausbruchmaterial - geologische und geotechnische Aspekte. Montanuniversität Leoben.
- Le Centre D'Etudes des Tunnels, C., 2016. Natural Geological Materials Excavated during Underground Works.
- Le Centre D'Etudes des Tunnels, C., 2017. Les notes de l'Observatoire des tunnels - les patrimoine des tunnels routiers en France.
- Le Centre D'Etudes des Tunnels, C., 2019. Les MEMENTO de l'Observatoire des tunnels - les travaux en tunnel.
- Locher, F., 2000. Zement - Grundlagen der Herstellung und Verwendung. Verlag Bau & Technik.
- Magnusson, S., Lundberg, K., Svedberg, B., Knutsson, S., 2015. Sustainable management of excavated soil and rock in urban areas – a literature review. *J. Clean. Prod.* 93, 18–25. <https://doi.org/10.1016/j.jclepro.2015.01.010>.
- Marzouk, M., Azab, S., 2014. Environmental and economic impact assessment of construction and demolition waste disposal using system dynamics. *Resour. Conserv. Recycl.* 82, 41–49. <https://doi.org/10.1016/j.resconrec.2013.10.015>.
- Merlini, D., Stocker, D., Falanesca, M., Schuerch, R., 2018. The Ceneri base tunnel: construction experience with the southern portion of the flat railway line crossing the Swiss alps. *Engineering* 4, 235–248. <https://doi.org/10.1016/j.eng.2017.09.004>.
- Minder, P., Puzrin, A.M., Plötze, M., 2016. Enhanced delivery of chemical agents in soil improvement applications. *Geotechnique* 66, 469–480. <https://doi.org/10.1680/jgeot.15.P.127>.
- Moreno, B., García-Álvarez, M.T., 2018. Measuring the progress towards a resource-efficient European Union under the Europe 2020 strategy. *J. Clean. Prod.* 170, 991–1005. <https://doi.org/10.1016/j.jclepro.2017.09.149>.

- Moscariello, A., Guglielmetti, L., Omodeo-Salé, S., De Haller, A., Eruteya, O.E., Lo, H.L., Clerc, N., Makloufhi, Y., Do Couto, D., Ferreira De Oliveira, G., Perozzi, L., DeOliveira, F., Hollmüller, P., Quiquerez, L., Nawratil De Bono, C., Martin, F., Meyer, M., 2020. Heat production and storage in Western Switzerland: advances and challenges of intense multidisciplinary geothermal exploration activities, an 8 years progress report. In: Proceedings World Geothermal Congress 2020, Reykjavik, Iceland, April 26 – May 2, p. 12.
- Oxburgh, E.R., 1981. R. Trümpy geology of Switzerland: a guide-book. Part A: an outline of the geology of Switzerland. Basel and New York (Wepf & Co.), 1980. 104 pp., 46 figs., 1 coloured pl. Price Sfr. 35.00. - Part B: geological excursions. Ibid 230. <https://doi.org/10.1180/minmag.1981.044.335.28>, 204 figs. Pri. Mineral. Mag. 44, 366.
- Panagos, P., Van Liedekerke, M., Jones, A., Montanarella, L., 2012. European soil data centre: response to European policy support and public data requirements. Land Use Pol. 29, 329–338. <https://doi.org/10.1016/j.landusepol.2011.07.003>.
- Piffner, A.O., 2014. Geology of the Alps, Revised and updated translation of Geologie der Alpen, second ed.
- Posch, H., Murr, R., Huber, H., Kager, M., Kolb, E., 2014. Tunnel excavation - the conflict between waste and recycling through the example of the Koralm Tunnel, contract KAT2. Geomech. Tunnelbau 7, 437–450. <https://doi.org/10.1002/geot.201400036>.
- Posch, H., Nahold, M., Kager, M., Kolb, E., Bauer, F., Huber, M., 2015a. Responsible handling of tunnel spoil through the example of Koralm Tunnel contract KAT2/Verantwortungsvoller Umgang mit Tunnelausbruch am Beispiel Koralmtunnel. Baulos KAT2. Geomech. Tunnelbau 8, 503–517. <https://doi.org/10.1002/geot.201500037>.
- Posch, H., Otto, R., Huber, H., Murr, R., Kager, M., Wagner, H., 2015b. Recycling of tunnel excavation using the example of the Koralm Tunnel, contract KAT2 - status April 2015. Geomech. Tunnelbau 8, 340–347. <https://doi.org/10.1002/geot.201500013>.
- Read, A., Hudgins, M., Harper, S., Phillips, P., Morris, J., 2001. The successful demonstration of aerobic landfilling: the potential for a more sustainable solid waste management approach? Resour. Conserv. Recycl. 115–146.
- République de Canton Genève, 2016. Guide pour la réutilisation des matériaux d'excavation non pollués, 1ère édit. In: Service de géologie, sols et déchets (GESDEC), République et Canton de Genève. GESDEC.
- République Française, 2003. Code de l'environnement. L'état Paris, Paris [WWW document]. <https://www.legifrance.gouv.fr/affichCode.do?cidTexte=LEGITEXT000006074220>.
- République Française, 2015. La loi du transition énergétique. L'état Paris, Paris [WWW document]. <https://www.legifrance.gouv.fr/affichTexte.do?cidTexte=JORFTEXT000031044385>. (Accessed 24 February 2020).
- Resch, D., 2012. Verwendung von Tunnelausbruchmaterial - Entscheidungsgrundlagen, PhD thesis. Montanuniversität Leoben, pp. 1–211.
- Resch, D., Lassnig, K., Galler, R., Ebner, F., 2009. Tunnel excavation material - high value raw material. Geomech. Tunnelbau 2, 612–618. <https://doi.org/10.1002/geot.200900047>.
- Reynard, E., Estoppey, E., 2020. The Lavaux world heritage terraced vineyard, pp. 111–121. https://doi.org/10.1007/978-3-030-43203-4_8.
- Rios, F.C., 2018. Beyond Recycling: Design for Disassembly, Reuse, and Circular Economy in the Built Environment.
- Ritter, S., Einstein, H., Galler, R., 2013. Planning the handling of tunnel excavation material – a process of decision making under uncertainty. Tunn. Undergr. Space Technol. 33, 193–201. <https://doi.org/10.1016/j.tust.2012.08.009>.
- Ritzén, S., Sandström, G.Ö., 2017. Barriers to the circular economy – integration of perspectives and domains. Procedia CIRP 64, 7–12. <https://doi.org/10.1016/j.procir.2017.03.005>.
- Robben, C., Wotruba, H., 2019. Sensor-based Ore sorting technology in mining—past, present and future. Minerals 9, 523. <https://doi.org/10.3390/min9090523>.
- Robinson, G., Kapo, K., 2004. A GIS analysis of suitability for construction aggregate recycling sites using regional transportation network and population density features. Resour. Conserv. Recycl. 42, 351–365. <https://doi.org/10.1016/j.resconrec.2004.04.009>.
- Rodríguez, G., Alegre, F.J., Martínez, G., 2007. The contribution of environmental management systems to the management of construction and demolition waste: the case of the Autonomous Community of Madrid (Spain). Resour. Conserv. Recycl. 50, 334–349. <https://doi.org/10.1016/j.resconrec.2006.06.008>.
- Röhling, S., Eifert, H., Jablinski, M., 2012. Betonbau - Band 1: Zusammensetzung, Dauerhaftigkeit, Frischbeton. Fraunhofer IRB Verlag.
- Saathof, L., Ketelaars, M., 1999. Re-use of excavated soil from large diameter tunnels in The Netherlands, Balkema. In: Twelfth European Conference on Soil Mechanics and Geotechnical Engineering (Proceedings). Amsterdam, Netherlands, pp. 1301–1307.
- Savage, G.M., Golueke, C.G., Stein, E.L. von, 1994. Landfill Mining: Past and Present. BioCycle (USA).
- Schubel, D., Schaffer, R., 2020. The Koralm Tunnel - mastering the challenges of reusing excavated materials. In: FCCIS Kick-Off Week. Geneva, Switzerland, p. 18.
- Simion, I., Fortuna, M., Bonoli, A., Gavrilescu, M., 2013. Comparing environmental impacts of natural inert and recycled construction and demolition waste processing using LCA. J. Environ. Eng. Landsc. Manag. 21, 273–287. <https://doi.org/10.3846/16486897.2013.852558>.
- Skuk, S., Schierl, H., 2017. Brenner Base Tunnel: first results of the exploratory tunnels from a geological and geomechanical point of view: case studies of four fault zones. Geomech. Tunnelbau 10, 275–290. <https://doi.org/10.1002/geot.201700012>.
- empa swiss federal laboratories for materials science and technology, 1998. Die Auswirkungen von freien Schichtsilikaten im Zuschlag auf die Eigenschaften von Mörtel und Beton, Internes Bereichsprojekt, Untersuchungsbericht 166'184. EMPA.
- Tamparopoulos, A., 2012. Cost Estimation of Large Construction Projects with Dependent Risks - a Study on the Brenner Base Tunnel. PhD Thesis. Universität für Bodenkultur Wien.
- T.E.L.T. consortium, 2018. Tunnel Euralpin Lyon-Turin: the Project and Status of the Works, July 2018. Ed. Tunnel Euralp Lyon Turin Consortium. TELT.
- T.E.L.T. consortium, 2020. Challenges in environment - the Lyon-Turin project. TELT [WWW document]. <https://www.telt-sas.com/en/challenges/environment/> (accessed 10.22.20).
- Teuscher, P., Thalmann, C., Fetzner, A., Carron, C., 2007. Alpenquerende Tunnel: materialbewirtschaftung und Betontechnologie beim Lötschberg-Basistunnel. Beton-Stahlbetonbau 102, 2–10. <https://doi.org/10.1002/best.200600526>.
- Thalmann, C., 1996. Beurteilung und Möglichkeiten der Wiederverwertung von Ausbruchmaterial aus dem maschinellen Tunnelvortrieb zu Betonzuschlagstoffen, PhD thesis. Eidgenössische Technische Hochschule (ETH), Zurich, pp. 1–115.
- Thalmann, C., Schindler, C., Kruse, M., Basler, E., 2003. Aggregates for high quality concrete and shotcrete made out of excavated rock material – experiences gained on the alptransit tunnel projects. In: Proceedings of Industrial Minerals and Buildings Stones. Istanbul, Turkey, pp. 1–12.
- Vernus, E., Bonnet, J., Gonzalez, L., Roche, L., Serpeau, J., 2017. Etude n°15-0159/1A: Gestion et réutilisation des matériaux excavés - comment favoriser l'économie circulaire?.
- Voiron, J., Haas, M., Amiot, J.-B., 2020. CERN HL-LHC POINT 1, Gestion des matériaux d'excavation potentiellement pollués aux hydrocarbures. AFTES Congr, Paris, 2020 (postponed to 2021), Submitt.
- Voit, K., 2013. Einsatz und Optimierung von Tunnelausbruchmaterial des Brenner Basistunnels, PhD thesis, Application and optimization of tunnel excavation material of the Brenner Base Tunnel, PhD thesis, Universität für Bodenkultur Wien. Guthmann-Peterson Verlag.
- Voit, K., Kuschel, E., 2020. Rock material recycling in tunnel engineering. Appl. Sci. 10 <https://doi.org/10.3390/AP10082722>.
- Voit, K., Zimmermann, T., 2015. Characteristics of selected concrete with tunnel excavation material. Construct. Build. Mater. 101, 217–226. <https://doi.org/10.1016/j.conbuildmat.2015.10.016>.
- Voit, K., Zeman, O., Murr, R., Bergmeister, K., Arnold, R., 2015. Aufbereitung und Wiederverwertung von Tunnelausbruchmaterial beim Brenner Basistunnel. Beton-Stahlbetonbau 110, 832–844. <https://doi.org/10.1002/best.201500023>.
- Vollprecht, D., Sattler, T.M., Döschek-Held, K., Galler, R., Schimek, J., Kasper, T., Daul, J., Pomberger, R., 2019. Innovative Deponierung sowie Recycling von Mineralwolleabfällen im Bergversatz, in der Zementindustrie und in der Mineralwolleindustrie – das Projekt RecyMin. In: Berliner Konferenz Mineralische Nebenprodukte Und Abfälle, p. 480.
- Wenighofer, R., Galler, R., 2017. Digitale Ortsbrustbilder mittels Kamerabefahrung eines TBM-Bohrkopfs Digital Imaging of the Tunnel Face Through the Cutter Head Using Cameras. BHM Berg- Hüttenmännische Monatsh. 162, 568–572. <https://doi.org/10.1007/s00501-017-0684-6>.
- Wood, A., Agency, E., 2017. Crossrail project : environmental management during delivery of London's Elizabeth Line 170, 49–55.
- Ziegler, H.-J., Isler, A., 2013. Zusammenfassender geologischer Schlussbericht Lötschberg-Basistunnel. Landesgeologie (Bundesamt für Landestopografie swisstopo). Wabern, Switzerland.
- Zumsteg, R., Plötze, M., Puzrin, A.M., 2013. Effects of dispersing foams and polymers on the mechanical behaviour of clay pastes. Geotechnique 63, 920–933. <https://doi.org/10.1680/geot.12.P.044>.
- Zuo, C., Birkin, M., Clarke, G., McEvoy, F., Bloodworth, A., 2013. Modelling the transportation of primary aggregates in England and Wales: exploring initiatives to reduce CO2 emissions. Land Use Pol. 34, 112–124.

A.3 Integrated geo-engineering rock characterisation for CERN's Future Circular Collider subsurface infrastructure (Geneva Basin, Switzerland-France) from well-log, field and laboratory data

Table A.3: Overview of authorship and metadata of the presented publication.

Title	Integrated geo-engineering characterisation for CERN's Future Circular Collider subsurface infrastructure (Geneva Basin, Switzerland-France) from well-log, field and laboratory data
Author names	Maximilian Haas, Davide Carraro, Dario Ventra, Michael Plötze, Antoine De Haller, Andrea Moscariello
First author	Maximilian Haas
First author's contributions	Conceptualization; data digitisation; rock core inspections in the field; all laboratory work; data analysis; modelling; petrophysical calculations; all visualizations; writing – original draft; writing – review & editing
Scientific value	Petrophysical (well-logging) and mineralogical (laboratory) results for the derivation of lithotypes across the Geneva Basin for the FCC; geological-sedimentological (field) rock descriptions of glaciogenic deposits, Molasse Rouge, Grès et Marnes Gris à gypse and Jura limestone formations in the Geneva Basin as encountered by the FCC; identification of geological and environmental hazards for the FCC construction; sand-silt-clay model for evaluation of swelling potential and sand management
Status	Published in <i>Swiss Journal of Geosciences</i>
Peer-reviewed journal	Yes
Full citation	Haas M., Carraro D., Ventra D., Plötze M., De Haller A., Moscariello A., Integrated geo-engineering characterisation for CERN's Future Circular Collider subsurface infrastructure (Geneva Basin, Switzerland-France) from well-log, field and laboratory data, <i>Swiss Journal of Geosciences</i> , Volume 115, 16 (2022). https://doi.org/10.1186/s00015-022-00407-y .

Haas et al. *Swiss Journal of Geosciences* (2022) 115:16
<https://doi.org/10.1186/s00015-022-00407-y>



ORIGINAL PAPER

Open Access



Integrated stratigraphic, sedimentological and petrographical evaluation for CERN's Future Circular Collider subsurface infrastructure (Geneva Basin, Switzerland-France)

Maximilian Haas^{1,2,3*} , Davide Carraro³, Dario Ventra³, Michael Plötze⁴, Antoine De Haller³ and Andrea Moscariello³

Abstract

The European Organization for Nuclear Research (CERN) is currently undertaking a feasibility study to build the next-generation particle accelerator, named the Future Circular Collider (FCC), hosted in a 90–100 km subsurface infrastructure in the Geneva Basin, extending across western Switzerland and adjacent France. This article represents a preliminary, basin-scale stratigraphic and lithotype analysis using state-of-the-art Swiss and French stratigraphic terminology, set in context with the FCC. Existing stratigraphic information, rock cores and well reports, laboratory analyses and geophysical well-logs from 661 wells representative for the construction area have been integrated to pave the way for a multidisciplinary approach across several geoscientific and engineering domains to guide the FCC's upcoming technical design phase. Comparisons with well-log data allowed the identification of rock formations and lithotypes, as well as to formulate a preliminary assessment of potential geological hazards. Regional stratigraphic evaluation revealed the FCC's intersection of 13 geological formations comprising 25 different lithotypes across the Geneva Basin. A lack of data remains for the western to south-western subsurface region of the FCC construction area shown by well-density coverage modelling. The main geological hazards are represented by karstic intervals in the Grand Essert Formation's Neuchâtel Member, Vallorbe and Vuache formations, associated to fractured limestone lithotypes, and Cenozoic formations represented by the pure to clayey sandstone-bearing Transition zone and Siderolithic Formation. Potential swelling hazard is associated to the presence of anhydrite, and claystone lithotypes of the Molasse Rouge and Grès et Marnes Gris à gypse formations, yielding up to 17.2% of smectite in the Molasse Rouge formation. Hydrocarbon indices in both gaseous and bituminous forms are encountered in the majority of investigated wells, and bear a potential environmental hazard associated with the Molasse Rouge deposits and fractured limestones of the Mesozoic Jura formations.

Keywords: Lithotypes, Geophysical well-logs, Laboratory analyses, Field data, Tunnelling, Swelling, Karst, Future Circular Collider (FCC), CERN, Molasse, Siderolithic, Cretaceous, Geneva Basin

1 Introduction

The construction of subsurface infrastructure has gained increasing public attention, as manifested by the Gotthard, Lötschberg and Brenner Base tunnels, following extensive geological investigations prior to construction approval (Burdin et al., 2017; Ehrbar, 2008; Fachgruppe für Untertagebau (FGU), 2016; Haas et al., 2021;

Editorial handling: Wilfried Winkler

*Correspondence: maximilian.mathias.haas@cern.ch

¹ European Organization for Nuclear Research (CERN), Espl. Des Particules 1, 1211 Geneva, Switzerland

Full list of author information is available at the end of the article



© The Author(s) 2022. **Open Access** This article is licensed under a Creative Commons Attribution 4.0 International License, which permits use, sharing, adaptation, distribution and reproduction in any medium or format, as long as you give appropriate credit to the original author(s) and the source, provide a link to the Creative Commons licence, and indicate if changes were made. The images or other third party material in this article are included in the article's Creative Commons licence, unless indicated otherwise in a credit line to the material. If material is not included in the article's Creative Commons licence and your intended use is not permitted by statutory regulation or exceeds the permitted use, you will need to obtain permission directly from the copyright holder. To view a copy of this licence, visit <http://creativecommons.org/licenses/by/4.0/>.

Thalman, 1996; Voit, 2013; Voit et al., 2015; Ziegler & Isler, 2013) and environmental impact assessment studies (e.g. Haas et al. 2020a, b). Despite their purpose being commonly aimed at transport infrastructure, tunnelling constitutes an essential part of construction operations for large underground laboratories. Extensive subsurface tunnel excavations have been part of engineering solutions for the Large Electron Positron (LEP) particle collider built in 1988 for the European Organization of Nuclear Research (CERN) across the Swiss and French border close to the city of Geneva (Switzerland) as well as for its successor, the Large Hadron Collider (LHC). The LHC used LEP's existing subsurface infrastructure and extended it by the construction of *A Toroidal LHC Apparatus (ATLAS)* and *Compact Muon Solenoid (CMS)* particle detector caverns for first particle collisions in 2008. Simultaneous stipulations agreed on an upgrade of the LHC, named the High-Luminosity Large Hadron Collider (HL-LHC), adding larger caverns and extending tunnel galleries to the existing ca. 27 km LHC subsurface infrastructure, to be scheduled for first physics experiments in 2027 (Voiron et al., 2020).

For high-energy particle collision experiments, CERN initiated a feasibility study in 2013 aiming at a next-generation particle accelerator, the Future Circular Collider (FCC), to be hosted in a new 90–100 km-long, quasi-circular subsurface infrastructure within the Geneva Basin, starting construction after 2030. An essential part of the FCC's current feasibility phase is a thorough understanding of the subsurface conditions for tunnelling construction, usage and disposal of an estimated ca. 10 million m³ of excavated regolith, rock and soil, and the assessment of geological and environmental hazards (Haas et al., 2020a, b; Haas et al., 2021). In its current construction layout across the Swiss-French geographical area defined herein as the Geneva Basin (GB), about 90% of the FCC's encountered rock is estimated to be represented by interstratified sandstone, marlstone, and conglomerate attributed to the Oligocene Molasse Rouge and Grès et Marnes Gris à gypse formations, 6% by Mesozoic limestone formations of the Jura and marly freshwater limestone as part of the Molasse Rouge formation, and 4% by unconsolidated morainal debris of Quaternary age. In this study the term Geneva Basin is used in a geographical context (Moscariello, 2019), emphasizing the region around the city of Geneva as part of the western Swiss Molasse Basin and its surrounding French departments Ain and Haute-Savoie.

During the past decades, the GB has been the subject of vast geological research with a strong focus on hydrocarbon exploration from the 1970's to the 1990's (Bachmann et al., 1982; Lemcke, 1967), as potentially economic reservoirs were identified in the Austrian and German

Molasse basins as part of the Northern Alpine Foreland Basin (NAFB) (Bartenstein, 1978; Berger, 1996; Brink et al., 1992; Doppler, 1989; Gross et al., 2018; Gusterhuber et al., 2014; Sachsenhofer et al., 2010; Schulz et al., 2002; Wehner et al., 1983; Ziegler, 1990). This early phase of applied research was followed by renewed interest for groundwater resources (Keller, 1992) and hydrocarbon distribution (Do Couto et al., 2021). Much predictive and interpretive research on the regional geology and stratigraphy has been guided by concepts linking the evolution of orogenic processes to foreland-basin stratigraphic and depositional evolution (Sinclair & Allen, 1992; Sinclair et al., 1991). During the past decade, research has concentrated on the potential importance of carbonate formations for geothermal exploration and subsurface heat storage (Chelle-Michou et al., 2017; Clerc et al., 2015; Makhloufi et al., 2018; Moscariello, 2018, 2019; Moscariello et al., 2020; Rusillon, 2018). Based on these extensive scientific and industrial explorations, available well-log and rock core datasets from adjacent basins have been accumulated to decipher the stratigraphic evolution, phases of basin uplift and erosion (Amir et al., 2020; Brink et al., 1992; Kaelin et al., 1992).

Despite a recent classification into six geotechnical classes (sandstones and marls) based on rock mechanics tests on Molasse Rouge samples taken during CERN's HL-LHC's construction (Fern et al., 2018), a distinct lack of stratigraphic analyses and lithotype identification remains for depths ranging from 0 to 1'000 m above sea level (m ASL) in the GB's subsurface, compared to the knowledge amassed on corresponding sectors of the NAFB in Austria, Germany, eastern Switzerland and eastern France (e.g. Amir et al., 2020). This lack of high-resolution information on stratigraphy and lithotypes for the GB's formations greatly hampers subsurface prediction for applied purposes, such as the FCC construction.

In particular, geo-engineering hazards such as swelling rocks, karstic intervals, aquifer horizons and presence of hydrocarbons considering environmental impact, and active fault regimes have remained undeciphered for the GB. Swelling depicts a significant hazard when tunnelling in clay-rich sedimentary deposits (Anagnostou, 1993; Anagnostou et al., 2010; Einfalt et al., 1979; Einstein, 1996; Kovári et al., 1987) and has led to severe problems at tunnel construction sites worldwide, e.g. in the Jura of Switzerland and France, southern Germany, Spain, Poland, Italy and the U.S.A. (Alonso & Olivella, 2008; Berdugo et al., 2009; Kovári et al., 2002; Steiner, 1993; Vrakas & Anagnostou, 2016; Yilmaz, 2001). Another type of geological hazard is posed by karstic features that have caused water flooding at several subsurface construction sites (Alija et al., 2013; Li et al., 2020; Lv et al., 2020; Su et al., 2021), while aquifer tables and associated groundwater flow (Butscher et al., 2011; Hasegawa et al., 1993)

have been well integrated in required environmental impact assessment studies (Huang et al., 2015) and contemplate together with seismic activity (Rehbock-Sander & Jesel, 2018) distinct hazards for subsurface construction projects.

This article aims to provide a detailed evaluation of the shallow subsurface across the Geneva Basin (Fig. 1) by reviewing existing stratigraphic and geophysical well-log data from former research and industrial activities preceded by their digitization and associated sedimentological and petrographical descriptions of lithotypes by means of inspected core material. This yet unpublished data are further integrated with performed mineralogical, geochemical and petrophysical laboratory analyses in order to (1) infer potential geological hazards, (2) establish a robust predictive approach addressing engineering uncertainties, and (3) optimize well placement prior to site investigations within the scope of the FCC's transition into the subsequent technical design phase in the upcoming years.

2 Geological setting

The western part of the Northern Alpine Foreland Basin (NAFB) has been thoroughly investigated along country borders, which makes it common to use different geographical terms in the literature, such as the *Basin Franco-Genevois* or *Savoy Molasse Basin* (Deville et al., 1994) in French-speaking countries when referring to the westernmost Swiss Molasse Basin (SMB) and to the adjacent French Molasse Basin (FMB). This article uses the term Geneva Basin (GB) (Moscariello, 2019) to emphasise the geographical area as part of both the SMB and FMB, and is bordered by the Jura mountains in the north/northwest, the Prealps in the east, the Salève massif in the south and the Vuache Fault system in the south/southwest. Stratigraphically, the Geneva Basin covers the Molasse and Quaternary deposits of the SMB and FMB, as well as the sediments of the Jura, and is delimited by the latter and by the Helvetic and Penninic units.

The following sections first derive the tectonic evolution of the NAFB and the Mesozoic deposits of the Jura,

followed by a stratigraphic description related to the GB marking the essential geological formations intersected by the FCC. A profound understanding of the spatial distribution of Mesozoic, Molasse and Quaternary deposits and of the temporal succession of depositional paleoenvironments are crucial for subsurface geo-engineering prospection in view of the construction of the FCC. This allows a reasonable extrapolation of the lithostratigraphic and lithological/-technical information (lithotypes) from available wells to nearby areas that have not yet been investigated directly in the subsurface.

2.1 Tectonic evolution of the Northern Alpine Foreland Basin (NAFB)

The NAFB is located north of the Alps and extends approximately from Lake Geneva (Lac Léman) in western Switzerland, across Bavaria in southern Germany, to the east towards Vienna in Austria, reaching up to 700 km in lateral extent for its Oligocene–Miocene infill (Kempf & Pross, 2005). The NAFB evolved from a foredeep to a negative-alpha basin controlled by rollback mechanisms of a proposed European slab (Schlunegger & Kissling, 2015) during the Paleogene and Neogene due to flexural bending of the European Plate under increasing orogenic load by the advancing Alpine thrust wedge (Allen et al., 1991; Burkhard & Sommaruga, 1998; Homewood et al., 1986; Karner & Watts, 1983; Pfiffner, 1986, 2021). The term “negative-alpha” describes a basin that formed on top of an orogenic wedge (Fuller et al., 2006; Willett & Schlunegger, 2010). The NAFB's tectonic origin relates to crustal loading in proximity of the uplifting Alpine orogen (Mock & Herwegh, 2017; Schlunegger & Mosar, 2011). The basin and the associated orogenic belt show different tectonic patterns along their east–west extent, distinguishing Swiss, southern German and Austrian sectors (Willett & Schlunegger, 2010). Sommaruga et al. (2012) described a notable decrease in structural complexity expressed in Mesozoic lithologies from west to east along the NAFB, substantiated by different deformation styles. In the western, wedge-top part

(See figure on next page.)

Fig. 1 A Overview of tectonic realms in the Geneva Basin for the FCC construction with analysed well and outcrop locations. Geophysical well-logs were digitized and analysed together with available rock core data from these wells. See Table 1 for well numbers and full well-IDs. The overlying Quaternary deposits are neglected for increased readability. The blue line depicts cross section A, the green line refers to cross section B (Figs. 5, 6). Note that the Salève and Mandallaz limestone as commonly referred to in technical reports are part of the Jura. *FTB* fold-and-thrust belt. **B** The white profile X–Y displays a large-scale cross section through the Geneva Basin and is based on chronostratigraphic units representing the vertical and spatial relationships of age-defined packages of lithologies in a geo-historical picture. The FCC's current subsurface tunnel alignment is currently foreseen at a depth interval between 100 to 300 m ASL. The Burdigalian Molasse belongs to the Upper Marine Molasse and is hereby noted Marine Molasse. Data compiled, amended and modified after Bachmann & Müller, 1991; Charollais et al., 2013; Clerc & Moscariello, 2020; Deville et al., 1994; Haq et al., 1987; Kuhlemann & Kempf, 2002; Lemcke, 1988; Mastrangelo & Charollais, 2018; Moscariello, 2019, 2021; Zweigel et al., 1998

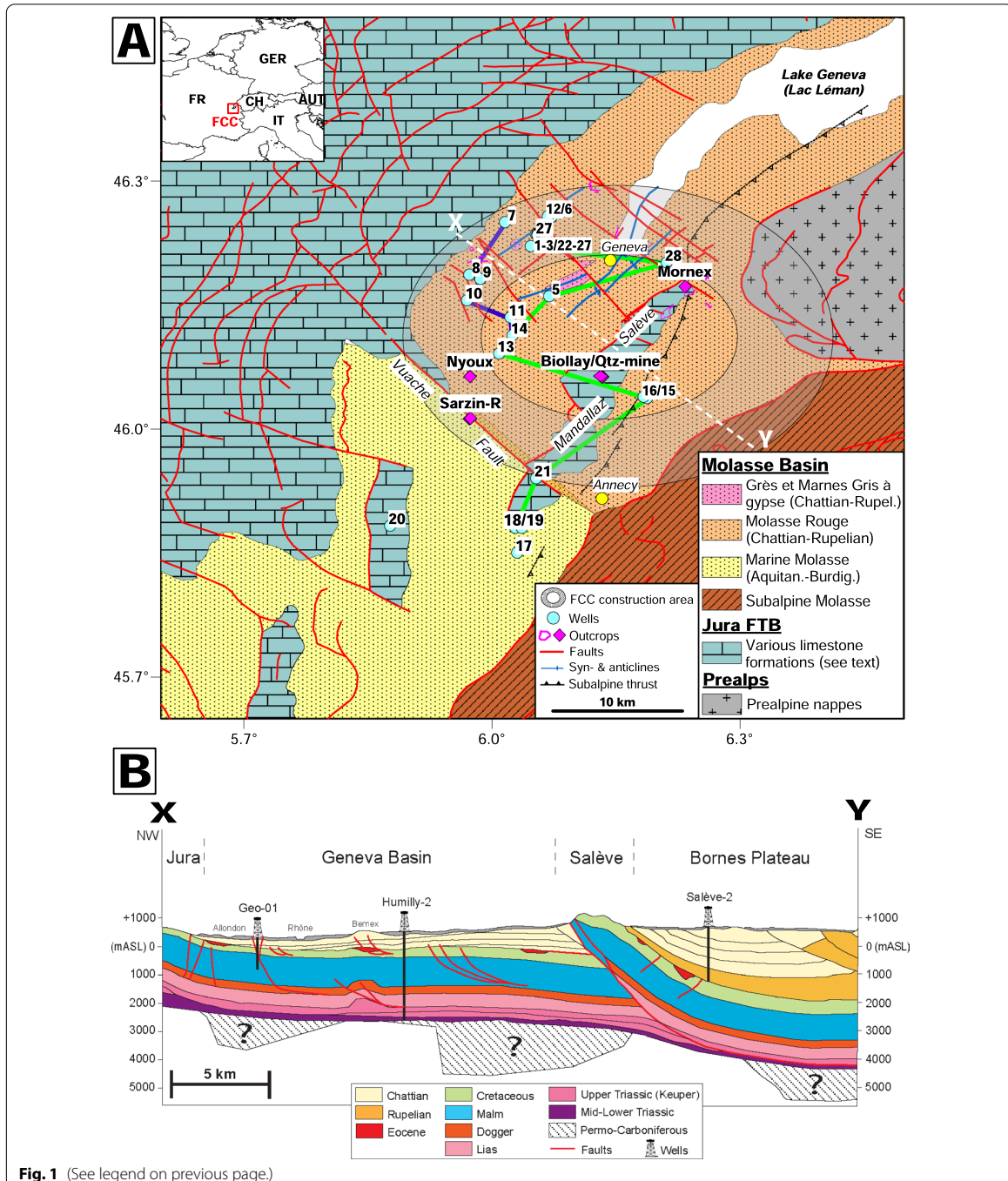


Fig. 1 (See legend on previous page.)

of the basin, thrusting and long-wavelength, evaporite-cored detachment folds relate to thin-skinned detachment tectonics (Sommaruga, 1999, 2011; Sommaruga et al., 2012), whereas the eastern, non-detached part is

comprised of normal faults related to Jurassic extension and subsidence of the epicontinental European shelf (Sommaruga et al., 2012; Stauble & Pfiffner, 1991; Wetzel et al., 2003). The *Fernschub* hypothesis,

originally proposed by Buxtorf (1916), confirmed a detachment of foreland sediments along a Triassic evaporite unit (Laubscher, 1961), leaving the SMB as the NAFB's westernmost area relatively undeformed compared with its conjugate eastern German and Austrian equivalents. Predominant conjugate NNE-SSW and NW-SE-trending strike-slip fault zones cut the western SMB and extend into the Jura fold-and-thrust belt (FTB), e.g. Vuache Fault (Fig. 1) (Gorin et al., 2003; Ibele, 2011; Sommaruga, 1999), limited to the sedimentary cover (Courboux et al., 1999; Thouvenot et al., 1998). Therefore, the Alpine orogen forms a tapered, double-vergent wedge to the NNW and SSE, with both the Jura FTB and SMB being decoupled from the basement over a basal *décollement* (Mosar, 1999). The Vuache and Dent de Vaulion Fault systems extend from the SMB into the Jura and are conjugate with SE-NW-striking dextral faults (Burkhard, 1990; Burkhard & Sommaruga, 1998; Sommaruga, 1997, 1999, 2011; Sommaruga et al., 2017). The Mesozoic deposits of the Jura form the substrate of the Cenozoic NAFB, which lies passively on top (cross-section X-Y in Fig. 1). Today both the Mesozoic and the Cenozoic deposits structurally form a single tectonic unit. From a tectonic point of view, there are two major structural units in the impacted FCC construction area: the Mesozoic of the Jura plus the Cenozoic (Molasse) of the Geneva Basin in the northwest, and the thrust Mesozoic of the Salève plus the Cenozoic (Molasse) of the Bornes Plateau in the southeast. The geographical GB is tectonically delimited by the Jura and the Mesozoic sedimentary Helvetic and Penninic units, and is internally divided into two tectonic subunits, the Plateau Molasse and the Subalpine Molasse, respectively (Burkhard, 1990; Mock & Herwegh, 2017; Pfiffner, 1986). The slightly deformed Plateau Molasse is up to 50 km wide and is affected by faults and folds (Gorin et al., 2003), with exemptions towards the west suggesting a convergence of Alpine and Jura structures (Burkhard, 1990). This required progressive sedimentation within the basin to guarantee mechanical integrity (Fuller et al., 2006). Thrusting of the Subalpine Molasse started in the Oligocene (Schlunegger et al., 1997) and lasted until approximately 5 Ma (Von Hagke et al., 2012). After an early deformation phase in the Late Oligocene (Kempf & Pross, 2005; Kuhlemann & Kempf, 2002), principal tectonic shortening occurred in the Jura FTB between 12 and 4 Ma (Becker, 2000), followed by progressive minor deformation in Pliocene-Quaternary times (Madritsch et al., 2010).

Two predominant hypotheses persist on the creation of accommodation for Molasse deposits: the first one is the argument of sea-level changes impacting sediment

supply, reflected by the two mega-sequences of marine to terrestrial deposits (Bachmann & Müller, 1991, 1992; Lemcke, 1984); the second one attributes the main role to tectonics and Alpine uplift in driving sediment accumulation, whereby the establishment of terrestrial environments would have followed increased sediment supply from the orogen, and marine conditions would have been tied to lesser sediment influx (Kuhlemann, 2000; Oxburgh, 1981; Schlunegger & Hinderer, 2001; Schlunegger et al., 2001). Both hypotheses hinge on sediment supply as proximate control on patterns of deposition (Kuhlemann & Kempf, 2002; Schlunegger & Mosar, 2011). For the Central Alps, a third hypothesis favours a slab-rollback mechanism to explain foreland plate flexure and accommodation space creation (Schlunegger & Kissling, 2015), substantiated by a delayed rebound-type, erosional response to surface uplift, and represented by larger sediment fluxes and shifts to more proximal facies (Schlunegger & Castelltort, 2016). Large sediment influx could have controlled the establishment of (fluvial) fans. These fans further prograded over several tens of kilometres, merging distally with an axial fluvial system, which linked the Tethys to the Black Sea (Kuhlemann & Kempf, 2002; Sinclair et al., 1991).

Early post-collisional Alpine history was characterized by increased sedimentation rates at the Rupelian/ Chattian transition, attributed to isostatic readjustment (Kuhlemann et al., 2002). Further increases in sedimentation rate took place later during the Aquitanian (23–21 Ma) and late Burdigalian (ca. 18–16.4 Ma), followed by decreased rates in early to middle Burdigalian (21–19 Ma) and Langhian to Serravalian times (16.4–12 Ma) (Kuhlemann et al., 2002). While the swift increase in sediment discharge in the Eastern Alps is explained by the termination of E-W extension (Dunkl & Demény, 1997) and subsequent minor uplift recorded by a regional regression (Winkler-Hermaden, 1958), the Western Alps record a rather slower reduction (Kuhlemann et al., 2002) due to extensional tectonics (Pfiffner, 1986; Schlunegger, 1999; Schmid et al., 1996). Basin inversion of the SMB between 11 and 10 Ma (Kaelin, 1997) changed the drainage pattern to an easterly direction and was intensified by folding and thrusting of the Swiss Jura Mountains (Kuhlemann et al., 2002). Still ongoing basin uplift started in latest Miocene times in the Swiss and Western Alps (Kuhlemann et al., 2002).

2.2 Stratigraphic framework of the Swiss Molasse Basin

The Jura and the Swiss Molasse Basin (SMB) consist of folded Mesozoic and Cenozoic successions, which are detached from the pre-Triassic basement (Sommaruga,

1997). During the Mesozoic, the Jura and the western SMB were part of the Alpine Tethys passive margin and comprised approximately 2 km of alternating limestone and marl (Sommaruga et al., 2012). Oligocene and Miocene alternating fluvial, lacustrine and marine Molasse sediments onlap the underlying Mesozoic rocks towards the northwest (Sommaruga, 1997, 1999; Sommaruga et al., 2012). For the present study and the GB's geographical realm, the Jura's subdivision into the external and internal Jura domains plays an important role, while the third subdivision as the Tabular Jura is significant for the realms only around the southern Black Forest and Vosges basement. With the external Jura consisting of flat areas and plateaus delimited to the north, the internal Jura, also referred to as folded Jura or *Haute Chaîne*, represents thrust-related folds and sinistral faults, whose orientation gradually changes from a N-S in the eastern Jura to a WNW-ESE direction in the western Jura (Sommaruga, 1997, 1999). The Mesozoic formations describe the general evolution from a shallow, peritidal platform to deep-water shelf environments followed by the evolution of a carbonate platform, and its subsequent drowning in order to prevail in pelagic conditions (Sommaruga, 1997; Strasser et al., 2016). Lower Cretaceous units, formerly termed *Urgonien*, are dominated by carbonate sedimentation, and marked by increasing clastic input associated to Valanginian sea-level fall (Haq, 2014). Variations of relative sea-level of both tectonic and eustatic origin drastically controlled the development of depositional environments. The common lateral and vertical changes in facies and sedimentation rates as well as numerous hiatuses within the formations witness a complex interplay of tectonics, climate, and sea level that controlled the Jura during the Cretaceous (Strasser et al., 2016). One of these hiatuses reflects 72 My separating rocks of Aptian age in the GB (Brentini, 2018; Rusillon, 2018) from the overlying Siderolithic Formation of proposed Late Eocene age (Charollais et al., 2007). This hiatus resulted probably from subaerial exposure and consequent development of an erosive and deep karst system at the top of the Mesozoic series, which play a predominant role in the aquifer drainage systems of the Cretaceous and Jurassic limestone across the GB (Moscariello, 2018), as well as for 6% of the FCC's current subsurface perimeter.

The infill of the SMB comprises two regressive, coarsening-upward sedimentary mega-sequences, each marking a transition from marine to continental conditions (Matter, 1980; Sinclair & Allen, 1992; Sinclair et al., 1991). The two mega-sequences are composed of four predominant lithostratigraphic units (Matter et al., 1980; Lemcke, 1988), namely the Lower Marine Molasse (LMM), the Lower Freshwater Molasse (LFM), the Upper

Marine Molasse (UMM) and the Upper Freshwater Molasse (UFM). Informal terms often used in a regional context of the LFM also refer to the *Molasse Rouge* and *Marnes bariolées* as well as the *Grès et Marnes Gris à gypse*, whereas the latter shows an increased content of gypsum (Haas et al., 2020a). For the northern/northeastern SMB, Freshwater-Brackish Molasse (SBM) evolved between the UMM and UFM (Bachmann & Müller, 1992; Lemcke et al., 1953). The eastern German and Austrian Molasse basins were subjected to marine conditions until Burdigalian times (Lemcke, 1984), which makes the LFM terminology for terrestrial deposits only reasonable for the SMB and western Bavaria due to prevailing marine conditions to the east (Kuhlemann & Kempf, 2002). The total sedimentary cover in the western SMB consists of up to 5'000 m of Mesozoic and Cenozoic successions overlying the basin's crystalline basement (Clerc & Moscariello, 2020; Gorin et al., 1993). Molasse deposition started in the Rupelian (34–30 Ma) as LMM and Chattian to Aquitanian (30 – 20 Ma) as LFM, respectively (Strunck & Matter, 2002), marking the transition from an underfilled to an overfilled foreland basin (Erdős et al., 2019; Sinclair & Allen, 1992). A Burdigalian (20 – 17 Ma) transgression that established the “Burdigalian Seaway”, was probably caused by reduced sediment discharge (Kuhlemann & Kempf, 2002) and marked the start of the second mega-sequence, with accumulation of the UMM (Keller, 1989, 1992) under marine conditions onto a truncated surface of LFM (Allen et al., 1991; Herb, 1988; Kempf & Pross, 2005; Matter, 1980; Sinclair & Allen, 1992). Molasse deposition in the Langhian to Serravallian (<17 Ma) accumulated fluvial floodplain and braidplain to lacustrine siliciclastics of the UFM in an overfilled basin, terminating marine conditions (Diem, 1986; Sinclair & Allen, 1992). Fluvial deposits of large alluvial megafans not only in the western SMB, but particularly in the central/eastern SMB were formed during the overfilled stage (Frisch et al., 1998; Kaelin & Kempf, 2009; Ortner et al., 2015; Schlunegger & Castellort, 2016) despite decreasing sediment discharge until 11 Ma (Kuhlemann & Kempf, 2002). After 11 Ma, sedimentation terminated in the western part of the NAFB due to folding and uplift of the Swiss Jura (Kuhlemann & Kempf, 2002). The Freshwater units (LFM and UFM) were accumulated in terrestrial settings, consisting mainly of alluvial and fluvial-fan deposits along the southern basin margin and fluvio-lacustrine sediments in the central and external parts of the SMB (Kempf & Pross, 2005). Kilometre-thick conglomerate successions were deposited by alluvial fans at the basin margin, while sand- and mud-dominated successions extended farther basinward (Kempf & Matter, 1999; Schlunegger et al., 1997; Spiegel et al., 2001). Marine units are predominantly composed

of shallow-marine siliciclastics deposited in tide- and storm-influenced environments (Kempf & Pross, 2005). To the east, the SMB persisted in an underfilled stage until at least 17 Ma, when sedimentation of sandstone and marlstone occurred under brackish to shallow-marine conditions (Hinsch, 2013; Lemcke et al., 1953; Mock et al., 2020). Alluvial fans were missing in the eastern part of the NAFB due to the paleo-Inn river transporting clastic debris further to the east (Frisch et al., 1998; Kuhlemann & Kempf, 2002). During UFM deposition, sediments originated from the central Alps and from massifs adjoining to the basin (Füchtbauer, 1959). Molasse and Quaternary deposits accumulated on top of 2 km of Lower Triassic to Upper Cretaceous shallow-marine sediments, which are not outcropping in the eastern SMB (Charollais et al., 2007, 2013; Sommaruga, 1997; Sommaruga et al., 2012).

The identification of the four Molasse lithostratigraphic units was based on biostratigraphic, magnetostratigraphic and palynostratigraphic data that constrained the marine to terrestrial transition (LMM to LFM) to about 31 Ma for the Wilhelmine Alps section in the German Molasse Basin (Kempf & Pross, 2005). Magnetostratigraphically correlated sections from central and eastern Switzerland indicate a diachronous regression of the LMM between 31.5 and 30 Ma during the LMM, associated with enhanced clastic input from the rising Alps (Kempf & Pross, 2005). Biostratigraphic information confirms a Chattian age for the equivalent LMM-LFM transition in the German Molasse Basin (Reichenbacher et al., 2004; Uhlig et al., 2000). Magnetostratigraphic data of the LFM-UFM resulted in a calibration chart for the NAFB within a timeframe of 28–13 Ma (Kempf & Matter, 1999; Kempf et al., 1997; Schlunegger et al., 1996; Strunck & Matter, 2002).

A drastic base-level drop (Brenchley, 1992; Lemcke, 1988) of possible eustatic origin occurred around 28.5 Ma (Abreu & Anderson, 1998; Haq et al., 1987) and caused an LMM regression towards the east (Bachmann & Müller, 1992; Lemcke, 1988; Zweigel et al., 1998). The LMM and lowermost LFM lithostratigraphic successions define a shallowing trend towards the top, indicated by an increase in sediment grain size (Diem, 1986). The LMM-LFM transition in the western SMB is part of the Subalpine Molasse, documenting conditions at the southern basin margin (Kempf & Pross, 2005). The study by Kempf and Pross (2005) emphasised the role of sediment supply for the transition of marine to terrestrial sedimentation in the northern Alpine foreland. In contrast to its eastern continuation, the western SMB lacks UFM units, which suggests complete erosion of this lithostratigraphic unit. Several researchers derived erosion thickness maps for the Late Miocene and

post-Miocene times using apatite fission tracks, vitrinite reflectance, shale compaction and porosity measurements (Kaelin et al., 1992; Mazurek et al., 2006; Schegg, 1993); Cederbom et al. (2004) proposed erosion up to 1,500 m for the Swiss Molasse Plateau and 3'000 m for the Subalpine Molasse as part of the SMB. They further mark the onset of erosion at 5 Ma, shortly before tectonic basin inversion.

In the GB, the Cenozoic succession consists explicitly of Oligocene to Early Miocene LFM deposits. The overlying UMM is found in the adjacent Bellegarde and Rumilly basins to the west and southwest of the Vuache Fault (Amir et al., 2020; Charollais et al., 2007; Paolacci, 2012). At the Bornes Plateau, the thrust Subalpine Molasse is encountered at the front of the Subalpine units (Charollais et al., 2007; Paolacci, 2012) continuing in front of the Prealpine units into the Lake Geneva encountering lacustrine sediments as inferred from seismic data (Dupuis, 2009). Accumulation of Molasse sediments took place during Jura deformation and in Late Miocene as the basin was detached from its basement (Cederbom et al., 2008). This suggests that erosion did not start before Pliocene times (Cederbom et al., 2004), but was associated to the 10–4 Ma Jura FTB shortening phase (Ziegler & Fraefel, 2009). These Molasse deposits are composed of sandstone, marl and intercalations of anhydrite/gypsum and conglomerates (Wildi et al., 2017) tied to erosion of the Western Alps (Oxburgh, 1981), sea-level changes (Bachmann & Müller, 1992) or possibly a combination of both (Schlunegger & Mosar, 2011). They constitute more than 90% of the subsurface domain to be intersected by the FCC's current layout.

Glacial erosion and deposition shaped the central part of the GB during the Middle and Late Pleistocene (Arn, 1984). Associated Quaternary deposits comprise the GB's cover as intersected by about 4% of the current FCC subsurface layout. A recent revision of the old nomenclature for Switzerland's glacial periods (*Günz*, *Mindel*, *Riss*, *Würm*) introduced the terms post-glacial and interglacial deposits with a new stratigraphic classification taking into account not only lithological but also geomorphological features of these deposits (Graf & Burkhalter, 2016). A distinct geomorphological element in the GB depicts the *Petit Lac* at the southwestern termination representing the remains of a subglacial tunnel valley, which formed underneath the Rhone Glacier by subglacial meltwater (Fiore, 2007; Moscariello, 1996; Moscariello et al., 1998; Van der Vegt et al., 2012). Borehole data gave hints that the Rhone Glacier was responsible for incising and removing older Quaternary sediments reaching the underlying Molasse deposits during the Last Glacial Maximum (LGM). In the subsurface, this incision deviates towards the SE. On

the surface, the buried incision is observed by the narrow Aire valley reflecting a branch of the Arve River located SE of the elongated Molasse ridge (*Bernex*). It is assumed that the Rhone Glacier tunnel valley was gradually filled by a thick succession of proglacial lake deposits (Moscariello, 1996) and accumulated in the large lake formed at the front of the melting LGM glacier (Moscariello, 2018). The downstream segment was filled with a mixed succession of subglacial, lacustrine, and proglacial deposits generated by the Arve Glacier (Moscariello, 2018). Low-relief ridges, perpendicular to the main valley axis represent the subaqueous frontal moraines formed during temporary re-advances of the glacier during the glacial withdrawal phase. Large, flat-bottomed incision bordering the Soral–Laconnex subaqueous moraine resulted from meltwater discharge generated by the Arve Glacier, which carved a narrow spillway between the glacier and the northern slope, and merged with the proglacial/lacustrine deposits that formed the flat morphology of the SW part of the Geneva area. The natural separation between the buried tunnel valley and its partly filled portion (*Petit Lac*) depicts a narrow ridge today. To the SE, this ridge forms an apron dipping to the SW, interpreted as a frontal moraine related to the Rhone Glacier, most likely formed in subaqueous(?) and subglacial(?) conditions (Moscariello, 1996, 2018). The proglacial and paraglacial lake caused by the melting of the Rhone, Arve, and Jura glaciers gradually reduced its volume, which is represented in the terraced surfaces on both sides of the Lake Geneva (Burri, 1981). These kame terraces formed in ephemeral lakes related to the LGM glacier at the ice front (Donzeau et al., 1997) in correspondence with probably lateral tributaries or supraglacial stream mouths (Moscariello et al., 1998). Lacustrine terraces formed during the evolution of syn- and post-glacial lake levels after the disappearance of the Rhone Glacier, ultimately charging the sinuous Rhone River that incised cemented gravel deposits, which are locally known as the *Alluvion Ancienne*. Progressive incision of both the Rhone and Arve rivers shaped the central GB by various slopes of glacial origin towards the main axial drainage system represented by the *Petit Lac*. The Allondon River is likely associated with karst and fractured networks, whereby its associated deposits are the subject of current research.

3 Materials and methods

3.1 Review of existing boreholes and database setup

Boreholes were reviewed across the Geneva Basin and selected within a 2 km range outside the FCC's planned quasi-circular perimeter (Abada et al., 2019; Benedikt et al., 2020). Geology not covered by the FCC's current footprint but likely to be encountered inside the

FCC construction ring was accounted in case available reported wells contained useful stratigraphic or geophysical well-log data. Over 2'000 boreholes were drilled in the Geneva Basin by Swiss (e.g. *Services Industriels de Genève, SIG*) and French (e.g. *Bureau de Recherches Géologiques et Minières, BRGM*) state surveys, as well as various oil and gas companies for geothermal, hydrocarbon and hydrogeological exploration. Among all well reports and datasets available from BRGM's online Infoterre database, Swisstopo's subsurface database, the literature, industrial exploration, and drilling campaigns (Brentini, 2018; Chablais & Rusillon, 2018; Chablais & Savoy, 2019; Clerc et al., 2015; Doumer and British Petrol (France), 1983f; Doumer and (France), 1983; Doumer and British Petrol (France), 1983b, 1983d, 1983a, 1983e, 1983c; Etat de Genève, 1994; Gervaise, 1972; Géotechnique Appliquée Dériaz & SA (GADZ), 1981a, 1981b, 1982b, 1982a, 1992, 1993a, 1993b, 1996a, 1996b, 1997, 2015a, 2015b, 2015c, 2015d, 2016a, 2016b, 2016c; Jenny et al., 1995; Lanterno et al., 1981; Pierdona, 2018; Rusillon, 2018; Schegg, 1993; Services Industriels de Genève (SIG), 2019; Wegmüller et al., 1995), 661 wells have been presently considered useful for the FCC's subsurface layout. Digitisation of ca. 37 km of cumulative geophysical well-log curves was performed on 28 selected boreholes (Fig. 1, Table 1), which comprised geophysical well-log data, rock core samples and both sedimentological and petrographical descriptions from well reports. Well-log data was further correlated to available core material by analyses on cuttings and plugs, the latter drilled from full-cores, half-cores and samples collected from outcrops. Core sample measurements were extrapolated from nearby wells to the Geo-01 well at similar depth levels for consecutive petrophysical well-log calculations.

The full datasets of reviewed and digitised well reports as well as laboratory results were stored in a dedicated database created in Microsoft ACCESS referencing each sample and well geospatially (longitude, latitude, elevation, depth) in non-projected coordinate system (World Geodetic System 1984). The database contains metadata of well-ID, drilling purpose, measured and true vertical depth, available third-party samples and samples taken within the scope of this study, as well as performed laboratory analyses. Furthermore, associated digitized stratigraphic data such as chronostratigraphic range (era, period, series/epoch, stage/age), top and bottom depth of encountered geological formations, lithostratigraphy, geological hazards (karstic intervals, hydrocarbon indices, swelling rocks), rock type and rock type description from logs as well as an appositely devised unified terminology to homogenize different (old) stratigraphic terms spanning over the past 70 years were added into the database.

Table 1 List of boreholes containing digitized and analysed geophysical well-logs used for petrophysical calculations and lithotype correlations

Map-ID (Fig. 1)	Well-ID	Measured depth (m)	Longitude (WGS 1984)	Latitude (WGS 1984)	Digitized well-logs	Cumulative length of digitized logs (m)	Year of drilling	Drilling purpose	Sample type
1	C1	90.70	6.05307890	46.23646280	CALI, GR, Vp, Vs	336.00	2015	SI	Plugs
2	C2	81.50	6.05455910	46.23617420	CALI, GR, Vp, Vs	167.00	2015	SI	Plugs
3	C3	81.70	6.05745850	46.23575360	CALI, GR, Vp, Vs	156.00	2015	SI	Plugs
4	Geo-01*	744.06	6.04687090	46.22162423	CALI, GR, URAN, THOR, POTA, SP, DT, RHOB, RHOMAA, DRHO, NPHI, RS, RD, PEF	-	2018	GX	Cuttings****
5	Geo-02*	1130.00	6.06917612	46.16099600	CALI, GR, URAN, THOR, POTA, SP, RHOB, DRHO, NPHI, RS, RD, PEF	-	2020	GX	Cuttings****
6	Gex-CD-01	290.5	6.07202053	46.25699268	CALI, GR, SP, DT, RHOB, ILD, NPHI	1358.00	1983	E&P	Cuttings, plugs
7	Gex-CD-02	403.20	6.01576270	46.25072090	DT	341.00	1983	E&P	Cuttings, plugs
8	Gex-CD-03	294.00	5.97257804	46.18706358	CALI, GR, SP, DT, SFL	1465.00	1982	E&P	Cuttings, plugs
9	Gex-CD-04	291.70	5.98583792	46.18190859	CALI, GR, SP, DT, SFL	1458.00	1982	E&P	Cuttings, plugs
10	Gex-CD-05	560.00	5.96985080	46.15607813	no logs	-		E&P	Cuttings, plugs
11	Gex-CD-06	422.00	6.02225030	46.13546971	CALI, GR, SP, SN, LN, NPHI	892.00	1983	E&P	Cuttings, plugs
12	Gex-CD-07	256.00	6.06751781	46.25758598	CALI, GR, SP, MSFL, LLS, LLD	1412.04	1983	E&P	Cuttings, plugs
13	Humilly-1	905.00	6.00864530	46.09165386	CALI, SP, Vp, SN	3481.00	1960	E&P	-
14	Humilly-2***	3051.00	6.02487400	46.11363102	CALI, GR, DT, RHOB, DRHO, LLD, NPHI	-	1969	E&P	Cuttings****
15	Salève-1	1175.60	6.18749460	46.03768763	SP	970.00	1959	E&P	-
16	Savève-2	1985.80	6.18334960	46.03921755	SP	815.00	1959	E&P	-
17	Savoie-101	2064.00	6.03042100	45.85043460	GR, SP, SN, LN, LAT, LIM	6000.00	1952	E&P	-
18	Savoie-104	1903.00	6.02818960	45.88050040	CALI, SP, SN, LN	4405.00	1953	E&P	-
19	Savoie-105	690.70	6.03605080	45.88042220	SP, SN, LN, INV	2280.00	1953	E&P	-
20	Savoie-107	2116.00	5.87683480	45.88302440	GR, SP, SN, LN	6000.00	1954	E&P	-
21	Savoie-109	1260.90	6.05337210	45.94061902	SP, SN, LN	3252.00	1959	E&P	-
22	SLHC20	120.20	6.05507350	46.23585973	GR, DT, RHOB, FORE	445.00	1995	SI	-
23	SLHC21	120.00	6.05551840	46.23579456	GR, DT, RHOB, FORE	406.00	1995	SI	-
24	SLHC22	120.00	6.05552590	46.23549085	RHOB	118.87			-
25	SLHC23	110.18	6.05494650	46.23530551	GR, Vp, RHOB, FORE	400.00	1995	SI	-
26	SLHC24	110.30	6.05526740	46.23526275	GR, Vp, RHOB, FORE	419.00	1995	SI	-
27	SLHC25	109.40	6.05502810	46.23494617	GR, Vp, RHOB, FORE	401.00	1995	SI	-
28	Thônex-1*, ***	2580.00	6.21131960	46.20183865	CALI, GR, SP, DT, RHOB, ILD, ILM, LLD, LLS, NPHI	-	1993	GX	Cuttings****

Well-logs: GR gamma-ray, URAN/THOR/POTA spectral GR as uranium, thorium and potassium concentration curves, SP spontaneous potential, DT sonic travel-time, RHOB bulk density, RHOMAA apparent matrix density, DRHO corrected bulk density, PEF photoelectric factor, NPHI neutron porosity, SN/RS short normal resistivity, LN/RD long normal resistivity, SFL spherically focused, MSFL micro-spherically focused resistivity, LLS shallow latero-log, LLD deep latero-log, FORE focused resistivity, LAT medium lateral resistivity, LIM micro-inverse resistivity, INV inverse lateral resistivity, ILD deep induction, ILM medium induction, Vp compressional wave velocity, Vs shear wave velocity. Drilling purposes: E&P hydrocarbon exploration, SI site investigations within the scope of regional civil engineering projects, GX geothermal exploration. *No well-log digitisation required. **Vp & DT performed on rock core samples (Hefny, et al., 2020). ***Deviated well. ****Samples taken as part of geothermal studies

3.2 Modelling of the FCC's well density coverage

Besides the digitized geophysical logs from 28 selected wells, the 661 boreholes relevant to the FCC were gridded and modelled to account for its well density coverage supporting future site investigations in favour of optimal well placement. The SURFER software package by GoldenSoftware was used to grid and model the data using Kriging and Nearest-Neighbour algorithms. A grid size of 41×100 m was created with 4'100 nodes. X-spacing was chosen to 0.014° ranging from 5.5°E to 6.9°E , while Y-spacing was set to 0.018° from 45.77°N to 46.5°N in World Geodetic System (WGS 1984) coordinate system.

3.3 Digitisation of geophysical well-logs and petrophysical calculations

Digitisation of well-logging intervals between 0 and ca. 1'000 m ASL, depending on elevation and corresponding intersection with the FCC depth interval, was performed on 28 selected wells (Table 1) to address the FCC's construction depth interval currently ranging from 100 to 300 m ASL. Sedimentological and geological core descriptions were carried out on analysed samples to establish a reference lithotype scheme assisting in the interpretation of geophysical well-log information. These lithotypes were defined based on macroscopical features such as texture, colour, consistency, composition, and sedimentary structures, cross-checked with well report documentation and further linked to geophysical well-logs to identify associated well-log patterns.

Geophysical well-logs such as gamma-ray (GR), sonic transit-time (DT), compressional (Vp) and shear-wave (Vs) velocity, caliper (CALI), spontaneous potential (SP), bulk and matrix densities (RHOB, RHOMMA), photoelectric factor (PEF) and corrected density (DRHO), neutron porosity (NPHI) as well as different types of resistivity logs, i.e. short normal (SN), long normal (LN), latero-log shallow (LLS), latero-log deep (LLD) and micro-spherically focused (MSFL) were digitized and quality-checked using the NeuraLog software. Data was outputted in LAS file format for further processing and interpretation in Schlumberger's Techlog software. Boreholes Gex-CD-01 to -07 were drilled by British Petrol France between 1982 and 1983 to constrain the depth domains and properties of the LFM formation (Chattian/Oligocene) and calcareous basement bedrock (Lower Cretaceous, formerly also known as *Urgonien*) for hydrocarbon exploration. The wells extend across the two French departments Ain and Haute-Savoie at the western edge of the GB along the Jura. The cumulative length of well data amounts to 2'517.32 m, of which 749.04 m were exposed as available rock cores. Encountered stratigraphic units belong chronologically to the Quaternary, Oligocene (Chattian), Eocene, and Early Cretaceous

(Hauterivian and Barremian). Note that the Barremian stage (Cohen et al., 2013) is commonly named "Urgonian" in traditional western European stratigraphy referring to the Early Cretaceous. Hence, the occasional adoption of the term in this article is to refer to regional geological features. In the northern part of the GB close to the city of Geneva, wells Geo-01, Geo-02 and Thônex-1 were drilled for geothermal exploration and were used as reference datasets for gamma-ray log calibration. SPL-, SLHC- and C-wells were drilled for site investigations in the framework of the LEP, LHC and HL-LHC civil engineering projects on behalf of CERN, whereas the latter wells allowed sampling of rock cores.

During digitisation, some mis-fit and log-shift was compensated via stretching and squeezing of log curves but could not be completely solved due to bad original paper quality, often loosely glued, or poorly scanned. Furthermore, NPHI, Vp and Vs well-logs were limited to specific intervals ranging between 5 to 100 m, especially for wells addressing hydrocarbon exploration (E&P). Each well-log type and its associated digitisation, data processing and analyses are described in the following sub-sections.

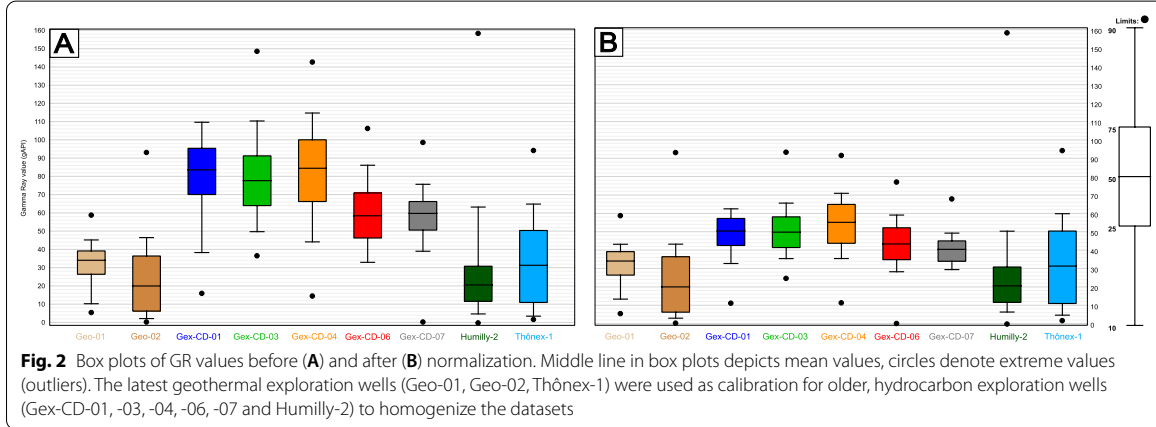
3.3.1 Lithology logs: Gamma ray (GR) and spontaneous potential (SP)

Despite different well-logging campaigns tailored for different exploration purposes, either a GR or SP logging tool, mostly deployed by companies Schlumberger, Hydrolog or Hydro-Geo Environnement, were run in most of the wells, excluding well Gex-CD-02 (only DT log). This allowed a first distinction of sand- and shale-dominated depth intervals. Respective SP log measurements were run and displayed in increments of 20, 10 or 5 mV.

Due to the variability of GR log measurements within a timeframe of 70 years, different log units hampered the process of homogenizing the data set. Some of the GR logs were formerly measured in microgram Radon per ton ($\mu\text{gR/t}$), which required re-calculation to common log units (Eq. 1) adopted by the American Petroleum Institute (gAPI). Hence, unit conversion between $\mu\text{gR/t}$ and gAPI was applied according to (Crain, 2021):

$$GR_{\log} = GR_{\mu\text{gR/t}} \cdot 10 \quad (1)$$

with GR_{\log} being the converted gamma ray log value in gAPI and $GR_{\mu\text{gR/t}}$ being the original gamma ray log value in $\mu\text{gR/t}$. Different GR tool calibrations among older (mostly E&P) wells required normalization based on newer (GX) wells. While the new wells offered higher tool sensitivity, the old wells were adapted accordingly



despite removing potential shale- and sand-influenced (geological) trends (Fig. 2).

The gamma ray index (I_{GR} , Eq. 2) was calculated based on GR logs applying different models depending on geological formations for the derivation of the shale volume (V_{sh}): the Stieber Miocene/Pliocene Model (Eq. 3) for the Quaternary deposits, the Tertiary Larionov Model (Eq. 4) for the Molasse Rouge, Grès et Marnes Gris à gypse, and Siderolithic formations, and the Larionov Model (Eq. 5) for the underlying Mesozoic rocks according to (Schön, 2015):

$$I_{GR} = \frac{GR - GR_{min}}{GR_{max} - GR_{min}} \quad (2)$$

$$V_{sh} = \frac{I_{GR}}{3 - 2 \cdot I_{GR}} \quad (3)$$

$$V_{sh} = 0.083 \cdot \left(2^{(3.7 \cdot I_{GR})} - 1\right) \quad (4)$$

$$V_{sh} = 0.33 \cdot \left(2^{(2 \cdot I_{GR})} - 1\right) \quad (5)$$

where the GR_{min} -value of 10 gAPI was defined as the maximum sand-dominated zone, and the GR_{max} -value of 100 gAPI as the maximum shale-dominated zone, respectively. Due to the heterogeneity of the Molasse Rouge and Grès et Marnes Gris à gypse formations, X-Ray diffraction (XRD) and/or automated mineralogy and petrography scanning (QEMSCAN) laboratory analyses were performed to identify and support decisions for respective GR_{min} and GR_{max} values. High quartz value intervals were chosen as clean (sand) zones, respectively in the same manner for high fractions of clay minerals in shaly zones. A $GR_{cut-off}$ sand/shale cut-off value of 57 gAPI was chosen for all normalized GR logs.

3.3.2 Porosity & lithology cross-over logs: bulk density (RHOB), apparent matrix density (RHOMMA), corrected density (DRHO), photoelectric factor (P_e), neutron (NPHI) and sonic travel-time (DT)

Bulk density logs were run in a vast number of boreholes, while apparent matrix density was run explicitly in the geothermal well Geo-01. For the GX well-logs, corrected density logs (DRHO) were used to verify the original bulk density log run, whereas a value above 0.2 g/cm^3 was considered erroneous (Asquith et al., 2004) and the RHOB log was discarded in such intervals. RHOB and NPHI logs run in wells Thônex-1, Humilly-2, Geo-01 and Geo-02 allowed the identification of porous and likely more permeable zones. An overlap of these two curves indicated permeable, i.e. possible sand(stone)-dominated depth intervals, whereas a clear separation denoted low porosity and permeable, i.e. possible shale-dominated intervals. In addition, neutron porosity versus bulk density enabled the derivation of clay types, i.e. occurrences of laminated, dispersed or structural shale. This was further used for the calculation of the sand-silt-clay model and the identification of clay type distribution.

Based on low-energy gamma ray interaction measurements, the photoelectric index (P_e , Eq. 6) was derived from the PEF log in well Geo-01. This allowed for an advanced lithology distinction based on atomic numbers (Z) according to (Ellis & Singer, 2007):

$$P_e = \left(\frac{Z}{10}\right)^{3.6} \quad (6)$$

Total (PHIT) and effective (PHIE) porosities were calculated using the sonic log and were calibrated to laboratory measurements in the Molasse Rouge formation. While RHOB and NPHI logs offer additional methods of porosity calculations, in most wells full log intervals were

restricted to the sonic log, while NPHI logs were run only in short depth intervals. Therefore, the sonic log was used as the main indicator for all porosity calculations using the Wyllie time-average equation (Wyllie et al., 1956, Eq. 7):

$$\Delta t = \Delta t_{\text{solid}}(1 - \phi) + \Delta t_{\text{fluid}}\phi \quad (7)$$

with an average Δt_{solid} of 47.5 $\mu\text{s}/\text{ft}$ and Δt_{fluid} of 189 $\mu\text{s}/\text{ft}$. For effective porosity, the shale volume was subtracted from total porosity. No porosity calculations were performed in the Mesozoic limestone formations. Fig. 3 exemplarily depicts the full workflow output for petrophysical calculations and incorporation of all laboratory analyses including an updated, re-drawn stratigraphic log for well Gex-CD-01.

3.3.3 Resistivity logs: induction (ILD, ILS) and latero-log (LLD, LLS)

These logs were obtained by company Schlumberger deploying the 6FF40 induction log deep (ILD) tool, a short normal (SN) 16-inch, a long normal (LN) 64-inch log as well as shallow (15' 0) and medium (18' 8") latero-logs. The logs were run along specific intervals (E&P wells) for hydrocarbon detection and used for water resistivity calculation and quality control across logged formations. Unless provided (GX wells) or stated in well reports, the gradient method (Crain, 2021) was used to calculate the formation temperature FTEMP, assuming a surface temperature of 15 °C with a gradient of 3 °C per 100 m. This seemed reasonable since in-situ temperature for the exploitation of geothermal energy significantly increases at ca. 1'000 m below surface in the GB's Mesozoic limestone formations (Chelle-Michou et al., 2017), which is not intersecting the FCC's depth intervals in its current subsurface layout. Water resistivity was calculated for the derivation of the sand-silt-clay model in the Molasse Rouge formation considering FTEMP, and element concentrations of Na, K and Ca measured in the laboratory via inductively coupled plasma optical emission spectroscopy (ICP-OES). Analyses yielded average values of 0.5 Na, 0.2 K and 1.6 mg/g Ca, respectively, whereas chloride (Cl) concentration was assumed for 0.16 mg/g (Kafkafi et al., 2001). True, uninvaded resistivity (R_t) was taken from deep resistivity curves (LN, LLD, ILD), while invaded resistivity (R_i) was derived from shallow resistivity logs (SN, LLS). Flushed zone resistivity (R_{xo}) is commonly taken from a micro-spherically focused (MSFL) log, which was only available in well Gex-CD-07. Due to data limitations, the flushed zone was assumed for the invaded zone in all other wells, hence $R_{xo} = R_i$.

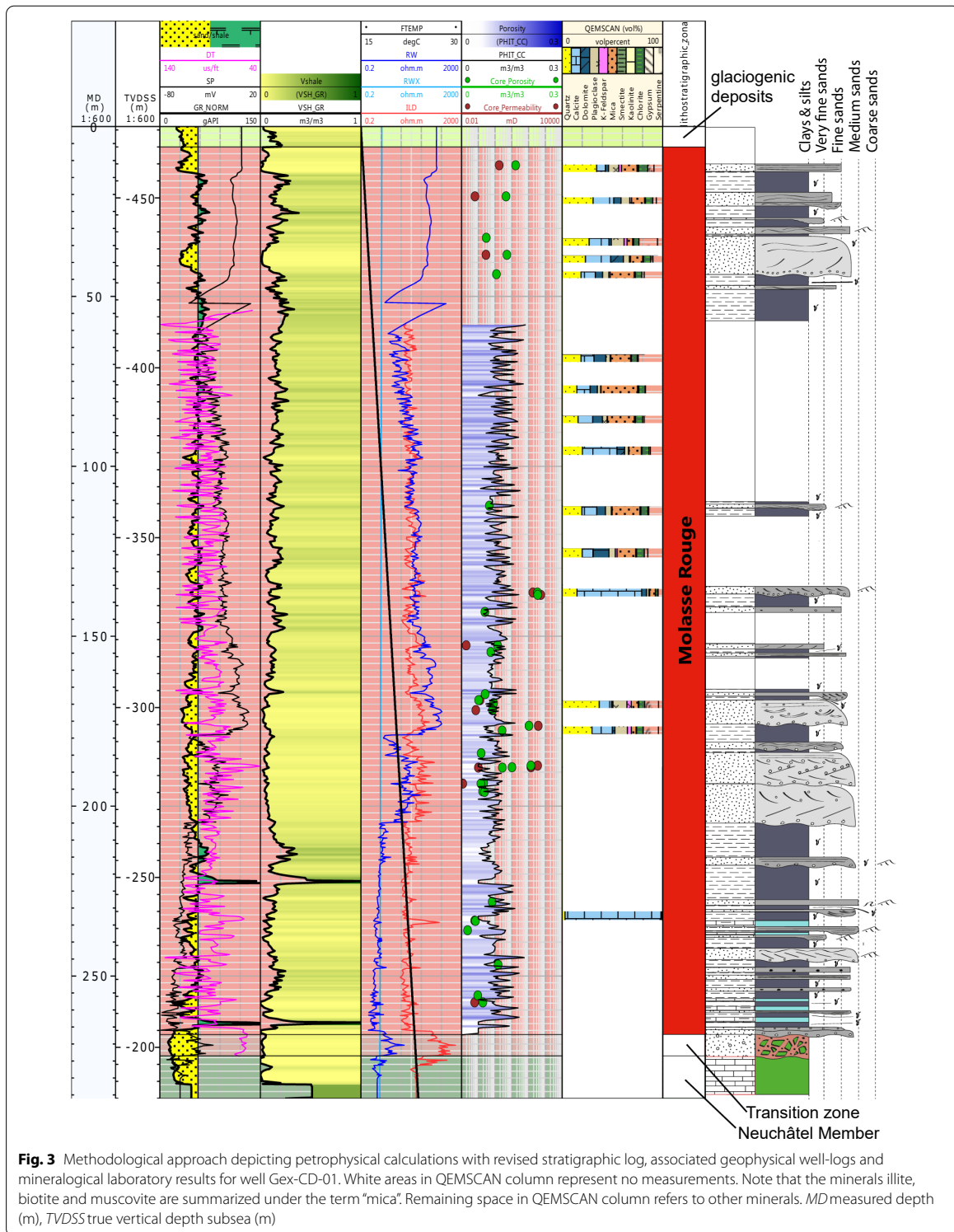
3.4 Sampling and laboratory analyses

A total of 930 samples across all geological formations in the Geneva Basin were analysed. Out of 930 samples, 785 were taken explicitly as part of the present study, and 145 samples during other geothermal studies (Brentini, 2018; Pierdona, 2018; Rusillon, 2018). QEMSCAN measurements included 418 samples in total, and 79 for XRD. A particular focus was hereby set on the Quaternary, Molasse Rouge and Grès et Marnes Gris à gypse formations restricted by the FCC construction depth.

Plugs with 2.5 cm in diameter and 2 to 8 cm in length were drilled from full-, half-cores and outcrops, and were prepared using abrasive tables to polish the top and bottom of each plug into planar surfaces, and subsequently split into different fractions for lithotype analysis. For well Geo-02, cuttings were consecutively taken during drilling progress. These were washed, sieved under water, and dried at 45 °C for ca. 60 h to prevent clay degradation. The dried samples were crushed in an agate mortar and sieved through a <400 μm sieve. Consequently, these cuttings were used to create thin sections that were analysed via QEMSCAN, and produced under vacuum impregnation with epoxy resin. The brick was cut and flattened on one side before mounting on a glass plate with epoxy resin. After cutting the sample down to a thickness of a few 100 μm , it was further abraded before fine polishing down to 30 μm using silicon carbide abrasives. The final step included polishing with alumina by hand and a polishing machine.

3.4.1 Automated mineralogy and petrography scanning (QEMSCAN)

An FEI QEMSCAN Quanta 650F instrument was used to identify the modal mineralogy, texture, and lithotype of 273 thin sections, 26 samples from Thônex-1, 87 from Geo-01 (Pierdona, 2018) and 32 from Humilly-2 (Brentini, 2018; Rusillon, 2018) along the current FCC layout. Measurements were based on a scanning electron microscope (SEM) equipped with two energy-dispersive X-Ray (EDX) spectroscopy detectors, and used for correlations with well-logs. This non-destructive analytical technique enabled in-situ high-resolution (analytical point of <2 μm) mapping (Pirrie et al., 2004). Mineral phase identification stemmed from the combination of back-scattered electron (BSE) contrast and EDS spectra providing information about the elemental composition (Gottlieb et al., 2000). Individual X-Ray spectra were compared to a library of known spectra comprising a specific mineral name and assigned to each individual acquisition point. The X-Ray EDS spectra library was initially provided by the manufacturer and has been further developed in-house using a variety of natural standards.



Measurements were performed at an acceleration voltage of 15 kV with a 10 nA probe current on polished thin sections, which were carbon-coated before scanning using a Quorum Q150T S/E/ES graphite coating device. X-Ray acquisition time was 10 ms per pixel using a point-spacing of 2.5 and 5 μm . Each section was scanned on a 1.5×1.5 cm area at 10 μm resolution to define textural parameters, mineralogical composition, and rock petrographic classification. Up to 122 individual view fields were measured in each sample, depicting 1.5 mm per single field. Data processing and analysis were performed using the FEI iDiscover software. Due to interstratified clay minerals and grain boundaries, which were not necessarily in compliance with the compared QEMSCAN mineral database, results contained a certain portion of unclassified minerals and limitations for clay minerals and interstratified clay minerals.

3.4.2 X-Ray diffraction (XRD)

A jaw crusher was used to crush the plug samples down to a fraction of < 400 μm , followed by a vibrating McCrone mill with agate balls to receive a < 20 μm fraction for subsequent XRD analysis. Samples were analysed according to standard DIN EN 13,925-1/-2 (European Norm (EN), 2003) using two different types of samples measured with a Bragg-Brentano X-ray diffractometer (D8 Advance, Bruker AXS/D). For quantitative XRD analyses, randomly oriented (Zhang et al., 2003), Ca-exchanged samples were scanned from 4 to 80° 2 θ with steps of 0.02° 2 θ at 2 s intervals. Oriented specimens were used for enhancement of the basal reflexes of layer silicates thereby facilitating their identification. The changes in the reflex positions in the XRD pattern by intercalations of organic compounds (e.g. ethylene glycol) and after heating were used for the identification of smectite (Brindley & Brown, 1980). The XRD instrument used CoK α -radiation generated at 35 kV and 40 mA and operated with dynamic beam optimisation using an automatic theta compensating divergence slit and a motorised anti-scatter screen. The diffractometer was equipped with primary and secondary soller slits, and an energy-dispersive LynxEye XE-T line detector. Qualitative phase analysis was conducted with the DIFFRAC.EVA v4.3 (Bruker AXS) software. The minerals were identified by peak positions and relative intensities in the X-Ray diffraction pattern compared with the PDF2 database. Mineral quantification was performed via Rietveld analysis of the XRD patterns using the Profex/BGMN V4.2.4 software (Doebelin & Kleeberg, 2015). This full pattern-fitting method calculates X-Ray diffraction patterns based on crystallographic data of each mineral

phase and its iterative adjustment (least-square fit) to the measured diffractogram. For final refinement, phase specific parameters and the phase content were adapted to minimize the difference between the calculated and the measured X-Ray diffractogram. XRD results in wt.% of the n-th mineral were converted into percentage by volume (%), Eq. 8) using respective averaged and normalized mineral grain densities ρ , according to:

$$\text{vol\%}_{\text{mineral}} = \frac{\frac{\text{wt\%}_{\text{mineral}}}{\rho_{\text{grain}}}}{\sum_n \frac{\text{wt\%}_n}{\rho_n}} \quad (8)$$

Depending on available well-logs, either XRD, QEMSCAN or both analyses were used for correlations of sandy and shaly intervals. Shale volume derived from GR logs was compared with results of XRD analyses, which provided a more robust result for fine-grained clay particles (< 2 μm) compared to QEMSCAN measurements. Mineral abbreviations in respective figures were used after Whitney and Evans (2010).

3.4.3 Effective cation exchange capacity (CEC)

With the Cutrien complex method at pH 7-8 according to Meier and Kahr (1999), the effective cation exchange capacity (CEC) of Molasse Rouge samples was analysed. No measurements were conducted for samples from the Quaternary or Mesozoic deposits. The extinction at 578.0 nm was analysed in the Spectral-Photometer DR6000 (Hach Lange) and compared with the extinction value of the blind solution without added sample material. Effective CEC in meq/100 g was then calculated according to (Eq. 9):

$$\text{CEC} = \frac{(\text{Ext}_{\text{blind}} - \text{Ext}_{\text{sample}}) \cdot 200 \cdot 100}{m_{\text{sample}}} \quad (9)$$

whereas $\text{Ext}_{\text{blind}}$ and $\text{Ext}_{\text{sample}}$ depicted respective extinction values in nm of the blind and real sample, and m_{sample} gave the sample mass in grams. Calculations were corrected by the water content of each < 63 μm sample. The exchange cations per unit pore volume, Q_V , was calculated (Eq. 10) from selected plug samples based on laboratory CEC values, core porosity ($\phi_{\text{eff,core}}$) and core grain density ($\rho_{\text{grain,core}}$) measurements for wells C1, C2, C3, Gex-CD-02 and Gex-CD-04 to Gex-CD-07 (see below), and were extrapolated to Geo-01 for the Molasse Rouge formation. Q_V calculations were conducted according to (Darling, 2005):

$$Q_V = \frac{\text{CEC} \cdot \rho_{\text{grain,core}}}{100 \cdot \phi_{\text{eff,core}}} \quad (10)$$

3.4.4 Exchangeable cations via Inductively Coupled Plasma Optical Emission Spectrometry (ICP-OES)

Sample preparation continued with the centrifuged supernatant of the previous CEC measurement. The solution was filtered with $0.45\ \mu\text{m}$ PES vaccine filters and acidified with 2% HNO_3 . Exchanged Na, K, Mg, Ca and further leachable elements (e.g. Ni, Cr) were quantified via ICP-OES using an Agilent 5110 ICP-OES device. Condition settings were adapted to 10 s of reading and 15 s stabilization time. Viewing mode was radial with a viewing height of 15 mm. For each sample run, a blank sample and 3 standards were used for calibration, followed by a quality control spike blank sample and a copper blank sample.

3.4.5 Water uptake capacity via Enslin-Neff

The Enslin-Neff analysis was performed to measure the water uptake capacity under free swelling conditions (Neff, 2005) and its associated time evolution of rock-water interaction following standard DIN 18,132 (Deutsches Institut für Normung (DIN), 2012). About 1 g of a $400\ \mu\text{m}$ sample was placed in an Enslin-Neff apparatus and its free water uptake over time until maximum was recorded (up to 1'440 min). The maximum water absorption reading (w_{max}) served for the calculation of the water absorption capacity, w_a in wt.% (Eq. 11) corrected by the dry mass, m_{dry} , according to:

$$w_a(\%) = \frac{w_{\text{max}}}{m_{\text{dry}} \cdot 100\text{wt}\%} \quad (11)$$

3.5 Core porosity, core permeability, and core grain density

The unsteady state pressure-decay technique after the modified Darcy's law was applied to measure effective porosity and absolute (single fluid) permeability with an AP-608 Automated Permeameter & Porosimeter (Chablais & Moscariello, 2012; Coretest Systems Inc., 2008, 2011) on a total of 170 Siderolithic, Molasse Rouge and Quaternary plug samples, and were further used for respective well-log calibration. The device measured porosity (percentage) and permeability (milli-Darcy, mD) in respective gas atmospheres. Plugs were analysed with nitrogen, and for selected samples with helium gas. The latter served as an ideal gas optimized for medium to high permeability values, whereas nitrogen was used for fine-grained Molasse Rouge samples expecting permeability values below 0.05 mD. The measurement analysed the equivalent liquid permeability, slip and turbulence factors. Pore volume measurements were retrieved using the gas expansion model based on Boyle's law. Grain densities were measured using the device's grain volume

chamber. Before a set of measurements, a reference volume inside the grain volume chamber, which was filled with calibrated metal cylinders, was calculated yielding an average value of $10.99\ \text{cm}^3$. During each measurement, temperature was maintained constant at $58.3\ ^\circ\text{C}$. Nitrogen and helium viscosities were used for appropriate calculations. Results were corrected for the Forchheimer (Forchheimer, 1901) and Klinkenberg (Klinkenberg, 1941, Eq. 12) effects, with the latter providing a robust approximation of liquid permeability based on measured gas permeability, following Tanikawa and Shimamoto (2006):

$$k_g = k_l \left(1 + \frac{4cl}{r} \right) = k_l \left(1 + \frac{ck}{\pi\sqrt{2r^3}} \frac{T}{p} \right) = k_l \left(1 + \frac{b}{p} \right) \quad (12)$$

with:

$b = \frac{ck}{\pi\sqrt{2r^3}}$, whereas k_g is the permeability of gas (m^2), k_l depicts the permeability of liquid (m^2), l is the mean free path of gas molecules (m), r is the pore radius (m), κ the Boltzmann's constant (JK^{-1}), T the temperature (K), c is a constant, p is the pore pressure (Pa) and b is the Klinkenberg slip factor (Pa). In contrast to flowing liquids, the velocity of gas flowing through a porous medium is not zero at the wall but shows a slight increase. This correction factor compensates for gas slippage within pores when gas flows along pore walls.

4 Results

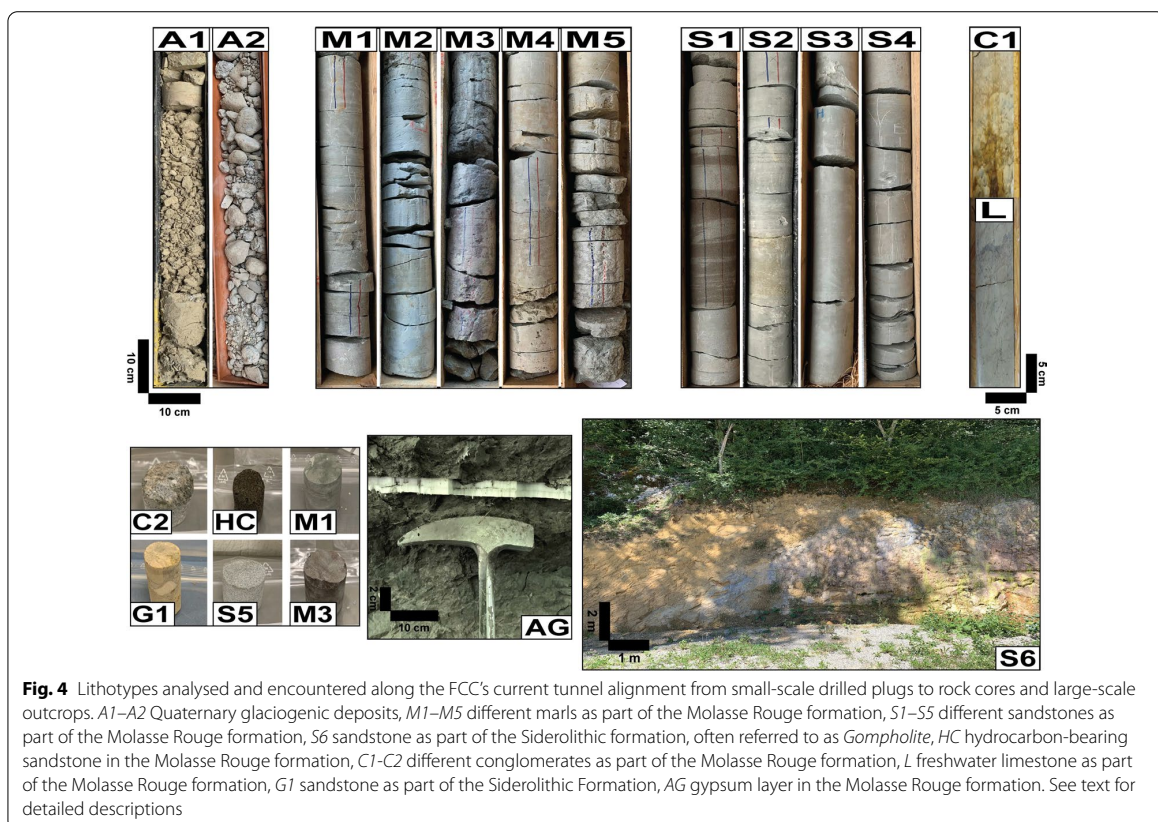
The FCC's ongoing feasibility phase requires the identification of encountered geological formations and the investigation of rock characteristics at its currently planned construction depth intervals between 100 and 300 m ASL for its main tunnel and experimental caverns. While subsurface designs are still subject to changes as additional information is collected from a wide range of well-log data and laboratory analyses, the current results impact admission into the subsequent technical design phase, associated environmental impact assessments, and ultimately, optimal well placement for upcoming site investigations.

Each data type is presented separately in the following sub-sections from local to regional scales. Visual geological rock core inspections show the highest resolution in the order of millimetres. Consecutive decrease in resolution is given by the geophysical well-logs with an average point density of 15.24 cm. A lithostratigraphic overview is depicted at outcrops within a few tens of meters (Fig. 4), followed by two distinct well correlation panels among the northern Gex well series (Fig. 5) and selected deeper wells along a NE-SW trend (Fig. 6), both within a few hundreds of meters in vertical and a few tens of kilometres in lateral extent.

4.1 Stratigraphy across the Geneva Basin

In the Geneva Basin, 22 geological formations and sub-units featuring 31 lithotypes are encountered across 661 wells distributed within the FCC's construction area. These are described in the following sub-sections in order of decreasing geological age, and the FCC's intersected 13 geological formations and associated 25 lithotypes (Table 2), of which some are exposed in the field and analysed on rock samples. Fig. 4 shows the encountered lithotypes: A1 represents Quaternary unconsolidated deposits at a depth between 4 to 5 m in C5 well (close to CERN's HL-HLC Point 1), while A2 is comprised of gravelly Quaternary deposits at a depth from 32.25 to 39.25 m in well Montfleury-2. M1-M5 lithotypes depict different marl- and siltstones that vary in colour and grain size from very fine to fine-grained (M1-M2) in well Peissy-I at depth levels from 125.12 and 126.12 m and between 42.30 and 42.90 m, respectively. A brownish-violet, often referred to as *lieu de vin* (M3), marl lithotype is encountered e.g. in well Gex-CD-01 at a depth from 40.96–41.90 m, and beige (M4) coloured lithotype is encountered in Peissy-I at a depth

between 82.50 and 83.46 m. Conglomeratic, low sphericity grains in a clayey matrix of siltstone (M5) are located at a depth between 124.12 and 125.12 m in well Peissy-I. S1-S4 show partly hydrocarbon-impregnated sandstone (S1) at a depth between 100.69 and 101.51 m, fine-laminated silty sandstone (S2), massive, compact sandstone (S3) at a depth between 58.95 and 59.90 m, and porous, fine-grained sandstone (S4), all cored in well Peissy-I. HC depicts a hydrocarbon saturated sandstone lithotype in Gex-CD-01 at a depth of 188.10 m, and very fine-grained, laminated sandstone (S5) is encountered in well Gex-CD-04 at 120.22 m. C1 and C2 represent conglomeratic lithotypes differentiated by colour and grain size at depth levels 233.20 m and 188.70 m in Gex-CD-01, respectively. G1 depicts the Siderolithic Formation, often referred to as *Gompholite*, drilled from an outcrop close to Mornex in the northern part of the GB (Fig. 1). The L lithotype depicts Molasse Rouge freshwater limestone encountered in Gex-CD-07 at a depth of 234.7 m. The AG lithotype depicts a fine layer of gypsum in an outcrop close to Nyoux, while S6 represents the Siderolithic Formation outcropping near Sarzin close to an abandoned quartzite



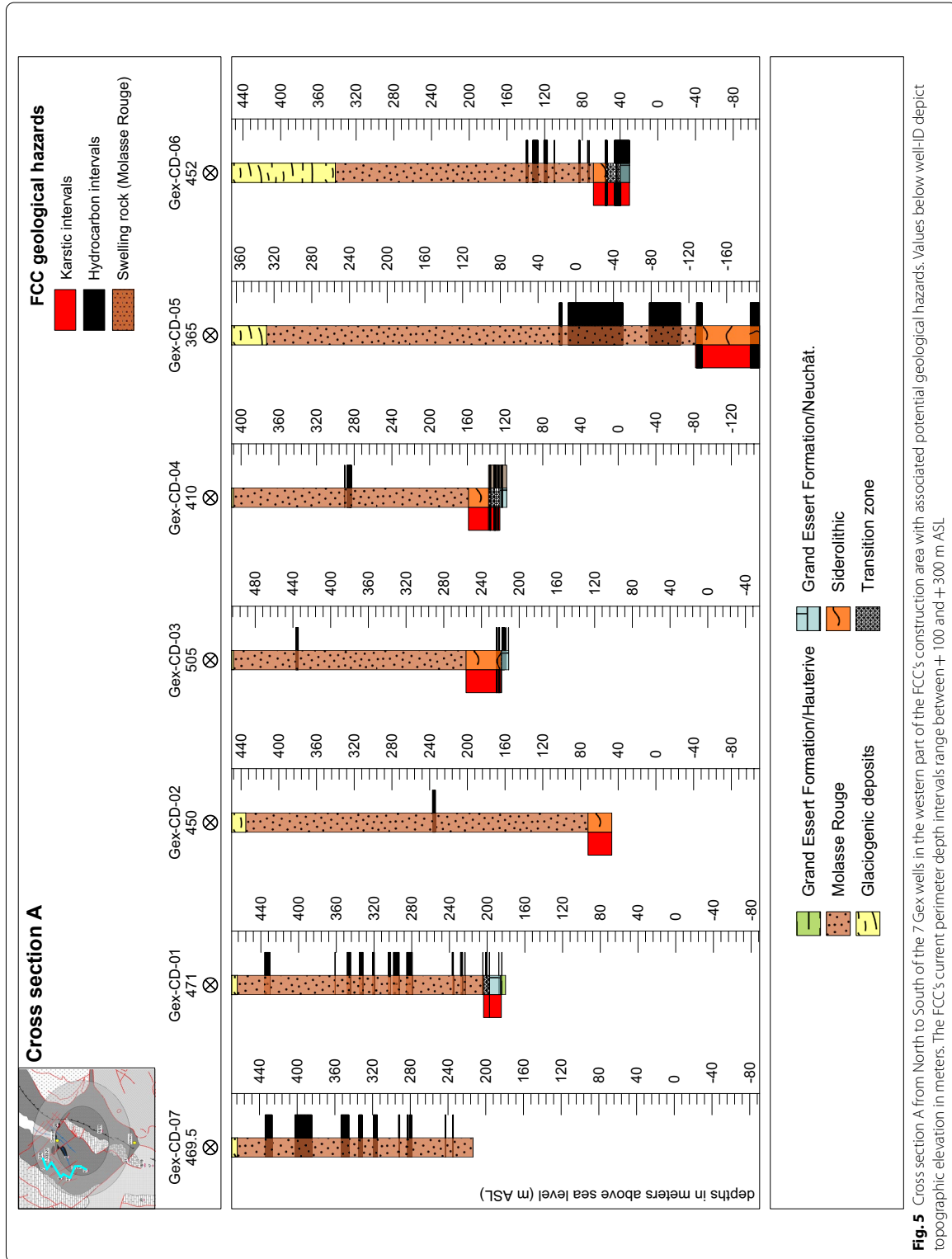


Fig. 5 Cross section A from North to South of the 7 Gex wells in the western part of the FCC's construction area with associated potential geological hazards. Values below well-ID depict topographic elevation in meters. The FCC's current perimeter depth intervals range between +100 and +300 m ASL

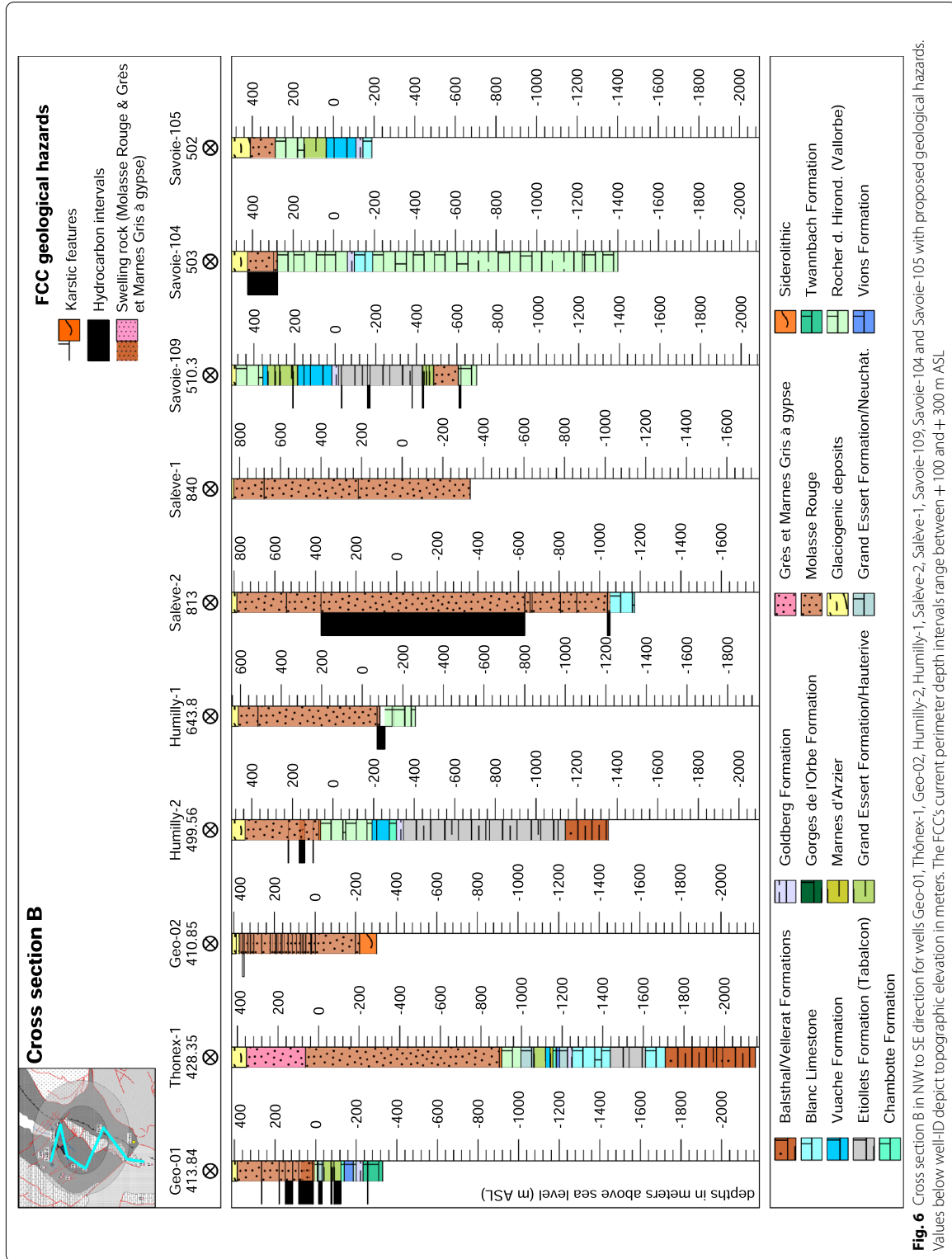


Table 2 Lithostratigraphic column for the Geneva Basin and geological tunnelling hazards linked to different lithotypes potentially relevant for FCC construction

Period	Epoch	Stage	Rock types	Lithostratigraphic notations	lithostratigraphy (this study)	lithotypes (this study)	abbreviation of lithotypes (see Fig. 4)	FCC's geological hazards (this study)
Quaternary	Pleistocene	Holocene	Absent	Absent	Topsoil	Topsoil	Topsoil	Active faults
		Late	Silty-Clayey Gravel, Conglomerate	Glaciogenic deposits, LGM moraines	Post-glacial sediments, LGM moraines	Sandy to (sometimes) clayey gravel mixtures, clast with grey-beige plastic consistency	A3	
Paleogene	Oligocene	Middle			Cemented & unconsolidated, interglacial sediments	dark grey, clayey mud- and wackestone with pollen traces	A2	Water-bearing aquifers
					Pre-glacial sediments	Mixture of fine sand and sandstone embedded in clayey matrix	A1	Water-bearing aquifers
Paleogene	Serravalian		Conglomerate	Upper Freshwater Molasse (UFM)	Absent	Absent	Absent	Absent
					Absent	Absent	Absent	Absent
					Absent	Absent	Absent	Swelling clays, anhydrite (AG), hydrocarbons (HC), active faults
Paleogene	Aquitainian		Molasse Grise	Lower Freshwater Molasse (LFM), (Molasse Rouge*, Grès et Marnes Gris à gypse*)	Absent	Absent	Absent	Swelling clays, anhydrite (AG), hydrocarbons (HC), active faults
					Grès et Marnes Gris à gypse, Molasse Rouge as part of LFM	Upper succession: sandstone with intercalations of marly siltstone lower succession: clayey limestone, breccia, sandstone, alternating thin beds of very fine to fine sandstone, laminated clayey siltstone Anhydrite/gypsum layers Hydrocarbon-bearing sandstone. Limestone	S1, S2, S3, S4, S5; M1, M2, M3, M4, M5; AG; HC; L	Swelling clays, anhydrite (AG), hydrocarbons (HC), active faults
Paleogene	Chattian		Grès et Marnes Gris à gypse, Molasse Rouge (upper and lower succession)					
Eocene	Eocene	Rupelian	Sandstone, conglomerate	Lower Marine Molasse (LMM)			C1, C2	Swelling clays, anhydrite (AG), hydrocarbons (HC), active faults
					Siderolithic	Conglomerate with quartz and limestone in clayey cement	C1, C2, S6, G1	Karst, hydrocarbons, active faults
Transition zone (Perte-du-Rhône Formation)**					Transition zone	Not stratified, karstic sandstone alternations(?)	KS	Karst, hydrocarbons, active faults

Table 2 (continued)

Period	Epoch	Stage	Rock types	Lithostratigraphic notations	lithostratigraphy (this study)	lithotypes (this study)	abbreviation of lithotypes (see Fig. 4)	FCC's geological hazards (this study)
Cretaceous	Early	Barremian	Limestone, often marly	Vallorbe Member of the Rocher des Hironnelles Formation and Gorges de l'Orbe Formation (both formerly represented by the Urgonien)	Vallorbe Member of the Rocher des Hironnelles Formation	Massive limestone	ML	Karst, hydrocarbons, active faults
				Vallorbe Member of the Rocher des Hironnelles Formation and Gorges de l'Orbe Formation (both formerly represented by the Urgonien), Grand Essert Formation (Hauterive Member and Neuchâtel Member)	Vallorbe Member of the Rocher des Hironnelles Formation, Grand Essert Formation (Hauterive Member and Neuchâtel Member)	Marly-sandy limestone, sometimes dolomitic, mud-/wackestone; limestone with siltstone	MSLd, MLs	Karst, hydrocarbons, active faults
Jurassic	Late	Tithonian	Limestone	Grand Essert Formation (Hauterive Member), Vuache Formation	Grand Essert Formation (Hauterive Member), Vuache Formation	Marly-sandy limestone, sometimes dolomitic	MSLd	Karst, hydrocarbons, active faults
				Goldberg Formation, Chamboite Formation, Pierre-Châtel Formation, Vions Formation, Neuchâtel Member	Goldberg Formation, Chamboite Formation, Pierre-Châtel Formation, Vions Formation, Neuchâtel Member	Massive limestone; marly-sandy limestone, biomicrite and wacke-/packstone	ML, MSL	Karst, hydrocarbons, active faults
Jurassic	Late	Tithonian	Limestone	Twannbach Formation	Twannbach Formation	Massive, dolomitic, partly fine-grained limestone; dolomitic limestone, massive dolomite	L, Ld, MD	Karst, hydrocarbons, active faults
				Twannbach Formation, Etiollets Formation (Tabalcon sub-unit), Blanc Limestone	Twannbach Formation, Etiollets Formation (Tabalcon sub-unit), Blanc Limestone	Dolomitic, clayey limestone, sometimes massive limestone	DCL, ML	Karst, hydrocarbons, active faults
Jurassic	Late	Tithonian	Limestone	Balsthal Formation, Vellerat Formation***	Balsthal Formation, Vellerat Formation***	Clayey to marly limestone and malistone	CVL, M1	Karst, hydrocarbons, active faults
				Twannbach Formation, Etiollets Formation (Tabalcon sub-unit), Blanc Limestone	Twannbach Formation, Etiollets Formation (Tabalcon sub-unit), Blanc Limestone	Clayey to marly limestone and malistone	CVL, M1	Karst, hydrocarbons, active faults

Bold area refers to the geology encountered by the FCC in its current subsurface layout. Rock types and lithostratigraphic notations after Blondel, 1984; Brentini, 2018; Burkhard & Sommaruga, 1998; Charollais et al., 2007; Deville et al., 1994; Graf & Burkhalter, 2016; Jaquet, 1966; Kissling, 1974; Moscarello, 2019; Strasser et al., 2016

*Molasse Rouge and Grès et Marnes Grès à gypse are commonly referred to informal but valid names as part of the LFM. **Currently under discussion but might imply new insights on the Mesozoic-Cenozoic boundary(?) as part of imminent research results for the GB. ***Currently under discussion, not yet fully defined. LGM Last Glacial Maximum

mine (Fig. 1). They substantially vary in vertical and lateral extent (Fig. 5, Fig. 6) and bear critical geological hazards and environmental contaminations as discussed and summarized in Table 2.

4.1.1 Balsthal Formation and Vellerat Formation

This Oxfordian interval is encountered by wells Brizon-1, Chaleyriat-1, Charmont-1 and Chatillon-1D close to the Jura in the western part of the GB, and by Humilly-2, La-Chandelière-1, La-Tailla, Musiège-1 and Thônex-1 comprising limestone, clayey to marly limestone and marl lithotype alternations. Except for well Chaleyriat-1 and La-Chandelière-1 with a starting depth at 18 m and 330 m extending down to 933 m and 726 m, respectively, average top depths among these wells range between 500 and 600 m. The exact stratigraphic terminology of these formations is currently debated.

4.1.2 Blanc Limestone Formation

This Kimmeridgian (Portlandian) formation is encountered in wells Faucigny, La-Chandelière-1, La-Tailla, Mont-de-Boisy-1, Musiège-1, Salève-2, Savoie-104 and Savoie-105 and Thônex-1, as dolomitic, often clayey limestone lithotype. While wells close to the Jura encounter this formation at shallow depths of about 67 m, wells distributed towards the South of the FCC perimeter intersect it between 600 and 800 m and extend down to about 1'986 m. Savoie-104 contains dolomitic limestone, whereas in its neighbour, Savoie-105, the lithotype becomes more massive and less dolomitic, starting at a depth of 605 m and 647 m, respectively. In Thônex-1, the formation is encountered as marly limestone of supposedly Portlandian age at a depth of 1'678.60 m and extends down into the Oxfordian from 2'038.60 to 2'136 m as massive limestone.

4.1.3 Etiollets Formation with Tabalcon Limestone sub-unit

Massive, often dolomitic limestone banks of Kimmeridgian age in the Etiollets Formation comprise the Tabalcon Limestone sub-unit encountered in wells Chapery-1, Humilly-2, La-Balme-1, La-Chandelière-1, Musiège-1, Savoie-106, -107, -109 and Thônex-1. The formation makes up a substantial portion of wells Savoie-106 and Savoie-107 starting from the top of the well down to 860 and 950 m depth, respectively, while for the other wells starting depths range between 846 and 1'100 m extending down to depths between 860 and up to 1'800 m in the Savoie wells, Humilly-2, Musiège-1, Chapery-1, Thônex-1 and La-Balme-1. The Etiollets Formation without

the Tabalcon Limestone sub-unit differs due to the absence of dolomitic composition, making it a pure, massive limestone.

4.1.4 Twannbach Formation and Goldberg Formation

The Late Kimmeridgian to Tithonian Twannbach Formation is comprised of dolomitic limestone and massive dolomite. The Goldberg Formation is of Early to Middle Berriasian age and bears massive, dolomitic, partly fine-grained limestone. Wells encountering these formations are Chapery-1, Geo-01, Humilly-2, La-Tailla, Musiège-1, Savoie-105, -107, -108, -109 and Thônex-1, restricted to the FCC's western region, terminated by the Salève and Mandallaz lineaments to the east and south-east. Average depths start at about 420 m and extend down to 1'680 m in Thônex-1.

4.1.5 Pierre-Châtel Formation

This Middle Berriasian formation consists of oolitic, often bioclastic, white to reddish limestone and marly interstratifications, and tends to become more massive towards the top yet impregnated by oolitic and bioclastic intercalations. This formation is encountered in the wells closer to the Jura.

4.1.6 Chambotte Formation and Vions Formation

These two formations of Berriasian age are mainly encountered by the northern wells close to the Jura. The Chambotte Formation intersects wells Faucigny, Geo-01, Humilly-2 and Thônex-1 comprising massive limestone, while Brizon-1, Chapery-1, Geo-01, La-Balme-1 and Thônex-1 account for the Vions Formation, comprised of marly to sandy limestone. Top depths of the Chambotte Formation start between 530 and 812 m, and extend down to 600 to 800 m, with an exception in Thônex-1 ranging between 1'583 and 1'600 m. Adjacent thereto, the Vions Formation extends down to 1'000 to 1'300 m, with exceptions in Geo-01 to 600 m and Thônex-1 to 1'615 m.

4.1.7 Vuache Formation

This Valanginian formation, formerly referred to as the *Calcaire Roux* (Limestone Formation) (Charollais et al., 2007; Strasser et al., 2016), includes predominantly sandy to marly limestone, sometimes dolomitic, and is encountered in Brizon-1, Chapery-1, Humilly-2 and La-Balme-1 at depths between 700 and 1'000 m, while in the SPM and L135 wells, top strata are exposed at shallower depths between 72 and 160 m in the northern part of the FCC's construction area. The Savoie, La-Tailla and Musiège-1 wells encounter these formations at depths

varying between 342 and 470 m. In Thônex-1, the formation is restricted to the interval between 1'546.90 and 1'568.10 m.

4.1.8 Grand Essert Formation with Hauterive Member and Neuchâtel Member

This formation consists of two members: the Late Valanginian to Early Hauterivian Hauterive Member, formerly referred to as the *Marnes d'Hauterivian* facies (Brentini, 2018; Charollais et al., 2007) and the Early to Late Hauterivian Neuchâtel Member, formerly referred to as the *Pierre Jaune de Neuchâtel* facies (Charollais et al., 2007). The former is comprised of marly to sandy limestone, sometimes dolomitic, and predominantly ochre, bioclastic mudstone (Potter et al., 2005) and highly recrystallized wackestone. The formation is encountered at 370 m in Brizon-1, 864 m in Chapery-1, 453 m in Geo-01, 286 m in Gex-CD-01, at 0 m in La-Chandelière-1, at 1'647 m in La-Tailla, 263 m in Musiège-1, at 356 m in Savoie-105, at 45 m in Savoie-108, 177 m in Savoie-109, at 107 m and 76.5 m in SPM1 and SPM15, and at 1'488 m in Thônex-1, respectively, becoming richer in clay before the overlying Neuchâtel Member. The Neuchâtel Member consists of limestone with minor associated marl, and ochre-coloured, glauconite-bearing, bioclastic wackestone/packstone, encountered in wells Chapery-1, Geo-01, Gex-CD-01 and -06, L130, La-Balme-1, La-Tailla, Musiège-1, SPM2, SPM11, SPM15 and Thônex-1. Typical for this formation is its richness in bivalve shell fragments. Top depths range in the GB's northern wells between 120 and 430 m, whereas Thônex-1 marks an exception starting at 1'425 m. Top depths of about 800 m are common due to the adjacent Jura mountains (Chapery-1) and associated elevated topography.

4.1.9 Rocher des Hirondelles Formation with Vallorbe Member

This Late Hauterivian to Late Barremian formation is encountered in wells Brizon-1, Chapery-1, Faucigny, Geo-01, Gex-CD-03, -04, -06, Grilly, Humilly-1, Humilly-2, L112, La-Balme-1, La-Tailla, Messery-1, Mont-de-Boisy-1, Musiège-1, Savoie-104, -105, -108, -109, SPM1-3, SPM5 and Thônex-1. In some well reports the differentiation between the Vallorbe Member and the Neuchâtel Member is not clear and refers to Barremian age. The main lithotype of this formation is massive limestone, often associated with sandstone and calcareous marlstone. Sandy-marly limestone is associated to the Vallorbe Member as well, when combined with the Neuchâtel Member. Together with the Late Hauterivian to Late Barremian

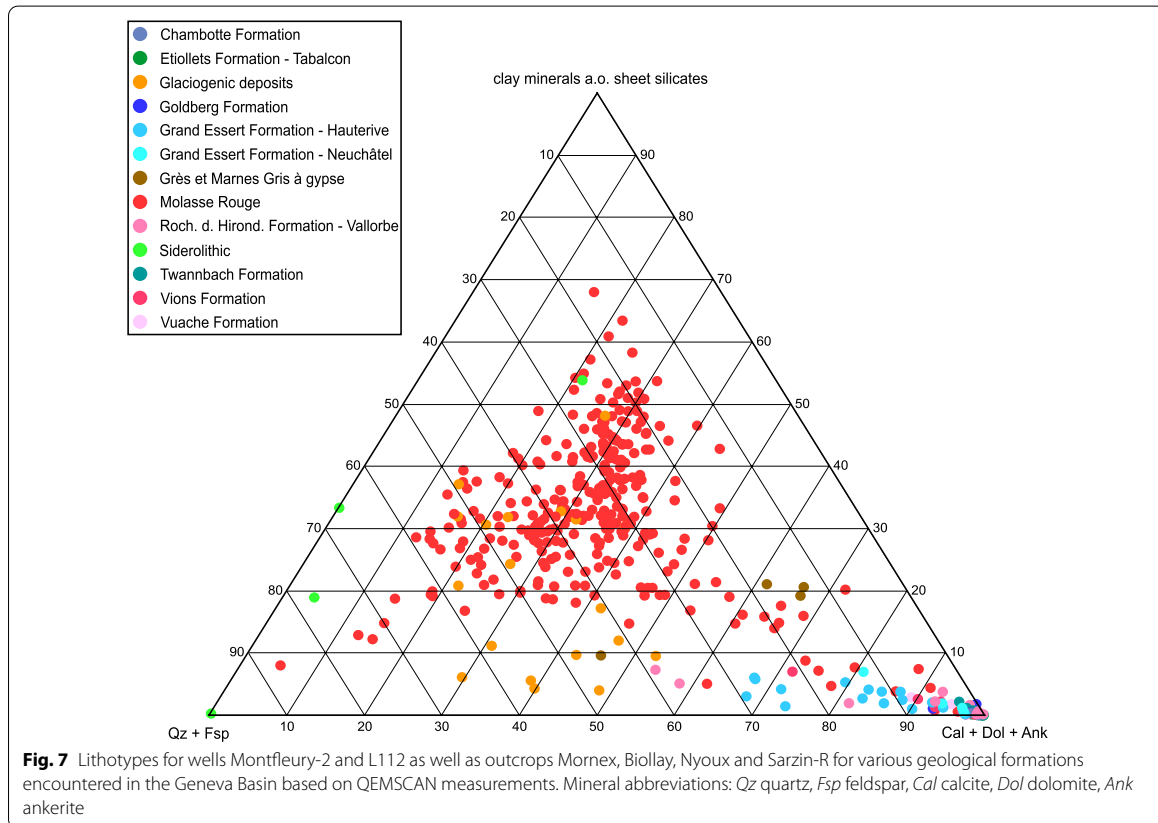
Gorges de l'Orbe Formation, these two formations today represent the former *Urgonien*, as referred to in older well reports.

4.1.10 Transition zone and Siderolithic Formation

The Mesozoic-Cenozoic(?) Transition zone has been extensively researched in the past years. Its temporal relationship is not yet scientifically proven—as is its informal name used here—but the sandstone-bearing unit comprises an Eocene(?) siliciclastic formation including karstic alterations, which have been erroneously combined with the Siderolithic Formation in older well reports. Latest considerations suggest that these lithologies could be part of the *Perte-du-Rhône* Formation, also referred to as *Gault*.

The Siderolithic Formation consists of continental sandstone likely deposited in a fluvial environment with the sedimentary source derived from the detrital Triassic of the eastern edge of the Central Massif (Conrad & Ducloz, 1977). This zone has yet not been fully investigated, and ongoing, unpublished studies in conjunction with the Transition zone characterize it as an assembly of centimetric blocks of beige, glauconitic, bioclastic limestone of the Mesozoic basement, cemented by marly, glauconitic sandstone, with angular quartz on a multi-decimetre-scale, primarily encountered in all Gex wells at depths between 230 to 290 and 395 to 412 m, respectively, in well Geo-02 between 630 and 714 m. Very fine cemented sandstone is associated with this limestone lithotype. Certain core samples in Gex-CD-02 show the presence of polygenic conglomerates with quartz and limestone, embedded or perforated in a ferruginous, ochre clay cement. The Siderolithic Formation has been formerly referred to as the *Gompholite* facies (Charollais et al., 2007, 2013) and is encountered in wells Charmont-1, Chatillon-1D, Faucigny, Geo-02, Gex-CD-02 to -06, Humilly-2, La-Chandelière-1, Musiège-1, Savoie-106 and 107 as well as Thônex-1. Figure 4 (S6) shows an outcrop of the Siderolithic Formation in the northern part of the FCC construction area, yielding a high content of quartz (appr. 99%).

The GR log indicates a distinct offset to lower values in the respectively logged well-logs, while the SP log increase up to 10 mV across all wells for the Transition zone. The LN resistivity log shows a high offset from 20 to 2000 Ohm*m, similar to the SN although in the order of 2 to 20 Ohm*m. Both logs, along the SP log, associate increased values to a higher clay content. The DT log depicts a decrease of travel-time, making the Siderolithic Formation a slow formation in terms of compressional wave velocity, substantiating its potentially karstic,



porous characteristics. GR values (<57 gAPI) indicate sand-dominated intervals, which partly increase for a few meters when cemented with higher amounts of shale. This is also reflected by high resistivity values across all wells.

Mineralogical analyses (QEMSCAN) of related outcrops (Fig. 7) reveal an associated limestone lithotype. The Sarzin and Biollay outcrops (Siderolithic Formation) show a sandstone lithotype exceeding 90% in quartz by volume, with varying claystone content from 0 up to 34%. In contrast, the Mornex and Nyoux outcrops show a tendency towards a limestone lithotype. A characteristic feature compared to the overlying Molasse Rouge sandstone lithotypes, is the fact that Siderolithic sandstones do not appear stratified on both a micro- and macroscopic scale. This facilitates their identification in the field.

4.1.11 Molasse Rouge

The Molasse Rouge, often informally referred to as *Marnes bariolées*, comprising a subset of the LFM (Charollais et al., 2007, 2013; Kissling, 1974), is dated

to Chattian age (Early Oligocene) and split into an Upper and Lower unit. The lower succession is dominated by clayey to partly silty limestone, making the Lower unit rich in clayey limestone from ca. 240 m down to the Transition zone in the Gex wells. Alternating thin beds of very fine to fine sandstone occur, rarely with medium and laminated, clayey siltstone or green, marly claystone. Nodular, highly bioturbated limestone with mollusc fragments were formerly correlated to the *Grilly* Formation (well Grilly) and interpreted as deposits of a palustrine environment (Charollais et al., 2007). The upper succession is comprised predominantly of sandstone with intercalations of marlstone across all wells, excluding those closer to the Jura. Freshwater limestone intermingled with palustrine breccias is associated with the lower succession. The sandstone of constant thickness is fine to medium-grained, showing a gradual decrease in grain size from top to bottom, with rather subangular grains and weak strength. This green-grey sandstone is comprised of quartz, feldspar, muscovite, and biotite,

sometimes occurring with soft, clayey pebbles dispersed in a clayey matrix in layers.

Encountered along the measured depth, the Savoie-109 well does exceptionally not transition into the Molasse Rouge, but directly into the limestone-bearing Rocher des Hirondelles' Vallorbe Member, equivalent to those encountered in the adjacent Rumilly and Valserine basins further to the south of the Geneva Basin. This well only shows Molasse Rouge at its base, which is also reflected by its higher drilling altitude compared to that of adjacent wells in this cross section.

The Molasse Rouge formation shows 13 lithotypes across all sampled wells (Figs. 5, 6, Table 2). This implies the necessity to define ranges for each mineral as measured by QEMSCAN and XRD analyses. Quartz, calcite and dolomite (ankerite) make up most of the formation with average values up to 80%, 50% and 25% by volume, respectively, but vary laterally across all wells from North to South. Calcite values reach up to 100% in Gex-CD-04 and -07 at about 200 m, representing the freshwater limestone lithotype (Fig. 8) associated to the Molasse Rouge. Total clay mineral volumes are quantified up to 60% (Fig. 9), constituting swelling potential in the Molasse Rouge.

GR log values vary between 5 to 100 gAPI across all wells with heterogeneous log patterns. The DT log remains at averaged constant values of 50 $\mu\text{s}/\text{ft}$, decreasing up to 20 $\mu\text{s}/\text{ft}$ before entering the underlying Siderolithic Formation and Transition zone in e.g. the Geo-01 well. Resistivity logs remain at average values between 20 and 200 $\text{Ohm}\cdot\text{m}$, except for thin depth intervals of a few meters bearing hydrocarbons, hence showing increased values above 200 $\text{Ohm}\cdot\text{m}$. NPHI and RHOB logs show separated log curves, making the Molasse Rouge appear impermeable due to its shale content (Fig. 10). Permeable zones are only detected below the Molasse Rouge in the Transition zone and Siderolithic Formation, suggesting compacted, sandstone-bearing intervals (Figs. 9, 10).

4.1.12 Grès et Marnes Gris à gypse

The Grès et Marnes Gris à gypse is part of the LFM Molasse formation in the Geneva Basin, and an equivalent to the Molasse Grise towards the northern area of the western SMB around Lausanne preserved in the foredeep of the GB. According to various well reports, the Grès et Marnes Gris à gypse is encountered only in the Thônex-1 well (Fig. 10), making the northern part of the FCC construction area more likely exposed to the Grès et Marnes Gris à gypse, and suggesting complete erosion towards the south. The formation is dated

to Late Oligocene (Middle/Upper Chattian) and is characterized by an increased amount of anhydrite/gypsum, intercalated in sandstone and marlstone of various grain sizes. While the northern boreholes (e.g. Geo-01 and Salève-1) directly transition into Molasse Rouge, the Thônex-1 marks an exception with Grès et Marnes Gris à gypse being encountered between 73 and 364 m. This complies with the fact that Grès et Marnes Gris à gypse lenses have been geologically mapped in FCC's northern construction area and are delimited by the syn- and anticline structures (Fig. 1). Further wells encountering the Grès et Marnes Gris à gypse are Messery-1 and Mont-de-Boisy-1, ranging from 18 to 560.50 m and 748 to 1'774 m, respectively. On the contrary, the C1-C3 wells do not show any traces of gypsum in the north-northwestern part of the basin.

In the Thônex-1 well, QEMSCAN measurements yield up to 30% of gypsum by volume, occurring as anhydrite in the subsurface, and decreasing towards the underlying Molasse Rouge. This is a decisive characteristic, as the FCC entirely crosses this formation in its currently planned subsurface alignment, raising concerns for operations and maintenance due to anhydrite swelling potential in this formation (Fig. 9).

Log differences between the Molasse Rouge and Grès et Marnes Gris à gypse are difficult to establish, and only slightly visible in lower averaged SP values ranging around -20 mV in the Grès et Marnes Gris à gypse formation, compared to the Molasse Rouge of -10 to $+20$ mV. The distinctive characteristic remains the increased anhydrite/gypsum content in the Grès et Marnes Gris à gypse formation.

4.1.13 Glaciogenic deposits

Glaciogenic sediments of Quaternary age, often mistakenly grouped as the "Moraine Formation" in technical reports, summarise terminologically deposits that were influenced by glaciers, glacial erosion/deposition or subsequent geomorphological processes, and formed during last pre-glacial, post-glacial, glacial and interglacial periods. They consist of compacted till made of sandy to clayey gravel mixtures, often with 0.5 to 2 cm-sized clasts of grey-beige plastic consistency and a mixture of fine-grained sand, embedded in a beige, clayey matrix. These sediments are encountered by all wells and range from about 2 m to up to 110 m depth, overlying the Molasse Rouge or Grès et Marnes Gris à gypse in e.g. wells Thônex-1, Messery-1 and Mont-de-Boisy-1. The greatest thicknesses are encountered in wells Gex-CD-05 and Gex-CD-06 with 37 and 110 m, respectively. However, these glacial deposits are typically irregular in thickness and lateral changes

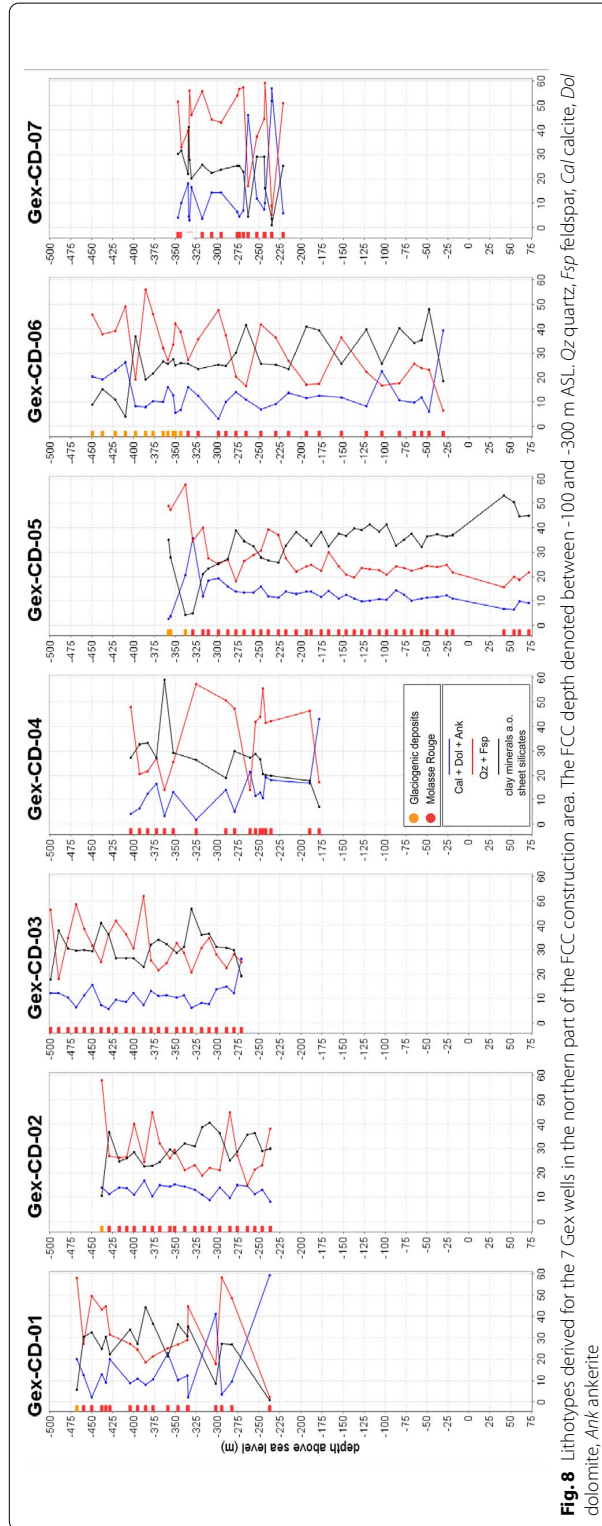


Fig. 8 Lithotypes derived for the 7 Gex wells in the northern part of the FCC construction area. The FCC depth denoted between -100 and -300 m ASL. Qz quartz, Fsp feldspar, Cal calcite, Dol dolomite, Ank ankerite

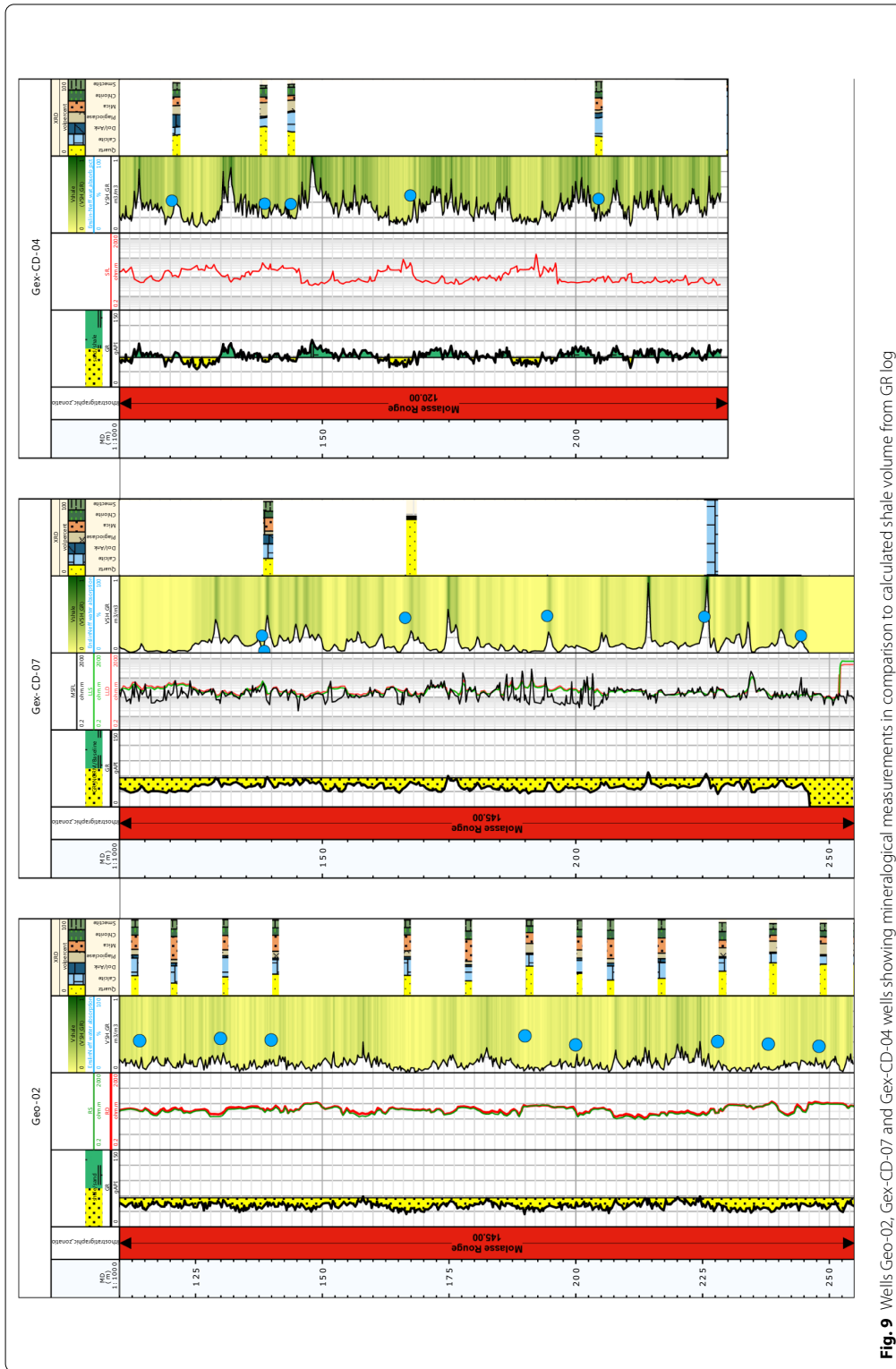
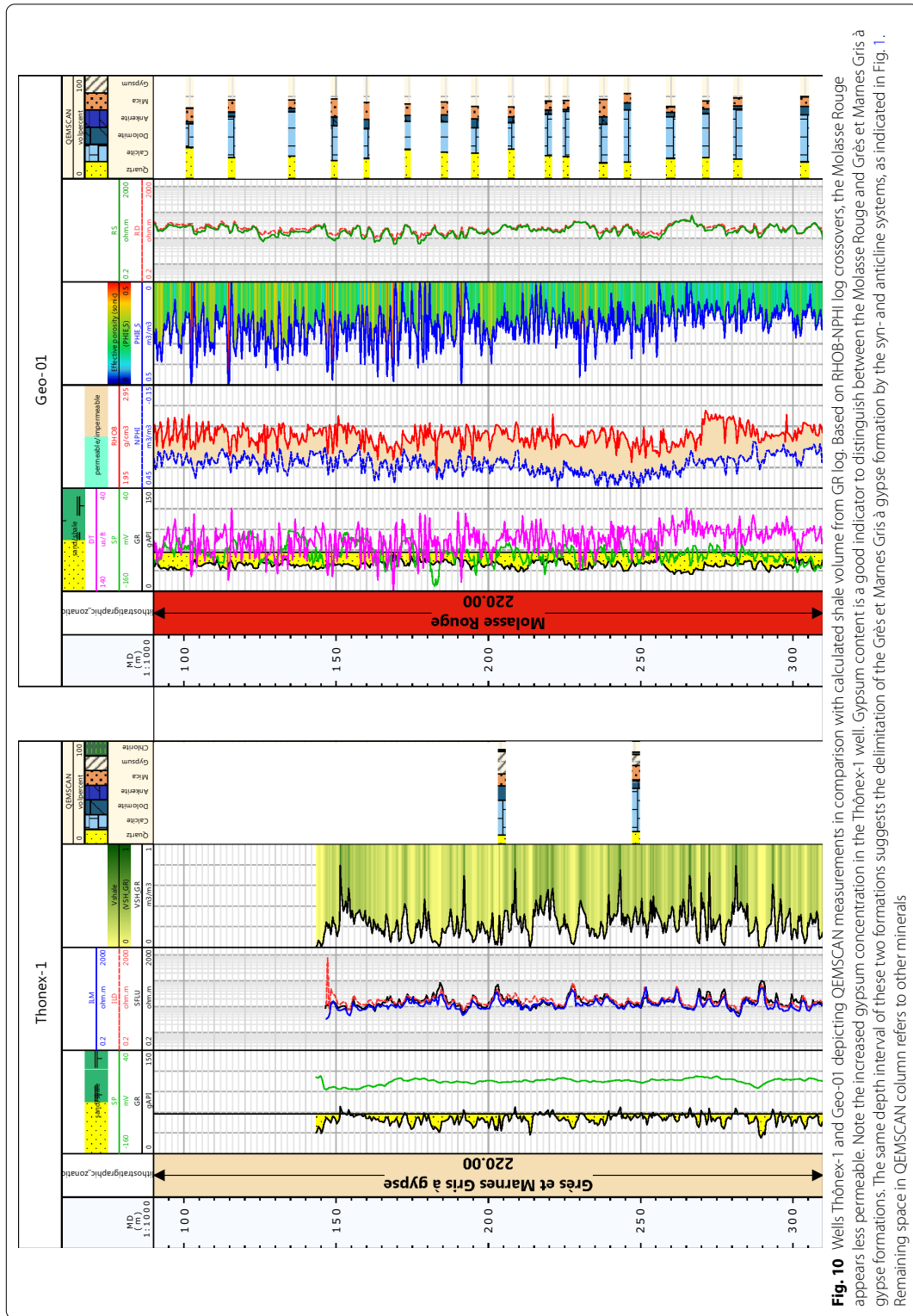
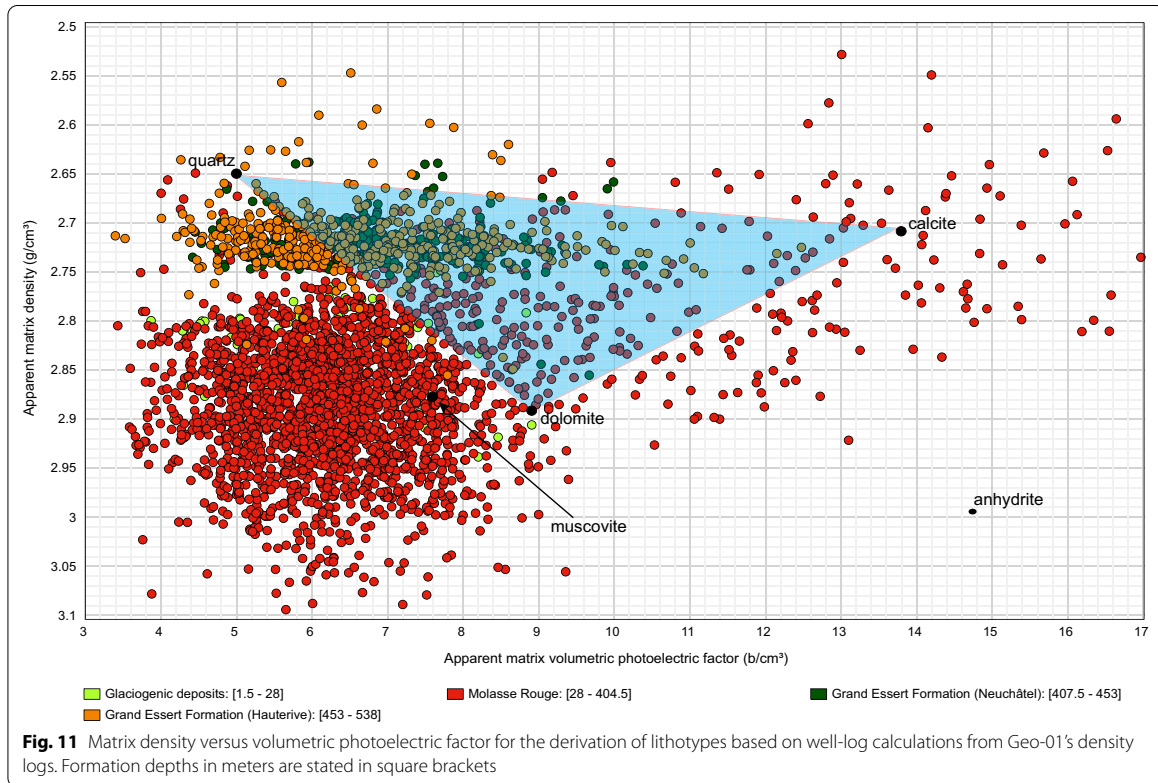


Fig. 9 Wells Geo-02, Gex-CD-07 and Gex-CD-04 showing mineralogical measurements in comparison to calculated shale volume from GR log





are caused by depositional or erosional processes. The post-glacial sediments are mostly fluvial and lacustrine and show a harder consistency, while the LGM moraines depict till and show a more loose but sticky consistency.

Interglacial deposits were formed between the glacial periods in the Late/Middle Pleistocene and occur either in cemented or unconsolidated form, while post-glacial deposits overlay these interglacial deposits. The latter consist of coarser gravel and sand, also commonly referred to as *Alluvion Ancienne*, which overlay fine-grained sediments in e.g. the Montfleury-2 well (Wegmüller et al., 1995). The post-glacial deposits consist of thick packages of variably cemented coarse gravel and sand, most likely deposited in a pro-glacial fluvial environment. These deposits are in-situ intercalated with dark-grey, clayey mudstones with traces of pollen.

GR logs show a tendency towards sandy intervals (low values) compared to the underlying Molasse Rouge, similar to the unconsolidated glacial sediments. Related DT logs show high values of 120 $\mu\text{s}/\text{ft}$, indicating loose, unconsolidated characteristics of these deposits. However, most logs show erroneous values

since their data processing and theoretical analyses are based on consolidated rather than loose and unconsolidated rock.

4.1.14 Topsoil

Holocene (recent) topsoil commonly marks the first 2 m of wells, represented by gravelly to sandy, unconsolidated material. Among the well reports depicting topsoil descriptions over a period of 70 years, two terms are interchangeably used: the term "colluvium" referred to a mixture of eroded, unconsolidated slope deposits, while the obsolete term "alluvium" was used to indicate fluvial deposits. These intervals are not logged.

4.2 Petrophysical lithotyping

Based on gamma-ray interaction logs (RHOB, PEF) and preceding calculated petrophysical parameters, lithotypes from logging curves are derived (Fig. 11) for well Geo-01 in the northern part of the basin, with a focus on the FCC's encountered Quaternary, Molasse Rouge, Grand Essert Formation's Neuchâtel and Hauterive members. A three-mineral model is assumed depicting quartz, calcite, and dolomite. The log lithotype model shows a quartz-dominated interval in the Hauterive

Member and Neuchâtel Member, with a matrix density between 2.70 and 2.75 g/cm³ and a volumetric photoelectric factor between 4 to 8 b/cm³, influenced by silty to clayey components. The Molasse Rouge formation shows a heterogeneous matrix density distribution between 2.55 and 3.13 g/cm³ with volumetric photoelectric factors of 4 up to 16 b/cm³. Occurrences of muscovite are observed in log lithotypes, and the mineral variations are well represented in the mineralogical analyses. The calcareous formation contains dolomite and calcite, which are both well captured by the PEF log. The glaciogenic deposits reflect a similar behaviour, with less variations for the matrix density ranging up to 2.95 g/cm³, and showing lesser abundance in muscovite.

5 Discussion

5.1 Geological formations encountered by the FCC

The number of geological formations possibly encountered by excavation and engineering operations for the FCC construction depends on its final tunnel alignment but is hereby established and discussed on the current layout (Abada et al., 2019) and available information. Understanding the basin's geological history is important for the FCC as it enables making reasonable assumptions and stratigraphic concept extrapolations to regions which might have not yet been investigated but would be targeted in future investigations.

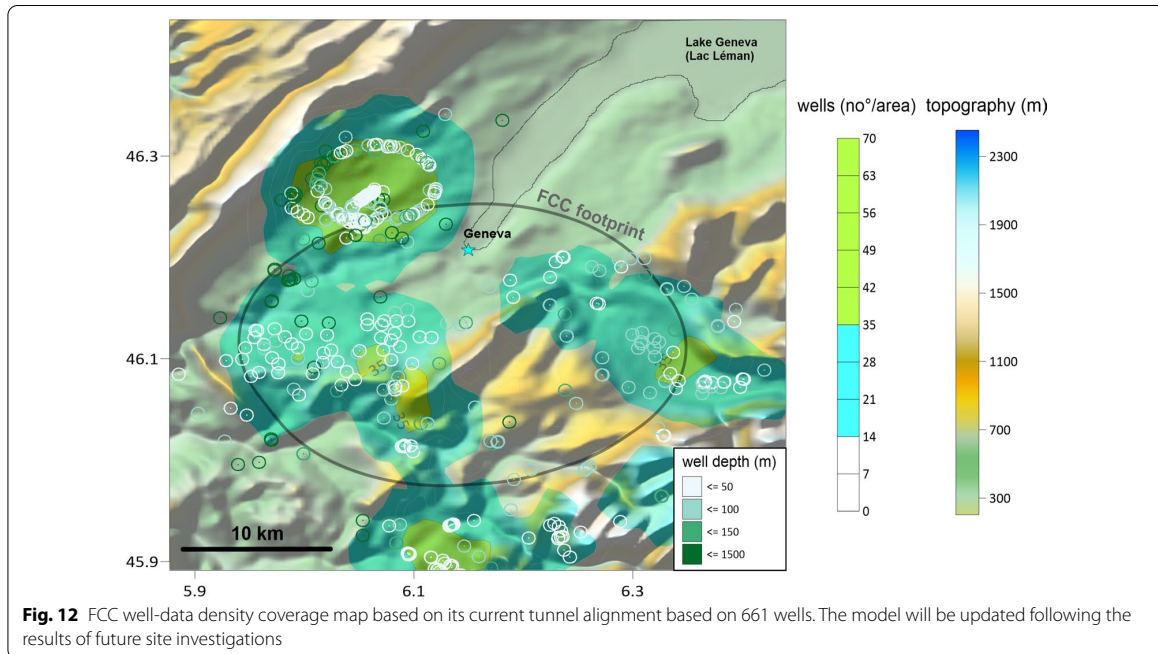
The latest feasibility phase layout ranges at depth intervals between the highest topographic level (shaft construction) and 100 to 300 m ASL (main tunnel and experimental cavern construction), and intersects 13 geological units comprising 25 lithotypes. With respect to the basin's architecture, the LFM Molasse Rouge sediments seem to overlap the Cretaceous formations in the Salève wells, while the Vuache Fault might have acted as a separation of continental and marine lithostratigraphic Molasse formations, separating the Chattian and Rupelian successions in the western part of the Geneva Basin. This suggests that the region to the west of the Salève may have been uplifted relative to the adjacent eastern Bornes Plateau (Fig. 1), potentially having caused less exposure to humid climate at the Bornes Plateau and complying with proposed influences of Molasse Rouge erosion in the literature. As depicted in Fig. 1, the Rupelian formations were deposited next to the Subalpine chain in the eastern part, substantiating the view of uplift and causing erosion in the western part. However, the encountered Siderolithic Formation, which is likely to have been eroded to the east of the Salève, indicates thickening towards the Jura in the north-west. This would infer a (shallow) marine

environment during its deposition in the hinterland of the Geneva Basin and a continental environment in its foreland, likely to be part of karstic intervals and following an extension of the model proposed by Kaelin and Kempf (2009). Considerations on geological climate conditions could be significant at this point since hydrocarbon occurrences are predominantly linked to marine conditions. The Salève wells being positioned close to the Vuache Fault, encounter reduced thicknesses of Molasse Rouge sediments compared to the northern wells. This could infer two different settings across the Geneva Basin: a predominant continental environment in the north-east and a marine one in the south-west of Burdigalian(?) age, which might have been likely connected during the Chattian leading to thick accumulations of Molasse Rouge deposits in the north-eastern part of the Geneva Basin (Moscariello et al., 2014). This might hamper the FCC construction by increased hydrocarbon accumulations in the realm of the GB towards the south-southwest, where the proposed marine environment conditions prevailed during accumulation. Furthermore, these hydrocarbon indices might follow migration paths created along fault systems such as the Vuache Fault as well as the northern syn- and anticline structures that also seem to delimit the Grès et Marnes Gris à gypse formation in the northern part of the basin.

The identified hiatus of about 72 Ma (Allen et al., 1991; Sinclair & Allen, 1992; Sinclair et al., 1991; Trümpy, 1973) separates rocks of Aptian age in the Geneva Basin (Brentini, 2018; Rusillon, 2018) from the overlying Siderolithic Formation of estimated Eocene(?) age (Charollais et al., 2007). This hiatus resulted probably from subaerial exposure and consequent development of an erosive and deep karst system at the top of the Mesozoic series, which played a predominant role in the establishment of an aquifer drainage system within Cretaceous and Jurassic limestones across the GB, and implies karstic hazards for the FCC construction at these depth intervals.

5.2 Modelling of well density

The FCC's current feasibility phase requires the evaluation of existing wells, which allow the interpolation and extrapolation (modelling) of geophysical well-log data, stratigraphic information, and laboratory analyses to deduce subsurface information on regions with low or no data coverage. The modelling result aims for optimal well placement as part of upcoming site investigations. Consecutive site investigations are planned to narrow down final shaft placement and surface installations. Well density coverage modelling is based on wells located within a 2 km radius of the



FCC's current layout. Therefore, for this model wells located within the FCC ring perimeter and along a lateral extension of up to 2 km outside of the ring have been accounted for, filtered for a minimum depth of 10 m from topographic level to 300 m ASL (Fig. 12). There is a distinct lack of wells between the southernmost point (Jura, "Mandallaz limestone") and the easternmost point at the Bornes Plateau (Fig. 1), as well as to the east of Lake Geneva along the FCC footprint. It is suggested that future site investigations, e.g. seismic surveys and drilling campaigns, should first aim for these areas. Relevant correlation and laboratory data from this study should then be integrated with the gathered measurements. Assuming the encountered stratigraphy and similar rock behaviour, no additional laboratory analyses would have to be conducted, as the information compiled for this study is abundant.

5.3 Lithotype analysis

Based on rock core samples and well reports, the topsoil, post- and interglacial unconsolidated deposits comprise a mixture of conglomerate and sandy-gravelly clay of fluvio-glacial origin. The lithotypes associated to the Molasse Rouge formation consist of irregular alternations of sandstone, often bearing hydrocarbons (Figs. 7, 8), siltstone and claystone (Figs. 8, 13), divided into an upper sandstone succession (Upper Chattian)

and a lower clay-limestone succession (Lower Chattian), as well as layers of anhydrite/gypsum, then transitioning into pure limestone lithotypes in the underlying Mesozoic units of the Jura. The Grès et Marnes Gris à gypse comprises higher amounts of anhydrite/gypsum and shows higher volumes of limestone lithotypes (Fig. 13) in the northern part of the FCC construction area compared to the Molasse Rouge. The Siderolithic Formation and Transition zone consist of beige sandstones and karstic breccias with carbonate elements of the substratum embedded in clayey sands. The Cenozoic Neuchâtel and Hauterivian members of the Grand Essert Formation feature massive limestones and ochre, bioclastic, glauconitic marls. Karstic limestones are encountered in the Cretaceous Vallorbe Member of the Rocher des Hirondelles Formation towards the FCC's southern construction area. The goal of the sand-silt-clay model (Fig. 14) was to derive estimate volumes of sand, silt and dry clay, as well as respective clay bound water and formation water solely based on well-logs to set them into context with lithotypes derived from cores. This also includes qualification of the clay type, i.e. dispersed, laminated, or structural, to correlate and associate the quantified volume with swelling clays in both the Molasse Rouge and Grès et Marnes Gris à gypse formations.

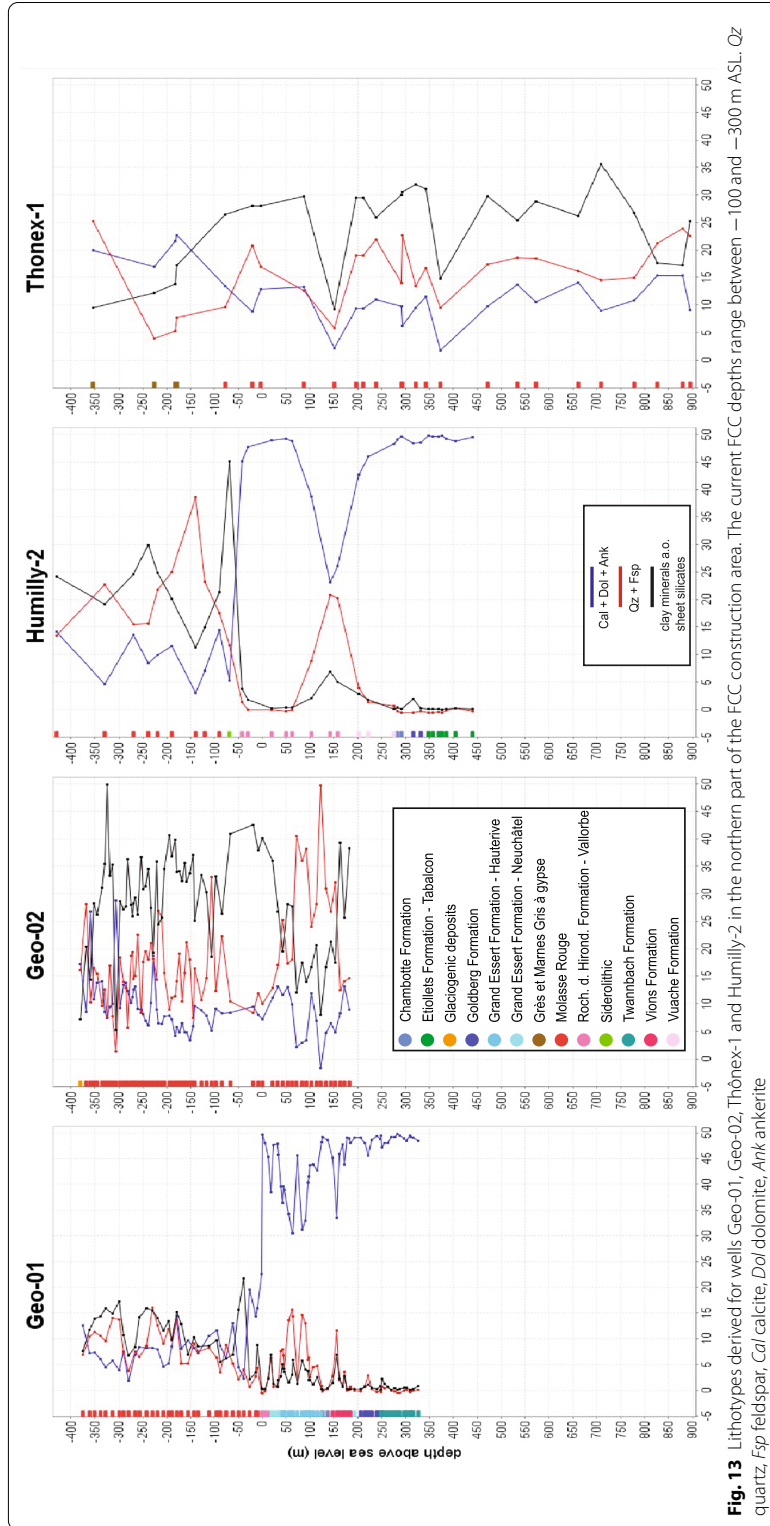


Fig. 13 Lithotypes derived for wells Geo-01, Geo-02, Thonex-1 and Humilly-2 in the northern part of the FCC construction area. The current FCC depths range between -100 and -300 m ASL. Qz quartz, Fsp feldspar, Cal calcite, Dol dolomite, Ank ankerite

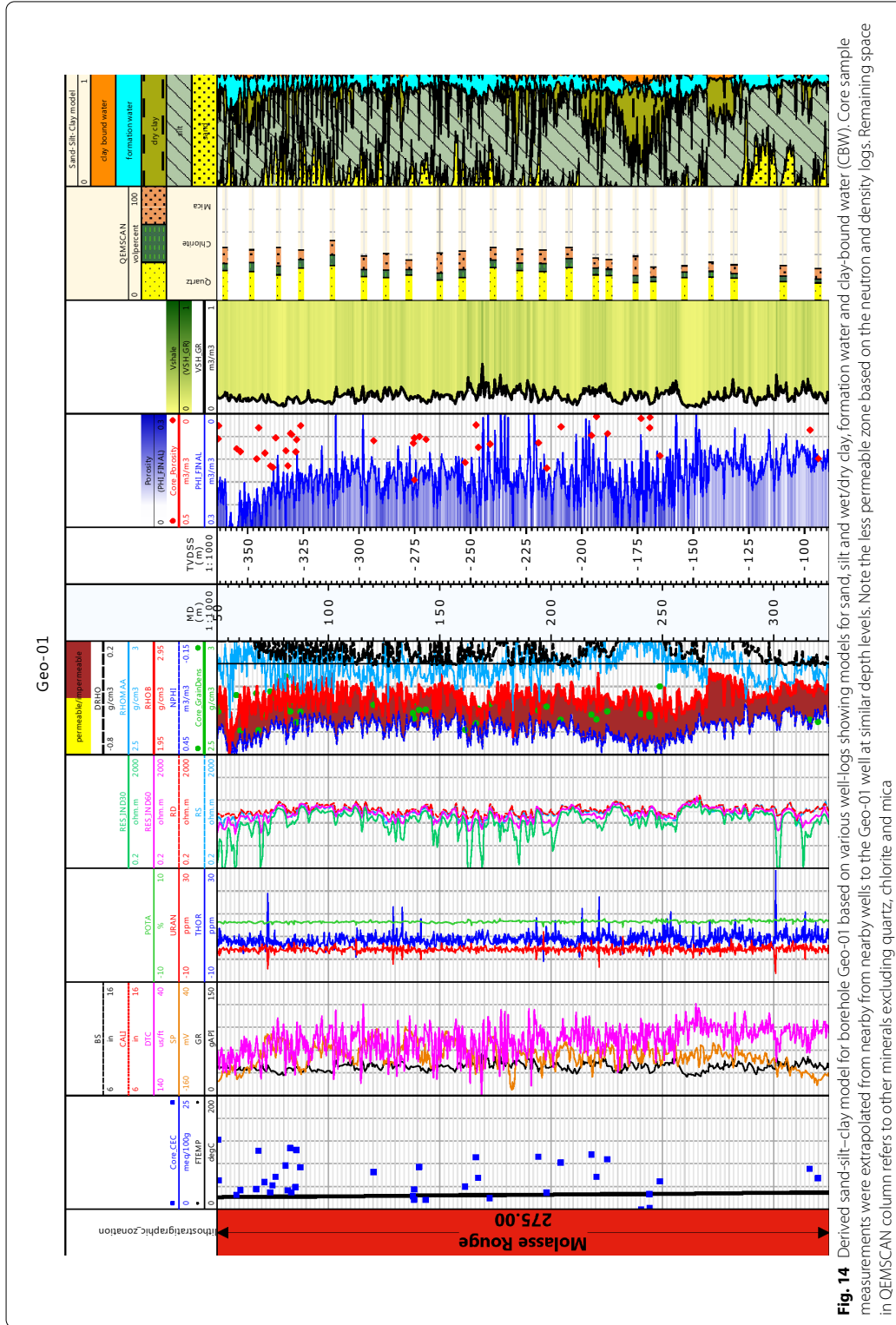
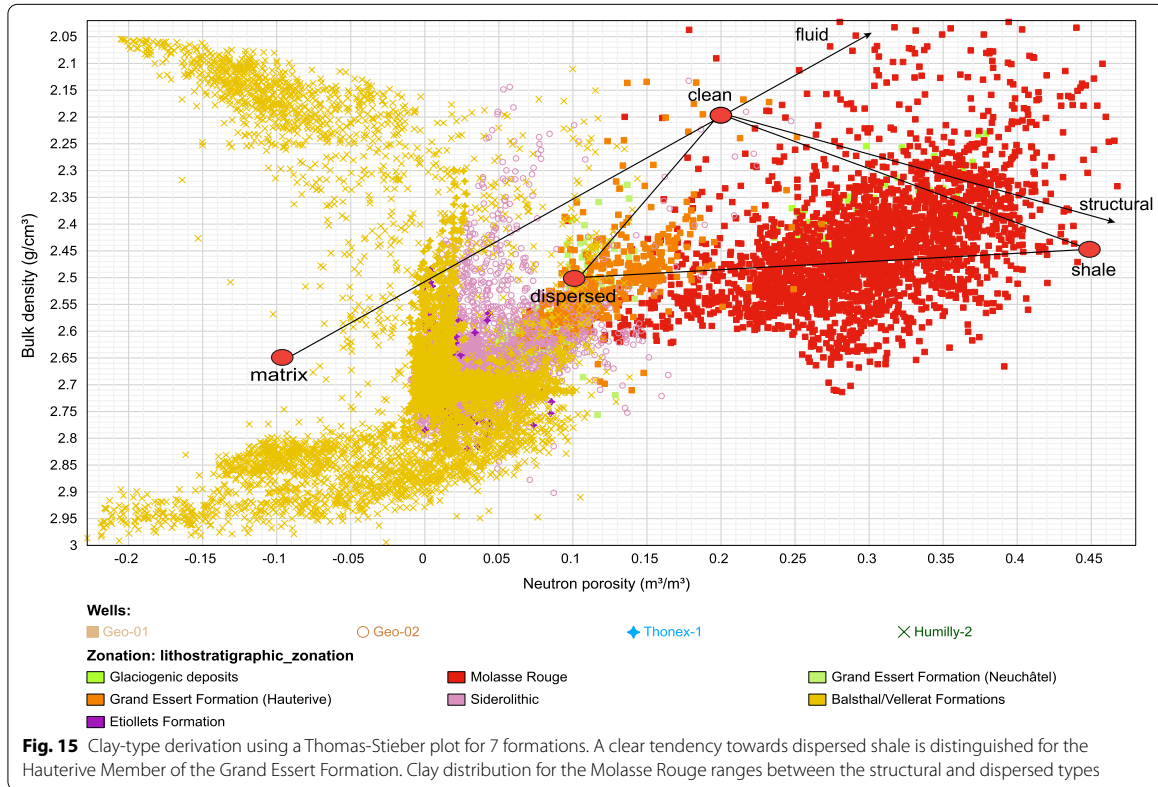


Fig. 14 Derived sand-silt-clay model for borehole Geo-01 based on various well-logs showing models for sand, silt and wet/dry clay, formation water and clay-bound water (CBW). Core sample measurements were extrapolated from nearby wells to the Geo-01 well at similar depth levels. Note the less permeable zone based on the neutron and density logs. Remaining space in QEMSCAN column refers to other minerals excluding quartz, chlorite and mica

Required inputs are neutron porosity, bulk density, true formation resistivity, flushed zone resistivity, formation temperature and water resistivity. The model is calculated based on available well-logs, petrophysical and geochemical laboratory data for well Geo-01 located in the northern part of the FCC construction area and shows high amounts of clay-bound water at depth intervals from 130 to 140 m ASL and 150 to 200 m ASL, together with a moderate amount of sand. Clay-bound-water decreases upwards towards ground level. Water content (formation water) remains constant from 375 to 80 m ASL but shows increased values between 70 and 20 m ASL, together with higher sand and reduced silt and clay content. The log solid rock volumes seem to correlate well with mineralogical analyses, also with respect to their volumes. This might suggest financial savings for upcoming FCC site investigations, as a first estimate of such a sand-silt-clay model and respective excavation volume estimates could be based on robust and proven well-logging analysis during site investigations prior to any laboratory analyses. QEMSCAN and sand-silt-clay model results follow similar trends in the Molasse Rouge: while QEMSCAN shows higher amounts of quartz, the

model includes all (clean) minerals making up sandstone, i.e. quartz. The high amount of silt could be associated to the indication of impermeable intervals in the NPHI-RHOB plot, as well as V_{sh} log calculations depicting a similar trend. Based on the derivation of clay type (Fig. 15) for subsequent logging analysis, this confirms the applicability of a solid predictive approach based purely on well-logs, neglecting mineralogical analyses, and requiring CEC, core porosity and core grain density measurements, which have already successfully been measured and could be taken as proxies for future investigations. CEC measurements proved to be useful for the calculations of exchange cations per unit pore volume (Q_V). At present, lithotyping solely based on petrophysical analyses would suggest successful log calibration applied to compensate for the Molasse Rouge's heterogeneity and adequately define sandstone- and shale-bearing intervals. A clear distinction between the Molasse Rouge and Grès et Marnes Gris à gypse could not be established without explicit laboratory data since the difference of SP values by -20 mV reflects the error to be overcome by mineralogical analyses. The Molasse Rouge tends between dispersed and structural shale,



with single samples showing clean zones. The Mesozoic clayey limestones show lesser content in clay.

5.4 Geological hazards

The FCC’s geological hazards are stated in Table 2, which provides a list of ascertained occurrences of swelling rocks, hydrocarbon-bearing and karstified intervals, active faults, and water aquifers based on a lithostratigraphic subdivision of the subsurface. The identification of geological hazards is discussed below and would impact all subsequent project phases spanning over a period of over roughly ten years. As such, these factors would affect environmental impact assessment in the current feasibility phase, optimal well placement prior to site investigations in the technical design phase, and excavation progress during the construction phase.

5.4.1 Swelling rocks

When dry clay is subjected to water, swelling occurs in two phases based on a layer structure, charge and exchangeable cations of clay minerals, i.e. smectite (montmorillonite). The first phase describes intra-crystalline swelling due to hydration of exchangeable

cations, while the second phase, osmotic swelling, stems from the difference of ion concentrations at the clay mineral surface compared to a lower concentration in the pore water solution. These two types of clay swelling are reversible, whereas the irreversible third type refers to anhydrite swelling incorporating water by the formation of gypsum. Intra-crystalline and osmotic swelling cause a volume increase of up to 200% (Jas-mund & Lagaly, 1993), while anhydrite swelling depicts volume increases up to 61% (Anagnostou, 2007; Steiner, 1993). In tunnelling, swelling is mostly associated with osmotic swelling, caused by the deconsolidation of clay minerals and their subsequent incorporation of water molecules.

The Grès et Marnes Gris à gypse contains a high amount of anhydrite/gypsum (Fig. 10), potentially leading to crystalline swelling. Note that QEMSCAN analyses chemical compositions, which do not allow a differentiation between anhydrite and gypsum. This fact favours XRD analysis, which allows to distinguish anhydrite and gypsum, and furthermore allows a quantitative approach and improved identification of fine-grained particles and clay mineral analysis. Based on clay minerals’ chemical behaviour, gypsum occurs on

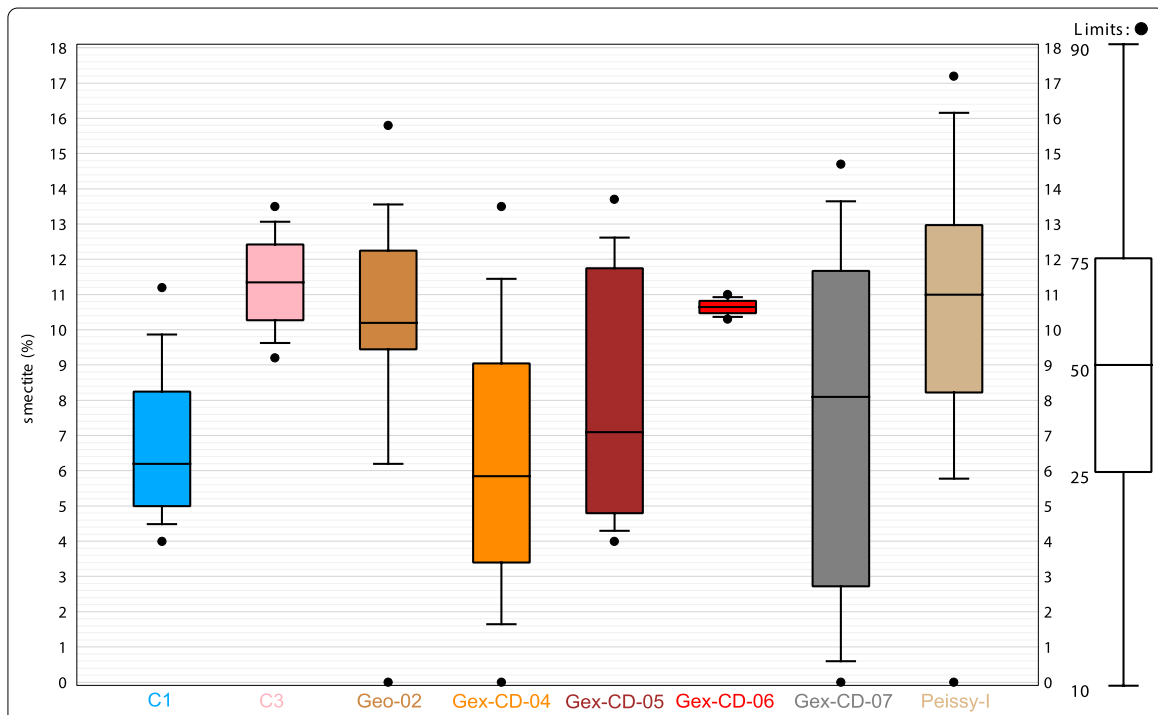


Fig. 16 Overview of swellable clay (smectite) from XRD measurements for 8 wells. The northern wells (Gex-CD-07 and Peissy-I) show a high variability, depicting maximum smectite values of 17.2%

surface while anhydrite is encountered in the subsurface (Wanninger-Huber, 2019). Anhydrite is encountered in the Savoie-104 well, and the Savoie wells as well as SPM2, SPM3 and SPM5 representing an anhydrite swelling hazard. The Balsthal/Vellerat formations might show a similar chemical composition as the Molasse Rouge for associated marl lithotypes, which bear swelling potential due to smectites, also encountered in the clayey limestone of the Etiollets Formation's Tabalcon Limestone sub-unit. The Molasse Rouge contains less anhydrite/gypsum but higher concentrations of smectite in clay, silty clay and clayey silt (Fig. 9) of up to 17.2% by volume (Fig. 16). With respect to anhydrite swelling, dedicated laboratory swelling tests are required for geotechnical design calculations of the FCC's tunnel infrastructure. Former research successfully used such swelling test results to numerically retrieve design value estimates of swelling pressures for final tunnel lining optimizations (Kovári & Vogelhuber, 2014).

Sandstone (S1–S6), mud- and siltstones (M1–M5) lithotypes show maximum Enslin-Neff water absorption of up to 58.9 wt.% (in Geo-02, Fig. 9) leading to swelling during construction. However, minimum Enslin-Neff water absorption values of 2.8 wt.% are represented by hydrophobic, hydrocarbon-bearing sandstone (HC). Detecting water absorption phenomena in geophysical well-logs is difficult, and only feasible in a qualitative manner via resistivity or neutron/density logs, potentially indicative of water/hydrocarbon-bearing rocks.

Log responses to detect swelling potential are related to (swellable) clay content in the SP log, which indicates slightly lower values in the Grès et Marnes Gris à gypse formation compared to the Molasse Rouge. This is most likely related to higher contents of anhydrite/gypsum in the Grès et Marnes Gris à gypse formation, as also measured by QEMSCAN, subjecting the type of voltage difference to the SP's membrane potential in the Molasse Rouge due to higher occurrences of clay, rather than the liquid junction potential. However, while logs might indicate qualitatively the hazard of swelling, mineralogical analyses remain crucial for its quantification. Both the Molasse Rouge and Grès et Marnes Gris à gypse formations bear a hazard for all three types of swelling.

5.4.2 Bituminous and gaseous hydrocarbons

An extensive overview of environmental thresholds for heavy-metal ions and hydrocarbons for usage and disposal of excavated rock has been reported in Haas et al. (2020a) and (b)). While these results are to be presented

in a future study, the lateral and vertical distribution of hydrocarbons are discussed from a stratigraphic point of view along the two cross sections (Figs. 5, 6).

Substantial amounts of hydrocarbons are detected in the massive dolostones in the Goldberg and Twannbach formations and are encountered in all wells featuring these two formations. The Vions Formation shows indices of hydrocarbons, as shared with the Grand Essert Formation's Neuchâtel Member. Although hydrocarbons occur predominantly as bitumen, well Geo-01-DAS located about 300 m next to the deeper Geo-01 well, shows the presence of gaseous hydrocarbons in the Molasse Rouge. This suggests that gas-bearing (hydrocarbon) horizons are likely to be encountered in the northern part of the construction area and should be addressed during site investigations. Cretaceous carbonates show indications of heavier oil and asphalt if they are fractured. With respect to their total well depths, the Gex-CD-01 and its neighbouring Gex-CD-07 well show the highest hydrocarbon indices in medium to coarse-grained sandstones in the Molasse Rouge (HC lithotype, Fig. 4) and in Mesozoic limestone formations (Fig. 5). For cross section B, all wells show indices of hydrocarbons (bitumen) with larger amounts in the Geo-01, Geo-02, and Salève-2 wells (Fig. 6). No traces of gas were observed in the cored intervals of the Gex wells. This suggests local gas accumulations rather than laterally extensive gas horizons and complies with minor industrial hydrocarbon exploration success across the basin in the past. In some rare occurrences (e.g. well L134B), the Quaternary deposits also contain bituminous hydrocarbons.

An increasing trend of large amounts of accumulated hydrocarbons is interpreted from south to north across the basin since the northern wells (Gex-CD-01, Gex-CD-07, Peissy-I, SLHC-wells, C-wells) contain most of the hydrocarbons within the studied area. An exception is marked by the Thônex-1 well, which, in the same area, crosses large amounts of the Grès et Marnes Gris à gypse formation. However, the Grès et Marnes Gris à gypse does not explicitly exclude hydrocarbon occurrences. Apart from the Molasse Rouge, deeper carbonate formations in the former *Urgonien* facies (Lower Cretaceous), Muschelkalk (Middle Triassic) and Buntsandstein sandstone (Lower Triassic) also show hydrocarbon indices in wells Chatillon-1 and Charmont-1, close to the Jura in the northwestern sector of the FCC's construction area. While these units are not primarily ranging within the projected FCC construction depths, adjacent faults might represent potential migration pathways for hydrocarbons toward the FCC depth intervals.

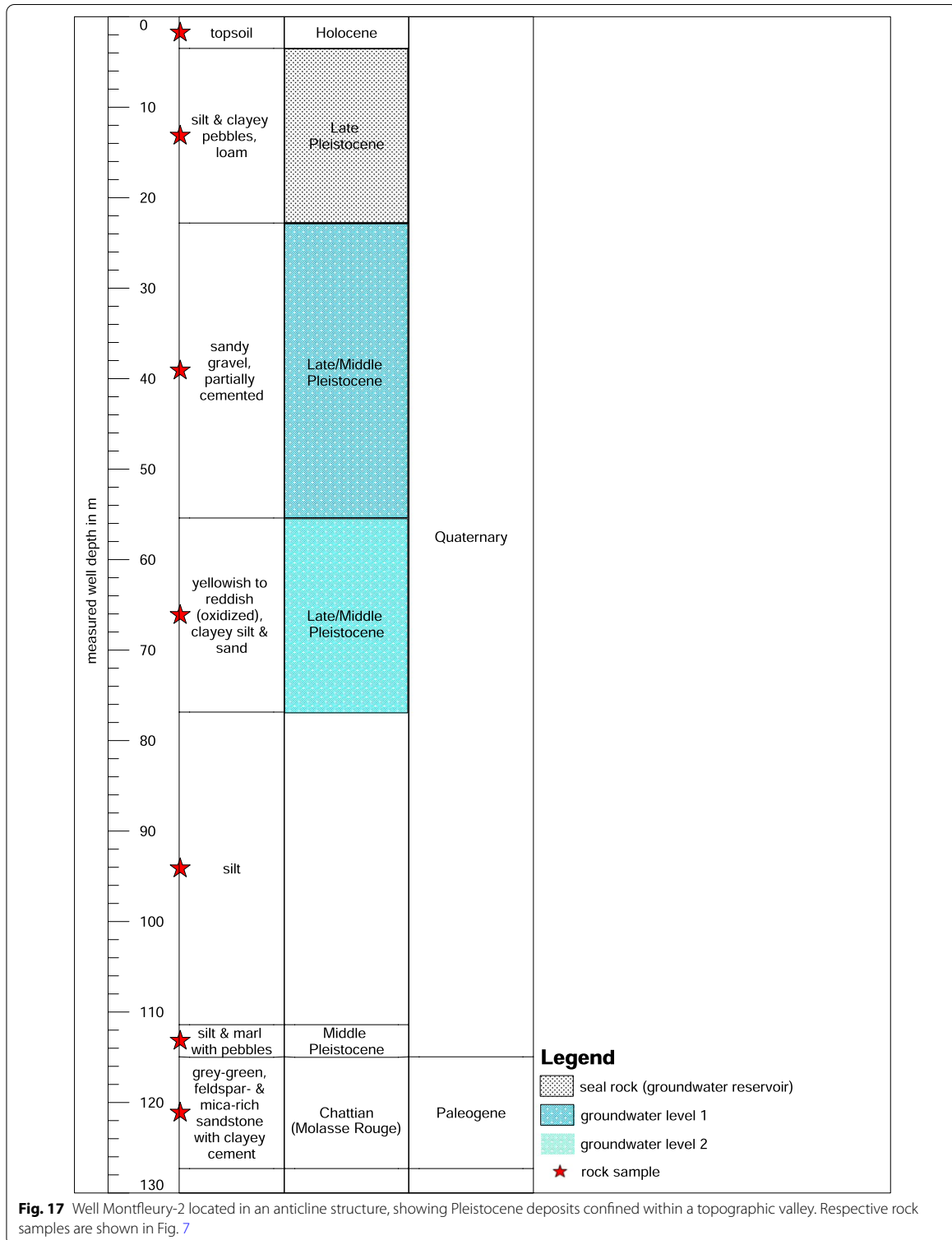


Fig. 17 Well Montfleury-2 located in an anticline structure, showing Pleistocene deposits confined within a topographic valley. Respective rock samples are shown in Fig. 7

5.4.3 Karstified intervals

Karst created a significant litho-technical hazard during LEP subsurface construction in the 1970's, substantiated in documentation from SPM wells. Reports of Salève wells document rapid loss of mud circulation into fractured limestones, which finally caused a forced well closure (Conrad & Ducloz, 1977; Géotechnique Appliquée Dériaz & SA (GADZ), 1981b, 1982b). This leads to the assumption that karst formations are not restricted to the northern FCC construction area but could be encountered also in fractured limestone formations in the south. Both the Chambotte Formation and Transition zone imply karstic occurrences, not necessarily excluding characteristics like those encountered in the porous Siderolithic Formation (Fig. 8). The Twannbach Formation, the Roches des Hirondelles Formation's Vallorbe Member, the Vions Formation and the Grand Essert Formation's Neuchâtel Member represent a substantial hazard for karst, extending across several tens of meters vertically. Since the FCC's current layout runs at several depth intervals through the Transition zone, geophysical seismic surveys should be conducted targeting these formation.

5.4.4 Fault structures and water aquifers

The FCC's current footprint crosses several active faults, synclines and anticlines, which bear a certain geological hazard of inducing an active stress regime around the tunnel perimeter during construction. This goes along with hydrocarbon migration paths along fault and fracture networks, which could lead to environmental contamination. The identification of faults and associated hydrocarbon migration paths should be investigated by future (3D) seismic surveys. One of the main active faults is represented by the sinistral strike-slip Vuache Fault in the southwestern corner of the FCC's planned construction area (Fig. 1). Another offset in geological formations is shown by the Subalpine Thrust, which per se is not active but indicates a displacement in the spatial arrangement of encountered formations. The syn- and anticline structures observed in the northern part of the proposed FCC perimeter do not reflect an active fault scenario. However, their geological trend is suggested to be studied with more accuracy, since it would allow better prediction of the Grès et Marnes Gris à gypse lateral and vertical distribution, a formation prone to swelling, as well as the distribution of unconsolidated glaciogenic deposits that are captured in between syn- and anticlines and that presently host important groundwater reservoirs. The large erosional valleys located at the Valley of Aire and at Petit Lac in the northern part of the FCC area are filled with unconsolidated, clayey sediments, usually referred to as mudstone of postglacial origin (Fiore et al.,

2002; Moscariello et al., 1998), and would pose a substantial hazard for the FCC shaft construction due to affected groundwater aquifers (Fig. 17). The Quaternary deposits represent one of the main water reservoirs in the Geneva Basin towards the northern part of the FCC construction, in close vicinity to syncline and anticline structures. Above these deposits, impermeable Late Pleistocene sediments seal the water reservoirs.

6 Conclusions

This study aims to provide the basis for a vast set of engineering and environmental undertakings as part of the Future Circular Collider project commissioned by the European Organization for Nuclear Research (CERN) in the Geneva Basin across the Swiss-French border. The objectives were to identify the geological formations in the subsurface of the Geneva Basin and link them to the geo-engineering construction of the FCC to address geological hazards and encountered lithotypes. A multidisciplinary approach was chosen by carrying out petrological, mineralogical and geochemical laboratory analyses from available rock cores in conjunction with digitized geophysical well-log analyses.

The geographically defined Geneva Basin consists in chronostratigraphic order of Holocene topsoil, Quaternary post-glacial deposits and LGM moraines, inter-glacial and pre-glacial sediments, which overlie the Oligocene Molasse Rouge and Grès et Marnes Gris à gypse (LFM) followed by the Eocene(?) Siderolithic Formation. The Transition zone (Perte-du-Rhône Formation?) marks the currently researched Cenozoic-Mesozoic stratigraphic boundary, before encountering the Jura units represented by the Cretaceous Vallorbe Formation, the Hauterive and Neuchâtel Members of the Grand Essert Formation and the Gorges de l'Orbe Formation (former *Urgonien*, Early Cretaceous) as well as the Vuache, Chambotte, Vions, Pierre-Châtel and Goldberg formations. The Twannbach, Etiollets and currently debated Balsthal and Vellerat formations complete the Jurassic units of the Jura. The FCC' stratigraphic evaluation revealed 13 geological formations excluding the Goldberg, Chambotte, Pierre-Châtel and Twannbach formations as well as the Etiollet Formation's Tabalcon Limestone sub-unit, the Blanc Limestone, Balsthal and Vellerat formations, and comprises 25 different lithotypes. A distinct lack of data remains in the western to south-western subsurface portions of the FCC's proposed construction area.

Associated geological hazards include karstic intervals in the Grand Essert Formation's Neuchâtel Member, Roches des Hirondelles Vallorbe Member and Vuache Formation associated to fractured limestone lithotypes, and Cenozoic formations represented by

the clayey sandstone-bearing Transition zone and Siderolithic Formation. The Molasse Rouge and Grès et Marnes Gris à gypse formations show presence of hydrocarbons and swelling potential due to smectite and anhydrite/gypsum occurrences, making these formations the most crucial ones for prevention of possible tunnelling issues. Hydrocarbon occurrences bear an environmental hazard encountered across all wells, mostly in the Molasse Rouge and Mesozoic formations, predominantly associated with fractured limestone. The Molasse Rouge was described and identified in north–south cross sections and divided into an upper sandstone-dominated and a lower clayey limestone succession, both of Chattian age. Encountered hydrocarbons are associated prevalently with the sandstone succession. The adopted interdisciplinary approach allowed to ascertain a set of geological hazards that may influence the projected engineering undertakings and environmental impact assessment for the FCC's final layout and subsequent technical design phase. The findings stipulate a robust predictive approach for large-scale subsurface construction and lithotyping, aimed at establishing a knowledge base for potential application scenarios of excavated material and engineering rock classifications. Moreover, future studies should also involve the careful investigation of rock mechanics data to derive geotechnical design calculations for the FCC's tunnel infrastructure.

Acknowledgements

The authors would like to thank the *Swiss Federal Office of Topography (Swisstopo)*, namely Dr. Peter Hayoz, for the permission of inspecting the core material at the Swiss core facility in Hochdorf (Switzerland). Company *TOTALEnergies* and its associated core facility service *STC (Carothèque)* represented by Gilles Graffin are kindly thanked for providing the well cores and enabling us to perform the rock core inspections under very welcoming conditions in Bousens (France). The *Services Industriels de Genève (SIG)* is sincerely thanked for the provision of geophysical well-logs for boreholes Geo-01 and Geo-02. Pieter Mattelaer and Jérémy Voiron are thanked for their administrative permissions to investigate the well cores stored at *CERN's HL-LHC Point 1* site. Anticipated gratitude is indebted to Dr. Michael Benedikt (CERN) for granting financial support on behalf of the FCC study to travel to respective core facilities. Finally, the first author would like to thank Ross Crain, PEng, for his valuable input. The results presented herein are part of the first author's PhD thesis conducted within the scope of the FCC study at CERN, Montanuniversität Leoben, ETH Zurich and the University of Geneva.

Authors' contributions

MH set up the concept together with AM, performed the data digitisation, rock core inspections and descriptions in the field, all laboratory analyses, corresponding data analysis (except for XRD and QEMSCAN raw data analysis) and full data interpretation, modelling, petrophysical calculations, all visualizations (except for the redrawn stratigraphic log of well Gex-CD-01), writing of the original draft as well as reviewing and editing of the manuscript. DC drew the stratigraphic log of Gex-CD-01. DV supervised the first author in editing the manuscript. MP performed the XRD raw data analysis, supervised the first author in the laboratory analyses performed at ETH Zurich (XRD, CEC, Enslin-Neff, ICP-OES), as well as reviewed and validated the manuscript. ADH performed the QEMSCAN raw data analysis, supervised the first author in QEMSCAN interpretation and validated the manuscript. AM set up the concept

together with MH, supervised during the stratigraphical, sedimentological and porosity-permeability interpretation as well as validated the manuscript.

Funding

This study has received funding from the European Union's Horizon 2020 research and innovation programme under grant agreement No. 951754.

Availability of data and materials

The datasets generated and/or analysed during the current study are available in the supplementary material. Geophysical well-log data are available from the corresponding author upon request, but certain third-party restrictions apply (SIG, GESDEC, CERN, UNIGE). The resulting Techlog (Schlumberger software) file used for well-log analysis is also available upon request of the corresponding author. The data have been partly published on the ZENODO platform (www.zenodo.org) under DOI's <https://doi.org/10.5281/zenodo.4725585>, <https://doi.org/10.5281/zenodo.4725517> and <https://doi.org/10.5281/zenodo.4725558>.

Declarations

Ethics approval and consent to participate

Not applicable. No inclusion of human participants, human data or human tissue.

Consent for publication

The manuscript does not contain any individual person's data in any form.

Competing interests

The authors declare that they have no competing interests.

Author details

¹European Organization for Nuclear Research (CERN), Espl. Des Particules 1, 1211 Geneva, Switzerland. ²Subsurface Engineering, Montanuniversität Leoben, Erzherzog-Johann-Strasse 3, 8700 Leoben, Austria. ³Geo-Energy Reservoir Geology and Sedimentary Basin Analysis, Université de Genève, Rue des Maraichers 13, 1205 Geneva, Switzerland. ⁴Institute for Geotechnical Engineering (ClayLab), ETH Zurich, Stefano-Franscini-Platz 3, 8093 Zurich, Switzerland.

Received: 27 October 2021 Accepted: 19 January 2022

Published online: 03 May 2022

References

- Abada, A., Abbrescia, M., AbdusSalam, S. S., Abdyukhanov, I., et al. (2019). FCC-ee: The lepton collider. *The European Physical Journal Special Topics*, 228, 261–623. <https://doi.org/10.1140/epjst/e2019-900045-4>
- Abreu, V., & Anderson, J. (1998). Glacial eustasy during the Cenozoic: Sequence stratigraphic implications. *American Association of Petroleum Geologists Bulletin*, 82, 1385–1400. <https://doi.org/10.1306/1D9BCA89-172D-11D7-8645000102C1865D>
- Alija, S., Torrijo, F. J., & Quinta-Ferreira, M. (2013). Geological engineering problems associated with tunnel construction in karst rock masses: The case of Gavarres tunnel (Spain). *Engineering Geology*, 157, 103–111. <https://doi.org/10.1016/j.enggeo.2013.02.010>
- Allen, P. A., Crampton, S. L., & Sinclair, H. D. (1991). The inception and early evolution of the North Alpine Foreland Basin, Switzerland. *Basin Research*, 3, 143–163. <https://doi.org/10.1111/j.1365-2117.1991.tb00124.x>
- Alonso, E., Olivella, S. (2008). Modelling tunnel performance in expansive gypsum claystone. In: The 12th international conference of international association for computer methods and advances in geomechanics, 2.
- Amir, K., Philippe, S., Philippe-Hervé, L., Vincenzo, S., Bastien, H., Albert, G., Jean-Loup, R., & Bernard, P. (2020). Changes in hydrodynamic process dominance (wave, tide or river) in foreland sequences: The subalpine Miocene Molasse revisited (France). *Sedimentology*, 67, 2455–2501. <https://doi.org/10.1111/sed.12708>
- Anagnostou, G. (1993). A model for swelling rock in tunnelling. *Rock Mechanics and Rock Engineering*, 26, 307–331. <https://doi.org/10.1007/BF01027115>
- Anagnostou, G. (2007). Design uncertainties in tunnelling through anhydritic swelling rocks. *Felsbau*, 25, 48–54.

- Anagnostou, G., Pimentel, E., & Serafeimidis, K. (2010). Swelling of sulphatic claystones—some fundamental questions and their practical relevance / Quellen von sulfatführenden Tonsteinen—Themen der Grundlagenforschung und ihre praktische Bedeutung. *Geomech. Tunn.*, *3*, 567–572. <https://doi.org/10.1002/geot.201000033>
- Arn, R. (1984). Contribution à l'étude stratigraphique du Pléistocène de la région lémanique. University of Lausanne.
- Asquith, G., Krygowski, D., Henderson, S., & Hurley, N. (2004). Basic well log analysis. *American Association of Petroleum Geologists*. <https://doi.org/10.1306/Mth16823>
- Bachmann, G.H., Müller, M. (1991). The Molasse Basin, Germany: evolution of a classic petroliferous foreland basin. In: Spencer (AM) (Ed.). University Press, Oxford, pp. 263–276
- Bachmann, G. H., & Müller, M. (1992). Sedimentary and structural evolution of the German Molasse Basin. *Ecolgæ Geologicae Helvetiae*, *85*, 519–530.
- Bachmann, G. H., Dohr, G., & Muller, M. (1982). Exploration in a classic thrust belt and its foreland: Bavarian Alps, Germany. *American association of Petroleum Geologists Bulletin.*, *66*, 2529–2542. <https://doi.org/10.1306/03b5ac69-16d1-11d7-8645000102c1865d>
- Bartenstein, H. (1978). Erdolvorkommen im Molassebecken. Erdol und Kohle—Erdgas Petrochemie Ver. mit Brennstoff-Chemie.
- Becker, A. (2000). The Jura Mountains—an active foreland fold-and-thrust belt? *Tectonophysics*. [https://doi.org/10.1016/S0040-1951\(00\)00089-5](https://doi.org/10.1016/S0040-1951(00)00089-5)
- Benedikt, M., Blondel, A., Janot, P., Mangano, M., & Zimmermann, F. (2020). Future Circular Colliders succeeding the LHC. *Nature Physics*, *16*, 402–407. <https://doi.org/10.1038/s41567-020-0856-2>
- Berdugo, I., Alonso, E., Romero, E., & Gens, A. (2009). Tunnelling and swelling in Triassic sulphate-bearing rocks. Part II—case studies from Jura Mountains. *Épsilon*, *12*, 39–53.
- Berger, J.-P. (1996). Cartes paléogéographiques-palinspastiques du bassin molassique suisse (Oligocène inférieur–Miocène moyen). *Neues Jahrbuch fuer Geologie Und Palaeontologie, Abhandlungen*, *202*, 1–44.
- Blondel, T. (1984). Étude tectonique de la partie septentrionale de la montagne du Vuache (Haute-Savoie, France).
- Brenchley, P.J. (1992). A geologic time scale 1989, Geological Journal. John Wiley & Sons Ltd. Doi: <https://doi.org/10.1002/gj.3350270220>
- Brentini, M., 2018. Impact d'une donnée géologique hétérogène dans la gestion des gisements: analyse intégrée et valorisation de la stratigraphie à travers le bassin genevois (Suisse, France). Université de Genève. <https://doi.org/10.13097/archive-ouverte/unige:103409>
- Brindley, G. W., & Brown, G. (1980). *Crystal structures of clay minerals and their X-ray identification*. Mineralogical Society of Great Britain and Ireland. <https://doi.org/10.1180/mono-5>.
- Brink, H. J., Burri, P., Lunde, A., & Winhard, H. (1992). Hydrocarbon habitat and potential of Swiss and German Molasse Basin: a comparison. *Ecolgæ Geologicae Helvetiae*, *85*(3), 715–732.
- Burdin, J., Monin, N., Thalmann, C. (2017). L'utilisation des matériaux extraits des ouvrages souterrains, Entrepren. ed. DOSSIER—MATEX.
- Burkhard, M. (1990). Aspects of the large-scale Miocene deformation in the most external part of the Swiss Alps (Subalpine Molasse to Jura fold belt). *Ecolgæ Geol* (pp. 559–583). Helv. Birkhäuser Verlag.
- Burkhard, M., & Sommaruga, A. (1998). Evolution of the western Swiss Molasse basin: structural relations with the Alps and the Jura belt. *Geological Society, London, Special Publications*, *134*(1), 279–298. <https://doi.org/10.1144/GSL.SP.1998.134.01.13>
- Burri, M. (1981). Les terrasses lémaniques: Géologie. *Arch. Sui. Anthr. Gén.*, *45*, 107–115.
- Butscher, C., Huggenberger, P., & Zechner, E. (2011). Impact of tunneling on regional groundwater flow and implications for swelling of clay–sulfate rocks. *Engineering Geology*, *117*, 198–206. <https://doi.org/10.1016/j.enggeo.2010.10.018>
- Buxtorf, A. (1916). Prognosen und Befunde beim Hauensteinbasis- und Grenchenbergtunnel und die Bedeutung der Letzteren für die Geologie des Juragebirges. *Verhandlungen. Naturforschende Gesellschaft (basel)*, *27*, 185–254.
- Cederbom, C., Sinclair, H. D., Schlunegger, F., & Rahn, M. K. (2004). Climate-induced rebound and exhumation of the European Alps. *Geology*, *32*, 709–712.
- Cederbom, C., Schlunegger, F., Sinclair, H.D., van der Beek, P. (2008). Late Neogene climatic, tectonic and geodynamic(?) forcing on the European Alps recorded by the erosion history of the North Alpine Foreland Basin. *Geophys. Res. Abstr.* *10*, EGU2008-A-01147.
- Chablais, J., Moscariello, A. (2012). Coretest Systems Inc., AP-608 Automated Permeameter-Perosimeter, Operator's Quick Manual. GE-RGBA Report 2012001. University of Geneva.
- Chablais, J., Rusillon, E. (2018). Fiche Forage—GEO-01.
- Chablais, J., Savoy, L. (2019). GEO-02 (SIG)—Litholog de forage—Litholog (LLR).
- Charollais, J., Weidmann, M., Berger, J.-P., Engesser, B., Hotellier, J.-F., Gorin, G., Reichenbacher, B., & Schäfer, P. (2007). La Molasse du bassin franco-genevois et son substratum. *Archives Des Sciences.*, *60*, 59–174.
- Charollais, J., Wernli, R., Mastrangelo, B., Metzger, J., Busnardo, R., Clavel, B., Conrad, M., Davaud, E., Granier, B., Martin, M. S., & Weipmann, M. (2013). Présentation d'une nouvelle carte géologique du Vuache et du Mont de Musièges (Haute-Savoie, France) stratigraphie et tectonique. *Archives Des Sciences.*, *66*, 1–63.
- Chelle-Michou, C., Do Couto, D., Moscariello, A., Renard, P., & Rusillon, E. (2017). Geothermal state of the deep Western Alpine Molasse Basin, France-Switzerland. *Geothermics*, *67*, 48–65. <https://doi.org/10.1016/j.geothermics.2017.01.004>
- Clerc, N., & Moscariello, A. (2020). A revised structural framework for the Geneva Basin and the neighboring France region as revealed from 2D seismic data: implications for geothermal exploration. *Swiss Bull. Appl. Geol.*, *25*, 109–131.
- Clerc, N., Rusillon, E., Moscariello, A., Renard, P., Paolacci, S., & Meyer, M. (2015). Detailed Structural and reservoir rock typing characterisation of the greater Geneva Basin, Switzerland, for Geothermal Resource Assessment, World Geothermal Congress 2015. *Melbourne, Australia*. <https://doi.org/10.1002/2017EF000724>
- Cohen, K., Finney, S., Gibbard, P., & Fan, J. (2013). The ICS International Chronostratigraphic Chart. *Episodes*, *36*, 199–204. <https://doi.org/10.18814/epiiugs/2013/v36i3/002>
- Conrad, M.-A., Ducloux, C. (1977). Nouvelles observations sur l'Urgonien et le Siderolithique du Salève. *Ecolgæ Geol. Helv.* *70*.
- Courboulex, F., Deichmann, N., & Gariel, J. C. (1999). Rupture complexity of a moderate intraplate earthquake in the Alps: The 1996 M5 Epagny-Anney earthquake. *Geophysical Journal International*. <https://doi.org/10.1046/j.1365-246X.1999.00931.x>
- Coretest Systems Inc. (2008). Coretest Systems Inc., Grain volume measurement system, operator's manual, supplement to operator's manual for AP-608 automated permeameter-porosimeter.
- Coretest Systems Inc. (2011). AP-608 Automated Permeameter-Porosimeter, Operator's Manual, V6g1.
- Crain, E.R. (2021). Crain's Petrophysical Handbook [WWW Document]. URL <https://spec2000.net/> (accessed 5.26.21).
- Darling, T. (2005). Well logging and formation evaluation. *First Edit. Ed. Gulf Professional Publishing*. <https://doi.org/10.1016/B978-0-7506-7883-4.X5000-1>
- Deutsches Institut für Normung (DIN) (2012). Soil, testing procedures and testing equipment—Determination of water absorption—DIN 18132.
- Deville, E., Blanc, E., Tardy, M., Beck, C., Cousin, M., & Ménard, G. (1994). Thrust propagation and syntectonic sedimentation in the Savoy Tertiary Molasse Basin (Alpine foreland). In *Hydrocarbon and petroleum geology of France* (pp. 269–280). Doi: https://doi.org/10.1007/978-3-642-78849-9_19
- Diem, B. (1986). Die Untere Meeresmolasse zwischen der Saane (Westschweiz) und der Ammer (Oberbayern). Universität Bern.
- Do Couto, D., Garel, S., Moscariello, A., Bou Daher, S., Littke, R., & Weniger, P. (2021). Origins of hydrocarbons in the Geneva Basin: Insights from oil, gas and source rock organic geochemistry. *Swiss Journal of Geosciences*. <https://doi.org/10.1186/s00015-021-00388-4>
- Doebelin, N., & Kleeberg, R. (2015). Profex: A graphical user interface for the Rietveld refinement program BGMN. *Journal of Applied Crystallography*, *48*, 1573–1580. <https://doi.org/10.1107/S1600576715014685>
- Donzeau, M., Wernli, R., Charollais, J., Monjuvent, G. (1997). Saint-Julien-en-Genevois Carte géologique de la France au 1:50 000, feuille 653 et notice explicative. BRGM, Orléans.
- Doppler, G. (1989). Zur Stratigraphie der nördlichen Vorlandmolasse in Bayrisch-Schwaben. *Geol. Bavarica*, *94*, 83–133.
- Doumer, P., British Petrol (France) (1983a). Société Française des Pétroles BP - Rapport 16.1219 de fin de sondages: Gex-CD-07 (géologie).

- Doumer, P., British Petrol (France) (1983b). Société Française des Pétroles BP - Rapport 16.1216 de fin de sondages: Gex-CD-04 (géologie).
- Doumer, P., British Petrol (France) (1983c). Société Française des Pétroles BP—Rapport 16.1214 de fin de sondages: Gex-CD-02 (géologie).
- Doumer, P., British Petrol (France) (1983d). Société Française des Pétroles BP—Rapport 16.1217 de fin de sondages: Gex-CD-05 (géologie).
- Doumer, P., British Petrol (France) (1983e). Société Française des Pétroles BP—Rapport 16.1218 de fin de sondages: Gex-CD-06 (géologie).
- Doumer, P., British Petrol (France) (1983f). Société Française des Pétroles BP—Rapport 16.1215 de fin de sondages: Gex-CD-03 (géologie).
- Doumer, P., (France), B.P., 1983. Société Française des Pétroles BP - Rapport 16.1213 de fin de sondages: Gex-CD-01 (géologie).
- Dunkl, I., & Demény, A. (1997). Exhumation of the Pannonian basin during Neogene extension. *Tectonophysics*, 272, 197–211.
- Dupuis, D. (2009). Etude des sédiments quaternaires, de la Molasse et sa tectonique, dans le Grand Lac (Leman) a partir de données sismiques 2D et 3D. Université de Genève.
- Ehrbar, H. (2008). Gotthard-Base-Tunnel—Experiences with different tunnelling methods, in: 2^o Congresso Brasileiro de Túneis e Estruturas Subterrâneas Seminário Internacional “South American Tunnelling”—2008Estruturas Subterrâneas Seminário Internacional “South American Tunnelling”—2008.
- Einfalt, H.-C., Fecker, E., Götz, H.-P. (1979). Das Dreiphasensystem Ton, Anhydrit, Gips und dessen zeitabhängiges Verhalten bei Zugabe von wässrigen Lösungen, in: 4. Internationaler Felsmechanik-Kongress, Montreux.
- Einstein, H. H. (1996). Tunnelling in difficult ground - Swelling behaviour and identification of swelling rocks. *Rock Mechanics and Rock Engineering*, 29, 113–124. <https://doi.org/10.1007/BF01032649>
- Ellis, D. V., & Singer, J. M. (2007). *Well logging for earth scientists* (2nd ed.). Springer. <https://doi.org/10.1007/978-1-4020-4602-5>
- Erdős, Z., Huismans, R. S., & van der Beek, P. (2019). Control of increased sedimentation on orogenic fold-and-thrust belt structure – insights into the evolution of the Western Alps. *Solid Earth*, 10, 391–404. <https://doi.org/10.5194/se-10-391-2019>.
- European Norm (EN) (2003). Non-destructive testing - X-ray diffraction from polycrystalline and amorphous material—Part 2: Procedures; German version EN 13925-2:2003
- Fachgruppe für Untertagebau (FGU) (2016). Bewirtschaftung und Wiederverwertung von Ausbruchmaterial—Inventar Schweizer Großprojekte. Fachgruppe für Untertagebau, Esslingen.
- Fern, E. J., Di Murro, V., Soga, K., Li, Z., Scibile, L., & Osborne, J. A. (2018). Geotechnical characterisation of a weak sedimentary rock mass at CERN, Geneva. *Tunnelling and Underground Space Technology*, 77, 249–260. <https://doi.org/10.1016/j.tust.2018.04.003>
- Fiore, J. (2007). Quaternary subglacial processes in Switzerland: Geomorphology of the Plateau and seismic stratigraphy of Western Lake Geneva. University of Geneva.
- Fiore, J., Pugin, A., & Beres, M. (2002). Sedimentological and GPR studies of subglacial deposits in the Joux Valley (Vaud, Switzerland): backset accretion in an esker followed by an erosive jökulhlaup. *Géographie Physique Et Quaternaire*, 56, 19. <https://doi.org/10.7202/008602ar>
- Forchheimer, P. (1901). Wasserbewegung durch Boden. *Zeitschrift Des Vereins Dtsch. Ingenieure*, 45, 1731.
- Frisch, W., Kuhlemann, J., Dunkl, I., & Brügel, A. (1998). Palinspastic reconstruction and topographic evolution of the Eastern Alps during late Tertiary tectonic extrusion. *Tectonophysics*. [https://doi.org/10.1016/S0040-1951\(98\)00160-7](https://doi.org/10.1016/S0040-1951(98)00160-7)
- Füchtbauer, H. (1959). Die Schüttungen im Chatt und Aquitan der deutschen Alpenvorlandmolasse. *Ecologae Geologicae Helveticae*, 73, 173–203.
- Fuller, C. W., Willett, S. D., & Brandon, M. T. (2006). Formation of forearc basins and their influence on subduction zone earthquakes. *Geology*. <https://doi.org/10.1130/G21828.1>
- Géotechnique Appliquée Dériaz & SA (GADZ) (1981a). Obturation des forages L133, L134, L134 BIS.
- Géotechnique Appliquée Dériaz & SA (GADZ) (1981b). Sondage SPM1; Sondage SPM2 (inclués SPM3 et SPM4); Sondages SPL 2.1 et 2.2; Sondage SPM5.
- Géotechnique Appliquée Dériaz & SA (GADZ) (1982b). Sondage SPL7.2; Sondage SPL8.1; Sondage SPL8.2; Sondage SPL8.7; Sondages SPL8.5 et 8.8, Sondages SPL8.9 et 8.13; Sondages SPL 8.10 et 8.12; Sondages SPL 8.14 et 8.15; Sondage SPM11; Sondage SPM15; Sondage SPM16.
- Géotechnique Appliquée Dériaz & SA (GADZ) (1982a). Sondage L135.
- Géotechnique Appliquée Dériaz & SA (GADZ) (1992). Sondage de reconnaissance SPL1.02.
- Géotechnique Appliquée Dériaz & SA (GADZ) (1993a). Projet LHC—Synthèse géologique et géotechnique—Rapport CERN-division-ST 3545/5. Geneva.
- Géotechnique Appliquée Dériaz & SA (GADZ) (1993b). Projet LHC (SLHC12).
- Géotechnique Appliquée Dériaz & SA (GADZ) (1996a). Projet LHC—LOT 1 (SLHC 20, SLHC 21, SLHC 22, SLHC 23, SLHC 24, SLHC 25).
- Géotechnique Appliquée Dériaz & SA (GADZ) (1996b). Projet LHC—LOT 3 (SLHC10, SLHC11, SLHC 42, SLHC 43, SLHC 44, SLHC 49, SLHC 50).
- Géotechnique Appliquée Dériaz & SA (GADZ) (1997). Statistique molasse (globale)—marnes standards, marnes altérées, marnes gruméleuses, marnes gréseuses, grès tendres, grès durs, grès très durs et marnocalcaires—synthèse LHC 1995–1997 (annexe 4g).
- Géotechnique Appliquée Dériaz & SA (GADZ) (2015a). High Luminosity LHC Point 1 - Sondage C2, 7222.102.
- Géotechnique Appliquée Dériaz & SA (GADZ) (2015b). High Luminosity LHC Point 1 - Sondage C4, 7222.104.
- Géotechnique Appliquée Dériaz & SA (GADZ) (2015c). High Luminosity LHC Point 1—Sondage C1, 7222.101.
- Géotechnique Appliquée Dériaz & SA (GADZ) (2015d). High Luminosity LHC Point 1—Sondage C3, 7222.103.
- Géotechnique Appliquée Dériaz & SA (GADZ) (2016a). High Luminosity LHC Point 1—Sondage C6, 7222.106.
- Géotechnique Appliquée Dériaz & SA (GADZ) (2016b). High Luminosity LHC Point 1—Sondage C7, 7222.107.
- Géotechnique Appliquée Dériaz & SA (GADZ) (2016c). High Luminosity LHC Point 1—Sondage C5, 7222.105.
- Etat de Genève (1994). Forage géothermique de Thônex—Rapport final, Géoproduction Consultants—Département des travaux publics et de l'énergie.
- Gervaise, J. (1972). *Études géologiques et géotechniques effectuées sur le site du synchrotron européen de 300 GeV—CERN/MC/61/Rev.*
- Gorin, G., Signer, C., & Amberger, G. (1993). Structural configuration of the western Swiss Molasse Basin as defined by reflection seismic data. *Ecologae Geologicae Helveticae*, 86, 693–716.
- Gorin, G., Morend, D., & Pugin, A. (2003). Bedrock, Quaternary sediment and recent fault activity in central Lake Neuchâtel, as derived from high-resolution reflection seismics. *Ecologae Geologicae Helveticae*. https://doi.org/10.1007/978-3-0348-7992-7_2
- Gottlieb, P., Wilkie, G., Sutherland, D., Suthers, S., Perera, K., Jenkins, B., Spencer, S., Butcher, A., & Rayner, J. (2000). Using quantitative electron microscopy for process mineralogy applications. *J. Miner. Met. Mater. Soc.*, 52, 24–25. <https://doi.org/10.1007/s11837-000-0126-9>
- Graf, H. R., & Burkhalter, R. (2016). Quaternary deposits: Concept for a stratigraphic classification and nomenclature—an example from northern Switzerland. *Swiss Journal of Geosciences*, 109, 137–147. <https://doi.org/10.1007/s00015-016-0222-7>
- Gross, D., Sachsenhofer, R. F., Bechtel, A., Gratzner, R., Grundtner, M. L., Linzer, H. G., Misch, D., Pytlak, L., & Scheucher, L. (2018). Petroleum systems in the Austrian sector of the north alpine foreland basin: an overview. *Journal of Petroleum Geology*. <https://doi.org/10.1111/jpg.12704>
- Gusterhuber, J., Hinsch, R., Sachsenhofer, R.F. (2014). Evaluation of hydrocarbon generation and migration in the Molasse fold and thrust belt (Central Eastern Alps, Austria) using structural and thermal basin models. American Association of Petroleum Geologists Bulletin. Doi: <https://doi.org/10.1306/06061312206>
- Haas, M., De Haller, A., Moscarriello, A., Scibile, L., Benedikt, M., Gegenhuber, N., Galler, R. (2020a). A mineralogical re-use classification model of molasse rock mass in the Geneva Basin. In: ISRM international symposium—EUROCK2020, June 14–19, 2020, Physical Event Not Held. Trondheim.
- Haas, M., Galler, R., Scibile, L., & Benedikt, M. (2020b). Waste or valuable resource – a critical European review on re-using and managing tunnel excavation material. *Resources, Conservation and Recycling*, 162, 105048. <https://doi.org/10.1016/j.resconrec.2020.105048>
- Haas, M., Mongeard, L., Ulrici, L., D'Alòia, L., Cherrey, A., Galler, R., & Benedikt, M. (2021). Applicability of excavated rock material: A European technical review implying opportunities for future tunnelling projects. *Journal of*

- Cleaner Production, 315, 128049. <https://doi.org/10.1016/j.jclepro.2021.128049>
- Haq, B. U. (2014). Cretaceous eustasy revisited. *Global and Planetary Change*, 113, 44–58.
- Haq, B. U., Hardenbol, J., & Vail, P. R. (1987). Chronology of Fluctuating Sea Levels Since the Triassic. *Science (80-)*, 235, 1156–1167.
- Hasegawa, M., Usui, M., & Gotoh, K. (1993). Geological prognosis ahead of a tunnel face. *Engineering Geology*, 35, 229–235. [https://doi.org/10.1016/0013-7952\(93\)90011-Z](https://doi.org/10.1016/0013-7952(93)90011-Z)
- Hefny, M., Zappone, A., de Makhloufi, Y., Haller, A., & Moscariello, A. (2020). A laboratory approach for the calibration of seismic data in the western part of the Swiss Molasse Basin: the case history of well Humilly-2 (France) in the Geneva area. *Swiss J Geosci*, 113, 11. <https://doi.org/10.1186/s00015-020-00364-4>.
- Herb, R. (1988). Eocaene Paläogeographie und Paläotektonik des Helvetikums. *Ecolgae Geologicae Helvetiae*, 81, 611–657.
- Hinsch, R. (2013). Laterally varying structure and kinematics of the Molasse fold and thrust belt of the Central Eastern Alps: Implications for exploration. *American Association of Petroleum Geologists Bulletin*. <https://doi.org/10.1306/04081312129>
- Homewood, P., Allen, P.A., Williams, G.D. (1986). Dynamics of the molasse basin of Western Switzerland. *Forel. Basins*, Wiley Online Books (pp. 199–217). Doi: <https://doi.org/10.1002/9781444303810.ch10>
- Huang, L., Bohne, R. A., Bruland, A., Jakobsen, P. D., & Lohne, J. (2015). Environmental impact of drill and blast tunnelling: life cycle assessment. *Journal of Cleaner Production*, 86, 110–117. <https://doi.org/10.1016/j.jclepro.2014.08.083>
- Ibele, T., 2011. Tectonics of the western Swiss Molasse Basin during Cenozoic times. *GeoFocus*.
- Jaquet, J.-M. (1966). Etude géologique de la région du Reculet. Diplôme thesis, Université de Genève.
- Jasmund, K., Lagaly, G. (1993). Tonminerale und Tone—Struktur, Eigenschaften, Anwendung und Einsatz in Industrie und Umwelt. Steinkopff Verlag, Darmstadt. <https://doi.org/10.1007/978-3-642-72488-6>
- Jenny, J., Burri, J.-P., Murali, R., Pugin, A., Schegg, R., Ungemach, P., Vuataz, F.-D., & Wernli, R. (1995). Le forage géothermique de Thônex (Canton de Genève): Aspects stratigraphiques, tectoniques, diagénétiques, géophysiques et hydrogéologiques. *Ecolgae Geologicae Helvetiae*, 88, 365–396.
- Kaelin, D. (1997). Litho- und Biostratigraphie der mittel- bis obermiozänen Bois de Raube-Formation (Nordwestschweiz). *Ecolgae Geologicae Helvetiae*, 90(1), 97–114.
- Kaelin, D., & Kempf, O. (2009). High-resolution stratigraphy from the continental record of the Middle Miocene Northern Alpine Foreland Basin of Switzerland. *Neues Jahrbuch Für Geologie Und Paläontologie - Abhandlungen*, 254, 177–235. <https://doi.org/10.1127/0077-7749/2009/0010>
- Kaelin, D., Rybach, L., Kempfer, E. H. K., Kaelin, B., Rybach, L., & Kempfer, E. H. K. (1992). Rates of deposition, uplift and erosion in the Swiss Molasse basin, estimated from sonic- and density-logs. *Bulletin Der Vereinigung Schweizerischer Petroleum-Geologen Und-Ingenieure*, 58, 9–22.
- Kafkafi, U., Xu, G., Imas, P., Magen, H., Tarchitzky, J., Johnston, A. (2001). Potassium and chloride in crops and soils: the role of potassium chloride fertilizer in crop nutrition. In: International Potash Institute. International Potash Institute, Basel, Switzerland, p. 220.
- Karner, G. D., & Watts, A. B. (1983). Gravity anomalies and flexure of the lithosphere at mountain ranges. *Journal of Geophysical Research: Solid Earth*, 88, 10449–10477. <https://doi.org/10.1029/JB088iB12p10449>
- Keller, B. (1989). *Fazies und Stratigraphie der Oberen Meeresmolasse (unteres Miozän) zwischen Napf und Bodensee*. Universität Bern.
- Keller, B. (1992). Hydrogeology of the Swiss Molasse Basin: A review of current knowledge and considerations for the future. *Ecolgae Geologicae Helvetiae*, 85, 611–651.
- Kempf, O., & Matter, A. (1999). Magnetostratigraphy and depositional history of the Upper Freshwater Molasse (OSM) of eastern Switzerland. *Ecolgae Geologicae Helvetiae*, 92, 97–103.
- Kempf, O., & Pross, J. (2005). The lower marine to lower freshwater Molasse transition in the northern Alpine foreland basin (Oligocene; central Switzerland-south Germany): Age and geodynamic implications. *International Journal of Earth Sciences*, 94, 160–171. <https://doi.org/10.1007/s00531-004-0437-0>
- Kempf, O., Bolliger, T., Kaelin, D., Engesser, B., Matter, A. (1997). New magnetostratigraphic calibration of early to middle Miocene mammal biozones of the North Alpine foreland basin. Me'm Trav EPHE Inst Montpellier (pp. 547–561).
- Kissling, D. (1974). L'Oligocène de l'extrémité occidentale du bassin molassique suisse: stratigraphie et aperçu sédimentologique. Université de Genève.
- Klinkenberg, L.J. (1941). The permeability of Porous media to liquids and gases. In: API drilling and production practices/drilling and production practices. New York (pp. 200–213).
- Kovári, K., Vogelhuber, M. (2014) Empirical basis for the design of tunnel linings in swelling rock containing Anhydrite. In: Proceedings of the World Tunnel Congress 2014—Tunnels for a Better Life. Foz do Iguaçu, Brazil (pp. 1–9).
- Kovári, K., Amstad, C., Anagnostou, G. (1987). Tunnelbau in quellfähigem Gebirge.pdf. In: Mitteilungen Der Schweizerischen Gesellschaft Für Boden- Und Felsmechanik, Frühjahrstagung 7. Mai, Biel (pp. 1–8).
- Kovári, K., Amberg, F., Ehrbar, H. (2002). Mastering of squeezing rock in the gothard base. *World Tunn* (pp 234–238).
- Kuhlemann, J. (2000). Post-collisional sediment budget of circum-Alpine basins (Central Europe). *Mem Sci Geol Padova*, 52, 1–91.
- Kuhlemann, J., & Kempf, O. (2002). Post-Eocene evolution of the North Alpine Foreland Basin and its response to Alpine tectonics. *Sedimentary Geology*, 152, 45–78. [https://doi.org/10.1016/S0037-0738\(01\)00285-8](https://doi.org/10.1016/S0037-0738(01)00285-8)
- Kuhlemann, J., Frisch, W., Székely, B., Dunkl, I., Kázmér, M., & Kazmer, M. (2002). Post-collisional sediment budget history of the Alps: Tectonic versus climatic control. *International Journal of Earth Sciences*, 91, 818–837. <https://doi.org/10.1007/s00531-002-0266-y>
- Lanterno, E., Kunzle, A., Gervaise, J., Bruderlein, J. (1981). Projet LEP—Sondages de reconnaissance: CERN SPS-SU-81-2.
- Laubscher, H. (1961). Die Fernschubhypothese der Jurafaltung. *Ecolgae Geologicae Helvetiae*, 54, 221–281.
- Lemcke, K. (1967). Zwölf Jahre Öl- und Gasförderung im süddeutschen Alpenvorland: Ein Überblick. *Bull. der Vereinigung Schweiz. Pet. Und -Ingenieure*, 33, 23–31.
- Lemcke, K. (1984). Geologische Vorgänge in den Alpen ab Obereozän im Spiegel vor allem der deutschen Molasse. *Geologische Rundschau*, 73, 371–397. <https://doi.org/10.1007/BF01820376>
- Lemcke, K. (1988). Geologie von Bayern.—I. Teil: Das bayerische Alpenvorland vor der Eiszeit. Stuttgart.
- Lemcke, K., Engelhardt, W. V., & Füchtbauer, H. (1953). Geologische und sedimentpetrographische Untersuchungen im Westteil der ungefalteten Molasse des deutschen Alpenvorlandes. *Beih. Geol. Jahrb.*, 11, 1–182.
- Li, J., Hong, A., Yuan, D., Jiang, Y., Deng, S., Cao, C., & Liu, J. (2020). A new distributed karst-tunnel hydrological model and tunnel hydrological effect simulations. *Journal of Hydrology*. <https://doi.org/10.1016/j.jhydrol.2020.125639>
- Lv, Y., Jiang, Y., Hu, W., Cao, M., & Mao, Y. (2020). A review of the effects of tunnel excavation on the hydrology, ecology, and environment in karst areas: Current status, challenges, and perspectives. *Journal of Hydrology*. <https://doi.org/10.1016/j.jhydrol.2020.124891>
- Madritsch, H., Preusser, F., Fabbri, O., Bichet, V., Schlunegger, F., & Schmid, S. M. (2010). Late Quaternary folding in the Jura Mountains: Evidence from syn-erosional deformation of fluvial meanders. *Terra Nova*. <https://doi.org/10.1111/j.1365-3121.2010.00928.x>
- Makhloufi, Y., Rusillon, E., Brentini, M., Moscariello, A., Meyer, M., & Samankasou, E. (2018). Dolomitization of the Upper Jurassic carbonate rocks in the Geneva Basin, Switzerland and France. *Swiss Journal of Geosciences*, 111, 475–500. <https://doi.org/10.1007/s00015-018-0311-x>
- Mastrangelo, B., & Charollais, J. (2018). Nouvelle conception de la structure du Salève. *Archives Des Sciences*, 70, 43–50.
- Matter, A., 1980. Flysch and Molasse of Western and Central Switzerland., in: Homewood, P., Trümpy, R. (Eds.), *Geology of Switzerland: A Guide Book. Part B Geological Excursions*. Wepf & Co., Basel, pp. 261–293.
- Mazurek, M., Hurford, A. J., & Leu, W. (2006). Unravelling the multi-stage burial history of the Swiss Molasse Basin: Integration of apatite fission track, vitrinite reflectance and biomarker isomerisation analysis. *Basin Research*, 18, 27–50. <https://doi.org/10.1111/j.1365-2117.2006.00286.x>
- Meier, L. P., & Kahr, G. (1999). Determination of the cation exchange capacity (CEC) of clay minerals using the complexes of copper(II) ion with triethylenetetramine and tetraethylenepentamine. *Clays and Clay Minerals*, 47, 386–388. <https://doi.org/10.1346/CCMN.1999.0470315>

- Mock, S., & Herwegh, M. (2017). Tectonics of the central Swiss Molasse Basin: Post-Miocene transition to incipient thick-skinned tectonics? *Tectonics*, 36, 1699–1723. <https://doi.org/10.1002/2017TC004584>
- Mock, S., Von Hagke, C., Schlunegger, F., Dunkl, I., & Herwegh, M. (2020). Long-wavelength late-Miocene thrusting in the north Alpine foreland: Implications for late orogenic processes. *Solid Earth*. <https://doi.org/10.5194/se-11-1823-2020>
- Mosar, J. (1999). Present-day and future tectonic underplating in the western Swiss Alps: Reconciliation of basement/wrench-faulting and decollement folding of the Jura and Molasse basin in the Alpine foreland. *Earth and Planetary Science Letters*, 173, 143–155. [https://doi.org/10.1016/S0012-821X\(99\)00238-1](https://doi.org/10.1016/S0012-821X(99)00238-1)
- Moscariello, A. (1996). Quaternary geology of the Geneva Bay: sedimentary record, palaeoclimatic and palaeoenvironmental reconstruction since the Last Glacial Cycle. University of Geneva.
- Moscariello, A. (2019). Exploring for geo-energy resources in the Geneva Basin (Western Switzerland): opportunities and challenges. *Swiss Bulletin for Applied Geology*, 24, 105–124.
- Moscariello, A. (2021). The Geomorphological Landscapes in the Geneva Basin. In E. Reynard (Ed.), *Landscapes and Landforms of Switzerland*. *World Geomorphological Landscapes*. Cham: Springer. https://doi.org/10.1007/978-3-030-43203-4_6
- Moscariello, A., Pugin, A., Wildi, W., Beck, C., Chapron, E., De Batist, M., Girardclos, S., Ivy Ochs, S., Rachoud-Schneider, A., Signer, C., & Van Clauwenberghe, T. (1998). Déglaciation würmienne dans des conditions lacustres à la terminaison occidentale du bassin lémanique (Suisse occidentale et France). *Eclogae Geologicae Helveticae*, 91, 185–201.
- Moscariello, A., Gorin, G., Rusillon, E., Charollais, J. (2014) Geology of Western Switzerland and nearby France in a geo-energy perspective—field trip B1 Guide Book. In: 19th international sedimentological congress Geneva, 18–22 August. p. 27.
- Moscariello, A., Guglielmetti, L., Omodeo-Salé, S., De Haller, A., Eruteya, O.E., Lo, H.L., Clerc, N., Makloufhi, Y., Do Couto, D., Ferreira De Oliveira, G., Perozzi, L., DeOliveira, F., Hollmuller, P., Quiquerez, L., Nawratil De Bono, C., Martin, F., Meyer, M. (2020). Heat production and storage in Western Switzerland: advances and challenges of intense multidisciplinary geothermal exploration activities, an 8 years progress report. In: Proceedings world geothermal congress 2020, April 26–May 2. Reykjavik.
- Neff, H.K. (2005). Der Wasseraufnahmeversuch nach Enslin-Neff in der erd- und grundbautechnischen Praxis. In: 5. Österreichische Geotechniktagung. 21.02. & 22.02.2005, Vienna (p. 27).
- Ortner, H., Aichholzer, S., Zerlauth, M., Pilser, R., & Fügenschuh, B. (2015). Geometry, amount, and sequence of thrusting in the Subalpine Molasse of western Austria and southern Germany, European Alps. *Tectonics*. <https://doi.org/10.1002/2014TC003550>
- Oxburgh, E.R. (1981). R. Trümpy geology of Switzerland: A guide-book. Part A: An outline of the geology of Switzerland. Basel and New York (Wepf & Co.), 1980. 104 pp., 46 figs., 1 coloured pl. Price Sfr. 35.00. - Part B: Geological Excursions. Ibid., 230 pp., 204 figs. Pri. Mineral. Mag. 44, 366. Doi: <https://doi.org/10.1180/minmag.1981.044.335.28>
- Paolacci, S. (2012). Seismic facies and structural configuration of the Western Alpine Molasse basin and its substratum (France and Switzerland). Université de Genève.
- Pfiffner, O.-A. (1986). Evolution of the North Alpine Foreland Basin in the Central Alps. Forel Basins, Wiley Online Books. Doi: <https://doi.org/10.1002/9781444303810.ch11>
- Pfiffner, O.-A. (2021). The geology of Switzerland (pp. 7–30). Doi: https://doi.org/10.1007/978-3-030-43203-4_2
- Pierdona, L. (2018). Chemical stratigraphy and petrography of the Molasse in the Geneva Basin (Master thesis). Université de Genève.
- Pirrie, D., Butcher, A.R., Power, M.R., Gottlieb, P., Miller, G.L. (2004). Rapid quantitative mineral and phase analysis using automated scanning electron microscopy (QemSCAN); potential applications in forensic geoscience. *Geol. Soc. London, Spec. Publ.* 232, 123 LP – 136. Doi: <https://doi.org/10.1144/GSL.SP.2004.232.01.12>
- Potter, P. E., Maynard, J. B., & Depetris, P. J. (2005). *Mud and Mudstones: Introduction and Overview*. Berlin: Springer.
- Rehbock-Sander, M., & Jesel, T. (2018). Fault induced rock bursts and micro-tremors—Experiences from the Gotthard Base Tunnel. *Tunneling and Underground Space Technology*, 81, 358–366. <https://doi.org/10.1016/j.tust.2018.07.003>
- Reichenbacher, B., Uhlig, U., Kowalke, T., Bassler, B., Matzke-Karasz, R., & Schenk, B. (2004). Biota, palaeoenvironments and biostratigraphy of continental Oligocene deposits from the south German Molasse basin (Penzberg Syncline). *Palaeontol.*, 47, 639–677.
- Rusillon, E. (2018). Characterisation and rock typing of deep geothermal reservoirs in the Greater Geneva Basin (Switzerland & France). Université de Genève. Doi: <https://doi.org/10.13097/archive-ouverte/unige:105286>
- Sachsenhofer, R.F., Leitner, B., Linzer, H.G., Bechtel, A., Čorić, S., Gratzner, R., Reichenbacher, D., Soliman, A., 2010. Deposition, erosion and hydrocarbon source potential of the Oligocene Eggerding Formation (Molasse Basin, Austria). *Austrian Journal of Earth Science*.
- Schegg, R. (1993). Thermal maturity and history of sediments in the North Alpine Foreland Basin (Switzerland, France). *Publ. du Département Géologie Paléontologie. Université de Genève*. Doi: <https://doi.org/10.13097/archive-ouverte/unige:110443>
- Schlunegger, F. (1999). Controls of surface erosion on the evolution of the Alps: Constraints from the stratigraphies of the adjacent foreland basins. *International Journal of Earth Sciences*. <https://doi.org/10.1007/s005310050265>
- Schlunegger, F., & Castellort, S. (2016). Immediate and delayed signal of slab breakoff in Oligo/Miocene Molasse deposits from the European Alps. *Science and Reports*. <https://doi.org/10.1038/srep31010>
- Schlunegger, F., & Hinderer, M. (2001). Crustal uplift in the Alps: Why the drainage pattern matters. *Terra Nov.*, 13, 425–432. <https://doi.org/10.1046/j.1365-3121.2001.00374.x>
- Schlunegger, F., & Kissling, E. (2015). Slab rollback orogeny in the Alps and evolution of the Swiss Molasse basin. *Nature Communications*, 6, 8605. <https://doi.org/10.1038/ncomms9605>
- Schlunegger, F., & Mosar, J. (2011). The last erosional stage of the Molasse Basin and the Alps. *International Journal of Earth Sciences*, 100, 1147–1162. <https://doi.org/10.1007/s00531-010-0607-1>
- Schlunegger, F., Burbank, D., Matter, A., Engesser, B., & Mödden, C. (1996). Magnetostratigraphic calibration of the Oligocene to Middle Miocene (30–15 Ma) mammal biozones and depositional sequences of the Swiss Molasse Basin. *Eclogae Geologicae Helveticae*, 89, 753–788.
- Schlunegger, F., Matter, A., Burbank, D. W., & Klaper, E. M. (1997). Magnetostratigraphic constraints on relationships between evolution of the central Swiss Molasse basin and Alpine orogenic events. *Bulletin Geological Society of America*. [https://doi.org/10.1130/0016-7606\(1997\)109%3c0225:MCORBE%3e2.3.CO;2](https://doi.org/10.1130/0016-7606(1997)109%3c0225:MCORBE%3e2.3.CO;2)
- Schlunegger, F., Melzer, J., & Tucker, G. (2001). Climate, exposed source-rock lithologies, crustal uplift and surface erosion: A theoretical analysis calibrated with data from the Alps/North Alpine Foreland Basin system. *International Journal of Earth Sciences*, 90, 484–499. <https://doi.org/10.1007/s005310100174>
- Schmid, S. M., Pfiffner, O.-A., Froitzheim, N., Schönborn, G., & Kissling, E. (1996). Geophysical-geological transect and tectonic evolution of the Swiss-Italian Alp. *Tectonics*, 15, 1036–1064. <https://doi.org/10.1029/96TC00433>
- Schön, J. H. (2015). *Physical properties of rocks—fundamentals and principles of petrophysics* (2nd ed.). Elsevier B.V.
- Schulz, H. M., Sachsenhofer, R. F., Bechtel, A., Polesny, H., & Wagner, L. (2002). The origin of hydrocarbon source rocks in the Austrian Molasse Basin (Eocene-Oligocene transition). *Marine and Petroleum Geology*, 19, 683–709. [https://doi.org/10.1016/S0264-8172\(02\)00054-5](https://doi.org/10.1016/S0264-8172(02)00054-5)
- Services Industriels de Genève (SIG), 2019. *Projet Géothermie 2020—Sondage de Satigny—GEO-1-DAS*. Well Rep. GEO-01-DAS.
- Sinclair, H. D., & Allen, P. A. (1992). Vertical versus horizontal motions in the Alpine orogenic wedge: Stratigraphic response in the foreland basin. *Basin Research*, 4, 215–232. <https://doi.org/10.1111/j.1365-2117.1992.tb00046.x>
- Sinclair, H. D., Coakley, B. J., Allen, P. A., & Watts, A. B. (1991). Simulation of Foreland Basin Stratigraphy using a diffusion model of mountain belt uplift and erosion: An example from the central Alps, Switzerland. *Tectonics*, 10, 599–620. <https://doi.org/10.1029/90TC02507>
- Sommaruga, A. (1997). *Geology of the Central Jura and the Molasse Basin: New insight into an evaporite-based foreland fold and thrust belt*. Mem. la société Neuchâtel. des Sci. Nat. Université de Neuchâtel.
- Sommaruga, A. (1999). Décollement tectonics in the Jura foreland fold-and-thrust belt. *Marine and Petroleum Geology*. [https://doi.org/10.1016/S0264-8172\(98\)00068-3](https://doi.org/10.1016/S0264-8172(98)00068-3)

- Sommaruga, A. (2011). From the central Jura Mountains to the Molasse Basin (France and Switzerland). *Bulletin Für Angewandte Geologie*, 16, 63–75. <https://doi.org/10.5169/seals-327746>
- Sommaruga, A., Eichenberger, U., Marillier, F. (2012). Seismic Atlas of the Molasse Basin. Beiträge zur Geol. der Schweiz—Geophys. 64 pp. PNR61
- Sommaruga, A., Mosar, J., Schori, M., Gruber, M. (2017). The role of the triassic evaporites underneath the North Alpine Foreland. In: Permo-Triassic Salt Provinces of Europe, North Africa and the Atlantic Margins. Doi: <https://doi.org/10.1016/b978-0-12-809417-4.00021-5>
- Spiegel, C., Kuhlmann, J., Dunkl, I., & Frisch, W. (2001). Paleogeography and catchment evolution in a mobile orogenic belt: The Central Alps in Oligo-Miocene times. *Tectonophysics*. [https://doi.org/10.1016/S0040-1951\(01\)00187-1](https://doi.org/10.1016/S0040-1951(01)00187-1)
- Stauble, M., & Pfiffner, O.-A. (1991). Processing, interpretation and modeling of seismic reflection data in the Molasse Basin of eastern Switzerland. *Eclogae Geologicae Helveticae*. <https://doi.org/10.5169/seals-166767>
- Steiner, W. (1993). Swelling rock in tunnels: Rock characterization, effect of horizontal stresses and construction procedures. *International Journal of Rock Mechanics and Mining Sciences*, 30, 361–380. [https://doi.org/10.1016/0148-9062\(93\)91720-4](https://doi.org/10.1016/0148-9062(93)91720-4)
- Strasser, A., Charollais, J., Conrad, M. A., Clavel, B., Pictet, A., & Mastrangelo, B. (2016). The Cretaceous of the Swiss Jura Mountains: An improved lithostratigraphic scheme. *Swiss Journal of Geosciences*, 109, 201–220. <https://doi.org/10.1007/s00015-016-0215-6>
- Strunck, P., & Matter, A. (2002). Depositional evolution of the western Swiss molasse. *Eclogae Geologicae Helveticae*, 95, 197–222.
- Su, M., Liu, Y., Xue, Y., Cheng, K., Ning, Z., Li, G., & Zhang, K. (2021). Detection method of karst features around tunnel construction by multi-resistivity data-fusion pseudo-3D-imaging based on the PCA approach. *Engineering Geology*. <https://doi.org/10.1016/j.enggeo.2021.106127>
- Tanikawa, W., & Shimamoto, T. (2006). Klinkenberg effect for gas permeability and its comparison to water permeability for porous sedimentary rocks. *Hydrology and Earth System Sciences Discussions*, 3, 1315–1338. <https://doi.org/10.5194/hessd-3-1315-2006>
- Thalmann, C. (1996). Beurteilung und Möglichkeiten der Wiederverwertung von Ausbruchmaterial aus dem maschinellen Tunnelvortrieb zu Betonzuschlagstoffen. PhD thesis, Eidgenössische Technische Hochschule (ETH), Zurich.
- Thouvenot, F., Frechet, J., Tapponnier, P., Thomas, J. C., Le Brun, B., Menard, G., Lacassin, R., Jenatton, L., Grasso, J. R., Coutant, O., Paul, A., & Hatzfeld, D. (1998). The M(L) 5.3 Epagny (French Alps) earthquake of 1996 July 15: A long-awaited event on the Vuache Fault. *Geophysical Journal International*, 135(3), 876–892. <https://doi.org/10.1046/j.1365-246X.1998.00662.x>
- Trümpy, R. (1973). The timing of orogenic events in the Central Alps. In K. A. DeJong & R. Scholten (Eds.), *Gravity and tectonics* (pp. 229–251). Wiley.
- Uhlig, U., Reichenbacher, B., & Bassler, B. (2000). Säugetiere, Fisch- Otolithen und Charophyten aus den Unteren Cyrenen-Schichten (Oligozän) der bayerischen Faltenmolasse (Murnauer Mulde). *Eclogae geol Helv* 93:503–516. *Eclogae Geologicae Helveticae*, 93, 503–516.
- Van der Vegt, P., Janszen, A., & Moscarriello, A. (2012). Tunnel valleys: current knowledge and future perspectives. In M. Huuse, J. Redfern, D. P. Le Heron, R. J. Dixon, A. Moscarriello, & J. Craig (Eds.), *Glaciogenic reservoirs and hydrocarbon systems* (pp. 75–97). Geological Society Special Publications.
- Voiron, J., Haas, M., Amiot, J.-B. (2020). CERN HL-LHC POINT 1, Gestion des matériaux d'excavation potentiellement pollués aux hydrocarbures. AFTES Congr. Paris 2020, Sept. 6–8, 2021.
- Voit, K. (2013). Einsatz und Optimierung von Tunnelausbruchmaterial des Brenner Basistunnels, PhD thesis, Application and optimization of tunnel excavation material of the Brenner Base Tunnel. Verlag Guthmann-Peterson.
- Voit, K., Zeman, O., Murr, R., Bergmeister, K., & Arnold, R. (2015). Aufbereitung und Wiederverwertung von Tunnelausbruchmaterial beim Brenner Basistunnel. *Beton- Und Stahlbetonbau*, 110, 832–844. <https://doi.org/10.1002/best.201500023>
- Von Hagke, C., Cederbom, C. E., Oncken, O., Stckli, D. F., Rahn, M. K., & Schlunegger, F. (2012). Linking the northern Alps with their foreland: The latest exhumation history resolved by low-temperature thermochronology. *Tectonics*. <https://doi.org/10.1029/2011TC003078>
- Vrakas, A., & Anagnostou, G. (2016). Ground response to tunnel re-profiling under heavily squeezing conditions. *Rock Mechanics and Rock Engineering*, 49, 2753–2762. <https://doi.org/10.1007/s00603-016-0931-2>
- Wanninger-Huber, T. (2019). Experimental investigations for the modelling of anhydritic swelling claystones. *ETH Zurich*. <https://doi.org/10.3929/ethz-b-000369625>
- Wegmüller, S., Amberger, G., & Vernet, J.-P. (1995). La formation de Montfleury près de Genève: Etude palynologique et sédimentologique d'une séquence du Pleistocène moyen. *Eclogae Geologicae Helveticae*, 88, 595–614. <https://doi.org/10.5169/seals-167689>
- Wehner, H., Hufnagel, H., Kuckelkorn, K., Schoell, M., Teschner, M. (1983). On the genesis of hydrocarbons in the German Alpine foreland.
- Wetzel, A., Allenbach, R., & Allia, V. (2003). Reactivated basement structures affecting the sedimentary facies in a tectonically "quiescent" epicontinental basin: An example from NW Switzerland. *Sedimentary Geology*. [https://doi.org/10.1016/S0037-0738\(02\)00230-0](https://doi.org/10.1016/S0037-0738(02)00230-0)
- Whitney, D. L., & Evans, B. W. (2010). Abbreviations for names of rock-forming minerals. *American Mineralogist*, 95, 185–187. <https://doi.org/10.2138/am.2010.3371>
- Wildi, W., Corboud, P., Gorin, G., 2017. Guide : géologie et archéologie de Genève Guidebook : geology and archaeology of Geneva. Société Phys. d'histoire Nat. Genève 93.
- Willett, S. D., & Schlunegger, F. (2010). The last phase of deposition in the Swiss Molasse Basin: From foredeep to negative-alpha basin. *Basin Research*, 22, 623–639. <https://doi.org/10.1111/j.1365-2117.2009.00435.x>
- Winkler-Hermaden, A. (1958). Geologisches Kräftepiel und Landformung. *GFF*. <https://doi.org/10.1080/11035895809447260>
- Wyllie, M. R. J., Gregory, A. R., & Gardner, L. W. (1956). Elastic wave velocities in heterogeneous and porous media. *Geophysics*, 21, 41–70. <https://doi.org/10.1190/1.1438217>
- Yilmaz, I. (2001). Gypsum/anhydrite: Some engineering problems. *Bulletin of Engineering Geology and the Environment*, 60, 227–230. <https://doi.org/10.1007/s100640000071>
- Zhang, G., Germaine, J. T., Martin, R. T., & Whittle, A. J. (2003). A simple sample-mounting method for random powder X-ray diffraction. *Clays and Clay Minerals*, 51, 218–225. <https://doi.org/10.1346/CCMN.2003.0510212>
- Ziegler, P.A. (1990). Geological Atlas of Western and Central Europe, Geological Atlas of Western and Central Europe. Shell Internationale Petroleum Maatschappij B.V.
- Ziegler, H.-J., Isler, A. (2013). Zusammenfassender geologischer Schlussbericht Lötschberg-Basistunnel. Landesgeologie (Bundesamt für Landestopografie swisstopo), Wabern, Switzerland.
- Ziegler, P., & Fraefel, M. (2009). Response of drainage systems to Neogene evolution of the Jura fold-thrust belt and Upper Rhine Graben. *Swiss Journal of Geosciences*. <https://doi.org/10.1007/s00015-009-1306-4>
- Zweigel, J., Aigner, T., Luterbacher, H. (1998) Eustatic versus tectonic controls on Alpine foreland basin fill: sequence stratigraphy and subsidence analysis in the SE German Molasse. Geological Society London Special Publications. 134, 299 LP – 323. Doi: <https://doi.org/10.1144/GSL.SP.1998.134.01.14>

Publisher's Note

Springer Nature remains neutral with regard to jurisdictional claims in published maps and institutional affiliations.

B Peer-reviewed conference articles

B.1 CERN HL-LHC POINT 1, Gestion des matériaux d'excavation potentiellement pollués aux hydrocarbures

Table B.1: Overview of authorship and metadata of the presented publication.

Title	CERN HL-LHC POINT 1, Gestion des matériaux d'excavation potentiellement pollués aux hydrocarbures
Author names	Jérémy Voiron, Maximilian Haas, Jean-Baptiste Amiot
Author's contributions	Conceptualization; literature review; on-site & subsurface investigations (HL-LHC Point 1); support of visualizations; writing (original draft) for abstract, geology & discussion chapters; writing (review & editing)
Scientific value	Identification of disposal and application potential of excavated tunnel material, and a first evaluation of chemical pollutants hampering disposal explicitly at the Swiss construction lot HL-LHC Point 1.
Status	Published in <i>AFTES2020, Conference Proceedings, Paris, France</i>
Peer-reviewed proceedings	Yes
Full citation	Voiron J., Haas M., Amiot J.-B., CERN HL-LHC POINT 1, Gestion des matériaux d'excavation potentiellement pollués aux hydrocarbures, AFTES2020 Congrès, September 6-8, Paris, France, 2020 (postponed to 2021), Click HERE, referring to the AFTES2021 conference homepage , under session "Circular economy: the challenges of materials management" presented by Jérémy Voiron on behalf of all co-authors.

CERN HL-LHC POINT 1, Gestion des matériaux d'excavation potentiellement pollués aux hydrocarbures

CERN HL-LHC POINT 1, Management of excavation materials potentially contaminated with hydrocarbons

Jérémy VOIRON, *setec, Genève, Suisse*

Maximilian HAAS, *CERN, Genève, Suisse & Montanuniversität, Leoben, Austria*

Jean-Baptiste AMIOT, *setec, Lyon, France*

Résumé

Le projet de grand collisionneur de hadrons à haute luminosité (HL-LHC) prévoit la construction d'infrastructures souterraines complexes (puits, cavernes, tunnels) dans le bassin genevois. Les travaux d'excavation ont débuté en été 2018 en méthode traditionnelle au sein de la Molasse Rouge du Chattien Inférieur, ils intéressent un volume d'environ 48'600 mètres cubes de matériaux.

La Molasse, de nature très hétérogène, est constituée d'une succession de couches subhorizontales de marnes à grès potentiellement pollués par des hydrocarbures. Dans les matériaux d'excavation molassiques, des concentrations en hydrocarbures supérieures aux seuils réglementaires en vigueur dans le canton de Genève ont été mises en évidence. Leur détection est basée sur des inspections olfactives et visuelles et des analyses en laboratoire. En raison de la forte représentativité de ces matériaux pollués (de l'ordre de 30 à 35% de la quantité totale de matériaux excavés), la gestion des déblais devient un enjeu majeur dans l'organisation du projet.

Les objectifs de cet article sont de présenter les méthodes développées et mises en œuvre pour répondre à cette problématique tant en termes d'organisation qu'en termes de suivi, et de présenter un retour d'expérience quant à l'identification et à la prévision quantitative au stade des reconnaissances géotechniques. Une telle évaluation préalable constitue un enjeu essentiel pour l'étude du futur collisionneur circulaire (FCC CERN), qui prévoit le creusement d'un tunnel circulaire d'environ 100 km de long, également en grande partie dans les matériaux molassiques.

Abstract

The High-Luminosity Large Hadron Collider (HL-LHC) project involves the construction of complex underground infrastructures (shafts, caverns, tunnels) in the Geneva basin. Excavation started in summer 2018 using conventional methods within the 'Molasse Rouge du Chattien Inférieur'. They represent about 50,000 cubic metres of excavated material.

The heterogeneous Molasse consists of a succession of sub-horizontal layers of marl and sandstone polluted by hydrocarbons. Hydrocarbon concentrations in molasse excavation can be found above the regulatory thresholds of the canton of Geneva. Detection of it is based on olfactory and visual inspections and laboratory tests. Due to the extent of these polluted materials in the area (about 30 to 35% of excavated materials), spoil management becomes a critical subject in the project organization.

The objectives of this publication are to present and explain the implemented spoil management plan in terms of organization and monitoring, and to further present lessons learned in the identification and quantitative forecasting during geological surveys. Such a preliminary assessment is a key information and experience for the Future Circular Collider (FCC CERN) study. A large part of this approximately 100 km long tunnel is foreseen to develop in molasse.

CERN HL-LHC POINT 1, Gestion des matériaux d'excavation potentiellement pollués aux hydrocarbures

CERN HL-LHC POINT 1, Management of excavation materials potentially contaminated with hydrocarbons

Jérémy VOIRON, setec, Genève, Suisse

Maximilian HAAS, CERN, Genève, Suisse & Montanuniversität, Leoben, Austria

Jean-Baptiste AMIOT, setec, Lyon, France

1 Introduction

Le projet de Grand collisionneur de hadrons à haute luminosité (HL-LHC) comprend la réalisation d'infrastructures souterraines complexes dans le bassin genevois. Côté Suisse, le Point 1 (cf. Figure 1) comprend la réalisation d'un puits de 10 à 12 m de diamètre intérieur et de 60 m de profondeur (PM17), d'une Caverne de 18 m de diamètre et de 45 à 50 m de longueur (US/UW17) et d'une galerie principale de 60 m² de section et d'environ 300 m de longueur, toutes deux connectées à des galeries secondaires de 50 à 70 m de longueur (UA/UPR 13 & 17 et UL 13 & 17). La totalité des excavations réalisées en méthode traditionnelle représente un volume de 48'600 mètres cubes en place.

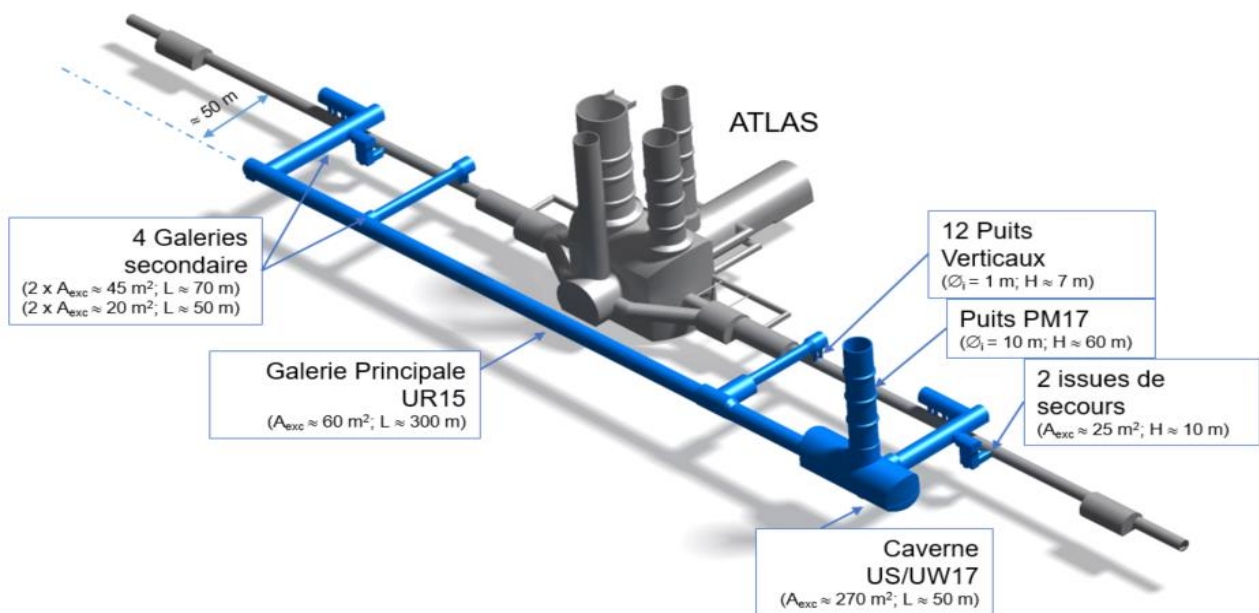


Figure 1. Structures souterraines existantes et nouvelles du CERN HL-LHC Point 1

2 La géologie au droit du projet

Le Bassin Molassique des Alpes Occidentales (Western Alpine Molasse Basin, WAMB), souvent appelé bassin de Genève, fait partie du Plateau Suisse limité par le Salève au Sud-est et le Jura au Nord-Ouest. Ces élévations géologiques particulières ont été influencées par les déformations tectoniques de l'avant-pays alpin, les glaciations associées du Pléistocène et les processus postglaciaires (Moscarello 2018).

Les zones molassiques présentes dans le bassin se développent le long des massifs du Salève, du Vuache et du Jura, et sont constituées de roches sédimentaires du Mésozoïque. La succession du Mésozoïque commence par des évaporites à la base, suivies d'une succession de calcaires et de marnes appartenant à la marge méridionale du continent européen et datant de l'océan Téthys. La séquence du Mésozoïque a été déposée au sommet du socle cristallin du Paléozoïque. Elle montre des structures de type graben remplies de sédiments siliciclastiques continentaux au Permien et au

Carbonifère, suite à l'orogénèse varisque (Moscariello et al. 2020). Le sommet de la séquence du Mésozoïque indique une vaste surface érodée formée pendant le soulèvement du bassin d'avant-pays lors de la compression de la ceinture alpine. Au-dessus de la surface érodée, des molasses siliciclastiques hétérogènes de l'Oligocène sont recouvertes de dépôts glaciaires à fluviatiles du Quaternaire, le plus souvent appelés Moraines. Les composants de la molasse ont été déposés sous forme de formations détritiques pendant l'orogénèse alpine (Trümpy et al. 1980).

Il existe deux modèles importants de classification de ces composants marneux et gréseux, basés sur la stratigraphie et l'analyse des paramètres physiques.

Une classification stratigraphique de la molasse est donnée par Trümpy (1980) selon : Molasse marine inférieure (UMM), Molasse d'eau douce inférieure (USM), Molasse marine supérieure (OMM) et Molasse d'eau douce supérieure (OSM). Dans la littérature, les abréviations de la molasse se réfèrent généralement à des termes allemands.

Les ensembles de données externalisées et recueillies par le CERN au cours des 70 dernières années ont servi à une deuxième classification géotechnique plus récente donnée par Fern et al. (2018), qui subdivise la molasse en : marnes très tendres (« very weak marl »), marnes tendres (« weak marl »), marnes moyennement tendres (« medium-weak marl »), grès tendres (« weak sandstone »), grès moyennement dur (« medium-strong sandstone ») et grès dur (« strong sandstone »). Ces différentes catégories sont basées sur la résistance à la compression uniaxiale et sur les différences dans les modules d'Young ou les limites d'Atterberg, en partie tirées des pré-études du point 1 du HL-LHC.

Ces matériaux molassiques peuvent présenter des hydrocarbures naturels. Ils sont dus à la dégradation naturelle de matières organiques produites il y a environ 25 millions d'années, lors du dépôt des formations molassiques, et peuvent concerner des lentilles ou des couches d'étendues et d'épaisseurs très variables. A noter que de telles lentilles avaient d'ailleurs déjà été rencontrées au CERN lors des travaux de génie civil pour le détecteur ATLAS (de 1999 à 2001), notamment lors de l'excavation des cavernes USA15 et UX15, avec des teneurs en hydrocarbures variant de 700 à 2800 ppm.

Ces matériaux potentiellement pollués pourraient nécessiter une dépollution pour être réutilisés dans le futur, et de ce fait, ces matériaux deviendraient une ressource pour l'industrie de la construction (Resch et al. 2009), ce qui fait actuellement l'objet d'une étude (Haas et al., soumis).

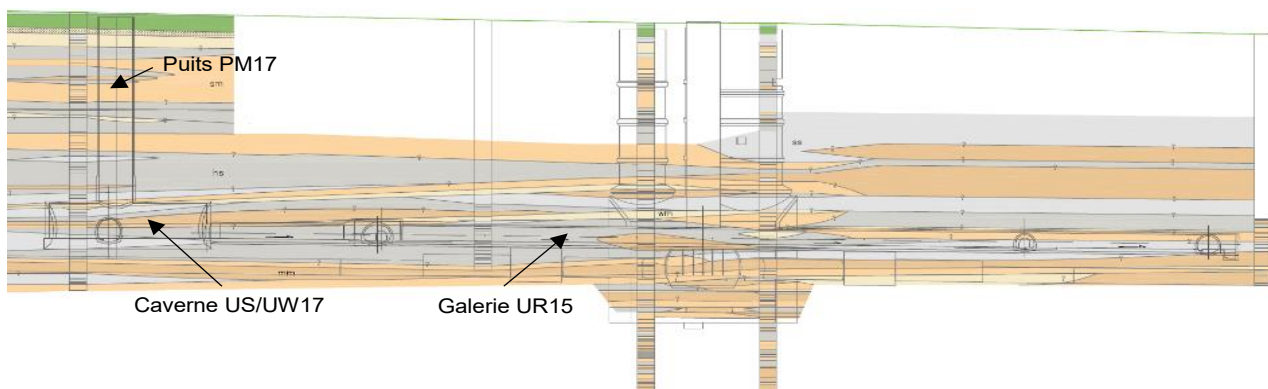


Figure 2. Profil en long géologique au droit du CERN HL-LHC Point 1

3 Le contexte réglementaire

3.1 Présentation de l'Ordonnance sur la Limitation et l'Élimination des Déchets

L'Ordonnance sur la Limitation et l'Élimination des Déchets (OLED ; RS 814.600 ; Confédération Suisse) est entrée en vigueur le 1^{er} janvier 2016. Elle a remplacé l'Ordonnance sur le Traitement des Déchets de 1990 (OTD ; Confédération Suisse).

L'OLED est une Ordonnance Fédérale qui a force de loi sur le Territoire Suisse. Elle fixe des principes de valorisation pour différentes catégories de déchets d'excavation, et s'adresse à tous les acteurs du domaine de la construction. Elle inclut les travaux d'excavation sur des sites pollués ou contaminés, que le site soit inscrit au cadastre des sites pollués ou non.

L'OLED permet notamment de classer les matériaux d'excavation et de percement en fonction de leurs degrés de pollution. L'article 19, alinéas 1 à 3 de la révision de l'Ordonnance définit une nouvelle nomenclature de décharges de type A à E (cf. Tableau 1).

Tableau 1. Destination des matériaux d'excavation et de percement en fonction de leur degré de pollution

Dénomination (selon OLED)	Ancienne dénomination (selon OTD)	Qualité (selon OLED)	Acceptables en décharges de...	Valorisation (selon OLED)
Non pollués	Non pollués « U »	« qualité A »	Type A	Article 19, alinéa 1
Faiblement pollués	-	« qualité B ⁻ »	-	-
Peu pollués	Inertes « DCMI »	« qualité B ⁺ »	Type B	Article 19, alinéa 2
Fortement pollués	Bioactifs « DCB »	« qualité E »	Type E	Article 19, alinéa 3

Les matériaux de type A sont les matériaux d'excavation et de percement non pollués, ils doivent autant que possible être valorisés comme matériaux de construction sur des chantiers ou dans des décharges, comme matières premières pour la fabrication de matériaux de construction, pour le comblement de sites de prélèvement de matériaux, ou pour des modifications de terrain autorisées.

Les matériaux de type B⁻ et B⁺ sont les matériaux d'excavation et de percement respectivement faiblement et peu pollués devant autant que possible être valorisés comme matières premières pour la fabrication de matériaux de construction aux liants hydrauliques ou bitumineux, comme matériaux de construction dans des décharges de types B à E, dans les travaux de génie civil sur le site pollué d'où proviennent les matériaux...

Les matériaux de type E sont les matériaux d'excavation et de percement fortement pollués devant autant que possible être valorisés ; à défaut, ils doivent être stockés dans des décharges de type E.

3.2 Cadre législatif applicable au projet

Le projet CERN HL-LHC Point 1 se situe sur la parcelle 13'450 sise sur le territoire de la commune de Meyrin (1217, Suisse). Cette parcelle n'est pas inscrite au cadastre cantonal des sites pollués.

Cependant, les investigations géotechniques effectuées préalablement au démarrage des travaux ont mis en évidence la présence de bancs de molasse gréseuse fortement pollués aux hydrocarbures.

Des hydrocarbures étaient identifiés dans trois des sondages carottés. Pour deux de ces sondages, au droit de la galerie UR15, le niveau de pollution se situait au-dessus du niveau du projet (environ 15 à 20 m au-dessus de la voûte de la galerie) ; en revanche, le troisième sondage, réalisé au droit du puits et de la caverne, identifiait deux horizons pollués (à des profondeurs de 59 m et de 67 m) interférant avec le projet au niveau de la base du puits et de la partie sommitale de la caverne, sans possibilité d'évaluer avec précision l'étendue de cette pollution et les teneurs en hydrocarbures associées.

Les matériaux issus de l'excavation étaient donc à considérer comme potentiellement pollués et devaient être traités en accord avec l'Ordonnance sur la Limitation et l'Élimination des Déchets présentée au chapitre précédent.

Selon l'OLED, les seuils réglementaires à considérer pour les hydrocarbures sont rappelés ci-après (cf. Tableau 2) :

Tableau 2. Exigences en termes de réglementation pour les matériaux d'excavation et de percement contenant des hydrocarbures (OLED, Annexe 3 – Chapitres 1 et 2)

Paramètres organiques		« Qualité A » [mg/kg]	« Qualité B ⁻ » [mg/kg]	« Qualité B ⁺ » [mg/kg]	« Qualité E » [mg/kg]
Hydrocarbures volatils	C ₅ – C ₁₀	1	-	10	100
Hydrocarbures	C ₁₀ – C ₄₀	50	100	500	5000

3.3 Dispositions prévues dans le contrat du marché de construction

Au moment de la rédaction des pièces du contrat de construction, il était donc établi que le projet aurait à traiter des matériaux potentiellement pollués par des hydrocarbures, mais sans possibilité à ce stade d'évaluer précisément ni les volumes concernés, ni les teneurs en hydrocarbures.

Les dispositions mises en œuvre dans l'appel d'offre puis dans le contrat de construction avaient donc pour but de pouvoir s'adapter aux conditions réelles rencontrées sur site :

- Définition d'un processus de tri des matériaux excavés, et prescription d'une aire dédiée au tri au sein des installations de chantier, avec une surface étanchée suffisante pour permettre la gestion par lots des matériaux excavés ;
- Spécifications concernant la ventilation et les méthodes d'excavation (interdiction du recours aux explosifs, détecteurs de gaz et équipements adaptés à la présence de gaz, procédures d'alerte et d'évacuation, etc.) pour la protection des travailleurs ;
- Spécifications concernant la membrane d'étanchéité des ouvrages souterrains (compatibilité avec les hydrocarbures) ;
- Intégration de ce risque de présence de matériaux pollués dans le bordereau des prix (prix d'excavation, et d'évacuation et de mise en décharge des matériaux), en fonction des teneurs par rapport aux seuils réglementaires ;
- Intégration de ce risque dans le mécanisme d'ajustement du délai d'exécution (sous-détail des cadences d'excavation contractuelles en fonction des seuils réglementaires, et prise en compte explicite des durées nécessaires à la ventilation des espaces souterrains en cas de présence de gaz).

Une bioremédiation sur site avait également été envisagée, à savoir un stockage provisoire sur site pendant environ 12 mois pour que les teneurs passent sous le seuil des 500 ppm, et permettent l'évacuation à un coût limité des matériaux. Mais cette solution avait été jugée incompatible avec les emprises disponibles pour les installations de chantier. De plus, un possible impact environnemental voulait être évité par le CERN du fait de la qualité des terres agricoles environnantes (label « agriculture biologique » des exploitations agricoles mitoyennes).

3.4 Les directives OLED, une opportunité pour le projet

Le GESDEC (Service de géologie, sols et déchets), est l'autorité compétente, dans le canton de Genève, pour ce qui concerne la gestion des déchets (y compris les matériaux d'excavation) et les sites pollués.

Dans le cadre de notre projet, en étroite collaboration avec cette entité, il a été étudié la possibilité de réutiliser sur place une fraction des matériaux faiblement pollués pour les raisons suivantes :

- L'origine de la pollution aux hydrocarbures est « géogène » (dont l'origine n'est pas due à une influence anthropique mais à une origine naturelle) ;
- La pollution de la fraction de matériau « faiblement pollués » envisagée d'être réutilisée, se trouvait dans la limite basse en terme de concentration en hydrocarbures C₁₀ – C₄₀ (seuil C₁₀ – C₄₀ compris entre 50 et 100 mg/kg) ;
- La nature des matériaux et les conditions de réutilisation sur site permettaient d'exclure une atteinte à l'environnement et en particulier aux eaux.

Selon l'OLED, les matériaux issus du chantier et présentant des concentrations en hydrocarbures ne sont pas considérés comme pollués du fait de l'origine naturelle du dépassement des valeurs limites de concentration observées.

Cependant, l'excavation de ces matériaux, les modifications physiques qu'elle engendre et leur déplacement dans un autre site impose d'assurer la sécurité environnementale de leur mode d'élimination. Ainsi, le GESDEC a proposé les règles suivantes pour la gestion de ces matériaux :

- Réutilisation sur place des matériaux « faiblement pollués » (jusqu'à la concentration maximale de $C_{10} - C_{40}$ de 100 mg/kg) et l'évacuation de préférence des matériaux « non pollués » de « Qualité A » aussi dans le but de ne pas surcharger les décharges de type B, dont les capacités dans le canton de Genève sont très limitées ;
- La réutilisation des matériaux « faiblement pollués » ne nécessite pas de réaliser d'essais de lixiviation ;
- Possibilité de réutiliser aussi sur place la fraction des matériaux faiblement pollués pour un seuil $C_{10} - C_{40}$ compris entre 100 et 250 mg/kg dans le cas de réalisation d'essais de lixiviation.

4 La détection des hydrocarbures

Les hydrocarbures peuvent se présenter sous différents aspects : gazeux, solide ou liquide. Les façons de les détecter sont donc multiples, et progressives au cours du cycle d'excavation et de maritage des matériaux.

4.1 Critères observationnels

4.1.1 Critères visuels

Les hydrocarbures de type $C_{10} - C_{40}$, peuvent être observés sous les aspects solide et liquide (cf. Figure 3) au cours des travaux d'excavation et notamment lors de l'établissement des levés de front géologiques.



Figure 3. Hydrocarbures observés lors de l'excavation de la base du puits PM17

4.1.2 Critères olfactifs

Les hydrocarbures de type $C_{10} - C_{40}$, peuvent avoir une perception olfactive remarquable même pour de faibles teneurs (teneurs exprimées en mg/kg, cf. Tableau 2), mesurées pour des concentrations en limite de matériaux non pollués et peu pollués (cf. Tableau 1).

4.2 Essais sur site – PetroFLAG®

Le PetroFLAG® est un appareil de terrain portatif peu coûteux et sans danger pour l'environnement permettant d'établir un ordre de grandeur de la quantité totale d'hydrocarbures pétroliers présente dans

un échantillon à partir d'un échantillon de sol de 10 grammes. Les mesures semi-quantitatives fournies par cet appareil doivent nécessairement être corrélées avec des analyses en laboratoire.

4.3 Essais en laboratoire

Les teneurs en hydrocarbures de type C₁₀ – C₄₀ sont évaluées dans un laboratoire spécialisé selon la Norme SN EN 14039 (Caractérisation des déchets – Détermination de la teneur en hydrocarbures par chromatographie en phase gazeuse dans la plage C₁₀ – C₄₀). Les résultats sont disponibles avec un délai de l'ordre de 3 à 10 jours, selon que l'on choisit une commande « express » ou normale.

Les teneurs en hydrocarbures de type C₅ – C₁₀ sont évaluées selon la méthode EPA 524.2 (mesure des composés organiques purgeables dans l'eau par chromatographie en phase gazeuse).

Au sens de l'OLED, ce sont les résultats d'essais effectués en laboratoire qui sont à considérer afin de statuer sur la qualité d'un matériau (cf. Tableau 2).

5 La démarche retenue

5.1 Recherche des traces d'hydrocarbures lors des travaux d'excavation

Un suivi conjoint par l'Entreprise et la maîtrise d'œuvre (« Engineer » selon terminologie du Contrat de Construction FIDIC) est effectué durant les travaux d'excavation. Ce suivi permet d'apprécier selon des critères visuels ou olfactifs la probabilité de présence d'hydrocarbures sous ses différents aspects (cf. chapitre 4.1.1 et 4.1.2).

Les éventuelles traces de pollutions sont évaluées à la fin de chaque cycle d'excavation par l'ingénieur géotechnicien en charge du suivi géologique du projet (maîtrise d'œuvre), et sont consignées dans la Fiche de Levé de Front associée.

5.2 Le tri des matériaux durant la phase de marinage

Les matériaux provenant de la caverne ou des galeries sont marinés du front d'attaque de l'ouvrage en cours de creusement vers la base du puits avec des chargeuses sur pneus.

Les matériaux sont ensuite acheminés vers la surface via une benne de six mètres cubes, et déversés dans une zone de stockage temporaire dans le hangar de protection du puits.

Sur la base des instructions données par le maître d'œuvre (point d'arrêt), les destinations des matériaux sont les suivantes :

- En cas de pollution jugée probable selon l'appréciation précitée, les matériaux sont acheminés vers la zone de stockage temporaire protégée des intempéries (hangar à matériaux) ;
- Dans le cas contraire (matériaux de « qualité A »), les matériaux sont autant que possible réutilisés sur site, en remblaiement de plateforme. A défaut (matériaux non pollués, mais excédentaires) ils sont évacués en tant que déblais non pollués en conformité avec l'article 19, alinéa 1 de l'OLED (cf. Tableau 1).

Cependant, il est important de noter qu'il a été mis en évidence sur une grande partie du projet (essentiellement lors de l'excavation des galeries), que des matériaux ne permettant aucune détection olfactive ou visuelle pouvaient contenir des hydrocarbures en quantités mesurables par les essais de laboratoire (cf. chapitre 4.3). A la suite de ce constat et suivant le principe de précaution, tous les matériaux provenant des excavations ont été considérés comme potentiellement pollués, et ont été acheminés vers la zone de stockage temporaire protégée des intempéries (hangar à matériaux), occasionnant ainsi une contrainte accrue en termes de gestion de l'espace.

5.3 Mise en stock temporaire des matériaux potentiellement pollués aux hydrocarbures

Les matériaux potentiellement pollués aux hydrocarbures sont stockés provisoirement sous le hangar à matériau. Les différents stocks sont définis en fonction de la provenance des matériaux (par cycle ou « tranche » d'excavation) et sont séparés dans le hangar par des blocs modulaires en béton.

Chaque lot est marqué et référencé par un panneau précisant (cf. Figure 4) :

- Nom de l'échantillon (provenance du matériau : ouvrage et points métriques de l'excavation)
- Date d'échantillonnage (cf. chapitre 5.4) ;
- Qualité du matériau (cf. Tableau 1).



Figure 4. Identification des stocks temporaires de matériaux potentiellement pollués aux hydrocarbures

5.4 Echantillonnage des matériaux

Les matériaux sont échantillonnés contradictoirement par l'ingénieur géotechnicien en charge du suivi géologique du projet (maîtrise d'œuvre) et par le responsable des travaux de l'Entreprise, selon une fréquence de l'ordre d'un échantillon tous les 250 mètres cubes de matériaux excavés.

Un lot de matériaux molassiques est composé de grès, de grès marneux et de marnes. Du fait de la méthode d'excavation retenue (excavation mécanique au brise-roche ou fraise), la granulométrie des lots est très variable, allant des fines à des blocs métriques (cf. Figure 4).

L'objectif est d'obtenir un échantillon global de qualité qui soit représentatif des propriétés moyennes du lot. Les échantillons sont donc constitués selon la méthodologie présentée dans la norme SN EN 932-1 (*Essais pour déterminer les propriétés générales des granulats - Partie 1 : méthodes d'échantillonnage*), norme applicable au prélèvement des échantillons de granulats.

Chaque lot fait l'objet de deux échantillons :

- « Echantillon testé » : envoyé par l'entreprise contractante vers un laboratoire spécialisé pour analyse (cf. chapitre 4.3) ;
- « Echantillon de référence » ou « copie » : conservé dans les bureaux de la maîtrise d'œuvre, pour permettre une nouvelle analyse si cela est jugé utile.

5.5 Réalisation des essais sur site et en laboratoire

Tous les échantillons prélevés ont fait l'objet d'essais en laboratoire (cf. chapitre 4.3).

En revanche, les essais PetroFLAG® n'ont été réalisés que sur une vingtaine des échantillons prélevés. En effet, l'utilisation du PetroFLAG® a été rapidement abandonnée du fait de la forte dispersion des mesures semi-quantitatives en comparaison aux résultats des essais menés en laboratoire (cf. Figure 5).

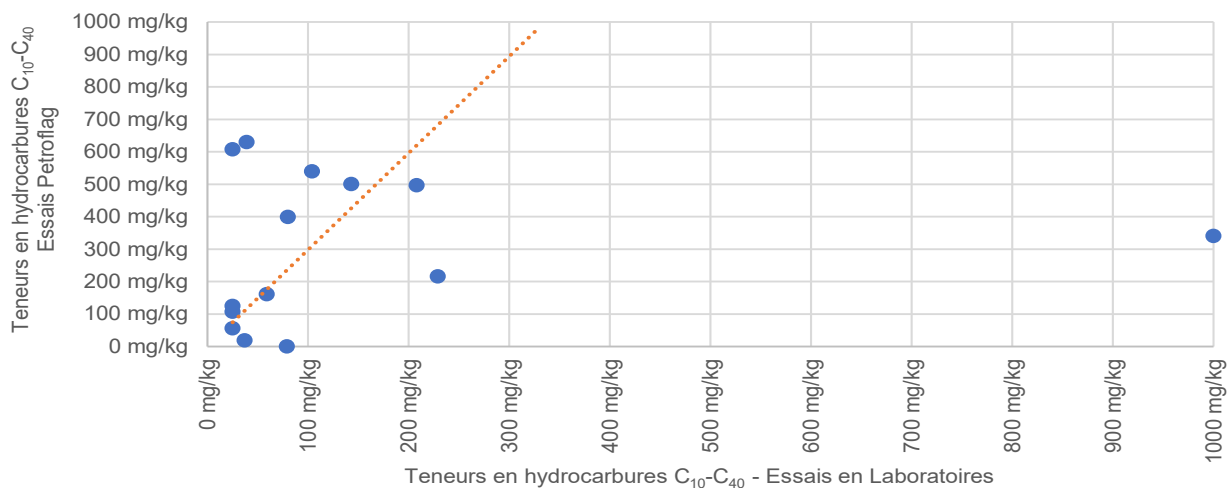


Figure 5. Tentative de corrélation entre les teneurs évaluées par essais Petroflag et par essais en laboratoires

Il est à noter que les essais par lixiviation n'ont pas été employés dans le processus précité. En revanche, de tels essais ont été menés sur des échantillons provenant du projet, par un organisme de contrôle indépendant ; une étude est en cours.

5.6 Obtention des résultats et définition de la destination des matériaux

A partir des résultats des essais menés en laboratoire (cf. chapitre 4.3) et transmis par l'Entreprise, et selon les seuils règlementaires définis par l'OLED pour les hydrocarbures (cf. Tableau 2), l'ingénieur géotechnicien en charge du suivi géologique du projet (maîtrise d'œuvre) confirme la destination à donner aux matériaux selon les classifications suivantes :

- Matériaux de « qualité A » : utilisation pour remblaiement sur le site du projet, ou évacuation en tant que déblais non pollués en conformité avec l'article 19, alinéa 1 de l'OLED (cf. Tableau 1) ;
- Matériaux de « qualité B⁻ » (matériaux « faiblement pollués », dans la limite basse) : utilisation pour remblaiement sur le site du projet selon l'accord du GESDEC ;
- Matériaux de « qualité B⁺ » (matériaux « peu pollués », dans la limite haute) : matériaux évacués vers des décharges de type B en conformité avec l'article 19, alinéa 2 de l'OLED (cf. Tableau 1) ;
- Matériaux de « qualité E » : matériaux évacués pour valorisation en conformité avec l'article 19, alinéa 3 de l'OLED (cf. Tableau 1).

Il est important de noter que l'ensemble des matériaux de « qualité E » issus du projet ont été évacués vers des cimenteries à proximité du projet pour être valorisés. Ces matériaux molassiques ont été intégrés au mix de préparation de la farine mise en œuvre dans le lit d'homogénéisation des fours (mix composé d'une fraction de l'ordre de 30 à 40% de matériaux molassiques issus du projet, et de matériaux calcaires et siliceux provenant d'autres carrières).

5.7 Contrôle extérieur

Alors que la présence ou non présence d'hydrocarbures dans les matériaux excavés s'est avérée assez conforme aux prévisions dans les premiers ouvrages excavés (puits et caverne), celle-ci est devenue beaucoup plus erratique et difficile à comprendre dans les galeries (cf. Figure 6). Comme indiqué plus haut, l'estimation initiale olfactive et visuelle s'est par ailleurs avérée non fiable pour juger de la présence ou non d'hydrocarbures.

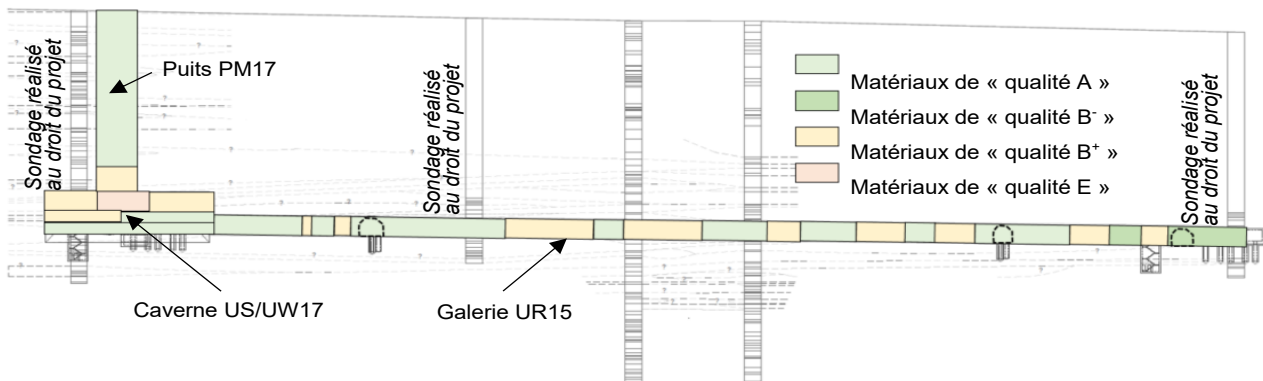


Figure 6. Organisation spatiale des matériaux excavés en fonction de leur degré de pollution

Dans le même temps, les concentrations dans les matériaux excavés des galeries étaient en général assez faibles et proches du seuil de qualification entre matériaux non pollués et matériaux pollués (50 mg/kg en C₁₀ – C₄₀). Cette situation mettait en doute la fiabilité du processus et la répétabilité des mesures.

Dans cette situation, le Maître d'ouvrage et la Maîtrise d'œuvre ont jugé utile de compléter le processus d'échantillonnage conjoint (Entreprise – Maître d'œuvre) et d'essais en laboratoire (pour le compte de l'Entreprise), en mettant en place un contrôle extérieur.

Ce contrôle extérieur intervenait alors sur demande de la maîtrise d'œuvre, de manière autonome, en procédant à ses propres échantillons, et en mandatant directement le laboratoire pour les réalisations des essais correspondants.

La comparaison des résultats d'essais (essais Entreprise – essais Contrôle extérieur) a fait apparaître certains écarts ou incohérences dans un premier temps, qui ont amené les intervenants à réexaminer les modalités d'échantillonnage, sans la modifier néanmoins. Les résultats ont été ensuite relativement homogènes. Lors d'écarts significatifs, la maîtrise d'œuvre en relation avec le contrôle extérieur pouvait décider d'invalider les résultats et de re-échantillonner de manière contradictoire avec l'Entreprise.

6 Les chiffres clefs

Le volume total des ouvrages souterrains à excaver était de l'ordre de 48'600 mètres cubes. A mi-janvier 2020, les excavations avaient atteint un avancement de 85%. Comme mis en évidence dans le Tableau 3, à cette même période, la part de matériaux de « qualité B » évacuée était de l'ordre de 30% (31'950 tonnes), celle de matériaux de « qualité E » de moins de 2% (1'370 tonnes). La valorisation des matériaux d'excavation « faiblement pollués » (seuil C₁₀ – C₄₀ géogènes compris entre 50 et 100 mg/kg) a permis de conserver sur chantier environ 5% (5'880 tonnes) de ces matériaux.

Tableau 3. Part des matériaux pollués par rapport aux volumes de matériaux excavés

A fin 2019 (Valeurs arrondies)	Volume total [m ³]	Volume excavé [m ³]	Part excavée [%]	« Qualité B ⁻ »		« Qualité B ⁺ »		« Qualité E »	
				[t]	[%]	[t]	[%]	[t]	[%]
Puits PM17	7'600	7'400	100	-	-	3'045	15	-	-
Caverne US/UW17	13'500	9'400	70	-	-	6'040	25	1'370	5
Galerie UR15	15'800	15'800	100	4'040	10	14'985	40	-	-
Galeries UA & UPR 13	4'400	2'000	45	1'840	35	-	-	-	-
Galerie UL13	1'900	300	15	-	-	-	-	-	-
Galeries UA & UPR 17	4'100	4'100	100	-	-	4'990	50	-	-
Galerie UL17	1'300	1'300	100	-	-	2'890	90	-	-
Total des ouvrages	48'600	40'300	85	5'880	5	31'950	30	1'370	< 2

Les quantités de matériaux pollués aux hydrocarbures (cf. Tableau 3) ont été comparées aux quantités estimées à partir des investigations géotechniques et prise en compte dans le contrat construction (cf. chapitre 3.2).

Tableau 4. Part des matériaux pollués par rapport aux volumes de matériaux évacués

	« Qualité B »	« Qualité E »	Au-delà de « Qualité E »
	[t]	[t]	[t]
Quantité de matériaux à évacuer prévues dans le contrat de marché de construction	12'500	6'250	6'250
Quantité de matériaux évacués à mi-janvier 2020	31'950	1'370	-

7 Conclusion et perspectives

La Molasse constituée de marnes et de grès est potentiellement polluée aux hydrocarbures. Ces derniers sont souvent retrouvés dans des concentrations parfois supérieures aux seuils réglementaires en vigueur, ce qui nécessite de traiter les matériaux d'excavation comme des matériaux pollués. La destination et le devenir de ces matériaux (valorisés ou mis en décharges) sont pilotés par leur degré de pollution, qu'il convient de mesurer par des essais en laboratoires réalisés sur des échantillons représentatifs des stocks associés.

Cette gestion des matériaux d'excavation potentiellement pollués nécessite un suivi accru durant les travaux d'excavation, et se poursuivant jusqu'à la réutilisation ou l'évacuation de ces matériaux.

La pollution de la molasse est un sujet avéré qu'il ne faut pas négliger lors de la préparation des contrats de construction, compte-tenu des enjeux financiers associés. La pollution aux hydrocarbures intéressant des lentilles gréseuses et des horizons étendus d'épaisseurs très variables de fraction molassique, il subsiste une part importante d'incertitude quant à la prévision d'une répartition de matériaux pollués par leur degré de pollution, et ce malgré la réalisation d'une campagne d'investigation géotechnique conséquente.

On retiendra que la pollution aux hydrocarbures peut intéresser une part importante des matériaux molassique excavés, qui fut de l'ordre de 30 à 35% dans le cas du CERN HL-LHC Point 1. Ce point sera donc à considérer comme une problématique majeure dans le cadre de l'étude du futur collisionneur circulaire (FCC CERN), qui prévoit le creusement d'un tunnel circulaire d'environ 100 km de long, également en grande partie dans des matériaux molassiques.

8 Références

- Fern, E.J., et al. 2018. Geotechnical characterisation of a weak sedimentary rock mass at CERN, Geneva. *Tunnelling and Underground Space Technology*, n°77, April 2018, pp 249-260
- Haas, M., et al. 2020. Hard Rock Engineering Conference ISRM International Symposium Eurock 2020 Trondheim, Norway. June 2020, pp 14-19, submitted
- Moscariello, A. 2018. The geomorphological landscapes in the Geneva basin. E. Reynard (Ed): *Landscapes and Landforms of Switzerland*. Springer Verlag, in press
- Resch, D., et al. 2009. Tunnel excavation material, high value raw material. *Geomechanics and Tunnelling* 2, n°5, pp 612-618
- Trümpy, R. 1980. Part A: An Outline of the Geology of Switzerland. Edit. by Trümpy, R., et al., Publishers, Basel, Switzerland

B.2 Geochemical challenges for the construction of CERN's 90-100 km subsurface infrastructure in the Geneva Basin, Switzerland/France

Table B.2: Overview of authorship and metadata of the presented publication.

Title	Geochemical challenges for the construction of CERN's 90-100 km subsurface infrastructure in the Geneva Basin, Switzerland/France
Author name	Maximilian Haas
Author's contributions	Conceptualization; data analysis; visualizations; writing (original draft); writing (review & editing)
Scientific value	Identification and discussion of chemical pollutants hampering disposal explicitly for the Future Circular Collider study, assuming disposal in Switzerland.
Status	Published in <i>2nd Geoscience & Engineering in Energy Transition EAGE Conference 2021</i>
Peer-reviewed proceedings	Yes
Full citation	Haas M., Geochemical challenges for the construction of CERN's 90-100 km subsurface infrastructure in the Geneva Basin, Switzerland/France, EAGE Conference Proceedings, 2nd Geoscience & Engineering in Energy Transition Conference, Nov 2021, Volume 2021, p.1-5, https://doi.org/10.3997/2214-4609.202121063 .



Geochemical challenges for the construction of CERN's 90-100 km subsurface infrastructure in the Geneva Basin, Switzerland/France

*M. Haas*¹

¹ European Organization for Nuclear Research (CERN), Esplanade Des Particules 1, 1211 Geneva, Switzerland.

Summary

The European Organization for Nuclear Research (CERN) is a world-wide leading organization in the field of particle physics carrying out a feasibility study for investigations on a next-generation particle accelerator, the Future Circular Collider (FCC), to be installed in a new 90-100 km subsurface infrastructure in the Geneva Basin, across the French and Swiss border. This requires a sustainable management plan for its ca. 9 million m³ of excavated rock and soil, comprised of sandstone, siltstone, conglomerate, and limestone lithotypes, to path the way for construction approval as part of environmental impact assessment. Rock samples from five wells along the FCC perimeter are presented in this study and were analyzed geochemically with an inductively coupled plasma optical emission spectroscopy (ICP-OES) to identify chemical pollutants and to compare with Swiss disposal legislation. The results show the presence of natural concentration of Ni with varying values between 0 and 330 ppm. Cd as well as Pb concentrations, both of natural occurrence, categorize the FCC construction interval between 100 and 300 m above sea level (mASL) as Swiss disposal class B. From 300 mASL to ground level, Gex-CD-02 shows higher amounts of Cd and Pb, which characterizes these intervals as disposal class E.

Introduction

Among the largest future tunnelling projects, the Future Circular Collider (FCC) project at the European Organization for Nuclear Research (CERN) ranks at the most ambitious undertakings by mankind, building a 90-100 km subsurface infrastructure of shafts, caverns, and surface site accesses in the Geneva Basin across eastern France and western Switzerland. About 9 million m³ of unconsolidated morainal debris, sandstones, siltstones, conglomerates and limestone will be excavated to host CERN's next-generation particle accelerator laboratory starting construction after 2030 [Abada et al., 2019; Benedikt et al., 2020]. Associated waste status and usage of excavated material are crucially linked to national and European legislation that state chemical pollutants and its respective thresholds [Haas et al., 2020]. In this article we identify chemical pollutants based on chemical laboratory measurements on plug and cutting samples, taken along the current FCC subsurface layout, which ranges between 100 and 300 m above sea level (mASL). We further elaborate on their environmental constraints originating from Swiss disposal classes, to substantiate future geo-engineering investigations for FCC marking an essential step into its technical design phase and, ultimately, construction approval.

Geological setting

FCC's current tunnel alignment passes through a quasi-circular 90-100 km subsurface infrastructure in the Geneva Basin (GB) as part of the Northern Alpine Foreland Basin (NAFB). The FCC construction area is geologically limited by the Vuache fault system [Gorin et al., 1993; Ibele, 2011; A. Sommaruga, 1999] in the south-west, the Jura Mountains in the north-west, the Lac Léman (Lake Geneva) in the north, and the mountain Salève towards the southeast [Burkhard, 1990; Mock and Herwegh, 2017; Pfiffner, 1986]. A thick succession of Red Molasse and Quaternary sediments [Charollais et al., 2007, 2013; Anna Sommaruga, 1997] overlies the Mesozoic sediments and is composed of sandstones, marls and intercalations of gypsum and conglomerates [Wildi et al., 2017] caused by either erosion of the Western Alps [Oxburgh, 1981], sea level changes [Bachmann and Müller, 1992] or a combination of both [Schlunegger and Mosar, 2011]. Morainal debris of Quaternary age were deposited on top of Red Molasse sediments as glacial and fluvio-glacial material [Charollais et al., 2013; Anna Sommaruga, 1997] consisting of gravel, sand, and marl [Wildi, 1997]. The high variability of the geological origin of the rocks and sediments that will cross the installation, concomitantly with the large dimensions of the infrastructure itself, increases the complexity of the excavation and of the management of the excavated rock.

Methods

Inductively coupled plasma optical emission spectroscopy (ICP-OES) was conducted on plug and cutting samples, taken at five distinct well locations along FCC's current subsurface perimeter. The samples were crushed to $\geq 70\%$ passing 2 mm and 250 g of the crushed material were pulverized $\geq 85\%$ to a fraction of 75 μm . The material was then dried in a 105°C oven for 48 h. For the identification of 59 elements (ultra-trace), four acid digestions with 0.25 g of the 75 μm sample fraction were produced and heated in HNO₃, HClO₄ and HF to fuming and consecutively dried. The residue was dissolved in HCl and analysed in a Perkin Elmer Sciex Instruments ELAN 9000 ICP-MS device. For the identification of Si, a Spectro Ciros Vision high-performance ICP-OES device (LiBO₂/LiB₄O₇ fusion analysis) was used.

Results

Table 1 gives an overview of the chemical pollutants for Swiss disposal classes [Schweizerischer Bundesrat, 2015], which are relevant for FCC's current subsurface layout. Predominant elemental pollutants depict lead (Pb), nickel (Ni), cadmium (Cd) and antimony (Sb), and are plotted for wells Geo-02, Gex-CD-01, -02, -05 and -06 depicting a north to south direction across the Geneva Basin. The Molasse sediments are composed of heterogeneous lithotypes, which have been identified in geophysical well-logs, calibrated to petrophysical and mineralogical laboratory analyses [Haas,



Carraro, et al., 2021]. They comprise mainly quartz, calcite, dolomite, Cr-spinel, gypsum and clay minerals, which are prone to polluting elements.

FCC's goal is to construct sustainable and environmental-friendly. This includes proper disposal for excavated material that might not be able to be used for the production of concrete, bricks, geopolymers or landfilling as suggested in a previous study [Haas, Mongeard, et al., 2021].

Figure 1 shows the five boreholes and their chemical distribution in elevation (mASL). Results show amounts of Ni varying between 0 and 330 ppm, respectively mg/kg. At depths below 300 mASL, the amount of Pb increases, showing high-peak values above 5000 ppm, which stays constant at about 2-5 ppm in FCC's range depth. Cd contents are in line with Pb contents, marking exceptions only in well Gex-CD-02 at depths of 375-400 mASL. Sb contents stay constant across all boreholes and respective depth intervals.

Table 1: Extract of required chemical thresholds for Swiss disposal classes [modified after Haas et al., 2021].

Disposal class	Asbestos	As	Cd	CN	Cr total	Cr-VI	Hg	Ni	Pb	Sb
-----mg/kg (dry substance) -----										
class-A	-	15	1	0.5	50	0.05	0.5	50	50	3
class-B	-	30	10	0.02	500	0.1	2	500	500	30
class-E	>0	50	10	0.03	1000	0.5	5	1000	2000	50

Conclusions

Interpretation is compared with Swiss disposal classes and its chemical pollutants for the Geneva Basin's Red Molasse and Quaternary morainal debris. In case the FCC's excavated material cannot be used properly, rock and soil will need to be disposed. ICP-OES analyses show that the FCC construction interval between 100 and 300 mASL would be associated to Swiss disposal class B. In the upper depth intervals, from 300 mASL to ground level, certain intervals are exposed to class E, being the most contaminated area and relevant for shaft construction to guarantee access to the main tunnel and physics equipment installation. While the depicted chemical pollutants are of uttermost significance, further comparisons with anion analyses and hydrocarbon contaminations will be elaborated in future studies.

This study delivers the basis for a vast set of engineering and environmental undertakings as part of the Future Circular Collider project, with results from upcoming site investigations consecutively updating the subsurface model. In addition to the ICP-OES analysis presented herein, rock samples have been further analysed geomechanically, whose results will be featured in a geotechnical-petrophysical rock characterisation for its encountered geology in a dedicated future study.

Acknowledgements

The author would like to thank Dr. Michael Plötze (ETH Zurich), Prof. Dr. Andrea Moscardello (University of Geneva) and Dr. Antoine De Haller (University of Geneva) for their supervision during laboratory measurements and input for this extended abstract.

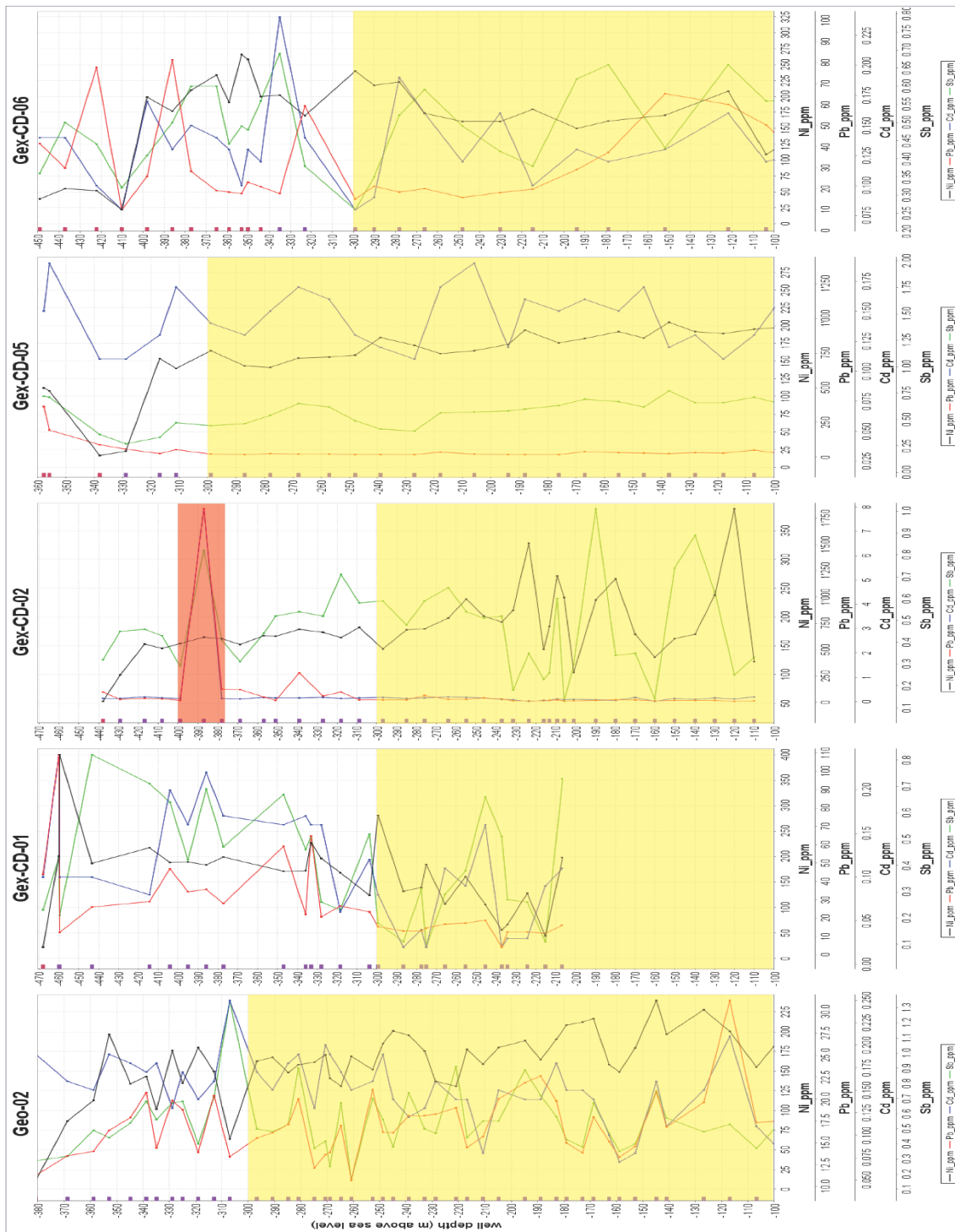


Figure 1 Overview of five boreholes along the FCC layout from north to south, depicting coloured Swiss disposal classes. Yellow = class B, red = class E. Coloured rectangles on the right-hand side depict lithostratigraphy: purple = Red Molasse, dark red = glaciogenic deposits (morainal debris).

References

- Abada, A., Abbrescia, M., AbdusSalam, S. S., Abdyukhanov, I., et al. [2019]. FCC-ee: The Lepton Collider. *The European Physical Journal Special Topics*, 228(2), 261–623. <https://doi.org/10.1140/epjst/e2019-900045-4>
- Bachmann, G. H., and Müller, M. [1992]. Sedimentary and structural evolution of the German Molasse Basin. *Eclogae Geol Helv. Eclogae Geol Helv*, 85, 519–530.
- Benedikt, M., Blondel, A., Janot, P., Mangano, M., and Zimmermann, F. [2020]. Future Circular Colliders succeeding the LHC. *Nature Physics*, 16(4), 402–407. <https://doi.org/10.1038/s41567-020-0856-2>
- Burkhard, M. [1990]. Aspects of the large-scale Miocene deformation in the most external part of the Swiss Alps (Subalpine Molasse to Jura fold belt). *Eclogae Geol. Helv.*, 83(3), 559–583.
- Charollais, J., Weidmann, M., Berger, J.-P., Engesser, B., Hotellier, J.-F., Gorin, G., Reichenbacher, B., and Schäfer, P. [2007]. La Molasse du bassin franco-genevois et son substratum. *Archives Des Sciences*, 60, 59–174.
- Charollais, J., Wernli, R., Mastrangelo, B., Metzger, J., Busnardo, R., Clavel, B., ... Weipmann, M. [2013]. Présentation d'une nouvelle carte géologique du Vuache et du Mont de Musièges (Haute-Savoie, France) stratigraphie et tectonique. *Archives Des Sciences*, 66(1), 1–63.
- Gorin, G. E., Signer, C., and Amberger, G. [1993]. Structural configuration of the western Swiss Molasse Basin as defined by reflection seismic data. *Eclogae Geologicae Helveticae*, 86, 693–716.
- Haas, M., Carraro, D., Ventra, D., Plötze, M., De Haller, A., and Moscariello, A. [2021]. Lithotype, well-log pattern and geo-engineering risk analyses for CERN's proposed 90-100 km Future Circular Collider subsurface infrastructure in the Geneva Basin. *Engineering Geology*, submitted.
- Haas, M., Galler, R., Scibile, L., and Benedikt, M. [2020]. Waste or valuable resource – a critical European review on re-using and managing tunnel excavation material. *Resources, Conservation and Recycling*, 162, 105048. <https://doi.org/10.1016/j.resconrec.2020.105048>
- Haas, M., Mongeard, L., Ulrici, L., D'Aloia, L., Cherrey, A., Galler, R., and Benedikt, M. [2021]. Applicability of excavated rock material: a European technical review implying opportunities for future tunnelling projects. *Journal of Cleaner Production*, 315.
- Ibele, T. [2011]. Tectonics of the western Swiss Molasse Basin during Cenozoic times.
- Mock, S., and Herwegh, M. [2017]. Tectonics of the central Swiss Molasse Basin: Post-Miocene transition to incipient thick-skinned tectonics? *Tectonics*, 36(9), 1699–1723. <https://doi.org/10.1002/2017TC004584>
- Oxburgh, E. R. [1981]. R. Trümpy Geology of Switzerland: A Guide-Book. Part A: An Outline of the Geology of Switzerland. Basel and New York (Wepf & Co.), 1980. 104 pp., 46 figs., 1 coloured pl. Price Sfr. 35.00. - Part B: Geological Excursions. Ibid., 230 pp., 204 figs. Pri. *Mineralogical Magazine*, 44(335), 366. <https://doi.org/DOI: 10.1180/minmag.1981.044.335.28>
- Pfiffner, O. A. [1986, December 22]. Evolution of the North Alpine Foreland Basin in the Central Alps. *Foreland Basins*, pp. 219–228. <https://doi.org/doi:10.1002/9781444303810.ch11>
- Schlunegger, F., and Mosar, J. [2011]. The last erosional stage of the Molasse Basin and the Alps. *International Journal of Earth Sciences*, 100(5), 1147–1162. <https://doi.org/10.1007/s00531-010-0607-1>
- Schweizerischer Bundesrat. [2015]. *Verordnung über die Vermeidung und die Entsorgung von Abfällen (Abfallverordnung, VVEA)*. 2015(April 2020), 1–46.
- Sommaruga, A. [1999]. Décollement tectonics in the Jura foreland fold-and-thrust belt. *Marine and Petroleum Geology*. [https://doi.org/10.1016/S0264-8172\(98\)00068-3](https://doi.org/10.1016/S0264-8172(98)00068-3)
- Sommaruga, Anna. [1997]. Geology of the Central Jura and the Molasse Basin. In *Memoire de la Société neuchateloise des sciences naturelles* (Vol. 12). https://doi.org/ZP_Brenets, PNR61
- Wildi, W. [1997]. Le site naturel de Genève. In Ph. Broillet, ed. (Ed.). *Les monuments d'art et d'histoire du Canton de Genève. Tome 1: La Genève sur l'eau*. Retrieved from <https://archive-ouverte.unige.ch/unige:90839>
- Wildi, W., Corboud, P., and Gorin, G. [2017]. Guide : géologie et archéologie de Genève Guidebook : geology and archaeology of Geneva. *Société de Physique et d'histoire Naturelle de Genève*, 93.

B.3 A mineralogical re-use classification model of Molasse rock mass in the Geneva Basin

Table B.3: Overview of authorship and metadata of the presented publication.

Title	A mineralogical re-use classification model of Molasse rock mass in the Geneva Basin
Author names	Maximilian Haas, Antoine De Haller, Andrea Moscariello, Luigi Scibile, Michael Benedikt, Nina Gegenhuber, Robert Galler
First author	Maximilian Haas
First author's contributions	Conceptualization; literature review; data analysis; visualizations; writing (original draft); writing (review & editing)
Scientific value	First concept proposal for application scenarios of excavated tunnel material as part of the Molasse formations in the Geneva Basin.
Status	Published in <i>ISRM International Symposium - EUROCK 2020, Conference Proceedings, Trondheim, Norway</i>
Peer-reviewed proceedings	Yes
Full citation	Haas M., DeHaller A., Moscariello A., Scibile L., Benedikt M., Gegenhuber N., Galler R., A mineralogical re-use classification model of molasse rock mass in the Geneva Basin, ISRM International Symposium, June 14-19, Trondheim, Norway, 2020, ISBN 978-82-8208-072-9.

A mineralogical re-use classification model of molasse rock mass in the Geneva Basin

M. Haas

*Chair of Subsurface Engineering, Montanuniversität, Leoben, Austria
European Organization for Nuclear Research (CERN), Meyrin, Switzerland
maximilian.mathias.haas@cern.ch (corresponding author)*

A. De Haller & A. Moscariello

Department of Earth Sciences, University of Geneva, Geneva, Switzerland

L. Scibile & M. Benedikt

European Organization for Nuclear Research (CERN), Meyrin, Switzerland

N. Gegenhuber & R. Galler

Chair of Subsurface Engineering, Montanuniversität, Leoben, Austria

Abstract

The Future Circular Collider (FCC) aims to become the largest and most powerful particle accelerator in the world located in parts of France and Switzerland. In order to host such an ambitious machine, a tunnel with a length of 97.75 km is currently under feasibility study at the European Organization for Nuclear Research (CERN). One of the study's main challenge is the handling of more than 9.1 million m³ of tunnel excavation material. As a matter of fact, this requires a sophisticated geo-scientific and technical classification of FCC's proposed excavated geological units, respectively the molasse rock mass, in terms of re-use and disposal scenarios and to generally considerate its environmental and economic impact. The paper casts a glance at the arising scientific opportunity to classify the excavated tunnel material in future using a mineralogical approach from macroscopic to microscopic scale.

Analyses show nickel and chromium minerals within the upper and anhydrite in the upper and lower molasse parts. Nickel and chromium concentrations pollute the molasse rock mass but could imply potential mining as a re-use scenario. Anhydrite likely causes tunnel construction issues when in contact with water. The proposed classification model serves as a link to French and Swiss legislation as well as an European technical guideline concerning re-use of tunnel excavation material on any international construction site. It simplifies and delivers the basis for future contractual models from a client's and contractor's perspective under conditions and protection of national, international and European Union legislation.

Keywords

Classification, mineralogical, re-use, soft rock



1 Introduction

Within the last decade, the European Organization for Nuclear Research (CERN) initiated several feasibility studies to build a future collider facing the physical challenges of the 21st century (Zimmermann 2015). A new collider should aim to supersede the current 27 km Large Hadron Collider (LHC) in terms of energy and luminosity. Currently, the High-Luminosity Large Hadron Collider (HL-LHC) project is upgraded to prepare for the next collider (Acar et al. 2017). However, looking beyond the next decade, a more powerful machine will be required. Hence, study efforts resulted in the final outcome named the Future Circular Collider (FCC) located in the canton Geneva, Switzerland and the French region Auvergne-Rhône-Alpes as depicted in Fig. 1. Its scope has been extensively examined with the intent to start physical measurements by 2040 (Abada et al. 2019a, b, c). The remaining time gap tends to investigate the subsurface being part of the geological Western Alpine Molasse Basin in terms of environmental, civil engineering and geological considerations and feasibility.



Fig. 1 The FCC ring layout in green with the LHC (large) and its predecessors (small) both in blue.

Social impact and environmental issues driven by civil engineering and geological constraints oblige to answer the question of how to handle 9.1 million m³ of a 97.75 km tunnel in circumference. Potential re-use and disposal options on future construction sites are essential and legally mandatory to preserve sustainability. A set of multi-disciplinary approaches such as mineralogy, geophysics, geomechanics and geology associated to stratigraphy is available to classify the material accordingly. Classification turns out to be essential for further analyses and treatment and to derive re-use and disposal scenarios for the material when compared to other projects. Several researchers have developed methods to characterise excavated material using different approaches. Specifically, on-line systems were installed for construction sites to clarify for potential re-use scenarios (Erben 2016; Michel et al. 2016; INDU et al. 2014; Tokgöz 2013; Resch et al. 2009) and the Gotthard Base tunnel successfully re-used 22 % analysing the excavated material in terms of chemistry for concrete aggregates, which seemed to be the ideal individual re-use case (Fabbri 2004). That being said, each tunnelling project requires specific re-use investigations that might be adaptable to other construction sites in terms of concept and planning, but not in terms of its underlying geology and technical feasibility. Classification is impeded by geological heterogeneity and this requires an adequate choice of reasonable parameters within a vast set of geo-scientific domains for potential re-use.

This paper addresses a mineralogical approach to characterise the molasse rock mass constituting more than 90 volume-% of FCC's proposed excavated material. Potential obstacles predicted by polluted material are introduced to imply first insights and suggestions to re-use scenarios and to cast a first glance at geological and civil engineering uncertainties. Moreover, a first investigation is presented for the proposed polluted material containing heavy metal ions that might hamper re-use and construction.

2 Geological setting

The Western Alpine Molasse Basin (WAMB) as depicted in Fig. 2, often referred to as the Geneva Basin in Western Switzerland, is part of the Swiss Plateau and limited by the Salève Mountain to the SE and the Jura mountains to the NW. These distinctive, geological elevations were influenced by tectonic deformation during the Alpine foreland emplacement, the associated glaciations of Pleistocene age and post-glacial processes (Moscariello 2018). The WAMB is divided into the Alpine foreland consisting of the Jura plateau and the Haute Chaîne as well as the Alpine units represented by the pre-alps (Penninic), the subalpine and Helvetic nappes, the external Crystalline massifs and the Penninic nappes (Chelle-Michou et al. 2017). The molasse rock units present in the basin crop out along the Salève, the Vuache and the Jura mountains, which consist of Mesozoic sedimentary rocks. The Mesozoic succession starts with evaporites at the base, followed by a succession of limestones and marls belonging to the southern margin of the European continent dated back to the Tethys Ocean. The Mesozoic sequence was deposited on top of the Palaeozoic crystalline basement. This shows graben-like structures filled with continental siliciclastic sediments during the Permian and Carboniferous, following the Variscan orogeny (Moscariello et al. 2020). The top of the Mesozoic sequence indicates an extensive erosive surface formed during the uplift of the foreland basin as the Alpine belt was compressed. Above the erosional surface, Oligocene heterogeneous siliciclastic Molasse are overlain by Quaternary glacial to fluvial deposits. These molasse packages were deposited as detrital formations during the Alpine orogeny (Trümpy et al. 1980) and represent FCC's targeted construction depth of 100 to 500 m.

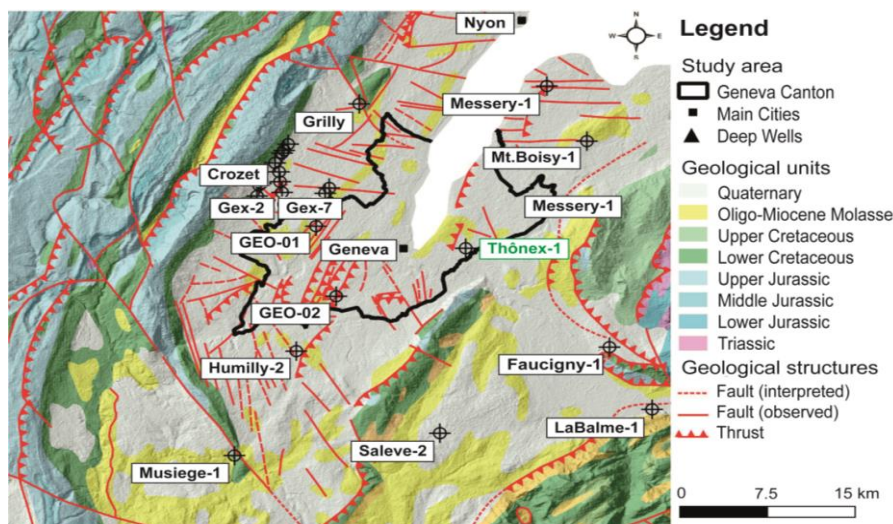


Fig. 2 Geological units with associated boreholes in the Geneva Basin. The well of Thônex chosen for this study is depicted in green. Modified after (Moscariello et al. 2020).

Two prominent classification models of its marl and sandstone components exist based on stratigraphy and the analyses of physical parameters. A stratigraphic classification of the molasse is given by Trümpy (1980) according to: Lower Marine Molasse (UMM), Lower Freshwater Molasse (USM), Upper Marine Molasse (OMM) and Upper Freshwater Molasse (OSM). In literature, molasse abbreviations usually refer to German terms. Data sets outsourced and gathered by CERN within the last 70 years served for a second and more recent geotechnical classification given by Fern et al. (2018), who subdivide the molasse into: very weak marl, weak marl, medium-weak marl, weak sandstone, medium-strong sandstone and strong sandstone. These categories increase in uniaxial compressive strength (UCS) and are further based on differences in e.g. Young's moduli or Atterberg limits, merely taken from HL-LHC Point 1. Even though these classifications led to a better understanding of molasse properties, a potential re-use classification was neither investigated nor demanded.

3 Data methodology

The mineralogical classification approach is based on data taken from the well of Thônex as depicted in Fig. 2. The samples were taken from cuttings, which typically contain sandstone, limestone and mudstone. In total, 113 samples each weighing between 100 to 200 g were chosen along a total

analysed borehole depth of 1323 m. 53 out of 113 samples were selected with an interval of 10 to 15 m to guarantee a regular profile resolution. X-ray fluorescence (XRF) and inductively-coupled plasma (ICP) analyses have been conducted to measure the elemental composition of molasse rock material. These results later served for oxide calculations. In addition, automated mineralogical scanning electron microscopy (QEMSCAN[©]) allowed calculation of grain density and modal mineralogical composition on polished thin sections. Lithotypes classification could be performed using mineralogical and textural information. Sample preparation included washing to remove drilling mud, hand-picking of coarse-grained particles and embedding in epoxy resin to create thin polished sections. QEMSCAN[©] measurements were performed using a beam voltage of 15 kV at 10 μ A, as typically applied for sedimentary rock. A 15 kV beam allows for a smaller analysis point ($< 3 \mu\text{m}$) compared to 25 kV at the expense of a less accurate determination of heavy elements. The small analytical point is preferred for sedimentary rocks, which predominant clay and fine-grained mineral mixtures, to minimize the number of mixed signal pixels (measured at the boundary between two minerals). The scans were performed applying a 10 μm grid on a 1.5x1.5 cm area. Measurements were performed with two fast EDS collectors, and each pixel was defined by an accumulation of 1000 counts, sufficient to identify the main components.

4 Results

QEMSCAN[©], XRF and ICP-MS measurements are presented below and a classification model, respectively lithotypes, are derived. A first look was taken at grain densities calculated from QEMSCAN[©] data as shown in Fig. 3.

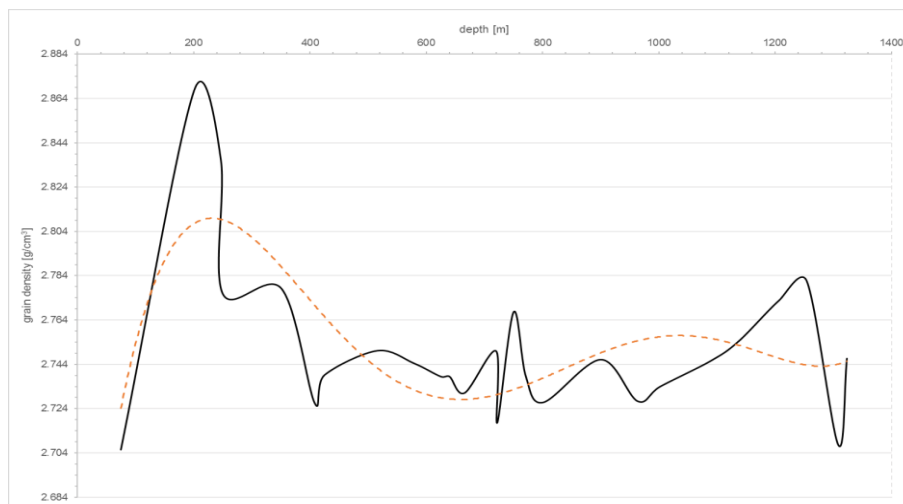


Fig. 3 Distribution of grain densities along borehole depth. Dashed line depicts a general trend.

After a first increase to around 2.87 g/cm^3 within the upper 240 m, the trend line shows density values dropping and stabilizing at around 2.73 g/cm^3 . Zooming in at each depth level, Fig. 4 shows the area-% proportions of different lithotypes recognized in the cuttings particles. Lithotypes were created based on modal mineralogy and textural information. It can be seen that phosphatic rock type is not-existent. Pyritic rock type only occurs between depths of 1254 and 1323 m. Evaporitic rocks are defined by the abundance of anhydrite (identified as gypsum/anhydrite) and are found between depths of 201 and 516 m as well as 1089 and 1323 m. Sandstone, limestone and claystone occur from top to bottom, whereas the area-% of limestone decreases until approximately 650 m to continuously increase towards the bottom. A similar behaviour can be seen with evaporitic rocks. Claystone completely misses out between depths of 250 to 425 m, while sandstone shows the same pattern. However, little concentrations seem to be present at depth 408 m. Except for depth 75 m, the mixed rock category is present at all levels. Fig. 5 (A) shows the modal volume-% distribution of each mineral at different borehole depths and in (B) anhydrite cleavage can be seen under the polarizing microscope. Fig. 6 shows a final comparison of QEMSCAN[©], XRF and ICP analyses. As proposed by lithotypes, gypsum/anhydrite (dark purple colour) is broadly distributed at certain borehole depths. QEMSCAN[©] data shows a fine-grained, compact texture with rather coarse-grained mineral compounds at depth 722 m. In XRF, SiO_2 (sandstone lithotype), CaO (limestone lithotype), Al_2O_3 and Cr_2O_3 are the most dominant oxides. ICP data shows element components such as nickel and

chromium correlated to serpentinite and Cr-spinel. Magnesium shows rather constant values, whereas uranium and thorium values constantly differ from one another in all samples.

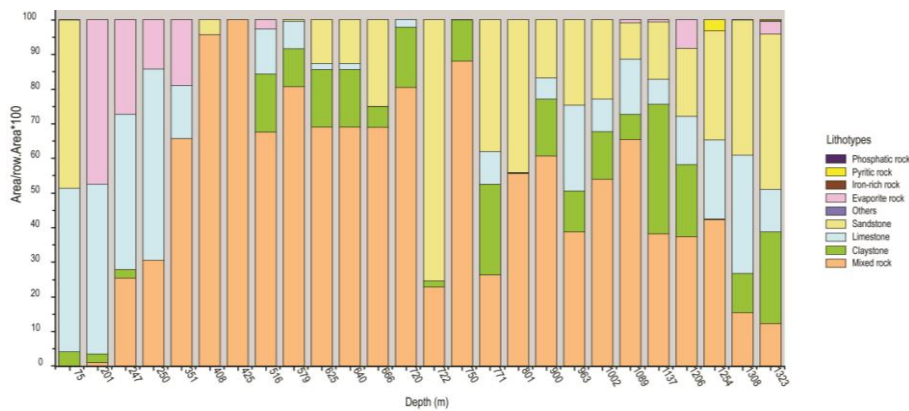


Fig. 4 Lithotypes derived from QEMSCAN© analyses at different borehole depths.

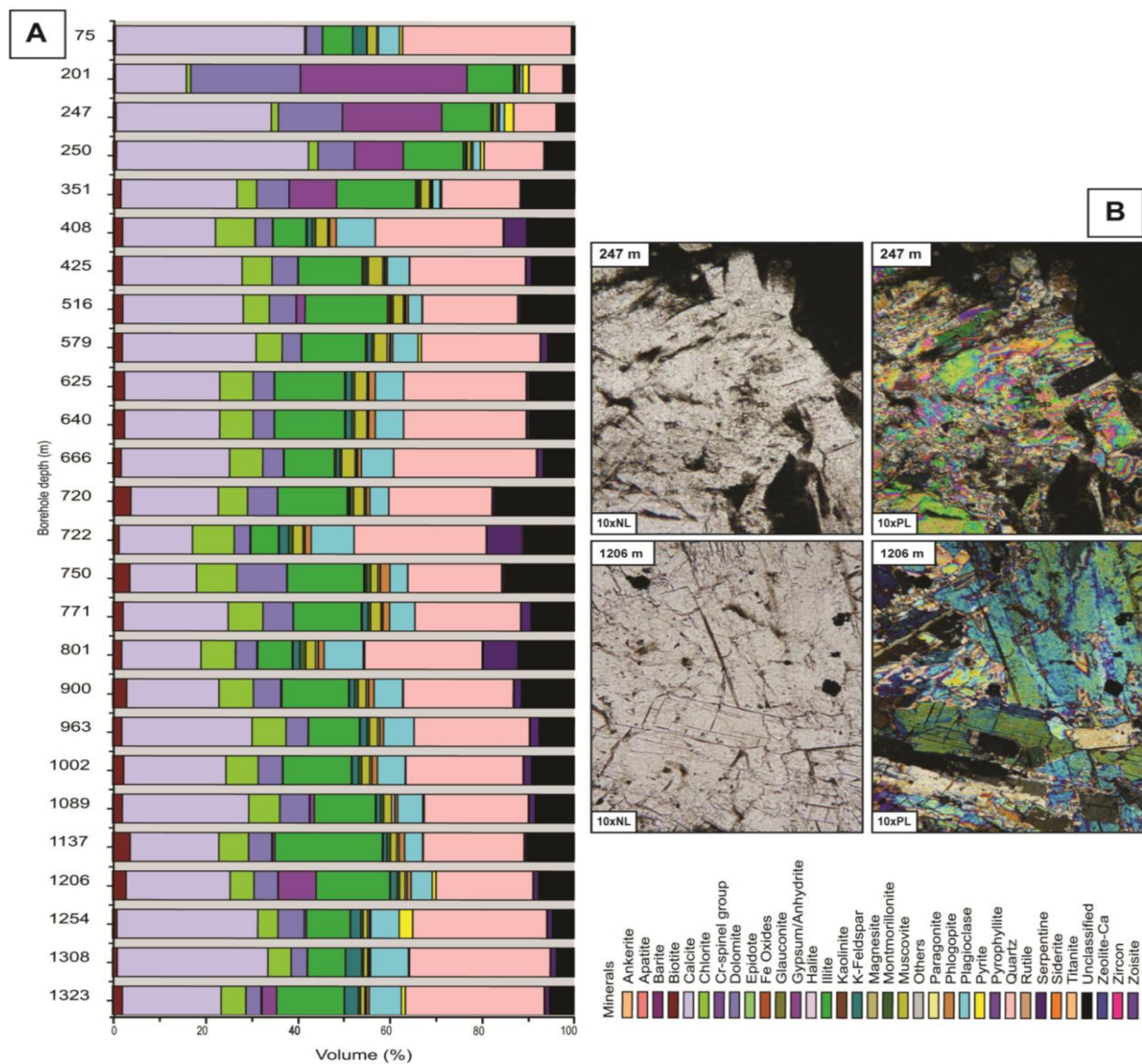


Fig. 5 A: Modal mineralogy at different borehole depths. B: Thin sections under polarizing microscope, in plane parallel (NL) and crossed polarized (PL) light. In contrast to QEMSCAN©, anhydrite is easily distinguished (birefringence, relief and cleavage) from gypsum under the polarizing microscope.

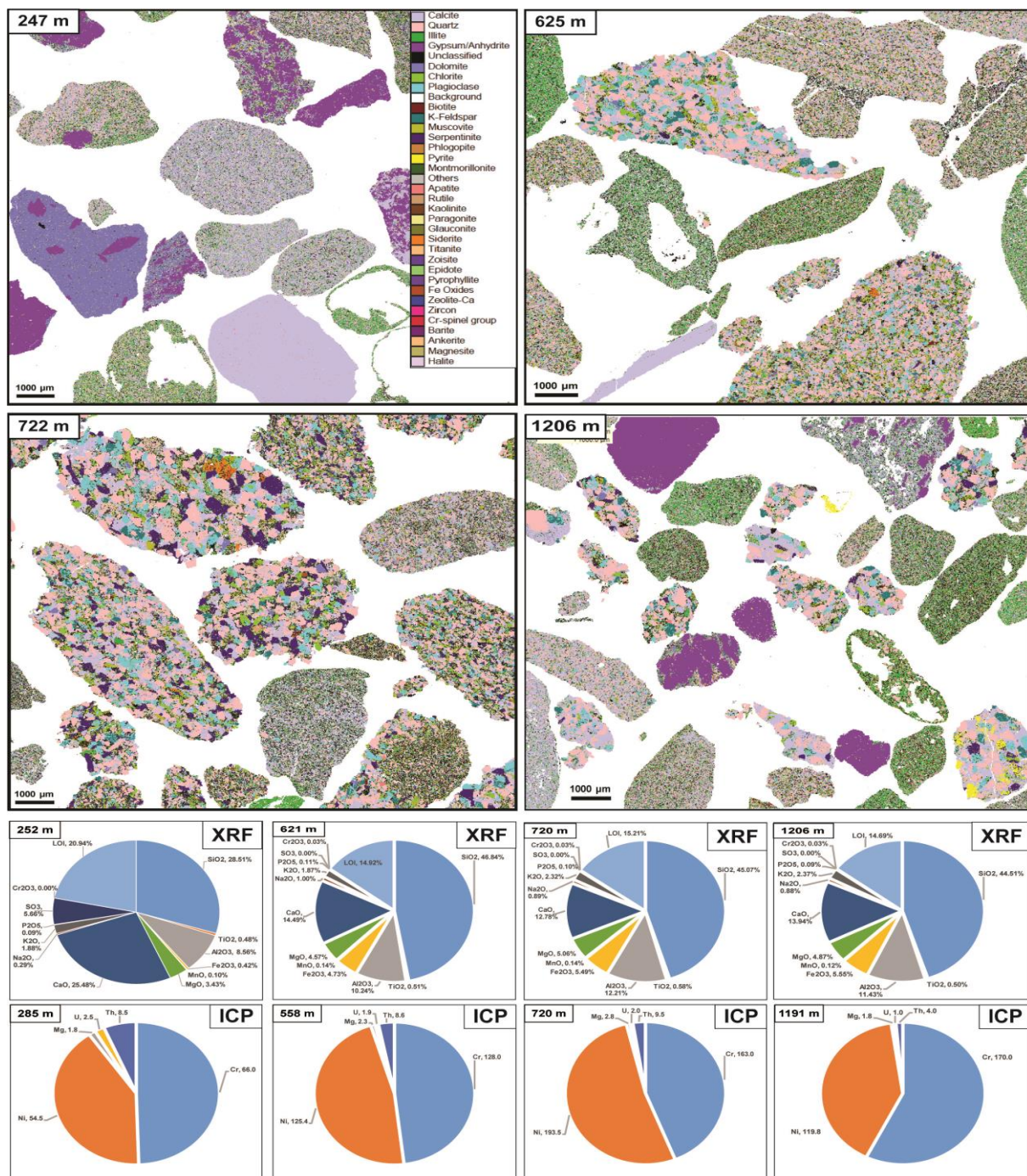


Fig. 6 QEMSCAN (top), XRF (middle) and ICP-MS (bottom) comparison at different borehole depths.

5 Discussion

Serried grain densities turned out to be not sufficient to derive a first classification model. They hardly allow a clear compositional classification. We created a few new definitions in the database (Cr-spinel, possibly also kaemmerite) but left quite a significant amount of unclassified that may correspond to either picotite or mixtures. Unclassified pixels in QEMSCAN© data could be an unknown mineral (not included in the data base) or a mixture of various minerals that cannot be solved. Typical cleavage depicted in the polarized light under the microscope clearly concludes anhydrite as the predominating mineral for all depths. Especially for mechanized tunnelling including different TBM types such as Slurry-TBM or Earth-Pressure-Balanced TBM, this bears a lot of issues when in contact with water.

The hydration of anhydrite produces gypsum constituting lower density but higher volume. This dilation can break tunnel structures and requires expensive support. If possible, anhydrite must be avoided during tunnelling. The occurrence of anhydrite at the top and bottom of the borehole might be in close relationship to different molasse types. Beyond Salève Mt. marine molasse is predominant that proceeds towards the Thônex well becoming continentally influenced. A major problem is faced when considering Ni and Cr present in Cr-spinel and serpentinite. Serpentine grains (up to 14 % volume) contained in molasse sandstone are probably the main carriers of these polluting elements. It is not known if any mechanical or chemical process are able to separate the serpentine fraction so that a minor volume of higher-grade Cr-Ni sand could be produced for disposal.

Extracting the Cr and Ni of the serpentinite might not be economic under normal mining conditions when considering its concentrations but may be viable taking the very high cost of polluted disposal into account. This might require processing the excavated material technically and/or biologically for different French and Swiss disposal classes. Detailed clearance can be stated when investigating samples with QEMSCAN® at 25 kV voltage, which allows to detect heavy metal ions such as Ni and Cr with higher precision, even though this comes to the account of lower resolution. Differences in natural radioactivity elements like uranium and thorium relate to different ratios of marl and sandstone within the molasse and open up opportunities to classify them accordingly with a strong practical advantage when considering gamma spectrometry along a conveyer belt.

6 Conclusion & future perspectives

A first classification model of the molasse rock mass was presented using QEMSCAN®, XRF and ICP data analyses based on lithotypes and modal mineralogy. It could be shown that the presence of anhydrite in the molasse rock mass likely causes construction issues during tunnelling. Its geological heterogeneity, respectively of cuttings, was overcome by using elemental, mineralogical and lithological indications. Natural radioactivity given in U and Th are able to classify molasse material as a first quick-look method. The mixed rock lithotype corresponds to a fine-grained, marly sandstone lithotype that implies sub-lithotype classifications among sandstone and marls within the molasse units bearing Cr-spinel and serpentinite. Ni and Cr concentrations tend to increase with depth and may be suited for a re-use scenario as mineral resources. This re-use scenario overcomes the legal issue of French and Swiss disposal classes since these elements significantly pollute the excavated molasse material and hence, requires purification. The classification proposes a first mineralogical link to a unified European, technical guideline concerning re-use of tunnel excavation material.

Since these preliminary results showed a mineralogical classification approach, future studies foresee further boreholes being taken into account along FCC's full quasi-elliptical layout considering all mineralogical data in different boreholes. Contextually, this data will be linked to existing geotechnical values as well as new measurements within the same survey area. Currently measured multi-disciplinary, especially geotechnical laboratory data as well as old archive data to be digitized is going to compare with geophysical borehole logs (e.g. sonic, resistivity, gamma-ray and induction log) to derive testing geotechnical parameters. These parameters are in preparation and will be presented in a forthcoming paper. Gamma-ray logs will be used to detect natural radioactive occurrences, compare them with laboratory measurements and calculate shale volumes prior to FCC site investigations and construction phases to establish a general prediction model. These cross-correlations will have to prove its accuracy, credibility and liability within the next study efforts.

References

- Abada A, Abbrescia M, AbdusSalam S S, et al (2019a) FCC Physics Opportunities. *Eur Phys J C* 79 (6): 474. 10.1140/epjc/s10052-019-6904-3.
- Abada A, Abbrescia M, AbdusSalam SS, et al (2019b) FCC-ee: The Lepton Collider. *Eur Phys J Spec Top* 228 (2): 261-623. 10.1140/epjst/e2019-900045-4.
- Abada A, Abbrescia M, AbdusSalam SS, et al (2019c) FCC-hh: The Hadron Collider. *Eur Phys J Spec Top* 228 (4): 755-1107. 10.1140/epjst/e2019-900087-0.
- Acar Y C, Akay A N, Beser S, et al (2017) Future circular collider based lepton–hadron and photon–hadron colliders: Luminosity and physics. *Nucl Instruments Methods Phys Res Sect A Accel Spectrometers, Detect Assoc Equip* 871: 47-53. 10.1016/J.NIMA.2017.07.041.
- Chelle-Michou C, Do Couto D, Moscariello A, Renard P, Rusillon E (2017) Geothermal state of the deep Western Alpine Molasse Basin, France-Switzerland. *Geothermics* 67: 48-65. 10.1016/J.GEOTHERMICS.2017.01.004.
- Erben H (2016) Real-Time Material Analysis and Development of a Collaboration and Trading Platform for Mineral Resources from Underground Construction Projects, Doctoral thesis at Montanuniversität Leoben, Austria.
- Fabbri C (2004) The Gotthard Base Tunnel – Project Overview, The 6th Annual Tunnelling Conference, Sydney, August 30-31.
- Fern E J, Di Murro V, Soga K, Li Z, Scibile L, Osborne J A (2018) Geotechnical characterisation of a weak sedimentary rock mass at CERN, Geneva. *Tunnelling and Underground Space Technology* 77: 249–260. 10.1016/j.tust.2018.04.003.
- Füchtbauer H (1988) *Sedimente und Sedimentgesteine, Sediment-Petrologie, Teil II*, 4th edition Schweizerbart Science Publishers, Stuttgart, Germany
- INDU, Himmelsbach C, Thalman C, Petitat M, Galler R, Barwart S, Erben H, Klein A, Zein A (2014) D3.2 Online analysis technology (publishable part), Development of Resource-Efficient and advanced underground technologies, http://www.dragonproject.eu/_pdf/555d7c674aa40.pdf, accessed at 10/24/2019.
- Michel P, Bertholet F, Neuenschwander M, Carron C (2016) Bewirtschaftung und Wiederverwertung von Ausbruchmaterial – Gestion et valorisation des matériaux d’excavation, inventaire de grands projets suisse, Fachgruppe für Untertagebau (FGU), Esslingen, Switzerland.
- Moscariello A (2018) The geomorphological landscapes in the Geneva basin. In E. Reynard (Ed): *Landscapes and Landforms of Switzerland*. Springer Verlag, in press.
- Moscariello A, Guglielmetti L, Omodeo-Salé S, et al (2020) Heat production and storage in Western Switzerland: advances and challenges of intense multidisciplinary geothermal exploration activities, an 8 years progress report. In: *Proceedings World Geothermal Congress 2020, Reykjavik Iceland, April 26 – May 2*.
- Resch D, Lassnig K, Galler R, Ebner F (2009) Tunnel excavation material – high value raw material, *Geomechanics and Tunnelling* 2 (5): 612-618. 10.1002/geot.200900047.
- Tokgöz N (2013) Use of TBM excavated materials as rock filling material in an abandoned quarry pit designed for water storage, *Engineering Geology* 153:152-162. 10.1016/j.enggeo.2012.11.007.
- Trümpy R (1980) Part A: *An Outline of the Geology of Switzerland*, edit. by Trümpy, R., Homewood, P.W., Ayrton, S., Fischer, H., Wepf & Co. Publishers, Basel, Switzerland.
- Zimmermann F (2015) High-energy physics strategies and future large-scale projects. *Nucl Instruments Methods Phys Res Sect B Beam Interact with Mater Atoms* 355: 4–10. 10.1016/j.nimb.2015.03.090.

C Non-peer-reviewed articles, data reports and database file

- C.1 Wiederverwertung ausgehobener Molasse basierend auf geologischer Untergrundmodellierung für den geplanten 100 km Teilchenbeschleuniger-Tunnel am CERN nahe Genf, Schweiz

Table C.1: Overview of authorship and metadata of the non-peer-reviewed *Berg- und Hüttenmännische Monatshefte*.

Title	Wiederverwertung ausgehobener Molasse basierend auf geologischer Untergrundmodellierung für den geplanten 100 km Teilchenbeschleuniger-Tunnel am CERN nahe Genf, Schweiz
Author name	Maximilian Haas
Author's contributions	Conceptualization; literature review; visualizations; writing (original draft); writing (review & editing)
Scientific value	Promotion of the FCC study and outline of research questions.
Status	Published in <i>Berg- und Hüttenmännische Monatshefte</i>
Peer-reviewed journal	no
Full citation	Haas M., Wiederverwertung ausgehobener Molasse basierend auf geologischer Untergrundmodellierung für den geplanten 100 km Teilchenbeschleuniger-Tunnel am CERN nahe Genf, Schweiz, <i>Berg- und Hüttenmännische Monatshefte</i> 2020, https://doi.org/10.1007/s00501-020-01026-6 .

Originalarbeit



Berg Huettenmaenn Monatsh
<https://doi.org/10.1007/s00501-020-01026-6>
© Der/die Autor(en) 2020

BHM Berg- und
Hüttenmännische
Monatshefte

Wiederverwertung ausgehobener Molasse basierend auf geologischer Untergrundmodellierung für den geplanten 100 km Teilchenbeschleuniger-Tunnel am CERN nahe Genf, Schweiz

Maximilian Haas^{1,2,3,4}

¹European Organization for Nuclear Research (CERN), Meyrin, Schweiz

²Subsurface Engineering, Montanuniversität Leoben, Leoben, Österreich

³Geo-Energy Reservoir Geology and Sedimentary Basin Analysis, Université de Genève, Genf, Schweiz

⁴Prévessin-Moëns, Frankreich

Eingegangen 24. September 2020; angenommen 29. September 2020

Zusammenfassung: Das CERN (Conseil Européen pour la Recherche Nucléaire bzw. European Laboratory for Particle Physics) ist eine weltweit führende internationale Forschungseinrichtung auf dem Gebiet der Hochenergie- und Teilchenphysik. Die Erforschung der grundlegenden Bausteine des Universums und ihrer Interaktionen lieferte in den vergangenen Jahrzehnten bahnbrechende Erkenntnisse, die im experimentellen Nachweis des Higgs-Boson im Juli 2012 gipfelten. Um die in diesem Zusammenhang erforderten Erkenntnisse weiter zu vertiefen und noch unbeantwortete Fragen nach dem Ursprung und der Funktion des Universums zu beantworten, hat eine internationale Gemeinschaft von über 150 Instituten weltweit am CERN eine Studie für ein Forschungsprogramm mit einer neuen, leistungsfähigeren Teilchenbeschleunigerinfrastruktur initiiert. Die Future Circular Collider (FCC) Studie schließt die dafür erforderlichen unterirdischen Tunnel, Kavernen und Schächte und die damit verbundenen Konstruktionen an der Oberfläche mit ein. Die Infrastruktur ist so ausgelegt, um im Zusammenschluss mit den bereits bestehenden Teilchenbeschleunigern am CERN (z. B. PSB, PS, SPS, LHC) zu funktionieren. Im Rahmen des Projekts wurden seit 2014 die ersten technischen Machbarkeitsstudien in den verschiedensten Gebieten, unter anderem Geologie und Konstruktion des Tunnels, der sich über ca. 100 km im teils westschweizerischen und teils französischen Molassebecken erstreckt, durchgeführt, sodass FCC nach derzeitigem Planungsstand um das Jahr 2040 in Betrieb gehen kann. Im Zuge dessen ist ein geologisches Untergrundmodell uner-

lässlich, um einen sicheren Bau unterirdischer Infrastruktur zu gewährleisten und die Baumethode auf die Geologie abzustimmen. Ein entscheidender Faktor neben dem geologischen Modell ist die Wiederverwertbarkeit des ausgehobenen Molasse-Materials mit einem Volumen von etwa 9 Mio. m³ sowohl aus technischer als auch rechtlicher, gesellschaftspolitischer und sozio-ökonomischer Sicht.

Dieser Artikel soll einen Einblick in diese beiden Machbarkeitsstudien des FCC Projekts geben, sowie Ansätze der geologischen, petrophysikalischen, geotechnischen und mineralogisch-chemischen Analysen präsentieren, die zur Beantwortung der Wiederverwertung dienen und in weiterer Folge in das geologische Untergrundmodell einfließen werden.

Schlüsselwörter: Molasse, Klassifizierung, Wiederverwertung, CERN

Re-use of Excavated Molasse Based on Subsurface Geological Modelling for a 100 km Particle Accelerator Tunnel at CERN near Geneva, Switzerland

Abstract: CERN (European Laboratory for Particle Physics or Conseil Européen pour la Recherche Nucléaire) is a world-leading international research institution in the field of high-energy and particle physics. During the past decades, research about the fundamental building blocks of the universe and their interactions has provided groundbreaking insights, culminating in the experimental detection of the Higgs boson in July 2012. In order to further deepen the knowledge and to answer yet unanswered questions about the origin and function of the universe, an international consortium of more than 150 institutes worldwide has initiated a study at CERN for a research

Dipl.-Ing. M. Haas, B.Sc. (✉)
Chemin Du Mail 97,
01280 Prévessin-Moëns, Frankreich
maximilian.mathias.haas@cern.ch

Originalarbeit

programme involving a new, more powerful particle accelerator infrastructure. The Future Circular Collider (FCC) study includes the necessary underground tunnels, caverns and shafts and the associated surface sites. The infrastructure is designed to work in accordance with existing particle accelerators at CERN (e.g. PSB, PS, SPS, LHC). Since 2014, the project has carried out first technical feasibility studies in a wide range of areas, including geology and tunnelling construction, which extends over ca. 100 km in the Molasse Basin, across both western Switzerland and France. According to current planning, FCC will be operational around 2040. With respect to these feasibility studies, a geological subsurface model is essential to ensure safe construction of underground infrastructure and to adapt excavation methods to the geology. In addition to the geological model, potential re-use of the excavated molasse material, which has a volume of around 9 million m³ proves to be an essential technical, legal, socio-political and socio-economic factor.

This article intends to provide first insights into the geological, petrophysical, geotechnical and mineralogical-chemical analyses, which will be used to answer the question of molasse re-use and will subsequently be incorporated into the geological underground model.

Keywords: Molasse, Rock mass characterisation, Re-use, CERN

1. Einleitung

Die Wiederverwendung von Tunnelausbruchmaterial ist aus ökologischen und ökonomischen Gründen zu einem entscheidenden Faktor in unterirdischen Bauprojekten geworden. Technische Machbarkeit und gesetzliche Rahmenbedingungen sind die beiden Hauptelemente, um diesen Sektor der Kreislaufwirtschaft umsetzbar zu machen. Bau- und Abbruchabfälle machen heute etwa ein Drittel des Gesamtabfallaufkommens in der Europäischen Union (EU) mit einer Wiederverwendungsrate von durchschnittlich 46% aus [1, 2]. Von nationalen Gesetzen gefordert, birgt die in Einklang mit der Natur und ökonomisch vertretbare Lösungssuche jedoch politische, rechtliche und technische Hürden in sich. Nach heutigem Stand wird Aushubmaterial als Abfall deklariert, was eine effiziente Wiederverwendung erschwert. Diverse Initiativen der EU und nationaler Organisationen (z. B. CETU und AFTES in Frankreich, GESDEC in der Schweiz, ÖBV in Österreich) haben dazu geführt, dass organisatorische und technische Richtlinien für die Wiederverwendung von Aushubmaterial in den letzten zwei Jahrzehnten entstanden sind. Eine sich verbessernde Situation hin zu einer einheitlichen europäischen Gesetzgebung fehlt [3].

Eine Vorreiterrolle nehmen die Staaten Schweiz, Frankreich und Österreich ein, die mit ihren großen Tunnelbauprojekten und unterschiedlichsten geologischen Formationen zu innovativer Lösungssuche gefordert sind. Die beiden erstgenannten Staaten sollen zukünftig den Unter-

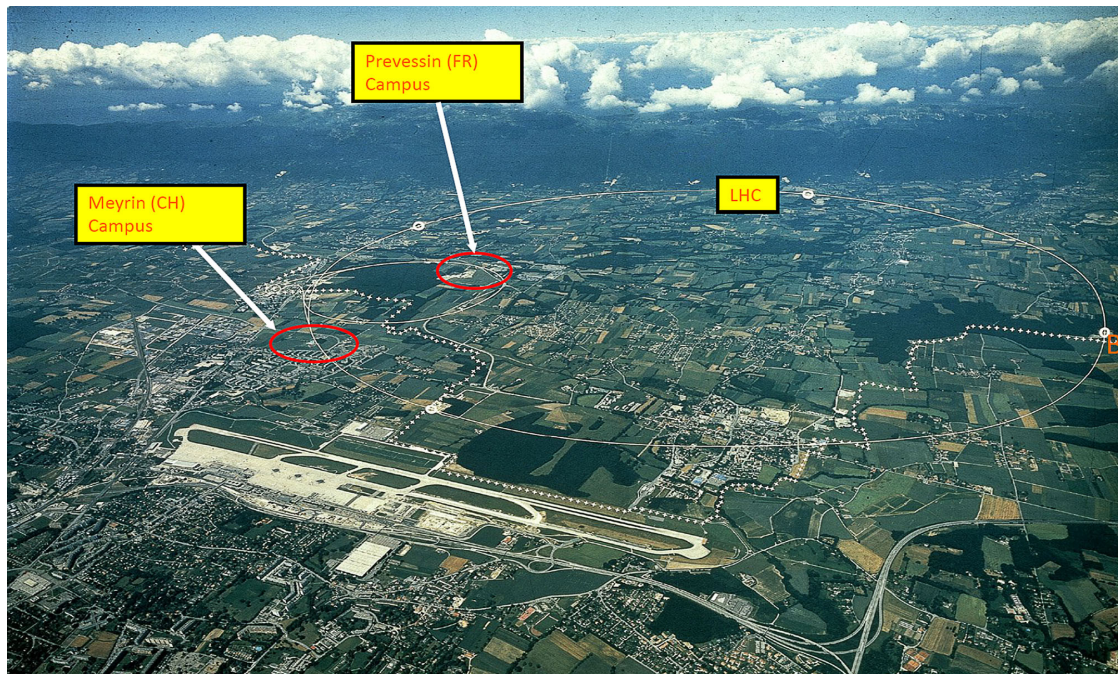


Abb. 1: Blick vom Genfer See aus auf die Hauptstandorte des CERN in der Schweiz (CH) und Frankreich (FR) und des im Untergrund verlaufenden LHC-Teilchenbeschleunigers

grund für den größten Teilchenbeschleuniger der Welt am CERN nahe Genf beherbergen. Er soll nicht nur das Standardmodell der Physik, sondern auch die Verwertbarkeit von etwa 9 Mio. m³ Aushubmaterial mit großem Molasse-Anteil in einem neuen, verbesserten geologischen Untergrundmodell revolutionieren. Da für dieses Material nach heutigem Stand der Technik keine ökonomisch relevante Wiederverwertungstechnologie im Einsatz ist, wurde im September 2018 ein Forschungsprojekt im Rahmen eines Doktorats am CERN in Zusammenarbeit mit der Montanuniversität Leoben, Österreich und der Université de Genève, Schweiz initiiert, über das in diesem Artikel berichtet werden soll.

2. CERN und die Future Circular Collider Studie

Das CERN erstreckt sich am Fuße des Genfer Sees auf schweizerischem (Meyrin, Kanton Genf) sowie französischem (Prévessin-Moëns, région Auvergne-Rhône-Alpes) Terrain und betreibt den derzeit mit 27 km Länge größten Teilchenbeschleuniger, den Large-Hadron-Collider (LHC) (siehe Abb. 1). Mit mehr als 3500 Wissenschaftlern vor Ort und über 10.000 weltweit stellt er eine der größten Forschungsinfrastrukturen überhaupt dar. Ab dem Jahr 2040 könnte ein 100 km langer neuer Teilchenbeschleuniger, dessen Projektname derzeit noch als Future Circular Collider (FCC) [4, 5] betitelt wird, in Betrieb gehen, um einer weltweiten Gemeinschaft von Wissenschaftlern ein Forschungsprogramm bis zum Ende des 21. Jahrhunderts zu ermöglichen. Hierfür müssen in den geologischen Formationen des lokalen Molassebeckens ein etwa 100 km langer, kreisförmiger Tunnel sowie 18 Schächte und 14 Kavernen gebaut werden (siehe Abb. 2). Im Jahr 2022 sollen erste Erkundungsbohrungen entlang der aktuellen Trassenwahl abgeteuft werden, die, zusammen mit bestehenden geologischen Daten wie Aufschluss- und Bohrprobenanalysen, seismischen Messungen und Bohrloch-Daten, ein erstes

geologisches Untergrundbild liefern. Diese Unternehmung ist Teil eines technischen Projektrisikomanagements, um Design und Umsetzungsplanung für den Bau der Infrastruktur zu optimieren.

Es soll hier ein erster Einblick in das Forschungsvorhaben gegeben und sowohl die rechtlichen Grundlagen von Wiederverwertung im europäischen und speziell französisch-schweizerischen Kontext dargelegt, als auch geomechanische, petrophysikalische sowie chemisch-mineralogische Analysen bestehender Bohrungen mitsamt Bohrloch-Logdaten für ein geologisches Modell erörtert werden.

3. Einblick in die Geologie

Das in Abb. 3 dargestellte Westalpine Molassebecken (WAMB), das in der Westschweiz oft als Genfer Becken oder „bassin franco-genevois“ bezeichnet wird, ist Teil des Schweizer Mittellandes und durch den Salève im Südosten und den Jura im Nordwesten begrenzt. Diese markanten geologischen Erhebungen wurden durch tektonische Deformationen während der Einlagerung im Alpenvorland, den damit verbundenen Vergletscherungen des Pleistozäns und nacheiszeitlichen Prozessen beeinflusst [6, 7].

Das WAMB gliedert sich in das Alpenvorland, bestehend aus der Jurahochebene und Haute Chaîne, sowie in die alpinen Einheiten, die durch die Voralpen bzw. penninischen, subalpinen und helvetischen Decken und äußeren kristallinen Massives repräsentiert werden [8]. Die im Becken vorhandenen Gesteinseinheiten der Molasse treten entlang des Salève, der Vuache und des Jura zutage, die aus mesozoischen Sedimentgesteinen bestehen. Die mesozoische Abfolge beginnt mit Evaporiten an der Basis, gefolgt von einer Sukzession von Kalksteinen und Mergeln, die zum südlichen Rand des europäischen Kontinents vor der alpinen Orogenese gehörten und auf den Tethys-Ozean zurück zu führen sind. Die mesozoische Abfolge wurde auf dem paläozoischen kristallinen Grundgebirge abgelagert. Diese zeigt grabenartige Strukturen, die mit kontinentalen,

Abb. 2: Nicht-maßstabsgetreue 3D Skizze des geplanten FCC Tunnels sowie dessen Schächte und Kavernen. (Modifiziert nach [4])

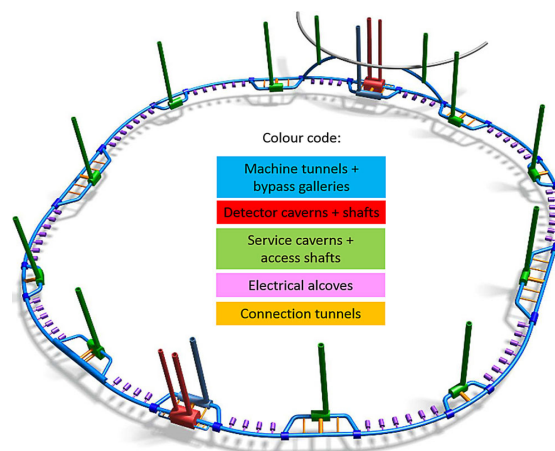
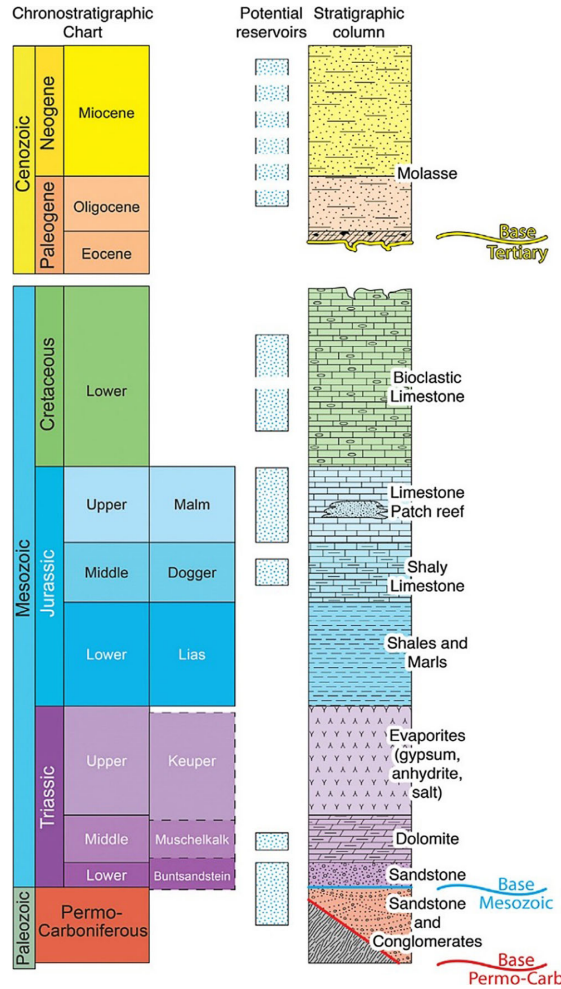




Abb. 3: Chronostratigraphische Abfolge des Molasse-Bekens in der Westschweiz und französischen Umgebung. Für das FCC-Projekt entscheidend sind die Formationen des Känozoikums (Molasse). (Modifiziert nach [7])



siliziklastischen Sedimenten während des Perm und Karbon im Anschluss an die variszische Orogenese gefüllt waren [9]. Die obersten Einheiten der mesozoischen Sequenz weisen auf eine ausgedehnte, erosive Oberfläche hin, die sich während der Hebung des Vorlandbeckens durch Komprimierung des Alpengürtels bildeten. Oberhalb der Erosionsoberfläche wird oligozäne, heterogene, siliziklastische Molasse von quartären glazialen bis fluvialen Ablagerungen überlagert. Die Molasseeinheiten wurden während der alpinen Orogenese als Detritalformationen abgelagert [10] und repräsentieren die von der FCC angestrebte Bautiefe bis in 250 m Tiefe.

4. Legale Aspekte der Wiederverwertung von Tunnelausbruchmaterial

In den Jahren 2000 bis 2010 schlug die Europäische Union (EU) eine klare Richtung für eine effiziente Wiederverwendung von Ressourcen ein, was zu einer verstärkten Einführung von nationalen Gesetzen und Richtlinien in diesem Zeitraum führte. Rechtliche Überlegungen und gesetzliche Verabschiedungen florierten, doch die daraus resultierende Heterogenität und mangelnde Kommunikation der Gesetzgeber untereinander sind noch bis heute eines der Schlüsselthemen, die es für eine effiziente Wiederverwertung zu beseitigen gilt.

Das Abfallkonzept der Europäischen Union ist in der Abfallrahmenrichtlinie 2008 definiert und legt Maßnahmen zum Schutz der Umwelt fest [11]. Gesteins- und Bodenaushub sind Teil des Abfallregimes und unterliegen damit der Gültigkeit des Abfallwirtschaftsgesetzes. Für Tunnel-

ausbruchmaterial, das nach EU-Richtlinien auf Baustellen wiederverwertet wird, ist die objektive Definition von Abfall nicht erfüllt. Um Ausbruchmaterial von Tunnelbaustellen wiederzuverwenden, ist es notwendig, das Ende des Abfallstatus zu erreichen. Abfälle können verwertet werden, wenn die gleichen Anforderungen wie an Primärrohstoffe erfüllt sind. Die Tatsache, dass das meiste Aushubmaterial nicht in einer Form zur sofortigen Wiederverwendung zur Verfügung steht und dass die Möglichkeiten der Wiederverwertung sorgfältig geprüft werden müssen, erfüllt die Definition des Ziels von Abfall. Die abfallrechtliche Terminologie wird durch Bundesregierungen und EU-Richtlinien geregelt, die in nationales Recht in den einzelnen Mitgliedsstaaten umgesetzt werden müssen. Eine umfassende Liste von europäischen Gesetzen, Richtlinien und Empfehlungen für Österreich, die Schweiz, Frankreich, Italien und die EU im Rahmen der Wiederverwertung von Gesteins- und Bodenaushub aus dem Untergrund können [3] entnommen werden.

Die Entwicklung in Richtung einer einheitlichen europäischen Gesetzgebung hat sich in den letzten fünf Jahren verbessert. Österreich, die Schweiz und Frankreich erweisen sich als Vorbilder bei der Wiederverwertung von Aushubmaterial, die durch eine solide Gesetzgebung und nationale Richtlinien untermauert ist, was durch die Tatsache, dass sich das FCC-Projekt um eine sowohl umweltfreundliche als auch ökonomisch wertvolle Wiederverwertung bemüht, unterstrichen wird. Einschränkungen für die Definition der relevanten Endverbraucher beinhalten eine mineralogische und geochemische Charakterisierung von Aushubmaterial und Boden sowie deren Positionierung in Bezug auf die

Grenzwerte für inerte Abfälle, wie sie in den verschiedenen nationalen Gesetzgebungen definiert sind. Eine Anpassung und Homogenisierung dieser Schwellenwerte wird unter den Alpenländern dringend empfohlen und könnte zu einer gemeinsamen europäischen Gesetzgebung führen, indem technische Messungen und rechtliche Ansätze standardisiert werden [3].

Im Rahmen des FCC-Forschungsvorhabens wird bereits heute an Verwertungskonzepten gearbeitet, deren zugrunde liegende Messkonzepte und Apparaturen einfach und schnell auf eine Tunnelbohrmaschine installiert und deren Messanalysen während des Materialstroms des Aushubs erste Einblicke in die zu verwertenden Möglichkeiten geben sollen. Im Zuge dessen ist auch ein Vergleich von on-line (on-site) und Laborergebnissen bezüglich Art der Vortriebsmethode sowie detaillierte geomechanische, petrophysikalische und chemisch-mineralogische Analysen von reinem oder kontaminiertem Ausbruchmaterial aus dem Untertagebau zu erstellen, die ein hochauflösendes geologisches Untergrundmodell liefern sollen.

5. Datenakquisition und Datenanalyse

Im Zuge der Erarbeitung eines geologischen Untergrundmodells und der Fragestellung zur potentiellen Wiederverwertung der Molasse werden entlang der möglichen FCC-Trassen Proben aus Bohrungen und Aufschlüssen chemisch-mineralogisch, geomechanisch und petrophysikalisch sowie mit weiteren in-situ-Bohrlochdaten wie geophysikalischen Logkurven, geomechanischen Tests oder

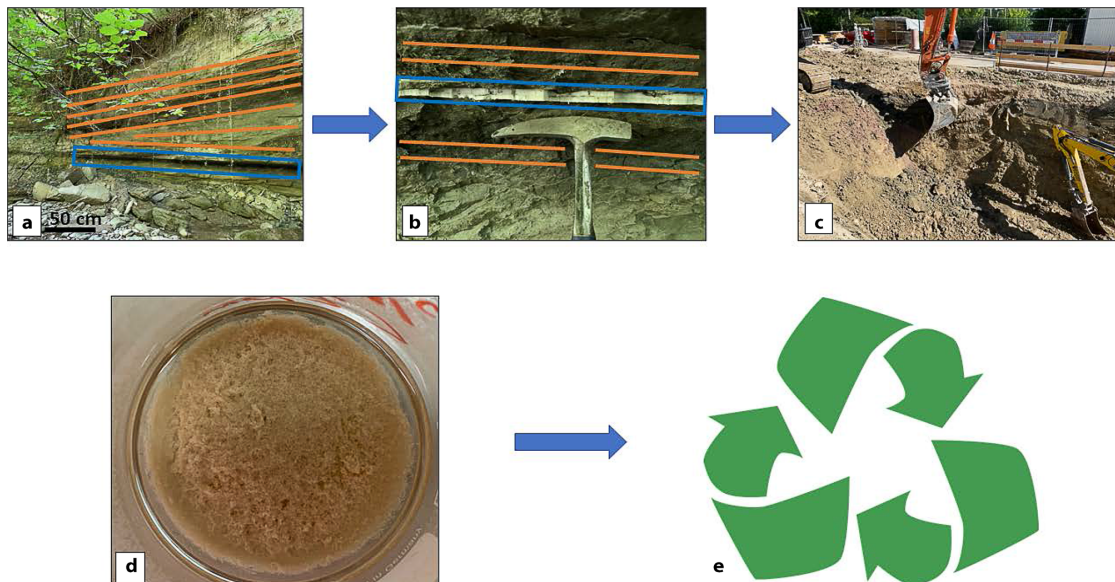


Abb. 4: Das Verfahren der Probenahme und Analyse wird gezeigt. a Molasse-Aufschluss entlang des zukünftigen Tunnels in Frankreich. Orange Linien stellen Molasse dar, blaue Linie heben Gipsschichten hervor (Heterogenität). b Nahaufnahme der Gipsschicht (blau) mit Molasse (orange Linien). c Probenahme in einer Baustelle nahe Genf. d Tonminerale, die aus Proben im Labor extrahiert wurden, um schließlich (e) potenziell für z. B. Geopolymere oder Ziegelherstellung wiederverwertet werden zu können

Originalarbeit

Abb. 5: Eine im Jahr 1944 durchgeführte Bohrung im FCC-Trassenbereich. Gesteinsproben in den 98 Kernboxen wurden geologisch (sedimentologisch), mineralogisch sowie geotechnisch und petrophysikalisch in Feldversuchen und Laboren untersucht



Abb. 6: Molasse-Aufschluss entlang der FCC-Trasse. Proben wurden aus dem Gesteinsverband entnommen und als vollständige Kerne oder als Plugs (kleine, zylinderförmige Proben) im Labor analysiert



seismischen Datensätzen verglichen und analysiert. Diese Tests beinhalten u. a. XRF-, XRD- und ICP-MS-Analysen, QEMSCAN®, TOC-Gehaltbestimmungen, Eluatversuche, FT-IR Spektren, Porositäts- und Permeabilitätsmessungen sowie LCPC, Cerchar, Point-Load und einaxiale Druckfestigkeitstests. Abb. 4 zeigt den Ablauf von einer genommenen Probe an einem Aufschluss in Frankreich, bis zur Extraktion von Tonmineralen und weiterer Wiederverwertung. Für eine interessante Entdeckung sorgte eine Bohrung im schweizerischen Kernlager aus dem Jahre 1944 (siehe Abb. 5), die Bohrkern exzellenter Qualität enthielt und für diverse weitere Tests verwendet werden konnte. Die Aufschlüsse – wie in Abb. 6 dargestellt – verteilen sich quer

über das gesamte Molassebecken und werden sukzessive beprobt und analysiert.

6. Technische Herangehensweise und erste Ergebnisse

Ein erstes Klassifizierungsmodell der Molasse-Gesteinsmasse wurde anhand von QEMSCAN®, XRF- und ICP-Datenanalysen auf Grundlage von Lithotypen und modaler Mineralogie vorgestellt. Erste Modelle zeigen, dass das Vorhandensein von Anhydrit in der Molasse Herausforderungen beim Tunnelbau darstellen könnte [12]. Die

geologische Heterogenität des Gesteins wurde durch die Verwendung elementarer mineralogischer und lithologischer Analysen überwunden, wobei die Radioaktivität von natürlich vorkommendem Uran und Thorium ermöglicht, Molasse als erste Schnellmethode zu klassifizieren.

Die Analysen zeigen Nickel- und Chromgehalte im oberen und Anhydrit im oberen und unteren Molassebereich der FCC-Konstruktionstiefen. Feinkörnige, mergelige Sandstein-Lithotypen enthalten Cr-Spinell und Serpentin. Dies ermöglicht einerseits eine Sub-Lithotyp-Klassifizierung zwischen Sandstein und Mergel. Andererseits steigen die im Serpentin enthaltenen Nickel- und Chrom-Konzentrationen mit zunehmender Tiefe und könnten somit eine Wiederverwertung aufgrund von Verschmutzung als äußerst schwierig und teuer gestalten. Die Klassifizierung schlägt eine mineralogische Brücke zu einer einheitlichen europäischen technischen Richtlinie zur Wiederverwertung von Tunnelausbruchmaterial vor. Das vorgeschlagene Klassifizierungsmodell dient als Bindeglied zur französischen und schweizerischen Gesetzgebung sowie zu einer europäischen technischen Richtlinie für eine Wiederverwertung von Tunnelausbruchmaterial auf internationalen Baustellen. Es liefert die Grundlage für zukünftige umweltfreundliche technische Vertragsmodelle aus Sicht des Auftraggebers und des Auftragnehmers unter den Bedingungen und unter dem Schutz der nationalen, europäischen und internationalen Gesetzgebung und Umwelt.

7. Fazit und Ausblick

Eine weltweite Zusammenarbeit von über 150 Instituten plant am CERN den weltweit größten Teilchenbeschleuniger in schweizerischem und französischem Untergrund. Der hierfür benötigte etwa 100 km lange Tunnel könnte noch vor Ende des Jahrzehnts in Bau gehen und wird seit 2014 von technischen, rechtlichen und sozio-ökonomischen Machbarkeitsstudien begleitet. Dies erfordert die Entwicklung eines neuen geologischen Untergrundmodells des westlichen Molassebeckens sowie die Darstellung der Wiederverwertbarkeit von Ausbruchmaterial. Das von der EU im H2020 Rahmenprogramm für Forschung kofinanzierte Projekt FCCIS (FCC Innovation Study) beinhaltet dazu konkret ein Evaluierungsprogramm. Im Zuge dessen wurden Proben aus Bohrlöchern und Aufschlüssen entlang der derzeit verlaufenden FCC-Trassen entnommen und mineralogisch-chemisch, petrophysikalisch und geomechanisch analysiert.

Technische Einschränkungen implizieren die physikalische und chemische Charakterisierung von Ausbruchmaterial sowie deren Positionierung im Verhältnis zu den Grenzwerten für inerte Abfälle, was eine ausgefeilte Materialflussanalyse erfordert und bereits bei einer beim FCC eingesetzten Tunnelbohrmaschine zukünftig eingesetzt werden könnte. Ein Materialflussanalysekonzept, das auf einer Tunnelbohrmaschine installiert wird und On-line-Analysen durchführt, die Konditionierung, Trennung und Transport von Ausbruchmaterial zu den Endverbrauchern effizient gestaltet, könnte als innovative Lösung für den Bau zukünftiger Tunnel am Paradebeispiel FCC dienen.

Da diese vorläufigen Ergebnisse einen mineralogisch-chemischen Klassifizierungsansatz zeigten, sehen zukünftige Arbeiten vor, dass weitere Bohrungen entlang des FCC unter Berücksichtigung aller Daten in verschiedenen Bohrlöchern in Betracht gezogen werden. Diese Daten sollen kontextbezogen mit bestehenden geotechnischen Werten sowie mit neuen Messungen innerhalb desselben Untersuchungsgebiets verknüpft werden. Gegenwärtig gemessene multidisziplinäre, insbesondere geotechnische und petrophysikalische Labordaten sowie alte Archivdaten, die digitalisiert werden, sollen mit geophysikalischen Bohrlochdaten (z. B. Schall-, Widerstands-, Gammastrahlen- und Induktionslogs) verglichen werden, um daraus geotechnisch relevante Parameter abzuleiten. Solche Korrelationen müssen im Rahmen der folgenden Arbeiten ihre Genauigkeit, Glaubwürdigkeit und Zuverlässigkeit unter Beweis stellen. Neue Daten werden im Zuge der im Jahr 2022 stattfindenden Erkundungsbohrungen verfügbar sein, die das geologische Untergrundmodell sukzessive vervollständigen.

Förderung. This project receives funding from the European Union's Horizon 2020 research and innovation programme under the European Union's Horizon 2020 research and innovation programme under grant agreement No 951754. Dieses Projekt wird im Rahmen des Horizon 2020 Forschungs- und Innovationsprogramms der Europäischen Union unter der Finanzhilfvereinbarung Nr. 951754 kofinanziert.

Funding. Open access funding provided by CERN (European Organization for Nuclear Research)

Open Access Dieser Artikel wird unter der Creative Commons Namensnennung 4.0 International Lizenz veröffentlicht, welche die Nutzung, Vervielfältigung, Bearbeitung, Verbreitung und Wiedergabe in jeglichem Medium und Format erlaubt, sofern Sie den/die ursprünglichen Autor(en) und die Quelle ordnungsgemäß nennen, einen Link zur Creative Commons Lizenz beifügen und angeben, ob Änderungen vorgenommen wurden.

Die in diesem Artikel enthaltenen Bilder und sonstiges Drittmaterial unterliegen ebenfalls der genannten Creative Commons Lizenz, sofern sich aus der Abbildungslegende nichts anderes ergibt. Sofern das betreffende Material nicht unter der genannten Creative Commons Lizenz steht und die betreffende Handlung nicht nach gesetzlichen Vorschriften erlaubt ist, ist für die oben aufgeführten Weiterverwendungen des Materials die Einwilligung des jeweiligen Rechteinhabers einzuholen.

Weitere Details zur Lizenz entnehmen Sie bitte der Lizenzinformation auf <http://creativecommons.org/licenses/by/4.0/deed.de>.

Literatur

1. European Commission: EU construction & demolition waste management protocol, Official Journal of the European Union (2016), pp. 1–22
2. Poulidakos, L.D.; Papadaskalopoulou, C.; Hofko, B.; Gschösser, F.; Cannone Falchetto, A.; Bueno, M.; Arraigada, M.; Sousa, J.; Ruiz, R.; Petit, C.; Loizidou, M.; Partl, M.N.: Harvesting the unexplored potential of European waste materials for road construction, Resources, Conservation & Recycling 116 (2017), pp. 32–44
3. Haas, M.; Galler, R.; Scibile, L.; Benedikt, M.: Waste or valuable resource—a critical European review on re-using and managing tunnel excavation material, Resources, Conservation & Recycling, 162 (2020). <https://doi.org/10.1016/j.resconrec.2020.105048>
4. Abada, A.; Abbrescia, M.; AbdusSalam, S.S. et al.: FCC-ee: The LEPton Collider. European Physical Journal Special Topics 228 (2019), pp 261–623
5. Offizielle Future Circular Collider Studie Homepage (CDR reports): <https://fcc-cdr.web.cern.ch/> (Zugriff: 06.10.2020)

Originalarbeit

6. Moscariello, A.: The geomorphological landscapes in the Geneva basin, In: Reynard, E. (Ed): Landscapes and Landforms of Switzerland, Cham: Springer, 2020, pp 83–96
7. Moscariello, A.: Exploring for geo-energy resources in the Geneva Basin (Western Switzerland): opportunities and challenges, Swiss Bulletin für angewandte Geologie, 24 (2019), no.2, pp 105–124
8. Chelle-Michou, C.; Do Couto, D.; Moscariello, A.; Renard, P.; Rusillon, E.: Geothermal state of the deep Western Alpine Molasse Basin, France-Switzerland, Geothermics, 67 (2017), pp. 48–65
9. Moscariello, A.; Guglielmetti, L.; Omodeo-Salé, S.; Haller, A.; Eruteya, O.; Ying Lo, H.; Clerc, N.; Makhloufi, Y.; Couto, D.D.; Oliveira, G. F.; Perozzi, L.; De Oliveira Filho, F.; Hollmuller, P.; Quiquerez, L.; Bono, C. N. D.; Martin, F.; Meyer, M.: Heat production and storage in Western Switzerland: advances and challenges of intense multidisciplinary geothermal exploration activities, an 8 years progress report, Proceedings World Geothermal Congress (2020), Reykjavik Iceland, April 26–May 2, <https://archive-ouverte.unige.ch/unige:127903> (Zugriff 28.09.2020)
10. Trümpy, R.: Geology of Switzerland, a guide book, Part A: An Outline of the Geology of Switzerland, edit. by Trümpy, R., with contributions by Homewood, P.W.; Ayrton, S.; Fischer, H. Basel: Wepf, 1980
11. European Commission: Directive 2008/98/EC on waste (waste framework directive), <https://ec.europa.eu/environment/waste/framework/> (Zugriff am 17.09.2020)
12. Haas, M.; De Haller, A.; Moscariello, A.; Scibile, L.; Benedikt, M.; Gegenhuber, N.; Galler, R.: A mineralogical re-use classification model of molasse rock mass in the Geneva Basin, ISRM International Symposium Eurock 2020—Hard Rock Engineering, Trondheim, Norway, in press

Hinweis des Verlags. Der Verlag bleibt in Hinblick auf geografische Zuordnungen und Gebietsbezeichnungen in veröffentlichten Karten und Institutsadressen neutral.

C.2 Microsoft Access database and data reports

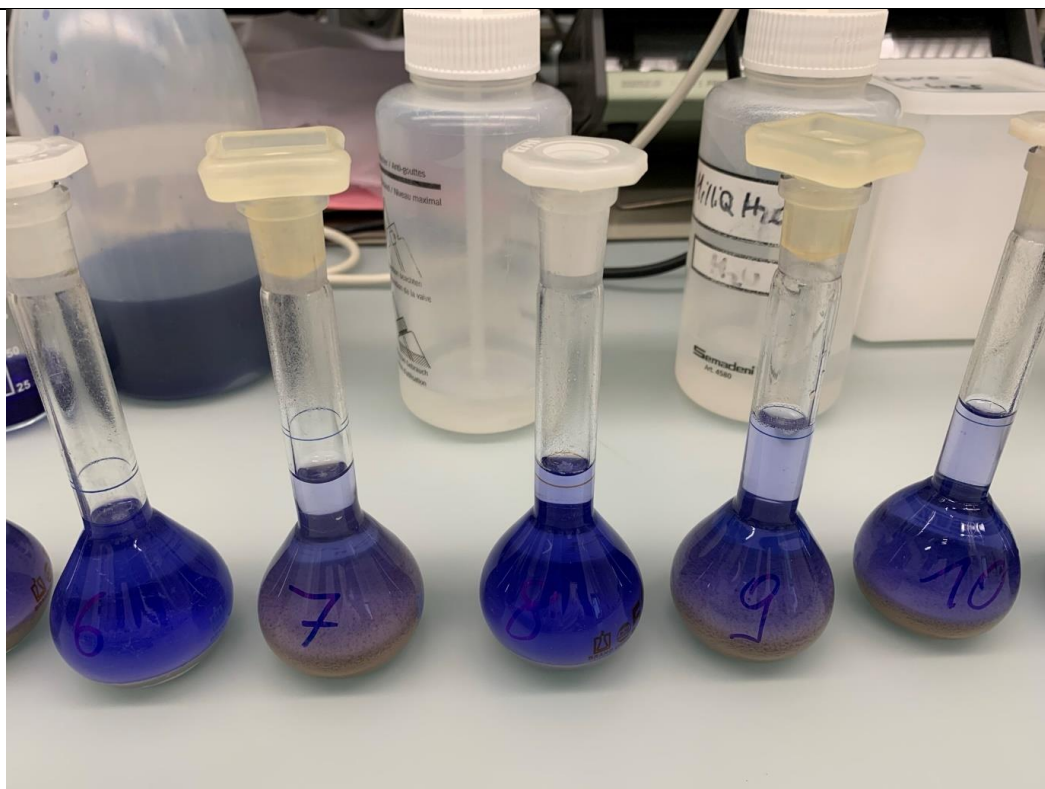
The full PhD data as well as reviewed and digitised stratigraphic information, well reports and rock sample pictures are accessible under the following OneDrive link upon password request by the author or a responsible person involved in the Future Circular Collider study at CERN:

<https://1drv.ms/u/s!AmfdD0Z-13USje5h9QAG01U4zzR5mQ?e=EfSa8O>

The following data reports have been published on the ZENODO platform, and state a simplified description of the laboratory analyses performed at the University of Geneva, Swiss Federal Institute of Technology Zurich and Montanuniversität Leoben. These three volumes have accompanied CERN's *Mining-the-Future* industrial competition, and are linked to a partial upload of the measured data of the present study under Haas, De Haller, Le Cottonnec, et al. (2021a) and Haas & Plötze (2021a) and Haas, Krainz, et al. (2021), respectively.


ETH zürich
FUTURE CIRCULAR COLLIDER STUDY / TECHNIAL PhD REPORT

Description of laboratory analyses performed at Eidgenössische Technische Hochschule (ETH) in Zurich, Switzerland



Revision no.	Date	Description	Written by	Edited by	Verified by
0	05/03/2021	Creation of document	Dipl.-Ing. Maximilian Haas		
1	28/03/2021	Revision of document		Dipl.-Ing. Maximilian Haas	
2 (final)	15/04/2021	Review & approval of document			Dr. Michael Plötze



Content

Important note	3
1. Introduction	3
2. Sample origin & sample number	4
3. Sample preparation	4
3.1. Milling of samples	4
3.2. H ₂ O content via 105 °C drying.....	5
4. Leaching characteristics (eluate) via ICP-OES.....	5
5. Anion analyses via cuvette tests.....	6
6. Effective CEC via [Cu(trien) ₃] ²⁺ complex.....	7
7. Exchangeable cation analyses via ICP-OES.....	8
8. Mineralogical analyses via FTIR and XRD	9
8.1. Fourier Transform Infrared spectroscopy (FTIR).....	9
8.2. X-Ray diffraction (XRD)	10
9. Surface analyses via gas adsorption	11
9.1. N ₂ -BET surface adsorption	11
9.2. Water vapour adsorption	12
10. Water absorption via Enslin-Neff	13
11. Pore size distribution & porosity analysis via mercury intrusion	14
12. Carbon content determination via acid and thermal treatment	15



Important note

The text used in this document is taken from the doctoral thesis written and performed by Dipl.-Ing. Maximilian Haas. Further use of text paragraphs for (scientific) publications, technical reports or FCC-related marketing must be permitted upon request by the author Dipl.-Ing. Maximilian Haas and ETH supervisor Dr. Michael Plötze, citing both the PhD thesis and this technical report.

1. Introduction

An essential part of the construction and molasse re-use as part of CERN's Future Circular Collider (FCC) subsurface infrastructure is a thorough understanding of its underlying geology. Hence, rock material has been tested at three distinct laboratories, respectively ETH Zurich, University of Geneva and Montanuniversität Leoben. Based on geomechanical, petrophysical, mineralogical and geochemical laboratory analyses, further implications are derived.

This document describes the laboratory measurements performed at the Eidgenössische Technische Hochschule (ETH) in Zurich, Switzerland from 18 January to 26 February 2021, within the scope of FCC's PhD study on "Geomechanical, petrophysical and sediment-petrographical classification of molasse rock in the Geneva Basin".

The laboratory measurements at the IGT ClayLab, ETH Zurich included:

1. Sample preparation,
2. Water content determination for <63 μm and <400 μm fractions,
3. Leaching characteristics (eluate),
4. Anion analyses,
5. Effective cation exchange capacity (CEC),
6. Exchangeable cations,
7. Fourier Transform Infrared (FTIR) spectroscopy,
8. X-Ray diffraction measurements as powder (XRD-P) and textured (XRD-S) samples,
9. N_2 -adsorption for BET surface,
10. Enslin-Neff free water uptake capacity (water absorption),
11. Specific (inner crystalline) surface (water vapour adsorption),
12. Mercury intrusion porosimetry (MIP) and
13. Carbon content determination.

For a detailed scientific description, the reader is referred to literature and technical data sheets cited at the end of each sub-chapter.

This laboratory report is dedicated to methodological descriptions only. Scientific interpretations and further conclusions are stated in the PhD thesis by Maximilian Haas.

For a general overview and further reading about clay analyses and clay minerals, the reader is referred to:



- Bergaya, F. et al. (Eds) (2013): Developments in Clay Science, v5, Handbook of Clay Science. Elsevier
- Jasmund & Lagaly (1993): Tonminerale und Tone: Struktur, Eigenschaften, Anwendungen und Einsatz in Industrie und Umwelt, Steinkopff Verlag Darmstadt (in German).
- Ulery, A.L. & Drees, L.R. (Eds.) 2008: Methods of Soil Analysis. Part 5 – Mineralogical Methods. SSSA Book Series.

2. Sample origin & sample number

Original samples were collected at Swiss (Lucerne) and French (Boussens) core facilities as well as from outcrops along the current FCC subsurface tunnel alignment according to CERN's CDR report (December 2018) featuring samples from Quaternary and Molasse (OSM) formations. Plugs with dimensions of 2-2.5 cm in diameter and 2-8 cm in length were drilled from half cores and outcrop blocks and split in <400 μm , <63 μm and <20 μm fractions for subsequent laboratory analyses. Table 1 gives an overview of the number of samples per analysis.

Table 1: Overview of analyses at the IGT ClayLab, ETH Zurich.

type of analysis	sample amount	sample location (wells & outcrops)
ICP-OES	74	Point 1, Geo-02, Peissy-I, Sarzin, Mornex, GEX-CD-4, GEX-CD-5, GEX-CD-7
CEC	76	
ICP-CEC	76	
Cuvette tests	42	
FTIR	31	
XRD	79	
BET surface	30	
Water vapour adsorption	59	
MIP	30	
Enslin-Neff	70	
Carbon content	70	

3. Sample preparation

Sample preparation was performed on drilled plugs starting with different milling devices to gain respective grain size fractions. After completion of milling, each sample has been dried to determine water content required as input for further calculations.

3.1. Milling of samples

As a first step, a jaw crusher was used to receive a fraction <400 μm for each sample. Second, an agate mill crushed the sample down to a fraction of <63 μm . For the FTIR and XRD measurements, a very fine-grained material (<20 μm) was necessary leading to a third milling



step of milling the <400 µm fraction in a vibrating McCrone mill, flushing them with ethanol and drying the sample-ethanol solution in a 65 °C oven between 2 to 5 hours depending on solution volume to receive a <20 µm fraction. For the <400 µm and <63 µm fractions, respective sieves are used to check the grain sizes after each milling step.



Figure 1: Overview of mills used for sample preparation. Left: jaw crusher for fraction <400 µm, middle: agate mill for fraction <63 µm, right: vibrating McCrone mill for fraction <20 µm.

3.2. H₂O content via 105 °C drying

For fractions <400 µm and <63 µm the water content was determined after DIN EN 12880, DIN EN ISO 17892-1 and DIN 18121-1 to calculate the dry mass. This excludes measurements for XRD and FT-IR using the <20 µm fraction as these analyses do not require dry mass input. The water content using humid and dry masses is calculated according to:

$$w(\%) = \frac{m_{\text{humid}} - m_{\text{dry}}}{m_{\text{humid}}} \cdot 100$$

Each sample was dried for 48h in a 105 °C oven until mass equilibrium. The present molasse samples showed rather low water contents ranging from 0.4 to 5.15 %.

4. Leaching characteristics (eluate) via ICP-OES

Inductively Coupled Plasma Optical Emission Spectrometry (ICP-OES) is a simple and high-precision state-of-the-art device for leaching (eluate) analyses, and successively supersedes the atomic absorption spectroscopy (AAS) analysis.

The measurements were performed using an Agilent 5110 ICP-OES device and followed DIN EN 12457-2 (leachate characterization waste), with minor changes made with respect to water content corrections and initial dry masses for the eluate solution/dry mass ratio. Each sample was measured for 20 s after 5 s stabilization time using a RF power of 1.2 KW in axial viewing mode with 8 mm viewing height and a plasma flow of 12 L/min. For each sample run, a blank sample and 4 standards have been used for calibration, followed by a quality control spike blank sample. The optimal ratio of eluate-dry mass according to the DIN standard should not exceed 10, which resulted in initial weights of 5 g of a <400 µm sample.



Results are given in mg/L and calculated according to DIN EN 12457-2:

$$A = C \cdot \left(\frac{L}{M_T} + \frac{FG}{100} \right)$$

With:

A = leaching substance at L/S ratio = 10, in mg/kg dry mass,

C = concentration of certain part in eluate solution, in mg/L,

L = volume leaching conditioning substance, in L,

FG = humid mass, in percentage related to dry mass.

M_T = dry mass of sample, in kg.

References & further reading:

- Leachate characterization waste, DIN EN 12457-2, <https://www.beuth.de/de/norm/din-en-12457-2/52065709>.

5. Anion analyses via cuvette tests

According to Swiss and French disposal classes (e.g. Ordinance on the Avoidance and the Disposal of Waste, version 01.01.2021) specific anions must not exceed legal thresholds as indicated in respective documents. While the ICP-OES method (see section 7) allowed the quantification of most cations, complementary anion analyses were performed as indicated in Table 2. For each anion, the company Hach Lange provides standardised cuvette tests in combination with its Spectral-Photometer DR 6000 (see section 5) analysed photometrically.

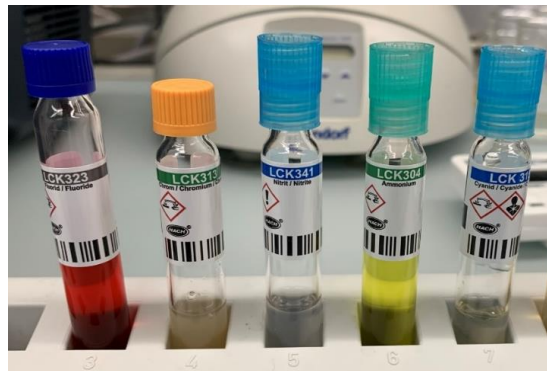


Figure 2: Overview of performed cuvette tests.

Table 2: Overview of measured anions complemented by ICP-OES analysis.

test-ID	parameter	measuring range	method	standard
LCK323	Fluoride, F ⁻	0.1 - 2.5 mg/L	SPADNS	-
LCK315	Cyanide free, CN ⁻	0.01 - 0.6 mg/L	Babituric Acid-Pyridine	-
LCK341	Nitrite, NO ²⁻ -N	0.015 - 0.6 mg/L	Diazotisation	EN ISO 26777, DIN 38405 D10
LCK304	Ammonium, NH ₄ -N	0.015 - 2.0 mg/L	Indophenol Blue	ISO 7150-1, DIN 38406 E5-1, UNI 11669:2017


ETH zürich

LCK313	Chromium-VI	0.03 - 1.0 mg/L	Diphenylcarbazide	EN ISO 11083, DIN 38405-D24
--------	-------------	-----------------	-------------------	--------------------------------

References & further reading:

- Hach LCK Cuvette Test System, Technical Data Sheet.
- Ordinance on the Avoidance and the Disposal of Waste, version 01.01.2021, <https://www.fedlex.admin.ch/eli/cc/2015/891/en>

6. Effective CEC via $[\text{Cu}(\text{trien})_3]^{2+}$ complex

The cation exchange capacity (CEC) via $[\text{Cu}(\text{trien})_3]^{2+}$ complex analyses effective cation exchange capacity of clay minerals at pH of 7-8 based on the method proposed by Meier & Kahr (1999). The sample solution was mixed with a $[\text{Cu}(\text{trien})_3]^{2+}$ complex and analysed via photometry to conclude on effective exchangeable cations in meq/100g.

800 mg of a <63 μm milled sample were treated in the ultrasound UP 200H device for 3 minutes to separate the clay minerals and destroy clay aggregates. The remaining volume was



Figure 4: Required measurement devices for CEC determination. Left: Spectral-Photometer DR 6000 by Hach Lange, middle: Eppendorf MiniSpin centrifuge, right: ultrasonic UP 200H.

filled up with millipore- H_2O . Each sample was shaken overhead 30 times and left for sedimentation and exchange for about 1-2 hours. After sedimentation, solution was filled into a centrifuge cup, which rotated at 13,000 RPM for 20 minutes in the Eppendorf Minispin centrifuge. Finally, the centrifuged solution was pipetted into the sample holder cuvette and analysed in the Spectral-Photometer DR 6000 by Hach Lange.

Calibration, i.e. determination of analysing wavelength was performed using a blind sample (millipore- H_2O). Wavelength at maximum extinction was given at 278.00 nm for the present samples, and the zero-baseline was set before running actual sample measurements. Effective CEC was then calculated according to:



Figure 3: Left sample depicting a low CEC compared to high CEC on right sample.



$$\text{CEC}(\text{mmol}/100\text{gclay}) = \frac{(\text{Ext.}_{\text{blind}} - \text{Ext.}_{\text{sample}}) \cdot 200 \cdot 100}{m_{\text{sample}}}$$

With:

- Ext._{blind} & Ext._{sample} = respective extinction values in nm of the blind and real sample,
- m_{sample} = sample mass in gram.

The calculation was corrected by the <63 µm fraction H₂O content for dry mass.

References & further reading:

- Meier, L.P., Kahr, G., 1999. Determination of the Cation Exchange Capacity (CEC) of Clay Minerals Using the Complexes of Copper(II) Ion with Triethylenetetramine and Tetraethylenepentamine. *Clays Clay Miner.* 47, 386–388.

7. Exchangeable cation analyses via ICP-OES

By measuring the copper-II-complex solution after cation exchange (see section 6), exchangeable cations are quantified via Inductively Coupled Plasma Optical Emission Spectrometry (ICP-OES). The same Agilent 5110 ICP-OES device was used as for the leaching analyses. Condition settings were adapted accordingly to 10 s of reading time and 15 s stabilization time. Viewing mode was changed to radial with a viewing height of 15 mm. Same settings for RF power were applied as for the leaching analyses. For each sample run, a blank sample and 3 standards have been used for calibration, followed by a quality control spike blank sample and a copper blank sample. Apart from a different centrifuge speed of 4,500 RPM in the Heraeus centrifuge, the same sample preparation procedure as for the ICP-eluate analysis (see section 4) was applied. Hence, sample preparation started with the CEC copper-II-complex solution being filtered with <0.45 µm PES vaccine filters and acidized with 2 % HNO₃.

References & further reading:

- Gaines, G.L., Thomas, H.C., 1953. Adsorption Studies on Clay Minerals. II. A Formulation of the Thermodynamics of Exchange Adsorption. *J. Chem. Phys.* 21.
- Harland, C.E., 1994. Ion Exchange, RSC Paperbacks. The Royal Society of Chemistry.
- Meier, L.P., Kahr, G., 1999. Determination of the Cation Exchange Capacity (CEC) of Clay Minerals Using the Complexes of Copper(II) Ion with Triethylenetetramine and Tetraethylenepentamine. *Clays Clay Miner.* 47, 386–388.
- Bergaya F, Lagaly, G., Vayer M.: Cation and Anion Exchange. In: Handbook of Clay Science (Eds. Bergaya, Theng, Lagaly) *Developments in Clay Science Vol. 1*, pp. 979-1001 and references therein.



8. Mineralogical analyses via FTIR and XRD

8.1. Fourier Transform Infrared spectroscopy (FTIR)

The FTIR spectroscopy derives mid-infrared spectra based on measured interferograms following Lambert-Beer's law. These interferograms are Fourier-transformed from time into frequency domain and allow conclusions about organic material as well as amorphous and crystallized mineral phases. The resulting spectra are displayed along 450 to 4000 cm^{-1} (wavenumber, x-axis) versus percentage of transmission (%T, y-axis).



Figure 5: Tools required for FTIR sample preparation. Left: agate mortar, funnel and desiccator (for sample conservation), middle: 1 mg of sample mixed with 199 mg KBr, right: pressing apparatus applying 10 tons onto the sample resulting in the pressed KBr pill.

A KBr (potassium-bromide) disc was prepared with 1 mg sample material $<20\text{ }\mu\text{m}$ dried at $105\text{ }^{\circ}\text{C}$ dispersed in 199 mg KBr. The spectra were measured with a Perkin Elmer Spectrum One device using the program Spectrum V5.3.1. Each analysis measured 20 runs and was summed up to a transmission spectrum.



Figure 6: Left: Perkin Elmer Spectrum One FTIR device used for analysis, right: close-up of sample holder inside the measuring device when turned

References & further reading:

- Farmer, V.C., 1974. The Infrared Spectra of Minerals. MinSoc Monograph 4.
- Van der Marel H.W., Beutelspacher H. 1976. Atlas of Infrared Spectroscopy of Clay Minerals and their Admixtures. Elsevier, Amsterdam.
- Smykatz-Kloss, W., Warne, S.S.J. (Eds.) 1991. Thermal Analysis in the Geosciences. Springer.
- Christidis, G.E. (Ed.) Advances in the Characterization of Industrial Minerals. EMU Notes in Mineralogy v9. Chapter 6: Madejova, J. et al. Application of vibrational spectroscopy to the characterization of phyllosilicates and other industrial minerals.



ETH zürich

8.2. X-Ray diffraction (XRD)

X-Ray diffraction (XRD) is the most common method to determine crystalline mineral phases qualitatively and quantitatively. The method was applied according to standard DIN EN 13925-1/-2. Two different types of samples were prepared and measured with a D8 Advance Bruker AXS/D XRD device. For quantitative XRD analyses, randomly oriented (Zhang et al., 2003) Ca-exchanged samples were scanned from 4 to 80° 2 θ with steps of 0.02° 2 θ at 2 s intervals using a Bragg-Brentano X-ray diffractometer (Bruker AXS D8 Advance, Germany). Oriented specimens were used for enhancement of the basal reflexes of layer silicates thereby facilitating their identification. The changes in the reflex positions in the XRD pattern by intercalation of different organic compounds (e.g. ethylene glycol) and after heating were used for identification in part of smectite. The XRD instrument worked with CoK α -radiation generated at 35 kV and 40 mA, and with dynamic beam optimisation using an automatic theta compensating divergence slit and a motorised anti-scatter screen. The diffractometer was equipped with primary and secondary soller slits, and an energy dispersive LynxEye XE-T line detector. Qualitative phase analysis was analysed with the software DIFFRAC.EVA v4.3 (Bruker AXS). The minerals were identified by peak positions and relative intensities in the X-ray diffraction pattern compared with the PDF2 database (ICDD 1998). Quantitative mineral analyses were performed with Rietveld analysis of the XRD patterns using the program Profex/BGMN V4.2.4 (Döbelin and Kleeberg, 2015). This full pattern-fitting method calculates X-ray diffraction pattern based on crystallographic data of each mineral phase and its iterative adjustment (least-square fit) to the measured diffractogram. In the refinement, phase specific parameters and the phase content were adapted to minimize the difference between the calculated and the measured X-ray diffractogram.



Figure 7: Left: XRD-device, right top: Powder (XRD-P) samples used for bulk analysis (Rietveld), right bottom: textured (XRD-S) samples used for clay mineral identification.



References & further reading:

- Moore, D.M., Reynolds, R.C., 1989. X-ray Diffraction and the Identification and Analysis of Clay Minerals, Clays and Clay Minerals. Oxford University Press.
- Döbelin, N., Kleeberg, R., „Profex: a graphical user interface for the Rietveld refinement program BGMN,, Journal of Applied Crystallography 48 (2015), 1573-1580.
- Christidis, G.E. (Ed.) Advances in the Characterization of Industrial Minerals. EMU Notes in Mineralogy v9. Chapter 3: Bish D., Plötze, M. X-ray powder diffraction with emphasis on qualitative and quantitative analysis in industrial mineralogy.

9. Surface analyses via gas adsorption

9.1. N_2 -BET surface adsorption

The method after DIN ISO 9277 measures specific surfaces via N_2 gas adsorption. Analysis preparation took about 1 day, while the second day was dedicated to actual sample measurement. On day one, the 150 °C dried sample was weighed in a sample tube, whose end was attached to a VacPrep 061 vacuum pump. Heating elements increased temperature gradually starting at 25 °C up to 150 °C and the sample was subjected to 150 °C for 15 h. Then, the sample tube was flushed with nitrogen gas for about 30 seconds at 0.5 bar. Afterwards, the sample was weighed on a medium-precision scale with 4 digits, and placed in the Quantachrome Autosorb-1^{MP} N_2 -adsorption measurement device for sample analysis.



Figure 8: Left: VacPrep 061 vacuum pump used for sample degassing, middle: Quantachrome Autosorb-1 device for measuring specific (outer) surface, right: close-up of liquid nitrogen tank, in which sample is immersed.

Data processing and analysis was performed using the ASiQwin Version 3.01 software applying the multipoint BET method (nitrogen on silicates as adsorbate), which included 11 points in a relative p/p_0 range of 0.1 to 0.3 to calculate specific surfaces.



References & further reading:

- Brunauer, S., Emmett, P.H., Teller, E., 1938. Adsorption of Gases in Multimolecular Layers. *J. Am. Chem. Soc.* 60, 309–319.
- Madsen, F.T., Kahr, G., 1992. Wasserdampfadsorption und spezifische Oberfläche von Tonen, in: Graf v. Reichenbach, H. (Hrsg.): Hydratation Und Dehydratation von Tonmineralen - Beiträge Zur Jahrestagung Hannover, DTTG. p. 8.
- Lowell, S., Shields, J.E., Thomas, M.A., Thommes, M. 2004: Characterization of porous solids and powders: surface area, pore size and density. Kluwer Academic, Dordrecht.
- Gregg, S.J., Sing, K.S.W. 1982: Adsorption, Surface Area and Porosity. Academic Press, London.

9.2. Water vapour adsorption

Vapor adsorption after Keeling et al. (1980) provides insights about the specific inner crystalline surface of clay minerals, respectively their water adsorption behaviour adsorbing H₂O molecules between their layers. The combination of Enslin-Neff (see section 10), BET and Keeling analyses provides powerful insights about a rock's water behaviour, respectively swelling potential. The latter further allows reasonable correlations with CEC (see section 6).

A <63 µm sample of 4 g was placed in a container with 75% relative humidity (RH) achieved above an oversaturated NaCl solution under atmospheric pressure. The sample's initial weight was compared to its conditioned and fully dried weight. Random samples were checked occasionally within 2-3 days for mass equilibrium after three weeks. Once no further adsorption was encountered, samples were weighted on a high-precision 5-digit scale. Afterwards, the sample was dried for 1 week in a 105 °C oven. The difference of humid, 75% RH adsorbed and dried masses (in mg) yielded the water adsorption according to:



Figure 9: 75% RH conditions for 3 continuous weeks.

$$w_{adsorption}(\%) = \frac{m_{75\%RH} - m_{dry}}{m_{dry} - m_{glass}} \cdot 100$$

References & further reading:

- Keeling, P.S., Kirby, E.C., Robertson, R.H.S., 1980. Moisture adsorption and specific surface area. *J. Brit. Ceram. Soc.* 79, 36–40.
- Madsen, F.T., Kahr, G., 1992. Wasserdampfadsorption und spezifische Oberfläche von Tonen, in: Graf v. Reichenbach, H. (Hrsg.): Hydratation Und Dehydratation von Tonmineralen - Beiträge Zur Jahrestagung Hannover, DTTG. p. 8.
- Lowell, S., Shields, J.E., Thomas, M.A., Thommes, M. 2004: Characterization of porous solids and powders: surface area, pore size and density. Kluwer Academic, Dordrecht.



- Gregg, S.J., Sing, K.S.W. 1982: Adsorption, Surface Area and Porosity. Academic Press, London.

10. Water absorption via Enslin-Neff

The Enslin-Neff analysis measures the water uptake capacity under free swelling conditions and its associated time evolution of rock-water interaction according to standard DIN 18132. About 1 g of a <400 µm sample was placed in the Enslin-Neff apparatus and its free water uptake capacity was recorded in a time interval of 0.25, 0.5, 1, 2, 4, 8, 15, 30, 60, 120, 240, 360 and 1440 minutes. Once the material reached its maximum absorption, the analysis was stopped, and water absorption was calculated according to:

$$w_a(\%) = \frac{W_{max}}{m_{dry} \cdot 100wt\%}$$

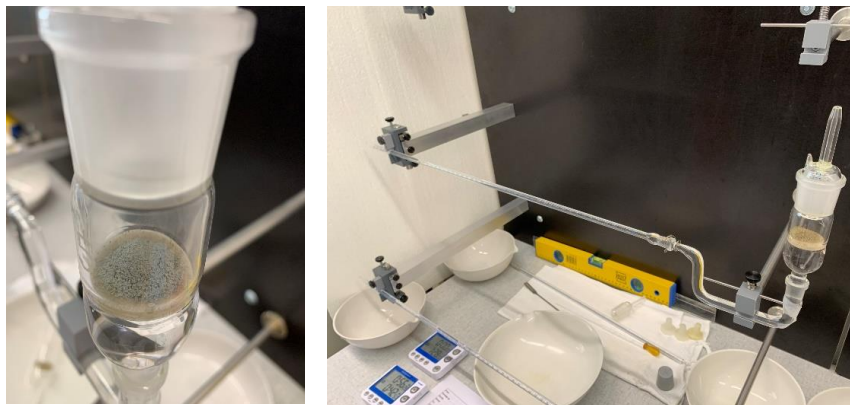


Figure 10: Left: close-up of sample burette with sample powder during water uptake, right: full Enslin-Neff apparatus including scaling burette to read absorbed water in ml.

References & further reading:

- Kaufhold, S., Dohrmann, R., 2008. Comparison of the traditional Enslin-Neff method and the modified dieng method for measuring water-uptake capacity. *Clays Clay Miner.* 56, 686–692.
- Kugler, H., Schwaighofer, B., Gruber, S., 2002. Die Modifizierung des Wasseraufnahmeversuches nach Enslin-Neff, in: Ottner, F., Gier, S. (Hrsg.): Beiträge Zur Jahrestagung Wien, Berichte Der DTTG, Band 9. p. 9.
 - Neff, H., 1959. Über die Messung der Wasseraufnahme ungleichförmiger bindiger anorganischer Bodenarten in einer neuen Ausführung des Enslingerätes. *Die Bautechnik* 11, 10.
 - Neff, H.K., 2005. Der Wasseraufnahmeversuch nach ENSLIN-NEFF in der erd- und grundbautechnischen Praxis, in: 5. Österreichische Geotechniktagung. 21.02. & 22.02.2005, Vienna, p. 27.



- Demberg, W. 1991: Über die Ermittlung des Wasseraufnahmevermögens feinkörniger Böden mit dem Gerät nach Enslin/Neff. Geotechnik 14, 125-131.
- Enslin-Neff apparatus after DIN 18132.

11. Pore size distribution & porosity analysis via mercury intrusion

The mercury intrusion porosimetry measures effective, total (i.e. non accessible pores) porosity and pore size distribution according to standard ISO 15901-1. To cover the full range of pore sizes, two POROTEC PASCAL devices with different pressure ranges were used. The low-pressure device used up to 400 kPa to inject mercury into the sample, while the high-pressure device used up to 400 MPa and high-pressure oil to further induce the mercury into the smallest pores down to 2 nm radius.

The samples were weighed into a dilatometer flask and evacuated in the macropore unit of the pressure porosimeter for 10 min. The dilatometer flask was filled with mercury under vacuum up to a certain volume in the measuring capillary. Then, the pressure of the low-pressure device was slowly increased up to 400 kPa. The dilatometer flask was removed from the macropore unit at air-out pressure, weighed and placed in the micropore unit of the pressure porosimeter. The pressure on mercury fluid in the dilatometer was gradually increased to 400 MPa in the second high-pressure device using a special oil in the autoclave of the micropore unit. As the pressure increases, the mercury intruded into smaller pores. The pore volume was derived from the amount of mercury intruded. The pore size distribution was determined according to the equation stated by Washburn (1921):

$$r = \frac{-2\gamma\cos(\theta)}{p}$$

With:

γ = mercury surface tension,
 p = applied, absolute pressure,
 r = pore radius,
 θ = wetting angle.



Figure 11: Low- and high-pressure chambers to analyse porosity and pore size distribution. Right: low-pressure device for mercury intrusion, left: high-pressure device to further induce the mercury into nanometer pores using high-pressure



Figure 12: Transfer of mercury injected sample from low-pressure to high-pressure device.



Assuming a mercury surface tension of 4800 N/m, a wetting angle for mercury of 141.3° and cylindrical pore shape, this results in the following equation:

$$r = \frac{7500}{p}$$

With:

r = pore radius in nm,

p = applied absolute pressure in kg/cm².

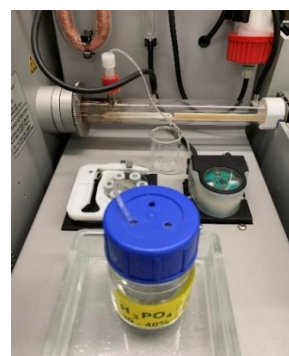
References & further reading:

- Washburn EW (1921) Note on a method of determining the distribution of pore sizes in a porous material. Proc Natl Acad Sci 7:115–116
- Giesche, H. 2006. Mercury Porosimetry: a General (Practical) Overview. Part. Part.Syst. Charact. 23, 1-11.
- Scrimgeour, C., 2008. Soil Sampling and Methods of Analysis (Second Edition), 2008/07/01. ed, Experimental Agriculture. Cambridge University Press.
- Kaufhold et al. 2016. Comparison of methods for the determination of the pore system of a potential German gas shale. CMS workshop lecture series vol21, ch13, 163-190. .

12. Carbon content determination via acid and thermal treatment

The total carbon (TC) and total inorganic carbon (TIC) methods were performed according to DIN EN 15936 in a multi-EA 4000 device and allowed conclusions about carbon content. For TC and TIC analyses, a 105 °C dried <400 µm sample was split into two sub-samples of different initial weight, respectively 50 mg for TIC and 300 mg for TC analysis. A CaCO₃ reference sample was used as a standard for all analyses. For the TIC analysis, the sub-sample was subjected to 35 %

H₃PO₄ acid and released CO₂ gas was detected via non-dispersive infrared (NDIR), which was used to calculate TIC content. For the TC content, the sub-sample was burned in a 1300 °C oven and release of CO₂ was detected by NDIR. The



total organic carbon (TOC) content was then derived indirectly via the difference method subtracting TIC from TC content in the multi-EA Analytik Jena software.

References & further reading:

- DIN-EN-15936 for carbon determination, <https://www.beuth.de/en/standard/din-en-15936/149052152>



**UNIVERSITÉ
DE GENÈVE**

FUTURE CIRCULAR COLLIDER STUDY / TECHNICAL PhD REPORT

**Description of laboratory analyses performed
at Université de Genève (UNIGE) in Geneva,
Switzerland**



Revision no.	Date	Description	Written by	Edited by	Verified by
0	10/03/2021	Creation of document	Dipl.-Ing. Maximilian Haas		
1	25/03/2021	Revision of document		Dipl.-Ing. Maximilian Haas	
2 (final)	08/04/2021	Review & approval of document			Prof. Dr. Andrea Moscariello, Dr. Antoine De Haller & Dr. Aymeric Le Cotonnec



UNIVERSITÉ
DE GENÈVE

Content

Important note.....	3
1. Introduction	3
2. Sample origin & sample number	3
3. Sample preparation	4
3.1. Drilling of plug samples	4
3.2. Washing of cutting samples	5
3.3. Polishing of thin sections.....	5
4. Geochemical analyses via XRF and ICP	5
4.1. Portable X-Ray fluorescence (pXRF).....	5
4.2. Ultra-trace inductively coupled plasma mass spectroscopy & emission spectrometer (ICP-MS/OES).....	7
5. Mineralogical analyses via QEMSCAN® and OMI	8
5.1. Integrated automated mineralogy and petrography (QEMSCAN®).....	8
5.2. Optical microscopy (OMI).....	9
6. Porosity, permeability & density analyses via gas expansion.....	10

**UNIVERSITÉ
DE GENÈVE**

Important note

The text used in this document is taken from the doctoral thesis written and performed by Dipl.-Ing. Maximilian Haas. Further use of text paragraphs for (scientific) publications, technical reports or FCC-related marketing must be permitted upon request by the author Dipl.-Ing. Maximilian Haas and UNIGE supervisors Prof. Dr. Andrea Moscariello and Dr. Antoine De Haller, citing both the PhD thesis and this technical report volume.

1. Introduction

An essential part of the construction and re-use of excavated material as part of CERN's Future Circular Collider (FCC) subsurface infrastructure is a thorough understanding of its underlying geology. Hence, rock material has been tested at three distinct laboratory locations, respectively ETH Zurich, University of Geneva and Montanuniversität Leoben. Based on geomechanical, petrophysical, mineralogical and geochemical laboratory analyses, further implications are derived.

This document describes the laboratory measurements performed at the Université de Genève (UNIGE) in Geneva, Switzerland from December 2019 to May 2021, within the scope of FCC's PhD study on "Geomechanical, petrophysical and sediment-petrographical classification of molasse rock in the Geneva Basin". Technical background of each laboratory analysis is briefly described, following a thorough description of measurement procedures.

The laboratory work includes:

1. Sample preparation,
2. Portable X-Ray fluorescence (pXRF),
3. Ultra-trace inductively coupled plasma mass spectroscopy & emission spectrometry (ICP-MS/ES),
4. Integrated automated mineralogy and petrography (QEMSCAN®),
5. Optical microscopy,
6. Gas expansion porosity, permeability, bulk & grain density.

For a detailed scientific description, the reader is referred to literature and technical data sheets cited at the end of each section. This laboratory report is dedicated to methodological descriptions only. Scientific interpretations and further conclusions are stated in the PhD thesis authored by Maximilian Haas.

2. Sample origin & sample number

Original samples were collected at Swiss (Lucerne) and French (Boussens) core facilities as well as from outcrops along the current FCC subsurface tunnel alignment according to CERN's



CDR report (December 2018) featuring samples from Quaternary and Molasse (OSM) formations. Plugs with dimensions of 2-2.5 cm in diameter and 2-8 cm in length were drilled from half cores and outcrop blocks and split in different fractions for subsequent laboratory analyses. Table 1 gives an overview of the number of samples per analysis.

Table 1: Overview of analyses performed at UNIGE with respective sample number and sampling location (well).

type of analysis	sample amount	sample location (wells & outcrops)
pXRF	42	Point 1, VSP-well, Geo-02, Montfleury-2, Peissy-1, Sarzin, Mornex, GEX-CD-1 to GEX-CD-7
ICP-MS/ES	378	
QEMSCAN	339	
Optical microscopy	339	
Poro/perm gas expansion	173	

3. Sample preparation

3.1. Drilling of plug samples

Plugs were drilled from well core samples and outcrop blocks using a driller machine and further prepared using abrasive tables to polish top and bottom of each plug for subsequent laboratory analyses.

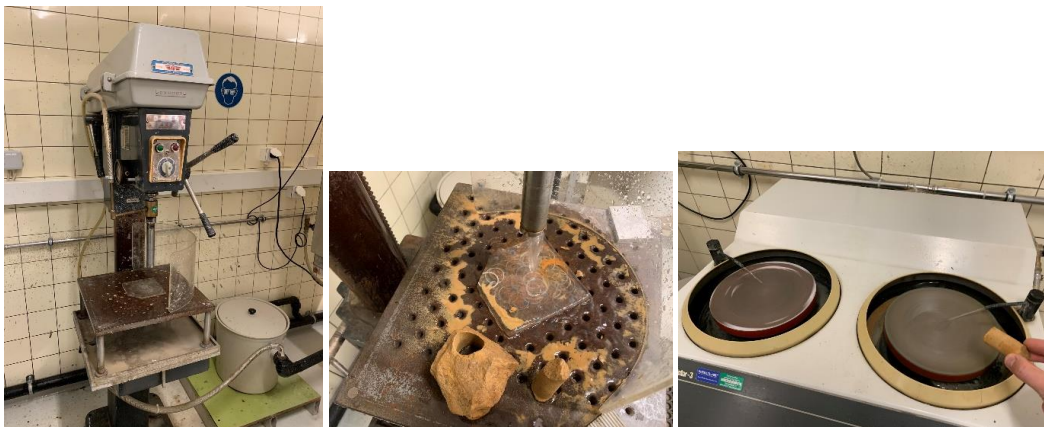


Figure 1: Overview of machine equipment to drill and prepare the plug samples. Left: Driller to drill plugs from blocks and/or cores, middle: result of a drilled plug, right: grinding of plug sample with rough (right table) and fine (left table) abrasives under flowing water.



UNIVERSITÉ
DE GENÈVE

3.2. Washing of cutting samples

For well Geo-02, sample cuttings were available and taken during drilling. These cutting samples were washed, sieved under water and dried at 45°C for 48h to prevent clay degradation. Afterwards, the dried samples were crushed by hand in an agate mortar and sieved with a <math><400\ \mu\text{m}</math> mesh. The powder is then used for clay analyses at the Eidgenössische Technische Hochschule (ETH) in Zurich, Switzerland (see CERN technical report “Haas, M.:



Figure 2: Washing and sieving steps of well cutting samples. Left: original sample as received from well site, middle: different mesh sizes of 8, 4, 1, 0.5 and 0.25 mm after washing, right: final, washed sample to be further dried in a 45°C oven.

Laboratory analyses performed at the Eidgenössische Technische Hochschule (ETH) in Zurich, Switzerland”) with further processing and milling steps, as well as for the analyses described in this document.

3.3. Polishing of thin sections

Representative cuttings samples were sent to Petrolab Sardegna in Sant’Antioco, Italy to create thin sections, which were further used for QEMSCAN and optical microscope analyses.

The thin sections were produced under vacuum impregnation with epoxy resin. The brick was cut and flattened on one side before mounting on a glass plate with epoxy resin. After cutting the sample down to a thickness of a few 100 μm it was further abraded before fine-polishing down to 30 μm using silicon carbide abrasives. The final step includes polishing by hand with alumina and a polishing machine.

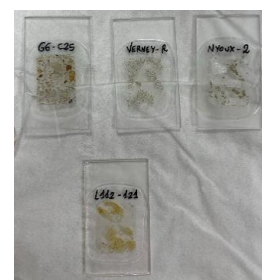


Figure 3: Extract of thin sections samples.

4. Geochemical analyses via XRF and ICP

4.1. Portable X-Ray fluorescence (pXRF)

Portable X-ray fluorescence allows fast and low-cost multi-elemental quantitative analysis of rocks (from Mg to U for best results). It can be used on any kind of material including cores,



rock chips or rock powder. Powder allows for better accuracy because any heterogeneity of the rock is homogenised. Portable XRF is of common use in mining (production and exploration) but also in the construction industry (e.g. to identify Pb-bearing paintings).

The device contains a detector and a radioactive (Caesium, Cs) source generating x-rays, which excite electrons in the atom's outer shell into higher states of energy, and ultimately pushing them out of their orbits. Electrons from the inner shell compensate the energy losses and occupy these orbits by emitting fluorescence. Hence, fluorescence depicts the difference of energy level by the two electrons, i.e. electromagnetic radiation (Bremsstrahlung X-rays). Counts and energy of X-rays are detectable via energy dispersive spectroscopy (EDS). The measurement is affected by erroneous sampling preparation, grain size, nugget effects, surface irregularities, sample thickness, weathering effects and depth of penetrating X-rays. The latter is usually in the range of sub-millimetres and depends on the element's atomic weight.

The analysis measures elemental composition on $<400 \mu\text{m}$ powder. A thorough sample preparation, i.e. washing, sieving and proper filling into the measuring cup is necessary (see section 3). About 2-3 g of $<400 \mu\text{m}$ powder was placed in a plastic cup, pressed with a plastic piston and then covered by a plastic foil. For the analysis, a Thermo Fisher Scientific Inc. NITON XL3t 900 Analyzer was used in conjunction with proper safety equipment. Each sample was analysed in three runs, each taking 120 seconds, whereas the average yields the result.

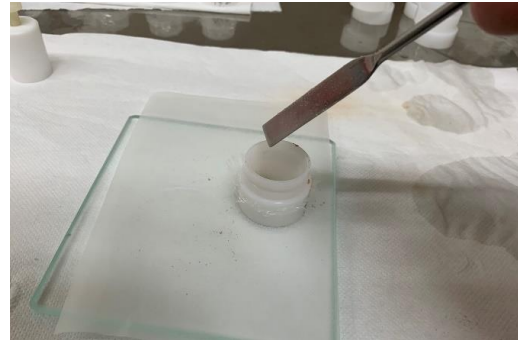


Figure 5: Filling $<400 \mu\text{m}$ sample powder in plastic cup.

Before each measurement, the beam hole (8 mm in diameter) and its surrounding area was thoroughly cleaned with $\text{C}_2\text{H}_5\text{OH}$ (ethanol). The device was used in Mining Cu/Zn Testing Mode specifically designed for soil and rock samples. This mode provides the best results for



Figure 4: Left: Measuring pXRF device with electronic equipment and laptop for machine controls and data processing, right: close-up of portable XRF device with powder sample on beam hole when device is turned off. pXRF can be directly used on outcrops or core samples with lesser precision than with powder on the desk system but with higher efficiency. This makes it a good measuring device also at the tunnel face or in a truck.



metal concentrations of analytes at 1% or higher. The following elements were measured: Mg, Al, Si, P, S, Cl, As, K, Ca, Ti, V, Cr, Mn, Fe, Co, Ni, Cu, Zn, W, Pb, Bi, Zr, Nb, Mo, Sn, Ba, Sb, Cd, Pd, Sr, Rb, Se, and Ag and Au. Portable XRF is not suited for elements lighter than Mg, also excluding sodium (Na). The detection limit is given by 3*sigma (standard deviation) of a measurement and depends on the composition of a sample. Precision is given by 2*sigma. An element is detected at a minimum of 1.5x the precision in parts per million (ppm) units.

References & further reading:

- Hall, G.E.M., Bonham-Carter, G.F., Buchar, A., 2014. Evaluation of portable X-ray fluorescence (pXRF) in exploration and mining: Phase 1, control reference materials. *Geochemistry Explor. Environ. Anal.* 14, 99–123.
- Mauriohooho, K., Barker, S.L.L., Rae, A., 2016. Mapping lithology and hydrothermal alteration in geothermal systems using portable X-ray fluorescence (pXRF): A case study from the Tauhara geothermal system, Taupo Volcanic Zone. *Geothermics* 64, 125–134.
- Roman Alday, M.C., Kouzmanov, K., Harlaux, M., Stefanova, E., 2018. Comparative study of XRF and portable XRF analysis and application in hydrothermal alteration geochemistry: The Elatsite porphyry Cu-Au-PGE deposit, Bulgaria. 16th Swiss Geosci. Meet. 2.
- Thermo Fisher Scientific Niton Analyzers: The XL3 Analyzer, Version 7.0.1 User's Guide, Revision C, November 2010.
- Thermo Fisher Scientific Niton XL3t 900Analyzer with GOLDD Technology, User's Guide, Version 6.5.

4.2. *Ultra-trace inductively coupled plasma mass spectroscopy & emission spectrometer (ICP-MS/OES)*

For ICP-MS/ES analyses samples were outsourced to the certified laboratory *Bureau Veritas* in Poland and Canada following analysing packages PRP70-250, EN004, PULSW, SHP-01, DY105, MA250, LF300-Si element, TC007 as specified in the lab's *Schedule of Services & Fees, 2019*. Multi-acid digestion for ultra-trace analysis via inductively coupled plasma mass spectroscopy (ICP-MS) was used for the identification of 59 elements. This covers most elements. However, implications are given by the fact that elements included in refractory minerals (e.g. zircon) are potentially detected at lower concentrations. Furthermore, total organic carbon content (excluding graphite C & CO₂) and silica (Si) were measured in respective analysing packages.

Original samples (plugs/cuttings) were crushed to $\geq 70\%$ passing 2 mm and 250 g of the crushed material were pulverized $\geq 85\%$ to a fraction of 75 μm . The material was then dried in a 105°C oven for 48h. For the identification of 59 elements (ultra-trace), four acid digestions with 0.25 g of the 75 μm sample fraction were produced and heated in HNO₃, HClO₄ and HF to fuming and dried. The residue was dissolved in HCl and analysed in a Perkin Elmer Sciex Instruments ELAN 9000 ICP-MS device. For the LF300-Si analysing package, a Spectro Ciros Vision high-performance ICP-OES device (LiBO2/LiB4O7 fusion analysis) was used for the



UNIVERSITÉ
DE GENÈVE

identification of silica. For the total organic carbon analyses, a Leco CS230 Carbon/Sulfur Series device was used on dried 75 μm samples.

References & further reading:

- Bureau Veritas – Dolomite-3 internal Reference Material for LOI determination, Revision 2018.1, May 16, 2018.
- Bureau Veritas – Metals, Minerals & Environmental, Schedule of Services & Fees, version 2019.
- Bureau Veritas – OREAS 25A-4A, Reference Material for Multi Acid Digestion, Revision 2019.2, February 9, 2019.
- Bureau Veritas – SO-19, Internal Reference Material for Whole Rock Analysis (LF300-Si), Revision 2015.3, August 10, 2015.
- Geostats PTY LTD Mining Industry Consultants, Reference Material Manufacture and Sales, Certified Pulp Graphite Reference Material, GGC-10.
- Geostats PTY LTD Mining Industry Consultants, Reference Material Manufacture and Sales, Certified Ore Grade Base Metal Reference Material, GBM309-15.
- Geostats PTY LTD Mining Industry Consultants, Reference Material Manufacture and Sales, Certified Sulphur and Carbon Reference Material, GS311-1.
- Geostats PTY LTD Mining Industry Consultants, Reference Material Manufacture and Sales, Certified Sulphur and Carbon Reference Material, GS910-4.
- Leco CS230 Carbon/Sulfur Series, Technical Data Sheet, R2.511-REV1, 2007.
- OREAS 45h, Ore Research & Exploration P/L, Lateritic Soil Lithochem., Certified Reference Material, Document-No. COA-1343-OREAS45h-R2, September 19, 2018.
- Perkin Elmer SCIEX Instruments, ELAN 9000 ICP-MS, Optimized for routine Ultra-trace Analysis, Technical Data Sheet.
- Spectro Ciros Vision, High-Performance second-generation ICP-OES-CCD spectrometer, Technical Data Sheet, 2004.

5. Mineralogical analyses via QEMSCAN[®] and OMI

5.1. *Integrated automated mineralogy and petrography (QEMSCAN[®])*

The FEI QEMSCAN[®] Quanta 650F instrument is used to identify the modal mineralogy, the texture, and the lithology based on a scanning electron microscope (SEM) equipped with two Energy-dispersive X-ray (EDX) spectroscopy detectors. This non-destructive analytical technique enables in-situ high-resolution (analytical point <2 μm) mapping. Mineral phase identification originates from the combination of back-scattered electron (BSE) contrast and EDS spectra providing information about the elemental composition. Individual X-ray spectra were compared to a library of known spectra comprising a specific mineral name and assigned to each individual acquisition point. The X-ray EDS spectra library was initially provided by the manufacturer and has been further developed in-house using a variety of natural standards. Measurements were performed on polished thin sections (see section 3.3) at an acceleration voltage of 15kV with a 10 nA probe current. These thin sections were carbon-coated by graphite before scanning using a Quorum Q150T S/E/ES coating device. X-ray



UNIVERSITÉ
DE GENÈVE

acquisition time was 10 ms per pixel using a point-spacing of 2.5 and 5 μm . Each section was



Figure 6: Carbon-coating of thin sections as prerequisite for QEMSCAN measurements. Left: thin sections without carbon-coating, middle: vaporizing graphite element, right: final carbon-coated samples.

scanned on a 1.5 x 1.5cm area at 10 μm resolution to define textural parameters, mineralogical composition, and rock nomenclature. Up to 122 individual fields of view were measured in each sample, depicting 1.5 mm per single field. Data processing was performed using the FEI iDiscover software.

The main limitations of the technique include the difficulty or impossibility to distinguish among polymorphs (e.g. calcite vs aragonite), and to identify minerals of very fine-grained mixture (grain size <5 μm), typically clay-rich. Complex minerals like clay interlayer are also challenging. When analysing amorphous material, QEMSCAN analyses the chemical composition but without a mineral name. For some subtle textural features including micropaleontological description, better results are obtained when using optical polarizing microscopy.

References & further reading:

- Quorum Technologies Q150T S/E/ES Sample Preparation System, Instruction Manual, Issue 4 10473.
- Gottlieb, P., Wilkie, G., Sutherland, D., Ho-Tun, E., Suthers, S., Perera, K., Jenkins, B., Spencer, S., Butcher, A., Rayner, J., 2000, Using quantitative electron microscopy for process mineralogy applications. *Journal of the Minerals, Metals and Materials Society*, v. 52, p. 24-25.
- Pierrie, D., Butcher, A., Power, M., Gottlieb, P., Miller, G., 2004, Rapid quantitative mineral and phase analysis using automated scanning electron microscopy (QEMSCAN®); potential applications in forensic geoscience. In: *Forensic Geoscience*, Pye, K., and Croft, D. (eds.), Geological Society, London, Special Publications 232, 328 p.

5.2. *Optical microscopy (OMI)*

Optical microscopy analysis allows the description and identification of transparent and opaque minerals and textures in transmitted and reflected polarized light using an OLYMPUS BX61 optical microscope operating with 2.5, 5, 10, 20, 40 magnification lenses. Photographic documentation was conducted with a mounted digital camera.



An overview of the sample area (gridding) was produced with the 2.5 magnification lens. Each picture taken on the grid was then combined to a full image. Samples were analysed in plain-polarized transmitted (T-PPL) and reflected light (R-PPL) as well as in cross-polarized transmitted (T-XPL) light using the OLYMPUS Stream Motion software. Image settings in these three specific modes were chosen depending on thin section glass thickness, as stated in the following using a 6.30x magnification (for GEO-02 well only) and 3.15x magnification (for rest of samples):

- R/PPL: on average 3.333 milliseconds (ms) exposure, white-balanced, 9V light source,
- T/PPL: on average 72.00 microseconds exposure, white-balanced, 12V light source,
- T/XPL: on average 1053 milliseconds (ms), white-balanced, 12V light source.

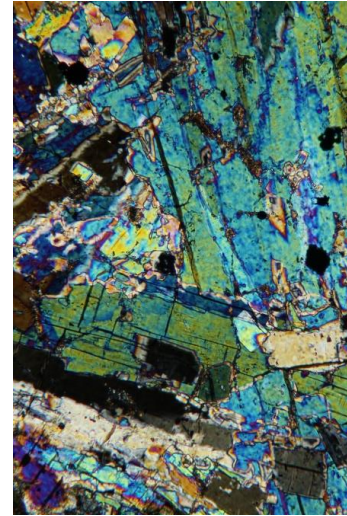


Figure 7: Sample extract in cross-polarized, transmitted light showing anhydrite.

Images were shot on an OLYMPUS DP27 digital camera mounted on the optical microscope with 1/80 of a second and ISO 100. Before image storage, proper scaling reference is implemented into the final image and then stored in TIFF-format with approx. 16262 x 10938 pixels yielding file size of 512 MB on average.

6. Porosity, permeability & density analyses via gas expansion

Porosity and permeability measurements were performed on an AP-608 Automated Permeameter & Porosimeter machine for 173 plug samples. Plugs of 2-8 cm in length and 2.5 cm in diameter were analysed with nitrogen, and for selected samples with helium gas. The latter served as an ideal gas optimized for medium to high permeability values, whereas nitrogen was used for low to very low permeability values, as this was the case for this fine-grained molasse material. For each geological unit, a reference sample was measured under different confining pressures ranging from 200, 500, 700 to 1000 psi to simulate increasing lithostatic pressure, which roughly correlates with sample depth.

Permeability measurements were conducted using the unsteady state pressure decay technique (modified Darcy's law). The measurement determines the equivalent liquid permeability, slip and turbulence factors.

Pore volume measurements were conducted using helium expansion based on Boyle's law. Boyle's law states that the pressure (P) of any ideal gas multiplied by its volume (V) yields a constant value at a given constant temperature, i.e. refers to the ability to determine an unknown volume by an expanding gas of a known pressure and temperature condition into a void space of known volume according to:

$$V_1 = \frac{P_2 \cdot V_2}{P_1}$$



UNIVERSITÉ
DE GENÈVE

Whereas P_1 and P_2 were measured values and V_2 was calculated using the volume formula for cylinders.

Grain densities were measured using the devices' grain volume chamber. Before a set of measurements, a reference volume of the grain volume chamber, which was filled with calibrated metal cylinders was calculated yielding an average value of 10.99 cm^3 . During measurement, a constant temperature of 137°F was kept.



Figure 8: Left: AP-608 Automated Permeameter & Porosimeter machine with attached gas bottles (N, He) in the back and grain volume chamber in the front, right: close-up of grain volume chamber and calibrated metal blocks plus sample (pointed finger).

Proper gas configurations such as nitrogen or helium viscosities were used in software calculations. For each sample, the device measured porosity (in percentage) and permeability (in milli-Darcy) in respective gas atmospheres. Results were corrected for the Klinkenberg effect. This correction factor compensates for gas slippage within pores when gas flows along the pores' walls. In contrast to flowing liquids, the velocity of flowing gas through a pore is not zero at the wall but represents a slight velocity increase. The Klinkenberg equation provides a solid approximation of the liquid permeability from a measured gas permeability.

References & further reading:

- Coretest Systems Inc., AP-608 Automated Permeameter-Porosimeter, Operator's Manual, V6g1, 2011.
- Coretest Systems Inc., AP-608 Automated Permeameter-Porosimeter, Operator's Quick Manual, edited by Jérôme Chablais and Andrea Moscariello, February 2012.
- Coretest Systems Inc., Grain Volume Measurement System, Operator's Manual, Supplement to Operator's Manual for AP-608 Automated Permeameter-Porosimeter, 2008.
- Tanikawa, W., Shimamoto, T., 2006. Klinkenberg effect for gas permeability and its comparison to water permeability for porous sedimentary rocks. *Hydrol. Earth Syst. Sci. Discuss.* 3, 1315–1338.
- Ahmed, A.S.D., Islam, S., 2015. Development Of Field Petrophysical Model Using Enhanced Data Analysis: A Case Study On Kailashtila Gas Field. *Int. J. Pet. Geosci. Eng.* 03, 41–55.



FUTURE CIRCULAR COLLIDER STUDY / DOCTORAL THESIS REPORT

Description of laboratory analyses performed at Montanuniversität (MU) in Leoben, Austria



Revision no.	Date	Description	Written by	Edited by	Verified by
0	16/03/2020	Creation of document	Dipl.-Ing. Maximilian Haas & Prof. Dr. Nina Gegenhuber		
1	07/04/2021	Revision of document		Dipl.-Ing. Maximilian Haas	
2 (final)	09/04/2021	Review & approval of document			Prof. Dr. Robert Galler



Content

Important note.....	3
1. Introduction	3
2. Sample origin, sample number & analyses.....	3
3. Sample shipment	4
4. Sample preparation	5
4.1. Drilling of plug samples.....	5
4.2. Preparation of drill cores.....	5
5. Compressional and shear wave velocity via ultrasonic measurements.....	5
6. Abrasivity behaviour via CERCHAR test	7
7. Tensile strength determination via Brazilian tensile test.....	7
8. Strength index determination via point load test	8
9. Abrasivity behaviour via Laboratoire Central des Ponts et Chaussee (LCPC) test 10	
10. Unconfined compressive strength via UCS test.....	11



Important note

The text used in this document is partly taken from the doctoral thesis written and performed by Dipl.-Ing. Maximilian Haas. Further use of text paragraphs for (scientific) publications, technical reports or FCC-related marketing must be permitted upon request by the author Dipl.-Ing. Maximilian Haas and MUL supervisors Prof. Dr. Robert Galler and Prof. Dr. Nina Gegenhuber, citing both the PhD thesis and this technical report volume.

1. Introduction

An essential part of the subsurface infrastructure construction and re-use of excavated rock material as part of CERN's Future Circular Collider (FCC) study is a thorough understanding of its underlying geology. Hence, rock material has been tested at three distinct laboratory locations, respectively ETH Zurich, University of Geneva and Montanuniversität Leoben. Based on geomechanical, petrophysical, mineralogical and geochemical laboratory analyses, further implications are derived.

This document describes the laboratory measurements performed at Montanuniversität Leoben, Austria from November 2020 to March 2021, within the scope of FCC's PhD study on "Geomechanical, petrophysical and sediment-petrographical classification of molasse rock in the Geneva Basin".

The laboratory measurements at Montanuniversität Leoben include:

1. Compressional (P) and shear (S) wave velocity,
2. Cerchar abrasivity (CER),
3. Brazilian tensile strength (BRA),
4. Point load (PL).
5. Laboratoire Central des Ponts et Chaussées (LCPC) and
6. Uniaxial compressive strength (UCS) tests.

For a detailed scientific description, the reader is referred to literature and technical data sheets cited at the end of each section. The purpose of this laboratory report is dedicated to methodological descriptions only. Scientific interpretations and further conclusions are stated in the PhD thesis by Maximilian Haas.

2. Sample origin, sample number & analyses

Original samples were collected at Swiss (Lucerne) and French (Boussens) core facilities as well as from outcrops along the current FCC subsurface tunnel alignment according to CERN's



CDR report (December 2018) featuring samples from the Quaternary and Molasse (OSM) formations.

Two sample types were analysed:

1. Drill cores (from Peissy-I well) and
2. Plug samples from
 - a. outcrops and
 - b. boreholes, namely Gex-CD-01 to -07 drilled from half-cores.

Plugs with dimensions of 2-2.5 cm in diameter and 2-8 cm in length were drilled from half cores and outcrop blocks and split in different fractions for subsequent laboratory analyses. Table 1 gives an overview of the number of samples per analysis.

Table 1: Overview of analyses performed at MUL with respective sample number and sampling location (well).

type of analysis	sample amount	sample location
P-wave ultrasonic velocity	498	Point 1 (C-wells), Peissy-I, Sarzin, Mornex, GEX-CD-1 to GEX-CD-7
S-wave ultrasonic velocity	470	
Cerchar	151	
Brazilian tensile strength	103	
Point load	185	
Laboratoire Central des Ponts et Chaussees (LCPC)	65	
Uniaxial compressive strength (UCS)	184	

All samples have been described sedimentologically and geologically prior to all subsequent analyses.

3. Sample shipment

Due to the COVID-19 pandemic, measurements could not be performed personally but were outsourced to the rock mechanics laboratory at Montanuniversität Leoben. Consequently, samples have been shipped to Leoben via truck transport for geomechanical and petrophysical analyses to compensate potential time delays. In total, about 512 kg of rock material were sent.



Figure 1: One out of two shipment boxes. Each sample was bubble wrapped to prevent any damage on rock samples.



4. Sample preparation

4.1. Drilling of plug samples

Plugs were drilled from well core samples and outcrop blocks using a driller machine and further prepared on abrasive tables to create planar surfaces for subsequent laboratory analyses.

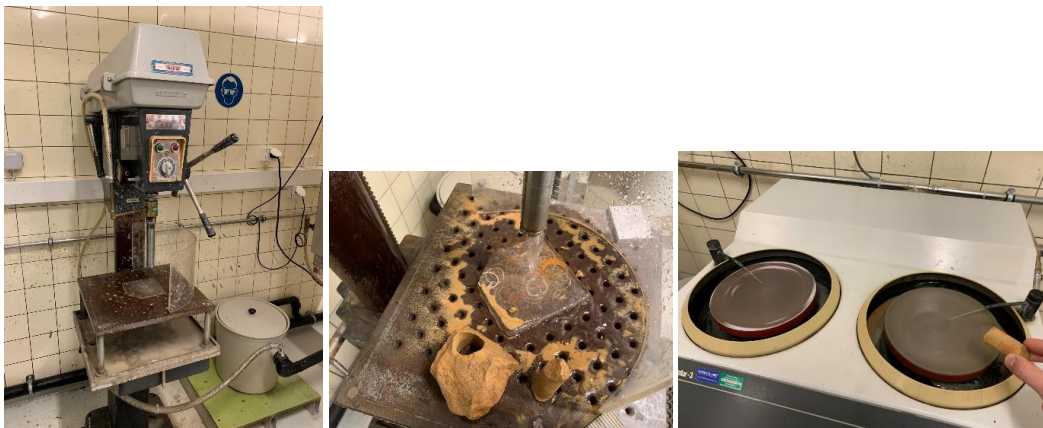


Figure 2: Overview of machine equipment to drill and prepare the plug samples. Left: Driller to drill plugs from blocks and/or cores, middle: result of a drilled plug, right: grinding of plug sample with rough (right table) and fine (left table) abrasives under flowing water.

4.2. Preparation of drill cores

Each drill core was prepared properly following standard procedures and norms in terms of length to diameter ratios and planar surfaces for each analysis as described in the following sections.

5. Compressional and shear wave velocity via ultrasonic measurements

In an isotropic elastic material two wave types, respectively V_p and V_s are observed. They are linked to elastic parameters such as Young's modulus, which is defined as the ratio of axial stress to axial strain in a uniaxial stress state, bulk modulus, k , as the ratio of hydrostatic stress to volumetric strain and shear modulus, μ , as the ratio of shear stress to shear strain. Further derivations using Poisson's ratio, which depicts the negative ratio of lateral strain to axial strain in a uniaxial stress state can be drawn. Wave velocity is controlled by elastic properties of rock forming minerals, their fractional volume, their contact, cementation, porosity, saturation, pressure, temperature and pore fluid. In magmatic and metamorphic rocks, it is mainly influenced by the effects of cracks, fractures and pores, their anisotropy, temperature and pressure. For sedimentary rocks, porosity and matrix are the most important factors. In



an anisotropic material a directional dependence can be indicated. With increasing pressure pore, fracture and crack closure occurs and velocities increase. With increasing temperature velocity decreases because of the change of the elastic properties of the rock forming minerals, the change of the pore filling and changes in contact conditions of the grains. Ultrasonic velocities are sensitive to fluids exhibiting strong influence on compressional wave velocity and a weak influence on shear wave velocity.

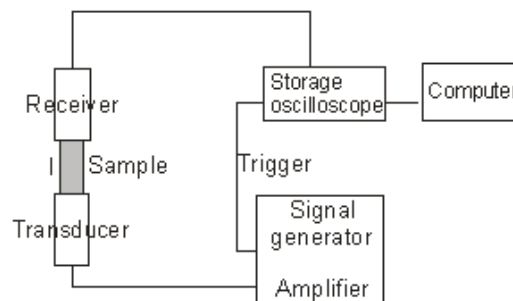


Figure 3: Ultrasonic device (left) and illustration of measurement procedure (right).

The compressional wave velocity was determined with an ultrasonic device. The sample was fixed between a transmitter and receiver with a contact agent on both sides (ultrasonic gel) and a pressure of 5 bar was applied continuously. Transducers comprised piezoceramic systems (Type: UPE, Geotron Elektrik, Germany) designed for compressional and shear wave measurements. A Dirac impulse was sent from a signal generator (Geotron Elektrik, Germany) to the transducer and resulted in a mechanical pulse passing through the sample. The arriving signal was visualized via a storage oscilloscope (Cleverscope, New Zealand). A program picked first arrivals and calculated velocities. At the start of each new measurement cycle, delay time between electrical impulse and mechanical pulse (dead time) was determined and corrected for all measurements. The onset of V_p and V_s were detected with the Akaike Information Criterion Picker (AIC). The AIC is an autoregressive method and assumes measurements, which are divided into local stationary segments, whereby the sections before and after an onset of a specific waveform state two different stationary processes. A phase onset is then identified by the position, where the AIC values show a minimum (least-square fit). A global minimum of AIC refers to the onset of a compressional wave arrival, a local minimum to an onset of a different phase is associated to the onset of the shear wave.

References & further reading:

- Gegenhuber, N. and Steiner-Luckabauer, C., 2012, v_p/v_s Automatic Picking of Ultrasonic Measurements and their Correlation of Petrographic Coded Carbonates from Austria, 74th EAGE Conference & Exhibition, Copenhagen. Anal. 14, 99–123.



- Mavko, G., Mukerji, T. and Dvorkin, J., 2009, The rock physics handbook, Cambridge University Press
- Schoen, J.H., 2015, Physical Properties of Rocks, Elsevier

6. Abrasivity behaviour via CERCHAR test

The CERCHAR (Laboratoire du Centre d'Etudes et Recherches des Charbonnages) abrasivity test is used to determine the CERCHAR Abrasivity Index (CAI). The CAI classification according to the International Society for Rock Mechanics (ISRM) ranges from 0.1 (extremely low abrasivity) to >5.0 (extremely high abrasivity). Measurement procedure follows standard NF P 94-430-1, AFNOR Paris 2000.

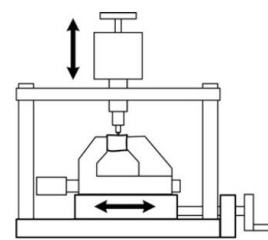


Figure 4: CERCHAR test apparatus depicting direction of weight movement (vertical) and steel pin (horizontal).

A sample's surface of a 10 mm rock piece was scratched 5 times for 1 mm/sec with a defined test pin (Rockwell hardness = HRC 54-56) along 5 different locations on the sample with a pin direction normal to the foliation on the sawn rock surface. The wear and tear of the testing pin was checked under a microscope with a computer-aided image processing program. Each individual test pin was examined 4 times at different angles (0°, 90°, 180°, 270°) and an average value was calculated. The mean total abrasion was calculated from these mean values, which were then divided by a factor of 100 to obtain the CAI.

References & further reading:

- Alber, M, Yrah, O, Dahl, F., Bruland, A., Käsling, H., Michalakopoulos, Th., Cardu, M., Hagan, P., Aydin, H., Özarslan, 2013, ISRM Suggested Method for Determining the Abrasivity of Rock by the CERCHAR Abrasivity Test, Rock Mechanics and Rock Engineering, <https://doi:10.1007/s00603-013-0518-0>

7. Tensile strength determination via Brazilian tensile test

The Brazilian tensile test is an indirect method to derive the uniaxial tensile strength of a material. A circular rock disc sample was prepared and subjected to compression between two curved platens in a servo-hydraulic rock testing system type MTS 815. During test procedure, it is assumed that the platens are rigid compared to the rock and follow a linear load distribution. This testing machine is ideal for uniaxial and triaxial compression tests as well as for direct and indirect tensile tests designed for testing rock samples up to 2850 kN axial compressive forces of up to 2850 kN and 1340 kN of tensile forces. The control mode was regulated at 3 mm/min. The uniaxial tensile strength σ_t (MPa) was calculated using the failure load F_a (kN) at which a tensile crack develops, according to:



$$\sigma_t = \frac{2F_a}{\pi Dt} = 0.636 \frac{F_a}{Dt}$$

With:

D = diameter (mm),

t = thickness (mm).

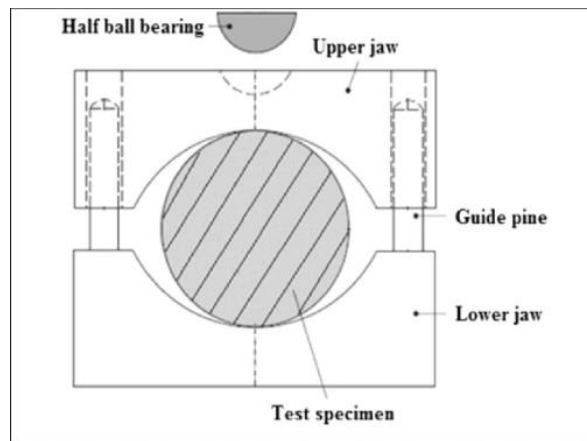
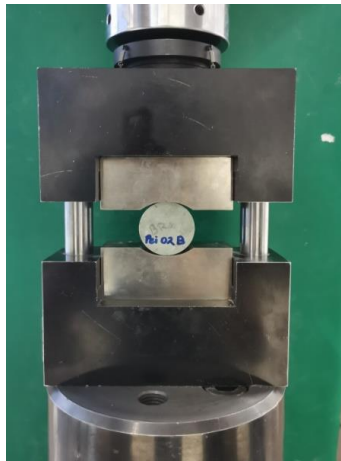


Figure 5: Brazilian testing apparatus (left) and illustration of measurement procedure (right), after Bieniawski and Hawkes, 1978.

References & further reading:

- Bieniawski, Z.T. and Hawkes, I. 1978. Suggested methods for determining tensile strength of rock materials. *International Journal of Rock Mechanics and Mining Sciences & Geomechanics Abstracts* 15(3): 99-103, [https://doi.org/10.1016/0148-9062\(78\)90003-7](https://doi.org/10.1016/0148-9062(78)90003-7).
- MTS Rock and Concrete Mechanics Testing System, Technical Description, MTS, Eden Prairie (USA)

8. Strength index determination via point load test

The point load strength index is determined using the point load test according to ISRM following the method after Franklin (1985). This index is further correlated with the uniaxial compressive strength (UCS). The testing device depicts the same as used for the Brazilian tensile strength test (see section 7) via a servo-hydraulic rock testing press type MTS 815, which applied an axial pressure with a control mode of 1,35 mm/min. The test specimen was clamped between two loading plates and pressure was applied until rock failure.

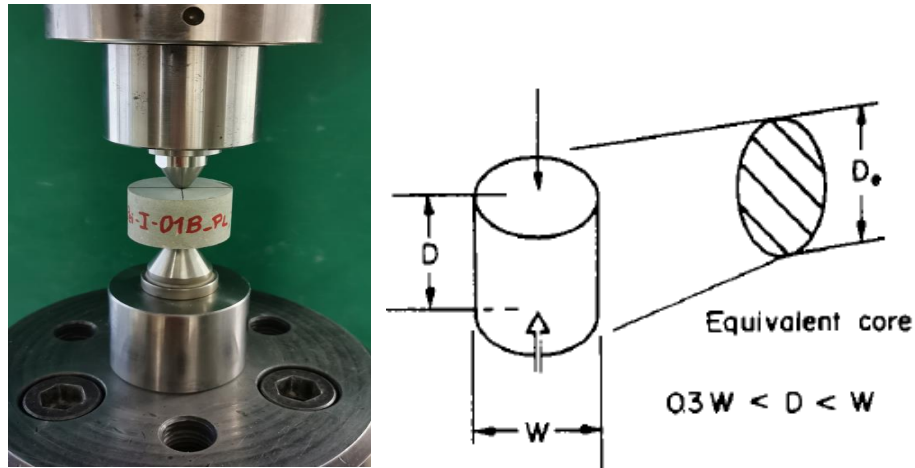


Figure 6: Point Load test (left) and schematic illustration (right) showing dimensions and direction for axial loading.

The load applied to the sample was converted to the uncorrected point load strength, I_s (MPa), according to:

$$I_s = \frac{P}{D_e^2}$$

With:

P = applied load (N),

D_e = equivalent core diameter (mm), calculated as:

$$D_e^2 = 4A/\pi$$

With:

A = minimum cross-sectional area (mm²) of a plane through the platen contact points.

Finally, the corrected point load strength index (MPa) equivalent to point load index for a 50 mm diameter sample, is calculated according to:

$$I_{s(50)} = FI_s$$

With

F = unitless geometric correction factor:

$$F = \left(\frac{D_e}{50}\right)^{0.45}$$

The mean value of $I_{s(50)}$ was calculated by removing the two highest and lowest values from 10 or more valid tests. When significantly fewer results were available, only the highest and lowest results were removed, and the mean was calculated from the remaining results.



To calculate mean values, test results were grouped according to similar sample locations and lithology. This provided mean values $I_{s(50)}$ on a location and lithology basis for further correlations with UCS values (see section 10), according to:

$$UCS = cI_{s(50)}$$

With:

c = unitless correlation factor ranging from 20 to 25, derived by plotting UCS and $I_{s(50)}$ values for different locations and lithologies.

References & further reading:

- Franklin, J.A. 1985. Suggested method for determining point load strength. International Journal of Rock Mechanics and Mining Sciences & Geomechanics Abstracts 22(2): 51-60, [https://doi.org/10.1016/0148-9062\(85\)92327-7](https://doi.org/10.1016/0148-9062(85)92327-7).

9. Abrasivity behaviour via Laboratoire Central des Ponts et Chaussee (LCPC) test

The LCPC test is used to derive the abrasivity of rock material. Test equipment consisted of an electric motor, which uses a rotating shaft to set a rectangular metal wing with a standardized steel hardness according to HRB 60-75 in rotation. The metal wing was immersed in a gravelly material with grain sizes of 4 - 6.3 mm in a steel container. The metal wing rotated at 4500 rpm for five minutes. To determine the abrasiveness, the metal wing was weighed before and after the measurement. The weight loss of the wing is a measure of the abrasiveness of the material. For each sample run, a new metal wing was used.

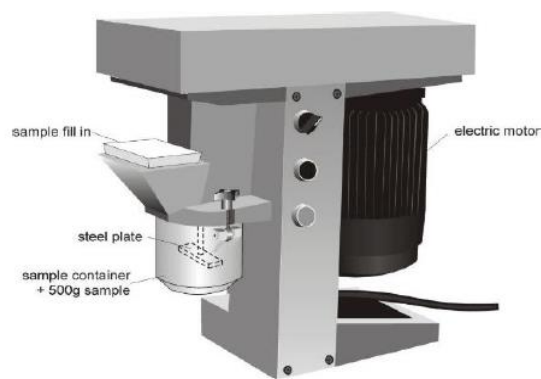


Figure 7: LCPC testing apparatus scheme as used for analysis.



10. Unconfined compressive strength via UCS test

The unconfined (sometimes also uniaxial) compressive strength (UCS) is used to measure the uniaxial rock strength of a rock sample. Cementations, i.e. bonding of solid components, anisotropy, porosity and fractures significantly influence the final results of the test.

The UCS test was carried out on a computer-controlled servo-hydraulic MTS 815 testing apparatus, with a load frame of type 315.02 and a machine rigidity of 9 MN/mm. The test specimens depicted a height-to-diameter ratio of 2:1 and were used without an intermediate layer or lubricant between the pressure plates. The upper plate was loaded with a low axial force and spherically supported. Loading up to rock failure was controlled with a rate of 0.5 mm/min. The UCS (MPa) was then calculated using the maximum force F_{\max} (N) and test specimen cross-sectional area A (mm²) according to:

$$\text{UCS} = F_{\max}/A$$



Figure 8: UCS testing apparatus with rock sample during loading.

References & further reading:

- Bieniawski, Z.T., Bernede, M.J. 1979. Suggested methods for determining the uniaxial compressive strength and deformability of rock materials: Part 1. Suggested method for the determination of the uniaxial compressive strength of rock materials. International Journal of Rock Mechanics and Mining Sciences & Geomechanics Abstracts 16(2) 137-138.
- Schoen, J.H., 2015, Physical Properties of Rocks, Elsevier

D Curriculum vitae



Dipl.-Ing. Maximilian Mathias Haas, B.Sc.

maximilian.haas@level8.info

Professional Experience

02/2022 to present	Geomechanics Engineer, Geomechanics Center of Excellence, Schlumberger, London Gatwick, United Kingdom
09/2018 – 06/2022	PhD Student at Montanuniversität Leoben and the European Organization for Nuclear Research, Geneva, Switzerland, in collaboration with the Swiss Federal Institute of Technology (ETH) Zurich and Université de Genève
03/2018 – 08/2018	Geophysics Associate, Geodata ZT GmbH, Leoben, Austria
06/2017 – 08/2017	Seismic Acquisition Student, Research Expedition (SONNE vessel, leg SO 258/2), Offshore Indian Ocean & Onshore, Sri Lanka
03/2017 – 09/2017	Master Student, Alfred Wegener Institute, Bremerhaven, Germany
09/2016 – 09/2016	Research Student, Alfred Wegener Institute, Bremerhaven, Germany
12/2015 – 12/2015	Temporary Associate, HOT-Engineering, Leoben, Austria
08/2015 – 12/2015	Bachelor Student, Zentralanstalt für Meteorologie und Geodynamik (ZAMG), Vienna, Austria
11/2015 – 03/2018	Research Student, Institute of Applied Geophysics, Montanuniversität Leoben
08/2014 – 04/2014	Intern, Rohöl-Aufsuchungs-AG (RAG), Vienna, Austria
04/2014 – 04/2014	Intern, GEO-5 (formerly Joanneum Research), Leoben, Austria
08/2012 – 09/2012	Intern, RHI Magnesita, Hochfilzen, Austria

Professional Affiliations, Skills, Training and Teaching

- Association Memberships: EAGE, AAPG, SPE, DGG, DTTG, ÖGG, SASEG, CHGEOL
- Responsibilities in Associations:
 - EAGE's Geoscience & Engineering in Energy Transition Conference, Technical Committee Member
 - DGG Public Relation & Outreach Committee, Team Leader
- SASEG Student Grant Award (2021)
- Full Scholarship Holder (2016-2018), Pro Scientia
- Language Skills: German, English, French, Spanish
- Software Skills: Techlog, Petrel, ArcGIS, Surfer, Strater, OriginPro, ioGAS, Echos Paradigm
- Programming Skills: MATLAB, R, Python, Generic Mapping Tool (GMT)
- Various Geological Field Trips and Excursions to e.g. South Africa, Crete, Cyprus
- Academic Co-Supervisor of 4 Seminar Theses
- Instructor & Co-Lecturer of Petrophysical & Mineralogical Laboratory Measurements for Graduate and Undergraduate Students at the Université de Genève and Montanuniversität Leoben

Education

Ongoing: **Dr.mont.**, Mining Sciences, European Organization for Nuclear Research (CERN), Swiss Federal Institute of Technology (ETH) Zurich, Université de Genève, Montanuniversität Leoben
2020: **Data Analyst Certificate**, Data Science & Geostatistical Analysis, Stanford University, California
2018: **Diploma Degree**, Applied Geophysics, Montanuniversität, Leoben
2016: **Bachelor's Degree**, Applied Geosciences, Montanuniversität, Leoben